# Characterisation of Lysozyme-Steroid Glucuronide Conjugates

A thesis presented in partial fulfilment of
the requirements for the degree of
Doctor of Philosophy in Chemistry
at Massey University.

Christopher Mark Smales

**February, 1997**

## Abstract

The steroid glucuronides estrone glucuronide and pregnanediol glucuronide were synthesised using the O-glycosylation reaction of a glycosyl donor with the appropriate steroid under standard Koenigs-Knorr conditions. X-ray crystallographic studies showed that the synthetic estrone glucuronide molecule had the correct stereochemistry. Estrone glucuronide and pregnanediol glucuronide conjugates of hen egg white lysozyme were prepared by both the mixed anhydride and active ester coupling procedures. Both methods gave good yields of conjugate but the active ester procedure gave a more diverse range of products. Unreacted lysozyme, which was present in all cases, was removed by a combination of cation-exchange and hydrophobic-interaction chromatography to give purified conjugate material whose lytic activity was inhibited by over 90% in the presence of excess anti-steroid glucuronide antibody. Steroid glucuronide-lysozyme conjugates purified in this way could be used in a homogeneous enzyme immunoassay system to measure the levels of urinary estrone and pregnanediol glucuronide encountered in a normal menstrual cycle. Chromatography of the conjugation reaction mixtures on an S-Sepharose (fast flow) column in the presence of 7 M urea allowed the isolation of the different conjugate products. Conjugation of lysozyme with estrone glucuronide by the mixed anhydride method gave one major derivative exclusively acylated at lysine residue 33 while acylation with pregnanediol glucuronide gave two major derivatives exclusively acylated at lysine residues 33 and 97 respectively. On the other hand, conjugation of lysozyme with the two steroid glucuronides by the active ester method gave six derivatives which were acylated at combinations of one or more of three lysine residues, 33, 97, and 116. The correlation of the protein environments of the lysine amino groups in the crystal structure of lysozyme with the acylation positions in the conjugate families suggested that these positions were determined not only by the surface accessibility and nucleophilicity of the lysine residues but also by the steroid glucuronide and the acylating reagent. Computer derived three dimensional structures of the estrone glucuronide-lysozyme and pregnanediol glucuronide-lysozyme conjugates suggested that the enzyme conjugate may be inactivated by the antibody in the immune complex by either providing a physical barrier to approach by the large bacterial substrate or by disrupting the binding of the bacterial cell wall polymer into the active site cleft. The lytic activity of the estrone glucuronide-lysozyme E3 conjugate was not inhibited in the presence of excess antibody when the small chitohexaose substrate was used, implying that the substrate could access the active site even when the conjugate was bound by antibody. The detailed characterisation of the mixed anhydride estrone glucuronide-lysozyme conjugate coupled with the current knowledge of the antigenic determinants of hen egg white lysozyme has made it possible to design, in principle, a novel sandwich solid phase immunoassay format for the measurement of estrone glucuronide levels.

# Acknowledgements

A large number of people have given me their time and advise during this thesis. As I can not mention everyone, thankyou to those of you not referred to below.

I am particularly indebted to my supervisor Associate Professor Len Blackwell for his support and guidance throughout the study presented (and for reading this thesis several times). Thanks must also go to Dr. Chris Moore (my second supervisor) who retired during the course of this study and Dr. Gill Norris for all her help and advice with crystallographic studies.

Others who have helped during this thesis that I wish to thank include;

Dr. Bryan Anderson for his help with Silicon Graphics modelling,

Associate Professor Dave Harding and Mr Dick Poll with chromatographic apparatus and advice,

Dr. Tony Burrell and Associate Professor Joyce Waters for solving the estrone glucuronide crystal structure,

Dr. Phil Jeffrey for solving the estrone glucuronide-lysozyme conjugate crystal structure,

Mr Dave Elgar for his advice on electrophoresis and related techniques, and

Dr. Roger Collin for his help with solid phase immunoassay colour test strips.

I must also thank all of the technical staff who have helped me during this study and the staff in stores who have always endeavoured to meet my needs. Of course such a study would be very dull indeed if it was not for the help, advice, humour and banter of my fellow postgraduate students within the Ovarian Monitor research group and the Departments of Chemistry and Biochemistry.

I am grateful to Massey University for a Massey University Postgraduate Scholarship.

A big thanks must also go to Mum and Dad who have supported me throughout my Ph.D. Finally, I would like to thank my wife Virginia to whom I am especially grateful to for all her support, help, and for putting up with the many highs and lows that come with scientific research.

# Acknowledgement of Published Work

The following work has thus far been published from that presented in this thesis:

Smales, C. M., Cooke, D., and Blackwell, L. F. (1994) Use of ion-exchange and hydrophobic-interaction chromatography for the rapid purification of lysozyme-estrone glucuronide conjugates, *J. Chrom. B* **662,** 3-14.

Smales, C. M., Blackwell, L. F., Waters, J. W., and Burrell, A. K. (1997) Crystal structure of an estrone glucuronide hydrate, Submitted to *Acta Cryst.*

# Table of Contents

---

## Chapter Two

## The Preparation and Purification of Estrone Glucuronide- and Pregnanediol Glucuronide-Lysozyme Conjugates

Conjugates Suitable for Use in a Homogeneous Enzyme Immunoassay System for the Measurement of Menstrual Cycle Levels of Urinary Estrone Glucuronide and Pregnanediol Glucuronide

---

## Chapter Three

## The Characterisation of Estrone Glucuronide- and Pregnanediol Glucuronide-Lysozyme Conjugates

---

## Chapter Four

## Structural Aspects of the Steroid Glucuronide-Lysozyme Conjugate-Anti-Hapten Antibody Immune Complexes



---

## Chapter Five

## The Kinetics and Mechanism of the Estrone Glucuronide-Lysozyme-Anti-Estrone Glucuronide Antibody Binding Reaction

---

## Chapter Six

## Studies Toward the Development of a Colour Test Immunoassay For the Detection of the Fertile Period

---

## Chapter Seven

## Crystallographic Studies

# List of Figures

# List of Tables

# List of Schemes

# Abbreviations

| | |
|---|---|
| $A_{280}$ | Absorbance at 280 nm |
| AB | Antibody |
| AE | Active ester |
| BBT | Basal body temperature |
| α-bromosugar | Methyl 1-bromo-1-deoxy-2,3,4-tri-O-acetyl-α-D-glucopyran-uronate |
| BSA | Bovine serum albumin |
| $C_B$ | Concentration of bound conjugate |
| $C_F$ | Concentration of free conjugate |
| $C_T$ | Total conjugate concentration |
| CDR | Complementary determining region |
| Conj | Lysozyme-steroid glucuronide conjugate |
| DCC | Dicyclohexylcarbodiimide |
| DMF | Dimethylformamide |
| DMPTU | N,N-dimethyl-N'-phenylthiourea |
| E1G | Estrone glucuronide |
| E1G-AB | Anti-estrone glucuronide antibody |
| E1G[H] | Estrone glucuronide (acid form) |
| E1G-HEWL | Estrone glucuronide-hen egg white lysozyme conjugate |
| E1G-HRP | Estrone glucuronide-horseradish peroxidase conjugate |
| E2-17β-3G | Estradiol-17β-3-glucuronide |
| E3-3G | Estriol-3-glucuronide |
| E3-16G | Estriol-16α-glucuronide |
| E3-17G | Estriol-17β-glucuronide |
| EDC | 1-ethyl-3-(3-dimethylaminopropyl) carbodiimide hydrochloride |
| EDTA | Ethylenediamine tetra-acetic acid |
| EIA | Enzyme immunoassay |
| ELISA | Enzyme-linked immunosorbent assays |
| EMIT | Enzyme-multiplied immunoassay technique |
| EPPS | N-(2-hydroxyethyl)piperazine-N'-(3-propane sulfonic acid) |
| Fab | Antigen binding fragment |
| FPLC | Fast protein liquid chromatography |
| FSH | Follicle stimulating hormone |
| GlcNAc | N-acetylglucosamine |
| $(GlcNAc)_2$ | Di-N-acetyl-chitobiose |
| $(GlcNAc)_3$ | Tri-N-acetyl-chitotriose |
| $(GlcNAc)_4$ | Tetra-N-acetyl-chitotetraose |
| $(GlcNAc)_5$ | Penta-N-acetyl-chitopentaose |

| | |
|---|---|
| $(GlcNAc)_6$ | Hexa-N-acetyl-chitohexaose |
| GnRH | Gonadotropin releasing hormone |
| HCG | Human chorionic gonadotrophin |
| HEPES | N-(2-hydroxyethyl)piperazine-N'-(2-ethane sulfonic acid) |
| HEWL | Hen egg white lysozyme |
| HEWL-AB | Anti-hen egg white lysozyme antibody |
| HPLC | High performance liquid chromatography |
| HRP | Horseradish peroxidase |
| HRP-E1G | Horseradish peroxidase-estrone glucuronide conjugate |
| I.D. | Internal diameter |
| IgG | Immunoglobulin G class of antibody |
| LH | Luteinizing hormone |
| MA | Mixed anhydride |
| MCAB | Estrone glucuronide monoclonal antibody |
| m.p. | Melting point |
| MurNAc | N-acetylmuramic acid |
| $NAD^+$ | Nicotinamide adenine dinucleotide phosphate (oxidised form) |
| NADPH | Nicotinamide adenine dinucleotide phosphate (reduced form) |
| NAG | N-acetylglucosamine |
| NAM | N-acetylmuramic acid |
| NFP | Natural Family Planning |
| NHS | N-hydroxysuccinimide |
| NMR | Nuclear magnetic resonance |
| PAGE | Polyacrylamide gel electrophoresis |
| PBS | Phosphate buffer saline |
| PdG | Pregnanediol glucuronide |
| PdG[H] | Pregnanediol glucuronide (acid form) |
| PEG | Polyethylene glycol |
| PIPES | Piperazine-N,N'-bis-(2-ethane sulphonic acid) |
| PITC | Phenylisothiocyanate |
| RIA | Radioimmunoassay |
| r.m.s. | Root mean square |
| µs | Microsphere |
| SDS | Sodium dodecyl sulphate |
| SDS-PAGE | Sodium dodecyl sulphate-polyacrylamide gel electrophoresis |
| $\Delta T$ | Change in transmission |
| TFA | Trifluoroacetic acid |
| TMB | Tetramethylbenzidine |
| TNBS | 2,4,6-trinitrobenzene 1-sulfonic acid |

| | |
|---|---|
| tris | Tris(hydroxymethyl)aminomethane |
| WHO | World Health Organisation |

## Amino Acid Abbreviations

| | | |
|---|---|---|
| A | Ala | Alanine |
| C† | | S-carboxymethylated cysteine |
| D | Asp | Aspartic acid |
| E | Glu | Glutamic acid |
| F | Phe | Phenylalanine |
| G | Gly | Glycine |
| I | Ile | Isoleucine |
| K | Lys | Lysine |
| K* | | Steroid glucuronide acylated lysine residue |
| L | Leu | Leucine |
| M | Met | Methionine |
| N | Asn | Asparagine |
| P | Pro | Proline |
| Q | Gln | Glutamine |
| R | Arg | Arginine |
| S | Ser | Serine |
| T | Thr | Threonine |
| V | Val | Valine |
| W | Trp | Tryptophan |
| Y | Tyr | Tyrosine |

# Chapter One

# Introductory Chapter

## The Framework for the Study Discussed in the Following Chapters

---

## 1.1 The Physiological Mechanisms and Control of the Menstrual Cycle

A prominent London Underground billboard in 1996 proclaimed:

> "God created man on the sixth day,
> when will be the best day for you"?

This thesis investigates methods for defining the fertile period during the female menstrual cycle. The ability to define the fertile period during a woman's menstrual cycle is a powerful tool for couples wishing to achieve pregnancy, as the best day (i.e. that day on which a single act of intercourse is most likely to result in pregnancy) can be accurately predicted and used for intercourse. Definition of the fertile period is also extremely useful for couples who wish to avoid pregnancy. Couples can minimise the chances of pregnancy by practising abstinence from intercourse during the potentially fertile period of the menstrual cycle.

### 1.1.1 The Menstrual Cycle and the Hypothalamic-Pituitary-Ovarian Axis

The key process in the regular and cyclic pattern of events known as the menstrual cycle in the primate order of the mammalian class is the rupturing of a mature follicle to release a viable ovum (egg) [1]. This process (the release of an oocyte from the ovarian follicle), which occurs once a month approximately mid-way through the menstrual cycle [2], is known as ovulation [3] and is the central event in reproduction [4]. Once a viable ovum has been released its life-span is relatively short, being of 12-24 hours duration [5], and hence the time during which fertilisation and conception may occur within a single menstrual cycle is extremely limited [6]. However, the actual fertile period is the time

during the menstrual cycle when coitus can result in the fertilisation of the ovum by a spermatozoon [4] and as a result the life-span of the male spermatozoa, which have a mean survival time of 3-4 days [7], must also be considered in measurements of the fertile period. Therefore, to define the potentially fertile period it is necessary to predict ovulation far enough in advance to allow for the life-span of both the spermatozoa and the ovum.

The menstrual cycle and ovulation take place as a result of a complex series of interactions between gonadotropin releasing hormone (GnRH), follicle stimulating hormone (FSH), luteinising hormone (LH) and the steroid hormones oestradiol and progesterone which are secreted by the hypothalamic-pituitary-ovarian axis [8]. By means of delicate mechanisms and interactions that are not well understood, these hormones control follicular growth, the release of the ovum from the follicle and the formation of the corpus luteum [8]. Both FSH and LH are large glycoproteins consisting of two subunits ($\alpha$ and $\beta$) of which the $\alpha$ subunits are very similar, but the $\beta$ subunits are distinctive and are responsible for the biological specificity of the hormones [1]. GnRH consists of ten amino acids linked together to form a decapeptide [1] while oestradiol and progesterone are members of a family containing the traditional steroid skeleton. A simplified summary of the complex interactions between the hypothalamic-pituitary-ovarian axis has been published by Wilson [9] and may be described as follows: the levels of the ovarian hormones estradiol and progesterone are initially sensed by the hypothalamus. In response the hypothalamus controls the pituitary gland through levels of GnRH in the blood which drains into the anterior lobe of the pituitary gland. In response to the levels of GnRH from the hypothalamus the anterior pituitary lobe releases various amounts of both follicle stimulating hormone and luteinising hormone which control the menstrual cycle [9]. To define and recognise the fertile period during the menstrual cycle it is necessary to understand the biochemical and physiological events which are occurring at the level of the ovary.

It has been estimated that the human female is born with somewhere between five hundred thousand and two million primordial follicles [2, 9]. This large supply of oocytes is exhausted once menopause is reached [10]. All of the primordial follicles, which consist of a single oocyte surrounded by a single layer of flattened spindle-shaped granulosa cells [10], have the potential to mature and ovulate [2]. However, in the human female over 99% of the primordial follicles formed during foetal life fail to ovulate and undergo atresia or degeneration [11, 12]. Although up to twelve preovulatory follicles may be initially recruited in each menstrual cycle, usually, in natural cycles, only one develops to the point of ovulation per cycle [12]. What therefore, is the physiological

basis which allows the recruitment and formation of a mature follicle through to the stage of ovulation from this initial cohort?

### 1.1.2 Recruitment, Selection and Emergence of the Dominant Follicle

Although the exact mechanism of selection of the dominant follicle is not yet fully understood [13] extensive information on the processes which occur during recruitment and selection has now been published. From this data, several models have been put forward in an attempt to explain the mechanisms occurring during the selection process. The most recent model suggests that during the continuous process, known as folliculogenesis, a given number of primordial follicles begin to develop each day [10]. This model is based on calculations involving changes in the total number of observed follicles rather than observation and tracking of individual follicles. The number of primordial follicles recruited into this growing pool is thought to vary with time, being greatest in early life and decreasing with age [12, 14]. The fraction of the primordial follicles recruited is also thought to be a function of the total pool available which can be influenced by a number of external and internal factors such as age, nutrition, activity of the thymus gland and opioid peptides [12].

After a gradual growth period of about 70 days [10] the primordial follicles become small antral follicles of 2-4 mm in diameter [11, 12] so that at the beginning of each menstrual cycle there are about 20 or so in the ovaries available for further development [2, 12]. This stage of follicular development, up to the small antral stage (2-4 mm), is believed to continue in a random and spontaneous manner which is unaffected by daily fluctuations in gonadotrophin levels. At the end of the 70 day slow growth period the small antral follicles of 2-4 mm in diameter are FSH dependent. While low levels of FSH are sufficient to enable the small antral follicles to develop normally, larger amounts are required for development to proceed beyond 4 mm diameter in size [11]. At the beginning of each new menstrual cycle there is a modest rise in the levels of FSH secreted by the pituitary gland which results in the recruitment of a cohort of up to 20 follicles to undergo further growth. This increased secretion of FSH by the pituitary gland constitutes the primary signal for preovulatory follicular development to begin [15-17]. The level of FSH which must be reached to stimulate a follicle to grow beyond 4 mm in size is known as the threshold level [15-16], with each follicle requiring a different level of exposure to FSH in order to begin further development. Zeleznik and Kubik [15] demonstrated experimentally using monkeys that there was a threshold for stimulation of follicles (to grow beyond 4 mm in size) by FSH, and upon reaching this threshold follicles readily entered their final stages of gonadotropin-dependent maturation [15]. If this threshold was not reached, individual follicles did not grow beyond 4 mm in size [15]. It is also

well documented that the FSH rise must be slow to prevent the possibility of large numbers of follicles carrying on to ovulation ("superovulation") [10].

The FSH secreted by the pituitary at the beginning of each cycle binds to the FSH receptor sites located on the surface of the granulosa cells of the small antral follicles [14]. This causes (1) the oocyte to enlarge and (2) the granulosa cells to divide and multiply and as a result the follicles grow rapidly. At sometime during this rapid growth phase, the granulosa cells of the developing follicle acquire aromatase activity due to the newly attained ability to express the cytochrome P450 enzyme known by the same name (aromatase). In natural cycles, normally only one follicle is destined to ovulate and it is thought that the follicle which most rapidly acquires this aromatase activity probably becomes the dominant follicle [12] while the remainder become degenerate or atretic [17]. Hence aromatase activity is a distinctive feature of the dominant follicle(s) (as clearly shown by McNatty [18]) and any proposed model must explain this.

*1.1.2.1 The Scheele and Schoemaker model [10] for the selection of the dominant follicle*
The recent (1996) model of Scheele and Schoemaker [10] (based on the available literature data) for the selection of the dominant follicle consists of three FSH related mechanisms of follicle selection working in concert during each menstrual cycle as shown in Fig. 1.1.1. The model has been termed the three-pillar cornet model whereby the mechanisms, or pillars, on which follicle selection is based act together to select the dominant follicle and non-dominant follicles are driven into atresia [10]. The model is really a pictorial summary of the events occurring during recruitment, selection and follicle dominance and not a complete explanation. The model is based on the threshold principle [15-17, 19-21] whereby for the small antral follicles (2-4 mm diameter) to grow further and develop, a certain level of FSH must be reached (the threshold level) for each follicle. The cohort of 20 or so follicles recruited at the beginning of each new menstrual cycle have different sensitivities to FSH and thus different threshold levels. The three pillar model is envisaged as follows;

(1) At the start of the new cycle the cohort of small antral follicles can be considered to be in a cornet whereby the most sensitive follicle with the lowest FSH threshold is situated at the bottom of the cornet. The FSH dependent growth of a cohort of follicles is initiated by a moderate rise in the level of FSH secreted by the pituitary which surpasses the FSH threshold of these follicles.

(2) The acquisition of aromatase activity by the growing follicles results in an increase in the levels of estrogen (see the following discussion for further details) which by a

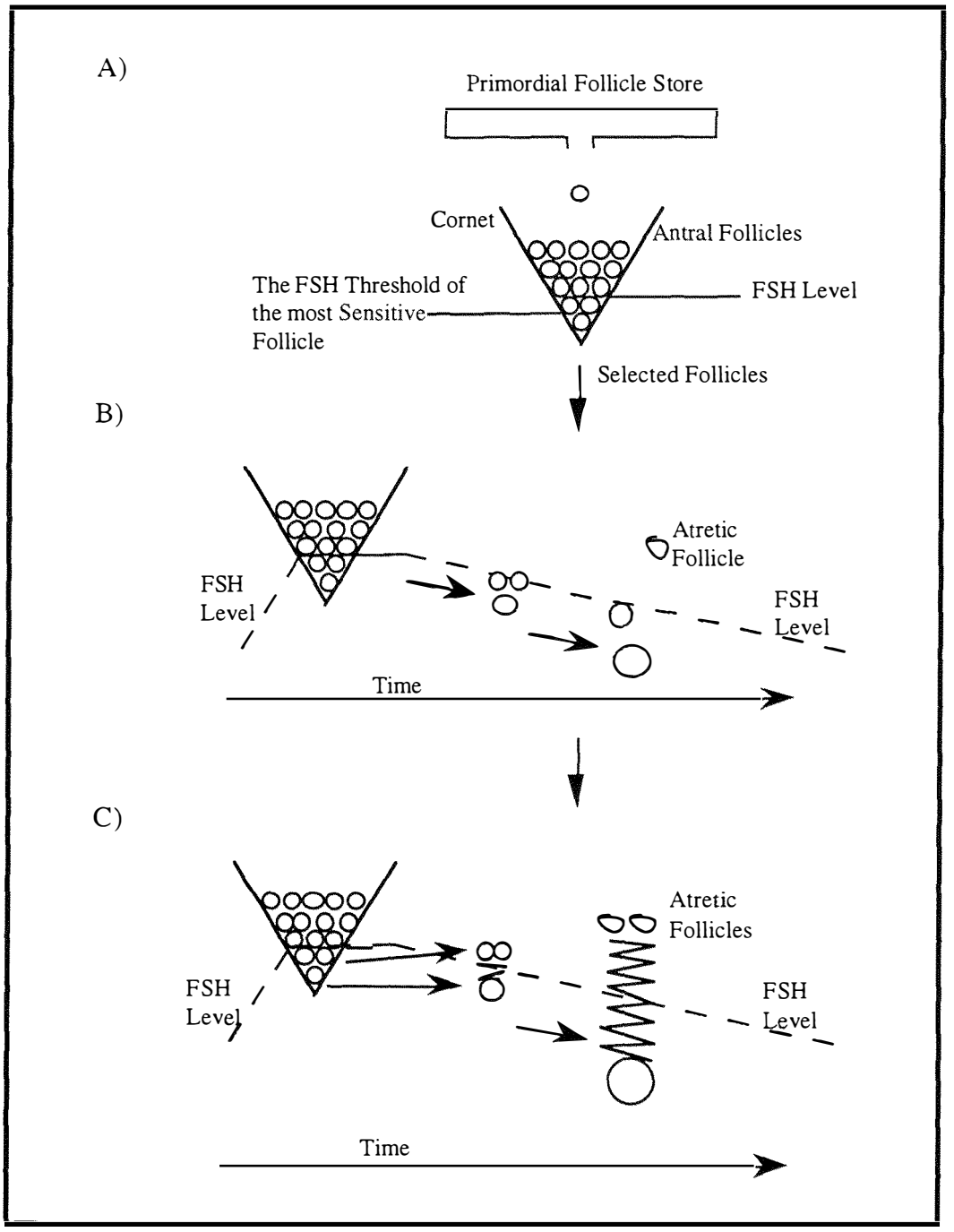


**Fig. 1.1.1** A schematic representation of the three-pillar cornet model for follicle selection in the normal menstrual cycle as proposed by Scheele and Schoemaker [10]. (A) The cornet in the centre contains a cohort of small antral follicles which are FSH dependent. Once the level of FSH rises, only follicles which are placed below the actual FSH-level are sensitive enough to continue growth. The remainder do not have sufficient sensitivity to FSH and undergo atresia. (B) The drop in FSH levels means only the follicles with the lowest FSH thresholds continue to grow out of those selected in (A). Follicles with higher FSH thresholds again dropout and undergo atresia. (C) Auto- and paracrine factors broaden the difference between the lower FSH threshold of the dominant follicle and the higher FSH threshold of the non-dominant follicle(s). As a result only the dominant follicle continues to grow while the others again drop out and undergo atresia. Note: Although step A appears to show that the latest follicle added to the cornet from the primordial follicle store has the highest threshold, this is not necessarily the case.

negative feedback mechanism to the hypothalamus dampens down the secretion of pituitary FSH. The decreased levels of FSH allow only the follicle(s) with the lowest FSH thresholds to thrive while those with higher FSH thresholds undergo atresia.

(3) In the mid and late follicular phase, autocrine and paracrine factors (manipulation by the dominant follicle of its own microenvironment), by a mechanism which is still only vaguely understood, increase the thresholds of the non-dominant follicles and decreases the FSH threshold of the dominant follicle resulting in an amplification of the difference between the FSH thresholds of the dominant and non-dominant follicles. This helps facilitate the discrimination between the follicles by the decreasing FSH levels and as a result the dominant follicle appears to inhibit the growth of the less mature follicles which become atretic. This stage, which is not well understood, is the key to the selection and dominance of the follicle destined to ovulate.

The dominant follicle which is destined to ovulate in the current cycle is thereby selected and at this stage is about 10 mm in diameter. The follicle has now acquired aromatase activity in the granulosa cells and converts aromatisable androgens into estrogens where estrogen refers to the sum of estrone, estradiol and estriol (as discussed in section 1.2). However, the granulosa cells are incapable of producing the precursor androgen substrates and must rely on the production of androgens from the theca cells [14]. As the dominant follicle continues to grow it requires an ever-increasing supply of aromatisable androgens and it is thought that the granulosa cell, by use of paracrine signalling, up-regulates thecal androgen synthesis [2] to keep pace with the ever increasing estrogen production.

### 1.1.3 Continued Growth of the Dominant Follicle and the Excretion of Ovarian Steroid Hormones

*1.1.3.1 The follicular phase of the menstrual cycle*

The dominant follicle is thus selected by about day seven of the cycle [10, 16] and continues to grow at a linear rate indicative of normal follicle development [14, 18]. As the diameter of the growing follicle increases, there is an associated logarithmic increase in the number of granulosa cells [18] which are directly responsible for the incremental increase in estrogen excretion observed at this time due to the aromatase activity of these cells. The principle estrogen excreted is estradiol [2] and a logarithmic increase in the levels of excreted estradiol is therefore indicative of a healthy, growing follicle. The rising level of circulating estradiol is sensed by the hypothalamic-pituitary-ovarian axis which exerts a negative feedback action on FSH release from the pituitary [22], further preventing the recruitment or growth of other follicles. The increased levels of estradiol

also stimulates the formation of further LH receptors and stimulates the cervical mucus glands to secrete fluid favourable to sperm survival and transport [22]. This rapid growth phase (characterised by the logarithmic excretion of estradiol) lasts about 5-6 days until a threshold level of estrogens is reached (the level of estrogen required to trigger the LH surge) [23-24] and the follicle is greater than 20 mm in diameter as shown in Fig. 1.1.2.

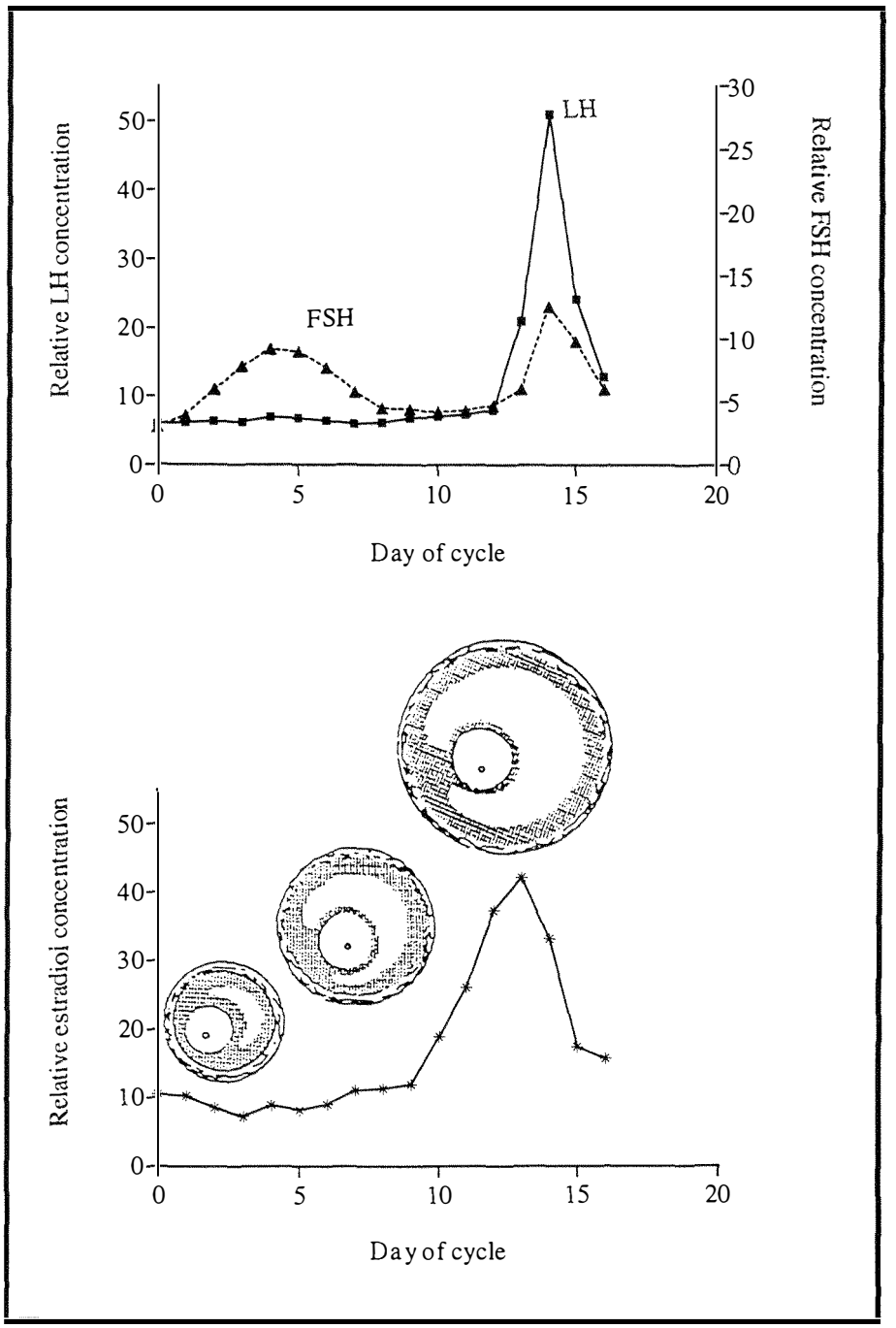


**Fig. 1.1.2** A schematic representation of pre-ovulatory follicular development in the menstrual cycle in relation to LH (■), FSH (▲), and estradiol (*) levels throughout the follicular phase of the menstrual cycle. Note the rises and falls of FSH, the LH surge, and the logarithmic increase in the levels of estradiol after day 9 of the cycle.

Androgens (see section 1.2) are not only synthesised in the theca cells but also in the adrenal glands. As a result there is always a background level of estrogens due to the peripheral aromatisation of these adrenal androgens. Because atretic follicles do not excrete estradiol the rapid and logarithmic rise in the rate of estradiol excretion from the dominant follicle as it enters into its rapid growth phase can be detected as a rise above the pre-ovulatory baseline (see Fig. 1.1.2). This point (the first significant rise in estradiol production above the baseline) can be used to mark the beginning of the potentially fertile phase [24].

The rapidly growing follicle continues to excrete estradiol which doubles in concentration about every 6.3 h [25] resulting in the logarithmic rise depicted in Fig. 1.1.2. About 4-6 days after the first detectable rise from the baseline the estradiol levels reach a maximum level which triggers the onset of the LH [26-27] and FSH surges [26]. This is often referred to as the midcycle gonadotropin surge. The surge is the result of the concentration of estradiol in the plasma exceeding a threshold level of about 600 pmol/L for more than 50 hours [23-24]. The surge in the concentration of plasma LH levels stimulates the resumption of meiosis in the oocyte and luteinises the theca and granulosa cells resulting in a dramatic decrease in the levels of estradiol secreted (see Fig. 1.1.2) while the levels of progesterone begin to rise [23, 25]. The surge in LH levels initiates the processes which lead to the rupturing of the mature follicle and ovulation (release of the ovum) occurs around 17 hours after the LH peak [16]. The day prior to ovulation is considered the day of maximum fertility as research has shown that an isolated event of intercourse is most likely to lead to conception on this day [28]. Detection of the LH surge can therefore be used for the immediate prediction of ovulation and is the best indirect parameter of impending ovulation [29], however this marker is too late to predict the onset of the fertile period [4]. The first significant rise from baseline levels in plasma estradiol concentration is therefore the best indicator for an advanced warning of ovulation which can allow for the sperm survival time.

*1.1.3.2 The luteal phase of the menstrual cycle*

The first part of the menstrual cycle known as the follicular phase is now complete. During this phase, which begins on day one of the cycle (the first day of menses), the dominant follicle is recruited, selected and then continues to grow and reach maturation until the follicular phase is completed with ovulation. The second part of the cycle from the day of ovulation to the day before the next menstrual bleed is known as the luteal phase. After the follicle has been luteinised the remnants of the follicle form a structure known as the corpus luteum [1]. As the corpus luteum develops it begins to secrete increasing amounts of the thermogenic steroid progesterone as well as estradiol and this can be seen in the cyclic variations of these hormones during the normal menstrual cycle

(see Fig. 1.1.3). This rise in the level of progesterone is clearly a suitable marker or indicator to signal the end of the potentially fertile period. However, studies undertaken by Hoff *et al.* [25] have shown that the rise in progesterone levels around the time of ovulation and immediately after ovulation is multiphasic (Fig. 1.1.4).

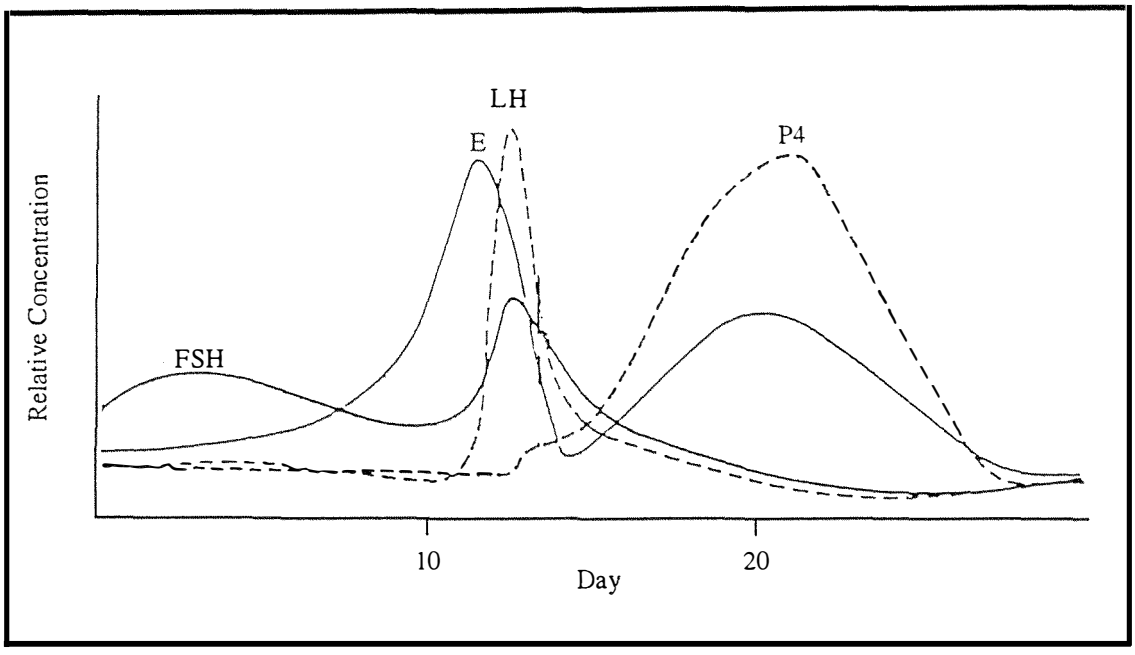


**Fig. 1.1.3** The mean values of serum luteinising hormone (LH), follicle stimulating hormone (FSH), estradiol (E), and progesterone ($P_4$) as seen in a normal human menstrual cycle

Fig. 1.1.4 shows that in the last 48 hours of the estradiol rise outlined above, before the peak concentration of estradiol is reached and the LH surge begins (zero point), the progesterone levels are also rising in parallel, initially at about the same rate as for estradiol. About 12 hours before the estradiol peak and the beginning of the LH surge a second phase in progesterone excretion begins with the progesterone levels rising sharply (four fold) until about 12 hours after the initiation of the LH surge when it reaches a plateau lasting from about 14 to 34 hours after the LH surge onset while the estradiol levels begin to plummet. This drop in estradiol levels can be used as a marker that ovulation is imminent. Following a plateau in the levels of progesterone (Fig. 1.1.4) is a fourth and final phase beginning 36 hours after the LH surge is initiated whereby there is a huge increase in the progesterone output due to the luteinisation of the follicle. Although this fourth phase rise does not look as large as the second phase rise in Fig. 1.1.4, the y-axis logarithmic scale shows that the last rise is almost three times that of the first. It is this last rise which can be associated with the end of the fertile period as the corpus luteum develops and secretes more and more progesterone. Hoff *et al.* [25] suggest that the first surge in progesterone levels during the second phase described above may augment estradiol action, influencing the timing, amplitude and duration of the LH surge.

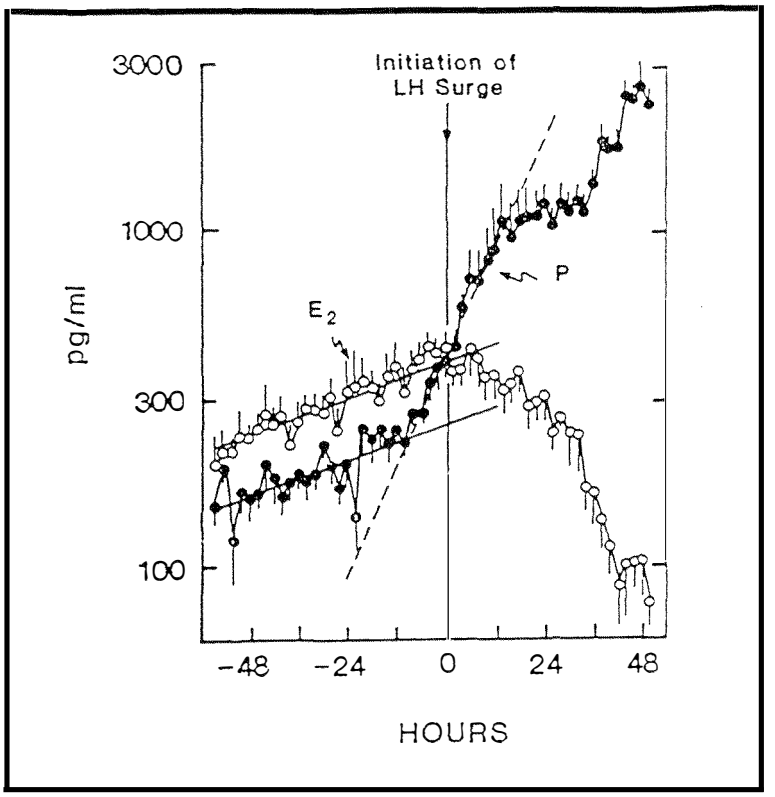


**Fig. 1.1.4** The mean serum estradiol ($E_2$) and progesterone (P) concentrations measured every two hours for five days during the midcycle in seven cycles as published by Hoff *et al.* [25]. The measurements are referenced to the initiation of the luteinising hormone (LH) surge as time zero and results are plotted on a logarithmic scale. The multiphasic rise in the progesterone levels before and after the estradiol peak and the initiation of the LH surge can be clearly seen.

After ovulation the corpus luteum continues to develop, increasing its secretion of progesterone and estrogen. The secretion of these steroids acts to stop the release of both LH and FSH for the remainder of the cycle. However, the corpus luteum requires a threshold level of LH to continue to develop and therefore brings about its own demise as the progesterone and estrogen levels from the corpus luteum prevent the release of sufficient LH to allow continued growth. Once the corpus luteum has regressed, the inhibitory effects of progesterone and estrogen are removed from the hypothalamic-pituitary-ovarian axis and the pituitary gland begins to secrete higher levels of FSH again and a new cycle begins. Before the new cycle begins menstruation occurs and the first day of the new cycle is regarded as beginning on the first day of menses.

The actual events occurring in the ovary are therefore reflected by the changes in hormone concentrations throughout the cycle. By monitoring these hormonal changes it is possible to eavesdrop on the activity of the ovary as it interacts with the hypothalamus and pituitary gland. As a result one can define the potential fertile period during a woman's

cycle using the steroid hormones estradiol and progesterone as biochemical markers to detect the beginning and end of the potentially fertile period respectively.

## 1.2 Biosynthesis of the Ovarian Steroid Hormones

### 1.2.1 The Synthesis of Progesterone

The classical pathway for the biosynthesis of the steroid hormones traditionally begins from the precursor cholesterol although other alternative pathways do exist [30]. The precursor cholesterol is itself synthesised in a series of reactions which begins from the combination of three molecules of acetic acid in the form of acetyl-CoA [30-31]. All 27 carbon atoms in the cholesterol molecule are derived from either these acetate precursor molecules [30] or dietary low-density lipoprotein cholesterol. The polypeptide adrenocorticotropic hormone synthesised by the anterior pituitary gland then stimulates the formation of pregnenolone from cholesterol as required [31].

Cholesterol consists of 27 carbon atoms, whereas the steroid hormones contain 21 or fewer carbon atoms and therefore the first step in the biosynthesis of the steroid hormones is the removal of the cholesterol side chain to form pregnenolone (scheme 1.2.1) [30-31]. Although there are several pathways by which this side chain may be removed, studies have shown that the major route involves the one step, direct enzymatic reaction from cholesterol to 20α,22β-dihydroxycholesterol from which the side chain is cleaved (scheme 1.2.1) [30]. The hydroxylation of the C-20 and C-22 groups requires the activation of molecular oxygen by the cytochrome P450 enzyme in the adrenal mitochondria cells and is NADPH dependent [31]. Following hydroxylation, the resulting 20α,22β-dihydroxycholesterol is converted to pregnenolone by the cleavage of the bond between C-20 and C-22 in a reaction catalysed by desmolase (scheme 1.2.1) [31]. It is thought that the side chain cleavage involves three consecutive *in situ* oxidations through a ferryl-atomic oxygen complex of P450 giving pregnenolone as the final product [32]. The $C_{21}$ steroid pregnenolone is the major precursor of steroid hormones in all endocrine tissues capable of *de novo* synthesis, that is, the ovary, testis and adrenal cortex [30].

Progesterone is synthesised from pregnenolone in two simple steps which occur in the microsomes [32]. It is necessary for the pregnenolone to be transported from the mitochondria for its conversion to progesterone as the enzymes required to undertake this transformation are located in the microsomes [32]. The 3-hydroxyl group of pregnenolone is oxidised to a 3-keto group and the $\Delta^5$ double bond is isomerised to a $\Delta^4$

double bond (scheme 1.2.1) by the enzyme 3β-hydroxy steroid dehydrogenase in the presence of $NAD^+$ [31]. Progesterone is then used as the precursor for the synthesis of all the androgens and estrogens (scheme 1.2.2). Pregnanediol is formed directly from the progesterone precursor as shown in scheme 1.2.1 by reduction of the 3- and 20-keto groups.

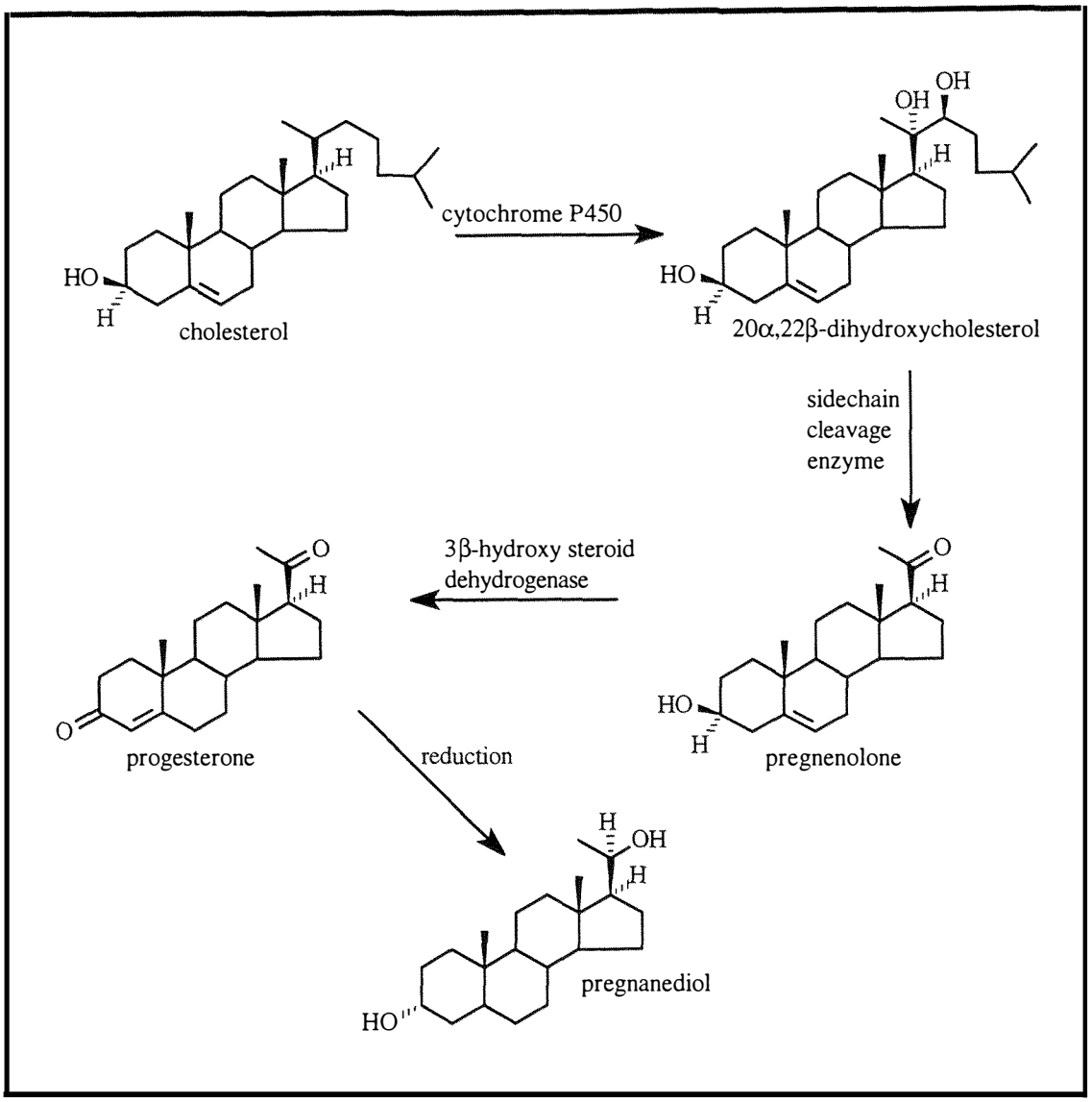


**Scheme 1.2.1** The synthesis of progesterone as described in section 1.2.1

## 1.2.2 The Synthesis of Androgens and Estrogens

The first step in the synthesis of estrogens begins with the formation of the androgen androstenedione as shown in scheme 1.2.2. Progesterone is hydroxylated at the C-17 position by the cytochrome P450 17α-hydroxylase enzyme and the side chain is then cleaved by desmolase to yield androstenedione (scheme 1.2.2). Androstenedione can

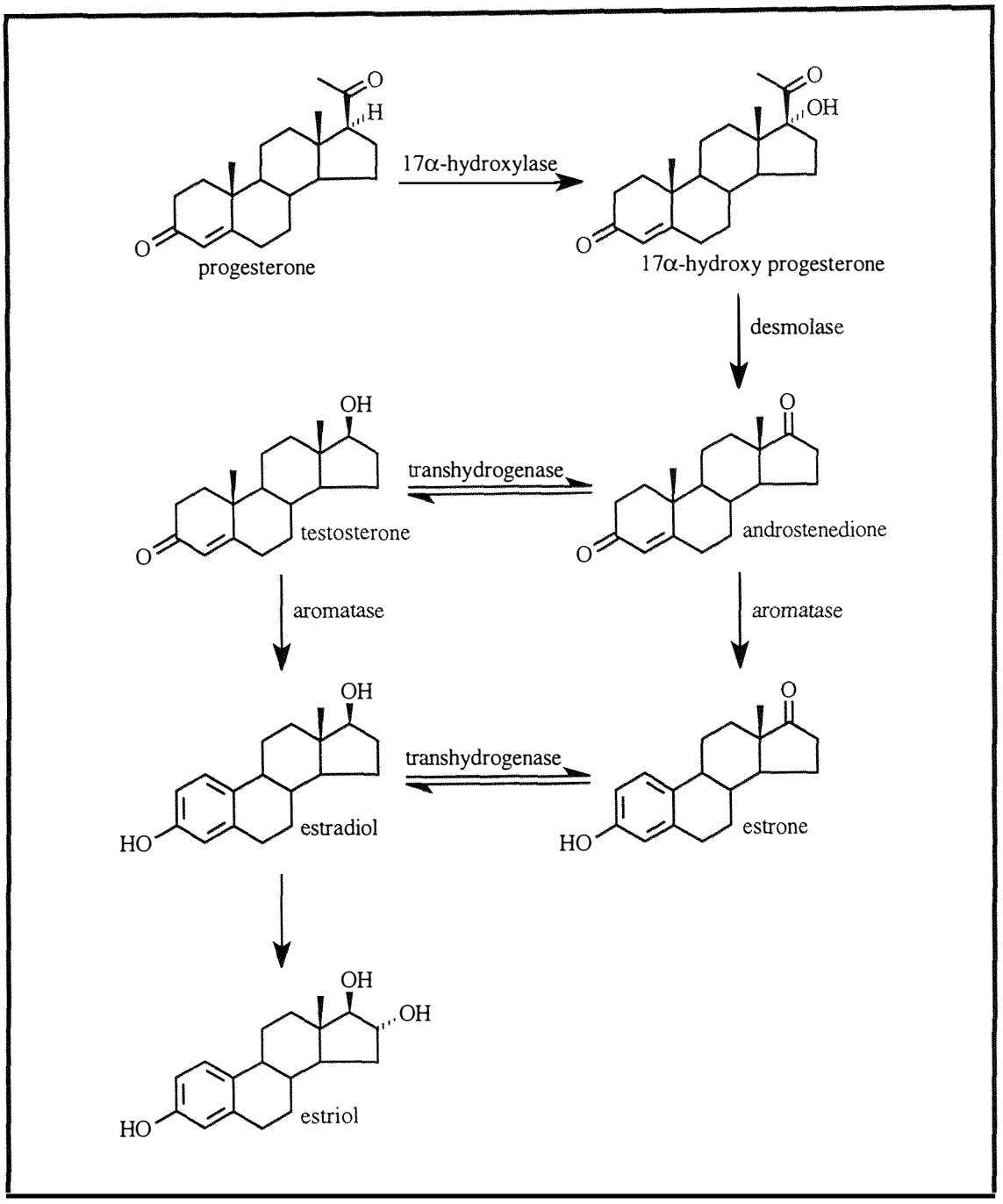


**Scheme 1.2.2** The synthesis of the estrogens from progesterone as described in section 1.2.2

then be reduced by a transhydrogenase enzyme in an equilibrium reaction which reduces the 17-keto group to a 17β-hydroxyl group to give another androgen, testosterone. In the growing follicle the conversion of progesterone to androgens takes place in the theca cells. It is at this point that the aromatase activity in the granulosa cell becomes important as discussed in section 1.1. The estrogens are synthesised from the androgens, a process which requires removal of the C-19 methyl substituent and aromatisation of the A ring. Estrone is derived from androstenedione while the more biologically active estradiol is synthesised from testosterone. The equilibrium which exists between the two (estrone

and estradiol) lies in favour of estradiol in the ovary and is thus the most biologically important estrogen.

Aromatisation of the androgens by the aromatase P450 enzyme requires the presence of molecular oxygen and NADPH [31] and is irreversible. The mechanism involves three hydroxylations, the first two of which take place at the C-19 methyl group of the androgen to give a diol at this position [33]. The diol is then converted to an aldehyde followed by a further hydroxylation at the C-2 position on the steroid A ring. Attack by an $OH^-$ group on the hydroxyl group at the steroid C-2 position results in aromatisation of the A ring and release of the ionic form of methanoic acid ($HCO_2^-$) [33]. Estradiol can also be converted to the less bioactive estriol moiety (scheme 1.2.2) by hepatic conversion of 17β-estradiol as well as conversion to the less reactive estrone molecule. Once estradiol has left the ovary the equilibrium between estradiol and estrone favours estrone formation and as a result estrone sulphate is the major circulating steroid derivative in the blood during the menstrual cycle.

### 1.2.3 Metabolism and Excretion of Ovarian Steroids

Ovarian steroid hormones are usually excreted in the urine as water soluble steroid glucosiduronates, sulfates or sulfoglucosiduronate conjugates [34]. The liver is the most active organ in which steroids are conjugated. It is generally accepted that conjugation of steroid hormones in this way is required for biological inactivation and excretion. While conjugation does produce molecules which are far more water soluble than the free steroids, the suggestion that the primary reason of conjugation is for excretion has been questioned [34]. It has been demonstrated that the plasma concentrations of the estrogens and progesterone does not exceed their aqueous solubility under normal conditions [34].

Progesterone has a large number of metabolites most of which are excreted *via* the bile and the gastrointestinal tract. Pregnanediol-3α-glucuronide (PdG, Fig. 1.2.1) is one of the major conjugated metabolites of ovarian progesterone (about 20%) to be excreted in the urine [35], although a baseline level of PdG is present due to the conversion of pregnenolone to PdG in the adrenal gland [36]. The rise from baseline levels of urinary PdG (which are directly related to the circulating levels of progesterone in the blood [37]) can therefore be used in principle to signal a rise in progesterone levels on formation of the corpus luteum.

Estradiol and the estrogenic steroid metabolites of estrone, estradiol and estriol are all excreted in the urine as glucuronide conjugates. Estradiol is the major estrogen produced by the ovary and the metabolite estradiol-17β-3-glucuronide (E2-17β-3G; Fig. 1.2.1) is

one of the first estrogen metabolites to be detected in the urine [38], but it is not a major metabolite of estradiol and is present in urine at very low concentrations making measurement difficult [39]. The estriol conjugated monoglucuronides (E3-3G, E3-16G, and E3-17G; Fig. 1.2.1) are excreted in relatively large amounts, which when summed together can be measured relatively easily [38]. Early work by Brown [40] has shown that although the estriol monoglucuronides are present in large amounts their excretion may be delayed due to a complex enterohepatic circulation involving biliary excretion and reabsorption. In contrast the metabolite of estrone, estrone glucuronide (E1G, Fig. 1.2.1), is excreted both rapidly (within a short time of its synthesis) and in relatively large amounts.

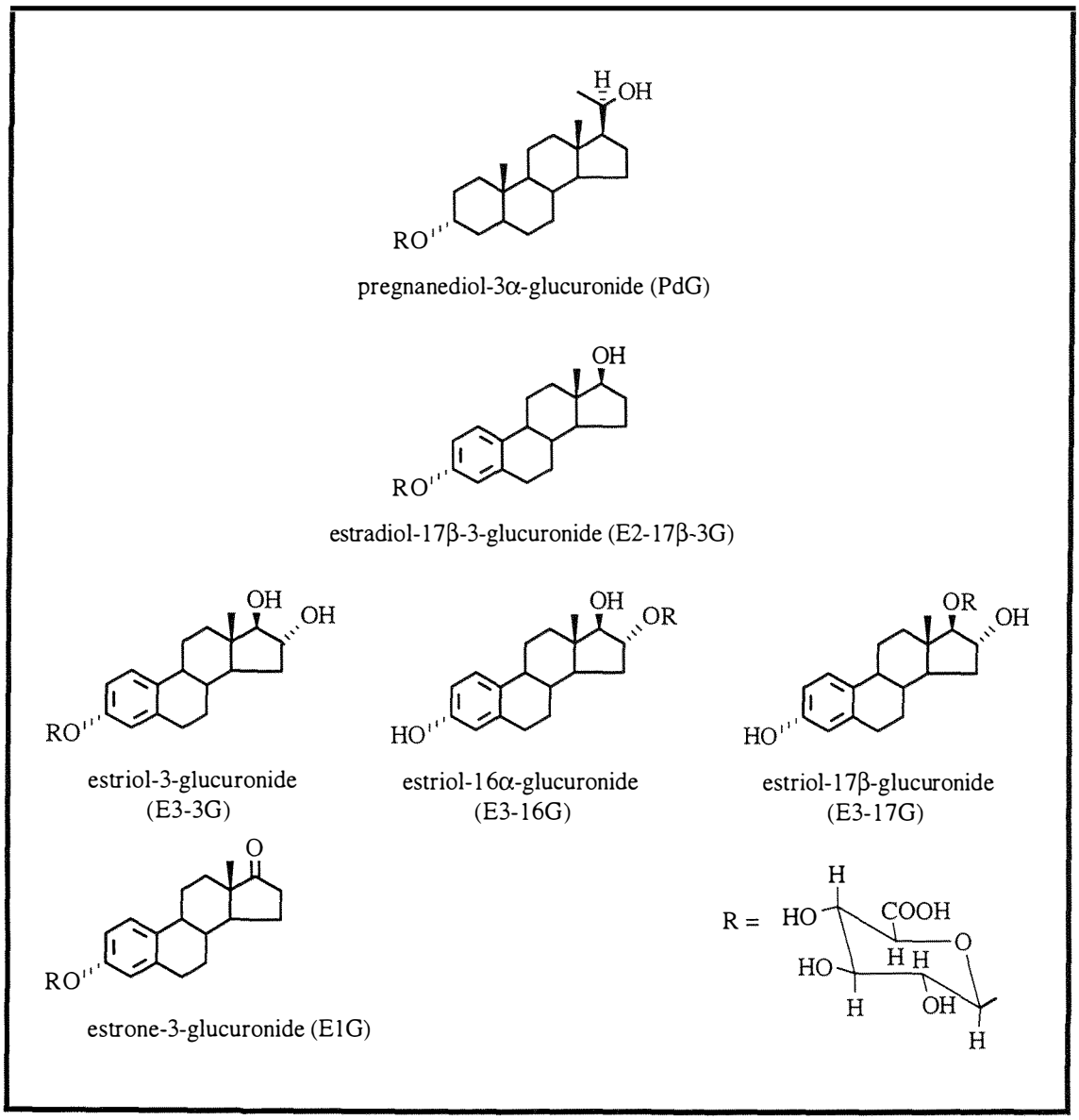


**Fig. 1.2.1** The conventional representation of the steroid glucuronide molecules discussed in section 1.2.3

Perhaps even more importantly it has been shown that the concentration of estrone conjugates and E1G secreted in the urine is closely related to the concentration of estradiol circulating in the plasma (Fig. 1.2.2) [41-42]. Thus the levels of E1G directly reflect what is happening at the level of the ovary. The measurement of the urinary concentrations of estrone glucuronide which signals the establishment of a dominant follicle and pregnanediol glucuronide which signals the establishment of the corpus luteum therefore allow the eavesdropping on the activity of the ovary as described in section 1.1 to predict the length of the fertile period during a typical menstrual cycle.

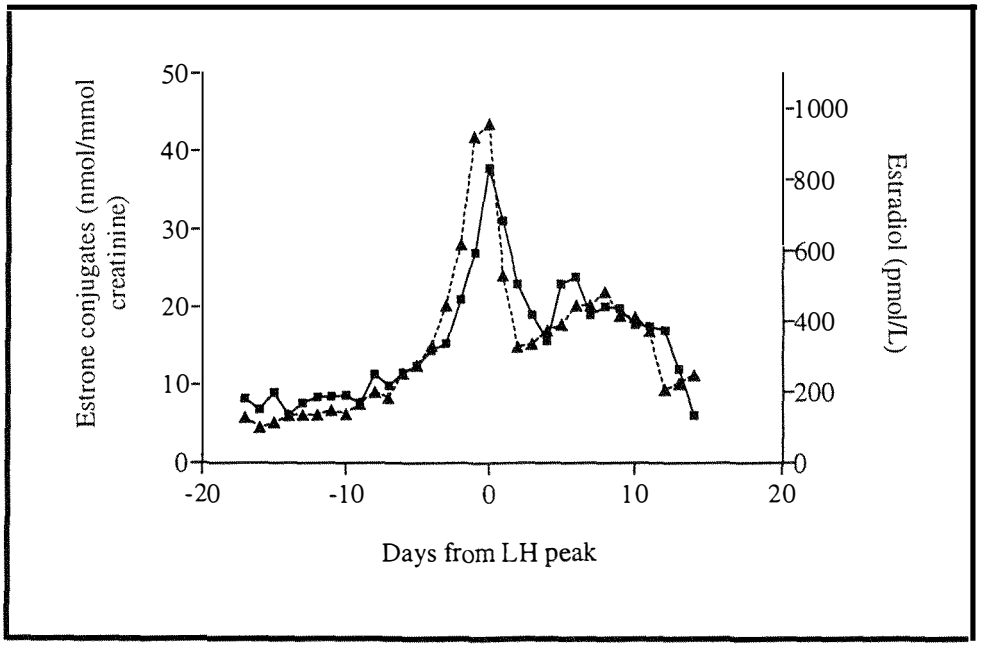


**Fig. 1.2.2** The daily mean serum estradiol (▲) and urinary estrone conjugates (■) concentrations in ten ovulatory menstrual cycles

## 1.3 Markers used for Definition of the Fertile Period

To predict and determine the fertile period, with the aim of either achieving or avoiding a pregnancy, it is necessary to know what is happening at the level of the ovary. Follicular development and release of the mature oocyte can be monitored by ultrasound techniques which have been used to predict the timing of ovulation [43]. Observation of the fertile phase in this way is obviously limiting both in terms of where the procedure can be used and in the number of women having access to this technique. Consequently, methods for defining the fertile period with the sole purpose of preventing or achieving pregnancy, and which can be applied to a wide cross-section of women, must be readily available, relatively cheap and most importantly, accurate. Any method will ideally be able to predict ovulation far enough in advance to allow for sperm survival time but will minimise the days of abstinence (from intercourse) required in each menstrual cycle.

### 1.3.1 Natural Family Planning (NFP)

Although many definitions of natural family planning exist the definition published by the World Health Organisation (WHO) is "the voluntary avoidance of intercourse by a couple during the fertile phase of the menstrual cycle to avoid pregnancy" [44]. The use of NFP therefore requires the accurate definition of the fertile period so that the days of potential fertility are known. The so called methods of natural family planning or NFP, all revolve around the observation of a woman's naturally occurring signs and symptoms of both the fertile and infertile phases of the menstrual cycle [45]. The observed physical symptoms are related to the hormonal changes discussed in section 1.1 which occur during the menstrual cycle.

NFP techniques include those of calendar (or rhythm) methods, basal body temperature (BBT), cervical palpation, the cervical mucus or Billings' method, and the symptothermal method which is currently recommended by New Zealand teachers from the Natural Family Planning Foundation. The oldest and least reliable of these methods is the calendar method which was first reported by Ogino in 1930 [46] although this method was undoubtedly in use before this date. This method estimates the probable days of fertility from previous cycle records and patterns and thus gives only a rough estimate of the fertile period [45] since it relies on the follicular phase being constant. Although this method is the least reliable, at present it is the most extensively used NFP method world wide.

The basal body temperature rise method monitors the rise in temperature associated with the thermogenic hormone progesterone which is secreted by the corpus luteum [45]. The

basal body temperature rises by 0.3-0.6°C following the surge in the rate of progesterone excretion and this elevation of the temperature lasts for at least three days and can therefore be used to delineate the end of the fertile period [4]. This method cannot determine the beginning of the fertile period and the temperature can be elevated by various other physical and psychological factors. The cervical palpation method follows cyclical changes in the opening of the cervix which occur during the menstrual cycle [47]. This method is the least popular of the NFP methods.

The ovulation method relies on a women following changes in her cervical mucus symptoms during the menstrual cycle [9]. Changes in the mucus secretion can be used by a woman to define the fertile period and it has been shown that these changes correlate well with the underlying hormonal changes. The method of NFP currently recommended in New Zealand by the Natural Family Planning Foundation is the symptothermal method. As the name suggests this method is a combination of the basal body temperature method (thermal), the cervical mucus secretion (ovulation method) and calendar calculations.

### 1.3.2 Steroid Hormone Metabolites as Markers of the Fertile Period

Although the symptothermal method can be very effective in defining the fertile period during a woman's menstrual cycle, the symptoms must be very clear. In many women the symptoms are not so clear and the fertile period cannot be precisely defined. As a result of the uncertainties associated with these symptoms, the defined fertile period is often longer than the true fertile period, thus requiring long periods of abstinence. A more precise definition of the fertile period would reduce the times of abstinence required. The most obvious way to identify the fertile period with precision is to follow the hormonal changes which occur during the menstrual cycle (see section 1.1).

The analysis and measurement of the first significant rises in urinary estrogen and progesterone metabolite concentrations as markers for the beginning and end of the potentially fertile period has long been a goal of researchers and in particular of the World Health Organisation. It is now universally accepted that the first significant rise either in the rate of excretion of plasma estradiol [7, 24, 48] or its urinary metabolites (such as E1G, E3-EG, or E3-16G) [6, 23, 37, 49-55] from baseline levels is useful as a biochemical marker for the beginning of the potentially fertile period. Therefore, considerable effort has been expended in developing methodologies which allow the recognition of the beginning of the fertile period from these first significant rises.

*1.3.2.1 Methods for the recognition of first estrogen rises to define the beginning of the fertile period*

Once a dominant follicle enters its rapid growth phase, successive estrogen observations are serially dependent and as a result a logarithmic increase in the levels of the urinary estrogens is observed. Although the first significant increase in total urinary estrogen

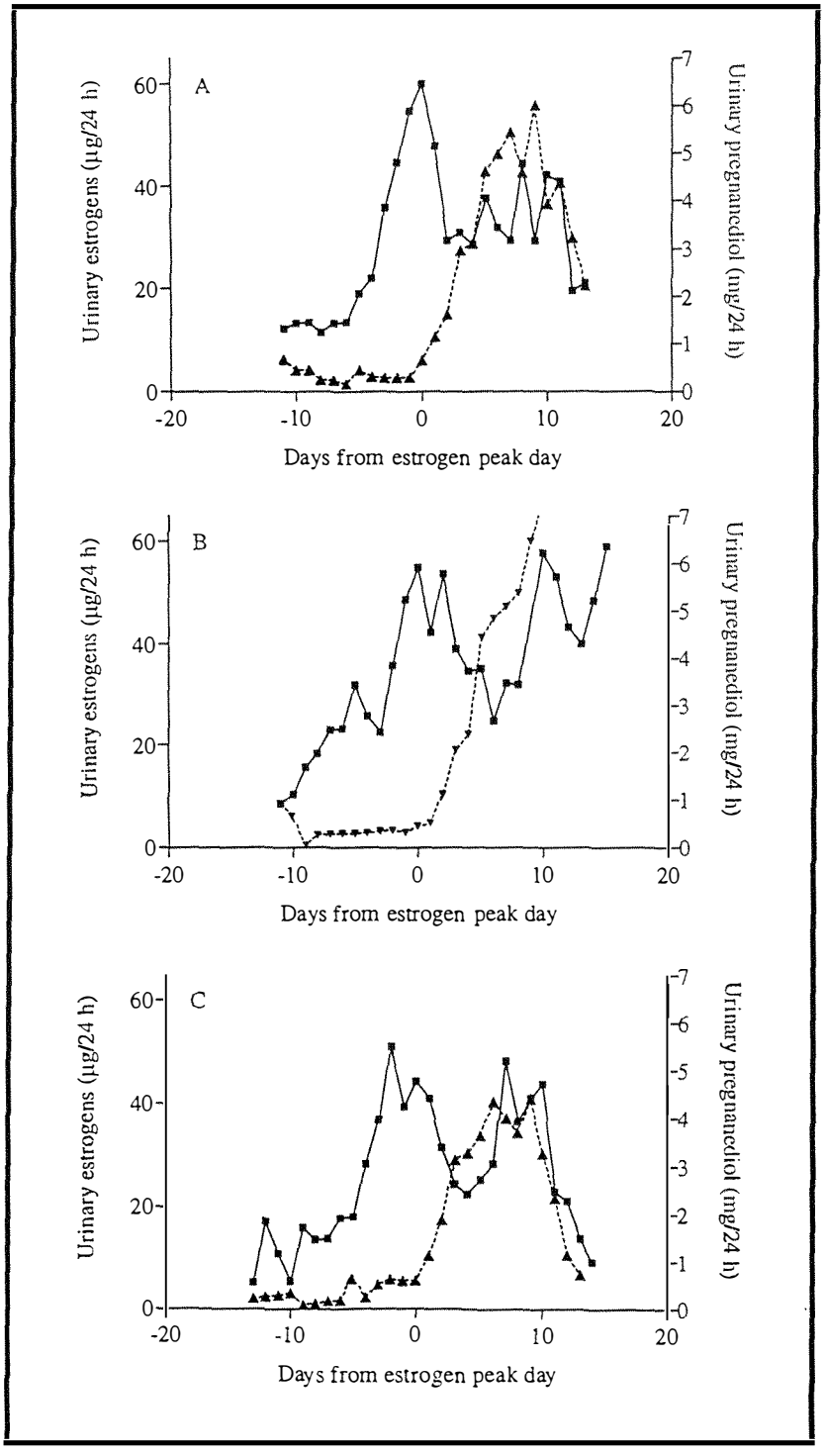


**Fig. 1.3.1** The most common urinary total estrogen (■) and pregnanediol (▲) value patterns observed in a normal menstrual cycle. A) most common pattern; B) cycle with an early rise, intermediate fall, and double estrogen peak, followed by pregnancy; and C) cycle with stable baseline and double estrogen peak.

levels is often easy to identify by visual inspection of the data (see Fig. 1.3.1) this is not recognised in scientific circles as an objective methodology. Blackwell and Brown [54] recognised the serial dependence of the urinary estrogen data and applied a new statistical method to a database of 142 menstrual cycles containing daily urinary total estrogen levels. The total estrogen concentration (or level) is a measurement of the sum of the three individual estrogen levels, that is, the sum of the urinary concentrations of estrone, estradiol and estriol conjugates.

The statistical approach applied by Blackwell and Brown [54] is known as time series or trend analysis. The method involves taking an exponentially smoothed average of the baseline data, which are the relatively unchanging days at the beginning of each menstrual cycle. The exponentially smoothed average is then used to predict or forecast the next observation. The difference between the forecast value and the real value is known as the forecast error. If there is no time-related change between two data points then the forecast value and the actual value should be approximately the same and the forecast errors will fluctuate around zero just as the real data has significant but random fluctuations around a mean baseline level. When a systematic change in the level of total urinary estrogens does occur the forecast error will become consistently more positive (for the ovarian steroid data under consideration). Application of the Trigg's method [56] using an exponentially smoothed forecast error, will measure the statistical significance of departures of the smooth forecast error from the established baseline levels. The Trigg's tracking signal is the normalised smoothed forecast error and is calculated by dividing the smoothed forecast error by the mean absolute deviation (where the mean absolute deviation is a measure of the amount of noise in the raw data). The Trigg's tracking signal is thus a prospective statistical measure of the significance of changes in the data from baseline levels (i.e. a statistically significant first rise) and varies between a value of $\pm 1$ where +1 means there is a 100% certainty that there has been a significant increase in the values being measured and -1 means there is a 100% certainty that there has been a significant decrease in the values being measured.

When Blackwell and Brown [54] applied a tracking signal decision level of 0.692 (equivalent to a 95% confidence interval, i.e. only five chances in 100 that the signal arises from random variability) to the 142 cycles in the data base, the first significant rise in total urinary estrogen levels was detected on average $4.03 \pm 1.4$ days before the total urinary estrogen peak day. This can be thought of as day one of the fertile period and as ovulation occurs about 36 hours after the total estrogen peak day this gives a mean warning of ovulation of about 6 days. A warning of this length of time would be far enough in advance of ovulation to prevent pregnancy from acts of intercourse except for the very longest sperm survival times. When this form of analysis was also applied to

urinary estrone glucuronide data it was found that once again the warning of ovulation was around 6 days in advance [57]. The definition of the first rise in total urinary estrogen levels or estrone glucuronide levels from an established baseline for an individual can therefore be used as a direct marker for the beginning of the potentially fertile period.

*1.3.2.2 Definition of the end of the fertile period*

The end of the fertile period can be identified by measurement of either luteinising hormone or pregnanediol concentrations. The luteinising hormone (LH) peak day occurs before ovulation. To allow for this and to define the fertile period by LH measurements it is necessary to predict the end of the potentially fertile time by estimating when ovulation has occurred. Although ovulation normally occurs within 24 hours of the LH peak day (in about three quarters of all cycles [4]) the end of the fertile period is not actually being measured and uncertainties may therefore arise. Further complications may arise due to the time delay between the secretion of the hormone (LH) from the corpus luteum and its urinary excretion when using urinary measurements [4]. The most accurate marker for detecting ovulation is likely to be by monitoring the levels of pregnanediol or pregnanediol glucuronide in urine since increases in its rate of excretion is the result of luteinisation of the dominant follicle and hence reflects what is happening at the level of the ovary, rather than anticipating what may occur. The first significant rise from baseline levels of pregnanediol can be clearly seen in all the cases presented in Fig. 1.3.1. However, when the Trigg's tracking signal was applied to a database of urinary pregnanediol glucuronide levels, the first significant rise above baseline levels was observed before the total estrogen peak day in about 25% of all cases, even at a 99% confidence level [57]. Obviously in these cases the first statistically significant rise cannot be related to the end of fertility and cannot therefore be used as a marker for the end of the fertile period.

The reason for these false positives is clearly demonstrated in Fig. 1.1.4 which shows that there is a peri-ovulatory rise in progesterone levels which is followed later by a much larger, second rise. It is this second rise which is associated with luteinisation and formation of the corpus luteum. The tracking signal is therefore working too well and detecting the smaller peri-ovulatory first rise in a large number of cases. However, if a threshold value of 6.3 μmol/24 h of pregnanediol glucuronide is applied to the urinary pregnanediol glucuronide data no false positives were detected and all of the rises equal to, or exceeding this threshold level were observed after the total estrogen peak day [57]. The measurement of the amount of urinary pregnanediol glucuronide can therefore be used as a marker for the end of the potentially fertile period when a threshold level is used.

Thus, in summary, measurement of the rate of excretion of estrone glucuronide (E1G) and pregnanediol glucuronide (PdG) in timed urine samples can be used to define the fertile period of the menstrual cycle with a high degree of certainty. It is necessary to use timed urine samples to allow for the variation in the rate of urine production throughout the day (as discussed in section 1.5). An idealised profile of the daily levels of E1G and PdG excreted during a normal menstrual cycle is shown in Fig. 1.3.2. The rise and fall of both steroid glucuronides is clearly shown and the peri-ovulatory PdG rise can also be seen. Ovulation is predicted to occur one day after the peak E1G day (day 15) and the PdG threshold cut off value (6.3 μmol/24 h) is reached between days 16 and 17 of the cycle. At this time ovulation has occurred and the potentially fertile period is over as the luteal phase begins. The day preceding ovulation (the peak E1G day) is said to be the day of maximum fertility (day when intercourse is most likely to result in conception) [28]. Accurate definition of the fertile period in this way can be used to avoid pregnancy, achieve conception, or assist in the transition of women to the menopause.

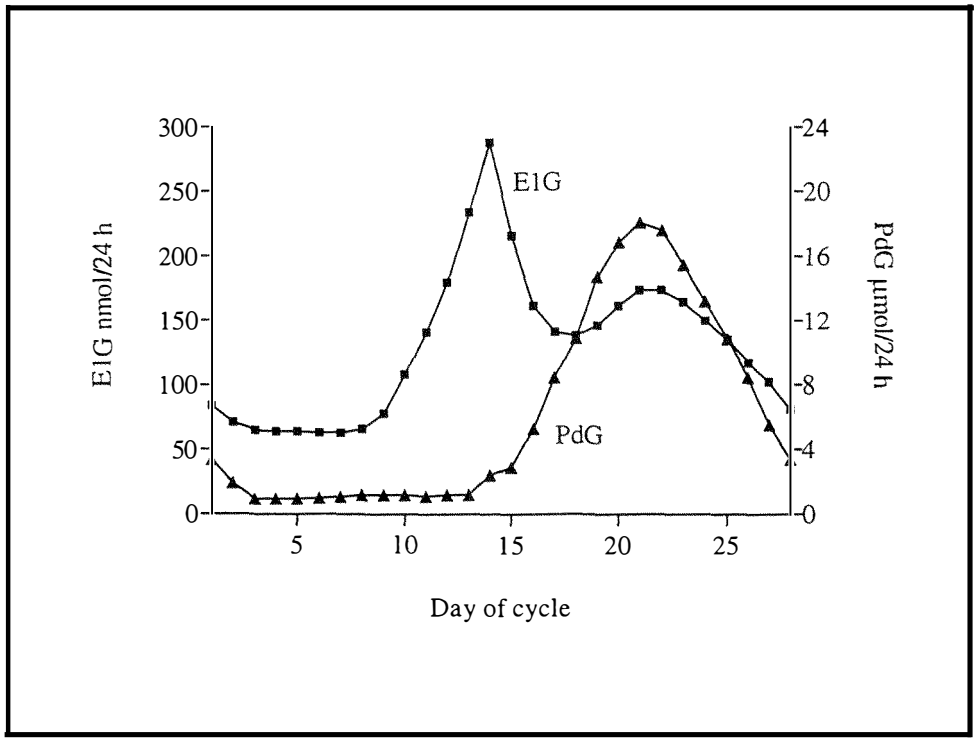


**Fig. 1.3.2** An idealised profile of the daily levels of urinary estrone glucuronide (E1G) and pregnanediol glucuronide (PdG) excreted during a normal menstrual cycle

## 1.4 Methods for the Measurement of Urinary Estrone Glucuronide and Pregnanediol Glucuronide as Markers of the Fertile Period

In principle, by monitoring the cyclic hormonal profiles which occur during a woman's menstrual cycle the periods of fertility and infertility can be determined with a high degree of certainty and precision. In designing a kit or clinical assay system which allows women in the home to follow their own menstrual cycle through the measurement of the circulating levels of ovarian steroids, it is necessary to consider from which body fluid the target analyte for measurement will be taken. The three most accessible fluids are serum (or blood), urine, and saliva. While serum sample assays measure the level of the circulating analyte at the time of sampling it requires invasive methods of sampling and the levels of the steroids in the blood are lower than that of the metabolites found in the urine. Urine samples however can be obtained using non-invasive sampling techniques and the steroid metabolites are present in relatively high concentrations. Collection of urine is far more convenient than the serial sampling of blood, and urine integrates the secretary episodes which can complicate the interpretation of blood sample measurements [37, 58]. Salivary steroids and their metabolites are also easily sampled and the concentrations correlate well with the circulating plasma levels. However, salivary concentrations of ovarian steroids and their metabolites are low [4] and as a result highly sensitive assays are required to measure their concentrations. The challenge for researchers over many years has therefore been to provide methods for the measurement of ovarian steroid glucuronide levels in the urine of menstruating women.

### 1.4.1 Early Measurements of Steroid Glucuronide Levels

Early methods for the measurement of steroids and steroid glucuronides in both urine and plasma involved time consuming chemical extractions and/or crystallisations for the purification of the analyte of interest so that its concentration could be measured by bioassay or chemical assay. As far back as the 1930's researchers were extracting or assaying for ovarian steroids [59-61]. One such method, now known as the Kober reaction [61], utilised the strong green fluorescence which results when any of the estrogens are heated with sulphuric acid in the presence of ethanol. In 1955 Brown [62] published an accurate but time consuming method for the measurement of estrogen levels in human urine which involved the hydrolysis of the estrogen glucuronides, several extractions and purifications, alumina columns for separation of the individual estrogens and finally determination of the extracted estrogens by the Kober method. The method was referred to as the split estrogen method, that is, the separate measurement of estrone, estradiol and estriol conjugates.

Several other extraction methods such as that published by Hashimoto and Neeman [63] for the characterisation of estriol 16α-glucosiduronic acid in human pregnancy urine were also developed in the 1960's. However, possibly the most important landmark in the measurement of steroid hormone concentrations and endocrinology was the advent of the radioreceptor [64] and radioimmunoassays [65] developed in the late 1960's. These methods resulted in unprecedented sensitivity (pmol/L), were highly specific and were relatively easy to perform [66]. As a result immunoassay became the way of the future for measuring picomolar or lower concentrations of steroid hormones, drugs and many other small analytes in both plasma and urine samples. More recently new instruments and technologies have allowed the separation and determination of ovarian steroid levels to be completed much faster by such methods as micellar electrokinetic chromatography [67].

### 1.4.2 Immunoassays

*1.4.2.1 Radioimmunoassay*

A large number of reviews and books have been written documenting immunoassay development, methodology and techniques (for example see references 68-69). Radioimmunoassay (RIA) was the first approach developed for the measurement of the concentration of small analytes and is still extensively utilised today. The principle behind the radioimmunoassay format involves the competitive binding of an antibody to both labelled and unlabelled antigen (or ligand) as shown in Fig. 1.4.1. An antibody, produced in response to an antigen, serves as a receptor or specific binder. The ligand (or analyte) in the test sample (urine or blood) competes with a fixed amount of labelled ligand (labelled antigen or suitable derivative) for the limited number of binding sites provided by the antibody molecules. After an equilibration period the amount of free labelled antigen is separated from the antibody bound labelled antigen and the radioactivity in either the free or bound state is measured. The amount of radioactivity observed can be compared to that observed with known concentrations of antigen (standards) and hence the concentration of analyte in the sample can be determined.

Radioimmunoassays are very sensitive and can detect concentrations of steroids at pmol/L levels or less. As a result they have been widely employed for the measurement of steroid hormones and steroid glucuronide metabolites in urine [41, 49, 53, 70-73]. Although radioimmunoassay works well in the laboratory, there are several inherent problems with the assay format, particularly when attempting to design an assay system for home use. The most obvious of these problems are 1) the need for specially equipped laboratories, 2) the expense of radioactive counting equipment, 3) some radioactive isotopes have a very limited shelf life, 4) the waste disposal problem, and 5) the ethical

and legal problems associated with radioactive materials. However, the greatest disadvantage of the radioimmunoassay format is the need to physically separate the bound and free labelled antigen. It is necessary to separate the bound and free labelled ligand as bound and free antigen cannot be distinguished from each other by radioactive methods. The free label concentration must be determined so that the analyte concentration can in turn be determined by reference to a standard curve. The separation of bound and free labelled ligand can be achieved by a variety of methods [68] but makes automation of any such assay system difficult. A variety of other immunoassay methods have been developed for the measurement of small analytes and have been utilised for the determination of levels of steroids and steroid glucuronides in plasma and urine. For example, numerous nonisotopic immunoassays have been developed [74], among which are chemiluminescence immunoassay [74-76] and fluoroimmunoassay [77-83]. Both of these methods have been used for the measurement of ovarian steroid and steroid glucuronide levels. These immunoassay systems use either a chemiluminescent or fluorophore tracer with which to label and measure the amount of bound or free antigen. A more convenient nonisotopic immunoassay method which has the potential to be used in either the laboratory or the home is the enzyme immunoassay (EIA).

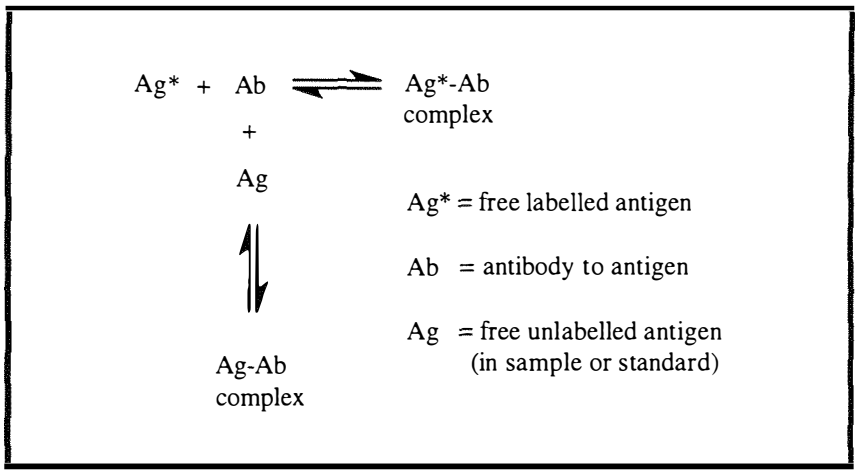


**Fig. 1.4.1** The principle reactions involved in radioimmunoassay

*1.4.2.2 Enzyme immunoassay*

There are now a large number of enzyme immunoassays based on the specific reaction between an antigen and antibodies raised to the antigen [84-85]. Enzyme immunoassays utilise 1) an enzyme labelled with hapten (or antigen), 2) the ability of antibodies to discriminate between structurally similar antigens, and 3) the specificity of enzymes. The reagents are on the whole relatively cheap, environmentally friendly, easy to dispose of, can be stored for lengthy periods of time and the assays are usually easy to perform. Enzyme immunoassay formats have other advantages over RIA's in that they eliminate

toxic and regulated substances, reduce the monetary and labour cost of analysis, and enhance the ability to expand the availability of such assay formats over a large population and geographic area due to the simplicity of the apparatus required to run an enzyme immunoassay. The EIA formats also provide the basis for the development of non-instrumental assays which could be used routinely in the home. Analysis of the results obtained by EIA in comparison with those obtained by RIA has shown that EIA can be just as sensitive and specific as RIA [86-87]. The ease of use of such assays, their accuracy, simplicity and relatively low cost has resulted in researchers developing a large number of enzyme immunoassays for the measurement of small analytes over the last 25 years. Many of these immunoassays have been developed for the measurement of the cyclic levels of ovarian and steroid hormones throughout a woman's menstrual cycle for use as biochemical markers of fertility or ovulation [88-101], or for monitoring pregnancy and fertility in various animal species [102-104].

Enzyme immunoassays can be divided into two broad groups, heterogeneous enzyme immunoassays and homogeneous enzyme immunoassays. Heterogeneous enzyme immunoassays (which include enzyme-linked immunosorbent assays or ELISA) are based on the same principles as radioimmunoassay. After incubation of the antigen and antibodies, the antigen-antibody complex is separated from the remaining free antigen and antibody. Instead of a radioactive label an enzyme label is used to measure the amount of bound and free label. The enzyme label (which is usually attached to the antibody) is equally active in both the bound and free state and the activity in one or both fractions is determined. It is therefore once again necessary, as in the case of RIA, to physically separate the bound and free enzyme label. In ELISA assay systems the enzyme is a passive passenger through the actual assay and development of such an assay system requires little knowledge of enzyme technology.

The advantage of homogeneous enzyme immunoassay systems is the ability to determine the amount of bound enzyme label (which depends on the analyte concentration) in solution by a simple kinetic measurement without the need for time consuming and technically demanding physical separation procedures [105-106]. Because the activity of the enzyme label is extensively inhibited (or sometimes activated) in the immune complex (when it is bound to the antibody) it is not necessary to separate the bound and free enzyme label. A simple rate measurement gives the free label concentration and hence the analyte concentration by reference to a standard curve. The simplicity of such assay systems gives the potential to develop accurate and fast assays which are easily automatable for use in clinical laboratories or adaptable for home assay systems.

The first published homogeneous immunoassay utilised an enzyme label in assays for low molecular weight ligands [107]. This type of enzyme immunoassay is known as an enzyme-multiplied immunoassay technique (EMIT). A typical EMIT assay format is shown in Fig. 1.4.2 whereby the bound enzyme label (often referred to as a conjugate) is inactivated in the bound form (immune complex). In the assay format the enzyme labelled hapten and the hapten in the sample of interest (which is unlabelled) compete for the limited number of antibody binding sites. As the concentration of hapten in the sample increases, the concentration of free enzyme labelled hapten at equilibrium increases, and an increase in enzymatic activity is detected. The observed enzymatic activity eventually reaches a maximum when all of the enzyme labelled hapten is in the free form (or alternatively all of the antibody is bound by the sample hapten). Hence, the inhibition levels are inversely proportional to the levels of free sample hapten in a stoichiometric manner as shown by Rubenstein *et al.* [107], or conversely, the enzymatic activity or rate

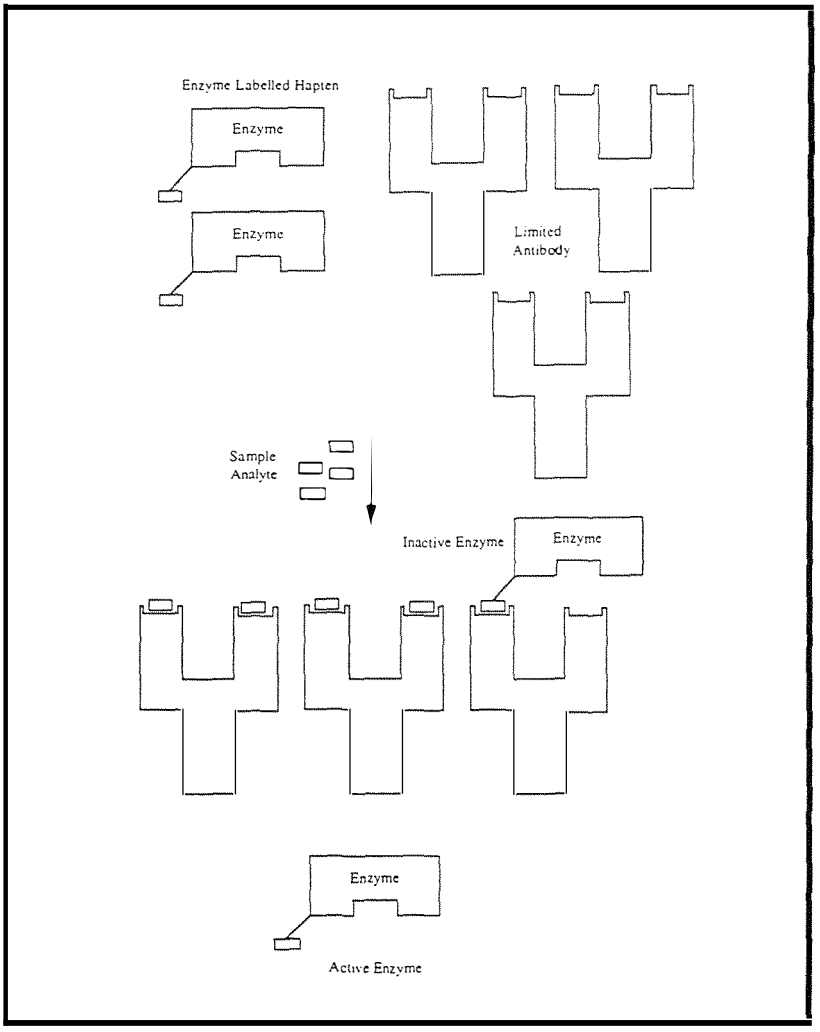


**Fig. 1.4.2** The principles behind the homogeneous enzyme immunoassay technique (enzyme-multiplied immunoassay technique). Sample hapten and enzyme labelled hapten compete for a limited amount of antibody. The enzyme-hapten is inactivated upon binding to antibody while free enzyme-hapten remains active.

is directly proportional to the free analyte concentration. Unlike the ELISA approach, EMIT requires an extensive knowledge of enzyme technology as enzymology is the key to the ultimate success or failure of any EMIT assay format.

The homogeneous enzyme immunoassay EMIT format is therefore ideally suited for the measurement of the urinary levels of the small hapten ovarian metabolites, E1G and PdG for the delineation of the fertile period. The EMIT format also has the potential to be developed into a home assay format to allow women the ability to detect their own fertile period accurately in the home.

---

## 1.5 The Ovarian Monitor

Although a large number of immunoassay formats have now been published for the measurement of ovarian steroid hormones and their metabolites (see section 1.4), the only system, which until now is both accurate and currently developed for use in the home situation, is the Ovarian Monitor. The Ovarian Monitor has been developed by Brown and colleagues [89, 91] over a number of years as a device for the home monitoring of the cyclic levels of the urinary metabolites of ovarian estradiol (estrone glucuronide) and progesterone (pregnanediol glucuronide) during a woman's menstrual cycle. This information can be gathered and used by women in the home to identify cyclical periods of fertility and infertility.

Only a limited number of enzymes have been employed in homogeneous enzyme immunoassay systems. Of these hen egg white lysozyme possesses an apparent specific activity with its bacterial substrate *Micrococcus lysodeikticus* which makes it ideal for the measurement of the levels of urinary estrone glucuronide (E1G) and pregnanediol glucuronide (PdG) encountered during the menstrual cycle [6]. Rubenstein *et al.* [107] also showed that the lytic activity of small hapten conjugates of hen egg white lysozyme could be extensively inhibited (up to 98%) by anti-hapten antibodies. As a result the concentration of a hapten such as PdG or E1G in any urine sample can be rapidly determined from a simple kinetic assay using the appropriate amounts of lysozyme conjugate (PdG or E1G) and anti-hapten antibodies (anti-PdG or anti-E1G antibodies).

The Ovarian Monitor consists of an Ovulation Meter and a specifically designed assay tube (Fig. 1.5.1). The Ovulation Meter contains a cell or tube holder with a built-in thermostat into which the assay tube is put during the immunoassay process to keep the reaction mixture at 40°C. The meter also acts as a spectrophotometer, measuring the transmission of the turbid *Micrococcus lysodeikticus* solution in the assay tube (at a

wavelength of 650 nm) and displaying the current value as a digital read out. In the laboratory situation where large numbers of samples may need to be analysed, a specifically designed heating block is used to hold the assay tubes and keep them at 40°C during the assay period. The plastic assay tube contains the required reagents for the immunoassay freeze dried onto the side of the tube so that sequential additions can be made and the various components mixed in the appropriate order. All of the assay tubes also contain a small glass bead which facilitates mixing. Separate tubes are used when assaying for E1G and PdG containing the appropriate reagents for each assay (E1G-lysozyme or PdG-lysozyme conjugate and anti-E1G or anti-PdG antibodies).

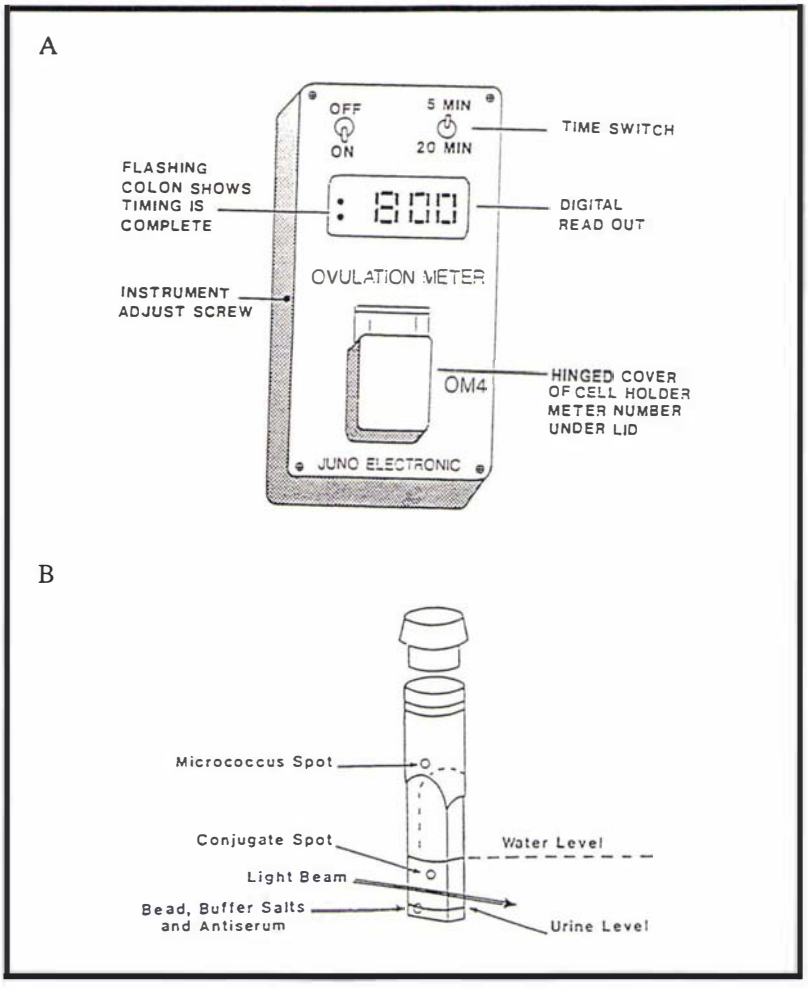


**Fig. 1.5.1** The components of the Ovarian Monitor assay system [89, 91]. A) A stylised diagram of the Ovulation Meter which consists of a small spectrophotometer, an in built timer, and a small, inexpensive thermostat. B) The assay tube used in the meter into which sequential additions are made to allow the three separate steps of the immunoassay to be performed in the same assay tube (for details see text).

The Ovarian Monitor assay is based on the classic enzyme-multiplied immunoassay technique (EMIT). The assay takes place in three discrete steps as shown in Fig. 1.5.2. In the first step the urine sample to be analysed is diluted to a volume of 150 mL per hour

of collection with tap water in a plastic jug. It is necessary to dilute the urine samples with respect to time to allow for the fluctuations in the rate of urine production and secretion which in turn is the result of factors such as varying fluid intake, temperature and intake of diuretics. After dilution, 50 μL of the urine sample is added to the bottom of the assay tube and the free E1G (or PdG) is allowed to react with the antibody raised against the hormone to be measured. Within the assay time frame the steroid glucuronide (E1G or PdG) in the urine sample binds irreversibly to the anti-steroid glucuronide antibody which is present in a slight excess. Because the steroid glucuronide-antibody binding

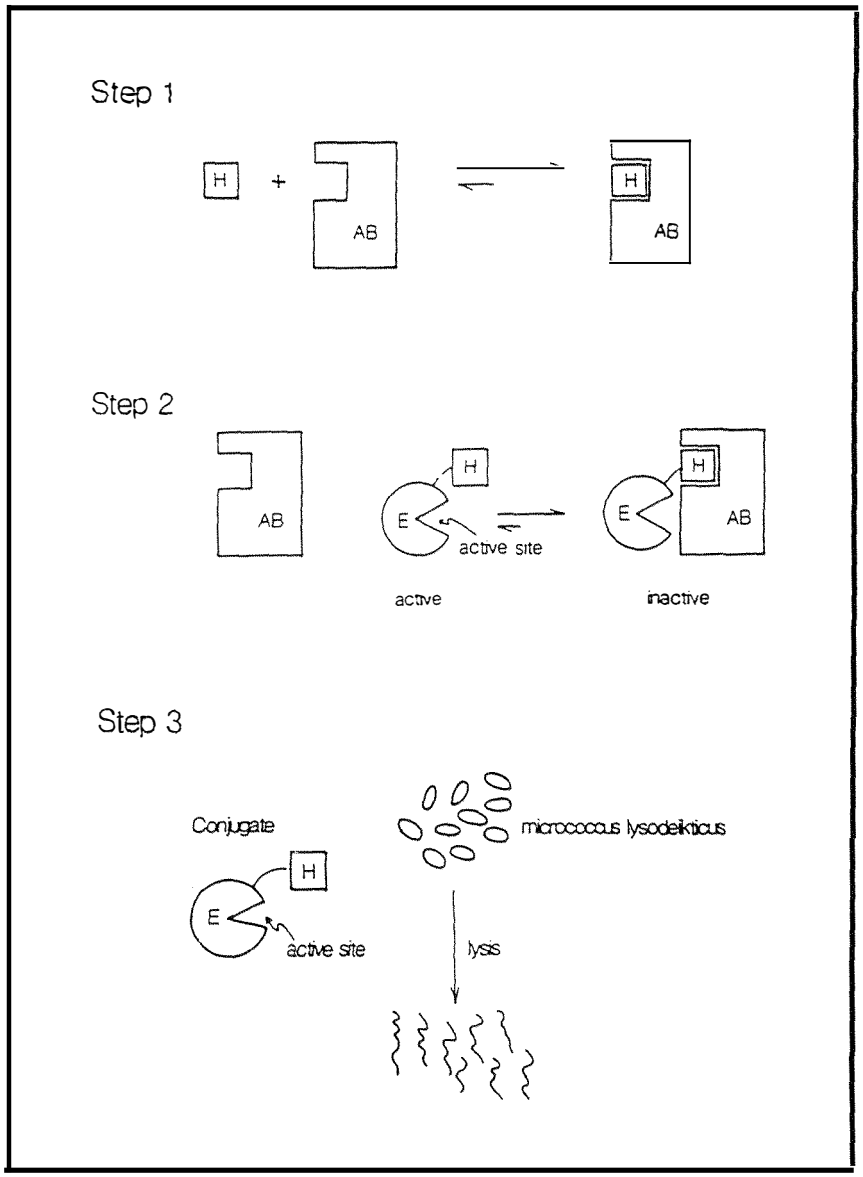


**Fig. 1.5.2** The three principle reactions involved in the measurement of the ovarian steroid metabolites estrone glucuronide and pregnanediol glucuronide by the homogeneous enzyme immunoassay system in the Ovarian Monitor [89, 91]. In the first step the steroid in the urine sample (H, either PdG or E1G, which ever is being assayed for) reacts with anti-steroid antibody (AB). In the second step the enzyme conjugate (E) is allowed to react with any anti-steroid antibody (inactivating the enzyme) which is not bound by steroid in the urine sample. In the third step the amount of enzyme-conjugate not bound by anti-steroid antibody (free conjugate) is measured by the rate of clearing of a turbid solution of the bacterial substrate *Micrococcus lysodeikticus*. For details see text.

reaction can be considered irreversible, the amount of antibody which is still free to react (i.e. not bound to an antigen moiety neutralising the antibody molecule) after this step is entirely dependent on the concentration of steroid glucuronide in the urine sample.

In the second step of the assay, water is added to dissolve the lysozyme conjugate spot (either PdG-lysozyme or E1G-lysozyme), which dissolves immediately. The conjugate is therefore allowed to react with any free antibody remaining after the first step. Binding of the conjugate to the anti-steroid glucuronide antibody (which can once again be considered irreversible within the assay time frame) results in almost complete inactivation (> 95%) of the enzymatic activity of the lysozyme conjugate. Thus, the amount of free (active) conjugate at the end of this step is dependent on the initial levels of free steroid glucuronide in the urine sample. If the urine sample contains a high concentration of steroid glucuronide then almost all of the antibody is neutralised and almost all of the conjugate remains in the free (active) state. For urine samples with low concentrations of steroid glucuronides the majority of the antibody remains free and as a result most of the enzyme conjugate is bound in the immune complex and inactivated.

In the third and final step of the immunoassay, the *Micrococcus lysodeikticus* spot, which is the usual lysozyme substrate, is dissolved and mixed in the reaction mixture by shaking and inverting the assay tube. The free lysozyme conjugates cleave (or lyse) the glycosidic C1-4 bond between the C-4 N-acetylglucosamine (NAG) and C-1 N-acetylmuramate (NAM) sugar units of the *Micrococcus lysodeikticus* cell wall. As a result of multiple cleavage of the cell wall by the lysozyme conjugates the strength of the cell is weakened and the cell bursts as a result of its internal osmotic pressure. The accumulated lysis of the bacterial cell walls results in the clearing of the initially turbid *Micrococcus lysodeikticus* solution. This clearing of the solution is measured as the change in transmission over 20 minutes (E1G) or 5 minutes (PdG). The two metabolites are measured over different time periods because urinary PdG is found in much higher concentrations than urinary E1G.

By using a set of known concentrations a standard curve may be generated which relates the steroid glucuronide concentration to the observed change in transmission (Fig. 1.5.3). The standard curve generated with any given batch of lysozyme-steroid glucuronide conjugate is extremely reproducible, negating the need to establish a new standard curve with each new analysis (unlike RIA where a new standard curve must be generated for each new batch of samples analysed). Hence, a simple rate measurement gives a direct measurement of the concentration of steroid glucuronide in any urine sample and thus couples can determine where in the fertility cycle a woman is. In practice a woman does not need to use the standard curve to determine her position in the current

menstrual cycle unless quantitative data are required. A simple monitoring of the rate of lysis, measured as a change in transmission ($\Delta T$) over a fixed period of time versus the cycle day serves as a direct measure of the urinary steroid concentration [91] (Fig. 1.5.4).

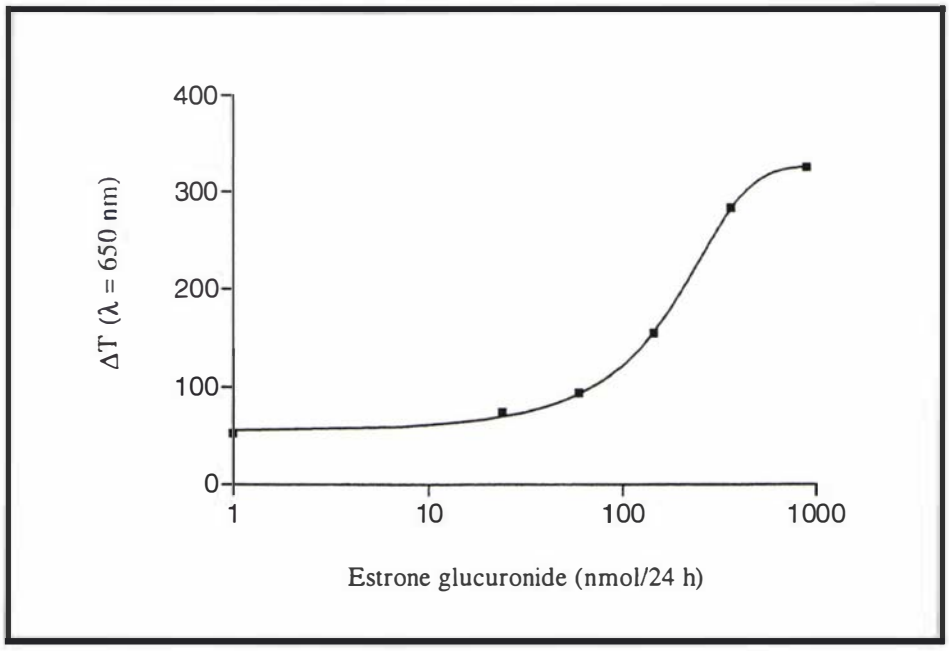


**Fig. 1.5.3** A standard curve generated for the measurement of urinary estrone glucuronide levels. For details see text.

Fig. 1.5.4 shows a typical profile of the menstrual cycle levels of urinary estrone glucuronide and pregnanediol glucuronide obtained using the Ovarian Monitor. The profiles are very similar to the idealised profile of the daily levels of E1G and PdG excreted during a normal menstrual cycle as shown in Fig. 1.3.2. The first significant E1G rise from baseline levels in Fig. 1.5.4 can be seen on day 9 of the cycle and thus the potentially fertile period begins on this day. The peak E1G day occurs on day 14 of the cycle and the most fertile day is therefore on day 15, the day of the E1G fall (from the peak day). If ovulation occurs on average 36 hours after the peak E1G day, then this data gives the woman 6-7 days advanced warning of ovulation which is long enough to prevent pregnancy for all but the longest sperm survival times.

The PdG marker for the end of fertility is clearly rising on day 17 of the cycle. However, the end of fertility is not reached until the threshold level of 6.3 μmol 24 $h^{-1}$ (1.75 μmol $L^{-1}$) is attained. This value is reached or surpassed on day 19 of the cycle. Thus, the data collected using the Ovarian Monitor is shown to define the potentially fertile period accurately. In the case given (Fig. 1.5.4) the potentially fertile period spans 11 days of the menstrual cycle during which time intercourse must be abstained from (or barrier

methods used) if pregnancy is to be avoided. For couples attempting to achieve pregnancy, in the example given the days of maximum fertility, the peak E1G day (day 14) and the day of the fall (day 15, predicted day of ovulation), are clearly defined.

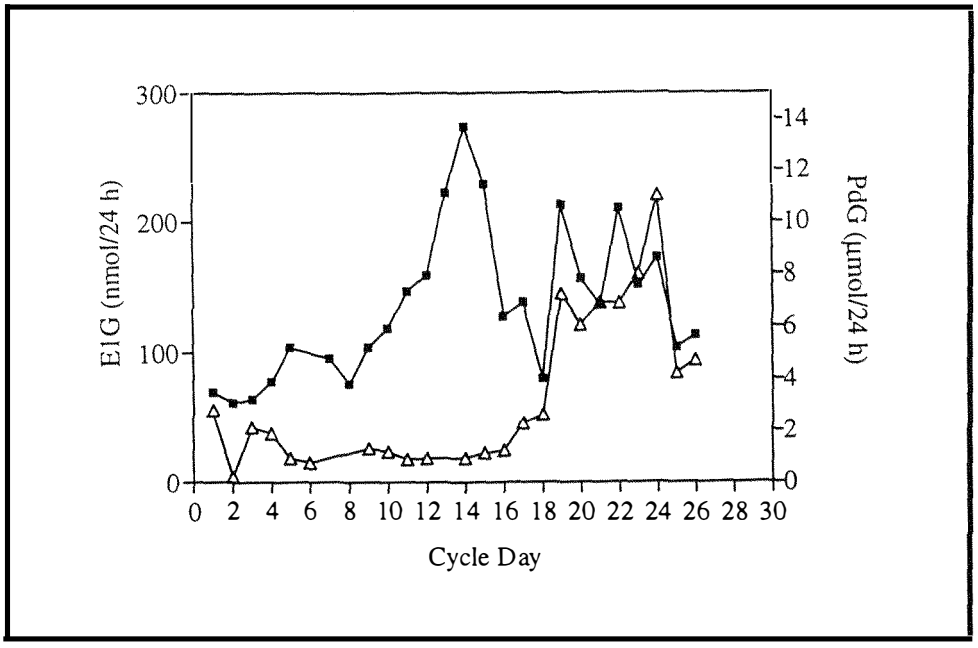


**Fig. 1.5.4** A normal menstrual cycle profile for the levels of urinary estrone glucuronide and pregnanediol glucuronide (■ = E1G, Δ = PdG) obtained using the Ovarian Monitor. For details see text.

The Ovarian Monitor is thus ideally designed for the measurement of urinary estrone glucuronide and pregnanediol glucuronide to identify the periods of fertility and infertility during the menstrual cycle. It may be used by both natural family planners who wish to prevent or space pregnancies without the use of chemical or barrier methods [108], or for those attempting to conceive. The accurate definition of the fertile period provided by the Ovarian Monitor greatly reduces the average number of days of abstinence required to prevent pregnancy from the 17 days per cycle reported [91] for couples using the ovulation method of natural family planning. The Ovarian Monitor may be of particular use to the sub-infertile couple who are having difficulty in conceiving so that the days (or period) of maximum fertility can be delineated accurately and precisely. Perhaps the biggest advantage of the Ovarian Monitor is its ease of use and the fact the tests can be undertaken by couples and women themselves within the comfort and privacy of their own homes.

Although the Ovarian Monitor enables women in the home to identify their own fertile period with great accuracy, some users of the system in a recent WHO study found the time requirements of the assay extreme [57]. Although the PdG assay takes only 15 minutes in total (with incubation steps) and the E1G assay around 35 minutes, users

perceived this as being rather too long to wait for the final result. There is also a market viewpoint that a colour dipstick type test, similar to many of the pregnancy tests now available [109], would be more acceptable to the general public both in terms of cost and ease of use.

---

## 1.6 New Systems for the Definition of the Fertile Period

### 1.6.1 The Problems Associated with the Development of New Colour Assay Systems

Any new system developed for the home measurement of steroid glucuronides as markers of the fertile period must be as accurate and reliable as the Ovarian Monitor. For this reason any new system must be validated against the current Ovarian Monitor system or something equivalent. The problem in developing new test systems, particularly colour test systems, is that to define accurately the fertile period the system must be able to detect and discriminate between the relatively small, but significant, increase in E1G from baseline levels on the first day of the potentially fertile period. This small change represents only a 20-25% total increase in the urinary concentration above the baseline E1G levels which are usually present in relatively low concentrations (nmol/L) at this time. Although lysozyme seems ideally suited in this sense, because lysozyme does not give a change in colour upon cleavage of its substrate, the lysozyme assay system cannot be used in its current format to give a colour test strip. In addition to this, the naked eye cannot detect these small but significant differences with the precision required and as a result a meter of some kind may be required which can follow the change in colour formation.

### 1.6.2 The Unipath Personal Contraceptive System

Although a new colour test strip assay is now available for the definition of the fertile period [110], the UNIPATH Personal Contraceptive System still requires a monitor to detect the first small, but significant rise in urinary E1G levels from baseline levels. The change in intensity of colour development on the test strip as a result of the first E1G increase is not easily detected visually. This E1G measurement is used only to confirm the beginning of the fertile period. The Unipath system uses the LH peak minus either 6 or 5 days to define the beginning of the fertile period based on a woman's previous history. The Unipath system also uses the mid-cycle surge in luteinising hormone (LH) as a marker of impending ovulation to delineate the end of the fertile period [110].

However, measurement of LH itself cannot be used as a marker for the end of fertility and a mathematical calculation is therefore required to predict the end of the potentially fertile period based on how long after the LH peak the ovum is no longer expected to be viable. The strip also gives a reverse colour change with increasing concentrations of urinary hormones. As the concentrations of the urinary hormones increase, the colour intensity development on the test strip decreases. If a visual test strip is to be designed, along the lines of the pregnancy confirmation test strips currently available, then an assay format whereby the intensity of the colour increases with increasing hormone concentrations is obviously much less confusing for couples in the home to use. A test strip which does not require a meter will also have considerable cost advantages. Development of a colour test strip which gives a positive signal (greater colour intensity with increasing hormone concentrations), using PdG as a marker for the end of fertility, and not requiring a monitor would offer an attractive alternative system to the UNIPATH system and the Ovarian Monitor.

### 1.6.3 Difficulties with Horseradish Peroxidase as an Enzyme for Producing a Colour Test

A number of enzymes capable of producing colour such as horseradish peroxidase (HRP) [98, 111-112] and alkaline phosphatase [98, 113] have now been linked to steroid glucuronides for use in enzyme immunoassays to measure urinary concentrations of these haptens. However, the vast majority of work undertaken with the aim of utilising a colour test has involved solid phase immunoassays or ELISA assays using horseradish peroxidase. Although horseradish peroxidase-hapten conjugates do retain a relatively high level of enzymatic activity after conjugation [113] the extensive degree of inhibition seen upon binding of the antibody to the hapten in lysozyme based immunoassays has not been observed for horseradish peroxidase based immunoassays. Hence, horseradish peroxidase has not been used for homogeneous enzyme immunoassays.

Several other problems have also been encountered in the use of HRP for enzyme immunoassay. It has proven difficult to obtain steroid glucuronide conjugates of HRP in good yield using traditional coupling procedures such as the mixed anhydride procedure or the active ester procedure [111]. As a result a large molar excess of steroid glucuronide is required to obtain HRP-steroid glucuronide conjugates with a reasonable level of coupling. The level of coupling influences both the immunoreactivity of the enzyme conjugate and the specific activity (relative to the native enzyme). However, it is not possible to control the position of attack or the number of sites attacked as most enzyme molecules will possess many more than one ε-amino group to which a hapten may be conjugated using the traditional coupling procedures. The need to use large amounts of

expensive steroid glucuronides to achieve coupling success also greatly increases the cost of producing the enzyme-conjugates.

HRP conjugates have also proven difficult to separate from unreacted starting materials (unreacted HRP and unreacted steroid glucuronide) after conjugation reactions. Although unreacted hapten can be removed by serial dialysis or gel filtration it is extremely difficult to separate conjugated HRP from native HRP. The reason for this is that the conjugation of one or two molecules of hapten to the large HRP molecule makes very little difference to the chemical nature or overall size of the HRP molecule. One further problem associated with HRP conjugates is the stability of the enzyme when stored in low concentrations. HRP-conjugates stored at relatively low concentrations very quickly lose their enzymatic and immunochemical activity when prepared using traditional coupling procedures.

Therefore, to obtain the maximum discrimination between similar hormone concentrations, as required for the delineation of the fertile period by a home assay, it is necessary to design a pure enzyme conjugate capable of producing a colour. The conjugate must be;

(1) relatively cheap,

(2) easy to produce, and

(3) purification procedures to separate unreacted enzyme and steroid glucuronide from the conjugation products must be simple and not overly demanding technically, or in terms of the time required to undertake the purification.

To design a conjugate which meets these needs is one of the long term goals of the Ovarian Monitor research group.

## 1.7 Aims of the Current Study

Although one of the long term goals of the Ovarian Monitor research group is to develop a new methodology based on homogeneous enzyme immunoassay and which produces colour, no suitable system currently exists. However, the Ovarian Monitor immunoassay lysozyme system does exhibit the extensive levels of inhibition required for the measurement of similar hormone concentrations and the delineation of the fertile period. Hence, a more thorough exploration of the Ovarian Monitor assay system may determine the parameters which are important in obtaining inhibitable enzyme conjugates. Although, the lysozyme-steroid glucuronide conjugates utilised in the Ovarian Monitor assay system [89, 91, 114-115] are extensively inhibited by anti-steroid glucuronide antibodies, their chemical composition remains unknown and hence the mechanism of inhibition is uncharacterised. An understanding of this system may help in the design of other homogeneous enzyme immunoassay systems using enzymes such as horseradish peroxidase. Consequently, a major aim of this thesis is to structurally characterise the steroid glucuronide-lysozyme conjugates used in the Ovarian Monitor in an attempt to identify the factors which are important in determining the mechanism of inhibition by the anti-steroid glucuronide antibodies. This thesis is therefore mainly concerned with the synthesis, purification and structural characterisation of the components of the Ovarian Monitor immunoassay system.

# Chapter Two

# The Preparation and Purification of Estrone Glucuronide- and Pregnanediol Glucuronide-Lysozyme Conjugates

## Conjugates Suitable for Use in a Homogeneous Enzyme Immunoassay System for the Measurement of Menstrual Cycle Levels of Urinary Estrone Glucuronide and Pregnanediol Glucuronide

---

## 2.1 Introduction

The Ovarian Monitor lysozyme-hapten conjugates are formed when a steroid glucuronide is attached to the ε-amino group (or the N-terminal amino group) of a lysine residue of the hen egg white lysozyme molecule *via* the carboxylic acid moiety on the glucuronide carbohydrate ring. The usual chemical procedure to activate the carboxylic acid group for coupling is the mixed anhydride acylating procedure of Erlanger *et al.* [116]. There are six lysine residues within the amino acid sequence of hen egg white lysozyme [117], all of which, including the N-terminal α-amino group, are found near the surface of the molecule [118], and hence the conjugation reaction may in principle acylate any of these amino groups to form a stable conjugate. It has been suggested that the site of acylation of haptens in enzyme conjugates is important in determining the recognition and strength of binding of the hapten by anti-hapten antibodies [119]. Although the mixed anhydride method is the usual method of conjugation, lysozyme can be acylated readily by a variety of acylating reagents [120] to give stable conjugates which retain lytic activity only if the total number of lysine residues acylated is less than four [121]. It is therefore necessary to use conjugation conditions which maximise the concentration of conjugates with low degrees of steroid substitution. This means that significant amounts of unreacted lysozyme will inevitably remain after completion of the conjugation reaction.

The sensitivity and precision of a homogeneous enzyme immunoassay is largely dependent on the purity of the enzyme-hapten conjugate used in the system [122]. This

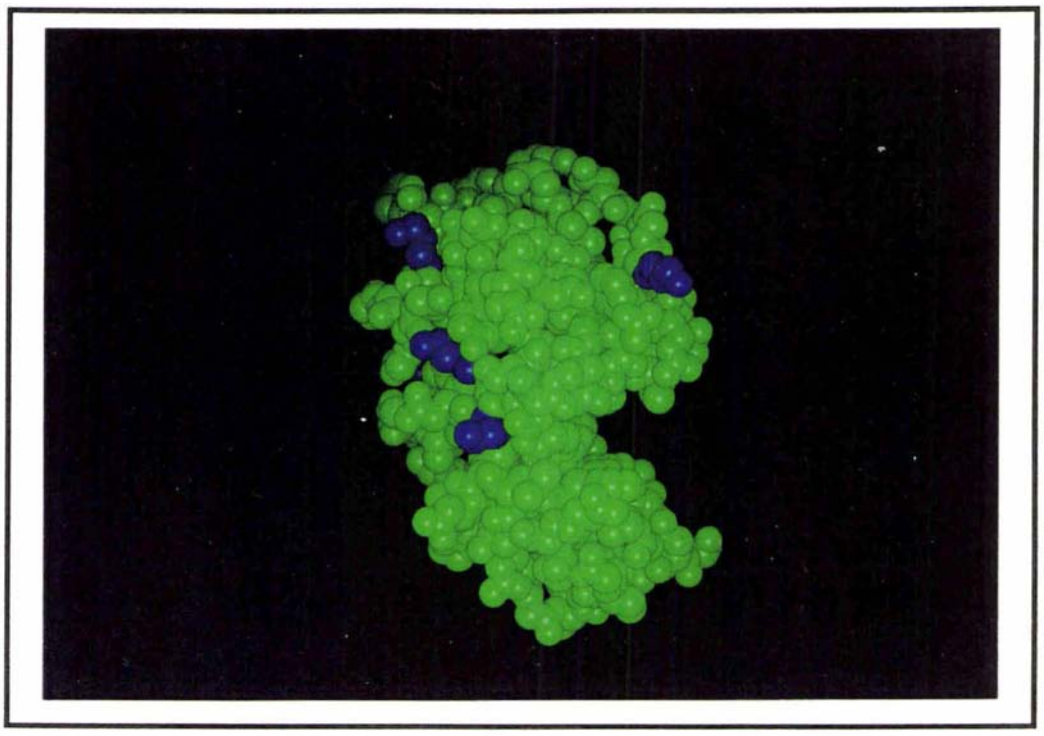

**Fig. 2.1.1** CPK space-filling representation of the three dimensional structure of hen egg white lysozyme as revealed by the crystallographic studies of Ramanadham *et al.* [118] with the active site cleft orientated to the right hand side of the molecule. Of the six lysine residues in the enzyme, four can be seen highlighted in blue. Three residues are located on one side of the molecule (when the active site cleft is orientated to the right hand side) and one residue is located above the active site cleft.

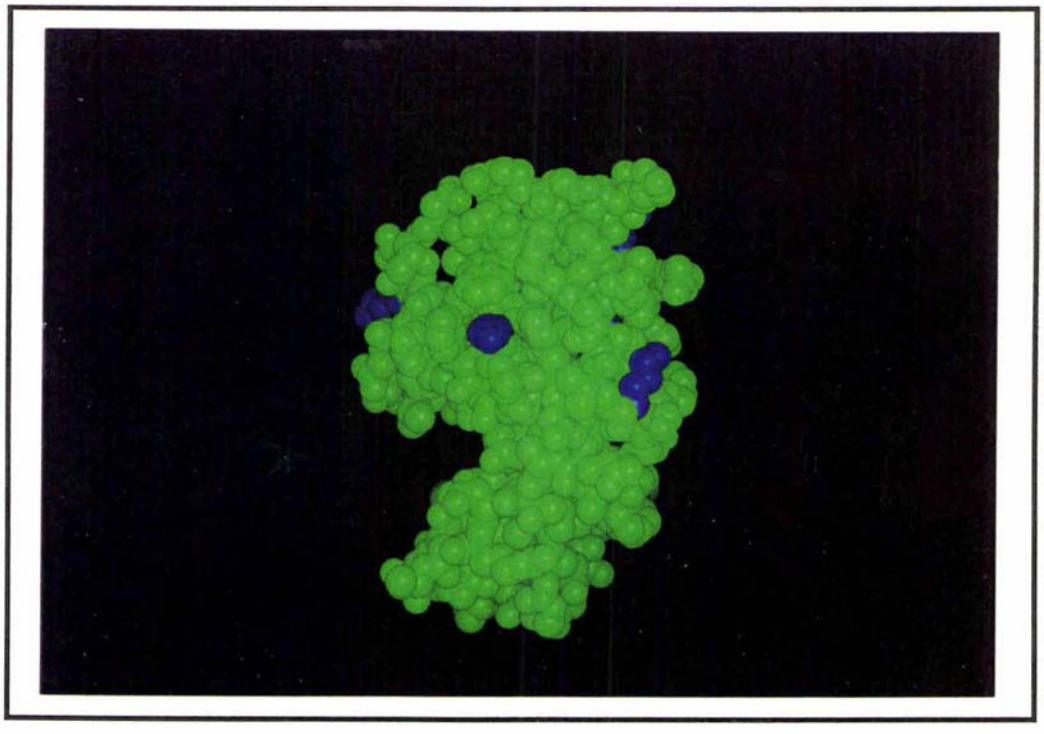

**Fig. 2.1.2** CPK space-filling representation of the three dimensional structure of hen egg white lysozyme as revealed by the crystallographic studies of Ramanadham *et al.* [118] with the active site cleft orientated to the left hand side of the molecule. Of the six lysine residues in the enzyme, two can be seen highlighted in blue from this orientation. The residue located above the active site cleft (as seen in Fig. 2.1.1) is partially visible in this orientation.

requirement necessitates that after conjugation any unreacted lysozyme is completely separated from the conjugated material. If unreacted enzyme remains in the conjugate material used for enzyme immunoassay, high baseline or background enzymatic rates are observed even in the presence of excess anti-hapten antibody as unconjugated enzyme is not inactivated.

To obtain the maximum assay discrimination between similar hormone concentrations, as is required for the delineation of the fertile period by a home assay [91], it is necessary to isolate an enzyme conjugate with a high degree of inhibition for baseline urinary hormone levels. Enzyme conjugates which display low degrees of inhibition in the presence of excess anti-hapten antibodies (< 90%) cannot discriminate between similar hormone concentrations with the accuracy required. Ideally the enzyme activity of the conjugate in the immune complex should be zero since the accuracy, working range and gradient of the standard curve are proportional to the difference in enzyme activity between the bound and free conjugate. Thus enzyme conjugates which are both free from unconjugated material and show a high level of inhibition (> 90%) in the presence of excess anti-hapten antibody must be prepared and purified for homogeneous enzyme immunoassay.

There have been few reports of chromatographic purification procedures for protein products after conjugation with small molecules apart from the use of a gel filtration step [90]. While such a step removes unreacted haptens or coupling reagents from the protein products, it does not remove unconjugated protein. The serial dialysis of conjugated material in 7 M urea solutions [123] is the only reported purification procedure for the separation of lysozyme conjugates from unconjugated lysozyme. While this procedure gives conjugates with high degrees of inhibition (> 90%), they are uncharacterised and the majority of the conjugated material is unsuitable for use in immunoassays either because it still contains lysozyme or the specific activities are too low.

The Ovarian Monitor system currently uses lysozyme-steroid glucuronide conjugates produced by acylation of lysozyme with estrone glucuronide or pregnanediol glucuronide by the mixed anhydride procedure [57]. The resulting conjugates are then purified by ion-exchange chromatography on a CM Sepharose column at pH 6.0 [57]. Both the mixed anhydride acylation procedure and the ion-exchange purification are difficult to undertake and are poorly reproducible in inexperienced hands. The details of these purification procedures have not yet been published. Although this system is not ideal, it has produced good quality lysozyme-steroid glucuronide conjugates which are currently used in the Ovarian Monitor homogeneous enzyme immunoassay system. The conjugated material is purified as the trailing edge of a single large peak eluted from a CM-Sepharose cation-exchange column with the conjugate fractions identified by their inhibition (>

90%) in the presence of excess anti-steroid glucuronide antibody. This single peak also contains unreacted lysozyme and other conjugated material which cannot be easily separated from the unreacted lysozyme material. As a result much of the conjugate material is either lost (under the lysozyme peak) or material must be rechromatographed several times in order to produce conjugates with high levels of inhibition (> 90%) in the presence of excess anti-hapten antibody. This chapter investigates new chromatographic procedures for the preparation and purification of large amounts of lysozyme-steroid glucuronide conjugates.

## 2.2 Experimental

### 2.2.1 Apparatus

Nuclear magnetic resonance spectroscopy (NMR) was performed on a JEOL GX-270 spectrometer. $^{1}H$ and $^{13}C$ spectra were obtained at operating frequencies of 270 and 67.9 MHz respectively. These were referenced relative to tetramethylsilane ($\delta$ = 0.0 ppm) as an internal standard and are reported as position (parts per million), multiplicity (s = singlet, d = doublet, dd = doublet of doublets, t = triplet), relative integral, coupling constant (J Hz) and assignment.

Melting points were determined on a Bausch and Lamb hot plate melting point apparatus. Mass spectra were obtained using a VG70-250S double focusing magnetic sector mass spectrometer. Major fragments are given as percentages relative to the base peak intensity. Microanalyses were performed by the microanalytical laboratory at the University of Otago. Silica gel 60 (Merck) particle size 0.04-0.063 mm, 230-400 mesh was used in flash column chromatography as described by Still *et al.* [124].

All chromatographic procedures were performed on a Pharmacia fast protein liquid chromatography (FPLC) system at room temperature. This system consisted of two P-500 pumps, an LCC-500 liquid chromatography controller, an MV-7 motor valve injector, a P-1 peristaltic pump, a Pharmacia mixer and a 280 nm single-path UV-1 monitor which was coupled to a two channel Pharmacia chart recorder. Purifications were performed on prepacked Mono-S strong cation-exchange and Alkyl Superose hydrophobic interaction columns HR 5/5 (50 x 5 mm I.D.). A Pharmacia HR 16/50 (500 x 16 mm I.D.) column packed with Pharmacia CM-Sepharose (fast flow) resin was also used.

### 2.2.2 Reagents

The following reagents were used and obtained from the sources indicated: Hen egg white lysozyme, grade 1, 3 times recrystallised and lyophilised, *Micrococcus lysodeikticus* , bovine thyroglobulin, 5$\beta$-pregnanediol-3$\alpha$,20S-diol diacetate, 3-hydroxy-estra-1,3,5(10)-triene-17-one, and glucuronolactone were all from Sigma Chemical Co. (St. Louis, MO, U.S.A.). All other chemicals and reagents were analytical reagent grade or better.

Ion-exchange and hydrophobic interaction chromatography buffers were prepared as described in figure legends. All buffers were filtered and degassed using 0.2 $\mu$m filters

(Millipore) before use. Samples were filtered through Millipore GVWP 013 00 filters (0.2 μm). Stock tris-maleate buffer (1.0 M), was prepared by mixing maleic acid (7.25 g), tris (19.80 g), NaCl (12.75 g), Tween 80 (20 mL of a 1/100 dilution in Milli-Q water), and HCl (2.8 mL of concentrated acid) in a total volume of 375 mL. The pH was adjusted to pH 7.0 with HCl as required.

### 2.2.3 Methods

*2.2.3.1 Synthesis of methyl 1-bromo-1-deoxy-2,3,4-tri-O-acetyl-α-D-glucopyranuronate*

The title compound was synthesised *via* a two step synthesis from glucuronolactone as previously reported by Bollenback *et al.* [125] and the final product recrystallised from absolute ethanol to give white crystals in 67% yield. m.p. 104-106°C (literature 106-107°C [125]); δH (270 MHz, $CDCl_3$), 2.05 (s, 3H, $OCOCH_3$), 2.06 (s, 3H, $OCOCH_3$), 2.11 (s, 3H, $OCOCH_3$), 3.77 (s, 3H, $COOCH_3$), 4.57 (d, 1H, J = 10.25 Hz, H-5), 4.86 (dd, 1H, J = 9.89, 4.03 Hz, H-2), 5.24 (t, 1H, J = 9.89 Hz, H-3), 5.61 (t, 1H, J = 9.89 Hz, H-4), 6.65 (d, 1H, J = 4.03 Hz, H-1).

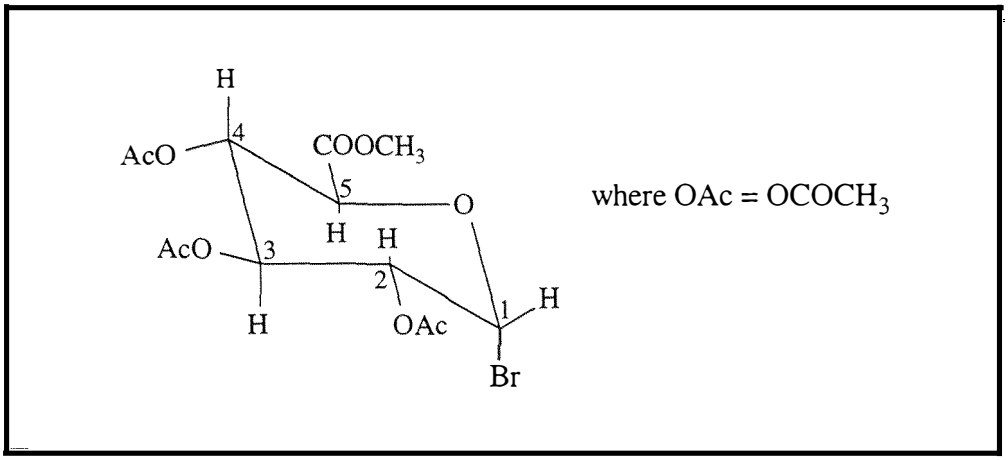


**Fig. 2.2.1** The structure of methyl 1-bromo-1-deoxy-2,3,4-tri-O-acetyl-α-D-glucopyranuronate (bromosugar)

*2.2.3.2 Synthesis of 17-oxoestra-1,3,5(10)-triene-3-yl-β-D-glucopyranosiduronic acid*

17-oxoestra-1,3,5(10)-triene-3-yl-β-D-glucopyranosiduronic acid (estrone glucuronide or E1G[H]) was synthesised in three steps from 3-hydroxy-estra-1,3,5(10)-triene-17-one (estrone) and methyl-1-bromo-1-deoxy-2,3,4-tri-O-acetyl-α-D-glucopyranuronate (α-bromosugar) essentially according to Conrow and Bernstein [126] to give a white crystalline product in 39% yield as shown in scheme 2.2.1. Typically estrone (II in scheme 2.2.1) was coupled with α-bromosugar (I in scheme 2.2.1) in dried toluene using cadmium carbonate as a catalyst in a molar ratio of 1:3:3 (estrone:bromosugar:cadmium carbonate) to give the desired β-glucuronide isomer (III in

scheme 2.2.1). The resulting methyl-[17-oxoestra-1,3,5(10)-triene-3-yl-2',3',4'-tri-O-acetyl-β-D-glucopyranosiduronate] (estrone glucuronide ester, III in scheme 2.2.1) was recrystallised firstly from 25% aqueous acetone and then twice from dichloroethane:ethanol (1:1). The estrone glucuronide ester was then hydrolysed in methanol using a molar ratio of 1:5 (ester:NaOH) to give sodium-[17-oxoestra-1,3,5(10)-triene-3-yl-β-D-glucopyranosiduronate] (estrone glucuronide sodium salt) which was recrystallised from methanol.

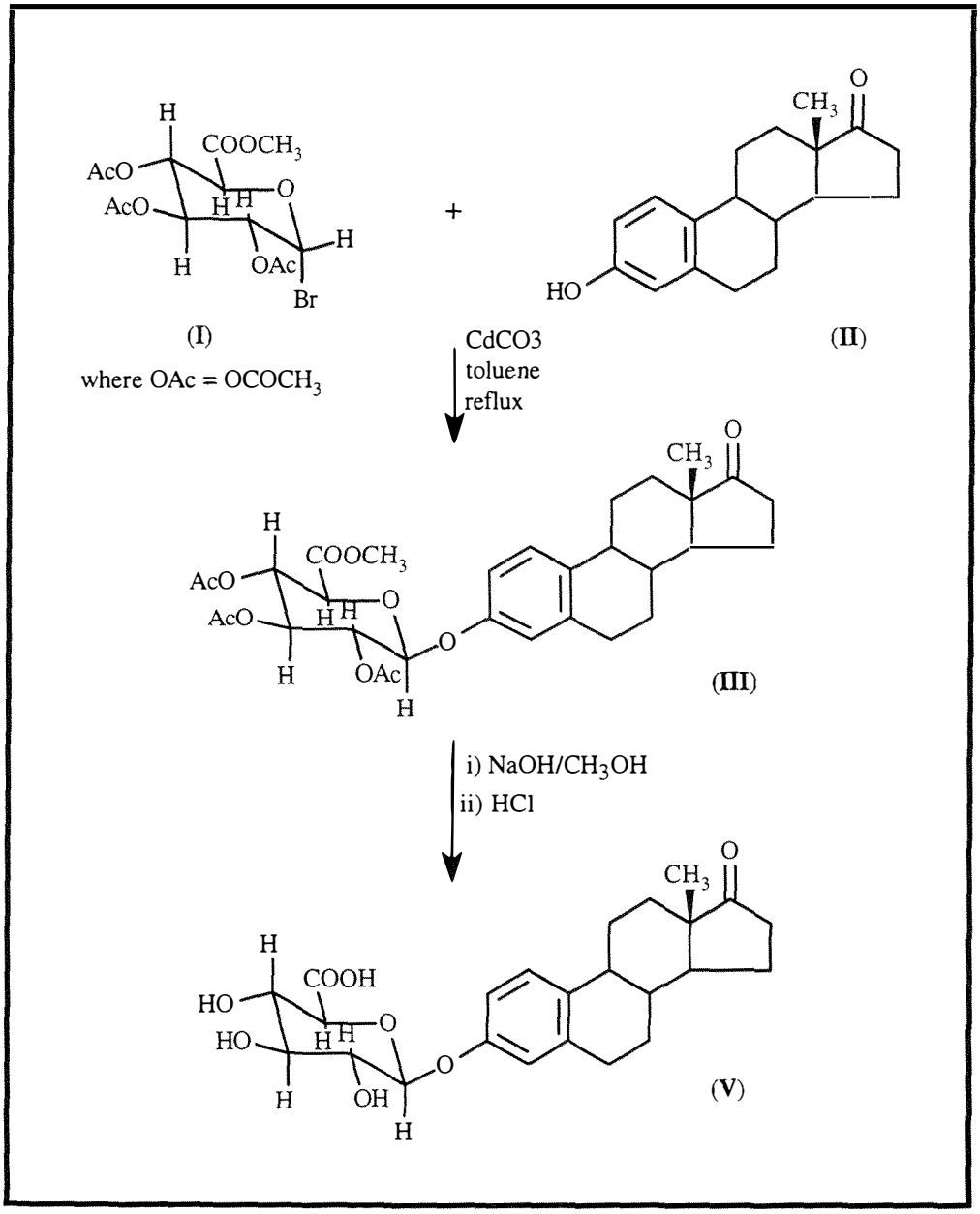


**Scheme 2.2.1** The synthesis of estrone glucuronide (V) as described in section 2.3.2.1

The acid form of estrone glucuronide (E1G[H]) was obtained by titrating the aqueous sodium salt to pH 2.4 with 0.5 M HCl to give a white precipitate of 17-oxoestra-

1,3,5(10)-triene-3-yl-β-D-glucopyranosiduronic acid (V in scheme 2.2.1) after standing overnight at 4°C. The estrone glucuronide acid form was purified by XAD-2 chromatography as described by Mattox *et al.* and Numazawa *et al.* [127-128] with the E1G[H] being eluted with a 75% aqueous methanol solution. The methanol was removed and the product freeze dried to give 17-oxoestra-1,3,5(10)-triene-3-yl-β-D-glucopyranosiduronic acid as a white solid. m.p. 168-170°C (literature 176.5-178°C [129]); Analysis calculated: C, 64.57; H, 6.73; found: C, 64.49; H, 6.60; δH (270 MHz, DMSO-$d_6$), 0.83 (s, 3H, 18-$CH_3$), 3.72 (d, 1H, J = 8.79 Hz, H-5'), 4.91 (d, 1H, J = 7.96 Hz, H-1'), 6.71 (s, 1H, H-4), 6.77 (d, 1H, J = 8.43 Hz, H-1), 7.17 (d, 1H, J = 8.43 Hz, H-2).

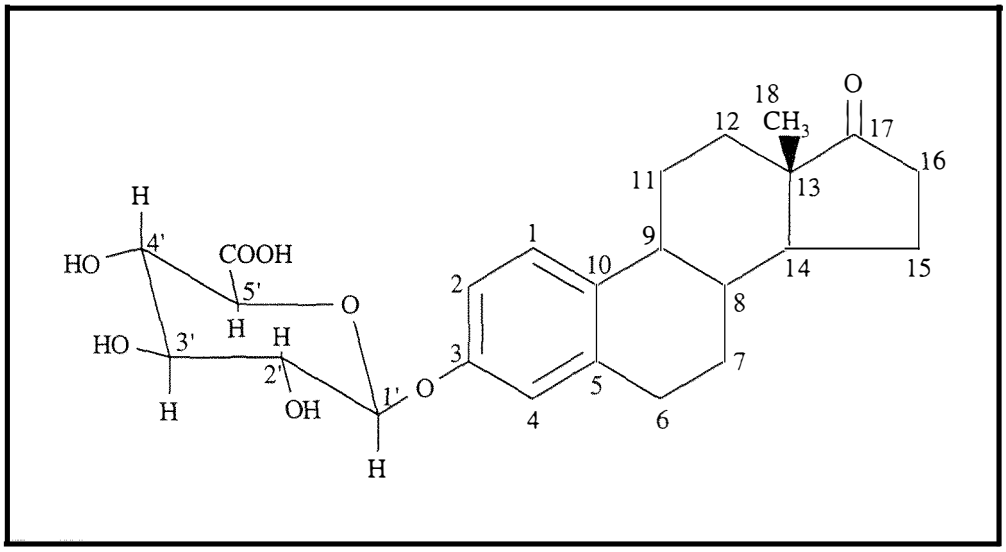


**Fig. 2.2.2** The structure of 17-oxoestra-1,3,5(10)-triene-3-yl-β-D-glucopyranosiduronic acid (estrone glucuronide) showing the conventional numbering system

*2.2.3.3 Synthesis of 5β-pregnane-3α,20S-diol-3-yl-β-D-glucopyranosiduronic acid*

5β-pregnane-3α,20S-diol-3-yl-β-D-glucopyranosiduronic acid (pregnanediol-3α-glucuronide or PdG[H]) was synthesised in four steps from 5β-pregnane-3α,20S-diol diacetate and methyl-1-bromo-1-deoxy-2,3,4-tri-O-acetyl-α-D-glucopyranuronate essentially according to Conrow and Bernstein [126] to give a white crystalline product in 36% yield. Typically, 5β-pregnane-3α,20S-diol diacetate was partially hydrolysed with methanolic potassium hydroxide using a molar ratio of 1:1 to give 5β-pregnane-3α-ol-20S-acetate which was purified by silica gel flash column chromatography. The 5β-pregnane-3α-ol-20S-acetate was then treated as for the estrone moiety, undergoing the same set of reactions as shown in scheme 2.2.1. 5β-pregnane-3α-ol-20S-acetate was coupled with methyl-1-bromo-1-deoxy-2,3,4-tri-O-acetyl-α-D-glucopyranuronate using the conditions specified in section 2.2.3.2 for the coupling of estrone to the α-bromosugar to give methyl-(5β-pregnane-3α-ol-20S-acetate-3-yl-2',3',4'-tri-O-acetyl-β-

D-glucopyranosiduronate) after purification by flash column chromatography. The pregnanediol-3α-glucuronide ester was hydrolysed in methanol using a molar ratio of 1:5 (ester:NaOH) to give the product sodium-(5β-pregnane-3α,20S-diol-3-yl-β-D-glucopyranosiduronate) (pregnanediol-3α-glucuronide sodium salt) which was recrystallised from methanol:water (3:2). The acid form of pregnanediol-3α-glucuronide (PdG[H]) was obtained by titrating the sodium salt to pH 2.5 in 60% aqueous methanol with 0.5 M HCl. A small amount of methanol was removed by rotary evaporation and the solution placed at 4°C to crystallise. The resulting crystals were removed by centrifugation, washed with water and then dried *in vacuo* to give 5β-pregnane-3α,20S-diol-3-yl-β-D-glucopyranosiduronic acid as a white crystalline solid. m.p. 194-197°C; Analysis calculated: C, 64.87; H, 9.29; found: C, 64.98; H, 9.13; δH (270 MHz, $CD_3OD$) 0.66 (s, 3H, 18-$CH_3$), 0.94 (s, 3H, 19-$CH_3$), 1.19 (d, 3H, J = 6.2 Hz, 21-$CH_3$), 4.45 (d, 1H, J = 7.69, H-5'); δC (270 MHz, $CD_3OD$) 13.69 (18-$CH_3$), 22.50 (19-$CH_3$), 24.66 (21-$CH_3$), 71.92 (4'-C), 73.96 (5'-C), 75.57 (2'-C), 77.36 (3'-C), 78.25 (20-C), 81.10 (3-C), 103.3 (1'-C), 173.40 (6'-C); m/z: 497 ($MH^+$, 21%), 285 ($C_{21}H_{33}$, 100%).

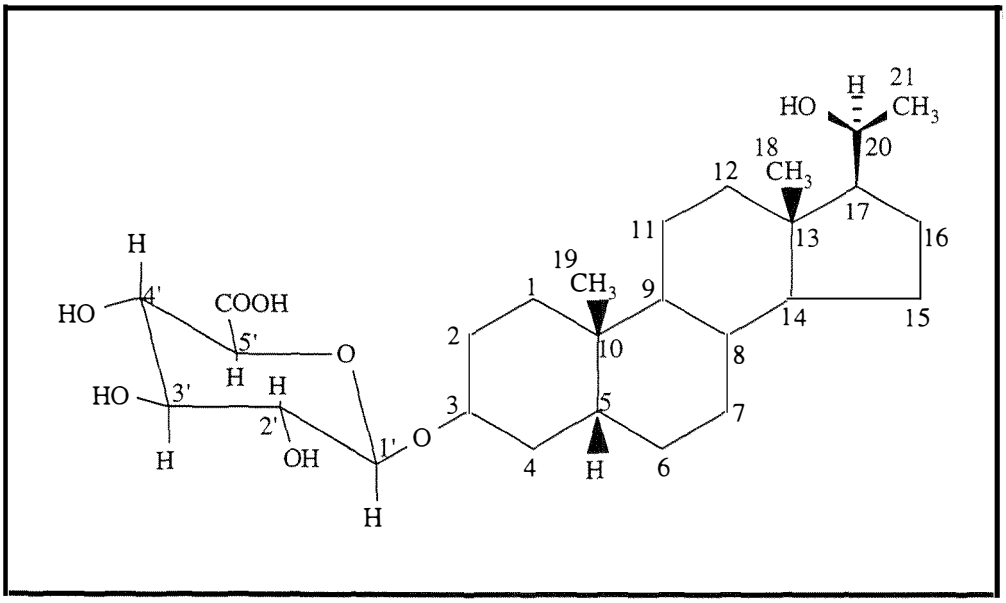


**Fig. 2.2.3** The structure of 5β-pregnane-3α,20S-diol-3-yl-β-D-glucopyranosiduronic acid (pregnanediol glucuronide) showing the conventional numbering system

*2.2.3.4 Purification of hen egg white lysozyme*

The commercial three times crystallised, dialysed and lyophilised lysozyme (2.6 g; 179 mmol) was further purified by loading onto a CM Sepharose (fast flow) column *via* a peristaltic pump in 10 mM pH 6.0 phosphate buffer (20 mL). Elution was effected with a 0.15 M to 0.6 M NaCl gradient, in the same buffer, over 600 minutes using a flow rate of 1.5 mL/min. The elution profile consisted of two peaks, a small impurity peak which

eluted first and was discarded, followed by the elution of a much larger peak containing the bulk of the lysozyme material. The peak fractions from the larger peak were pooled, exhaustively dialysed against Milli-Q water and freeze dried for storage as previous work has shown that lyophilisation of native lysozyme does not effect the structure or activity of the enzyme [130]. The freeze dried, purified lysozyme was then stored at -10°C until required for conjugation experiments.

*2.2.3.5 Preparation of steroid glucuronide-lysozyme conjugates by the active ester method*

Estrone glucuronide (E1G[H]) and pregnanediol-3α-glucuronide (PdG[H]) conjugates of

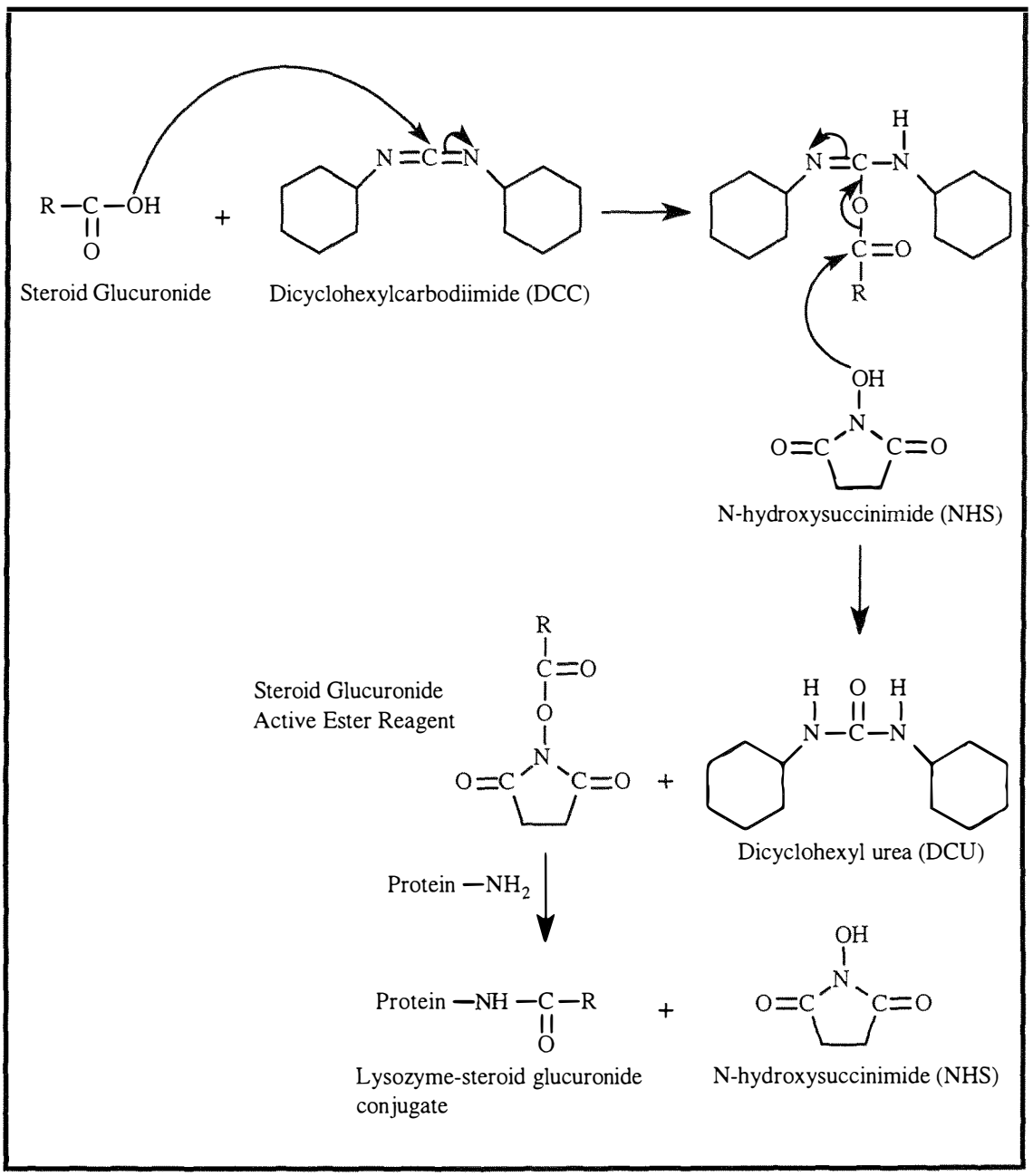


**Scheme 2.2.2** The synthesis of steroid glucuronide-lysozyme conjugates by the active ester method

lysozyme were prepared by the N-hydroxysuccinimide/dicyclohexylcarbodiimide coupling method [111] at a 1.6:1 molar ratio of steroid glucuronide to lysozyme (unless stated otherwise) as shown in scheme 2.2.2.

In a typical experiment an active ester reagent was prepared from E1G[H] (7.6 mg, 17.04 μmol) in dimethylformamide (52 μL). N-hydroxysuccinimide (22.5 mg, 195 μmol) and dicyclohexylcarbodiimide (29.9 mg, 145 μmol) were each separately dissolved in dimethylformamide (100 μL). From these stock solutions N-hydroxysuccinimide (20 μL, 39 μmol) was added to the E1G[H] solution followed by the addition of dicyclohexylcarbodiimide (20 μL, 29 μmol). After standing at room temperature for one hour the active ester reagent was added dropwise to a stirred solution of purified lysozyme (152 mg, 10.65 μmol) dissolved in 1% aqueous sodium hydrogen carbonate (6 mL, pH 9.10) at 0°C in an ice bath. After standing overnight with stirring at 4°C the reaction mixture, which appeared opaque, was dialysed against Milli-Q water (3 x 2 L) and then stored at -10°C.

*2.2.3.6 Purification of steroid glucuronide-lysozyme conjugates*

The success of the conjugation experiments and purity of the derivatives was determined by analytical chromatography on a Mono-S cation-exchange column in 7 M urea buffers as described in the figure legends (see Fig. 2.3.1 for example). Steroid glucuronide-lysozyme conjugates were purified in a two step procedure from the conjugation reaction mixture by Mono-S cation-exchange chromatography in pH 4.3 sodium dihydrogen phosphate buffers followed by Alkyl Superose hydrophobic interaction chromatography in pH 6.6 buffers as described in the figure legends.

*2.2.3.7 Lysine titrations*

The concentration of free lysine amino groups within the conjugate populations was determined essentially as previously described in the 2,4,6-trinitrobenzene 1-sulfonic acid (TNBS) procedure of Habeeb [131], Sashidar *et al.* [132] and Fields [133]. Typically, conjugate (0.6 mg/mL) was dissolved in 4% sodium hydrogen carbonate (1 mL) followed by the addition of aqueous TNBS (0.1%, 1 mL). The resulting solution was then incubated at 40°C in the dark for two hours. Upon the completion of the incubation period, an aqueous 10% (w/v) SDS solution (1 mL) was added, followed by the addition of 1 M HCl (0.5 mL). The absorbance of the solution was recorded at 336 nm and the number of moles of free lysine residues was calculated using a molar extinction coefficient of $1.4 \times 10^4$.

*2.2.3.8 Preparation of estrone glucuronide-thyroglobulin and pregnanediol-3α-glucuronide-thyroglobulin immunogen conjugates*

Steroid glucuronide-thyroglobulin conjugates were prepared using the active ester method described above in section 2.2.3.5. Typical conditions were as follows: E1G[H] (9.9 mg, 22.2 μmol), dimethylformamide (55 μL), N-hydroxysuccinimide (5.6 mg, 48.75 μmol) and dicyclohexylcarbodiimide (7.5 mg, 36.25 μmol) both dissolved in dimethylformamide (25 μL), and bovine thyroglobulin (52 mg) dissolved in 1% aqueous sodium hydrogen carbonate (3 mL). After dialysis against Milli-Q water (3 x 2 L) the resulting reaction mixture was freeze dried and stored at -10°C.

*2.2.3.9 Production of estrone glucuronide and pregnanediol-3α-glucuronide antisera*

Antisera were raised in sheep by Dr Keith Henderson, AgResearch, Wallaceville Animal Research Centre, Upper Hutt, New Zealand using the thyroglobulin-steroid glucuronide conjugates prepared above in section 2.2.3.8 and procedures essentially as described elsewhere [89].

*2.2.3.10 Standard curves for estrone glucuronide and pregnanediol-3α-glucuronide using lytic assays*

Lytic assays for the determination of the E1G and PdG standard curves were undertaken using an Ovarian Monitor essentially as described previously by Brown *et al.* [91] in pH 7.0 tris-maleate buffer (40 mM). Use was made of the inhibition of the lytic activity of the E1G-lysozyme and PdG-lysozyme conjugates by the presence in the assay of the appropriate anti-E1G and anti-PdG antiserum. The assay was performed in plastic 1 mL cuvettes (Adindas Plastics, Melbourne, Australia) designed specifically for the Ovarian Monitor. In generating the E1G standard curve 50 μL of E1G standard (0.5 to 1083 nM or 1.8 to 3899 nmol/24 h) and 50 μL of a blank urine sample diluted to 150 mL/h of collection and which contained 2.7 nmol/24h (0.75 nM) E1G (as determined by fluorescence [134]) was added to each tube. Antiserum (5 μL) was then added to each tube with vortex mixing followed by an aliquot of an appropriate dilution of E1G-lysozyme conjugate (5 μL). Finally 40 mM tris-maleate buffer (pH 7.0) was added to make the volume up to 340 μL. The mixture was then equilibrated for a minimum of 10 minutes at 40°C in a specifically designed heating block. At the end of the pre-incubation time a *Micrococcus lysodeikticus* suspension (10 μL of a 7.5 mg/mL suspension in 75 mM tris-maleate buffer, pH 7.0) was added with vortex mixing and the initial transmission noted. After 20 minutes the final transmission was recorded and the difference calculated. The rate of reaction was therefore calculated as the change in transmission (ΔT) per 20 minutes. The volume of conjugate per assay tube was calculated to give a change in apparent transmission of 350 units in 20 minutes in the absence of

antiserum. The concentration of antiserum added to each assay tube was calculated as that which just gave 90-95% inhibition of the lytic activity of the conjugate as determined from an antiserum titration curve. A standard curve for the determination of PdG was constructed in the same way using PdG standards (0 to 10 μM or 0 to 36 μmol/24h) but the end-point assay was determined over 5 minutes instead of 20 minutes.

## 2.3 Results

### 2.3.1 The Synthesis of Estrone Glucuronide (E1G[H]) and Pregnanediol Glucuronide (PdG[H])

Both estrone glucuronide (Fig. 2.2.2) and pregnanediol glucuronide (Fig. 2.2.3) were synthesised from the appropriate starting materials in good yields. Proton NMR spectra confirmed that for both estrone glucuronide and pregnanediol glucuronide the sugar ring was in the chair conformation, and that the steroid was attached to the sugar moiety in the desired β orientation. This was shown by the large coupling constants for the H-1' and H-5' protons of the sugar ring consistent with a trans configuration of the H-1' and H-2' protons, and for the H-4' and H-5' protons.

### 2.3.2 The Preparation and Purification of Estrone Glucuronide-Lysozyme Conjugates

The addition of the E1G[H] active ester reagent (prepared from synthetic E1G[H] as described in section 2.2.3.2) to a purified hen egg white lysozyme solution (at a molar ratio of 1.6:1) resulted in conjugation of 70% of the initial amount of lysozyme with E1G[H]. This was shown by analytical cation-exchange chromatography in 7 M urea buffers. After the reaction mixture had been dialysed against Milli-Q water, sufficient urea was added to an aliquot (100 μL) of the conjugate reaction mixture to give a 7 M urea solution which was loaded onto a Mono-S cation-exchange column for analysis (Fig. 2.3.1). The largest peak (30% of the total) consisted of unreacted lysozyme (L) as shown by comparison with the elution profile of a pure sample of lysozyme. The six peaks E1-E6 which eluted earlier consisted of different E1G-lysozyme conjugate fractions (comprising the remaining 70% of the yield) and are numbered relative to the elution position for lysozyme, E1 being the closest to lysozyme and E6 being the first conjugate to elute from the column (see Fig. 2.3.1). The two largest conjugate fractions, E1 and E3, were present in 22% and 18% overall yields respectively, and together comprised 57% of the total conjugate yield. The remaining 43% of the conjugate yield

consisted of fractions E2 (7.4% overall yield), E4 (7.0% overall yield), E5 (11% overall yield), and E6 (4.6% overall yield).

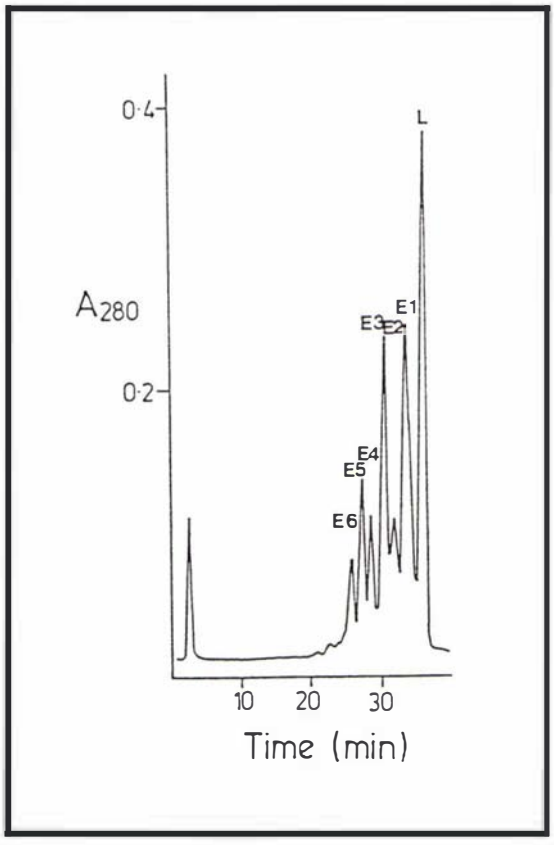


**Fig. 2.3.1** E1G-lysozyme active ester conjugation reaction mixture in 7 M urea on a Mono-S cation-exchange HR 5/5 column. Conditions: buffer A, 7 M urea + 50 mM $NaH_2PO_4$ buffer titrated to pH 6.0 with 1 M NaOH and buffer B, buffer A + 1 M NaCl titrated to pH 6.0 with 1 M NaOH; gradient, 0% B for 5 min, 0-30% B in 40 min at 0.5 mL/min; chart, 0.2 cm/min.

An aliquot of the active ester conjugation reaction mixture which had been dialysed against 0.2 M hydroxylamine (pH 8.50) was analysed by Mono-S cation-exchange chromatography in 7 M urea as described above. Table 2.3.1 shows the peak areas of the estrone glucuronide-lysozyme conjugates before and after dialysis against hydroxylamine relative to the unreacted lysozyme peak. The peak heights and areas of the estrone glucuronide-lysozyme conjugates did not change significantly relative to unreacted lysozyme after dialysis against hydroxylamine.

After filtration, 700 µL of the active ester conjugation mixture was loaded onto a Mono-S column equilibrated with 50 mM phosphate buffer (pH 4.3) and fractions were collected as shown in Fig. 2.3.2. Five fractions (a-e) were collected and each fraction was dialysed into Milli-Q water (3 x 2 L) and stored at -10°C. The fractions were then analysed for unreacted lysozyme by removing an aliquot from each, adding sufficient urea to give a 7

M urea sample and then loading onto the analytical Mono-S column and eluting as described in Fig. 2.3.1. The results are shown in Fig. 2.3.3.

**Table 2.3.1**

A comparison of the peak areas of the estrone glucuronide-lysozyme conjugates in the active ester reaction mixture relative to the unreacted lysozyme peak before and after dialysis against hydroxylamine

| Conjugate peak | Relative peak area before dialysis against hydroxylamine | Relative peak area after dialysis against hydroxylamine |
|---|---|---|
| Unreacted lysozyme | 1.00 | 1.00 |
| E1 | 0.66 | 0.65 |
| E2 | 0.26 | 0.30 |
| E3 | 0.61 | 0.58 |
| E4 | 0.26 | 0.24 |
| E5 | 0.33 | 0.30 |
| E6 | 0.16 | 0.16 |

The chromatogram of fraction a (Fig. 2.3.3A) consisted of three main peaks; an unreacted lysozyme peak (40% of the total) and two conjugate peaks (28% and 23% of the total respectively) while the chromatogram of fraction c (Fig. 2.3.3B) showed it to consist largely (71%) of unreacted lysozyme. Although the chromatogram of fraction e (Fig. 2.3.3C) contained all seven chromatographically distinct conjugate peaks (as seen in Fig. 2.3.1) there was only a small unreacted lysozyme peak (4%). The six conjugate peaks were present in about the same relative ratio's as prior to the purification step (cf. Fig. 2.3.1) with fractions E1 and E3 together constituting 54% of the total conjugate yield. Fraction b (Fig. 2.3.2) was almost identical to fraction c, and fraction d, as expected, consisted of relatively more unreacted lysozyme and less of the conjugate peaks (E1-E6) than fraction e. The lytic activity of conjugate fraction e was inhibited by 78% when excess E1G antibody was present in the assay mixture.

The relative order of elution of the bulk conjugate fraction e and the unreacted lysozyme fraction c changed greatly with pH, under non-denaturing conditions, on the Mono-S column. Table 2.3.2 shows the retention times for the bulk conjugate (fraction e) relative to the retention time for unreacted lysozyme (fraction c) as a function of pH. At pH 4.3 the bulk conjugate fraction eluted after the unreacted lysozyme fraction as shown in Fig. 2.3.2. However, at pH 6.0 the two peaks co-eluted and at pH 7.6 the elution

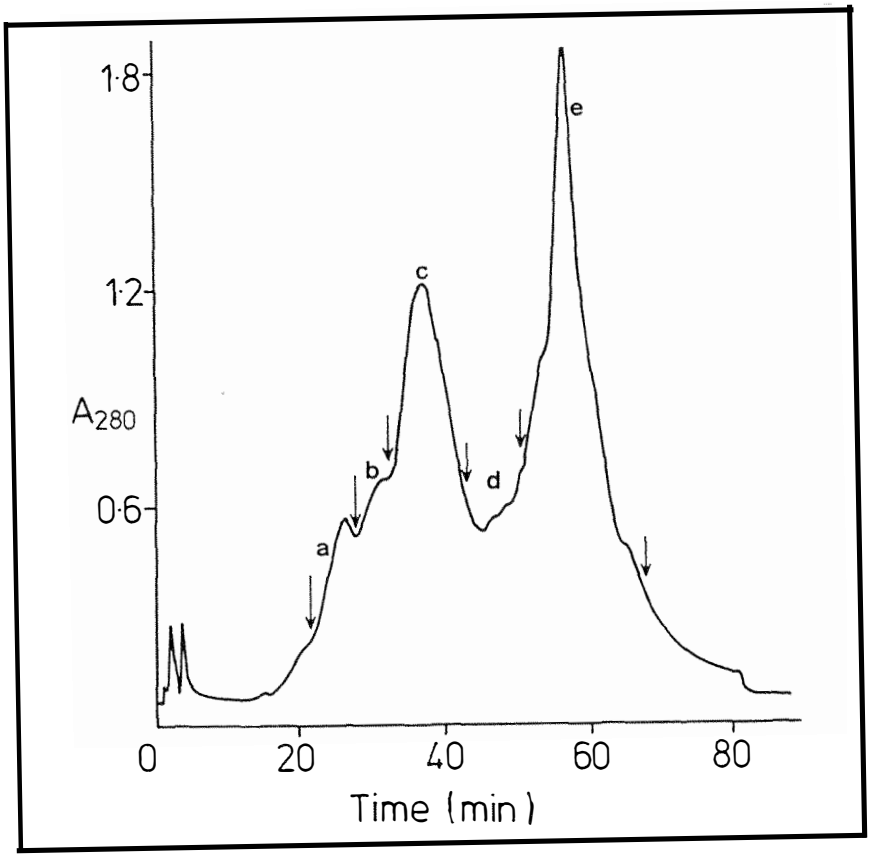


**Fig. 2.3.2** E1G-lysozyme active ester conjugation reaction mixture on a Mono-S cation-exchange HR 5/5 column. Conditions: buffer A, 50 mM $NaH_2PO_4$ and buffer B, 50 mM $NaH_2PO_4$ + 1 M NaCl; gradient, 0-35% B in 5 min, 35% B for 35 min, 35-37% B in 2 min, 37% B for 3 min, 37-40% B in 1 min, 40-45% B in 4 min, 45-75% B in 2 min, 75% B for 8 min, 75-100% B in 1 min, 100% B for 14 min at 0.5 mL/min; chart, 0.2 cm/min. Fractions were collected between the arrows as indicated.

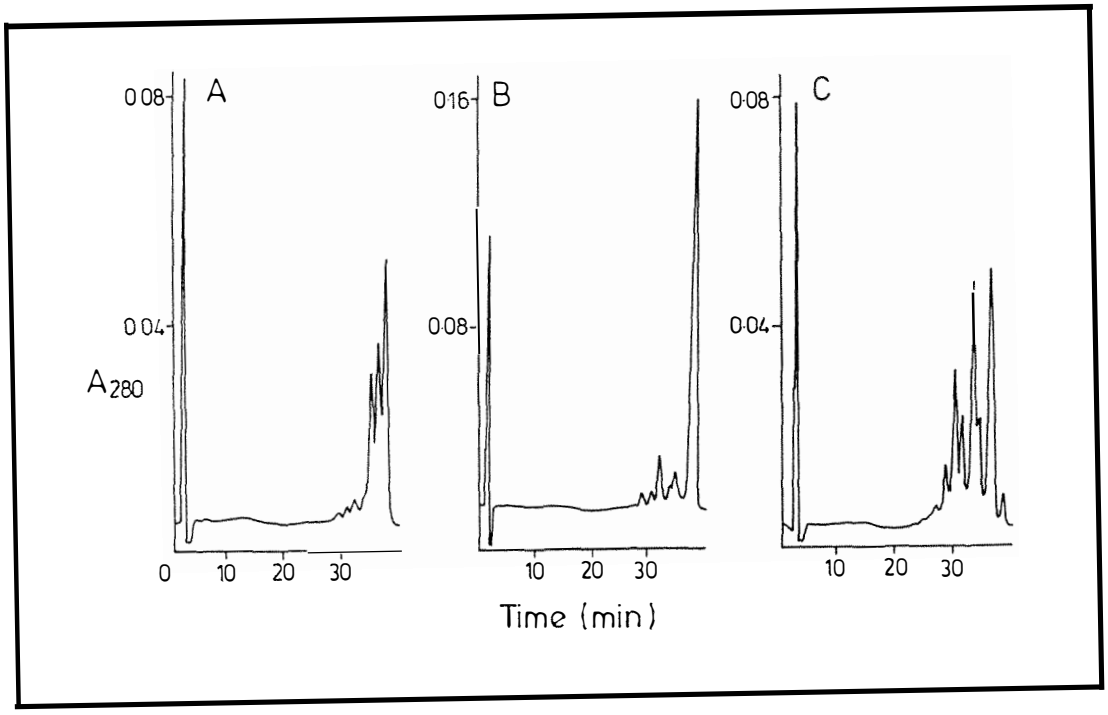


**Fig. 2.3.3** Fractions a (A), c (B), and e (C) from Fig. 2.3.2 in 7 M urea on a Mono-S cation-exchange HR 5/5 column. Conditions: buffers, gradient and chart as in Fig. 2.3.1.

positions of the unreacted lysozyme fraction c and the bulk conjugate fraction e had reversed, so that the conjugate fraction e now eluted slightly before the unreacted lysozyme. As the buffer pH was further increased, the conjugate fraction (fraction e) continued to elute earlier than the unreacted lysozyme fraction. Although the resolution between the two peaks increased with increasing pH, even at pH 10 the two peaks were not completely resolved. As the pH of the buffer system increased, the ionic strength required to elute the conjugate fraction decreased as shown in Table 2.3.2. Addition of 1.5% 2-propanol to the buffer system at pH 4.3 resulted in a greatly reduced retention time for the bulk conjugate fraction (fraction e) as shown in Fig. 2.3.4. However, the retention time for the unreacted lysozyme fraction c did not change significantly and the two fractions (c and e) co-eluted.

**Table 2.3.2**

Retention of E1G-lysozyme conjugate fraction e on a Mono-S column relative to unreacted lysozyme and the corresponding ionic strength at elution

| Buffer pH | [NaCl] at elution (mol/L) | Rf value of conjugate fraction e |
|---|---|---|
| 4.3 | 0.45-0.75 | 1.52 |
| 6.0 | 0.20 | 1.00 |
| 7.6 | 0.17 | 0.90 |
| 9.5 | 0.16 | 0.88 |
| 10.0 | 0.11 | 0.76 |
| 4.3 + 1.5% 2-propanol | 0.35 | 1.00 |

Sufficient ammonium sulfate was added to an aliquot of fraction e (from Fig. 2.3.2) to bring it to 1.4 M and the resulting solution was loaded onto an Alkyl Superose 5/5 column and eluted as shown in Fig. 2.3.5. The chromatogram consisted of an initial broad peak (f) (which passed straight through the column), followed later in the gradient by a series of peaks (combined as fraction g), as indicated in Fig. 2.3.5. The two fractions were then dialysed into Milli-Q water (3 x 2 L) and stored at -10°C. Both fractions were analysed by adding the appropriate amount of urea and loading onto a Mono-S column as previously described. The resulting analytical chromatographs are shown in Fig. 2.3.6. Fraction f (Fig. 2.3.6A) consisted mainly of a single peak whose lytic activity was not significantly inhibited when excess E1G antibody was present, while fraction g (Fig. 2.3.6B) consisted mainly of conjugate peaks E1-E5 and a small amount of material (5%) which eluted at the unreacted lysozyme position (L). The lytic

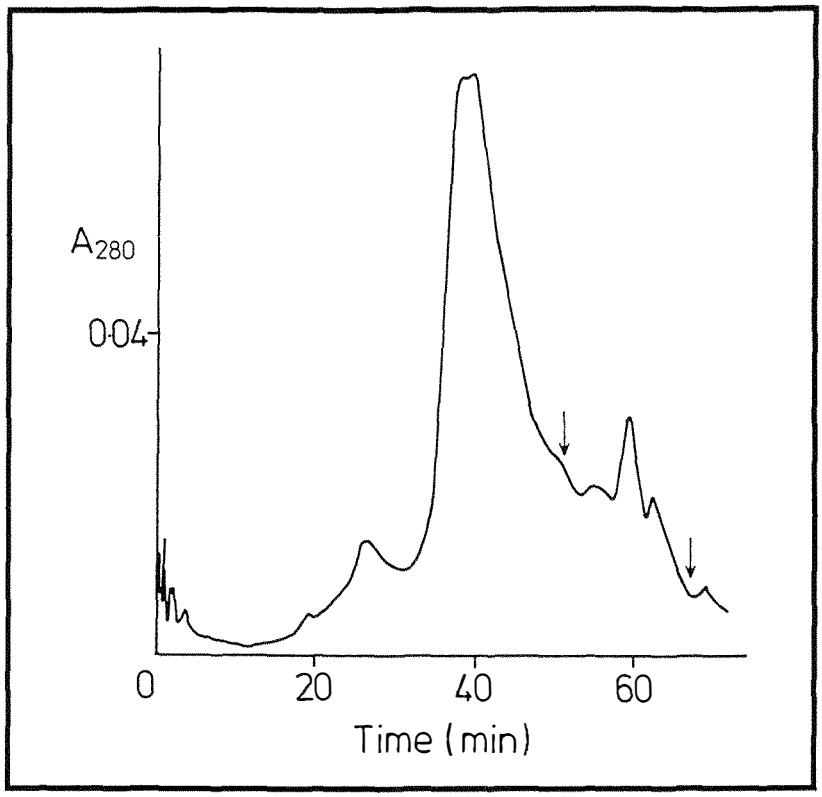


**Fig. 2.3.4** E1G-lysozyme conjugate reaction mixture on a Mono-S cation-exchange HR 5/5 column in the presence of 2-propanol. Conditions: buffers as in Fig. 2.3.2 + 1.5% 2-propanol in both buffers; gradient and chart as in Fig. 2.3.2. The position in which fraction e elutes in the absence of 2-propanol is indicated by arrows (cf. Fig. 2.3.2).

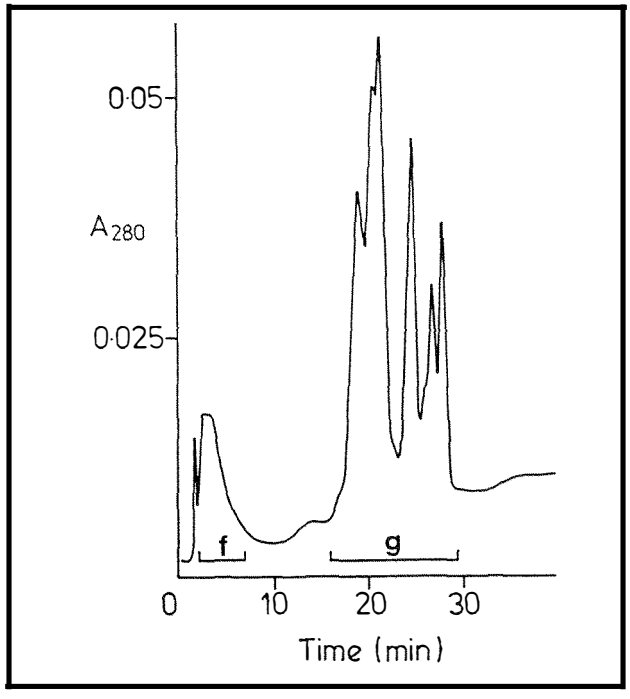


**Fig. 2.3.5** Fraction e from Fig. 2.3.2 in 1.4 M ammonium sulfate on an Alkyl Superose hydrophobic interaction HR 5/5 column. Conditions: buffer A, 50 mM $NaH_2PO_4$ + 1.4 M $(NH_4)_2SO_4$ titrated to pH 6.6 with 1 M NaOH and buffer B, 50 mM $NaH_2PO_4$ titrated to pH 6.6 with 1 M NaOH; gradient, 0% B for 10 min, 0-100% B in 20 min, 100% B for 15 min; chart, 0.2 cm/min.

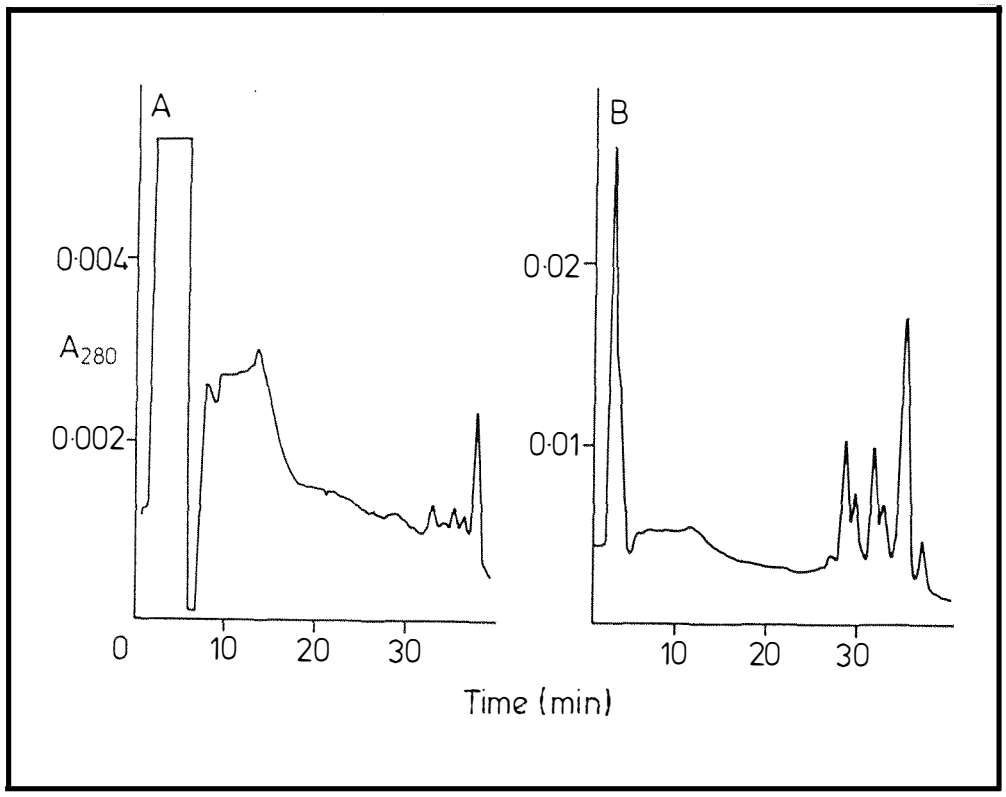


**Fig. 2.3.6** Fraction f (A) and g (B) from Fig. 2.3.5 in 7 M urea on a Mono-S cation-exchange HR 5/5 column. Conditions: buffers, gradient and chart as in Fig. 2.3.1.

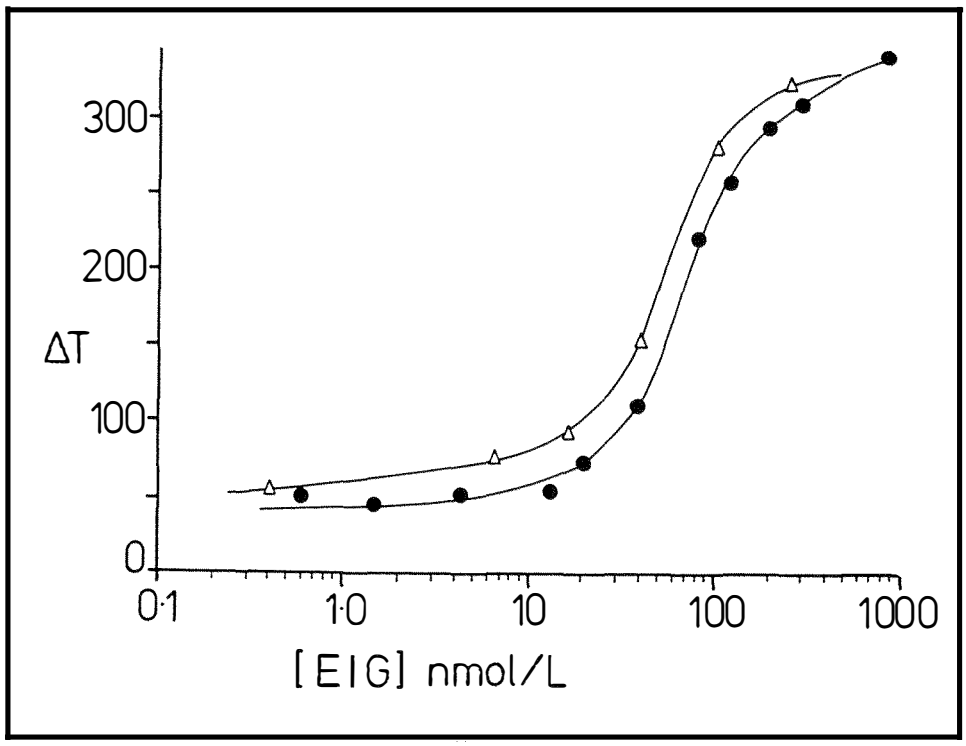


**Fig. 2.3.7** An EIG standard curve using (1) conjugate fraction g from Fig. 2.3.5 (●) and (2) the mixed anhydride conjugate from the Ovarian Monitor (Δ). For details see text.

activity of the combined fraction (g) was now inhibited by 93% when an excess of E1G antibody was present.

A standard curve suitable for the determination of urinary estrone glucuronide levels was established in pH 7.0 tris-maleate buffer by utilising the inhibition of the lytic activity of the E1G-lysozyme conjugates contained in fraction g by an E1G antibody as described in section 2.2.3.10. Assays carried out with variable amounts of E1G standards produced the sigmoidal standard curve shown in Fig. 2.3.7. The working range of the curve was 20 nM to 290 nM (76 nmol/24h to 1044 nmol/24h) which covered the range of E1G concentrations found in urine during a normal menstrual cycle. A typical menstrual cycle was then analysed using this system whereby the steroid standard in the assay was replaced by 50 µL of urine (diluted to 150 mL/h of collection). The resulting daily profile until the end of the first E1G peak (approximate day of ovulation) is shown in Fig. 2.3.8.

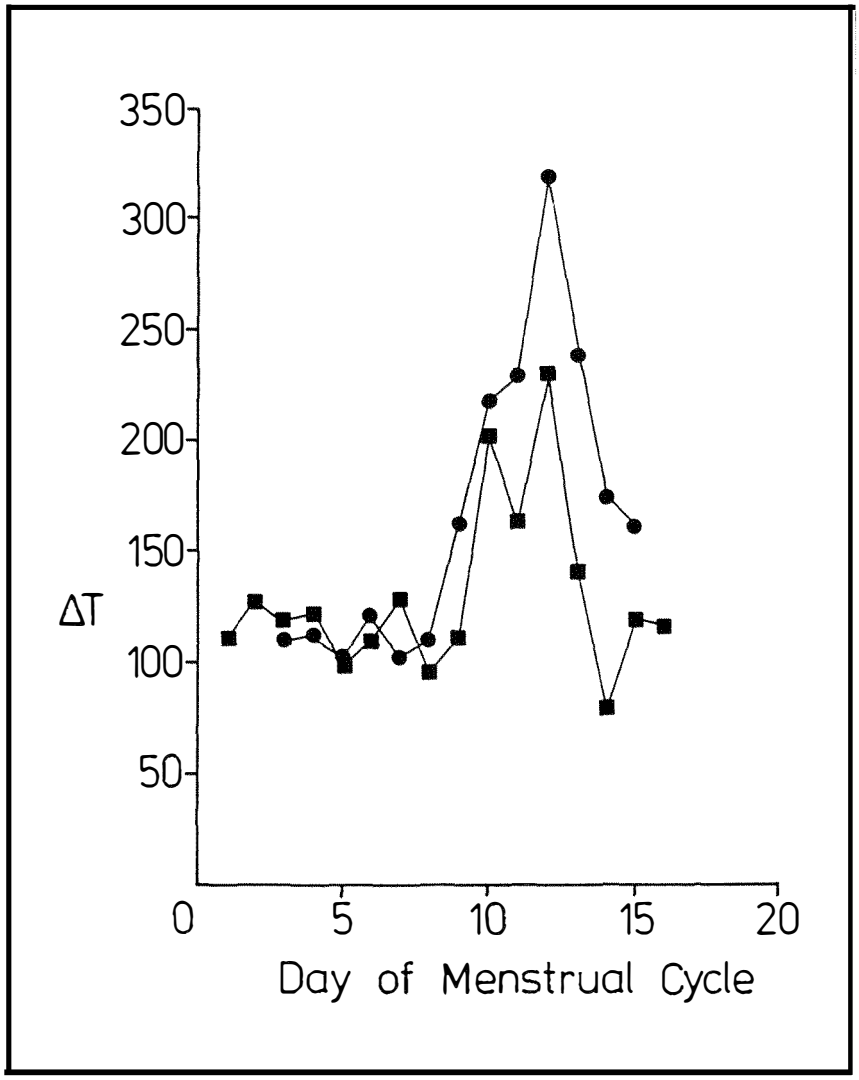


**Fig. 2.3.8** A typical example of a menstrual cycle pattern obtained using the standard curves described in Fig. 2.3.7 (see text). (●) woman's data using the Ovarian Monitor and (■) data using conjugate fraction g from Fig. 2.3.5.

### 2.3.3 The Preparation and Purification of Pregnanediol Glucuronide-Lysozyme Conjugates

The addition of the PdG[H] active ester reagent (prepared from synthetic PdG[H] as described in section 2.2.3.3) to a purified hen egg white lysozyme solution (at a molar ratio of 1.6:1) resulted in conjugation of 73% of the initial amount of lysozyme with PdG[H]. This was shown by analytical cation-exchange chromatography in 7 M urea buffers (Fig. 2.3.9) as for the E1G[H] conjugation described in section 2.3.2 above. The largest peak (26.70% of the total) consisted of unreacted lysozyme (L), while the six peaks (P1-P6) which eluted earlier consisted of different PdG-lysozyme conjugate fractions (comprising the remaining 73.3% of the yield). The peaks are numbered relative to the elution position for lysozyme as with the E1G-lysozyme conjugates (see Fig. 2.3.9). The largest conjugate fraction P1 was present in 26.6% overall yield and comprised 36.3% of the total conjugate yield. Conjugate fraction P3 was present in 13.6% overall yield and together with conjugate P1 comprised 55.2% of the total conjugate yield. The remaining 44.8% of the conjugate yield consisted of fractions P2 (9.18% overall yield), P4 (9.27% overall yield), P5 (8.62% overall yield), and P6 (6.14% overall yield).

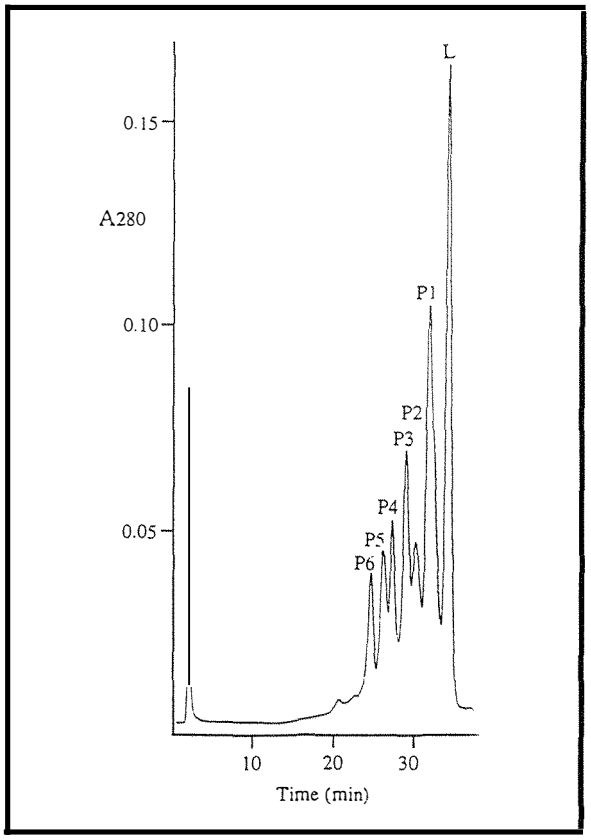


**Fig. 2.3.9** PdG-lysozyme active ester conjugation reaction mixture in 7 M urea on a Mono-S cation-exchange HR 5/5 column. Conditions: buffers, gradient and chart as in Fig. 2.3.1.

After filtration, 700 μL of the active ester conjugation mixture was loaded onto a Mono-S column equilibrated with 50 mM phosphate buffer (pH 4.3) and four fractions (h-k) were collected as shown in Fig. 2.3.10. Each fraction was dialysed against Milli-Q water (3 x 2 L) and stored at -10°C. The fractions were individually analysed for unreacted lysozyme as described in section 2.3.2 and the results are shown in Fig. 2.3.11. The

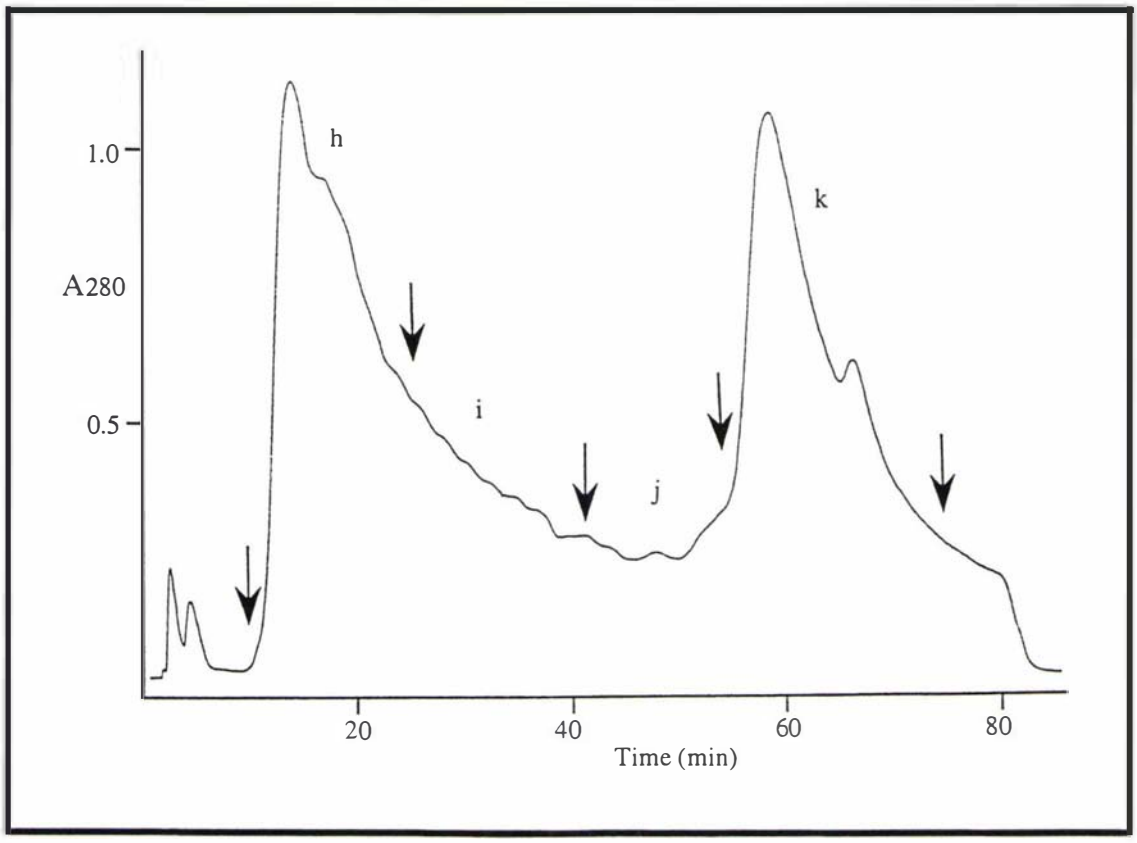


**Fig. 2.3.10** PdG-lysozyme active ester conjugation reaction mixture on a Mono-S cation-exchange HR 5/5 column. Conditions: buffers, gradient and chart as in Fig. 2.3.2. The fractions h-k were manually collected between the positions indicated by the arrows.

chromatogram of fraction h (Fig. 2.3.11A) consisted of a series of peaks, the largest being unreacted lysozyme (46.7% of the total peak area). The remaining material in fraction h was shown to be seven pregnanediol glucuronide-lysozyme conjugate peaks, of which the two peaks eluting closest to the unreacted lysozyme peak comprised 17.4% and 11.3% of the total peak area respectively. The remaining material in fraction h (24.6% of the total peak area) was comprised of five further conjugate peaks present in minor amounts (Fig. 2.3.11A). The chromatogram of fraction i (Fig. 2.3.11B) showed it to consist largely (48.8%) of unreacted lysozyme and one main conjugate peak (23%, P3) whereas fraction j was shown to consist of unreacted lysozyme (28%) and three main conjugate peaks (18.9%, 11.8%, and 27.1% of the total respectively) while

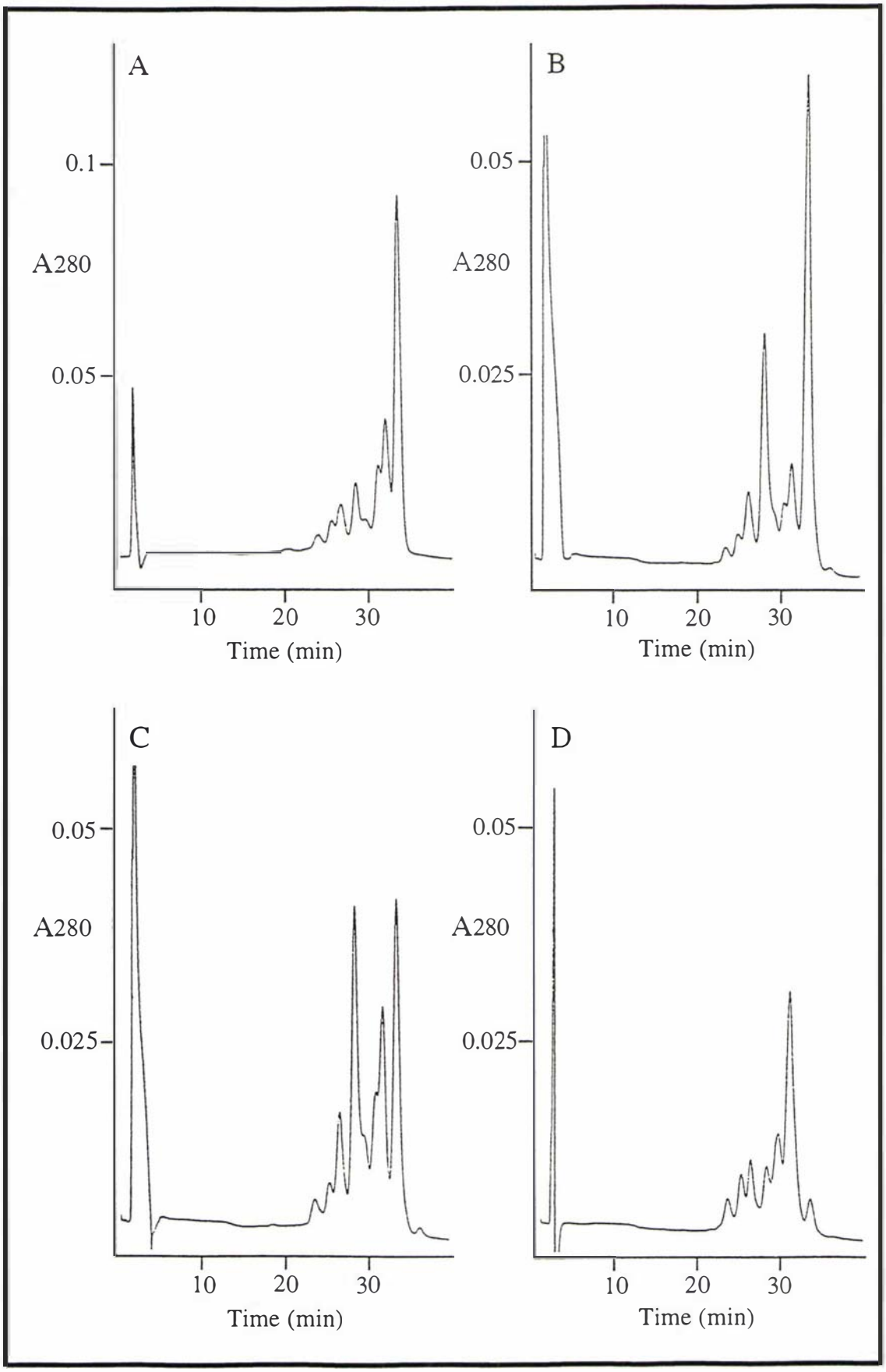


**Fig. 2.3.11** Fractions h (A), i (B), j (C), and k (D) from Fig. 2.3.10 in 7 M urea on a Mono-S cation-exchange HR 5/5 column. Conditions: buffers, gradient and chart as in Fig. 2.3.1.

all of the other conjugate peaks were present in minor amounts (Fig. 2.3.11C). Although the chromatogram of fraction k (Fig. 2.3.11D) contained all seven chromatographically distinct peaks (as seen in Fig. 2.3.9) there was only a small unreacted lysozyme peak (5.6%). The six conjugate peaks were all present in about the same relative ratio's as prior to the purification step (cf. Fig. 2.3.9) except for conjugate peak P3 which constituted only 8.1% of the total conjugate yield (cf. Fig. 2.3.9 where P3 constituted 18.9% of the total conjugate yield). The major conjugate peak (P1) constituted 30% of the total conjugate yield (cf. Fig. 2.3.9 where P1 comprised 36.3% of the total conjugate yield). The lytic activity of conjugate fraction k was inhibited by 75% when excess PdG antibody was present in the assay mixture.

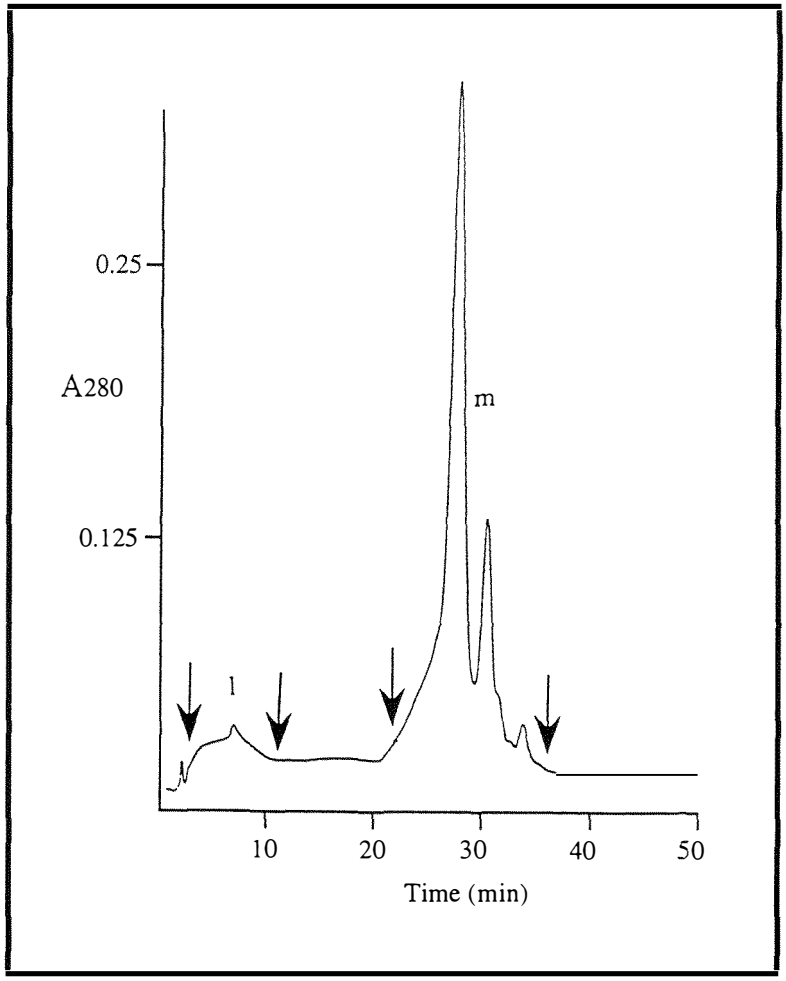


**Fig. 2.3.12** Fraction k from Fig. 2.3.10 in 1.4 M ammonium sulfate on an Alkyl Superose hydrophobic interaction HR 5/5 column. Conditions: buffers, gradient and chart as in Fig. 2.3.5. Fractions l and m were manually collected between the positions indicated by the arrows.

Sufficient ammonium sulfate was added to an aliquot of fraction k (from Fig. 2.3.10) to bring it to 1.4 M and the resulting solution was loaded onto an Alkyl Superose 5/5 column and eluted as shown in Fig. 2.3.5. The chromatogram consisted of a small initial broad peak (l), (which passed straight through the column) followed later in the gradient

by a series of three peaks (pooled as fraction m), as indicated in Fig. 2.3.12. The two bulk fractions were then dialysed against Milli-Q water (3 x 2 L) and stored at -10°C. Fraction m was analysed by adding the appropriate amount of urea and loading onto a Mono-S column as previously described. The resulting analytical chromatograph (Fig. 2.3.13) showed that fraction m consisted mainly of conjugate peak P1 (69%) and a small amount of conjugates P2 (10.7%), P3 (4.1%), P4 (9.4%), and P5 (5.3%). A small amount of material (1.5%) which eluted at the unreacted lysozyme position was also detected. The lytic activity of fraction g was now inhibited by 89% when an excess of PdG antibody was present.

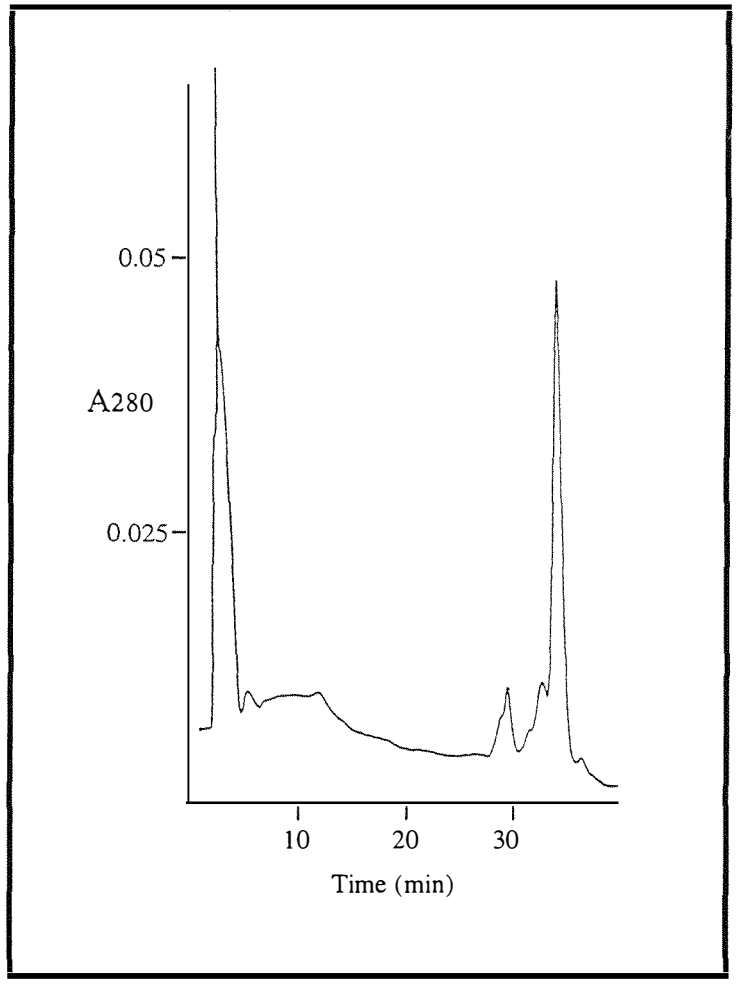


**Fig. 2.3.13** Fraction m from Fig. 2.3.12 in 7 M urea on a Mono-S cation-exchange HR 5/5 column. Conditions: buffers, gradient and chart as in Fig. 2.3.1. The largest peak consists of PdG conjugate family P1.

A standard curve suitable for the determination of urinary pregnanediol glucuronide levels was established as described in section 2.2.3.10. Assays carried out with variable amounts of PdG standards produced the sigmoidal standard curve shown in Fig. 2.3.14. The working range of the curve was 0.56 μM to 290 μM (2 μmol/24 h to 36 μmol/24 h) which covered the range of PdG concentrations found in urine during a normal menstrual

cycle. From a typical menstrual cycle which had previously been analysed with the Ovarian Monitor, the peak PdG excretion day was selected for re-analysis along with a PdG baseline day from early in the cycle (day 6). These two samples were then re-analysed for pregnanediol glucuronide using the standard curve described in Fig. 2.3.14 whereby the steroid standard in the assay mixture was replaced by 50 µL of urine (diluted to 150 mL/h of collection). A baseline PdG excretion day (as previously determined by the Ovarian Monitor assay system) gave a ΔT value of 85 while the PdG peak excretion day (as defined by the Ovarian Monitor assay system) gave a ΔT of 219 in a 5 minute assay.

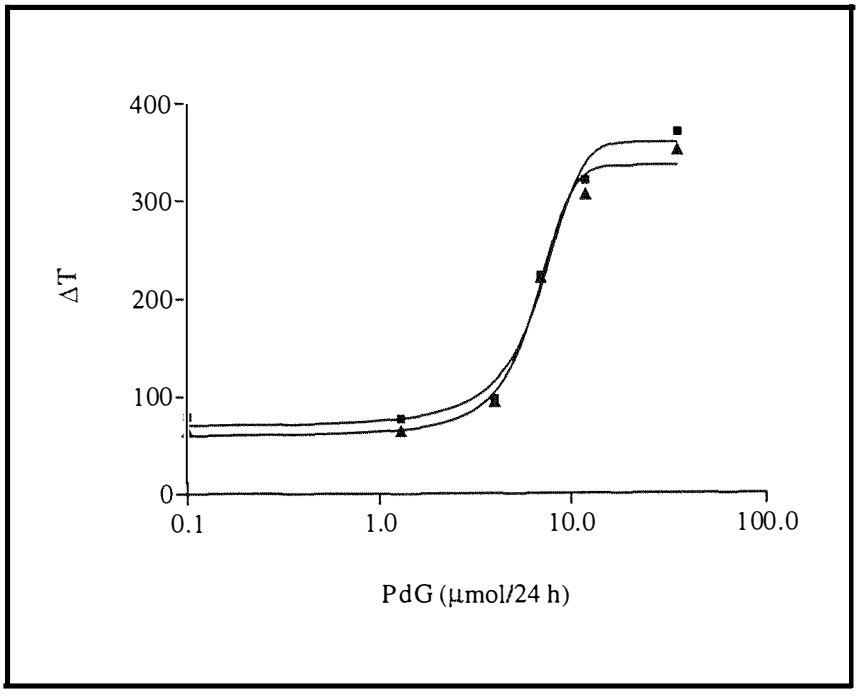


**Fig.2.3.14** A PdG standard curve using (1) conjugate fraction m from Fig. 2.3.12 (▲) and (2) the mixed anhydride conjugate from the Ovarian Monitor (■). For details see text.

## 2.4 Discussion

### 2.4.1 The Synthesis of Estrone Glucuronide and Pregnanediol Glucuronide

The NMR spectrum of both estrone glucuronide and pregnanediol glucuronide were as expected for the structures assigned and confirmed the correct stereochemistry at the anomeric carbon atom. The presence of the sugar ring in the correct orientation and the β orientation of the glucuronide moieties with respect to the steroid skeleton, was confirmed by the large coupling constants for the readily identified sugar C-1' and C-5' protons, thus indicating a trans configuration at these two positions. It is possible to unambiguously assign the H-1 and H-5 protons of the free, unconjugated, α-bromosugar from the proton NMR spectrum. Because the anomeric carbon (1-C) is linked directly to two electron withdrawing atoms (an oxygen and a bromine atom, see Fig. 2.2.1), the anomeric proton (H-1) has a higher chemical shift value (6.65 ppm) than that of the 5-proton (H-5, 4.57 ppm), as carbon-5 is linked directly to only one electron withdrawing atom (see Fig. 2.2.1). The H-1' and H-5' proton signals of the glucuronide ring can also be unambiguously assigned in the steroid glucuronide complexes for the same reason. In the steroid glucuronide complexes the anomeric carbon (1'-C) of the glucuronide ring is directly linked to two oxygen atoms (for example see Fig. 2.2.2) while the 5'-C carbon is directly linked to only one oxygen atom. As a result the anomeric proton (H-1') has a higher chemical shift value than that of the 5'-proton (H-5') e.g. for E1G the H-1' chemical shift is 4.91 ppm and the H-5' chemical shift is 3.72 ppm.

In the case of pregnanediol glucuronide, carbon 20 of the pregnanediol moiety (Fig. 2.2.3) is chiral and the stereochemical integrity of this position must be maintained. For the naturally occurring pregnanediol glucuronide to be recognised specifically by antibodies it is essential that the synthetic PdG material used to generate the antibodies has the same stereochemistry. Also, synthetic lysozyme-pregnanediol glucuronide conjugate(s) must have the same stereochemistry in the steroid moiety if a competitive assay is to be established. For these reasons pregnanediol-3α,20S-diol diacetate was selected as the starting material since it contains the required 20S configuration and this should not be affected by the chemical reactions shown in scheme 2.2.1.

The coupling of the bromosugar to the appropriate steroid was achieved using an excess of bromosugar, driving the reaction towards the desired product. To achieve the maximum yield all reagents used in the coupling reaction must be dry and the toluene solvent anhydrous. Anhydrous conditions were maintained during the addition of the α-bromosugar by distillation as described by Wu and Blackwell [135]. While the exact

mechanistic details of the reaction which results in the desired β-glucuronide stereoisomer are unclear [136-139], it is generally accepted that the bromosugar, which possesses a participating acetoxy group at C-2, reacts under Koenigs-Knorr conditions to initially yield a 1,2-acyloxonium intermediate [138] (scheme 2.4.1). The bromosugar, in the presence of the cadmium carbonate halide ion acceptor (catalyst), and under the driving force of the ring oxygen, forms an oxocarbonium-halide ion pair. Participation from the C-2 acetoxyl group leads to an acetoxonium ion [138] (scheme 2.4.1). In the product forming step the alcohol group at the 3 position of the steroid attacks the acetoxonium ion to give a 1,2-orthoester intermediate, which under proton catalysed isomerisation, yields the desired thermodynamic product [138] since the α-face is shielded by the acetoxonium group (see scheme 2.4.1).

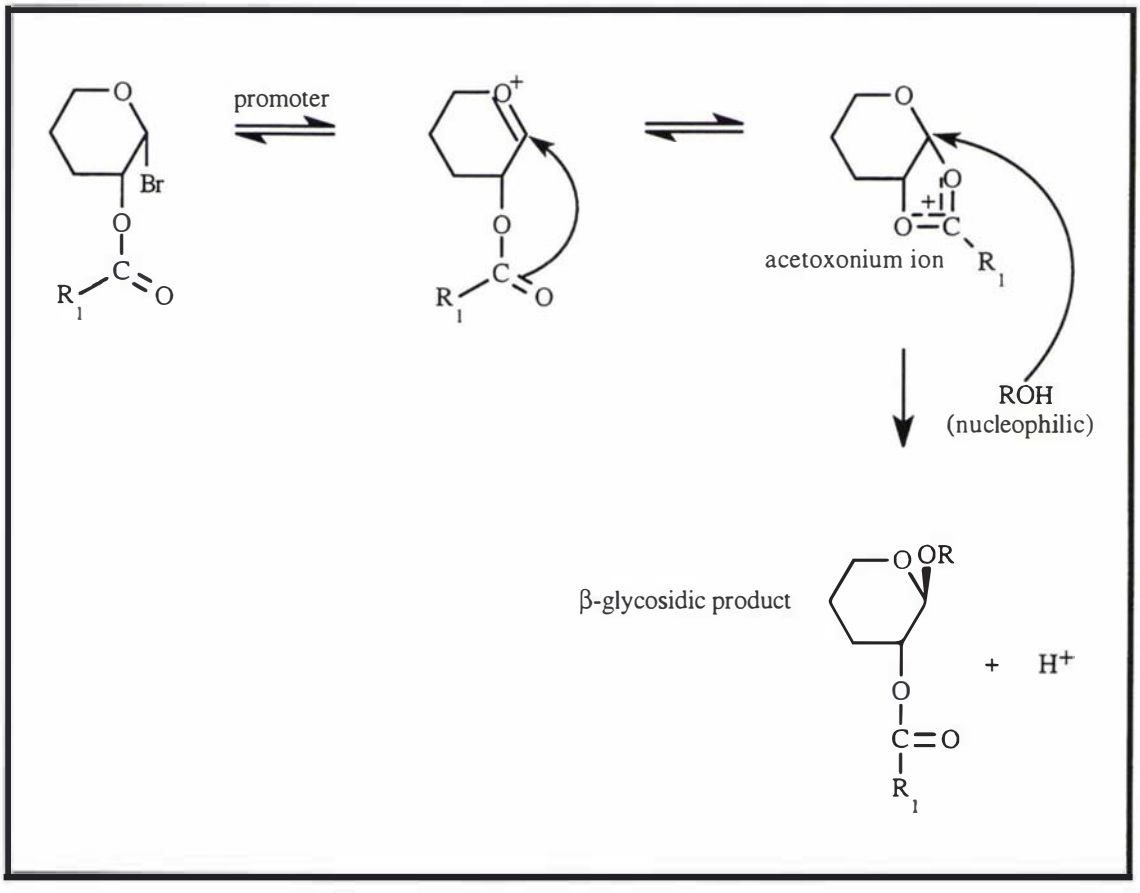


**Scheme 2.4.1** The proposed reaction pathway for the formation of 1,2-orthoester intermediates leading to the thermodynamically favoured β-glycosidic product under Koenigs-Knorr reaction conditions

## 2.4.2 The Synthesis and Purification of Estrone Glucuronide-Lysozyme and Pregnanediol Glucuronide-Lysozyme Conjugates

*2.4.2.1 The preparation of steroid glucuronide-lysozyme conjugates*

The synthetic steroid glucuronides were efficiently coupled to purified hen egg white lysozyme by the active ester coupling method resulting in the formation of stable E1G-lysozyme and PdG-lysozyme conjugates. The two steroids gave similar yields with approximately 70% of the total amount of lysozyme conjugated in both cases and similar conjugation patterns (Figs. 2.3.1 and 2.3.9) for the individual conjugates, except for the E3 and P3 conjugate families. Conjugation of lysozyme with estrone glucuronide by the active ester method resulted in preparation of E1G-lysozyme conjugate E3 in 18% yield. However, conjugation of lysozyme with pregnanediol glucuronide by the active ester method resulted in preparation of the PdG-lysozyme conjugate P3 in only 14% yield, a decrease of 25%. The reason for this difference is unclear but previous work with steroid glucuronides has shown that the mixed anhydride acylation procedure also gives rise to different results when different steroid glucuronides are used [111].

The preparation of the active ester reagent using the combined N-hydroxysuccinimide (NHS) / dicyclohexylcarbodiimide (DCC) method was preferred over the direct use of dicyclohexylcarbodiimide or 1-ethyl-3-(3-dimethylaminopropyl) carbodiimide hydrochloride (EDC). While DCC is a good leaving group, the steroid glucuronide-DCC complexes are insoluble in aqueous environments and the formation of the carbodiimide reagents is optimal at low pH (pH 4-5) where the amino groups are rather unreactive. Thus the NHS active ester reagent was preferred. The NHS steroid glucuronide active ester was quite stable and its hydrolysis is slow in aqueous media compared with the rate of reaction with amino groups at the reaction pH [140]. Reaction was almost immediate for the conjugation of lysozyme with steroid glucuronide active ester reagents since there was no difference between the FPLC traces in 7M urea at 5 minutes and after 24 hours reaction.

*2.4.2.2 Analytical Mono-S cation-exchange chromatography in 7 M urea of conjugation reaction mixtures*

The elution patterns for the conjugates on the Mono-S cation-exchange column in 7 M urea were highly reproducible, even after extensive dialysis and storage for several weeks at -10°C. Lysozyme is a very basic protein (isoelectric point 10.5 [141]) due to the presence of six lysine residues and eleven arginine residues [117] on the external surface of the enzyme [118]. In the stable conjugates (E1-E6 and P1-P6), the steroid glucuronide moieties are presumably attached to the protein by means of amide linkages *via* the α-amino and ε-lysine residues in the protein since the elution pattern was not changed even

after extensive treatment with hydroxylamine and no additional unreacted lysozyme could be detected relative to that present before treatment. Although linkages due to esterification of alcohol groups on aliphatic (serine and threonine) and phenolic (tyrosine) residues are possible, treatment with hydroxylamine should remove steroid glucuronide molecules linked to lysozyme in this way leaving unreacted lysozyme. This result suggests that there is no acylation of lysozyme by steroid glucuronides *via* esterification and that stable linkages between the steroid glucuronides and lysozyme were formed presumably *via* lysine amino groups. There are two possible reasons for the absence of any ester linkages between lysozyme and the steroid glucuronide moieties in the purified conjugates. These are (1) that while the conjugates are passing through the Mono-S column, interactions with the column matrix result in the hydrolysis of any unstable ester linkages, or alternatively, (2) that reaction of lysozyme with the steroid glucuronides under the conditions described at stoichiometric ratio's is specific for amino groups as previously reported for the reaction of lysozyme with 1-guanyl-3,5-dimethylpyrazole nitrate [121]. Whatever the explanation, the patterns obtained on Mono-S columns in 7 M urea (Figs. 2.3.1 and 2.3.9) serve as a simple, rapid system for analysis of lysozyme conjugation reactions. The success of purification steps and the purity of fractions can be analysed rapidly and in this way the removal of unreacted lysozyme and subsequent changes in conjugate composition of a fraction can be followed easily throughout a purification procedure.

The order of elution of each steroid glucuronide-lysozyme conjugate on a cation-exchange column in 7 M urea, when the enzyme is partially denatured, would be expected to be determined by the number of free lysine residues. Every free lysine residue in the enzyme is positively charged at the buffer pH (pH 6.0) and this positive charge is lost upon acylation. The order of elution of the steroid glucuronide-lysozyme conjugates should therefore be inversely related to the number of free lysine residues. Evidence that this is so was provided by titration of the lysine amino groups in the individual conjugate populations (E1-E6 and P1-P6). The titration procedure does not appear to titrate the N-terminal amino group since only six free amino groups were determined. Titration of the individual conjugate families showed that the conjugate families had the following number of free amino groups: conjugate E1, 5 free amino groups; conjugate E3, 5 free amino groups; and conjugate E6, 3.5 free amino groups. Similar results were obtained for the pregnanediol glucuronide conjugate families (P1, 5 free amino groups; P3, 5 free amino groups; P6, 3.3 free amino groups). The conjugates are therefore substituted in the order E6 > E3 > E1 and P6 > P3 > P1. Hence the extent of acylation of the amino groups on the protein is correlated directly with the elution position of the individual conjugate populations in 7 M urea on Mono-S columns as expected. The most highly substituted conjugates eluted first and unsubstituted, unreacted

lysozyme (L in Figs. 2.3.1 and 2.3.9) always eluted last with a characteristic elution time. Hence the presence of lysozyme could be recognised easily in the chromatograms.

The use of ion-exchange chromatography in 7 M urea would appear to be the ideal method for the removal of unreacted lysozyme from the reaction mixture. Not only are the conjugation products well separated from the unreacted lysozyme peak (see Figs. 2.3.1 and 2.3.9) allowing its removal, they are also well separated from each other allowing the purification of individual conjugate families if desired. However, conjugates purified in this way always gave lower inhibitions (< 90%) than required for homogeneous enzyme immunoassay even though they appeared to contain very little unreacted lysozyme (4-5%) by analytical FPLC. In the development of a viable purification procedure, with potential for scaling up, the ultimate test for purity of a conjugate has to be the degree of lytic inhibition observed when excess anti-hapten antibody is present. If the observed degree of lytic inhibition is not greater than 90% of the uninhibited rate, the conjugate is unsuitable for use in homogeneous enzyme immunoassays irrespective of the appearance of the FPLC profile.

It is difficult to explain the inadequate inhibition after exposure to denaturation in 7 M urea since it does not correlate with the amount of free lysozyme present. The two most obvious explanations are carbamylation and/or denaturation of the protein so that the enzyme cannot refold correctly. Carbamylation of lysine residues of lysozyme by cyanate ions present in the urea solution to produce enzyme forms with less positive charges is a possible source of contamination by non-inhibitable lysozyme. For example, a monocarbamylated lysozyme molecule would be eluted in the same position as a di-substituted E1G-lysozyme conjugate. While the monocarbamylated enzyme would possess lytic activity, it would show no immune response towards anti-hapten antibodies resulting in a lowering of the degree of inhibition and its presence would not be apparent in the FPLC profile. Also, the exposure of the E1G-lysozyme and PdG-lysozyme conjugates to urea results in their denaturation which must be reversed by dialysis before use in immunoassays. Hence, an incomplete or inaccurate refolding could explain the lower than expected inhibition of conjugates after purification by ion-exchange chromatography on Mono-S columns in 7 M urea. However, two studies in the literature rule out denaturation-renaturation as the source of the inadequate inhibition. In the first study lysozyme conjugates have been separated from unconjugated lysozyme using serial dialysis from 7 M urea solutions [123] to give highly inhibited conjugates. The second study by Maeda *et al.* [142] concluded that gentle removal of urea from denatured proteins, and in particular lysozyme, by means of dialysis, should effectively renature denatured protein.

*2.4.2.3 The purification of steroid glucuronide-lysozyme conjugates by Mono-S cation-exchange chromatography under non-denaturing conditions*

As a result of the loss in immune reactivity on chromatography of the steroid glucuronide-lysozyme conjugates on Mono-S cation-exchange columns in the presence of 7 M urea, attempts were made to effect a separation between unreacted lysozyme and the conjugates under non-denaturing conditions. The chromatographic behaviour of the conjugate fractions (a-e; Fig. 2.3.2 and h-k; Fig. 2.3.10) on the Mono-S column under such conditions was unexpected if only charge interactions with the column matrix were operating. The elution order at pH 4.3 (Figs. 2.3.2 and 2.3.10) clearly did not follow that predicted by charge interactions alone. Indeed, the bulk of the conjugate was found in fraction e (estrone glucuronide-lysozyme conjugates) and fraction k (pregnanediol glucuronide-lysozyme conjugates) which were eluted after the bulk of the unreacted lysozyme (fraction c, E1G reaction mixture; fractions h and i, PdG reaction mixture). If electrostatic factors were the only mode of interaction between lysozyme and the steroid glucuronide-lysozyme conjugates and the column matrix, then the order of elution should not change with pH (the strength of binding should change but the relative elution positions should remain the same). Because this was not the case (Table 2.3.2), non-electrostatic factors must also be contribute to the binding of the conjugates to the Mono-S column matrix.

The variation of the relative elution position with pH can be explained on the basis of two opposing effects [143]. As the pH of the buffer system was decreased, the retention time of lysozyme on the Mono-S cation-exchange column increased [144] because of the increasing charge on the protein, hence requiring a higher ionic strength to elute the lysozyme (Table 2.3.2). However, accompanying the increasing ionic strength is an increasing surface tension which would be expected to increase hydrophobic interactions between the protein and the column matrix [143]. It has been previously reported that the Mono-S Pharmacia cation-exchange column has very little, if any, hydrophobicity [144]. This conclusion was based on the observation that the retention time for lysozyme decreased by less than 5% in the presence of buffers spiked with 1% 2-propanol. However, no work has been reported for lysozymes acylated with hydrophobic steroids. The results reported here agree with those of Kopaciewicz *et al.* [144] in that addition of 1.5% 2-propanol to the buffer system (described in Fig. 2.3.4) resulted in very little decrease in the retention time for native lysozyme. However, there was a very significant decrease (ca. 25%) in the retention time for the major conjugate containing peak (fraction e). The exact magnitude of the decrease was difficult to determine as the unreacted lysozyme and the bulk of the E1G-lysozyme conjugate products eluted at virtually the same position (Fig. 2.3.4). However, this decrease in retention time for the bulk of the E1G-lysozyme conjugate products, in their native conformations, clearly indicates that

there is an important hydrophobic interaction occurring between the hydrophobic steroid moieties of the E1G-lysozyme conjugates and the Mono-S matrix.

Thus, the relative elution positions of the E1G-lysozyme conjugates, PdG-lysozyme conjugates and lysozyme on a Mono-S cation-exchange column are determined by both the electrostatic and hydrophobic interactions. In buffers of high pH where low salt concentrations are required for elution, hydrophobic interactions between the steroid moiety and the column matrix are minimised and thus play little part in the separation. In this case, as a result of the lower net positive charge, E1G-lysozyme was eluted prior to the unreacted lysozyme as expected, although the two peaks were not well resolved. This lack of resolution means that, in the native state, the E1G-lysozyme conjugates cannot be separated easily from unreacted lysozyme at pH values of 6.0 or above. However, in buffers of low pH, the stronger binding of lysozyme to the Mono-S column (Table 2.3.2) and the higher ionic strength required for elution results in significant hydrophobic interactions of the steroid moiety with the column. This additional factor causes the steroid glucuronide-conjugates to be eluted later than lysozyme. Hence, at pH 4.3 the hydrophobic interactions can be utilised to give a separation between unreacted lysozyme and the E1G or PdG-lysozyme conjugates (Figs. 2.3.2 and 2.3.10). Kopaciewicz and Regnier [145] have reported that a similar hydrophobic-ionic interaction property may be responsible for the variation in retention times of lysozyme found on a weak glutaric anhydride cation-exchanger. The separation between the bulk lysozyme containing fraction and the bulk conjugate containing fractions is greater for the PdG conjugates than the E1G conjugates (see Figs. 2.3.2 and 2.3.10), presumably due to the greater hydrophobic nature of the PdG moiety relative to the E1G moiety giving further evidence of hydrophobic interaction between the conjugates and the column matrix.

Conjugate fraction (e) (prepared by cation-exchange chromatography at pH 4.3 (Fig. 2.3.2)) consisted almost completely of E1G-lysozyme conjugates (peaks E1-E6) and very little unreacted lysozyme compared with the original reaction mixture (cf. Fig. 2.3.1) while conjugate fraction (k) (prepared by cation-exchange chromatography at pH 4.3 (Fig. 2.3.10)) consisted almost completely of PdG-lysozyme conjugates (peaks P1-P6) and very little unreacted lysozyme compared with the original reaction mixture (cf. Fig. 2.3.9). Hence, under these conditions there does not seem to be any evidence for associative interactions between the conjugates and lysozyme. Surprisingly, despite the fact that fraction e (E1G conjugates) and fraction k (PdG conjugates) which contained the bulk of the conjugate products and only low levels (4% and 5.6% respectively) of unreacted lysozyme, the lytic activity was still inadequately inhibited (being only by 78% and 75% respectively) when excess anti-hapten antibody was present. This occurred despite the absence of 7 M urea (see section 2.4.2.2), thus no real advantage was gained

by running the columns under non-denaturing conditions. Rechromatography of the fractions through the Mono-S column at pH 4.3 resulted in only a small increase in the degree of inhibition (2-3%), hence a second chromatographic step was still clearly required.

*2.4.2.4 The chromatography of steroid glucuronide-lysozyme conjugates on hydrophobic Alkyl Superose columns*

The strong retention of the E1G-lysozyme and PdG-lysozyme conjugates on an Alkyl Superose column (Figs. 2.3.5 and 2.3.12) was consistent with an increased hydrophobic interaction with the column matrix. It might be expected that passage of a conjugate reaction mixture through an Alkyl Superose column as a first purification step would remove the unreacted lysozyme and hence avoid the difficulties associated with ion-exchange chromatography. However, when this was done, despite the fact that chromatograms obtained after loading of a conjugate reaction mixture directly onto an Alkyl Superose column looked similar to Figs. 2.3.5 and 2.3.12 (although with a much larger lysozyme peak) the conjugate fractions all contained lysozyme. A second passage through the Alkyl Superose column did not significantly improve the extent of inhibition of the conjugate fraction showing that much of the lysozyme still remained. This result indicates that there is an association between the E1G-lysozyme conjugates, PdG-lysozyme conjugates and free lysozyme at high concentrations of both substances. The association results because lysozyme is known to possess hydrophobic patches on its surface which can be identified by examination of the crystal structure [118]. Hence, it is necessary to utilise a first step which reduces the unreacted lysozyme concentration otherwise all subsequent conjugate fractions are contaminated.

Analysis of the E1G conjugate fraction g after Alkyl Superose chromatography showed that it consisted mainly of the lower substituted E1G-lysozyme conjugates (Fig. 2.3.6). The lytic activity of the conjugate was now well inhibited (by 93%) when excess anti-hapten antibody was present, hence it was suitable for use in homogeneous enzyme immunoassays for E1G. Similarly analysis of the PdG conjugate fraction m after Alkyl Superose chromatography showed it consisted almost entirely of PdG-lysozyme conjugate P1 (Fig. 2.3.13). The observed inhibition of the lytic activity of fraction m was now also improved, being inhibited by 89% when excess antibody was present. The amount of lysozyme removed by this step (< 5%) cannot account for the increase in observed inhibition of the conjugates to approximately 90% after the Alkyl Superose chromatographic step. Thus, a combination of Mono S cation-exchange chromatography at pH 4.3, followed by hydrophobic interaction chromatography on an Alkyl Superose column, rapidly produced conjugate of sufficient quantity and immune reactivity for use in enzyme immunoassays. These procedures have the potential for scaling up and

represent the best procedures yet reported for purification of lysozyme-steroid conjugates. Conjugates purified using the described procedure lost activity slowly over time, even when stored at -10°C. This may be due to the very dilute concentrations at which these conjugates were stored as concentration of the purified conjugates resulted in better keeping qualities. This problem has also been observed in other enzyme systems [146-147]. It may be possible to increase the shelf life of the steroid glucuronide-lysozyme conjugates, even at low concentrations, by using stabilisation systems such as those previously reported for other enzyme systems and biosensors [146-149].

*2.4.2.5 Possible explanation for the lower than expected levels of inhibition of the lytic activity of conjugates separated from unreacted lysozyme by strong cation-exchange chromatography on a Mono-S column*

As discussed above, when the steroid glucuronide-lysozyme conjugates were separated from unreacted lysozyme by chromatography on a strong cation-exchange column the levels of inhibition in the presence of excess antibody were lower than expected, irrespective of whether the procedure was undertaken in 7 M urea conditions or under non-denaturing conditions (sections 2.4.2.2 and 2.4.2.3). Since this was observed in both systems, carbamylation due to the presence of urea (as discussed in section 2.4.2.2 in the urea system) can be excluded as a possible reason for the inadequate inhibition. The lower than expected inhibition therefore most probably arises from a column matrix-conjugate contact effect. Since this effect is seen in both the 7 M urea system (where the conjugate-matrix interactions are presumably electrostatic) and in the non-denaturing system (where the conjugate-matrix interactions involve both electrostatic and hydrophobic interactions) the column matrix-conjugate effect which results in the low levels of inhibition must be an ionic effect. Therefore, upon contacting the column matrix a significant level of the conjugate (~ 20%) must be altered in some way such that the antibody does not bind to the steroid glucuronide moiety or alternatively, the antibody binds in such a position and orientation that the lytic activity of the enzyme is no longer affected. This alteration in the conjugate most probably involves the movement and conformational rearrangement of the flexible lysine-steroid glucuronide moiety on the enzyme surface in some manner that does not destroy the enzymatic activity but removes the immune reactivity. Upon passing the conjugate through an Alkyl Superose hydrophobic interaction column the steroid glucuronide moiety presumably binds to the matrix, reorientating it and reversing the effect of the strong cation-exchange column so that the antibody can again bind to the steroid glucuronide and inactivate the enzymatic activity. These contact denaturation and renaturation effects are poorly understood and clearly should be investigated further.

*2.4.2.6 Standard curves for estrone glucuronide and pregnanediol glucuronide using lytic assays*

The standard curve obtained for the determination of E1G concentrations utilising the E1G-lysozyme active ester conjugate (Fig. 2.3.7) was found to be highly reproducible. It was in the correct working range and of suitable gradient ($d\Delta T/d[E1G]$) to allow the accurate measurement of estrone glucuronide. A menstrual cycle obtained using this system (Fig. 2.3.8) was compared with the results obtained for the same cycle by a woman using the Ovarian Monitor at home. The beginning of the fertile period was clearly defined by the first rise in urinary E1G and the day of the peak excretion rate of E1G was cycle day 12 in both cases. The response of the assay system to a given level of urinary E1G (Fig. 2.3.8) was greater for the Ovarian Monitor assay system which uses a conjugate preparation consisting mainly of E3 and prepared using a mixed anhydride reagent (see chapter 3). The difference in response was also apparent in the standard curves (Fig. 2.3.7) and may reflect the fact that the active ester conjugate contains the more highly substituted E4 and E5 conjugates in significant amounts. Previous consideration of the conjugate system has shown that maximum sensitivity is achieved by a 1:1 enzyme/steroid ratio [122]. Thus, higher levels of urinary E1G are required to give the maximum lytic response for these latter conjugates which will continue to be inhibited while the less substituted conjugates are no longer bound by the antibody. Hence, the mixed anhydride acylation procedure may be preferable to the active ester procedure for good quality conjugate. Irrespective of which coupling method is preferred, the purification procedures described here can be applied.

The standard curve obtained for PdG, utilising the PdG-lysozyme active ester conjugate (Fig. 2.3.14) was also found to be highly reproducible, in the correct working range and of suitable gradient for the accurate measurement of pregnanediol glucuronide. A small difference in the response of the active ester PdG-lysozyme conjugate and the mixed anhydride prepared conjugate (see chapter 3) used in the Ovarian Monitor was again apparent in the standard curves (Fig. 2.3.14). The purification of the PdG-lysozyme conjugates using the described purification procedure appears to remove the more highly substituted conjugates to a greater degree than does the purification of the E1G-lysozyme conjugates (see Figs. 2.3.6B and 2.3.13) and as a result the standard curves are much more alike than the E1G standard curves (Figs. 2.3.7 and 2.3.14). The system clearly showed the difference between a PdG peak excretion day and a baseline PdG excretion day and could be used to define the end of the fertile period using pregnanediol glucuronide as the marker. The combination of the E1G and PdG systems, using conjugates produced by the active ester method and purified as described above, can therefore be used in the Ovarian Monitor to define the entire fertile period.

## 2.5 Conclusions

Estrone glucuronide and pregnanediol glucuronide conjugates of hen egg white lysozyme were successfully prepared by the active ester coupling procedure. The conjugates were purified from unreacted lysozyme by a combination of cation-exchange and hydrophobic interaction chromatography to give conjugate mixtures whose lytic activity was well inhibited in the presence of the appropriate antibody. When used in a homogeneous enzyme immunoassay system these conjugates allowed the measurement of the urinary steroid glucuronide levels encountered in a normal menstrual cycle. However, the active ester and mixed anhydride conjugates appear to behave differently in the assay system as determined from the standard curves. The difference in the standard curves is probably a reflection of the different ratio's of conjugate families present.

The conjugates in the Ovarian Monitor system (derived from the mixed anhydride procedure) are also a mixture of different conjugate families [57] resulting from possible acylation at different lysine residues as are the conjugates prepared by the active ester method and utilised in the above systems (see Fig. 2.3.6B). Each of these conjugate peaks represents a family of conjugates with the same overall charge and substitution level, however the steroid glucuronide moiety may not be attached to the same lysine(s) in each one resulting in a heterogeneous mixture within a conjugate family. To investigate further the Ovarian Monitor assay system it is necessary to purify individual conjugate families from each other (for example E1 from E2 in Fig. 2.3.1) so that they can be studied and characterised.

## Chapter Three

# The Characterisation of Estrone Glucuronide- and Pregnanediol Glucuronide-Lysozyme Conjugates

## 3.1 Introduction

It is not clear from previous studies whether the individual conjugate families utilised in the Ovarian Monitor are heterogeneous (substitution at various lysine residues) or homogeneous (substitution of a single, or the same set of, lysine residues). The acetylation and carbamylation of lysozyme has been shown to lead to a series of groups or families, each of which is assumed to be a mixture of various species [150], further suggesting that the individual steroid glucuronide-lysozyme conjugates may also be heterogeneous mixtures. Identification of the amino groups modified in a protein by various acylating reagents has usually been undertaken by analysis of proteolytic digest patterns [151], mass spectrometric peptide mapping [152] and immunological studies [153]. From these studies selective acylation of the amino groups of proteins has often been observed [154].

It is well known that the steroid/enzyme ratio in a conjugation reaction effects the level of acylation [155] and that the coupling method has an influence on the resulting conjugation products and hence their usefulness for enzyme immunoassay [156]. Since the individual conjugate families in the Ovarian Monitor conjugate have never been isolated and purified, there has been no chemical characterisation of the different populations. As a result the effect of different acylating agents (such as the active ester and mixed anhydride procedures) on the quality of the conjugate has not been assessed. More importantly a detailed study of the antibody inhibition mechanisms has not been possible and hence the binding requirements for the anti-steroid glucuronide antibodies remain undetermined. It has been suggested that the acylation position and orientation of the haptens in enzyme conjugates is important in the recognition and binding of the hapten antibodies [119].

As a step towards this goal, lysozyme was acylated with estrone glucuronide and pregnanediol glucuronide and methods developed for the large scale isolation and characterisation of the individual conjugate products using cation-exchange

chromatography in 7 M urea. While the column procedures described in chapter two separate conjugated protein material from unconjugated lysozyme, the procedure does not separate the individual conjugate families from each other. Although the Mono-S 7 M urea column described in chapter two does separate the individual conjugates, only small amounts of material can be loaded onto the column and purified in this way. Limited proteolysis of the purified conjugates was then undertaken using the protease enzyme trypsin and standard procedures similar to those described by Charbonneau [157] were used to characterise the conjugate families.

Furthermore, the success of the Ovarian Monitor assay system depends on an analytical method to monitor the success of the purification procedures. The method utilising Mono-S cation-exchange chromatography in 7 M urea while constituting a good analytical procedure, involves the denaturing of the enzyme in 7 M urea. It is desirable for some purposes to have an analytical system which gives the same resolution but which utilises non-denaturing conditions and hence may be used to check on the structural integrity of the conjugates following urea denaturation. It has been demonstrated that basic proteins and peptides such as lysozyme can be separated from other basic proteins and peptides by acid-polyacrylamide or acid-urea-polyacrylamide gel electrophoresis [158-160]. Protein derivatives, such as alkylated proteins, have also been analysed by high and low pH discontinuous acrylamide slab electrophoresis to give discrete and distinctive bands which are well separated [161]. Various lysozyme derivatives have also been analysed by acid-urea-polyacrylamide gel electrophoresis [162] to give a ladder of distinct bands. However, this procedure involves the use of the denaturing agent urea used in the Mono-S cation-exchange method discussed in chapter two.

It has been shown that non-urea, high pH polyacrylamide gel electrophoresis can be used to give distinct bands when analysing certain lysozyme derivatives with good results [120-121]. However, this method did not give good resolution when applied to the estrone glucuronide-lysozyme conjugates. An alternative, non-denaturing system was therefore required for the analysis of steroid glucuronide-lysozyme conjugates. The alternative procedure is based on the fact that acylation of lysozyme at the ε-amino groups of lysine residues decreases the degree of positive charge. The system utilises non-denaturing, acid-polyacrylamide gel electrophoresis (acid-PAGE) to assess, analyse and purify small amounts of the individual E1G-lysozyme conjugates. The advantage of the system is that it is rapid, simple, non-denaturing and gives excellent resolution between different E1G-lysozyme conjugate families.

## 3.2 Experimental

### 3.2.1 Apparatus

All chromatographic procedures were performed on a Pharmacia fast protein liquid chromatography (FPLC) system at room temperature. The system was set up as described in section 2.2.1. The following columns were used; a prepacked Pharmacia Mono S HR 5/5 cation exchange column (50 x 5 mm I.D.); a Pharmacia HR 16/50 (500 x 16 mm I.D.) column which was packed with Pharmacia S-Sepharose (fast flow) cation-exchange resin, and; a (150 x 16 mm I.D.) column which was prepacked with Pharmacia hydrophobic interaction Butyl Sepharose resin. The refrigerated centrifuge used was a Sorvall Superspeed RC2-B model and the freeze drier was a Cuddon New Zealand model (patent numbers 145033/149129) unit. Minigels were run on a Mini-Protean® II dual Slab system while larger gels were run on a Protean® II xi system, both from Bio-Rad Laboratories, Richmond, CA 94804. All other apparatus used is described in the methods section.

### 3.2.2 Reagents

Estrone glucuronide (E1G) and pregnanediol glucuronide (PdG) were synthesised as described in sections 2.2.3.2 and 2.2.3.3 respectively. Hen egg white lysozyme (grade 1, 3 times recrystallised and lyophilised from Sigma) was purified as described in section 2.2.3.4. *Micrococcus lysodeikticus*, L-1-tosylamino-2-phenylethyl chloromethyl ketone treated trypsin and cytochrome c (from bovine heart) were from Sigma Chemical Co. (St. Louis, MO, U.S.A.). Ion-exchange and hydrophobic interaction chromatography buffers were prepared as described in the figure legends. All buffers were filtered and degassed using 0.2 μm filters (Millipore) before use. Samples were filtered through Millipore GVWP 013 00 filters (0.2 μm). Stock tris-maleate buffer was prepared as in section 2.2.2. All other reagents were analytical grade or better.

### 3.2.3 Methods

*3.2.3.1 Preparation of estrone glucuronide-lysozyme and pregnanediol glucuronide-lysozyme conjugates by the mixed anhydride method*

Conjugation of lysozyme with estrone glucuronide (E1G) and pregnanediol glucuronide (PdG) was achieved using the mixed anhydride procedure of Erlanger *et al.* [116] at a 1.6:1 molar ratio of steroid glucuronide to lysozyme, as shown in scheme 3.2.1. For the estrone glucuronide-lysozyme conjugation reaction the mixed anhydride reagent was prepared from E1G[H] (10 mg, 22.42 μmol) in dimethylformamide (160 μL) in a 0.5 mL reaction vial. The vial was placed in a specifically designed aluminium block pre-equilibrated at 10°C in a refrigerator and allowed to equilibrate for three hours. Tri-n-butylamine (6.25 μL, 26.31 μmol), pre-equilibrated at 10°C, was then added and the E1G[H] solution left for 5 minutes at 10°C before the aluminium block was cooled to 0°C in a freezer. Once the aluminium block had cooled to 0°C it was removed from the freezer and placed in a cold room at 4°C and left to equilibrate for 15 minutes.

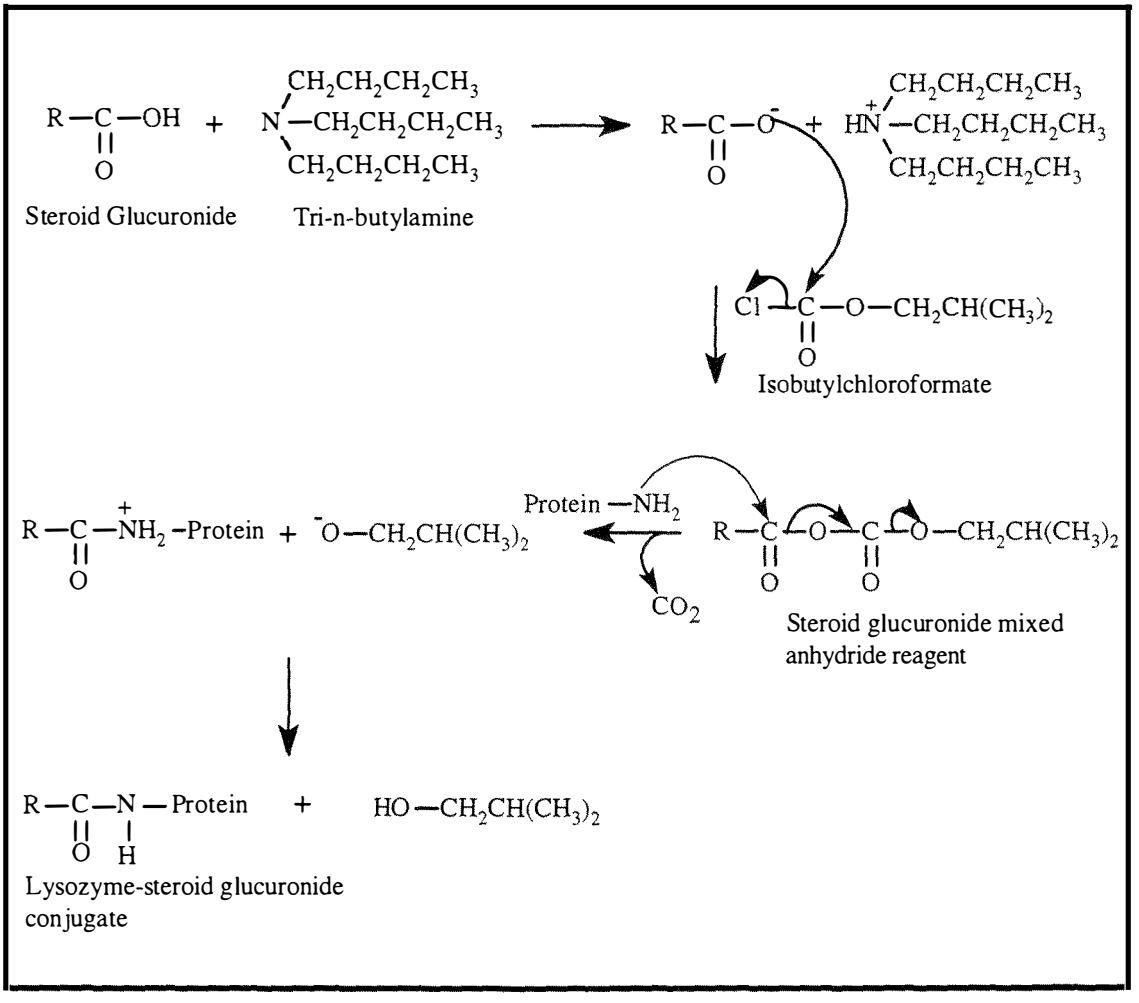


**Scheme 3.2.1** Synthesis of steroid glucuronide-lysozyme conjugates by the mixed anhydride method

Isobutylchloroformate (3.47 μL, 26.71 μmol) pre-equilibrated at 4°C was then added and the resulting E1G[H] solution left to stand for 30 minutes. The mixed anhydride reagent was then stabilised by placing the aluminium block at the bottom of a refrigerated centrifuge pre-equilibrated at approximately -15°C. Purified lysozyme (200 mg, 13.99 μmol) was dissolved in Milli-Q water (5 mL) with stirring and the pH adjusted to 8.00 with 0.5 M NaOH at room temperature. Ice was packed around the lysozyme reaction vessel, which was then placed in the cold room at 4°C and left to equilibrate for 45 minutes with stirring while the pH was monitored. The temperature setting of the pH meter was set at 0°C and stabilised at pH 8.54 after the equilibration period.

After standing at -15°C for one hour, the mixed anhydride reagent was added dropwise, with a dry 10 μL pipette tip at 4°C, to the stirred lysozyme solution over 15 minutes. Associated with each addition of mixed anhydride reagent was a drop in the pH of the lysozyme solution which was readjusted back to approximately 8.54 with 0.5 M NaOH. The lysozyme solution was left with stirring for two hours upon the final addition of mixed anhydride reagent (while 0.5 M NaOH was added as required to readjust the pH) after which time the reaction mixture, which appeared opaque, had stabilised at pH 8.39 and was stored at -10°C until purified by cation-exchange chromatography.

For the pregnanediol glucuronide-lysozyme mixed anhydride conjugation reaction procedure the conditions were as follows: PdG[H] (20 mg, 40.32 μmol), dimethylformamide (322 μL), tri-n-butylamine (11.88 μL, 50 μmol), isobutylchloroformate (6.50 μL, 50 μmol) and purified lysozyme (360 mg, 25.2 μmol) dissolved in 9.25 mL of Milli-Q water at 0°C, pH 8.49.

*3.2.3.2 Preparation of estrone glucuronide-lysozyme and pregnanediol glucuronide-lysozyme conjugates by the active ester method*

Estrone glucuronide (E1G) and pregnanediol glucuronide (PdG) conjugates of lysozyme were prepared by the N-hydroxysuccinimide/dicyclohexylcarbodiimide coupling method [111] as described in section 2.2.3.5 and shown in scheme 2.2.2. Upon completion of the active ester coupling reaction, the reaction mixtures were dialysed against Milli-Q water and stored at -10°C until purified by cation-exchange chromatography. The conditions for the E1G reaction were as described in section 2.2.3.5. For the PdG active ester conjugation reaction procedure the conditions were as follows: PdG[H] (12.4 mg, 25 μmol), dimethylformamide (100 μL), N-hydroxysuccinimide (3.23 mg, 28.06 μmol) and dicyclohexylcarbodiimide (5.75 mg, 27.86 μmol).both dissolved in dimethylformamide (17.5 μL), and purified lysozyme (222 mg, 15.5 μmol) dissolved in 1% aqueous sodium hydrogen carbonate (5.6 mL).

*3.2.3.3 Purification of individual estrone glucuronide-lysozyme and pregnanediol glucuronide-lysozyme conjugates*

The success of the conjugation experiments and purity of the derivatives was determined by analytical chromatography on a Mono-S cation-exchange column in 7 M urea buffers as described in section 2.2.3.6. Estrone glucuronide-lysozyme and pregnanediol glucuronide-lysozyme conjugates were purified from the reaction mixture by large scale cation-exchange chromatography in 7 M urea buffers on an S-Sepharose (fast flow) column. To the reaction mixture was added sufficient solid urea to give a 7 M solution and a calculated amount of solid sodium dihydrogen phosphate dihydrate to give a 50 mM phosphate solution. After the solution had been adjusted to pH 6.0 with 1 M NaOH it was loaded, with a peristaltic pump, onto the column pre-equilibrated with 7 M urea, 50 mM sodium dihydrogen phosphate dihydrate buffer (pH 6.0). The column was eluted with a linear salt gradient from 0 to 0.24 M NaCl in 792 minutes at a flow rate of 1.5 mL/min. The absorbance of the eluent fractions (6 mL) was read at 280 nm and the enzymatic activities were determined from the rate of lysis of *Micrococcus lysodeikticus* in the presence and absence of excess anti-steroid glucuronide antiserum using an Ovarian Monitor [91]. Fractions from each individual estrone glucuronide-lysozyme and pregnanediol glucuronide-lysozyme conjugate peak were combined, dialysed extensively against Milli-Q water and freeze dried before rechromatography on the same column. This procedure gave chromatographically homogeneous steroid glucuronide-lysozyme conjugates when re-analysed by Mono-S cation-exchange chromatography. The purified conjugates were extensively dialysed against Milli-Q water, freeze dried and then stored at -10°C until required for tryptic digestion experiments.

Each estrone glucuronide conjugate, after purification by cation-exchange chromatography on an S-Sepharose (fast flow) column, was dissolved in 1.4 M ammonium sulfate pH 6.6 buffer and loaded onto a Butyl Sepharose column pre-equilibrated with 1.4 M ammonium sulphate, 50 mM sodium dihydrogen phosphate dihydrate buffer (pH 6.6). The column was eluted as described in Fig. 3.3.3. The absorbance of the eluent fractions (5 mL) was read at 280 nm and the enzymatic activity determined as for the fractions collected from the S-Sepharose (fast flow) column. Fractions from each peak (I and II Fig. 3.3.1.3) were combined, dialysed extensively against Milli-Q water, concentrated through a Centricon® concentration membrane (Mr cut off 5 000) and stored at -10°C until required for digestion or lytic activity experiments.

*3.2.3.4 Enzyme assays for lytic activity of chromatography column fractions*

The assays for lytic activity of the various column fractions were performed using an Ovarian Monitor [91] as described in section 2.2.3.10. The volume of each fraction to be

used in the assay was calculated from the concentration of the peak tube as determined by the absorbance at 280 nm. The dilution of this peak tube required to give an apparent change in transmission of 350 units in 20 minutes was determined. The same dilution was then used for all of the other fractions to measure their relative lytic activities. The inhibition of the lytic activity of each eluent fraction by anti-steroid glucuronide antibodies was measured by adding a slight excess of the appropriate antiserum to the assay mixture and comparing it with the suitable control.

*3.2.3.5 Reduction and alkylation of estrone glucuronide-lysozyme and pregnanediol glucuronide-lysozyme conjugates with iodoacetic acid*

Conjugates were reduced and alkylated with iodoacetic acid essentially as described by Rutherfurd *et al.* [163-164]. Typically, conjugate (5 mg) was dissolved in a mixture of 8 M urea and 0.25 M tris-HCl buffer (pH 8.75, 300 μL) containing 1 mM EDTA, before the addition of dithiothreitol (0.84 mg, 5.4 μmol). The resulting solution was flushed with argon gas and the reduction allowed to proceed at 37°C for three hours, prior to the addition of iodoacetic acid (1.57 mg, 8.4 μmol). Alkylation was allowed to proceed in the dark at room temperature for 45 minutes. Excess β-mercaptoethanol was then added and the alkylated protein was dialysed against 8 M urea (3 x 200 mL).

*3.2.3.6 Tryptic digestion*

Tryptic digestion of the alkylated unmodified lysozyme, estrone glucuronide-lysozyme and pregnanediol glucuronide-lysozyme conjugates was carried out in 2 M urea solutions. After dialysis against 8 M urea the alkylated protein solutions were diluted with 1% ammonium bicarbonate buffer (pH 8.50) to give 2 M urea solutions, allowing for the volume of the trypsin solution. L-1-tosylamino-2-phenylethyl chloromethyl ketone treated trypsin (2 mg) was dissolved in 330 μL of 1% ammonium bicarbonate (pH 8.50) and then the appropriate volume was added to the digest solution so that an enzyme to substrate ratio of 1.5:100 (w/w) was achieved. Digestion was allowed to proceed for 3.5 hours at 37°C after which the reaction mixture was stored at -10°C until analysis by high performance liquid chromatography (HPLC).

*3.2.3.7 Separation of trypsin fragments*

The separation of the tryptic fragments was carried out on a Vydak C18 reverse-phase column (250 x 4.6 mm I.D.) using a Spectra Physics SP8800 high performance liquid chromatography system (HPLC). Aliquots from the completed native lysozyme and E1G-lysozyme tryptic digests were loaded onto the column pre-equilibrated with deionised, distilled water (containing 0.1% TFA) and then eluted using a linear gradient from 0 to 40% acetonitrile (containing 0.08% TFA) in 80 minutes at a flow rate of 1 mL/min. Aliquots from the completed PdG-lysozyme tryptic digests were eluted using a

linear gradient from 0 to 45% acetonitrile (containing 0.1% TFA) in 90 minutes at a flow rate of 1 mL/min. Detection of the tryptic peptides was carried out at 220 nm with a Spectra Physics SP8490 detector and they were collected manually into 1 mL Eppendorf tubes. Peptides were concentrated on a Savant Speed Vac Concentrator to a volume of approximately 15 μL and then stored at -10°C until analysed.

*3.2.3.8 Manual Edman sequencing*

Manual Edman sequencing was undertaken essentially as described previously [165]. Typically, a steroid glucuronide modified peptide (which was isolated by HPLC as described in section 3.2.3.7 above) was dried under vacuum to leave a white solid in a Pyrex screw top 5 mL test tube. The solid was redissolved in deionised, distilled water (150 μL) to which was added 5% (v/v) phenylisothiocyanate (PITC, 150 μL) in pyridine. The resulting solution was degassed with $O_{2(g)}$ free $N_{2(g)}$ and the tube incubated at 47°C for 90 minutes. The tube contents were then dried over $P_2O_5$ and NaOH pellets, under high vacuum, at 60°C for 30 minutes. Trifluoroacetic acid (200 μL) was then added, the tube degassed with $O_{2(g)}$ free $N_{2(g)}$ and incubated a further 30 minutes at 47°C to cleave the N-terminal phenylthiocarbamyl amino acid. The trifluoroacetic acid was removed under high vacuum over $P_2O_5$ and NaOH pellets. The resulting material was resuspended in deionised, distilled water (200 μL) and extracted three times with ethyl acetate. The ethyl acetate layer was discarded and the aqueous peptide layer concentrated on a Savant Speed Vac Concentrator. The resulting, cleaved peptide was then isolated by HPLC as described in section 3.2.3.7. A blank, containing water only, was also run.

*3.2.3.9 Analysis of tryptic peptides*

Tryptic peptides were analysed by both Edman N-terminal peptide sequencing [166] and electrospray mass spectrometry [167-170]. Peptide sequencing was undertaken on an Applied Biosystems Edman degrading gas phase 476A Protein Sequencer. Mass spectral analyses were obtained on a VG Platform II Electrospray Mass Spectrometer at Waikato University, Hamilton, New Zealand.

*3.2.3.10 Immunochemical analysis of estrone glucuronide-lysozyme E1 tryptic peptides*

Peptides obtained from the estrone glucuronide-lysozyme conjugate family E1 were screened for the presence of estrone glucuronide using the Ovarian Monitor [91]. An assay mixture was prepared containing amounts of estrone glucuronide-lysozyme conjugate and estrone glucuronide antibody such that a partially inhibited ΔT value of approximately 150 units in 40 minutes was obtained upon the addition of 10 μL of a 7.5 mg/mL solution of *Micrococcus lysodeikticus*. The enzymatic rate in the absence of estrone glucuronide antibody was 350 units in 40 minutes. To the assay mixture was

added 5 μL of the concentrated peptide and the change in transmission over 40 minutes was recorded. The difference between the ΔT value in the presence and absence of the peptide respectively in the partially inhibited assay mixture was calculated as the immune reactivity.

*3.2.3.11 Analysis of estrone glucuronide-lysozyme conjugates by acid polyacrylamide gel electrophoresis*

E1G-lysozyme conjugates were analysed by non-denaturing acid-polyacrylamide gel electrophoresis (acid-PAGE), at room temperature, on continuous acrylamide slab gels at pH 4.08 with reverse polarity (lower chamber cathode). The reservoir buffer in both upper and lower chambers consisted of glycine (28.1 g), glacial acetic acid (3.06 mL) and Milli-Q water as required to adjust the volume to 1 L at pH 4.08, as described previously by Hrkal [171]. This buffer was freshly prepared before use.

Both Mini gels and larger gels were prepared and run. Mini gels were prepared using commercially available Bio-Rad 40% acrylamide solution as follows; acrylamide (3.75 mL) to give a 15% final solution was mixed with pH 4.08 reservoir buffer (6.25 mL). After degassing N, N, N', N',-tetramethylethylenediamine (15 μL) and ammonium persulfate (100 μL of a freshly prepared 50 mg/500 μL solution) were added and mixed before the gel was poured. For larger gels (160 x 200 mm) a 40% acrylamide solution was prepared and the gels were mixed in the same ratio's as for the Mini gels. Mini gels were pre-run at 200 volts for 1.5 h or until a constant current was obtained, while larger gels were pre-run for 3.5 h. Following pre-running both the upper and lower chambers were refilled with fresh reservoir buffer.

The conjugate samples were then loaded in reservoir buffer which contained 20% glycerol. The gel was run with one lane containing cytochrome c so that its bright orange colour could be used as a tracking agent. Electrophoresis was undertaken at a constant voltage (200 volts) with the usual current reversed so that the polarity was from the anode (upper chamber) to the cathode (lower chamber), until the cytochrome c marker reached the bottom of the gel. All gels were stained with a 0.1% Coomassie blue R-250, 40% methanol, 10% acetic acid and 50% Milli-Q water solution. Gels were destained in the same solvent mixture without Coomassie blue.

## 3.3 Results

### 3.3.1 Preparation and Purification of Individual Estrone Glucuronide-Lysozyme Conjugates

The addition of the mixed anhydride reagent (prepared from synthetic E1G as described in section 3.2.3.1), to the purified hen egg white lysozyme solution (at a molar ratio of 1.6:1), resulted in conjugation of 41.9% of the initial amount of lysozyme with E1G. This was shown by analytical cation-exchange chromatography in 7 M urea buffers (Fig. 3.3.1A). The largest peak (58.1% of the total) consisted of unreacted lysozyme (L), as shown by comparison with the FPLC profile of a pure sample of lysozyme. Of the conjugated lysozyme, the predominant conjugate families were E3 (72%) and E1 (22%) with the remainder (6%) made up of small amounts of E4 and E5. Acylation of hen egg white lysozyme with estrone glucuronide by the N-hydroxysuccinimide/dicyclohexylcarbodiimide procedure resulted in a more complex reaction mixture, as previously shown (Figs. 2.3.1 and 3.3.1B). The conjugate families are numbered relative to the elution position for lysozyme as defined in section 2.3.2. It was assumed that conjugates obtained from the mixed anhydride reaction with retention times the same as those

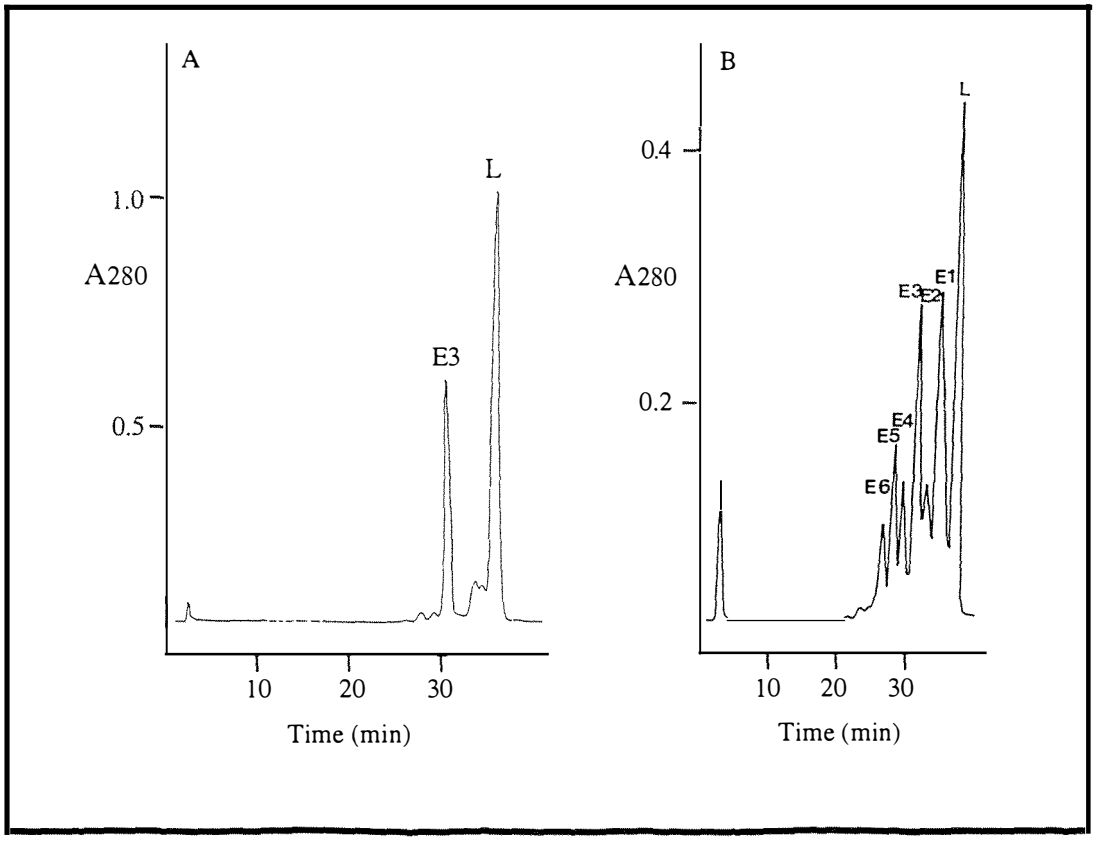


**Fig. 3.3.1** E1G-lysozyme conjugate reaction mixtures (mixed anhydride (A) and active ester (B) methods) in 7 M urea on a Mono-S cation-exchange HR 5/5 column. Conditions: buffer, gradient and chart as described in Fig. 2.3.1. Fig. B is the same as that presented in Fig. 2.3.1.

produced by the active ester reaction were equivalent (see characterisation details for confirmation) and hence were labelled using the same nomenclature.

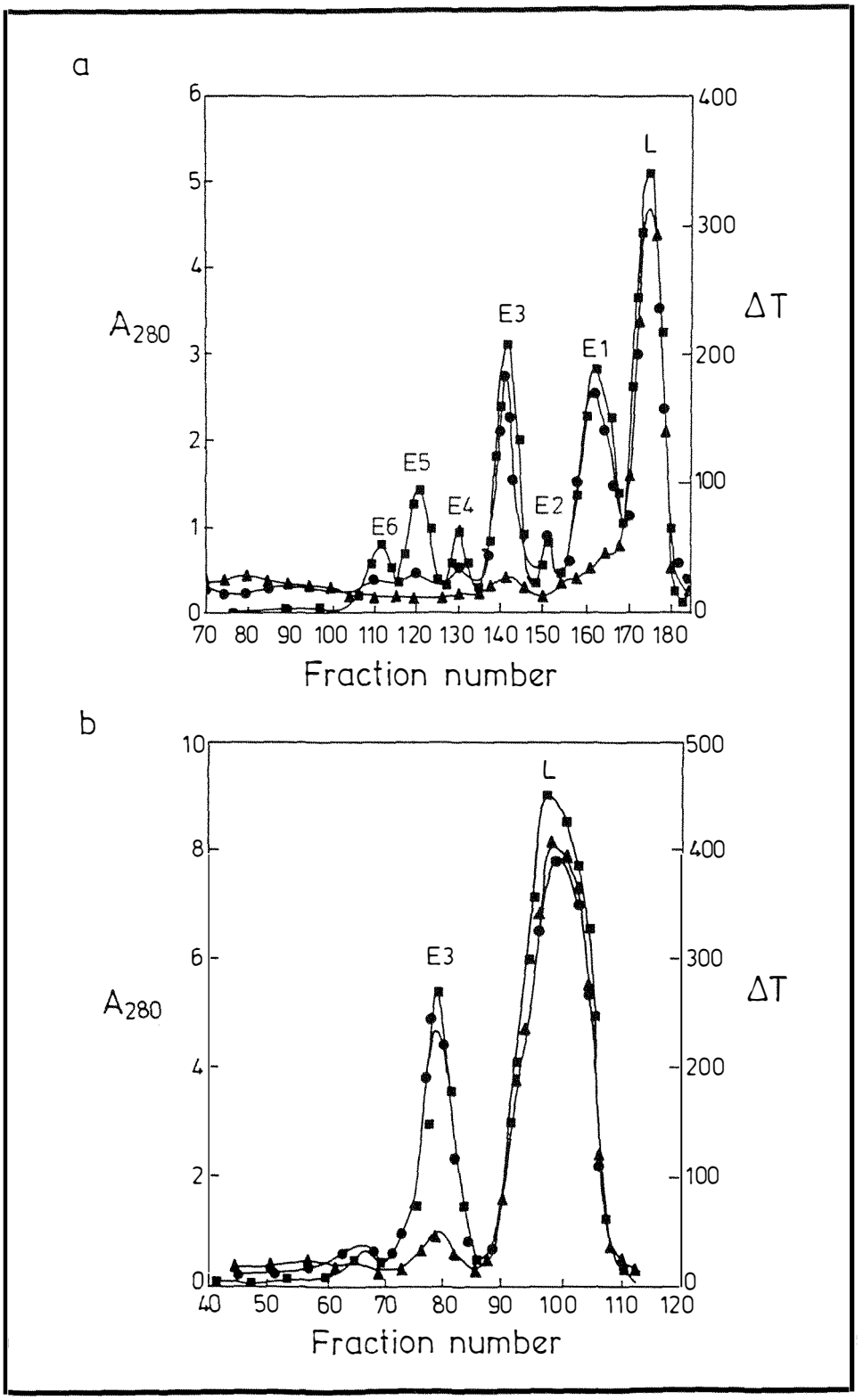


**Fig. 3.3.2** E1G-lysozyme conjugate reaction mixtures (active ester (a) and mixed anhydride (b) methods) in 7 M urea on an S-Sepharose (fast flow) column. The profiles show A280 (■), and lytic activity in the absence (●=ΔT) and presence (▲=ΔT) of excess E1G antibody. For conditions and details see text.

**Table 3.3.1**

Summary of yields and specific activities for estrone glucuronide-lysozyme conjugates purified by cation-exchange chromatography in 7 M urea on Mono-S and S-Sepharose (fast flow) columns

| Conjugate | Yield (1)* (% of total) | Yield (2)* (% of total) | Lysine residues acylated† | Specific activity†† |
|---|---|---|---|---|
| Lysozyme | 30.0 | 36.9 | 0 | 100 |
| AE E1 | 22.0 | 25.6 | 1 | 95.1 |
| AE E2 | 7.4 | 2.8 | 1.5 | 88.2 |
| AE E3 | 18.0 | 19.1 | 1 | 94.0 |
| AE E4 | 7.0 | 3.9 | 2 | 60.8 |
| AE E5 | 11.0 | 7.7 | 2 | 57.6 |
| AE E6 | 4.6 | 4.0 | 3 | 42.3 |
| Lysozyme | 58.1 | 73.5 | 0 | 100 |
| MA E1 | 9.2 | - | ¥ | ¥ |
| MA E3 | 30.2 | 24.3 | 1 | 99.5 |
| MA E4 | 1.1 | - | ¥ | ¥ |
| MA E5 | 1.5 | 2.2 | ¥ | ¥ |

**Key**
AE = active ester conjugate family
MA = mixed anhydride conjugate family
* = yield (1) is calculated from the Mono-S 7 M urea profiles; yield (2) is calculated from the S-Sepharose (fast flow) 7 M urea profiles
† = determined by titration of lysine groups with trinitrobenzenesulfonic acid (see chapter 2 for details) and proteolytic studies
†† = % relative to unreacted lysozyme
¥ = not determined

The mixed anhydride reaction mixture also produced two major chromatographically distinct peaks (Fig. 3.3.2b) when passed in bulk through an S-Sepharose (fast flow) column, the largest again being unreacted lysozyme (L). The material which eluted earlier consisted almost entirely of conjugate family E3. Conjugate family E1, which can be seen in Fig. 3.3.1A, eluted under the large unreacted lysozyme peak, explaining the higher yield of lysozyme as calculated from the S-Sepharose (fast flow) column compared with the Mono-S column (see Table 3.3.1). Peak E4 can be seen as a slight shoulder on the front edge of peak E3 while peak E5 was present in a small amount. On the other hand, when lysozyme was conjugated by the active ester procedure, seven chromatographically distinct peaks were obtained upon passing the reaction mixture in bulk through an S-Sepharose (fast flow) column (Fig. 3.3.2a) in yields similar to those calculated from the

Mono-S profiles (Figs. 2.3.1 and 3.3.1B) (Table 3.3.1). Once again the largest peak was unreacted lysozyme and of the six conjugate peaks (E1-E6) which eluted earlier, E1 and E3 together comprised over half of the total conjugate yield (Table 3.3.1). It was necessary to rechromatograph each conjugate family by passage twice through the S-Sepharose (fast flow) column to obtain derivatives which were chromatographically homogeneous on a Mono-S column in 7 M urea and by acid-polyacrylamide gel electrophoresis (see sections 3.3.6 and 3.4.4).

The estrone glucuronide-lysozyme conjugate family E1 did not elute under the lysozyme peak in the active ester profile, presumably due to the smaller amount of protein material loaded onto the S-Sepharose column in this case. As a result, the resolution between protein peaks was much greater for the active ester profile. This can be clearly seen in Fig. 3.3.2 where the lysozyme and E3 peaks elute closer together in the mixed anhydride profile than in the active ester profile. In addition to this, there was only a small amount of the estrone glucuronide-lysozyme conjugate family E1 produced by the mixed anhydride reaction procedure as confirmed by Mono-S 7 M urea cation-exchange chromatography. The combined effect of these two factors explains why conjugate family E1 elutes under the lysozyme peak in the mixed anhydride profile but not in the active ester profile.

All of the estrone glucuronide-lysozyme conjugate families (E1-E6) and unreacted lysozyme, from both conjugation procedures, had lytic activities which paralleled the $A_{280}$ profiles (Figs. 3.3.2a and 3.3.2b) and all were inhibited by 70-80% when excess E1G antibody was present in the assay mixture. The lytic activity of unreacted lysozyme (designated L) was not affected by the presence of excess anti-E1G antiserum as expected. Conjugate families E4, E5, and E6 had much lower specific activities than the E1, E2, and E3 conjugate families (Table 3.3.1) which had specific activities similar to that of native lysozyme.

The chromatogram of an E1G-lysozyme conjugate family population (which had initially been purified by cation-exchange chromatography on an S-Sepharose (fast flow) column to give a homogeneous product) when passed through a Butyl Sepharose hydrophobic interaction column, typically consisted of an initial small broad peak (I) followed later in the gradient by a much larger, conjugate containing second peak (II) (Fig. 3.3.3). Peak I, although containing no lysozyme when analysed by gel electrophoresis or chromatography in 7 M urea on a Mono-S column, was only inhibited by 75-85% when excess E1G-antibody was present in the assay system. However, the lytic activity of the major conjugate containing peak (II) was inhibited by > 90% when excess E1G-antibody was present in the assay system.

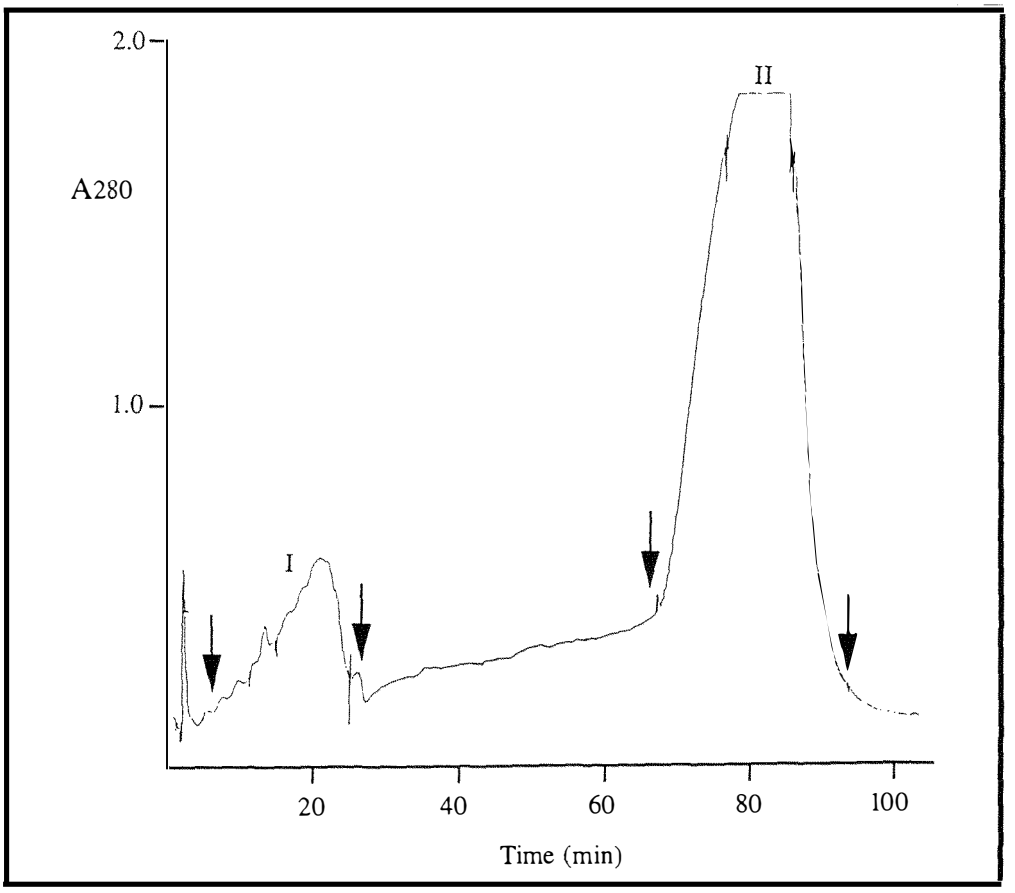


**Fig. 3.3.3** The A280 profile of E1G-lysozyme mixed anhydride conjugate family E3 (after purification in 7 M urea on an S-Sepharose (fast flow) column) on a Butyl Sepharose hydrophobic interaction column as described in the text. Conditions: buffer A, 50 mM $NaH_2PO_4$ + 1.4 M $(NH_4)_2SO_4$ titrated to pH 6.6 with 1 M NaOH and buffer B, 50 mM $NaH_2PO_4$ titrated to pH 6.6 with 1 M NaOH; gradient, 0-10% B in 5 min, 10% B for 40 min, 10-100% B in 20 min, 100% B for 45 min at 1.0 mL/min.

### 3.3.2 Preparation and Purification of Individual Pregnanediol Glucuronide-Lysozyme Conjugates

The addition of the mixed anhydride reagent (prepared from synthetic PdG as described in section 3.2.3.1) to the purified hen egg white lysozyme solution at a molar ratio of 1.6:1, resulted in conjugation of 46.5% of the initial amount of lysozyme with PdG (Table 3.3.2). This was shown by analytical cation-exchange chromatography in 7 M urea buffers (Fig. 3.3.4A). The largest peak (53.5% of the overall yield) consisted of unreacted lysozyme (L), as shown by comparison with the FPLC profile of a pure sample of lysozyme. Of the conjugated lysozyme, the predominant conjugate families were P1 (56% of the conjugate yield) and P3 (32% of the conjugate yield) with the remaining 12% of the conjugate yield made up of small amounts of P4 (6.1%), P5 (5.5%) and a very small amount of P6 (0.4%). As expected, the profile of the mixed anhydride PdG-lysozyme reaction mixture on an S-Sepharose (fast flow) column (Fig.

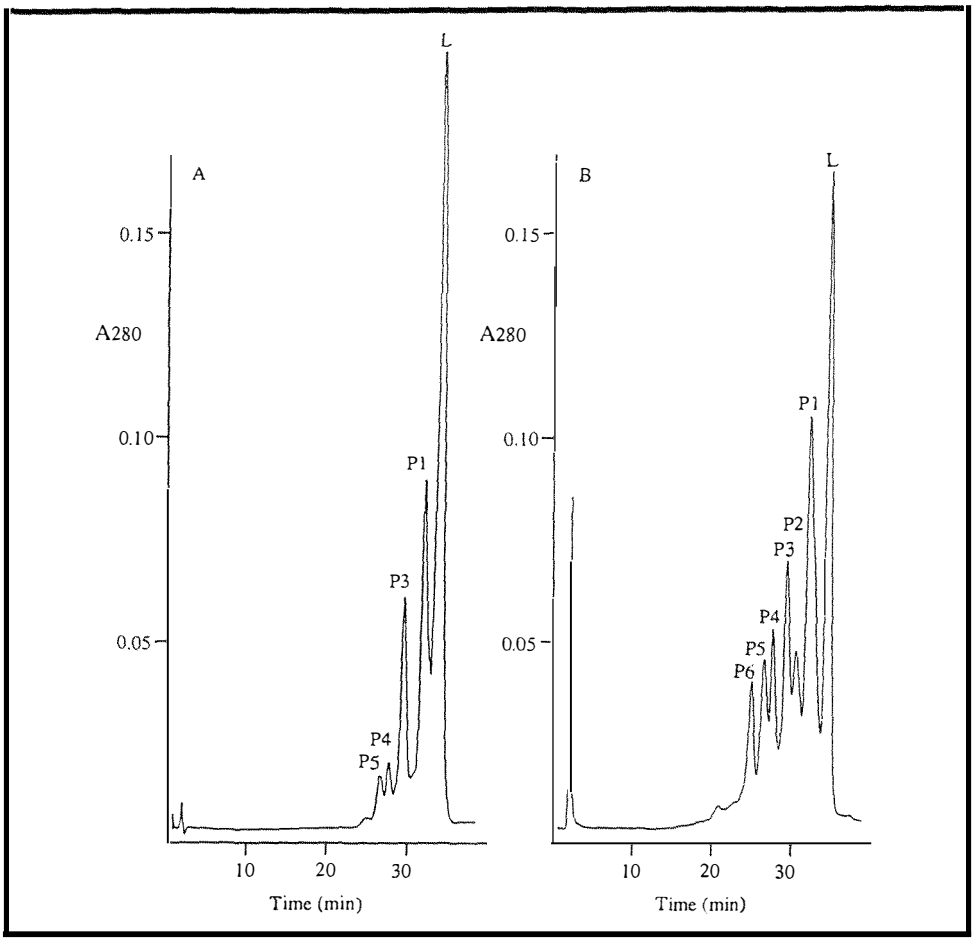


**Fig. 3.3.4** PdG-lysozyme conjugate reaction mixtures (mixed anhydride (A) and active ester (B) methods) in 7 M urea on a Mono-S cation-exchange HR 5/5 column. Conditions: buffer, gradient and chart as described in Fig. 2.3.1. Fig. B is the same as that reported in Fig. 2.3.9.

3.3.5A) was very similar to that obtained on the analytical Mono-S cation exchange column in 7 M urea (Fig. 3.3.4A). The conjugate families are numbered relative to the elution position for lysozyme as defined in section 2.3.3 and it was assumed that mixed anhydride conjugates with retention times the same as active ester produced conjugates are equivalent and hence were labelled using the same nomenclature.

On the other hand, when lysozyme was conjugated by the active ester procedure with pregnanediol glucuronide, seven chromatographically distinct peaks were obtained upon passing the reaction mixture through an S-Sepharose (fast flow) column (Fig. 3.3.5B) (as expected from the Mono-S 7 M urea profile (Figs. 2.3.9 and 3.3.4.B)). Once again the largest peak was unreacted lysozyme and of the six conjugate peaks (P1-P6) which eluted earlier, P1 was the predominant family comprising 36.3% of the total conjugate yield as calculated from the Mono-S 7 M urea profile. Conjugate fractions P1 (36.3% of the total conjugate yield) and P3 (18.9% of the total conjugate yield) together comprised 55.2% of the total conjugate yield as calculated from the Mono-S 7 M urea profile. The

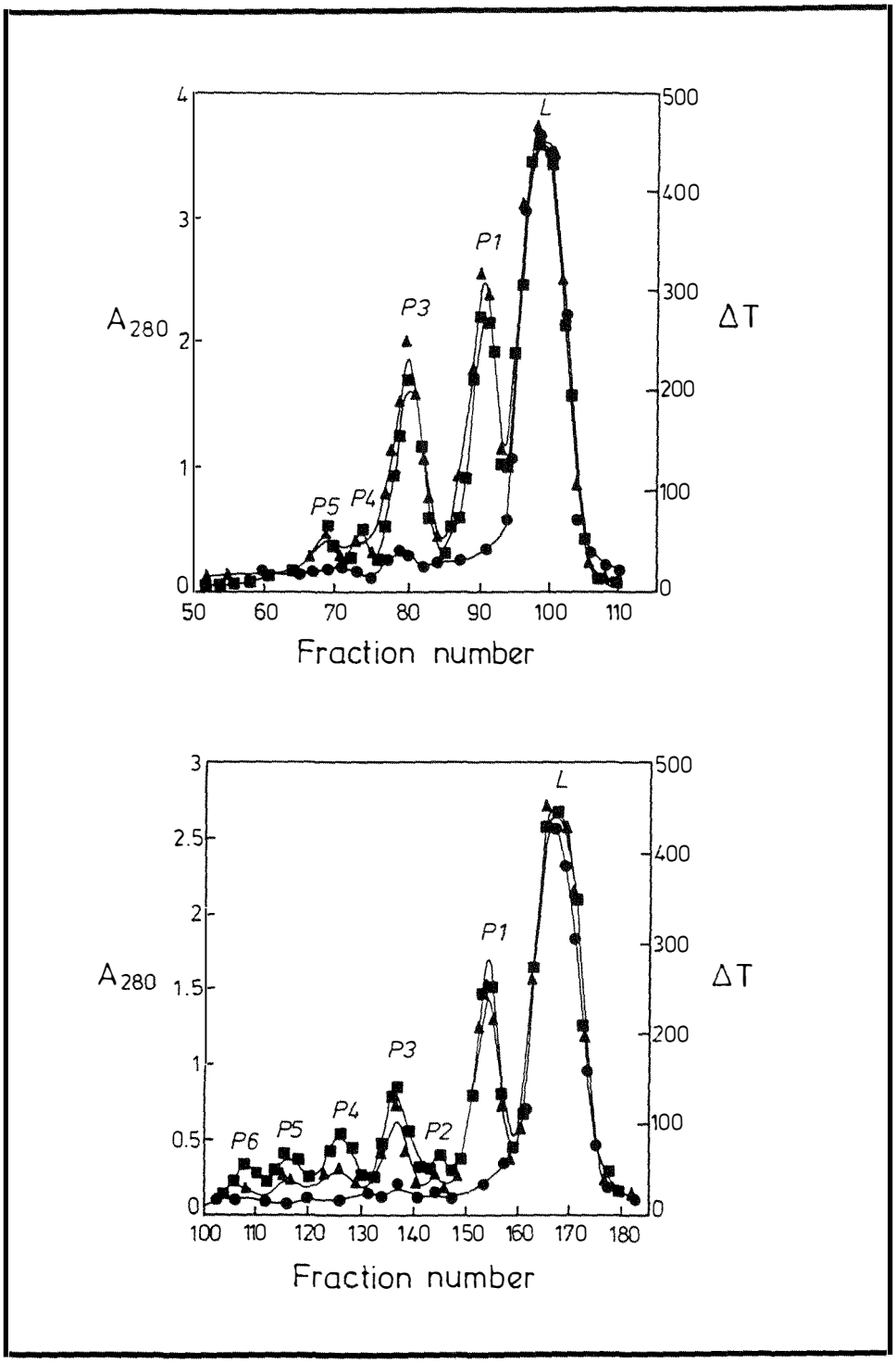


**Fig. 3.3.5** PdG-lysozyme conjugate reaction mixtures (mixed anhydride (A) and active ester (B) methods) in 7 M urea on an S-Sepharose (fast flow) column. The profiles show A280 (■), and lytic activity in the absence (▲=ΔT) and presence (●=ΔT) of excess PdG antibody. For conditions and details see text.

remainder of the conjugate yield consisted of small amounts of families P2 (12.5% of the total conjugate yield), P4 (12.6% of the total conjugate yield), P5 (11.8% of the total conjugate yield), and P6 (8.4% of the total conjugate yield). Similar yields were

**Table 3.3.2**

Summary of yields and specific activities for pregnanediol glucuronide-lysozyme conjugates purified by cation-exchange chromatography in 7 M urea on Mono-S and S-Sepharose (fast flow) columns

| Conjugate | Yield (1)* (% of total) | Yield (2)* (% of total) | Lysine residues acylated† | Specific activity†† |
|---|---|---|---|---|
| Lysozyme | 26.70 | 46.5 | 0 | 100 |
| AE P1 | 26.60 | 23.7 | 1 | 92 |
| AE P2 | 9.18 | 3.0 | 2 | 76 |
| AE P3 | 13.85 | 12.7 | 1 | 88 |
| AE P4 | 9.27 | 7.3 | 2 | 55 |
| AE P5 | 8.62 | 4.2 | 2 | 61 |
| AE P6 | 6.14 | 2.6 | 3 | 47 |
| Lysozyme | 53.5 | 54.5 | 0 | 100 |
| MA P1 | 27.6 | 23.3 | 1 | 92 |
| MA P3 | 13.7 | 16.3 | 1 | 93 |
| MA P4 | 4.0 | 3.0 | 2 | ¥ |
| MA P5 | 3.7 | 3.0 | 2 | ¥ |

**Key**
AE = active ester conjugate family
MA = mixed anhydride conjugate family
* = yield (1) is calculated from the Mono-S 7 M urea profiles; yield (2) is calculated from the S-Sepharose (fast flow) 7 M urea profiles
† = determined by titration of lysine groups with trinitrobenzenesulfonic acid (see chapter 2 for details) and proteolytic studies
†† = % relative to unreacted lysozyme
¥ = not determined

calculated from the S-Sepharose (fast flow) profile (Table 3.3.2). As in the case of the estrone glucuronide-lysozyme conjugates, it was necessary to rechromatograph each conjugate family by passage twice through the S-Sepharose (fast flow) column to obtain derivatives which were chromatographically homogeneous on a Mono-S column in 7 M urea.

As for the E1G conjugates, all of the PdG conjugate families (P1-P6) and unreacted lysozyme from both conjugation procedures had lytic activities which paralleled the $A_{280}$ profiles (Figs. 3.3.5A and 3.3.5B) and the conjugates were inhibited by 75-85% when excess PdG antibody was present in the assay mixture. The lytic activity of unreacted lysozyme (designated L) was not affected by the presence of excess anti-pregnanediol

glucuronide antiserum as expected. Once again the more highly substituted conjugate families (P4, P5, and P6) had much lower specific activities than the less highly substituted conjugate families (P1, P2, and P3) which again had specific activities similar to that of native lysozyme (Table 3.3.2). Pregnanediol glucuronide-lysozyme conjugates passed through a Butyl Sepharose hydrophobic interaction chromatography were inhibited by 89-90% in the presence of excess antibody.

### 3.3.3 Identification of Native, Unmodified Lysozyme Tryptic Digest Peptides

The identities of the lysine residues acylated by estrone glucuronide and pregnanediol glucuronide in the chromatographically and electrophoretically homogeneous lysozyme conjugates were determined by tryptic digestion of the reduced, S-carboxymethylated derivatives in 2 M urea solutions at pH 8.5 and 37°C. The resulting tryptic peptides were analysed by reverse phase chromatography and the elution profiles are shown in Figs. 3.3.7, 3.3.9, 3.3.10, 3.3.12, 3.3.13, and 3.3.14. The tryptic peptides from the native lysozyme digest are shown in Figs. 3.3.7a and 3.3.12a and are numbered in their order of elution from the reverse phase column. Twenty major peaks were observed in the

**Table 3.3.3**

The native lysozyme peptides containing lysine (K) residues

| Peptide peak number(s)* | Peptide assignment | Lysine (K) residue within the peptide |
|---|---|---|
| 2 | $T_{1+2}$ | Lys 1 |
| 7-10 | $T_{3+4}$ | Lys 13 |
| 15 | $T_6$ | Lys 33 |
| 16-18 | $T_{13}$<br>$T_{12+13}$ | Lys 97 |
| 20 | $T_{11}$ | Lys 96 |
| # | $T_{15}$ | Lys 116 |

**Key**

* = see Figs. 3.3.7 and 3.3.12

\# = this dipeptide ($T_{15}$) could not be detected in the tryptic maps as described in section 3.3.3

digest of native lysozyme (Figs. 3.3.7a and 3.3.12a) of which peaks 2 ($T_{1+2}$, K1), 7-10 ($T_3$ and $T_{3+4}$, K13), 15 ($T_6$, K33), 16-18 ($T_{13}$ and $T_{12+13}$, K97) and 20 ($T_{11}$, K96) contained lysine residues (Table 3.3.3) where T refers to the nomenclature of Canfield [172] for the tryptic peptides of hen egg white lysozyme. The small lysine dipeptide $T_{15}$ (K116) was not observed. Trypsin hydrolysed most of the lysyl and arginyl bonds completely although the potential cleavage sites between $T_1$ and $T_2$ and between $T_{17}$ and $T_{18}$ (under peak 3) could not be hydrolysed, as previously reported by Noda *et al.* [173] and Okazaki *et al.* [174] for S-carboxymethylated lysozyme derivatives in the absence of 2 M urea. The potential cleavage sites between $T_3$ and $T_4$, and $T_{12}$ and $T_{13}$ were only partially hydrolysed. The peak areas of $T_{12+13}$ and $T_{13}$ were added together because they result from the hydrolysis of two neighbouring cleavage sites. Peptide $T_{13}$ appeared as two peaks in the present work and Yamada *et al.* [175] have suggested that this is due to the presence of a monomer-dimer mixture which presumably persists in 2 M urea.

### 3.3.4 Characterisation of E1G-Lysozyme Conjugate Families

In the tryptic maps for each conjugate family, certain lysine containing peptides disappeared or diminished in height relative to the tryptic map of lysozyme. For example peaks 6, 15 and 16-18, which contained the tryptic peptides $T_7$ (6), $T_6$ (15) and $T_{13}$ + $T_{12+13}$ (16-18) respectively, were reduced in height in one or more of the conjugate digest profiles (Figs. 3.3.7, 3.3.9, and 3.3.10). New peaks appeared later in the HPLC gradient at much higher acetonitrile concentrations than the native peptides (after peak 20, Fig. 3.3.7a). The amino acid sequences of these later eluting lysine acylated peptides (c-m) were matched with the known sequences of the tryptic peptides from hen egg white lysozyme [117, 172]. However, the acylated peptides did not exhibit a lysine peak where expected from the known tryptic peptide sequence during sequence analysis. Instead a new peak, which eluted off the sequencer HPLC column after all of the other amino acid peaks, was observed (Fig. 3.3.6). This peak was always present when sequencing E1G modified peptides and is presumably due to an estrone glucuronide acylated lysine residue. Since the new peak eluted last from the sequencer HPLC column it did not interfere with detection of any of the other amino acids in the sequence. From the tryptic maps it was evident that lysine residue 96 was unmodified in all of the conjugates since the peptide peak T11 (residues 74-96, peak 20 Fig. 3.3.7a) did not change in height, area or elution characteristics.

N-terminal sequencing of the intact conjugates and the unmodified native lysozyme by gas phase Edman degradation through 36 steps, allowed direct monitoring of the first four possible acylation sites (lysine residues 1, 13 ,33 and the N-terminal amino group)

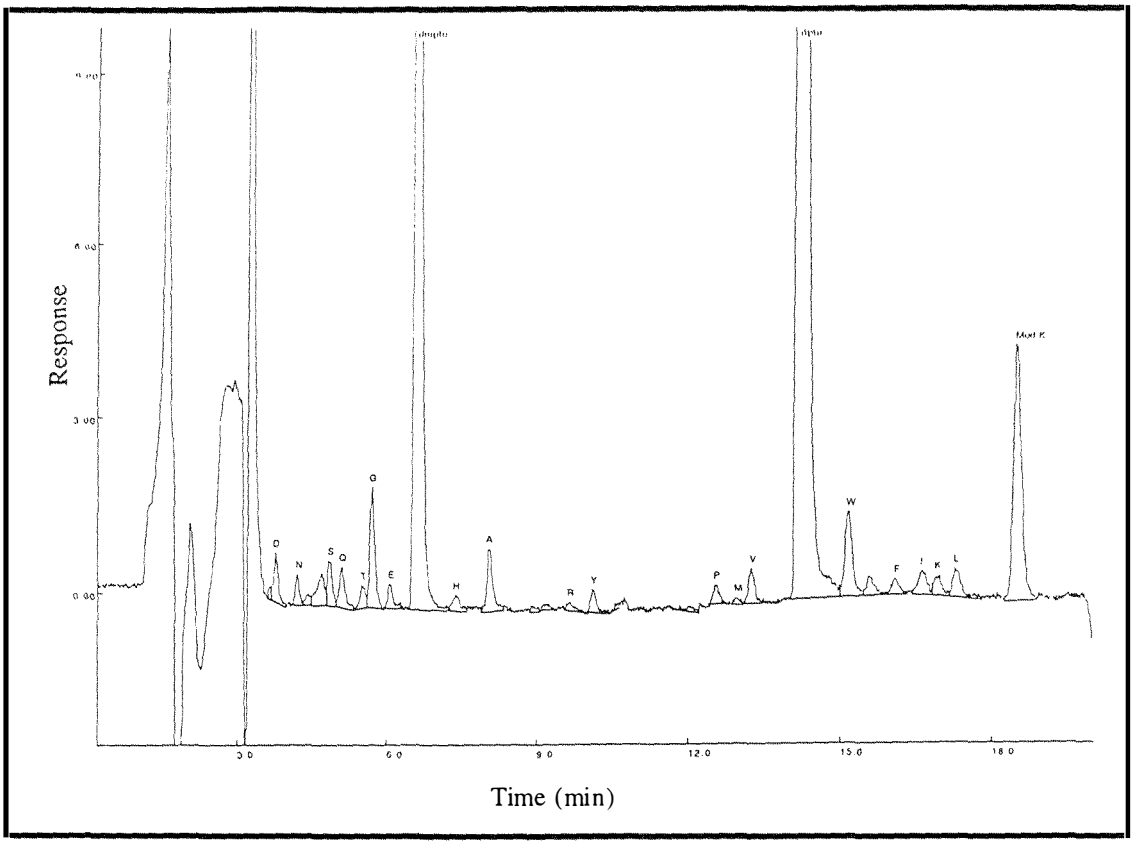


**Fig. 3.3.6** The HPLC profile from the amino acid sequencer when a lysine residue acylated with estrone glucuronide was sequenced. Instead of a lysine peak (K) a characteristically large peak, which always eluted later in the gradient than lysine (designated Mod.K on the profile), was observed. This peak eluted after all of the other amino acid peaks and is presumably due to an estrone glucuronide acylated lysine residue.

in the lysozyme sequence [117]. The consistent, reproducible yields obtained for all of the individual amino acids, of both the conjugated and native lysozyme sequences, showed that the N-terminal α-amino group and both the ε-amino groups of lysine residues 1 and 13 were unmodified. This was confirmed by the peptide mapping results. In all of the conjugate tryptic maps the peptide peaks $T_{1+2}$ (residues 1-5, peak 2 Fig. 3.3.7a) and $T_3 + T_{3+4}$ (residues 6-14, peaks 7-11 Fig. 3.3.7a) remained unchanged in height and area relative to the tryptic map for the lysozyme control.

*3.3.4.1 Tryptic digestion of estrone glucuronide-lysozyme conjugate families E1 and E2*

In the tryptic digest of conjugate E1 which was prepared by the active ester method (Fig. 3.3.7b) peaks 16-18 (peptides $T_{13}$, residues 98-112 and $T_{12+13}$, residues 97-112) had diminished in height by approximately 60% relative to the native lysozyme digest (Fig. 3.3.7a). Several major new peptide peaks (f, i and j) were eluted much later in the gradient, along with three minor peaks (c, d and m). Enzyme immunoassays carried out in the presence of the native lysozyme tryptic peptides (peaks 1-20, Fig. 3.3.7a) did not

**Table 3.3.4**

The acylation positions of lysozyme with estrone glucuronide in the lysozyme-estrone glucuronide conjugates characterised as described in the text

| E1G-lysozyme conjugate | Number of E1G molecules per lysozyme molecule* | Acylated peptide(s) | Corresponding peptide peaks† | Acylation position |
|---|---|---|---|---|
| AE E1 | 1 | $T_{12+13}$ | d, i, j | Lys 97 |
| | | $T_{15+16}$ | c, f | Lys 116 |
| AE E2 | 1.5 | $T_{12+13}$ | d, i, j | Lys 97 |
| | | $T_{15+16}$ | c, f | Lys 116 |
| AE E3 | 1 | $T_{6+7}$ | k, m, o | Lys 33 |
| AE E4 | 2 | $T_{6+7}$ | k, m, o | Lys 33 |
| | | $T_{15+16}$ | c, f | Lys 116 |
| AE E5 | 2 | $T_{6+7}$ | k, k', o | Lys 33 |
| | | $T_{12+13}$ | i, j | Lys 97 |
| AE E6 | 3 | $T_{6+7}$ | k, k', m | Lys 33 |
| | | $T_{12+13}$ | d, i, j | Lys 97 |
| | | $T_{15+16}$ | c, f | Lys 116 |
| MA E3 | 1 | $T_{6+7}$ | k, m, o | Lys 33 |

**Key**
AE = active ester conjugate family
MA = mixed anhydride conjugate family
* = determined from proteolytic studies and titration of lysine groups with trinitrobenzenesulfonic acid (see chapter two for details)
† = see Figs. 3.3.7, 3.3.9, and 3.3.10

significantly increase the lytic activity of the intact E1G-lysozyme conjugate in the presence of the E1G antibody (Fig. 3.3.8a). This same result was observed for peptide peaks 1-20 obtained from the tryptic digest of E1, which therefore did not contain E1G. However, assays carried out in the presence of the active ester E1 tryptic peptides f, i and j increased the enzymatic rates of lysis (to approximately 350 units per 40 minutes). This rate was the same as obtained for the control assay in the absence of the E1G antibody, thus the immune reactivities for these three peptides were high (Fig. 3.3.8b), confirming the presence of estrone glucuronide.

Peptides i and j were comprised of $T_{12+13}$ acylated with estrone glucuronide at lysine 97, as shown by amino acid sequencing and mass spectrometry (Table 3.3.5). The difference between peaks i and j was that peak j had undergone an amide/carboxylic acid interchange at residue 106 from asparagine (N, $-CH_2-CO-NH_2$) to aspartate (D, $-CH_2-COO^-$). A single cycle of manual Edman sequencing was undertaken on the acylated $T_{12+13}$

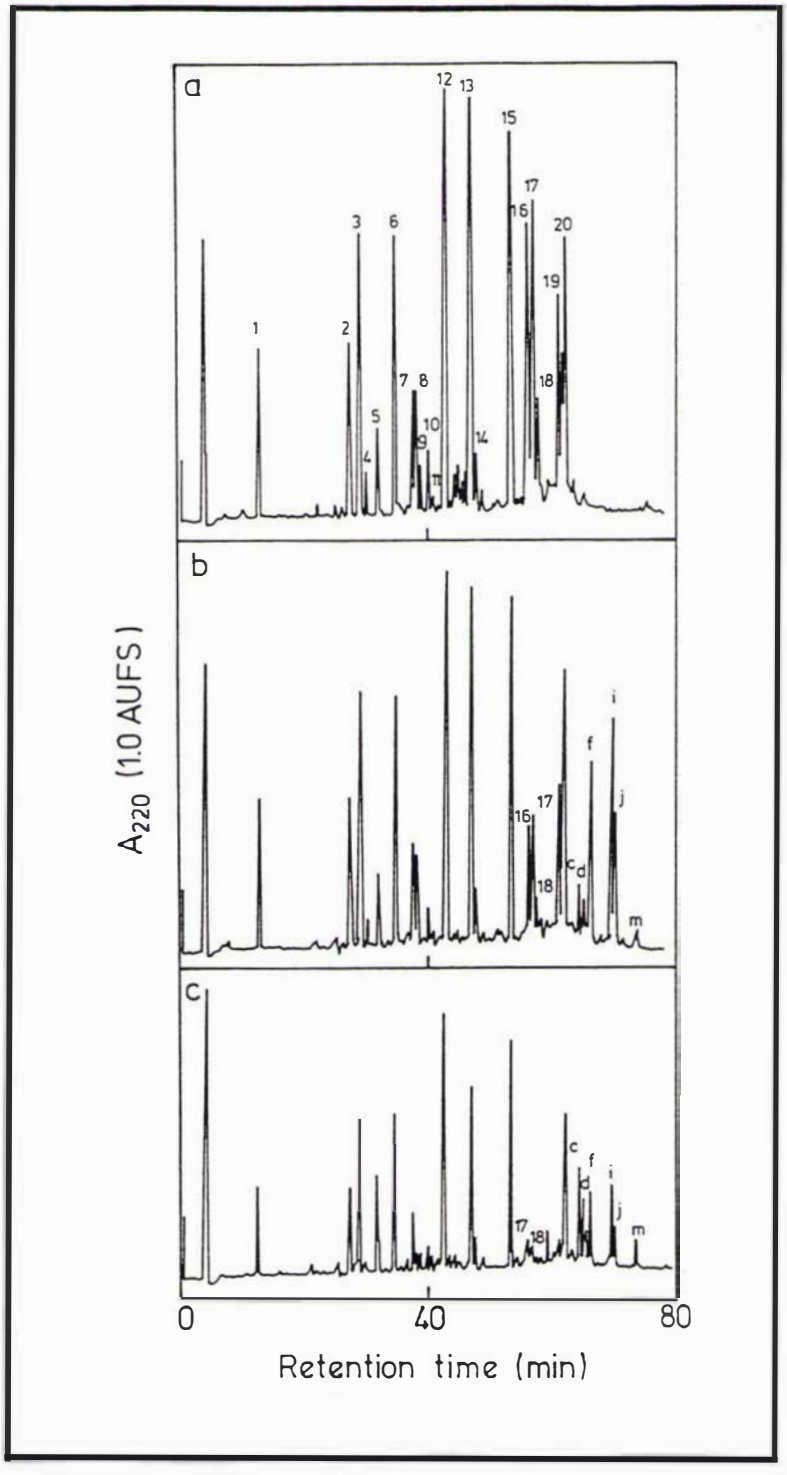


**Fig. 3.3.7** Reversed-phase HPLC separation of the tryptic peptides from tryptic digests of unmodified lysozyme (a), and active ester E1G-lysozyme conjugates E1 (b), and E2 (c). The numbers refer to unmodified tryptic peptides and the letters to acylated tryptic peptides. For conditions and details see text.

peptide. The result was a new peptide which corresponded to unmodified $T_{13}$ by mass spectrometry and sequence analysis. The difference in mass (556), between the Edman generated $T_{13}$ peptide and the original acylated $T_{12+13}$ peptide, corresponded to a lysine residue acylated with estrone glucuronide. This confirmed that the modification was due to acylation by estrone glucuronide at lysine residue 97. The minor peptide peak d was also the result of acylation at lysine residue 97. This peptide did not contain the complete sequence of acylated $T_{12+13}$ but was four residues shorter at the C-terminal end due to chymotryptic cleavage (Table 3.3.5). Peptide f consisted of $T_{15+16}$ (residues 115-125)

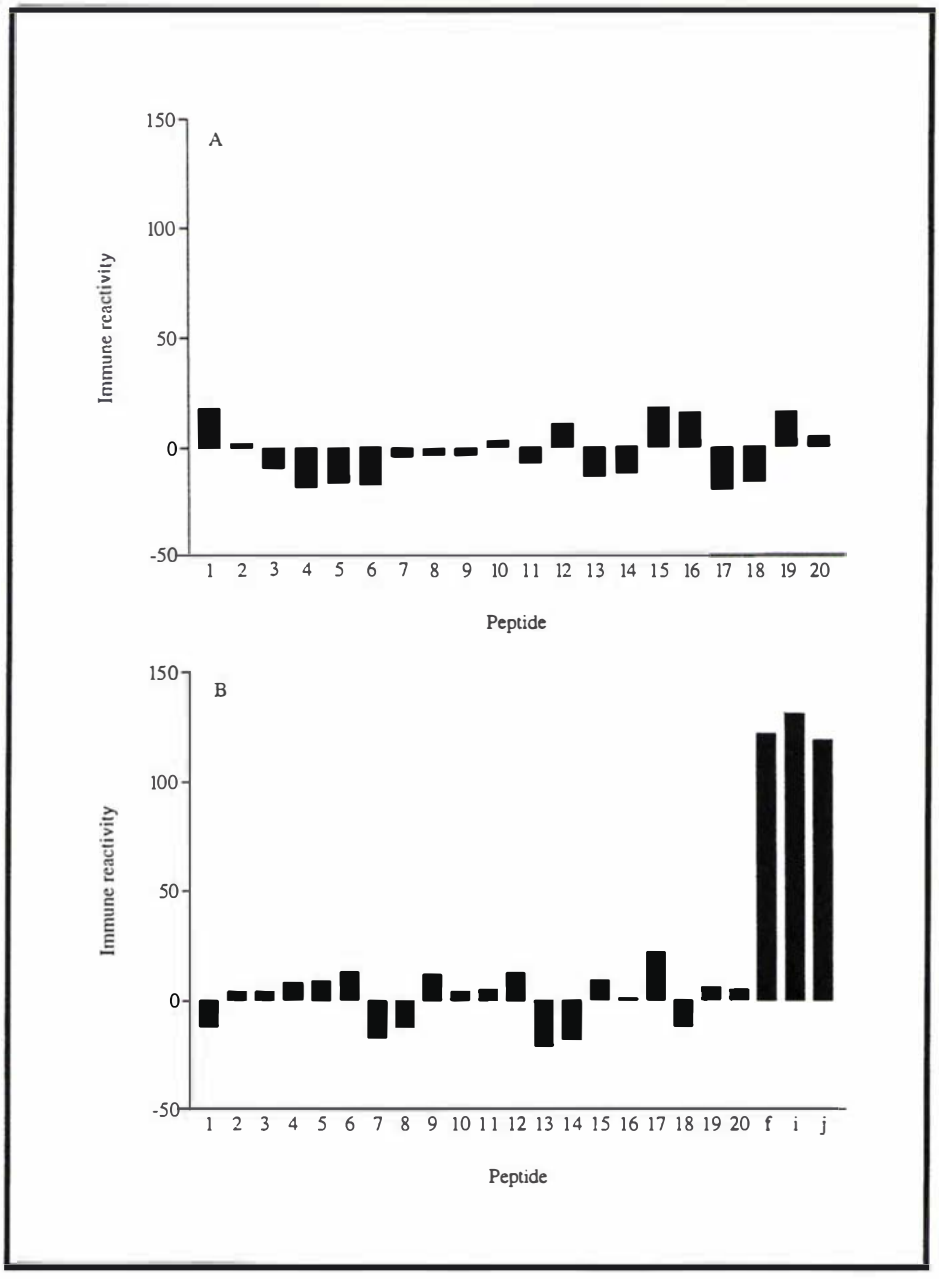


**Fig. 3.3.8** The immune reactivities of the tryptic peptides from unmodified lysozyme (A) and active ester E1G-lysozyme conjugate E1 (B) as measured using an Ovarian Monitor. The high immune reactivities of E1 peptides f, i, and j (B) confirmed the presence of E1G. For details see text.

acylated with estrone glucuronide at lysine residue 116 (Tables 3.3.4 and 3.3.5). Peptide c was also the result of acylation at lysine residue 116, but as in the case of peptide d, was not the complete $T_{15+16}$ peptide due to C-terminal chymotryptic cleavage (Table 3.3.5). A very small amount of peptide m (acylation at lysine residue 33) was also detected, however, a decrease in the height of peaks 6 and 15 from which peptide m is derived, could not be observed (see Fig. 3.3.7b).

The tryptic digest from the active ester conjugate E2 (Fig. 3.3.7c), showed that acylation had occurred at the same two lysine positions as for the E1 conjugate. Peptides i, j and d due to acylation of lysine residue 97 (Tables 3.3.4 and 3.3.5) were once again present. Peaks 16-18 had almost completely disappeared indicating that lysine 97 was acylated to a much greater extent in conjugate fraction E2 than in conjugate fraction E1. Peptides c and f due to acylation at lysine 116 were also present as in the E1 digest. A small amount of peptide m was once again detected.

*3.3.4.2 Tryptic digestion of estrone glucuronide-lysozyme conjugate family E3*

The elution patterns obtained for the tryptic digests of the estrone glucuronide-lysozyme E3 active ester and mixed anhydride conjugate families are shown in Figs. 3.3.9a and 3.3.9b. The digest patterns of the active ester and mixed anhydride E3 conjugate were nearly identical. In the mixed anhydride E3 digest (Fig. 3.3.9b) peptides $T_6$ (residues 22-33, peak 15) and $T_7$ (residues 34-45, peak 6) had considerably diminished in height, from the very large peaks exhibited in the native digest (Fig. 3.3.7a) to become minor peaks. The predominant new peptide peak (m) was comprised of peptide $T_{6+7}$ (residues 22-45) acylated with estrone glucuronide at lysine residue 33 (Tables 3.3.4 and 3.3.5). The other minor peaks, of which peptides k and o composed the bulk, were the result of chymotryptic cleavage of the acylated $T_{6+7}$ peptide (peak k) and amide/carboxylic acid interchange (peak o, Table 3.3.4) at residue 41 from glutamine (Q, $CH_2$-$CH_2$-CO-$NH_2$) to glutamate (E, $CH_2$-$CH_2$-$COO^-$). In the case of the active ester E3 digest (Fig. 3.3.9a) the predominant new peptide peak was again peak m, while minor amounts of peptides k and o were also detected. However, unlike the mixed anhydride E3 digest the peptide peaks corresponding to acylation at lysine positions 97 and 116 could also be detected, although only in very small amounts.

*3.3.4.3 Tryptic digestion of estrone glucuronide-lysozyme conjugate families E4, E5 and E6*

The elution patterns obtained for tryptic digestion of the estrone glucuronide-lysozyme active ester conjugate families E4, E5 and E6 are shown in Figs. 3.3.10a, 3.3.10b, and 3.3.10c. In the case of E4 (Fig. 3.3.10a), acylation had occurred at lysine residues 33

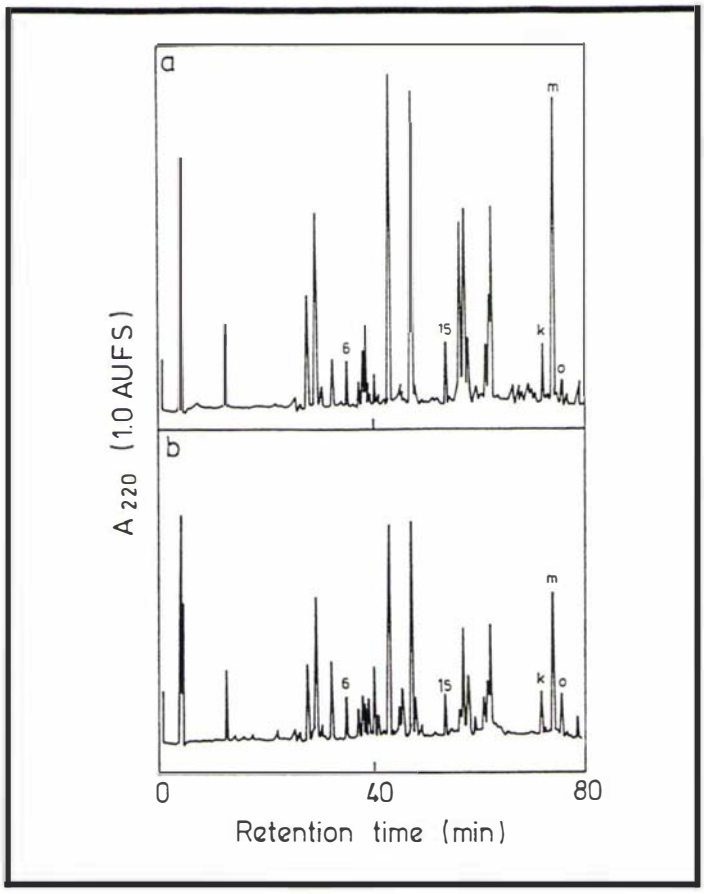


**Fig. 3.3.9** Reversed-phase HPLC separation of the tryptic peptides from tryptic digests of active ester E1G-lysozyme conjugate E3 (a) and mixed anhydride E1G-lysozyme conjugate E3 (b). The numbers refer to unmodified tryptic peptides and the letters to acylated tryptic peptides. For conditions and details see text.

and 116, as was shown by the appearance of the new peptide peaks c, f and m and the diminished heights of peaks 6 and 15. Minor amounts of peaks i and j were detected. The active ester conjugate E5 (Fig. 3.3.10b) was acylated with estrone glucuronide at lysine residues 33 and 97. Peptide peaks 6 and 15 had almost completely disappeared and the corresponding new acylated peaks k, k' and m eluted later in the gradient. Peak k' was the result of the same chymotryptic cleavage of acylated $T_{6+7}$ as found in peak k but it had also undergone an amide/carboxylic acid interchange (Table 3.3.5) at residue 41 as described in section 3.3.4.2. Peaks 16-18 had diminished considerably in size and the corresponding acylated peptides i and j could be detected. The most highly modified conjugate, active ester E6 (Fig. 3.3.10c), was found to be acylated at lysine residues 33, 97 and 116 (Tables 3.3.4 and 3.3.5). As previously described peptide peaks 6, 15 and 16-18 decreased in size while the corresponding acylated peptides eluted later in the gradient.

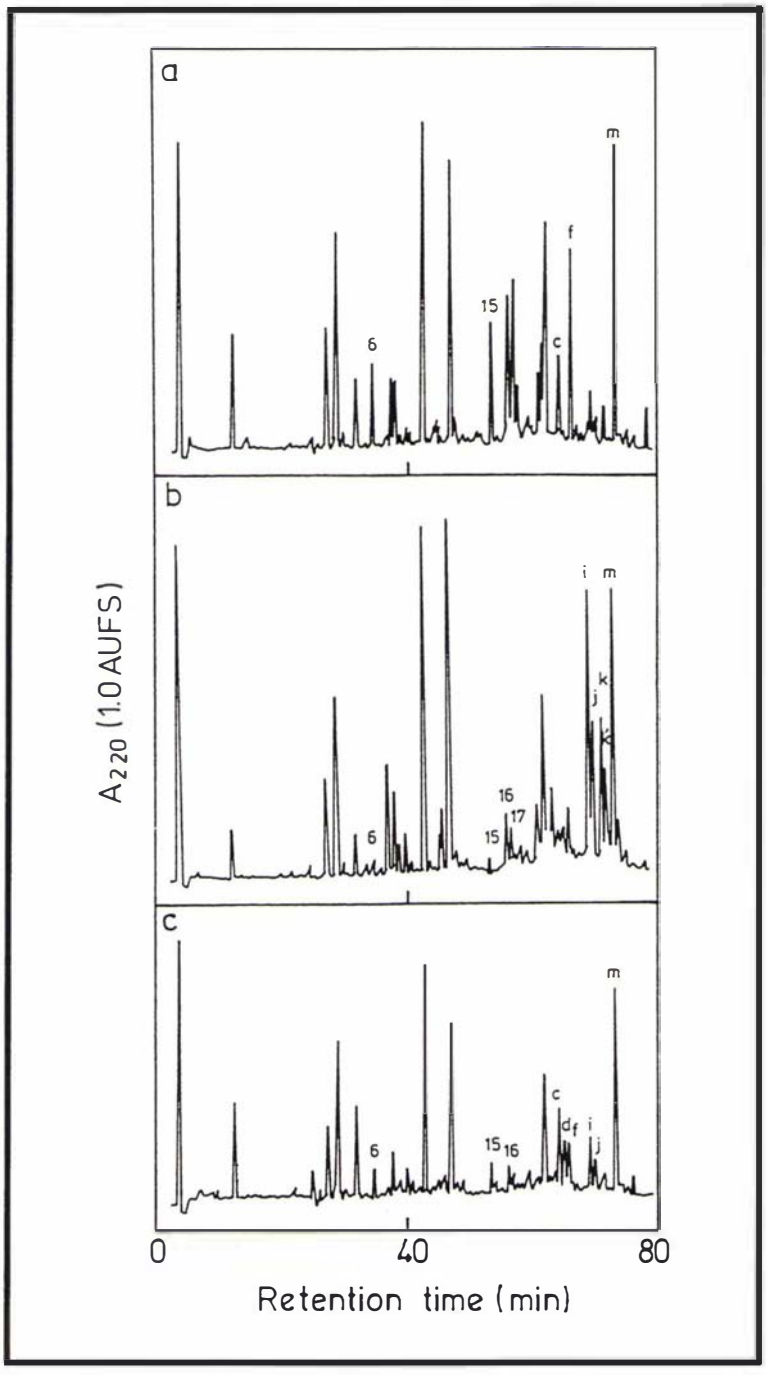


**Fig. 3.3.10** Reversed-phase HPLC separation of the tryptic peptides from tryptic digests of active ester E1G-lysozyme conjugates E4 (a), E5 (b), and E6 (c). The numbers refer to unmodified tryptic peptides and the letters to acylated tryptic peptides. For conditions and details see text.

*3.3.4.4 Mass spectral data for the estrone glucuronide acylated peptides*

The mass spectral data obtained for the estrone glucuronide acylated lysozyme tryptic peptides are reported in Table 3.3.5. As the amino acid sequence of lysozyme is known, the expected mass for tryptic peptides could be calculated. If an estrone glucuronide molecule was conjugated to a lysine residue within the peptide, the mass of the acylated peptide should be 428 mass units greater than the native peptide (i.e. if 428 is subtracted from the experimental m/z, a mass corresponding to a lysozyme peptide should be

obtained). By comparing calculated data with the experimental data, the acylated peptide, and thus the acylated lysine residue, could be assigned without the need for amino acid sequencing. In all cases the calculated and experimental results were in good agreement and unambiguously identified the assigned peptide, as confirmed by amino acid sequencing. A typical mass spectral analysis of a estrone glucuronide acylated peptide is shown in Fig. 3.3.11.

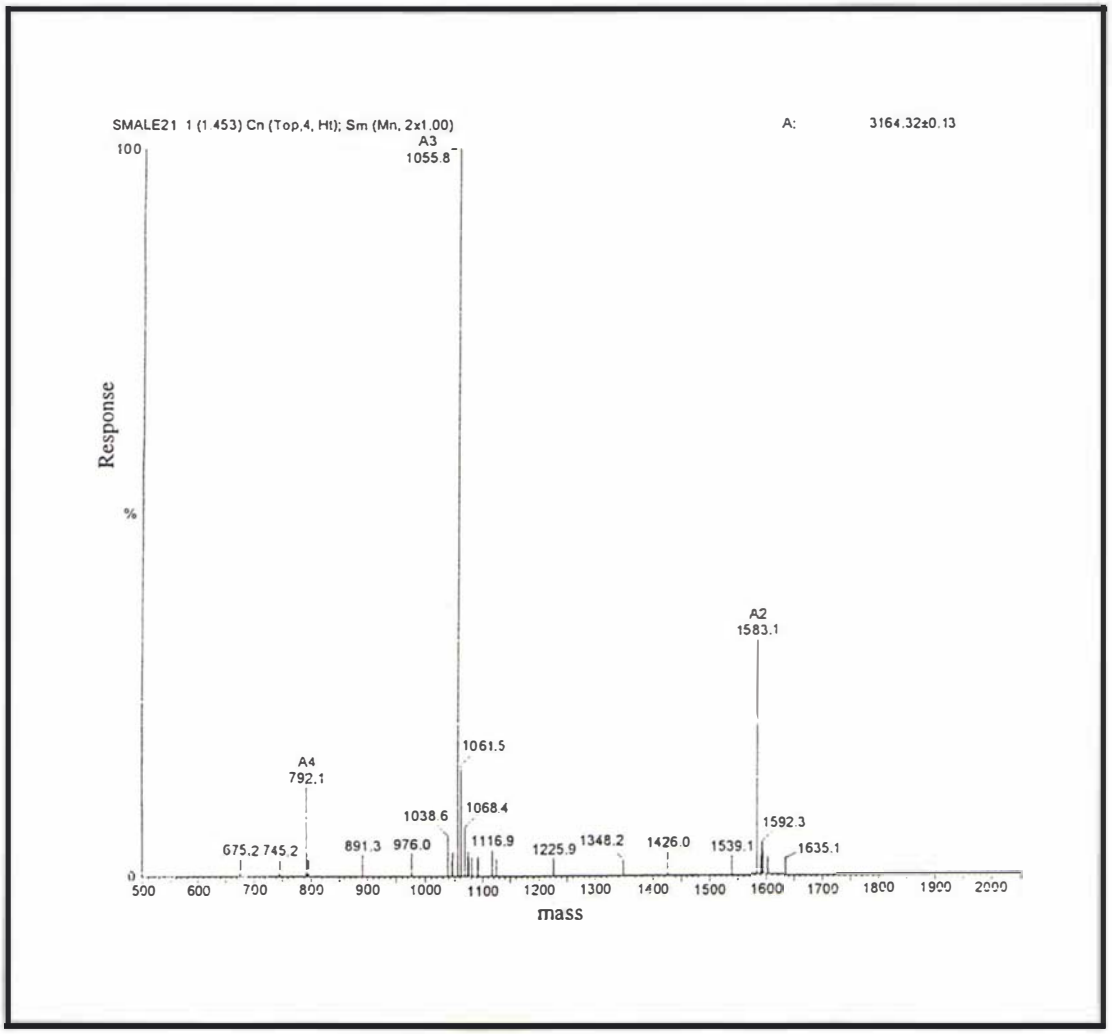


**Fig. 3.3.11** A typical electrospray mass spectrometry analysis as recorded for peptide peak m (see Table 3.3.4) derived from the tryptic digestion of E1G-lysozyme conjugates. The m/z charge ratio's are shown as A4 (m/4), A3 (m/3) and A2 (m/2) and the calculated mass for the peptide is shown in the top right hand corner (calculated mass = 3164.3).

**Table 3.3.5**

Sequence and mass spectral data for the estrone glucuronide acylated lysozyme tryptic peptides

| Peptide peak | Sequence data | Calculated m/z | Experimental m/z | Acylation location |
|---|---|---|---|---|
| c | $C^{\dagger}K^{*}$GTDVQAW$^{**}$ | 1492.7 | 1493.0 | Lys 116 |
| d | $K^{*}$IVSDGNGMNAW$^{**}$ | 1718.9 | 1719.3 | Lys 97 |
| f | $C^{\dagger}K^{*}$GTDVQAWIR | 1762.7 | 1762.5 | Lys 116 |
| i | $K^{*}$IVSDGNGMNAWVA WR | 2231.9 | 2231.5 | Lys 97 |
| j | $K^{*}$IVSDGNGM**D**AWVA WR | 2232.9 | 2233.5 | Lys 97 |
| k | $^{**}$SLGNWVC$^{\dagger}$AAK$^{*}$FE SNFNT**Q**ATNR | 2943.2 | 2943.9 | Lys 33 |
| k' | $^{**}$SLGNWVC$^{\dagger}$AAK$^{*}$FE SNFNT**E**ATNR | 2944.2 | 2944.7 | Lys 33 |
| m | GYSLGNWVC$^{\dagger}$AAK$^{*}$F ESNFNT**Q**ATNR | 3164.4 | 3164.3 | Lys 33 |
| o | GYSLGNWVC$^{\dagger}$AAK$^{*}$F ESNFNT**E**ATNR | 3165.2 | 3166.8 | Lys 33 |

**Key - for details see text**
$C^{\dagger}$ = S-carboxymethylated cysteine
$K^{*}$ = estrone glucuronide acylated lysine residue
$^{**}$ = chymotryptic cleavage at this site
Amino acid letters in **bold** are involved in amide/carboxylic acid interchanges (for details see text).

### 3.3.5 Characterisation of PdG-Lysozyme Conjugate Families

In the tryptic digest maps of the pregnanediol glucuronide-lysozyme conjugate families, certain lysine containing peptides disappeared, or diminished in height, relative to the tryptic map of lysozyme, as was the case for the estrone glucuronide-lysozyme conjugate digests. Again new peaks appeared later in the HPLC gradient at much higher acetonitrile concentrations than for the native peptides (after peak 20, Fig. 3.3.12a). These new peaks also eluted at higher acetonitrile concentrations than did the estrone glucuronide acylated peptides (see section 3.3.4), presumably due to the extra hydrophobicity associated with the pregnanediol glucuronide moiety. The amino acid sequences of these later eluting lysine acylated peptides (b-f) were again matched with the known sequences of the tryptic peptides from hen egg white lysozyme [117, 172]. As in the case of estrone

glucuronide, the acylated peptides did not exhibit a lysine peak where expected from the known tryptic peptide sequence during sequence analysis. However, unlike the estrone glucuronide acylated peptides, a new peak was not observed eluting off the sequencer HPLC column after all of the other amino acid peaks. From the tryptic maps it was also evident that lysine residue 96 was unmodified in all of the conjugate families as was the case for the estrone glucuronide conjugate families, since the peptide peak T11 (residues 74-96, peak 20 Fig. 3.3.12a) did not change significantly in height, area or elution characteristics (relative to the native peptide peaks 1 and 3, the areas and heights of which are not affected by acylation of any lysine residues in the lysozyme molecule).

N-terminal sequencing of the intact conjugates as described in section 3.3.4 showed that the N-terminal α-amino group and both the ε-amino groups of lysine residues 1 and 13 were unmodified in all of the PdG-lysozyme conjugate families, as found for the estrone glucuronide conjugates. This was confirmed by the peptide mapping results. In all of the conjugate tryptic maps the peptide peaks $T_{1+2}$ (residues 1-5, peak 2 Fig. 3.3.7a and 3.3.12a) and $T_3 + T_{3+4}$ (residues 6-14, peaks 7-11 Fig. 3.3.7a and 3.3.12a) remained unchanged in height and area relative to the tryptic map for the lysozyme control.

*3.3.5.1 Tryptic digestion of pregnanediol glucuronide-lysozyme conjugate families P1 and P2*

The tryptic digest of conjugate peak P1, prepared by the active ester method (Fig. 3.3.12c), was very similar to the map obtained for the tryptic digest of the estrone glucuronide conjugate E1 (section 3.3.4.1, Fig. 3.3.7b). Two sets of major new peptide peaks (b and c, d and e) were eluted later in the gradient than any of the native lysozyme tryptic peptides, while peptides 16, 17 and 18, from which peptides b-e are comprised, decreased in height. Peptides b and c were the result of acylation of lysine residue 116 with pregnanediol glucuronide (Tables 3.3.6 and 3.3.7). Peptide c consisted of $T_{15+16}$ (residues 115-125) acylated at lysine residue 116 while peptide b was also acylated at residue 116 but was not the complete $T_{15+16}$ peptide due to C-terminal chymotryptic cleavage (Table 3.3.7) and hence eluted just before peptide c. Peptides d and e were both the result of acylation at lysine residue 97 with pregnanediol glucuronide. The difference between the two peaks was that peak e had undergone an amide/carboxylic acid interchange at residue 106 from asparagine (N, $-CH_2-CO-NH_2$) to aspartate (D, $-CH_2-COO^-$) as confirmed by amino acid sequencing and electrospray mass spectrometry (Table 3.3.7).

In contrast, the tryptic digest of conjugate family P1 prepared by the mixed anhydride method (Fig. 3.3.12b) contained only one major set of new peptide peaks. Once again

**Table 3.3.6**

The positions of acylation of lysozyme with pregnanediol glucuronide in the lysozyme-pregnanediol glucuronide conjugates characterised as described in the text

| PdG-lysozyme conjugate | Number of PdG molecules per lysozyme molecule* | Acylated peptide(s) | Corresponding peptide peaks† | Location of acylation position |
|---|---|---|---|---|
| AE P1 | 1 | $T_{12+13}$ | d, e | 97 |
| | | $T_{15+16}$ | b, c | 116 |
| AE P2 | 2 | $T_{12+13}$ | d, e | 97 |
| | | $T_{15+16}$ | b, c | 116 |
| AE P3 | 1 | $T_{6+7}$ | f | 33 |
| | | $T_{12+13}$ | d (minor amounts) | 97 |
| | | $T_{15+16}$ | b (minor amounts) | 116 |
| AE P4 | 2 | $T_{6+7}$ | f | 33 |
| | | $T_{15+16}$ | b, c | 116 |
| AE P5 | 2# | $T_{6+7}$ | f | 33 |
| | | $T_{12+13}$ | d, e | 97 |
| | | $T_{15+16}$ | b | 116 |
| AE P6 | 3 | $T_{6+7}$ | f | 33 |
| | | $T_{12+13}$ | d, e | 97 |
| | | $T_{15+16}$ | b, c | 116 |
| MA P1 | 1 | $T_{12+13}$ | d, e | 97 |
| MA P3 | 1 | $T_{6+7}$ | f | 33 |
| MA P4 | 2 | $T_{6+7}$ | f | 33 |
| | | $T_{15+16}$ | b, c | 116 |
| MA P5 | 2 | $T_{6+7}$ | f | 33 |
| | | $T_{12+13}$ | d, e | 97 |

**Key**

AE = active ester conjugate family
MA = mixed anhydride conjugate family
* = determined from proteolytic studies and titration of lysine groups with trinitrobenzenesulfonic acid (see chapter two for details)
† = see Figs. 3.3.12, 3.3.13 and 3.3.14
\# = although for the active ester conjugate family P5 there are only two PdG molecules per lysozyme molecule, there are three acylation positions. This is because none of the three lysine positions are completely acylated in all of the lysozyme molecules. As a result the residues are only partially acylated and the sum of these gives an overall substitution ratio of two PdG molecules per lysozyme molecule as determined by titration with trinitrobenzenesulfonic acid (see text for details).

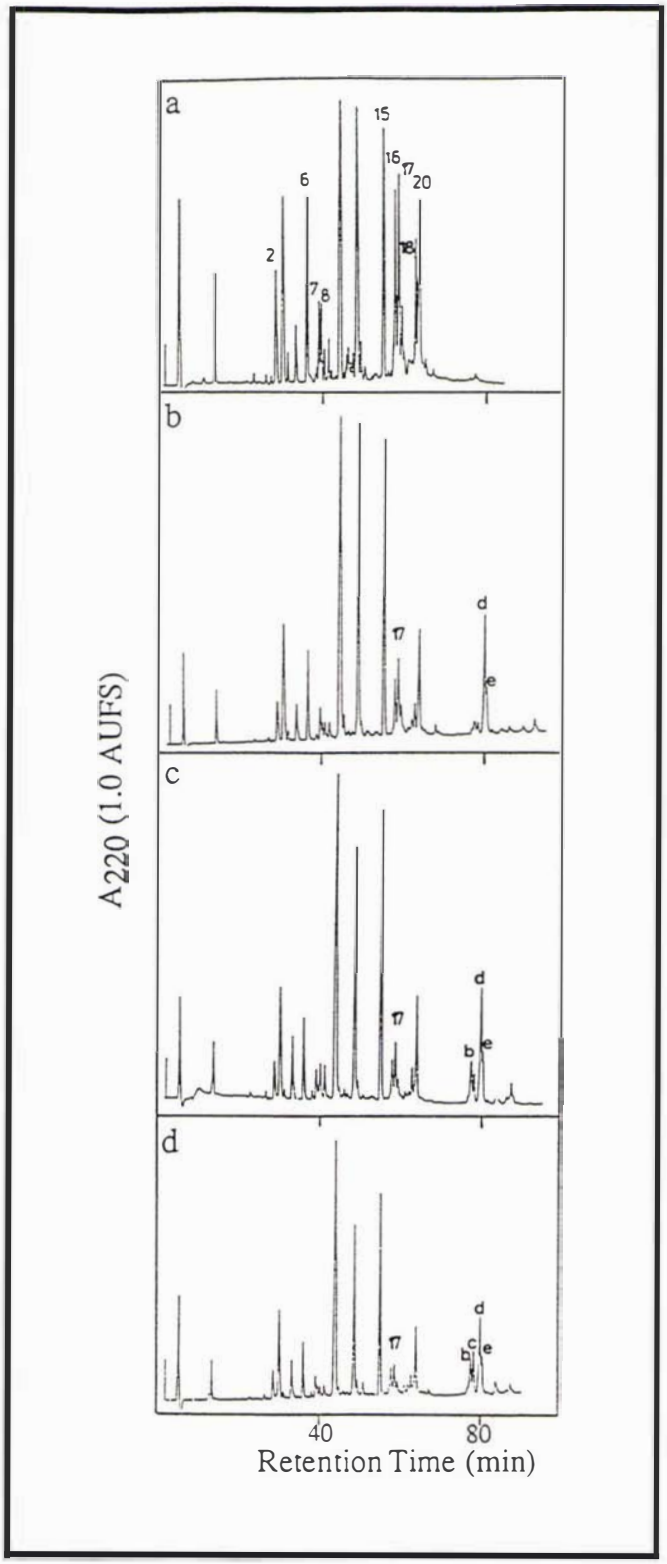


**Fig. 3.3.12** Reversed-phase HPLC separation of the tryptic peptides from tryptic digests of unmodified lysozyme (a), mixed anhydride PdG-lysozyme conjugate P1 (b), and active ester PdG-lysozyme conjugates P1 (c), and P2 (d). The numbers refer to unmodified tryptic peptides and the letters to acylated tryptic peptides. For conditions and details see text.

the presence of peaks d and e, along with the decrease in height and area of peaks 16, 17 and 18 (by approximately 70-75% relative to the native digest), showed acylation had

occurred at lysine residue 97. This was confirmed by amino acid sequencing and electrospray mass spectrometry (Table 3.3.7) as described for the estrone glucuronide acylated peptides. Only very small amounts of peptides b and c resulting from the acylation of lysozyme with pregnanediol glucuronide at lysine residue 116 were detected.

The tryptic digest of the pregnanediol glucuronide-lysozyme active ester conjugate P2 (Fig. 3.3.12d) showed that acylation had occurred at lysine residues 97 and 116 as in the active ester conjugate P1. The areas of the new peaks (b-e) and the diminished heights of peaks 16-18, compared to the decrease in height in the P1 active ester digest, showed that lysine residues 97 and 116 were acylated to a greater extent in conjugate family P2 than in conjugate family P1, consistent with the lysine titration data in Table 3.3.6.

*3.3.5.2 Tryptic digestion of pregnanediol glucuronide-lysozyme conjugate families P3 and P4*

The elution patterns obtained for the tryptic digests of the P3 and P4 active ester and mixed anhydride conjugate families are shown in Fig. 3.3.13. In the case of the P3 conjugate digests, differences were observed between the active ester and mixed anhydride conjugate tryptic maps. In the tryptic map of the active ester P3 conjugate (Fig. 3.3.13b), peptides $T_6$ (residues 22-33, peak 15), $T_7$ (residues 34-45, peak 6) and $T_{12}$ + $T_{12+13}$ (residues 97-112) had diminished in height compared to the native digest and the new peptide peaks b, d and f were present. Peak f was comprised of peptide $T_{6+7}$ (residues 22-45) acylated at lysine residue 33 with pregnanediol glucuronide (Tables 3.3.6 and 3.3.7). Peptide peaks b and d were the result of acylation at lysine residues 116 and 97 as previously described. In the mixed anhydride P3 conjugate digest (Fig. 3.3.13a) only one predominant new peak was observed (peak f), while peaks 6 and 15 had diminished in height from major peaks (as seen in the native digest), to minor peaks. The mixed anhydride P3 conjugate was therefore almost exclusively acylated at lysine residue 33.

The digest patterns of the active ester and mixed anhydride P4 conjugates are shown in Figs. 3.3.13c and 3.3.13d. The tryptic maps for the two P4 digests were very similar. In both cases the peptide peaks 6 ($T_7$) and 15 ($T_6$) had diminished considerably in height and the major new peak was peak f, comprising the peptide $T_{6+7}$ acylated at lysine residue 33 as previously described. Significant amounts of peptide peaks b and c were also observed in the tryptic maps due to the acylation of lysine residue 116. A small amount of peptide d was also detected, corresponding to acylation at lysine residue 97 (Table 3.3.7).

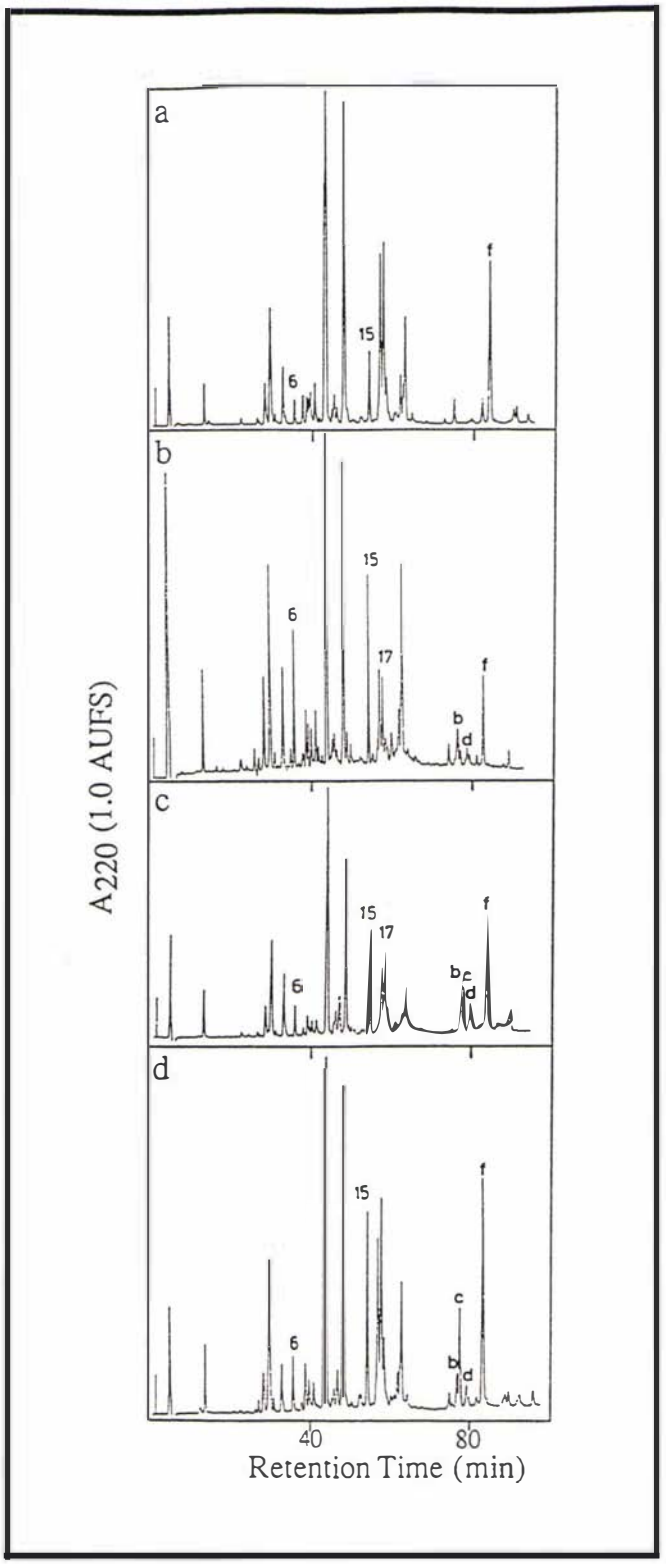


**Fig. 3.3.13** Reversed-phase HPLC separation of the tryptic peptides from the tryptic digests of mixed anhydride PdG-lysozyme conjugates P3 (a), and P4 (d), and active ester PdG-lysozyme conjugates P3 (b) and P4 (c). The numbers refer to unmodified tryptic peptides and the letters to acylated tryptic peptides. For conditions and details see text.

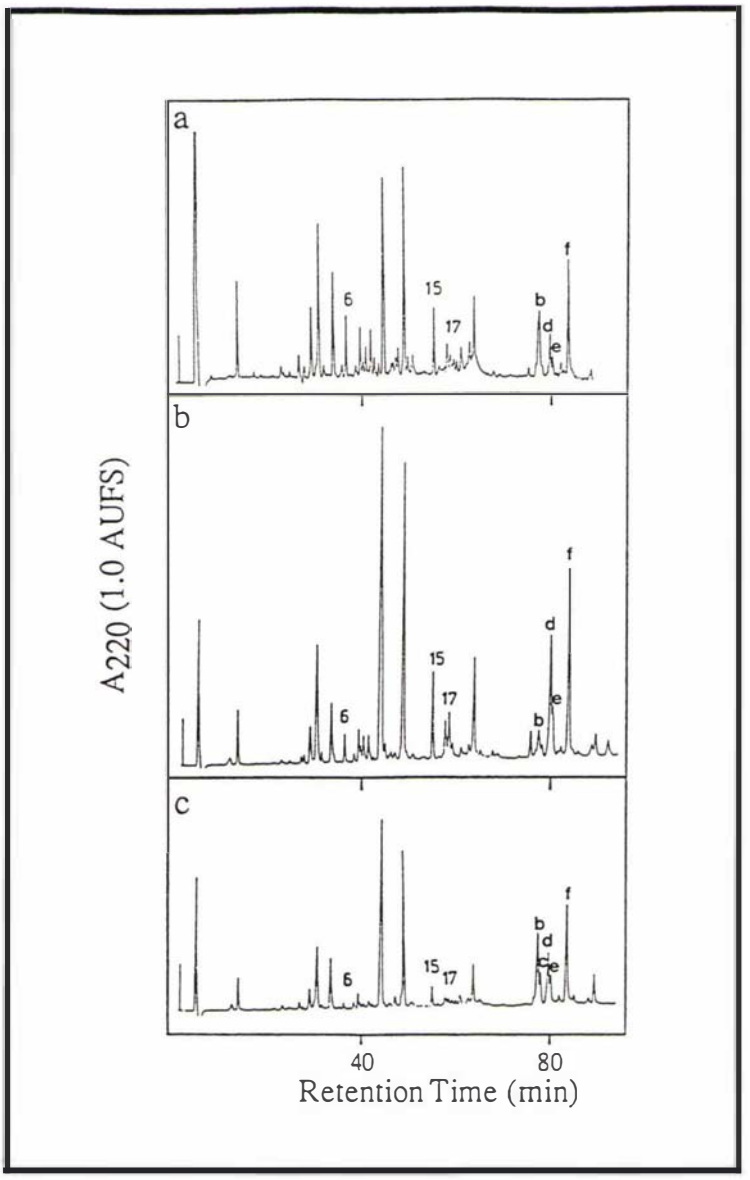


**Fig. 3.3.14** Reversed-phase HPLC separation of the tryptic peptides from the tryptic digests of active ester PdG-lysozyme conjugates P5 (a), and P6 (c), and mixed anhydride PdG-lysozyme conjugate P5 (b). The numbers refer to unmodified tryptic peptides and the letters to acylated tryptic peptides. For conditions and details see text.

### *3.3.5.3 Tryptic digestion of pregnanediol glucuronide-lysozyme conjugate families P5 and P6*

The elution profiles obtained for tryptic digestion of the active ester conjugate P5, mixed anhydride conjugate P5 and active ester conjugate P6 are shown in Figs. 3.3.14a, 3.3.14b and 3.3.14c. In the case of the P5 conjugates, the major new peptide peak for both the mixed anhydride and active ester conjugates was peak f, corresponding to acylation at lysine residue 33 (Table 3.3.7). However, there was a difference between the active ester and mixed anhydride P5 conjugates in the appearance of the other new peptide peaks. The mixed anhydride P5 tryptic map contained large amounts of peaks d and e arising from the acylation of lysine residue 97 however, there was only a very

small peak (peak b) arising from the acylation of lysine residue 116. On the other hand, the tryptic map of the active ester P5 conjugate contained the peptide peaks b, d, and e (Fig. 3.3.14a). Lysozyme peaks 16, 17 and 18 had almost disappeared suggesting lysine residue 97 was almost completely acylated. Peptide peak b was also present in large amounts, indicating significant acylation at lysine residue 116 in this case. The most highly modified conjugate, active ester conjugate P6, was found to be almost completely acylated at all three lysine residues (33, 97 and 116). The new peptide peaks (b-f) were all present (Fig. 3.3.14c) while the peaks from which these new peptides are derived (peaks 6, 15, 16-18) had all diminished in size so as to be barely detectable.

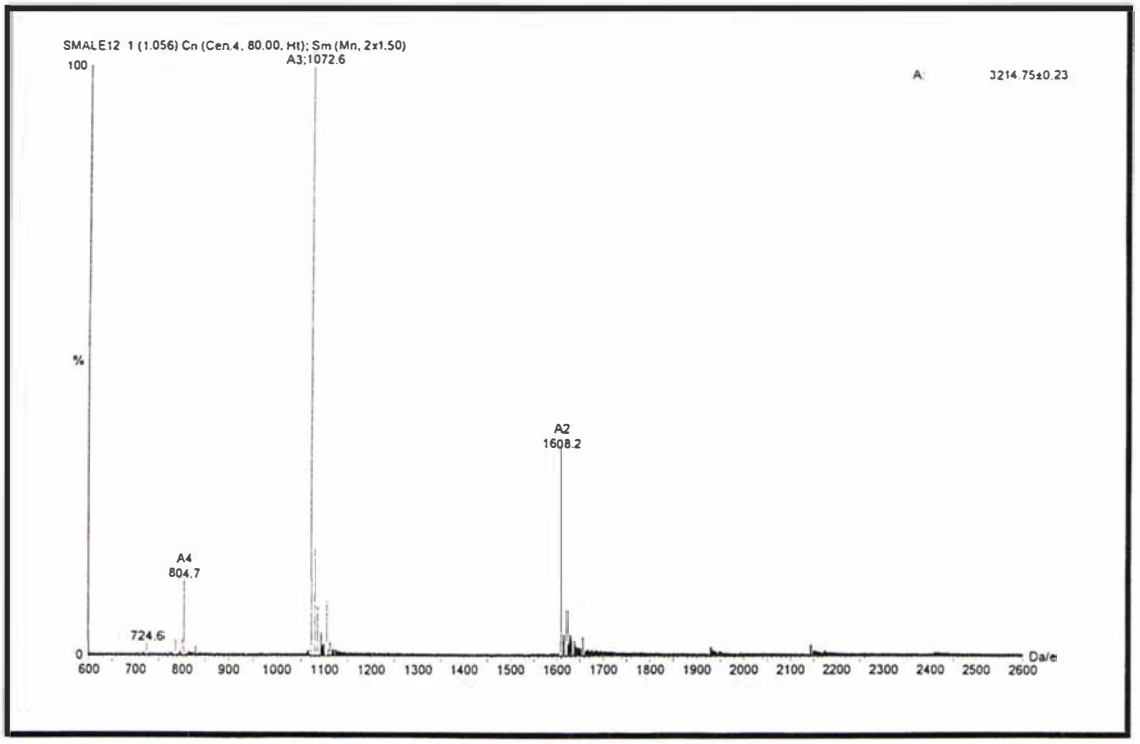


**Fig. 3.3.15** A typical electrospray mass spectrometry analysis recorded for peptide peak f derived from the tryptic digestion of PdG-lysozyme conjugates. The m/z charge ratio's are shown as A4 (m/4), A3 (m/3) and A2 (m/2) and the calculated mass for the peptide is shown in the top right hand corner (calculated mass = 3214.8).

*3.3.5.4 Mass spectral data for the pregnanediol glucuronide acylated peptides*

The mass spectral data obtained for the pregnanediol glucuronide acylated lysozyme tryptic peptides are reported in Table 3.3.7. The mass spectral data were calculated and interpreted as described for the estrone glucuronide-lysozyme conjugate data in section 3.3.4.4, except that the mass of an acylated peptide was 478 mass units greater than the native, unmodified peptide, due to the presence of PdG. In all cases the calculated and experimental results were in good agreement and unambiguously identified the assigned peptide as confirmed by amino acid sequencing. A typical mass spectral analysis of a pregnanediol glucuronide acylated peptide is shown in Fig. 3.3.15. Because the mass

spectral data unambiguously identified the peptides with lysine 97 acylated with PdG it was not necessary to undertake manual Edman sequencing as described in section 3.3.4.1.

**Table 3.3.7**

Sequence and mass spectral data for the pregnanediol glucuronide acylated lysozyme tryptic peptides

| Peptide peak | Sequence data | Calculated m/z | Experimental m/z | Acylation location |
|---|---|---|---|---|
| b | $C^{\dagger}K^{*}$GTDVQAW** | 1542.7 | 1543.4 | Lys 116 |
| c | $C^{\dagger}K^{*}$GTDVQAWIR | 1812.7 | 1812.4 | Lys 116 |
| d | $K^{*}$IVSDGNGMNAWVA WR | 2281.9 | 2281.8 | Lys 97 |
| e | $K^{*}$IVSDGNGMDAWVA WR | 2280.9 | 2280.4 | Lys 97 |
| f | GYSLGNWVC$^{\dagger}$AAK$^{*}$F ESNFNTQATNR | 3214.4 | 3214.8 | Lys 33 |

**Key - for details see text**
$C^{\dagger}$ = S-carboxymethylated cysteine
$K^{*}$ = pregnanediol glucuronide acylated lysine residue
** = chymotryptic cleavage at this site

### 3.3.6 Analysis of Estrone Glucuronide-Lysozyme Conjugates by Acid-Polyacrylamide Gel Electrophoresis

The estrone glucuronide-lysozyme conjugates prepared by the active ester method were used in the development of an acid-polyacrylamide gel electrophoresis (acid-PAGE) system for the analysis of conjugation products. The acid-PAGE analysis was then compared with the analysis of the conjugates by Mono-S cation-exchange chromatography in 7 M urea, as described in chapter two. Acid-PAGE electrophoresis showed evidence of seven distinct conjugate populations (Fig. 3.3.16) for the active ester E1G-lysozyme conjugates as previously seen on the Mono-S cation-exchange column in 7 M urea (Fig. 3.3.1B). Positive identification of the acid-PAGE populations was achieved by diffusing each band from the gel and running it through the Mono-S 7 M urea system, or alternatively by collecting each conjugate fraction from the Mono-S 7 M

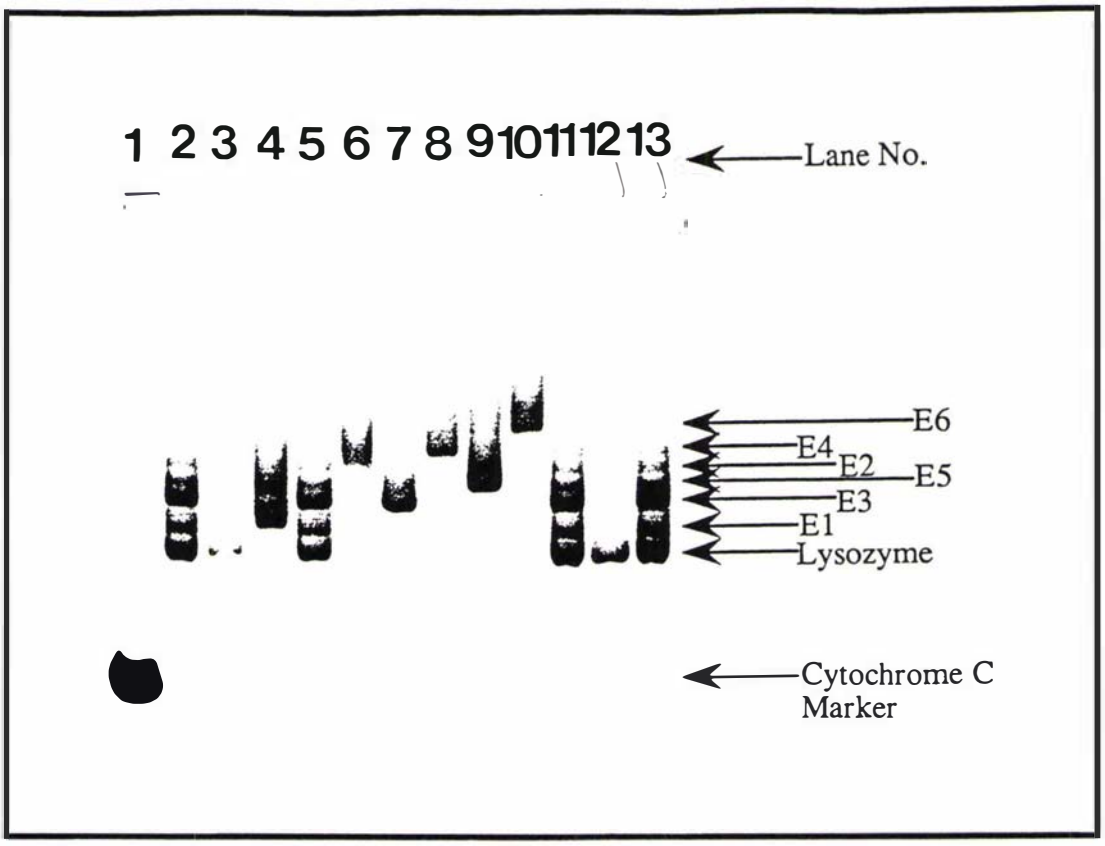


**Fig. 3.3.16** Analysis of E1G-lysozyme active ester conjugates by acid-PAGE as described in the text. Cytochrome C was run as a marker (lane 1) while the E1G-lysozyme active ester conjugation reaction mixture was run in lanes 2, 5, 11, and 13. The individual conjugate peaks as collected off the Mono-S column (as shown in Fig. 3.3.1B) were also analysed on the gel. Unreacted lysozyme (lane 3), conjugate families E1 (lane 4), E2 (lane 6), E3 (lane 7), E4 (lane 8), E5 (lane 9), and E6 (lane 10) were also run along with a sample of pure lysozyme which had not been involved in a conjugation reaction (lane 12).

urea column and running it on the acid-PAGE system (Fig. 3.3.16). The order of separation of the E1G-lysozyme conjugates by acid-PAGE was not a simple correspondence between the degree of substitution and the distance travelled towards the negative electrode down the gel. Based on the data of Figure 3.3.1B, the distance each conjugate travels on the acid-PAGE system should decrease in the order L > E1 > E2 > E3 > E4 > E5 > E6, this being the order of increasing positive charge as deduced from the Mono-S 7 M urea column. On the acid-PAGE system (Fig. 3.3.16) lysozyme, which migrated the furthest, followed the expected order. However, the order of migration of conjugates E2-E5 was in fact E3 > E5 > E2 > E4. In effect conjugates E3 and E5 both migrated further down the gel than expected from their chromatographic behaviour. Conjugate E1 migrated in two bands, one travelling to the expected position, its distance travelled being only second to lysozyme, while a second band was also detected. The distances relative to unreacted lysozyme that the conjugates travelled by acid-PAGE, compared to their elution positions in 7 M urea on a Mono-S column are summarised in Table 3.3.8.

**Table 3.3.8**

Retention of the E1G-lysozyme conjugates prepared by the active ester method on a Mono-S column in 7 M urea and the distance migrated by the E1G-lysozyme conjugates by acid-PAGE relative to unreacted lysozyme

| Conjugate peak | Rf value by cation-exchange chromatography in 7 M urea | Rf value by acid-PAGE analysis |
|---|---|---|
| unreacted lysozyme | 1.00 | 1.00 |
| E1 (acylated at lysine 97) | 0.93 | 0.92 |
| E1 (acylated at lysine 116) | 0.93 | 0.81 |
| E2 | 0.87 | 0.73 |
| E3 | 0.82 | 0.86 |
| E4 | 0.77 | 0.69 |
| E5 | 0.74 | 0.78 |
| E6 | 0.69 | 0.64 |

It has been reported that silver stains detect proteins on acrylamide gels with one hundred times higher sensitivity than the more traditional Coomassie blue stain [176]. The acrylamide gels were therefore stained using either of the silver stain procedures of Tsai and Frasch [177], or Dubray and Bezard [178]. However, when the estrone glucuronide-lysozyme conjugates were stained using either silver stain procedure [177-178] the sensitivity was lower than that observed using the Coomassie blue stain. Several of the higher modified conjugates could not be detected at all, or only very weakly, when using the silver stain. The reason for this is not clear. As a result the silver stain procedures were not used for the detection of the estrone glucuronide-lysozyme conjugates and all gels were stained with Coomassie blue stain. The migration positions of the PdG-lysozyme conjugates when analysed by acid-PAGE have not yet been determined.

## 3.4 Discussion

### 3.4.1 The Effect of the Acylating Agent on the Preparation of Estrone Glucuronide-Lysozyme and Pregnanediol Glucuronide-Lysozyme Conjugates

At first sight there does not appear to be much difference between the active ester and mixed anhydride reagents (see schemes 2.2.2 and 3.2.1). Since the active ester methodology is easier to perform, it is used more often in protein conjugation reactions, especially in the hands of non-organic chemists. However, the present data show that there are significant differences between the two methods and hence careful consideration needs to be given to the choice of reagent, depending on the aims of the study.

Attachment of the hydrophobic estrone glucuronide moiety to the ε-amino groups of lysine residues in hen egg white lysozyme, modified both the charge properties of the protein (see Figs. 3.3.1A and 3.3.2a for example), and its overall polarity. The active ester reagent was more reactive than the mixed anhydride reagent as it gave a more diverse range of conjugate products at the same ratio of steroid glucuronide to lysozyme (Figs. 3.3.1A and 3.3.1B). Amongst the six conjugate families E1 and E3 predominated. The mixed anhydride method was clearly much more selective than the active ester method giving mainly conjugate family E3 (Fig. 3.3.1A). Mattox *et al.* [179] also found that active ester reagents result in a much greater degree of substitution than conjugates produced with the isobutylchloroformate mixed anhydride method when coupling steroidal glucosiduronic acids to bovine serum albumin. The difference in the reactivity of the two reagents (active ester and mixed anhydride), is possibly due to the difference in solubility. The N-hydroxysuccinimide ester is likely to be much more soluble than the mixed anhydride reagent, when added to the aqueous lysozyme solution, and as a result would be expected to react faster, acylating more residues and to a greater extent. In support of this suggestion, the active ester reaction was almost instantaneous, as was shown by analysis of the reaction mixture after 2, 5, 60, 180 minutes and an overnight reaction aliquot. Analysis of the timed aliquots from the reaction mixture by Mono-S 7 M urea cation-exchange chromatography showed that no additional conjugation products were formed after the first 2 minutes and the relative peak heights were unchanged, indicating that the reaction between the active ester reagent and lysozyme must be very fast. On the other hand, the mixed anhydride reagent reacted much more slowly over several hours and evidence that this was the case was seen in the slow pH drop as the reagent reacted with lysozyme. The amount of NaOH required to readjust the pH was usually approximately equal to the number of moles of steroid glucuronide (or amount of

mixed anhydride reagent) and this volume was added over several hours, indicating the on going, slow reaction of the mixed anhydride reagent with lysozyme.

Acylation of hen egg white lysozyme with pregnanediol glucuronide using the mixed anhydride procedure was also more specific than the active ester method, resulting in two main conjugate peaks (P1 and P3), although small amounts of conjugate peaks P4 and P5 were also present (Fig. 3.3.4A). The active ester method again gave a more diverse range of conjugate products at the same molar ratio of pregnanediol glucuronide to lysozyme (Fig. 3.3.4B). Conjugate families P1 and P3 also predominated in the active ester conjugation mixture (as discussed in chapter two) however, quite large amounts of conjugate families P2, P4, P5 and P6 were also present (Fig. 3.3.4B).

The active ester reagent resulted in a greater conjugate yield than the mixed anhydride reagent in both the estrone glucuronide and pregnanediol glucuronide reactions and could be carried out at room temperature. It was also less time consuming and technically less demanding than the mixed anhydride procedure but the complexity of the product mixture makes purification and study of the conjugates more difficult. For use in immunoassays the extra complexity of the product mixture was an undesirable feature since the relatively large amounts of the more highly substituted conjugates produced (E4, E5, and E6) had low specific activities. Because of the extra number of steroid glucuronide moieties, these conjugates required more antiserum to inhibit their lytic activity, making them less suitable for homogeneous enzyme immunoassay. However, the greater conjugate yield from the active ester reagent was a positive factor in the characterisation of the individual conjugate families since more of each was available for purification than with the mixed anhydride reaction. The mixed anhydride reaction gave a more selective range of conjugates which had low substitution levels and could be purified easily. However, the mixed anhydride reaction is difficult to control and although the reagent can be stabilised by cooling, disproportionation [180] is also possible which can result in a halving of the conjugate yield.

### 3.4.2 The Purification of Individual Estrone Glucuronide-Lysozyme and Pregnanediol Glucuronide-Lysozyme Conjugates

*3.4.2.1 Isolation and purification of individual estrone glucuronide-lysozyme conjugate families*

The estrone glucuronide-lysozyme conjugate profiles obtained on the S-Sepharose column correlated directly with those from an analytical Mono-S cation exchange column as described previously (section 2.2.3.6), except for the small mixed anhydride conjugate

peak E1, which eluted under the large lysozyme peak on the S-Sepharose (fast flow) column. The S-Sepharose column in 7 M urea is the first procedure reported which allows the separation and purification of large quantities of individual conjugate populations. As a result, sufficient amounts of the conjugate populations could be purified so that they could be studied individually and this has previously not been possible. Although the procedure outlined in chapter two gave E1G-lysozyme conjugate suitable for use in homogeneous enzyme immunoassays the product was still a mixture of conjugate families (see Fig. 2.3.6B).

The specific activities of the active ester conjugates E1, E2, and E3 were similar to those of native lysozyme (Table 3.3.1). However E4, E5, and E6 had much lower specific activities than lysozyme, or E1, E2, and E3 (Table 3.3.1). The decrease in specific activities of the conjugate families E1-E6 mirrors the increasing substitution ratio of conjugates E1-E6. Conjugate E6 is the most highly substituted with three estrone glucuronide molecules per enzyme molecule (Table 3.3.4) and has the lowest relative specific activity (Table 3.3.1), while conjugates E1 and E3 have the lowest substitution ratio (Table 3.3.4), with one estrone glucuronide molecule per enzyme molecule, and the highest relative specific activities (Table 3.3.1). Other lysozyme conjugates, such as the palmitic acid-lysozyme conjugates of Nakamwa *et al.* [181] produced by the active ester method, resulted in a conjugation mixture with an average of two palmitic acid molecules per enzyme molecule and a specific activity of 71% (relative to a lysozyme control), once again showing a decrease in the specific activity upon acylation at lysine residues. It is well established that the loss in the specific activity of lysozyme conjugates acylated at lysine amino groups is due to a decrease in the enzymatic positive charge when measured using *Micrococcus lysodeikticus* as substrate [182-184]. It has been proposed that this loss in specific activity reflects an alteration in the electrostatic interaction between the positively charged enzyme and the negatively charged cell wall [185]. The mixed anhydride E3 conjugate, with a substitution level of only one estrone glucuronide per enzyme molecule (Table 3.3.4), had a specific activity, within experimental error, the same as unmodified, native lysozyme (Table 3.3.1).

Despite the chromatographic and electrophoretic analysis (see section 3.3.6) of the estrone glucuronide-lysozyme conjugate families purified using the S-Sepharose (fast flow) column showing each conjugate to be homogeneous and to contain no unpurified lysozyme, the lytic activities were again only inhibited by 75-80% in the presence of excess E1G-antibody. Exposure to 7 M urea denaturing conditions cannot be responsible for the inadequate inhibition observed as previously discussed in sections 2.4.2.2 and 2.4.2.5. Clearly the same contact denaturation is occurring between the conjugates and

the packing material (in this case the S-Sepharose (fast flow) matrix) as described in section 2.4.2.5.

Passage of the purified conjugates through a Butyl Sepharose hydrophobic interaction column gave conjugate products which were adequately inhibited (> 90%) in the presence of excess E1G-antibody. This was consistent with the fact that conjugates passed through an Alkyl Superose hydrophobic interaction column (as described in chapter two) also showed increased inhibition. A small amount of material does elute first from the column which is not adequately inhibited by anti-E1G antibodies (inhibited to the same extent as after cation-exchange chromatography) however, the removal of this small amount of material from the bulk conjugate fraction would not be expected to increase the inhibition level to the extent observed experimentally. Thus, the early eluting peak may be due to column overloading and as a result the conjugates within this peak are not binding to the column matrix and the column effect is not felt by these conjugates. The column effect reversing the deleterious effect of the cation-exchange column interaction is presumably the same as that between the conjugates and an Alkyl Superose column as discussed in sections 2.4.2.4 and 2.4.2.5.

*3.4.2.2 Isolation and purification of individual pregnanediol glucuronide-lysozyme conjugate families*

The individual pregnanediol glucuronide-lysozyme conjugate families were successfully isolated from each other and unreacted lysozyme by large scale chromatography on an S-Sepharose (fast flow) column in 7 M urea solutions (Fig. 3.3.5). The resulting $A_{280}$ profiles correlated directly with those obtained from an analytical Mono-S cation-exchange column (see Fig. 3.3.4). Again the specific activities of the mixed anhydride conjugates P1 and P3, were similar to unreacted lysozyme (Table 3.3.2) although the activity of conjugate P3 was lower than the corresponding estrone glucuronide E3 conjugate reported in section 3.3.1 (93 v 99.5%). Active ester conjugates P1 and P3 also had specific activities similar to unreacted lysozyme (Table 3.3.2) however, once again, the activities were lower than the corresponding estrone glucuronide conjugates (92 v 95.1% for the P1 and E1 conjugates; 88 v 94% for the P3 v E3 conjugates). Titration of the free amino groups showed that all of the conjugates P1, E1, P3 and E3, were acylated at a level of one steroid glucuronide molecule per lysozyme molecule.

The specific activity of the active ester P2 conjugate family, with a substitution ratio of two steroid glucuronide molecules per lysozyme molecule, was only 75% of that of unreacted lysozyme (Table 3.3.2). Since the active ester estrone glucuronide E2 conjugate reported in section 3.3.1 had a specific activity 88% that of unreacted lysozyme, attachment of PdG to lysozyme decreased the lytic activity of the enzyme to a

greater extent than attachment of E1G. The effect could be due to the greater hydrophobicity associated with the pregnanediol glucuronide moiety, but a mechanism based on this factor is not obvious since precise details of the structure of the *Micrococcus lysodeikticus* surface are unknown. The conjugation of a PdG moiety to lysozyme must however result in greater interference (than an E1G molecule) between the processes of binding and association of the negatively charged *Micrococcus lysodeikticus* cell wall substrate [186] to the net positively charged lysozyme enzyme. If this is true, $K_M$ (the substrate concentration at which the reaction rate is half of its maximal value) for the PdG-lysozyme conjugates may be higher than for the E1G-lysozyme conjugates, however data to confirm this is not presently available. The more highly substituted active ester PdG conjugates (P4, P5 and P6) all had much lower specific activities than unreacted lysozyme (Table 3.3.2) as expected from the specific activities of the corresponding more highly substituted E1G conjugates (E4, E5 and E6). Overall, the results again show that the mixed anhydride reagent is preferable to the active ester reagent for the production of conjugates suitable for homogeneous enzyme immunoassay as it generates conjugates with low substitution ratio's. The major conjugate products in both the E1G and PdG reaction mixtures consisted of monosubstituted products. However, in the case of PdG, the mixed anhydride procedure did give a more diverse range of conjugate products when compared with the conjugate products resulting from acylation of lysozyme with E1G.

For the identification of the acylation sites of lysozyme with pregnanediol glucuronide, the relatively low inhibition of the lytic activities of the conjugate families in the presence of excess anti-PdG antibody was not considered a concern. While passage through a Butyl Sepharose hydrophobic interaction column increased the lytic inhibition of the conjugates from 80-85% to 90%, this step was not deemed necessary for the characterisation of the conjugates. The work reported on the characterisation of estrone glucuronide-lysozyme conjugates showed that the extra chromatography step did not affect the observed substitution ratio's, amounts or positions of acylation within conjugate families. Therefore the pregnanediol glucuronide conjugates purified by S-Sepharose (fast flow) chromatography were used for characterisation experiments without further purification, provided that each was homogeneous as shown by Mono-S 7 M urea cation-exchange chromatography.

### 3.4.3 Characterisation of Individual E1G-Lysozyme Conjugate Families

The positions of acylation in the estrone glucuronide-lysozyme conjugate families were determined from tryptic digestion experiments. The serine protease, trypsin cleaves on the C-terminal side of positively charged lysine (K), arginine (R) and modified, amino

ethyl cysteine residues [187]. It will not cleave N-terminal lysine, arginine or amino ethyl cysteine residues and generally will not cleave on the C-terminal side of a Lys-Pro or Arg-Pro sequence. Trypsin should therefore cleave on the C-terminal side of lysine and arginine residues in hen egg white lysozyme to give eighteen tryptic peptides. However, in the estrone glucuronide-lysozyme conjugate digests an acylated lysine residue is no longer positively charged and therefore trypsin no longer recognises this as a cleavage site. This results in the disappearance of the two peptides on either side of the acylated lysine residue which are seen in the native lysozyme digest and the appearance of a new peak in the conjugate digest consisting of the modified lysine residue linked to two peptides (i.e. a new, larger peptide containing an uncleaved, modified lysine residue). In this way the acylation positions of lysozyme with estrone glucuronide could be determined.

In the tryptic digestion experiments it was necessary to use 2 M urea to maintain solubility of the hydrophobic reduced and S-carboxymethylated acylated conjugates and peptides. These precipitated out of aqueous solutions in the absence of 2 M urea and could not be resolubilised easily. Under the 2 M urea conditions used for the digestion experiments trypsin was active [188] and highly reproducible tryptic digests were obtained (Figs. 3.3.7, 3.3.9, and 3.3.10). The tryptic maps of native S-carboxymethylated lysozyme in the presence of 2 M urea (Fig. 3.3.7a) were similar to those which have been obtained previously in the absence of urea [173-174, 189-191]. After calibration of the peaks by sequence and mass spectral analysis, visual inspection of the HPLC traces allowed ready identification of the major sites of acylation, under the reaction conditions used, from a combination of the loss in amplitude of the lysine containing tryptic peptides in the native digest and the appearance of new characteristic acylated peptides in the conjugate digest (peaks i, j etc.). Acylation with E1G could be readily determined in this way and it was shown that conjugates resulting from both the active ester and mixed anhydride procedures, which eluted in the same place (e.g. AE E3 and MA E3) were indeed equivalent. It was also shown that the acylation positions and relative molar ratio's of steroid to lysozyme were unchanged between conjugates purified using the S-Sepharose (fast flow) column in 7 M urea alone and those which were also passed through the Butyl Sepharose hydrophobic interaction column. This confirmed that the running of the S-Sepharose purified conjugate families through the Butyl Sepharose hydrophobic interaction column was not necessary. The tryptic digests also confirmed the earlier hydroxylamine experiment (discussed in section 2.4) showing that there was no evidence for esterification of lysozyme with estrone glucuronide in the conjugate products. While esterification would not effect the digestion of lysozyme by trypsin, any peptide which was esterified with estrone glucuronide would elute later in the gradient off the HPLC than the native peptide due to the extra hydrophobicity of the steroid moiety.

Acylation of lysozyme with estrone glucuronide was specific for the ε-amino groups of lysine residues at positions 33, 97 and 116 when using the active ester method and for the ε-amino group of lysine 33 when the mixed anhydride reagent was used (Table 3.3.4). As the coupling reactions were carried out under limiting conditions of reagent the fact that conjugate E3 (lysine 33) was the major product of the mixed anhydride reaction indicates that lysine 33 was the most reactive residue at pH 8.0 and 0°C. The elution position of the mixed anhydride minor conjugate peak (Fig. 3.3.2b) suggests that it is E5 with both lysines 33 and 97 acylated (Table 3.3.4) which in turn indicates that lysine 97 is the next in the order of reactivity. The active ester coupling procedure was carried out at pH 9.1, which results in a greater effective nucleophilicity for the ε-amino groups since the extent of deprotonation is greater. Nevertheless, the reactivity order suggested from the mixed anhydride reaction holds. Conjugate E3 is still one of the major peaks and of the two disubstituted conjugate fractions (E4 and E5 of Table 3.3.4) E5 is present in the greatest amount. Hence, lysine 97 which is the second lysine to be acylated in E5 may be more reactive than lysine 116 which is the second acylated lysine in E4.

Free lysine residues in the enzyme are positively charged at the buffer pH of 6.0 and this charge is lost upon acylation. Hence the most highly substituted conjugates are expected to elute first and unmodified, native lysozyme always elutes last with a characteristic elution time. However, there was not a simple correspondence between the degree of substitution and the elution position. For example, the three peaks which eluted nearest to lysozyme (E1-E3) all had a substitution ratio of 1-1.5 as determined by lysine titrations, and the clearly separated peaks E4 and E5 both had a substitution ratio of 2 (as described in chapter 2). Previous work has shown that hen egg white lysozyme is resistant to urea denaturation, even in the presence of 8 M urea [192] and structural changes are slight. Therefore, the elution characteristics of the conjugate peaks can be understood if the contribution of the acylated lysine residues to the positive field of lysozyme in 7 M urea decreases in the same order as their reactivity in the native protein (33 > 97 > 116). Thus, chemical modification of lysine residue 33 causes earlier elution of this conjugate than the conjugates resulting from the single modification of lysines 97 and 116 because lysine 33 is the most exposed to the solvent. From the relative elution positions of the disubstituted conjugate fractions, E4 and E5, it can be deduced that acylation of lysine 97 has a bigger effect on the positive charge density than does acylation of lysine 116, also in agreement with the reactivity order.

Previous work involving the acylation and modification of amino groups of hen egg white lysozyme has also shown a differential selectivity in the reactivity of the lysine residues [151-152]. It has been established by crystallographic studies that the terminal

α-amino group and six lysine ε-amino groups in hen egg white lysozyme are in different protein environments [193]. Nuclear magnetic resonance studies have suggested that the solution environments of the amino groups in lysozyme are likely to be similar to those in the crystalline protein [194]. Hence the difference in the reactivities of the lysine residues can be related to the different protein environments as revealed by crystallography. When Suckau *et al.* [152] aminoacetylated lysozyme with acetic anhydride and characterised the derivatives by electrospray mass spectroscopy, the reactivities of the amino groups showed an order Lys 97 = 33 > 1 (ε-$NH_2$ and α-$NH_2$) > 13 = 116 > 96. The accessibility of the lysine side chain ε-amino groups, as determined from their degree of extension in the crystal structure, decreases in the order 97 > 33 >> 1 (ε-$NH_2$) > 13 > 116 > 96 > α-$NH_2$ [152] which is consistent with the experimentally determined order.

The ready acylation of lysozyme with estrone glucuronide at lysines 33 and 97 found in the present work is also consistent with the reactivity preference shown in the data of Suckau *et al.* [152] as lysines 33 and 97 are by far the most accessible of the seven. However, according to the results of Suckau *et al.* [152] acylation of lysine 116 with estrone glucuronide should not have occurred until after the acylation, or partial acylation, of lysine 1 (α and ε-$NH_2$) and lysine 13. Acylation at these three amino groups was not observed in the present work. Succinylation of lysozyme with succinic anhydride [151] resulted in six derivatives which suggested that the reactivities of the amino groups decreased in the order 116 > N-terminal α-$NH_2$ > 33 > 96 > 13 = 1 (ε-$NH_2$) > 97. However, these results were obtained with high concentrations of acylating agent and Suckau *et al.* [152] also found that lysines 13 and 116 were not significantly modified until the molar ratio of acetic anhydride to lysozyme was 1600:1. The acylation of residue 116 with estrone glucuronide in preference to lysine 1 (α and ε-$NH_2$), lysine 13 or lysine 96 may therefore be the result of a relatively high local concentration of the E1G reagent in the vicinity of lysine 116. This could be achieved if E1G has an affinity for one or more of the sugar binding sites in the active site cleft since lysine 116 is situated just above this.

The apparent resistance of lysozyme to acylation with estrone glucuronide at lysine residue 96 can be explained on the basis of its limited accessibility. This residue is the least accessible of the lysine residues [152] and prior acylation of the much more accessible, neighbouring lysine residue 97 would result in the partial shielding of lysine 96. The N-terminal α-amino group is the least accessible of the amino groups, being partially shielded by Thr 40 [185], hence explaining the apparent resistance to modification of this amino group as previously shown by Fujita and Noda [193] during acylation of lysozyme. The amino groups of both lysine 1 and lysine 13 are involved in ion pair interactions and Fujita and Noda [193] have suggested that this ion pair

interaction is responsible for the extreme resistance to acylation of these two residues. It is presumably for these reasons that lysine 1 ($\alpha$ and $\varepsilon$-$NH_2$) and lysine 13 are not acylated with estrone glucuronide under near stoichiometric conditions by either of the acylation methods reported.

### 3.4.4 Analysis of Estrone Glucuronide-Lysozyme Conjugates by Acid-Polyacrylamide Gel Electrophoresis

Lysozyme and lysozyme derivatives have previously been analysed and separated by polyacrylamide gel electrophoresis [120-121, 162]. Hirose *et al.* [162] utilised discontinuous acid-polyacrylamide gel electrophoresis in the presence of 8 M urea for the analysis of alkylated lysozyme derivatives. The use of acid-urea gel electrophoresis allowed the alkylated lysozyme families to be separated into distinct bands of n + 1 where n was the integral number of total half-cystines [162]. However, when estrone glucuronide acylated lysozyme conjugates were run on this system there was no resolution of conjugate families into distinct bands. The system was therefore abandoned as a possible alternative method to the Mono-S 7 M urea column for the analysis of estrone glucuronide-lysozyme conjugates.

Non-urea, disc gel electrophoresis in tris-glycine buffer at pH 8.9 has been used previously by Habeeb and Atassi to analyse derivatives of lysozyme obtained by modification of lysine amino groups [120-121]. The amino groups were modified by reaction with either diketene, tetrafluorosuccinic anhydride, maleic anhydride or citraconic anhydride [120], or by guanidation, acetylation, succinylation and maleylation [121] to give heterogeneous populations of lysozyme derivatives. When the resulting reaction mixtures were analysed by non-urea, disc gel electrophoresis in tris-glycine buffer at pH 8.9, a series of discreet bands forming a ladder was observed in all cases, regardless of whether the anode was at the top or the bottom of the tube [120-121]. The resolution was much better when the anode was at the bottom of the tube so that more negatively charged derivatives would migrate further down the gel towards the positively charged electrode. However, when the estrone glucuronide-lysozyme conjugates were analysed by this system distinct bands were not observed and there was no visible separation between the conjugates and unreacted lysozyme. Habeeb and Atassi have suggested that esterification and not amino group modification may be responsible for the laddering effect and apparent heterogeneity seen by disc electrophoresis of their modified lysozyme derivatives [120]. This could explain why there was no separation observed between unreacted lysozyme and the individual estrone glucuronide-lysozyme conjugate families when the mixture was run on the acrylamide gel electrophoresis tris-glycine buffer system at pH 8.9 as the acylation of lysozyme with estrone glucuronide (by the

active ester method) gives stable conjugate derivatives *via* modification at lysine amino groups only (see section 3.4.3). There is no evidence for modification by esterification at hydroxyl groups and therefore the laddering effect and heterogeneity seen by Habeeb and Atassi [120] should not be present for the estrone glucuronide-lysozyme conjugates.

It was therefore decided to try using a similar system but at low pH values where all of the ionisable groups in the protein molecule would be protonated and hence the more positively charged derivatives would migrate down the gel towards the negative electrode. The low pH, non-denaturing acid-polyacrylamide gel electrophoresis system developed here to utilise the charge differences between lysozyme and estrone glucuronide-lysozyme conjugates gave a ladder of conjugate families (see Fig. 3.3.16). Since it was necessary to run the gels from the positive electrode (anode) to the negative electrode (cathode) bovine cytochrome c was used as a marker since it also has a high isoelectric point (10.0 [195] v 10.5 for lysozyme [141]), a molecular weight similar to hen egg white lysozyme (13 000 [196] compared to lysozyme 14 300) and its bright orange colour was easy to identify on the running gel.

Analysis of the estrone glucuronide-lysozyme conjugate reaction mixture using the active ester coupling method showed evidence of seven distinct populations within the reaction mixture (Fig. 3.3.16) similar to the results obtained by cation-exchange 7 M urea chromatography (Fig. 3.3.1B). Once again the order of separation of the E1G-lysozyme conjugates was not a simple correspondence between the degree of lysine acylation and the distance travelled towards the negative electrode down the gel. Based on the separation of the conjugates shown in Fig. 3.3.1B, the expected order of migration of the E1G-lysozyme conjugates by acid-PAGE should be L > E1 > E2 > E3 > E4 > E5 > E6, this being the assumed order of increasing positive charge. However, the order of migration was L > E1(97) > E3 > E1(116) > E5 > E2 > E4 > E6 (Fig. 3.3.16 and Table 3.3.8) where E1(97) is acylation at lysine residue 97 and E1(116) acylation at lysine residue 116 with estrone glucuronide as described in section 3.4.3.

Comparison of the predicted (calculated from Mono-S 7 M urea analysis) and observed orders of migration of the E1G-lysozyme conjugates by acid-PAGE shows that in effect conjugates E3 and E5 both migrate further down the gel suggesting a higher degree of positive charge than expected from their chromatographic behaviour. Why is this so? Denaturation or conformational changes in the presence of concentrated urea solutions are unlikely to be variables affecting the separation of the estrone glucuronide-lysozyme conjugates by cation-exchange chromatography, as lysozyme crystals grown in the presence of high urea concentrations (up to 9 M) are essentially isomorphous with the structure of native crystals grown in the absence of urea [192]. It has also previously

been shown that hen egg white lysozyme is very resistant to urea denaturation and that even in the presence of 8 M urea solutions structural changes in lysozyme are slight [192, 197]. In the presence of urea, the crystal structure of hen egg white lysozyme showed no evidence of carbamylation of the free amino groups [192] also ruling out this possibility as a variable affecting the separation of the conjugates by cation-exchange chromatography in the presence of urea .

The observed differences between the migration orders of the E1G-lysozyme conjugates when analysed by acid-PAGE and cation-exchange chromatography in the presence of 7 M urea may be explained on the basis of the characterisation of the conjugate families. Neither of the two estrone glucuronide-lysozyme conjugate families E3 or E5 are acylated at lysine 116 (section 3.4.3). In the partially denaturing, 7 M urea conditions used for the cation-exchange analysis, it has been reported that a urea molecule hydrogen bonds to lysine residue 116 [192]. Urea has a pronounced effect on the high-performance cation-exchange chromatography behaviour of hen egg white lysozyme, significantly reducing its retention time over that observed in the absence of urea [198]. Although this result is expected on the basis of the increase in the solvent dielectric constant in the presence of urea, it is also possible that the large decrease in retention time may be due, in part, to the binding of a urea molecule to lysine residue 116 since this would reduce the apparent positive charge on hen egg white lysozyme. Thus, in the urea system, the contribution of lysine 116 to the positive electrostatic field may have been underestimated. As a result, in the non-denaturing acid-PAGE system, when this effect is absent, conjugates E3 and E5 both migrate further than their counterparts E2 and E4 in which lysine 116 is acylated by the steroid glucuronide. The acid-PAGE system may therefore give a truer reflection of the apparent positive charge of each lysine residue than does the denaturing 7 M urea system.

Hence, non-denaturing acid-polyacrylamide gel electrophoresis (acid-PAGE) can be used to assess, analyse and purify small amounts of the individual E1G-lysozyme conjugates under non-denaturing conditions. The advantage of the system is that it is rapid, simple, and gives excellent resolution between different E1G-lysozyme conjugate families without the use of denaturing agents such as urea. The use and development of systems such as the acid-PAGE system described above are important when considering the sensitivity of immunoassays utilising enzymes other than lysozyme. One of the major hurdles facing scientists developing new immunoassays is the separation of conjugated protein products from unconjugated protein. To obtain the maximum assay discrimination between similar hormone concentrations in homogeneous enzyme immunoassays it is necessary to isolate enzyme conjugates with a high degree of inhibition as discussed in chapter two. It is therefore essential that after conjugation, any unreacted enzyme is

separated and removed from the conjugated material. Unfortunately many immunoassays developed in the last twenty years have utilised enzymes such as horseradish peroxidase where the separation of unreacted enzyme from conjugated material is extremely difficult. However, the acid-PAGE system described above has shown promising preliminary results in the separation of directly conjugated horseradish peroxidase material from unconjugated protein material. It may therefore be possible to apply PAGE techniques, or modified PAGE techniques, to some of the wider problems encountered in attempting to separate conjugated and unconjugated protein products from each other.

### 3.4.5 Characterisation of Individual PdG-Lysozyme Conjugate Families

As in the case of the estrone glucuronide-lysozyme conjugate families it was necessary to undertake the tryptic digestion experiments of pregnanediol glucuronide-lysozyme conjugate families in 2 M urea to maintain the solubility of the hydrophobic reduced and S-carboxymethylated acylated conjugates and peptides. It was necessary to take care when diluting the 8 M urea solutions to 2 M urea solutions using 1% ammonium carbonate buffer (pH 8.50) as the 2 M urea conditions were on the threshold of solubility for several of the more highly substituted pregnanediol glucuronide-lysozyme conjugates. Dilution of the solution below 2 M urea resulted in the precipitation of the conjugates out of solution resulting in incomplete tryptic digestion even after long digestion periods (> 24 hours) and the addition of fresh trypsin solution. The use of more concentrated urea solutions (for example 2.5 and 3 M urea) changed the digestion patterns of native lysozyme slightly at 2.5 M urea and significantly at 3 M urea, presumably due to the effect of urea on trypsin. Therefore 2 M urea conditions were employed for the tryptic digests of the PdG conjugates and this gave good reproducible results provided the dilutions were correct. The use of 2 M urea also meant that the control native lysozyme digest described earlier, did not have to be repeated. Visual inspection of the tryptic maps of the conjugate families again allowed ready identification of the major sites of acylation from a combination of the loss in amplitude of the lysine containing tryptic peptides in the native lysozyme digest and the appearance of new characteristic acylated peaks later in the tryptic digest map. The tryptic digests also confirmed that there was no esterification of lysozyme with pregnanediol glucuronide in the conjugate families for the reasons discussed in section 3.4.3.

Characterisation of the pregnanediol glucuronide-lysozyme conjugate families as described in the methods section, showed that the acylation of lysozyme with pregnanediol glucuronide was also specific for the ε-amino groups of the same three lysine residues 33, 97 and 116 (Table 3.3.6). The acylation of lysozyme with pregnanediol glucuronide by the active ester method resulted in similar conjugates which

were acylated in the same positions as the corresponding estrone glucuronide conjugates discussed in section 3.4.3 (Tables 3.3.6 and 3.3.4). The major difference between the two sets of steroid glucuronide conjugate families was that the active ester P5 conjugate was partially acylated at three lysine residues 33, 97 and 116 (instead of only two (K33 and K97) in the active ester E5 conjugate family). Complete acylation had obviously not occurred at any of these lysine residues as the overall molar ratio of PdG to enzyme in the P5 family was two PdG molecules per lysozyme molecule (Table 3.3.6).

The selectivity and reactivity of the amino groups discussed in section 3.4.3, for the acylation of lysozyme with estrone glucuronide, therefore seems to hold for the acylation of lysozyme with pregnanediol glucuronide by the active ester method as well. The ready acylation of lysines 33 and 97 was again consistent with the reactivity preference as these lysine residues are by far the most accessible of the seven amino groups [152]. The extra level of acylation of lysine residue 116 may result from a greater affinity of the more hydrophobic PdG molecule (relative to the E1G molecule) for the lysozyme in the vicinity of this amino group. As discussed in section 3.4.3, the resistance to acylation of lysine residues 1, 13 and 96 and the N-terminal α-amino group can be explained on the basis of limited accessibility (lysine 96, [152]), shielding (N-terminal α-amino group [185]) and ion pair interactions (lysines 1 and 13 [193]), all making these lysine residues unfavourable as acylation sites.

The acylation of lysozyme with pregnanediol glucuronide by the mixed anhydride method gave a different conjugation reaction mixture compared to the corresponding estrone glucuronide reaction mixture. Instead of only one major derivative (conjugate family E3 which constituted 72% of the total conjugate yield) exclusively acylated at lysine residue 33 (see section 3.4.3 for details) acylation of lysozyme with pregnanediol glucuronide by the mixed anhydride method gave two major derivatives, P1 and P3 (Fig. 3.3.4A). The total amount of lysozyme acylated was similar to that found in the E1G reaction. The largest peak (P1) was due to acylation exclusively at lysine residue 97 with pregnanediol glucuronide and constituted almost 60% of the total conjugate yield. The other major derivative was conjugate P3, which was due to acylation at lysine residue 33 but constituted only 30% of the total conjugate yield. Therefore less than half the amount of conjugate produced resulted from the acylation of the most reactive lysine residue (residue 33) when using the pregnanediol glucuronide mixed anhydride reagent. Now the major conjugation site for the PdG reagent was the amino group situated at lysine residue 97.

The best explanation for this lies in the nature of the pregnanediol glucuronide moiety. The pregnanediol glucuronide steroid moiety is much more hydrophobic in nature than

the estrone glucuronide steroid moiety and as a result is less suited to aqueous environments. Therefore, when the pregnanediol glucuronide mixed anhydride reagent is introduced into the aqueous lysozyme solution for reaction, it may accumulate at a small hydrophobic patch on the surface of the enzyme near lysine residue 97 in an attempt to find a less polar environment. If this is the case there would be a relatively large concentration of the PdG mixed anhydride reagent in the vicinity of, and available to react with, the amino group of lysine 97. As a result the pregnanediol glucuronide mixed anhydride reagent could react with both the most reactive amino group at lysine 33 (as in the case of the estrone glucuronide reagent) and lysine residue 97 due to the hydrophobic effect.

The final composition of conjugation products resulting from the coupling of a steroid glucuronide to lysozyme is therefore not governed by a single parameter, but is the result of a combination of several variables when using stoichiometric ratio's of hapten to enzyme. The two biggest effects dictating the selectivity of the position(s) of acylation are the surface accessibility of the lysine amino groups and the coupling reagent used to link the hapten to the enzyme. However the physical and structural properties of both the hapten and the enzyme may also influence the coupling position(s) and substitution ratio's. Further evidence that the hapten influences the coupling procedure and results has been observed in the conjugation of estriol monoglucuronides to lysozyme which give different conjugation patterns again to those found with estrone glucuronide and pregnanediol glucuronide when using the mixed anhydride method [57].

## 3.5 Conclusions

Chromatography of the estrone glucuronide-lysozyme conjugates prepared by both the mixed anhydride and active ester coupling procedures on an S-Sepharose (fast flow) column allowed the large scale isolation of individual conjugate families. Passage of the isolated families through a Butyl Sepharose hydrophobic interaction column gave highly inhibited conjugates (> 90%) in the presence of anti-estrone glucuronide antibodies which were suitable for use in homogeneous enzyme immunoassay systems. Conjugation of lysozyme by the mixed anhydride procedure gave one major derivative while conjugation by the active ester method gave six derivatives. Characterisation of the conjugate families showed the major mixed anhydride derivative to be acylated at lysine residue 33 while the active ester conjugates were acylated at one or more of lysine residues 33, 97, and 116 showing that the acylating reagent influences the yield and composition of the protein products. The mixed anhydride reagent is thus preferable to the active ester reagent as a source of conjugates for homogeneous enzyme immunoassay as it gives an almost pure conjugate in good yield.

Estrone glucuronide-lysozyme conjugates were analysed by both Mono-S 7 M urea cation-exchange chromatography and acid-polyacrylamide gel electrophoresis. The difference in the behaviour of the individual conjugate families when run on the two chromatographic systems can be accounted for by the hydrogen binding of a urea molecule to lysine residue 116 in the 7 M urea cation-exchange system. The binding of a urea molecule to lysine residue 116 masks the contribution of this residue to the enzymatic positive surface charge of hen egg white lysozyme. While both the chromatographic and acid-PAGE systems gave excellent resolution between the E1G-lysozyme conjugate families and unreacted lysozyme, the acid-PAGE system has the added advantage of being a non-denaturing system which can be important when handling proteins and enzymes particularly when it is necessary to retain the biological activity of the protein or enzyme of interest.

As for the estrone glucuronide-lysozyme conjugates, acylation of lysozyme with PdG was shown to be selective for the three lysine residues 33, 96 and 116. Once again the mixed anhydride reagent was found to be preferable to the active ester reagent for the production of conjugates for homogeneous enzyme immunoassay as it gave a less diverse range of conjugate products. The correlation of the protein environments of the amino groups in the crystal structure of lysozyme with the acylation positions of both the estrone glucuronide and pregnanediol glucuronide conjugates suggested that the surface accessibility and secondary interactions of lysine residues are largely responsible for determining the reactivity of individual residues and the resulting acylation positions.

It was interesting that acylation of only lysine residues 33, 97 and 116 was detected in the lysozyme conjugates of both estrone glucuronide and pregnanediol glucuronide synthesised at stoichiometric ratio's of steroid to enzyme. The explanation of this is clearly outlined above. The acylation positions may play an important part in the recognition and binding of the anti-steroid antibodies when used in enzyme immunoassays which may in turn determine the inhibition mechanisms at work in the antibody-conjugate immune complex. For example, the small residual activity involved in the Ovarian Monitor assay system (about 5%), when all of the conjugate would be expected to be bound to the appropriate antibody and thus inactive, could be explained if a small amount of steroid was coupled to a lysine residue on the rear surface of hen egg white lysozyme with respect to the active site. If steric hindrance of the bacterial cell wall substrate by the antibody in the immune complex was the sole cause of the lytic inhibition of the steroid glucuronide-lysozyme conjugate (as suggested by Rubenstein *et al.* [107]), the binding of an antibody molecule to a steroid coupled to a lysine residue at the back of the active site should not interfere with the active site and thus some lytic activity would still be observed. The rate at which the antibody-conjugate complexes dissociate (the displacement off-rate constants) can also account for small amounts of residual activity due to equilibration during the assay and this effect is investigated further in chapter five.

With the advent of apparatus such as the SMART Fast Protein Liquid Chromatography system from Pharmacia, which can detect very small amounts of material, it will be possible to undertake a tryptic finger print on any given steroid glucuronide-lysozyme conjugate family with a small aliquot of sample. Several tryptic digests of conjugate families run through a C18 reverse phase column on the SMART system showed tryptic maps very similar to those obtained on the HPLC system used in this study. Once the SMART system was calibrated with a native lysozyme digest it should be a simple matter to analyse other conjugate families by visual inspection of their tryptic finger prints. The only factor which may limit the use of this system, as opposed to the present system, is the physical problem of dealing and handling such small amounts of material.

To study the physical binding, mechanisms, and parameters of the anti-hapten antibody inhibitory effect on the lytic activity of the Ovarian Monitor conjugates, it is necessary to look at tertiary structures of the conjugates and antibodies. By using the known crystal structure of lysozyme and the known acylation positions in the characterised conjugates, three dimensional tertiary structures of the steroid glucuronide-lysozyme conjugates can be generated. By examining these models and antibody crystal structures we can predict the effect of the substrate size, enzyme size, length and rigidity of the link between the hapten and enzyme, and the orientation of the hapten with respect to the active site on the inhibition of the lysozyme conjugates. A further understanding of the relative importance

of these factors may help in the rational design of other inhibitable enzyme conjugate systems.

# Chapter Four

# Structural Aspects of the Steroid Glucuronide-Lysozyme Conjugate-Anti-Hapten Antibody Immune Complexes

## 4.1 Introduction

Perhaps the most important characteristic of an enzyme-hapten conjugate to be utilised in an homogeneous enzyme immunoassay system, is the ability of excess anti-hapten antibody to extensively inhibit the enzymatic activity of the enzyme conjugate. However, little is known about the binding of conjugated haptens to anti-hapten antibodies, or the mechanisms by which the binding of these antibodies can inhibit the activity of the conjugated enzyme. Rubenstein *et al.* [107] have long ago suggested that the binding of an antibody to a hapten coupled to a lysine residue of lysozyme inhibits the lytic activity of the enzyme by steric hindrance. Although this view is universally accepted, the actual mode of action, or degree of steric hindrance within enzyme-hapten conjugate anti-hapten antibody complexes is unknown.

The basic immunoglobulin G (IgG) antibody structure consists of two types of polypeptide chain, a heavy type 50 kilodalton (kd) polypeptide chain (designated H) and a light type 25-kd polypeptide chain (designated L). Each antibody molecule consists of two heavy and two light polypeptide chains. Each L chain is linked to an H chain by a disulfide bond, and the two H chains are bonded to each other by at least one disulfide bond to give the Y-shaped molecule typical of immunoglobulin G antibodies (Fig. 4.1.1). At the N-terminal end of both the light and heavy chains is a variable region of amino acid residues, which differ between antibodies, and these hypervariable regions form the antigen binding sites. Each heavy-light chain dimer forms an antigen binding site at these variable positions, and each immunoglobulin molecule therefore contains two antigen binding sites, one at the end of each heavy-light chain dimer as depicted in Fig. 4.1.1. Immunoglobulins therefore bind antigens at the end of each H-L dimer arm in the binding pocket formed between the variable segments (known as the complementarity determining regions) of the L and H polypeptide chains. The C-terminal end of both the heavy and light chains is known as the constant region and as the name implies is remarkably similar in amino acid composition between all immunoglobulins.

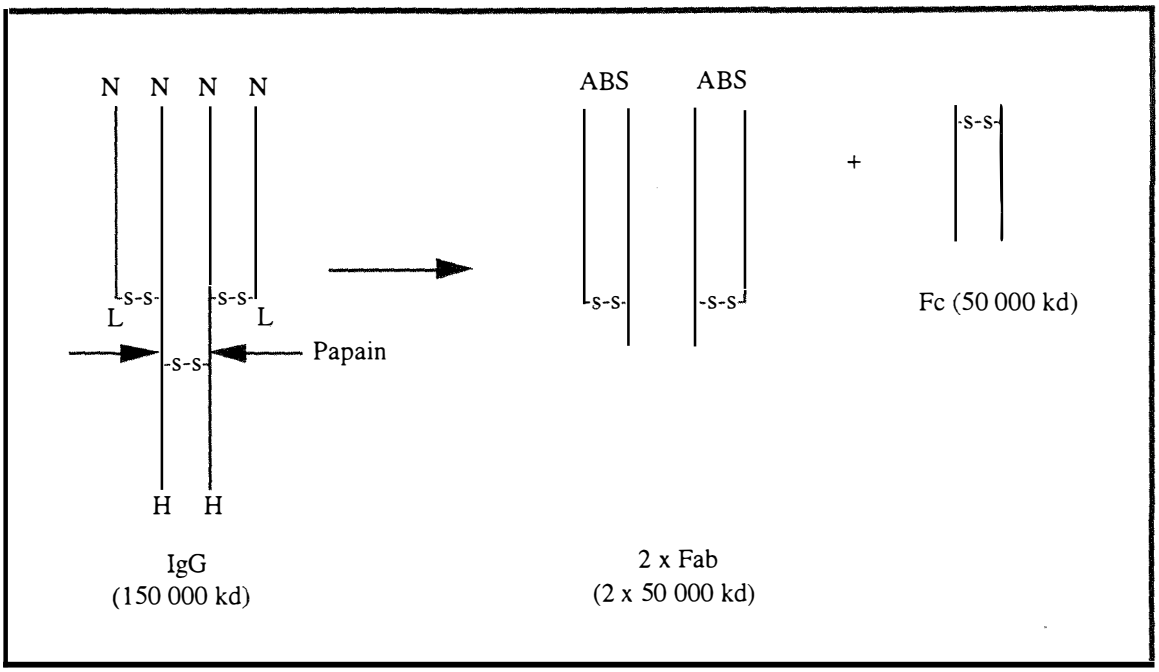


**Fig. 4.1.1** The conventional schematic representation of the basic Y-shaped immunoglobulin molecule (left hand side). The light and heavy chains are indicated by the letters L and H respectively. The N-terminal end of the polypeptide chains is indicated by the letter N. The position at which the enzyme papain cleaves the immunoglobulin molecule is also indicated by arrows. The Fab and Fc fragments, resulting from papain cleavage of the intact immunoglobulin molecule, are also shown. The positions of the antigen binding sites (ABS) are indicated in the Fab representations.

The immunoglobulin molecule can be split into three fragments that retain immunological activity by the limited proteolytic action of papain (see chapter five and Fig. 4.1.1). Papain cleaves the immunoglobulin molecule on the N-terminal side of the disulfide bond(s) that hold the two heavy chains together resulting in the production of three antibody fragments. Two of these fragments contain antigen binding sites and these are known as Fab (ab stands for antigen-binding, F for fragment) fragments, each fragment having a molecular weight of 50 kd. Each Fab contains one combining site for antigen or hapten, and has a similar binding affinity for hapten as does the whole molecule. The remaining fragment (also having a molecular weight of 50 kd), called Fc because it crystallises readily, does not bind antigen, but mediates effector functions such as complement fixation. When studying antibody-hapten complexes by X-ray crystallography, crystallographers separate the Fc and Fab fragments. Only the Fab fragments are used in crystallisation experiments as they are much smaller than the intact immunoglobulin molecule and have only one antigen binding site. More detail on the preparation of Fab fragments and the crystallisation of Fab-antigen complexes is reported in chapters five and seven.

The effect of the hapten location and orientation in the enzyme conjugates upon the binding of the anti-hapten antibodies has not been investigated. Furthermore, the binding

requirements of the anti-hapten antibodies have not been determined for protein conjugated haptens, and in order to successfully design enzyme systems which are likely to produce colours and possibly show inhibition by anti-hapten antibodies, an understanding of the structural parameters at work within the immune complex is essential.

In order to investigate the structures of the steroid glucuronide-lysozyme conjugate-anti-hapten antibody immune complexes, three dimensional models of the estrone glucuronide and pregnanediol glucuronide conjugates were generated using computer graphics packages. The three dimensional structures of the immune complexes were then built using the known crystal structures of lysozyme and a progesterone antibody Fab fragment, so that the effects of hapten location and orientation on the lytic activity could be investigated. The results are discussed and compared to the known binding requirements and parameters of other protein-antigen complexes as revealed by X-ray crystallographic studies.

---

## 4.2 Experimental

The building and modelling of the three dimensional structures of estrone glucuronide, pregnanediol glucuronide, estrone glucuronide-lysozyme conjugates and pregnanediol glucuronide-lysozyme conjugates was performed on a Silicon Graphics Workstation using the software package INSIGHT II (Biosym Technologies). The crystal structure of triclinic lysozyme [118] (file 2LZT of the Brookhaven Protein Data Bank) was examined using INSIGHT II. The structures of E1G and PdG were built using the builder module of INSIGHT II and then submitted to energy minimisation calculations to obtain the thermodynamically most likely structures. Energy minimisations were undertaken using the program Discover which was run from within the INSIGHT II software package. For energy minimisations the number of iterations was set at 1000 and the derivative for convergence at 0.01. The steroid glucuronide models were attached to the appropriate amino groups within the hen egg white lysozyme structure using INSIGHT II to give model three dimensional tertiary structures of the lysozyme conjugates.

Several crystal structures of lysozyme-Fab immune complexes were also examined using the INSIGHT II software package on a Silicon Graphics Workstation (files 1fdl [199], 1mlc [200], 2hfl [201] and 3hfm [202] of the Brookhaven Protein Data Bank). A progesterone-Fab complex [203] was also examined (file 1dbb of the Brookhaven Protein Data Bank). The steroid moieties of the estrone glucuronide-lysozyme and pregnanediol glucuronide-lysozyme conjugate models were placed into the anti-

progesterone antibody binding pocket by matching the appropriate steroid atoms of the models with the bound progesterone atoms using a general least squares fit program.

## 4.3 Results and Discussion

### 4.3.1 Structural Modelling of the Estrone Glucuronide and Pregnanediol Glucuronide Moieties

The crystal structure of many steroids have been solved in the last 40 years, all of which are characterised by a basic carbon skeleton or nucleus consisting of three six membered rings and one five membered ring [204-205] as shown in Fig. 4.3.1. Steroids and steroid derivatives all differ from each other in the conformation of the ring systems and the presence, or absence, of additional functional groups and substituents attached at various positions in the ring systems. Although the crystal structures of many steroid derivatives have been solved [206-207], very few crystal structures of steroid glucuronides have appeared due to the difficulty in producing good quality crystals. The three dimensional crystal structures of estrone-3-glucuronide and pregnanediol-3α-glucuronide were not available at the time this work was undertaken. It was therefore necessary to produce models of the three dimensional crystal structures of the estrone glucuronide and pregnanediol glucuronide moieties so that they could be attached to the lysozyme crystal structure to provide models of the individual steroid glucuronide-lysozyme conjugate families.

More recently, the crystal structure of estrone glucuronide has been solved, the details of which are reported in chapter seven. However, it did not prove necessary to recalculate the estrone glucuronide-lysozyme conjugate models using the actual crystal structure as the three dimensional estrone glucuronide model (generated as described in the methods section) used in generating the conjugate structures was almost identical to the actual estrone glucuronide crystal structure. A least squares fit of the estrone glucuronide crystal structure (as reported in chapter seven) with the structure of the computer generated estrone glucuronide model, showed that the crystal structure and the computer generated estrone glucuronide structure were virtually isomorphous. This was shown by the very small root mean square deviations calculated for the fit of the individual atoms in the steroid glucuronide structures (actual and generated), indicating a very close fit between the two steroid structures. It was therefore considered unnecessary to recalculate the estrone glucuronide-lysozyme conjugate structures using the actual three dimensional crystal structure of E1G (as reported in chapter seven) as this would have made very

little, if any, difference to the model structures for the estrone glucuronide-lysozyme conjugates.

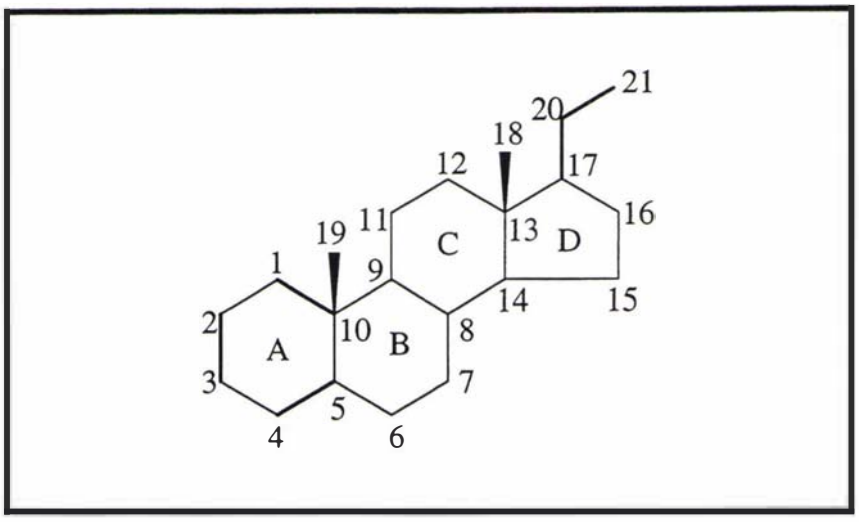


**Fig. 4.3.1** The basic steroid skeleton structure, numbering system and ring designations

The final estrone glucuronide and pregnanediol glucuronide model tertiary structures, after building and energy minimisation calculations, are shown in Figs. 4.3.2 and 4.3.3 respectively. Oxygen atoms in Figs. 4.3.2 and 4.3.3 are shown in red while hydrogen atoms are coloured white. The views of the steroid glucuronides from above (the β-face) are shown in the top left hand corner of Figs. 4.3.2 and 4.3.3. The bottom left hand views of the two steroid glucuronides show the planar geometry of the estrone A ring (Fig. 4.3.2) and the more saturated nature of the pregnanediol steroid skeleton (Fig. 4.3.3) relative to the estrone steroid skeleton. The view of the steroid glucuronides shown on the right hand side of Figs. 4.3.2 and 4.3.3 represents a more side-on view of the structures. This right hand side view clearly shows that a kink will result when one of the steroid glucuronide moieties is conjugated to another molecule *via* the COOH group of the carbohydrate glucuronide ring as the COOH group protrudes at right angles to the steroid skeleton (right hand views, Figs. 4.3.2 and 4.3.3).

The geometry of the estrone ring system in the computer generated estrone glucuronide three dimensional structure (Fig. 4.3.2) was as expected from the study of similar steroid skeletons solved by X-ray diffraction studies [204, 206-209]. The major features of the computer generated model are the expected aromaticity and planarity of the estrone A ring, the β orientation of the sugar moiety with respect to the steroid moiety, and the chair conformation of the sugar ring. The non-planar geometries of the estrone B, C and D rings are also easily recognised, and as expected, by comparison with other similar steroid molecules [204, 206-209].

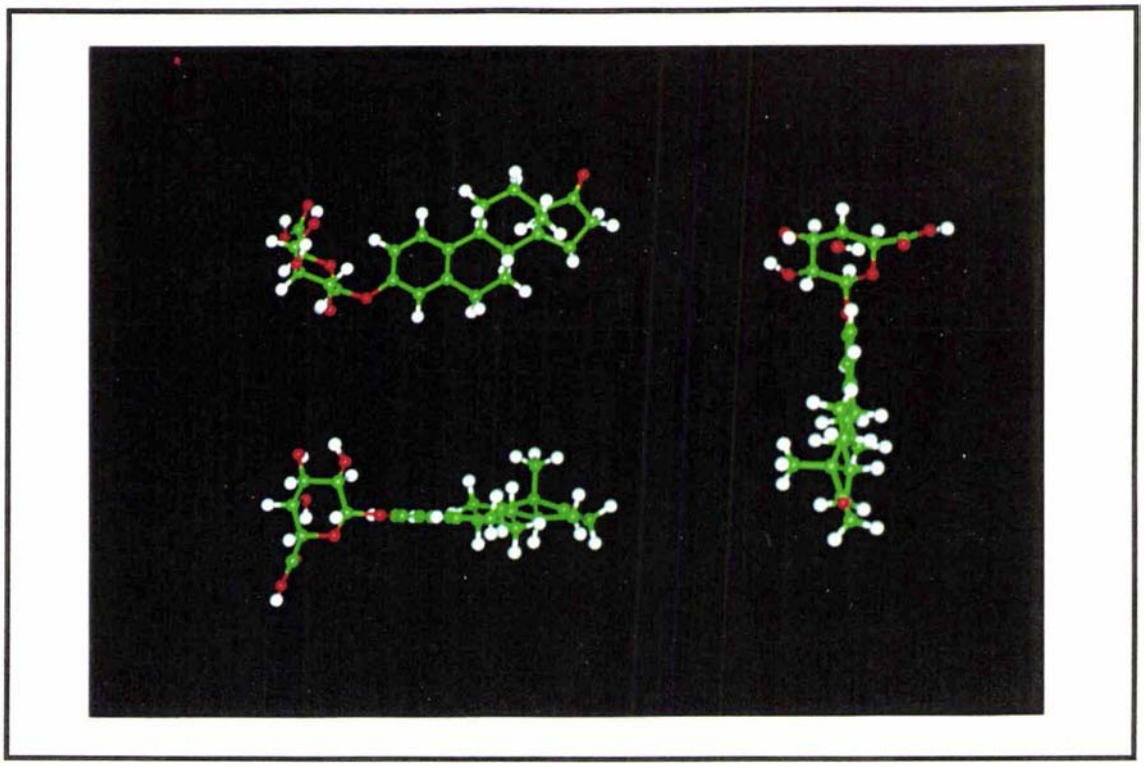

**Fig. 4.3.2** Computer generated three dimensional structures of the estrone glucuronide moiety after energy minimisation as described in the text. Oxygen atoms are shown in red and hydrogen atoms in white. The β-orientation of the glucuronide linkage the aromaticity of the steroid A ring and the non-planar geometries of the B, C and D rings can be seen in the bottom left hand figure.

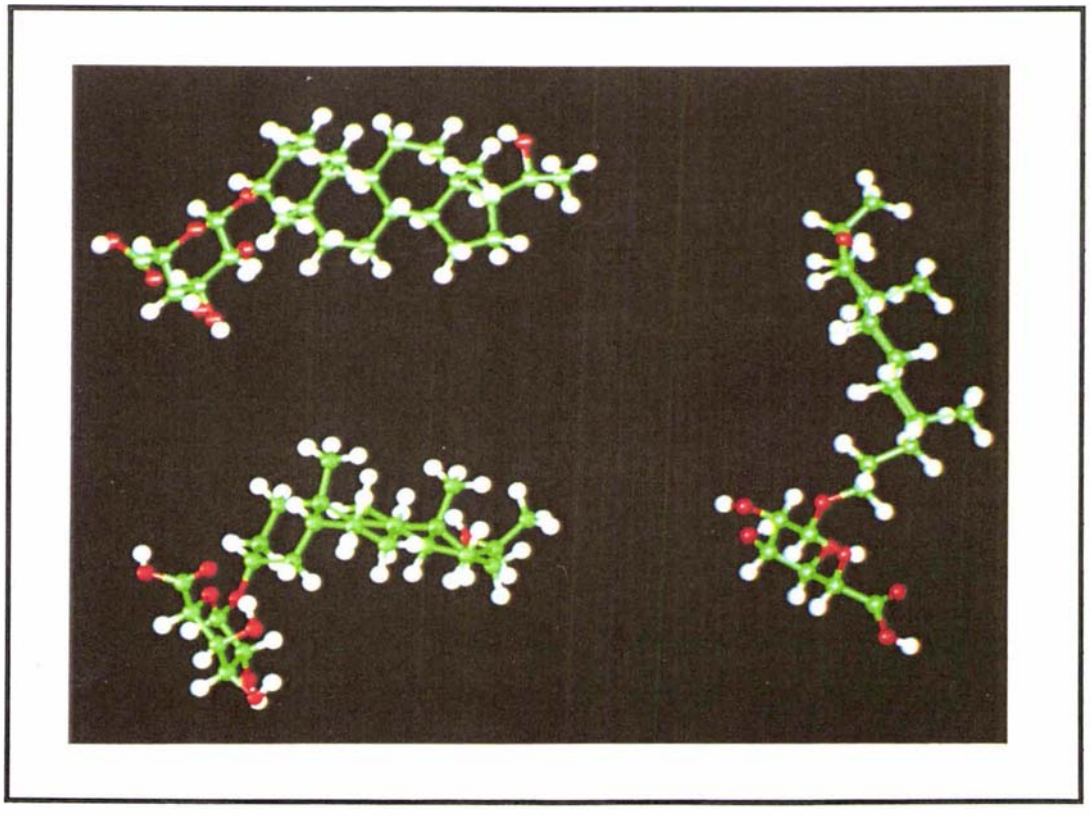

**Fig. 4.3.3** Computer generated three dimensional structures of the pregnanediol glucuronide moiety after energy minimisation as described in the text. Oxygen atoms are shown in red and hydrogen atoms in white. The non-planar geometries of the steroid ring system and the cis A-B ring junction can be seen in the bottom left hand and right hand side figures.

The pregnanediol glucuronide three dimensional structure generated by computer graphics (Fig. 4.3.3) also exhibited the major geometrical features as expected from a comparison with other non-aromatic steroid skeletons which have been solved by X-ray diffraction studies [204, 210-212]. The non-planar geometry of the steroid A, B, C and D rings and the cis conformation of the A-B ring junction were clearly visible. The β orientation of the sugar moiety with respect to the steroid and the chair conformation of the sugar ring were once again clearly shown. The glucuronide ring was attached *via* a β-1 acetal linkage to the steroid moiety at the 3 hydroxyl position and the carbohydrate ring was in the correct chair conformation. As both of these geometries were present and correct in the generated PdG structure the model was considered an appropriate representation of the real structure for the modelling of the pregnanediol glucuronide-lysozyme conjugates utilised in the Ovarian Monitor assay system [91].

### 4.3.2 The Importance of the Chemical Bridge Linking Hapten and Protein in Enzyme Immunoassay

Before the steroid glucuronide-lysozyme conjugate models and immune complex models are discussed, several other structural factors influencing any homogeneous enzyme immunoassay system warrant discussion. Haptens are small chemical compounds which on their own are not usually immunogenic, and it is therefore necessary to covalently couple them to a protein carrier (different than the enzyme utilised in the immunoassay system, lysozyme in this case) in order to elicit an immune response [213]. As a result, antibodies which recognise both the steroid hapten and/or the chemical bridge structure may be produced.

To obtain the best antibodies, the immunising hapten for the target analyte should be as close a copy of that molecule as possible. Preferably, the immunising hapten should be identical to the target analyte in structure, geometry, electronic and hydrophobic properties [214]. This is not a problem in the present work since the immunising hapten is the same as the analyte measured in the assay system. It is also important that when the hapten is covalently attached to the carrier protein, it is attached at such a position and orientation that the unique antigenic determinant groups are optimally presented to the immune system [214].

The hapten moiety is usually linked to the protein carrier *via* a chemical bridge and there have been many studies published on the effect of both the bridge length, and the site of attachment of the bridge to the hapten, on the specificity of the resulting antibodies [155, 215-218]. Previous work has shown that the optimum length of the bridge (or linker) appears to be between 4 and 6 carbon atoms, since a further increase in the length of the

linker does not increase the antibody specificity [219-220]. Of course it is not necessary to add a bridge to the steroid glucuronides in the present work in order to attach them to a carrier protein for the production of antibodies. The glucuronide ring itself can be utilised as both the bridge and the attachment of the steroid glucuronides to the carrier protein, and is equivalent in length to between 4 and 6 carbon atoms. The free carboxyl group of the glucuronide ring is conjugated directly to the carrier protein to form a covalent amide linkage as discussed in chapters two and three.

The use of the glucuronide ring as the linker in the steroid glucuronide-lysozyme conjugates has two possible drawbacks. The first is that the glucuronide structure and geometry is conserved in all of the steroid glucuronides and thus the glucuronide ring in one steroid glucuronide could in theory be recognised by antibodies to a different steroid glucuronide giving an unwanted cross reaction. However, the glucuronide ring is wedged between the steroid and the protein moieties in the conjugate products and as a result, the presentation of the glucuronide ring system to antibodies is limited due to the shielding effect of the steroid moiety, thus reducing the cross reactivity. The glucuronide ring therefore has little influence on the specificity or cross reactivity of antibodies for steroid glucuronides and it is the difference in the steroid skeleton and its substituents which determines the specificity and cross reactivity. As can be seen from the structural models of E1G and PdG (Figs. 4.3.2 and 4.3.3), the attachment of the steroid glucuronide to the carrier protein, *via* the free carboxyl group of the carbohydrate ring means that the steroid moiety is far enough removed from the protein surface that the binding of antibody to the steroid moiety is not effected by the proximity of the protein surface. The differences in the shape (geometry) of the steroid moieties in the different glucuronide structures mean that the antibody binding pocket for one steroid glucuronide will most likely be different to the antibody binding pocket of another steroid glucuronide. Therefore, even if a given steroid-glucuronide antibody does recognise the glucuronide ring of a different steroid glucuronide, it is unlikely that the antibody will be able to correctly accommodate the steroid moiety.

The major structural differences between the two steroid glucuronide structures shown in Figs. 4.3.2 and 4.3.3 are found in the steroid A ring and the D ring and its substituents. Bermúdez *et al.* [221], and Podestá and Montagnoli [222], have both shown that the steroid A and D rings are the important determinants in conferring specificity to steroid antibodies. Presumably, this is also the case for the specificity determination for anti-steroid glucuronide antibodies. It is therefore of vital importance that the A and D rings are presented to the immune system in the same orientation and conformation in both the conjugates and the protein carrier system used to elicit the antibodies. The use of covalent amide bonds derived from the glucuronic acid carboxyl group in both the lysozyme-

steroid glucuronide conjugates and the immunogen conjugates (for producing the antibodies) ensures a common orientation for the steroid glucuronide moiety as far as possible.

### 4.3.3 Computer Models of the Tertiary Structures of the Estrone Glucuronide-Lysozyme Conjugate Family E6

Tertiary structures of the steroid glucuronide-lysozyme conjugates used in the Ovarian Monitor immunoassay are not currently available. However, computer models have been generated by attaching the estrone glucuronide and pregnanediol glucuronide structures generated in section 4.3.2 above to the known crystal structure of hen egg white lysozyme [118] at lysine residues 33, 97 and 116 producing a model of conjugate family E6. The orientations of the estrone glucuronide moiety at the individual lysine residues is presumably the same in all of the conjugates. For example, an estrone glucuronide moiety attached to lysine residue 33 will presumably have the same orientation and conformation in conjugate family E3 as in conjugate family E6. The tertiary structure of the estrone glucuronide-lysozyme E6 conjugate generated in this way are shown in Figs. 4.3.4-4.3.7. In previous studies chemical modification of the lysine residues of hen egg white lysozyme by reductive methylation was shown to have very little structural effect on the enzyme, as revealed by X-ray crystallography [223]. Even though estrone glucuronide is much larger than a methyl group, it is difficult to see how the acylation of lysozyme at the amino groups of lysine residues with estrone glucuronide could lead to major structural perturbations of the enzyme. Hence, the structures shown in Figs. 4.3.4-4.3.7 are likely to be good representations of the actual three-dimensional arrangements of the E1G-lysozyme conjugates.

After the estrone glucuronide moiety modelled in section 4.3.2 had been attached to the appropriate lysine residue and energy minimisation calculations completed, the steroid glucuronide was virtually parallel to, and quite close to, the protein surface in each model (Figs. 4.3.4-4.3.7). This conformation is the result of the cis arrangement of the β-1 acetal linkage of the carbohydrate ring to the steroid, and the β-6 linkage of the carboxyl group of the glucuronide ring to the protein. Fig. 4.3.4 shows the computer generated three dimensional structure of estrone glucuronide-lysozyme conjugate E6 oriented to show the steroid glucuronide moiety attached at lysine residue 33. The lysozyme molecule is coloured green (except for the lysine residues which are coloured blue) and the active site of the enzyme can be clearly seen on the left hand side. The carbon atoms of the estrone glucuronide molecule are coloured yellow, the hydrogen atoms white and the oxygen atoms red. The aromatic A ring of the steroid skeleton can be clearly seen

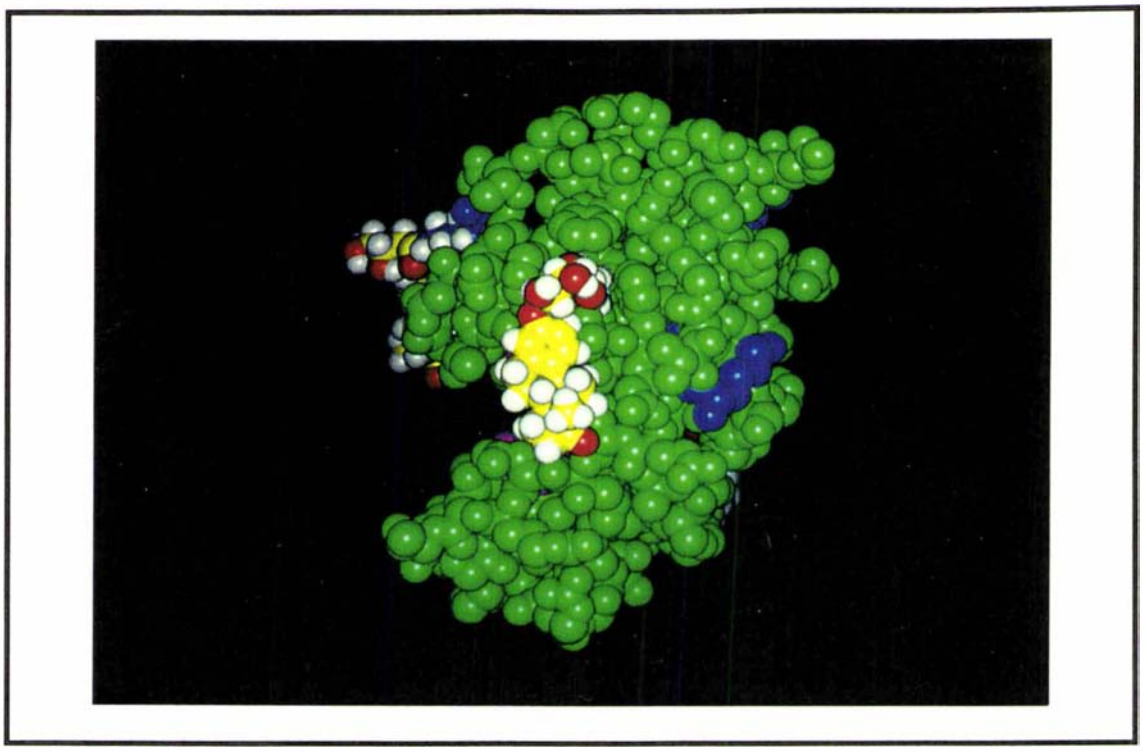

**Fig. 4.3.4** CPK space-filling representation of the computer generated estrone glucuronide-lysozyme conjugate tertiary structure showing the positions of acylation and orientation of the E1G moiety relative to the lysozyme molecule and the active site cleft when acylation occurs at lysine residues 33, 97 and 116 as in the active ester E6 conjugate family. The E1G moiety is coloured yellow with hydrogen atoms coloured white and oxygen atoms red. The lysine residues of hen egg white lysozyme are highlighted in blue. Acylation can be seen at lysine residue 33 when the active site cleft is oriented to the left hand side. The steroid moieties due to acylation at lysine residues 97 and 116 can be seen in the background.

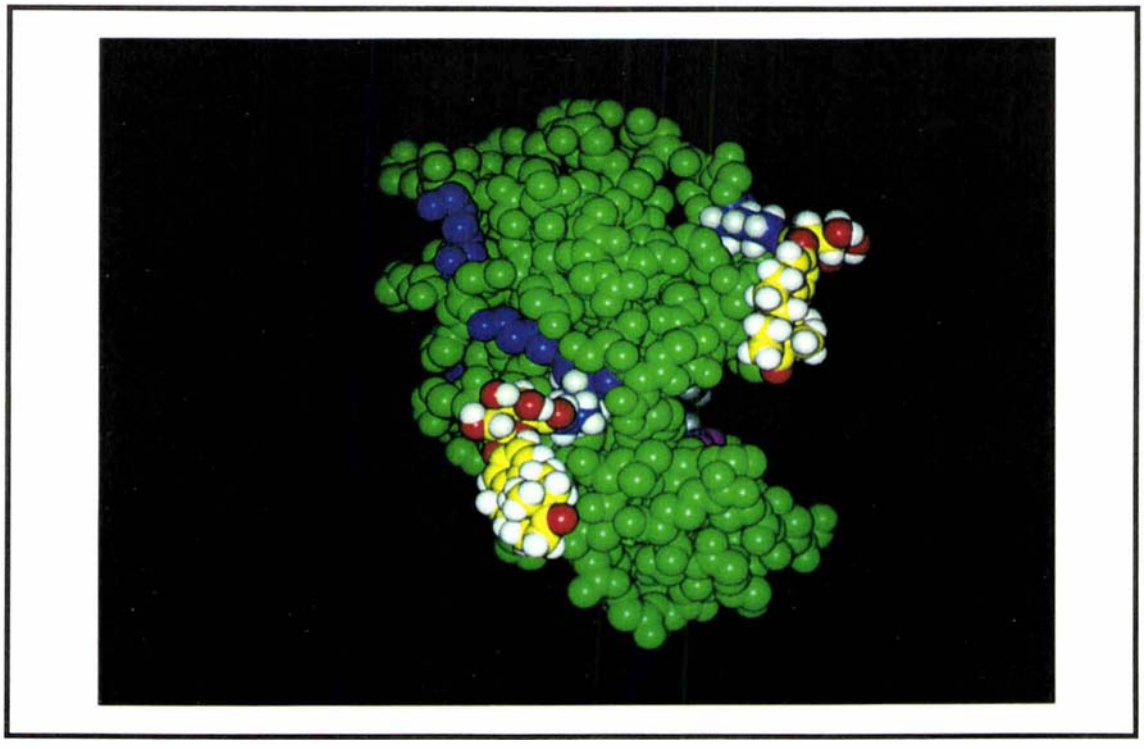

**Fig. 4.3.5** CPK space-filling representation of the computer generated estrone glucuronide-lysozyme conjugate E6 tertiary structure described in Fig. 4.3.4 with the active site cleft oriented to the right hand side of the molecule. The left hand steroid molecule is attached to lysine residue 97 while the steroid above the active site cleft is attached to lysine residue 116.

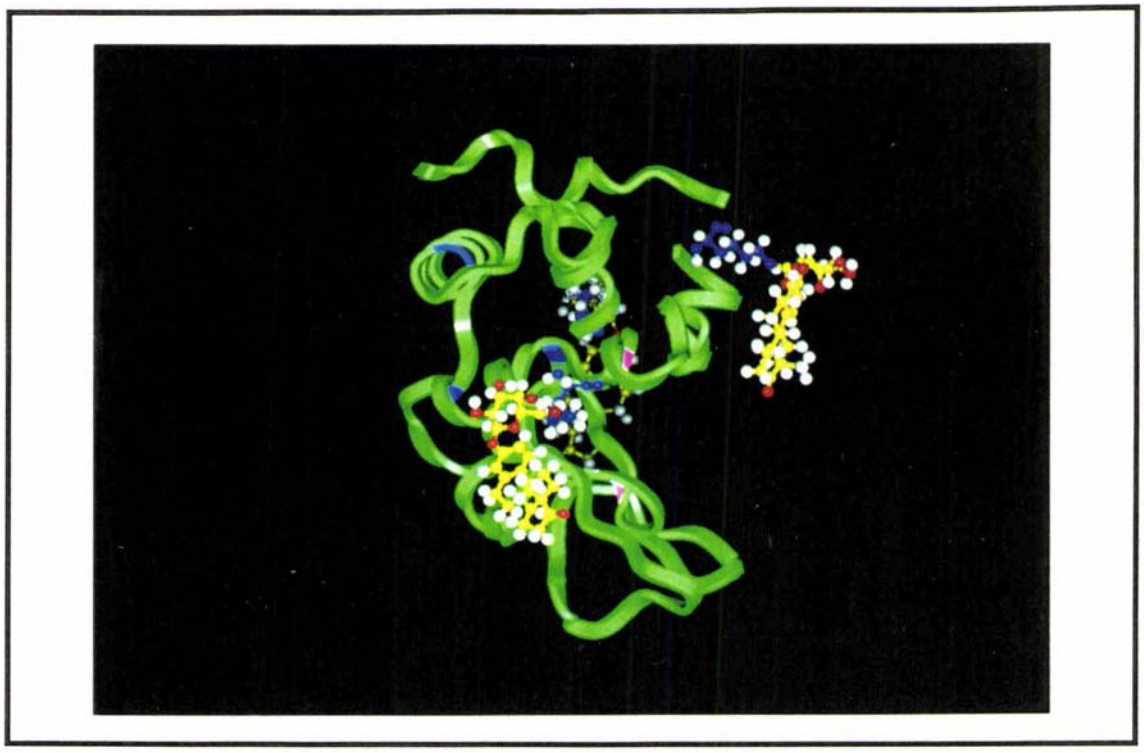

**Fig. 4.3.6** Ribbon diagram representation of Fig. 4.3.5 which clearly shows the dog leg formed between the acylated lysine residue and the steroid glucuronide moiety as seen above the active site cleft when acylation occurs at lysine residue 116. The steroid moiety attached at lysine residue 97 can also be seen in the foreground.

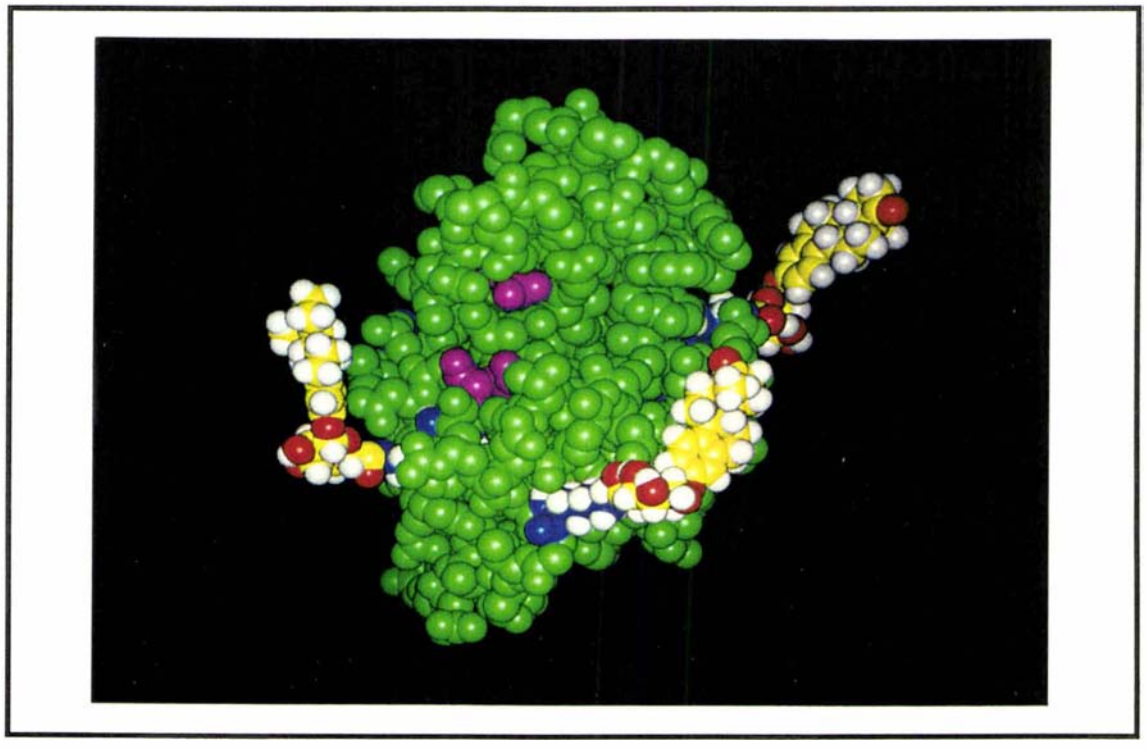

**Fig. 4.3.7** CPK space-filling representation of the computer generated E6 conjugate family tertiary structure when looking directly into the active site cleft. The two catalytic residues Glu 35 (upper) and Asp 52 (lower) are highlighted in pink. All three acylation positions can be clearly seen from this orientation.

parallel to the protein surface and the D ring 17-keto oxygen atom substituent is pointing away from the active site. The steroid skeleton of the steroid glucuronide molecule is therefore presented to the anti-estrone glucuronide antibody so that the unique specificity determinants (the A and D rings) can be bound by the antibody. The tightness of the binding will depend on the distance between the steroid nucleus and the protein surface since the antibody binding surface has a depth to it. An estrone glucuronide moiety linked to lysine residue 116 can also be seen in the background of Fig. 4.3.4.

Fig. 4.3.5 gives a different orientation of the conjugate showing the estrone glucuronide molecules relative to the lysozyme surface when acylation occurs at lysine residues 116 (steroid glucuronide molecule above the active site) and 97 (lower, left hand side steroid glucuronide molecule). Once again the unique determinants of the steroid moiety can be clearly seen. The dog leg bend orientation of the steroid glucuronide moiety relative to the enzyme surface can also be seen clearly, the bend being the result of the peptide linkage formed between the COOH group of the glucuronide ring and the $NH_2$ group of the lysine residue. There is little space between the plane of the steroid and the protein surface in the vicinity of lysine residue 116. Fig. 4.3.6 shows a different representation of E6 (Fig. 4.3.5) whereby the dog leg bend effect can be seen more prominently when the steroid glucuronide molecule is attached to lysine residue 116 situated above the active site. Fig. 4.3.7 shows an orientation of E6 showing the steroid glucuronide molecules at all three acylation positions (lysine 33, right hand side; lysine 97, left hand side; lysine 116, centre) when looking directly into the active site of the enzyme. The two catalytically active residues in the active site of lysozyme (Glu 35, upper residue and Asp 52, lower residue, for more details see chapter five) are highlighted in pink. Once again the dog leg effect and the proximity of the steroid glucuronide moiety to the protein surface can be seen.

In generating the estrone glucuronide-lysozyme conjugate models, non-covalent interactions between the estrone glucuronide moiety and the protein surface were not considered. Nevertheless, the model depicted in Figs. 4.3.4 and 4.3.7 showed that for acylation at lysine 33, the closest protein-steroid interaction was between the aromatic phenol A ring of the steroid and Asn residue 37 of the protein situated 4.43 Å away. The closest contact between the steroid and the protein surface when acylation had occurred at lysine residue 97 was between the non-planar B ring of the steroid and Asn residue 77, a distance of 6.55 Å. Conjugation at residue 116 resulted in a close approach between the D ring of the steroid and Gly residue 102 of the enzyme which were only 3.97 Å apart. However, it is possible that in the actual three dimensional conjugate structures, secondary interactions such as hydrogens bonds and van der Waals contacts between the

protein surface and the steroid glucuronide molecule pull the steroid glucuronide moiety in closer to the protein surface.

Thus, conjugation of the three lysine residues 33, 97 and 116, with estrone glucuronide *via* the free carboxyl group on the carbohydrate ring, results in the presentation of the steroid A and D rings so that the approach by an antibody to the unique determinants is unhindered, as can be seen clearly in Figs. 4.3.4-4.3.7. However, the steroid glucuronide moieties lie parallel to, and quite close to, the protein surface (see Figs. 4.3.4-4.3.7) and the close proximity of the protein to the steroid glucuronide moiety might be expected to hinder the approach of the large anti-hapten antibody. Nevertheless, the anti-estrone glucuronide antibody obviously can bind to the E1G moiety in all of the orientations shown for E6. This conclusion is drawn since extensive inhibition of the lytic activity is observed at stoichiometric ratios of antibody in all cases (see chapter two) but especially for the monosubstituted conjugates which presumably have the same orientation of the E1G moieties as represented by the E6 structures (Figs. 4.3.4-4.3.7).

### 4.3.4 The Molecular Basis for the Immune Recognition of an Antigen by Anti-Antigen Antibodies

Little is known about the molecular basis of the immune recognition by an antibody for a conjugated hapten, or about the three dimensional structures of antibodies and Fab fragments bound to conjugated haptens in immune complexes. More is known about the binding and immune recognition of antibodies to protein antigens [224-226] and much of this work has centred on the mapping of the antigenic epitopes of lysozyme [227-229], and the X-ray structural analysis of anti-lysozyme antibody-lysozyme complexes [199-202, 229-231]. As far back as 1972 Rubenstein *et al.* [107] suggested that the mode of inhibition, when the lytic activity of lysozyme was inhibited by the binding of anti-hapten antibodies to conjugated haptens, was steric hindrance. Thus, the binding of the large antibody to the conjugated hapten is proposed to block the approach of the even larger *Micrococcus lysodeikticus* substrate molecule to the lysozyme active site preventing lysis of the substrate.

X-ray structural analysis of anti-lysozyme antibody-lysozyme complexes has shown that no significant or gross conformational changes are observed in the lysozyme structure upon the binding of a Fab antibody fragment to the protein surface [224]. The Fab structure also undergoes very little structural change upon binding to the lysozyme molecule. Only small, local conformational changes are seen in a few side chains which are required to accommodate the binding of the antibody fragment [224]. Inactivation of

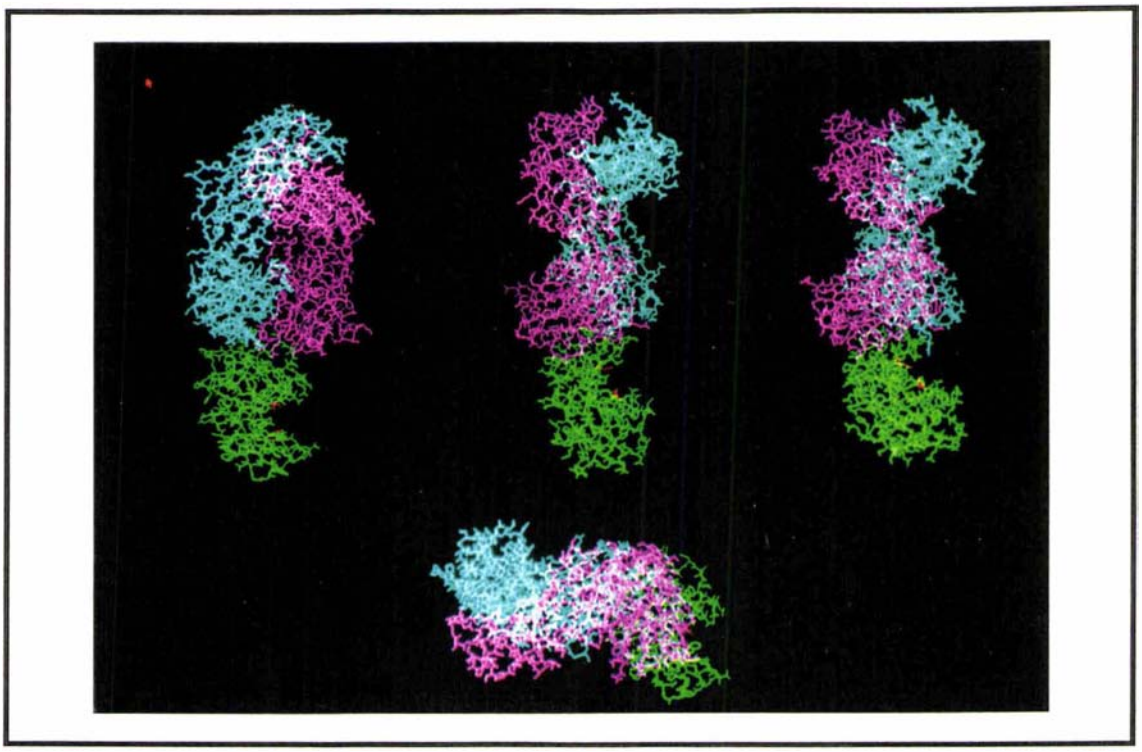

**Fig. 4.3.8** Three dimensional structures of four lysozyme-Fab complexes solved by X-ray crystallographic studies. The structures are those of a) Fischmann *et al.* [199] (top left hand side); b) Braden *et al.* [200] (top centre); c) Sheriff *et al.* [201] (top right hand side); and d) Padlan *et al.* [202] (bottom centre). The lysozyme molecule is shown in green and the active site can be clearly seen on the right hand side in all cases. The heavy chain of the Fab fragment is shown in pink and the light chain in pastel green.

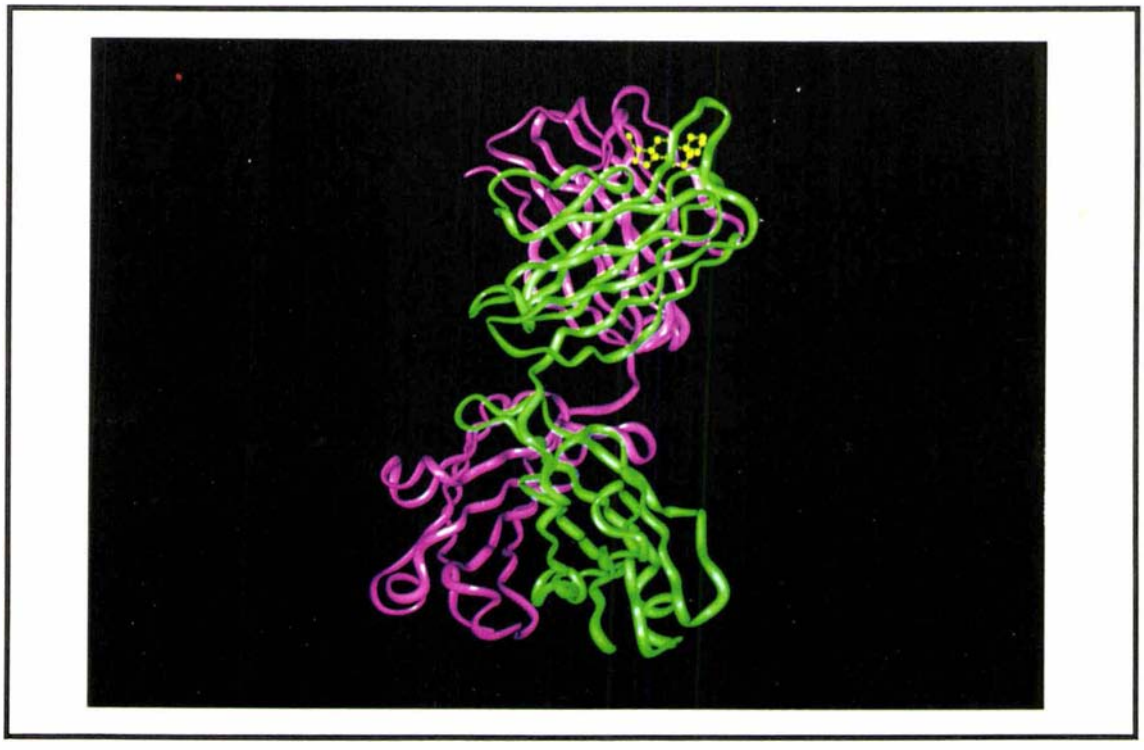

**Fig. 4.3.9** Ribbon diagram representation of the three dimensional structure of the progesterone-Fab complex published by Arevalo *et al.* [203]. The heavy chain of the Fab structure is shown in purple and the light chain in green. The progesterone moiety (coloured yellow) is bound at the top of the Fab fragment in a hydrophobic pocket formed by the hypervariable loops of the heavy and light chains.

lysozyme as a result of a conformational change in the structure of the enzyme upon the binding of the antibody, is therefore unlikely to be responsible for the inhibition of the lytic activity.

Four of the lysozyme-Fab structures solved by X-ray crystallographic studies are shown in Fig. 4.3.8. The antibody Fab fragments in Fig. 4.3.8 are highlighted so that the heavy chain of the fragment is coloured pink and the light chain of the fragment is coloured pastel green. In all of the structures presented (Fig. 4.3.8) the lysozyme molecule is highlighted in green, with the active site oriented so that it is clearly visible on the right hand side of the molecule. The Fab antibody fragment is therefore not completely blocking the active site in any of the structures shown in Fig. 4.3.8 as it can still be seen in all cases despite the presence of a Fab fragment. However, the anti-lysozyme Fab fragments still inhibit the lytic activity of lysozyme very effectively. The inhibitory effect on the lytic activity of the enzyme must therefore be more subtle than simple blocking of access or approach of a substrate to the enzymatic active site. The inhibitory effect of the antibody (or Fab fragment) must still be due to steric hindrance as very little conformation change is expected for the reasons discussed above. Because the lysozyme molecule is so much smaller than the large bacterial substrate (*Micrococcus lysodeikticus*), the presence of the bound Fab fragment, in effect, makes the lysozyme substrate a much larger molecule, stretching out laterally beyond the lysozyme molecule itself. The extra size of the bound Fab fragment must therefore physically prevent the large bacterial substrate approaching close enough to the enzymatic active site of the lysozyme molecule to bind productively. As a result, the enzyme cannot bind and cleave the large bacterial substrate in the presence of anti-lysozyme antibodies or anti-lysozyme Fab fragments.

The major difference between Fab-hapten and Fab-protein antigen structures is likely to be in the actual binding site, as depicted in Fig. 4.3.10. The binding sites of small unconjugated haptens are characterised by the presence of a binding cavity or pocket within the Fab structure into which the hapten fits [230]. The binding sites tend to be rather small in size. However, in protein antigen-Fab X-ray structures, the most relevant structural feature of the combining site tends to be the large irregular, rather flat surface, where the two molecules fit together [230]. The binding sites tend to be large in size and the two molecules interact in the classical lock and key manner, fitting together without the need for gross conformational changes [230]. The lock and key principal is regarded as too static for many steroid-antibody complexes with the overall flexibility of these complexes regarded as being important in the overall binding events [220].

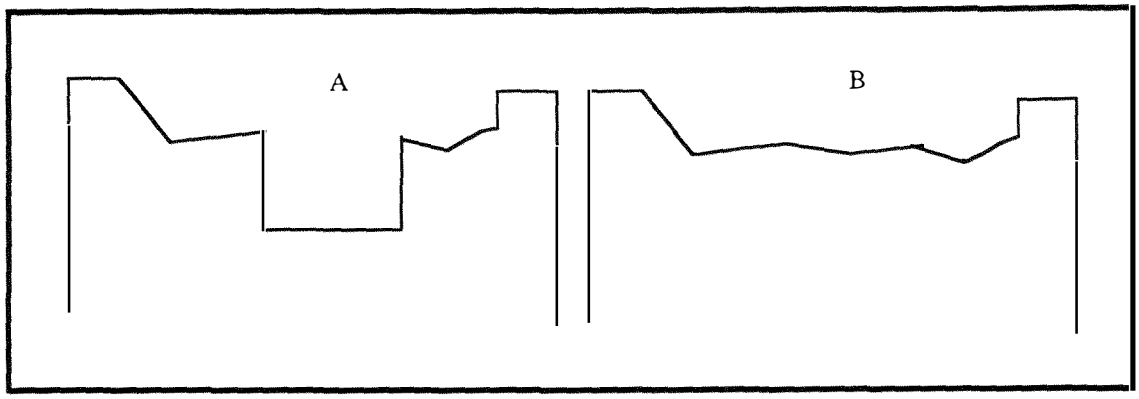


**Fig. 4.3.10** A schematic representation of the differences in Fab-hapten and Fab-protein antigen binding sites. Fab-hapten binding sites (A) tend to be well defined binding cavities or pockets while Fab-protein binding sites (B) tend to be large irregular, rather flat surfaces. The binding sites of Fab-hapten complexes are also much smaller than the binding sites for Fab-protein complexes.

Previous work investigating the binding of steroids to proteins has tended to approach the problem using dilute water miscible organic solvents [232] then followed the binding reaction by monitoring the dielectric and hydrogen bonding properties. The basic idea is that comparing the effects of the solvents would permit the importance of hydrophobic and hydrogen bonding to be differentiated, and give information on the effects of the environment on the binding reaction [232]. Recently however, the X-ray structure of a progesterone-Fab complex has been reported which has revealed important information about steroid-protein binding interactions [203]. A ribbon diagram representation of the structure, as shown by X-ray crystallographic studies (Fig. 4.3.9) shows that the progesterone moiety (coloured yellow) binds at one end of the Fab fragment in a cleft formed between the heavy (purple) and light (green) chains of the Fab molecule. The progesterone moiety can be seen clearly in the binding pocket of the Fab fragment, lying more or less parallel to the combining site surface. The binding site consists of a very hydrophobic pocket which is form by the loop regions of the complementary determining regions (CDR) H1, H2, and H3 hypervariable loops of the heavy chain and the L1 and L3 hypervariable loops of the light chain [203]. The steroid, when bound by the antibody, is almost completely buried in the hydrophobic binding pocket (89% buried) with a total buried surface area of ~ 241 $Å^2$ [203] which is only about a third of the area reported for the binding contact area of the lysozyme-Fab structures [229].

The steroid moiety in the published progesterone-Fab crystal structure is bound in a narrow slot formed by two aromatic tryptophan residues (heavy chain residues Trp 50 and Trp 100). The binding pocket has two conformations, an open and closed conformation, whereby the heavy chain tryptophan 100 residue moves to expose the hydrophobic binding pocket to the incoming steroid [203]. In this way the hydrophobic binding pocket can be hidden from the aqueous solvent when the antibody is in its free,

unbound conformation, and the solubility and stability of the antibody is not compromised.

Both the A and D rings of the progesterone moiety are involved in hydrogen bonds within the complex, the 3-keto group of the A ring hydrogen bonding to a histidine residue and the 20-keto group of the D ring hydrogen bonding to an asparagine residue. The D ring of the steroid is buried much deeper in the binding pocket than the A ring as it is enclosed not only by the two tryptophan residues but also by two extra aromatic rings (heavy chain residues tyrosine 97 and phenylalanine 100b) [203]. Although the steroid obviously occupies a far smaller contact area in the antibody binding site than is the case for the binding of antibodies to protein antigens [199-202], it is still surrounded by the remainder of the antibody combining site which may therefore exert large proximity effects. The recognition and binding of estrone or pregnanediol, which is chemically linked to lysozyme *via* the glucuronide ring, by anti-estrone glucuronide or anti-pregnanediol glucuronide antibodies, probably occurs in the same general manner.

### 4.3.5 Modelling of the Tertiary Structures of the Steroid Glucuronide-Lysozyme-Anti-Steroid Glucuronide Antibody Immune Complexes

Models of the tertiary structures of the steroid glucuronide-lysozyme-anti-steroid glucuronide antibody immune complexes were built by overlapping the steroid moiety of the lysozyme conjugates with the steroid coordinates from the progesterone-Fab complex using a least squares fit program which ensured that the target steroids were oriented into the binding site in the same manner as the progesterone moiety. Only carbon atoms which were conserved in both the progesterone structure and the estrone or pregnanediol moieties were overlapped as shown in Fig. 4.3.11. Fitting of carbon atoms which were not conserved may have changed the orientation of the target steroid in the Fab binding site relative to the orientation of the progesterone molecule.

The root mean square (r.m.s.) deviations between the steroid glucuronide steroid carbon atoms and the progesterone carbon atoms were small (0.163), indicating a good fit between the overlapped structures. Although the progesterone antibody does not recognise the bridging glucuronide ring, the resulting orientation of the antibody, relative to the lysozyme molecule, is likely to be similar to that in the actual three dimensional structure of the conjugate-antibody immune complex. The reasoning behind this expectation is that the steroid-antibody interactions are likely to be the key interactions holding and aligning the steroid glucuronide in the antibody pocket with the glucuronide ring being oriented outwards where few interactions are likely. The glucuronide ring is also in quite close proximity to the lysozyme surface (as discussed in section 4.3.3) and it

is unlikely that the anti-steroid glucuronide antibody can approach close enough to the lysozyme surface to bind all of the glucuronide ring in any case.

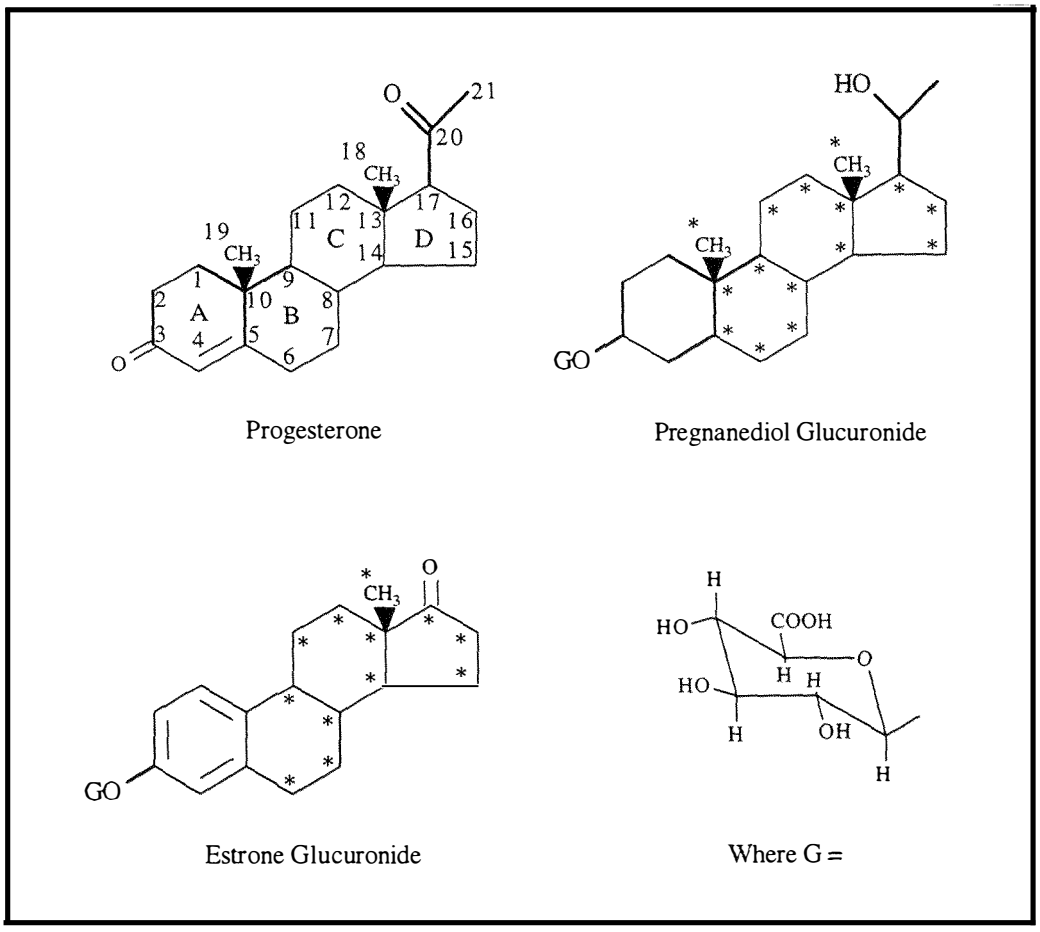


**Fig. 4.3.11** The structures of a) the progesterone steroid moiety (top left hand side) from the progesterone-Fab complex, b) pregnanediol glucuronide, and c) estrone glucuronide showing the carbon atoms of the steroid glucuronides used in the least squares fit to the progesterone structure (those marked with an asterix (*)). For details see text.

The calculated three dimensional structures for the PdG-lysozyme conjugate immune complexes, obtained by inserting the pregnanediol glucuronide moiety into the binding pocket of the Fab fragment of the progesterone-Fab complex are shown in Figs. 4.3.12-4.3.15. In Figs. 4.3.12-4.3.15 the PdG moiety is coloured yellow, the lysozyme molecule green, and the light and heavy chains of the Fab fragment pastel green and purple respectively. The two catalytically active residues in the active site of lysozyme (Glu 35 and Asp 52, see chapter 5) are coloured red. When the antibody binds to a pregnanediol glucuronide moiety which is attached to lysine 116 (as in Fig. 4.3.12), the Fab fragment does not completely cover the lysozyme active site which lies more or less directly below the pregnanediol glucuronide moiety. The Fab moiety does however protrude outwards almost at right angles from the lysozyme surface, and hence the close

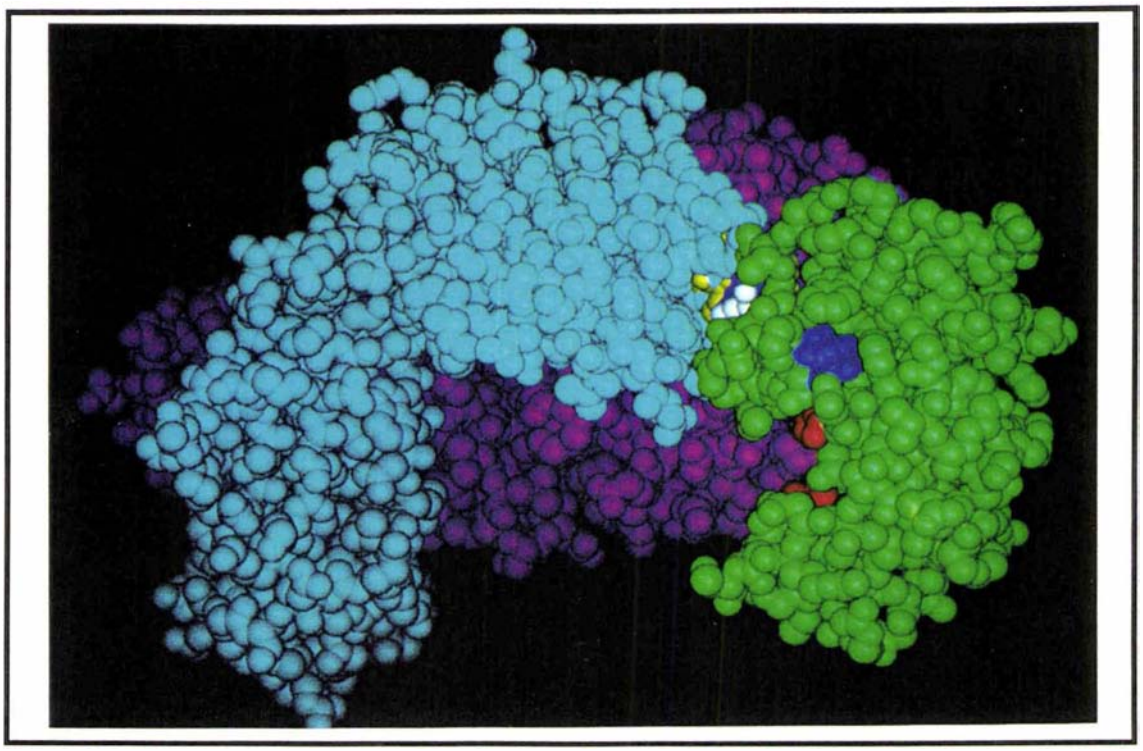

**Fig. 4.3.12** CPK space-filling representation of the computer generated three dimensional structure of the PdG-lysozyme-anti-hapten antibody immune complex when the PdG moiety is attached at lysine residue 116, and the active site cleft is oriented to the left hand side. The lysozyme molecule is shown in green, the PdG moiety is coloured yellow, and the two catalytic residues of lysozyme are highlighted in red. The heavy chain of the Fab fragment is coloured purple and the light chain is coloured pastel green. Lysine residue 33 is highlighted in blue. For details see text.

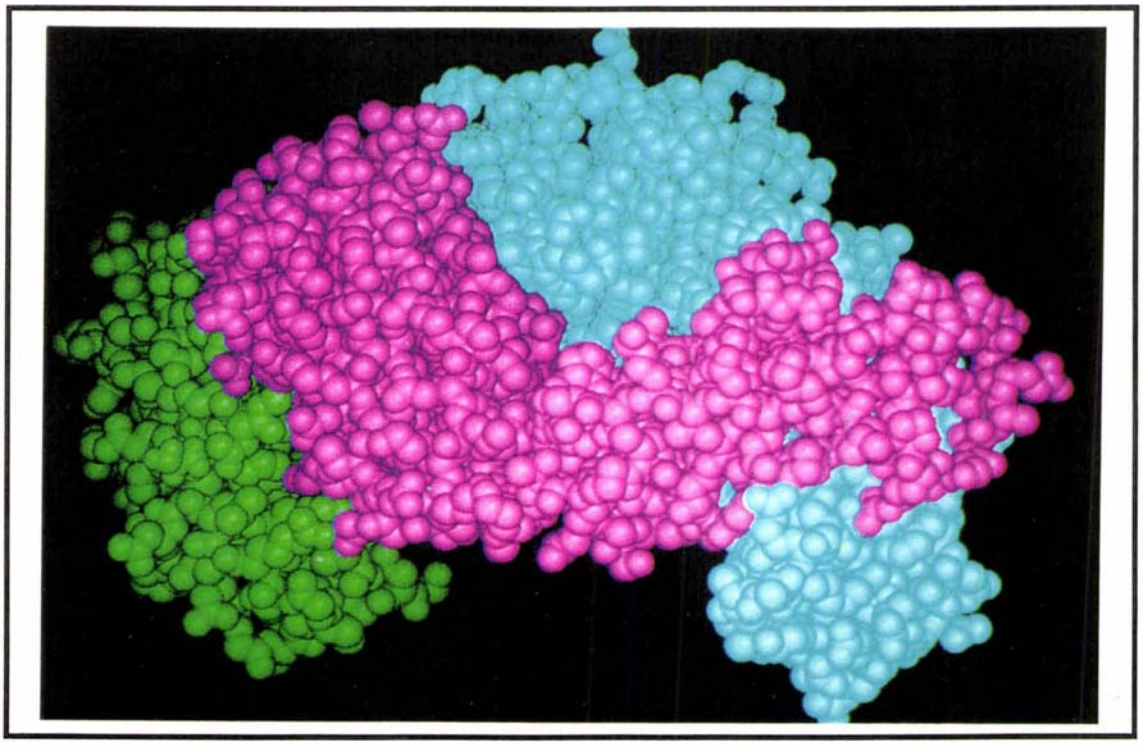

**Fig. 4.3.13** CPK space-filling representation of the computer generated three dimensional structure of the PdG-lysozyme-anti-hapten antibody immune complex when the PdG moiety is attached at lysine residue 116 and the active site cleft is oriented to the right hand side. The colours are coded as described in Fig. 4.3.12.

approach required by the bacterial substrate *Micrococcus lysodeikticus* must be physically prevented. Hence binding of the cell wall into the lysozyme active site is impossible. This is shown more clearly in Fig. 4.3.13 where the immune complex shown in Fig. 4.3.12 is viewed from the other side of the lysozyme molecule, and the Fab structure can be seen to protrude out a considerable distance directly in front of the active site cleft.

When the Fab fragment is bound to the PdG moiety attached at lysine residue 97 (Fig. 4.3.14), the majority of the antibody structure lies in a similar orientation to that seen when the Fab fragment binds to lysine residue 116 (Figs. 4.3.12 and 4.3.13). Fig. 4.3.14 also shows that several amino acid residues from the Fab light chain (shown in pastel green) are in close proximity to the active site cleft. Again, although the Fab fragment does not actually block the active site of the enzyme, approach of the bacterial substrate close enough for insertion of the cell wall NAM-NAG polymer into the active site cleft is not possible. Certainly, the antibody does prevent lysis very effectively as this conjugate is highly inhibited by anti-pregnanediol glucuronide antibodies.

When the Fab fragment is bound to the PdG moiety which is attached to lysine residue 33 of the lysozyme molecule (Fig. 4.3.15) it lies so that it is almost in the same plane as the enzyme. In this case the light chain (coloured purple) of the Fab fragment protrudes slightly outwards and forward from the lysozyme surface with respect to the active site. This may however be sufficient to physically prevent the close approach required of the bacterial substrate to allow productive binding of the cell wall and subsequent lysis of the substrate. At the same time several amino acid residues of the heavy chain of the Fab fragment (coloured purple) are again in close proximity to the enzymatic active site and the catalytically important lysozyme residues (coloured red). As in the case of PdG-lysozyme conjugates, where the steroid is attached at lysine residue 97, this intrusion of the protein may be sufficient in itself to prevent or seriously impair the cell wall of the large bacterial substrate binding productively into the active site cleft. The lytic activity of the conjugate may therefore be inactivated, in this case, by a combination of two different steric inhibition modes, that is, by both preventing (1) the close approach of the bacterial substrate and (2) the productive binding required for substrate lysis. It is not possible to predict from the structure which mode may play the more dominant role in the lytic inhibition of the conjugate when the PdG steroid is attached at lysine residue 33.

The estrone glucuronide-lysozyme conjugate, where the steroid moiety was attached at lysine residue 33, was also placed into the binding site of the progesterone Fab structure and the resulting three dimensional immune structure is shown in Fig. 4.3.16. The resulting orientation of the Fab structure, with respect to the lysozyme active site, is

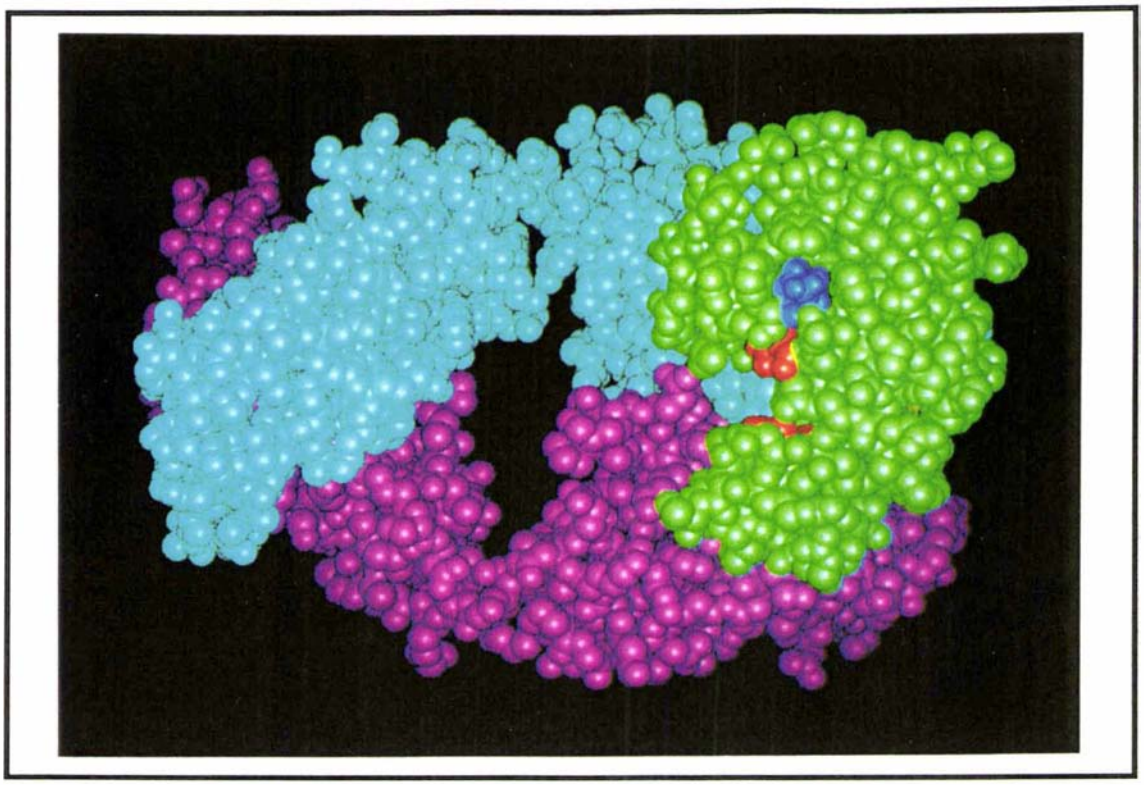

**Fig. 4.3.14** CPK space-filling representation of the computer generated three dimensional structure of the PdG-lysozyme-anti-hapten antibody immune complex when the steroid glucuronide moiety is attached at lysine residue 97. The colour coding is as described in Fig. 4.3.12. Lysine residue 33 is highlighted in blue. The PdG moiety cannot be seen as it is obscured by the lysozyme molecule. For details see text.

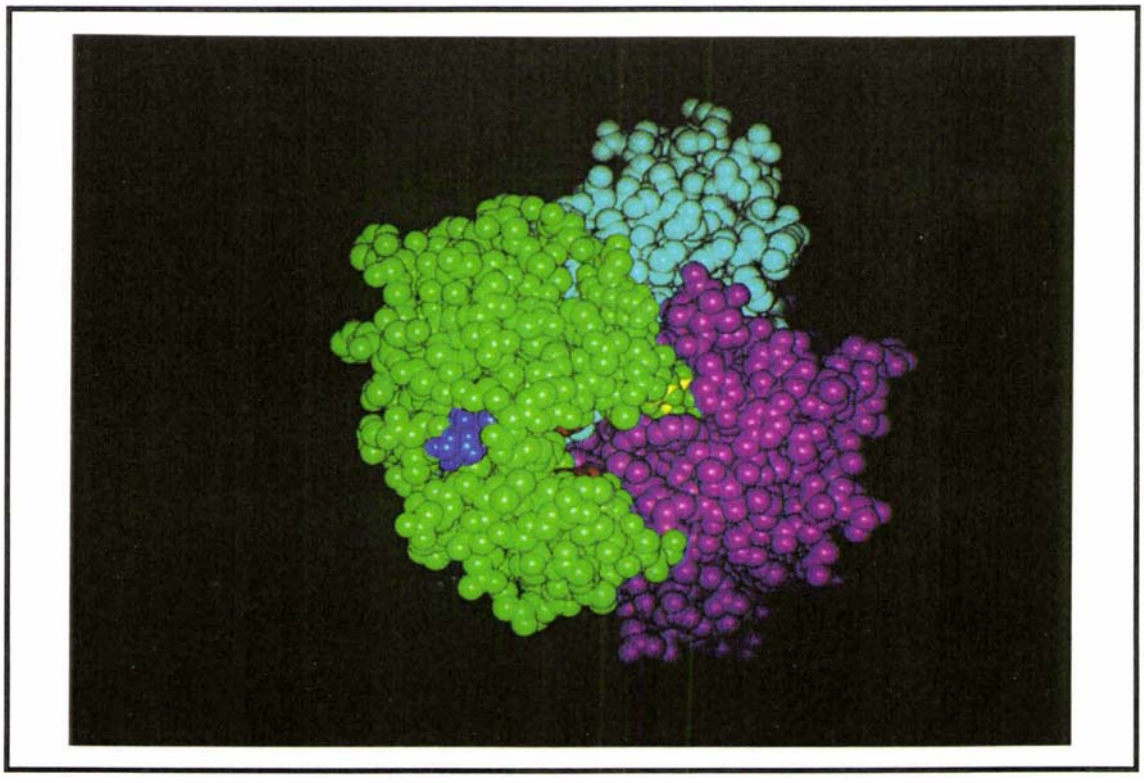

**Fig. 4.3.15** CPK space-filling representation of the computer generated three dimensional structure of the PdG-lysozyme-anti-hapten antibody immune complex when the PdG moiety is attached at lysine residue 33. The colour coding is as described in Fig. 4.3.12. Lysine residue 97 is highlighted in blue. The PdG moiety cannot be seen as it is obscured by the lysozyme molecule. For details see text.

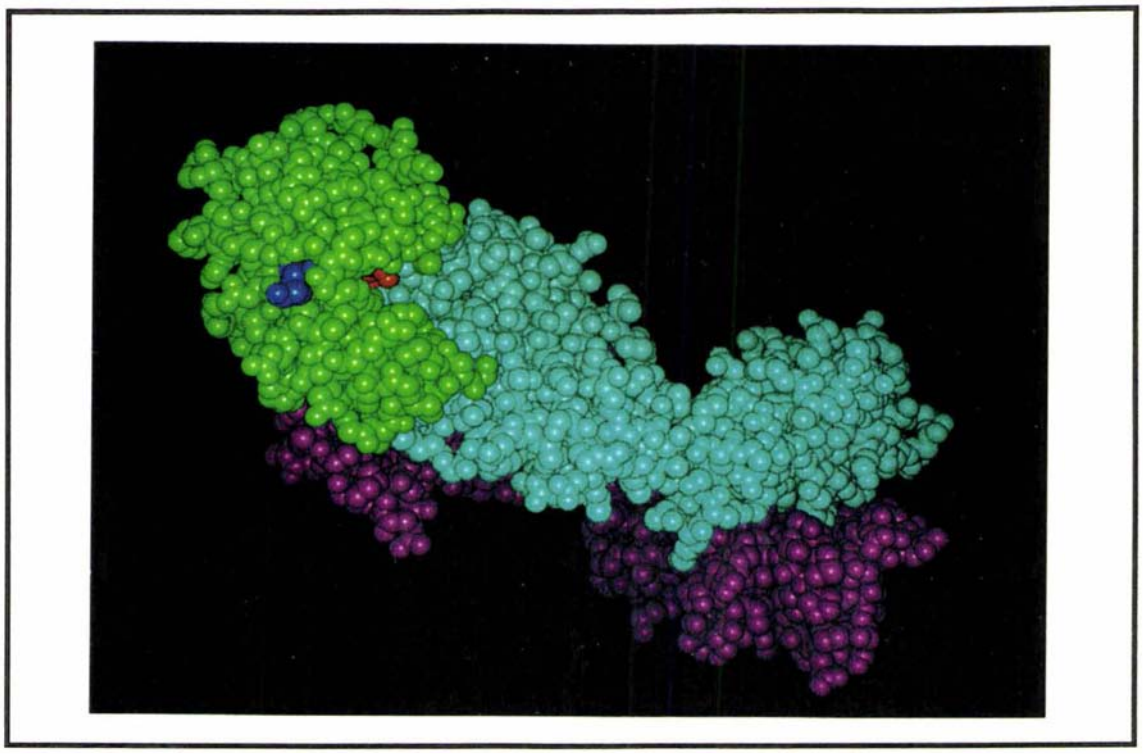

**Fig. 4.3.16** CPK space-filling representation of the computer generated three dimensional structure of the E1G-lysozyme-anti-hapten antibody immune complex when the E1G moiety is attached to lysine residue 33. The lysozyme molecule is shown in green and the two catalytic residues are highlighted in red and can be seen in the active site cleft. The heavy chain of the Fab fragment is coloured purple and the light chain is coloured pastel green. Lysine residue 97 is highlighted in blue. The E1G moiety cannot be seen as it is obscured by the lysozyme molecule. For details see text.

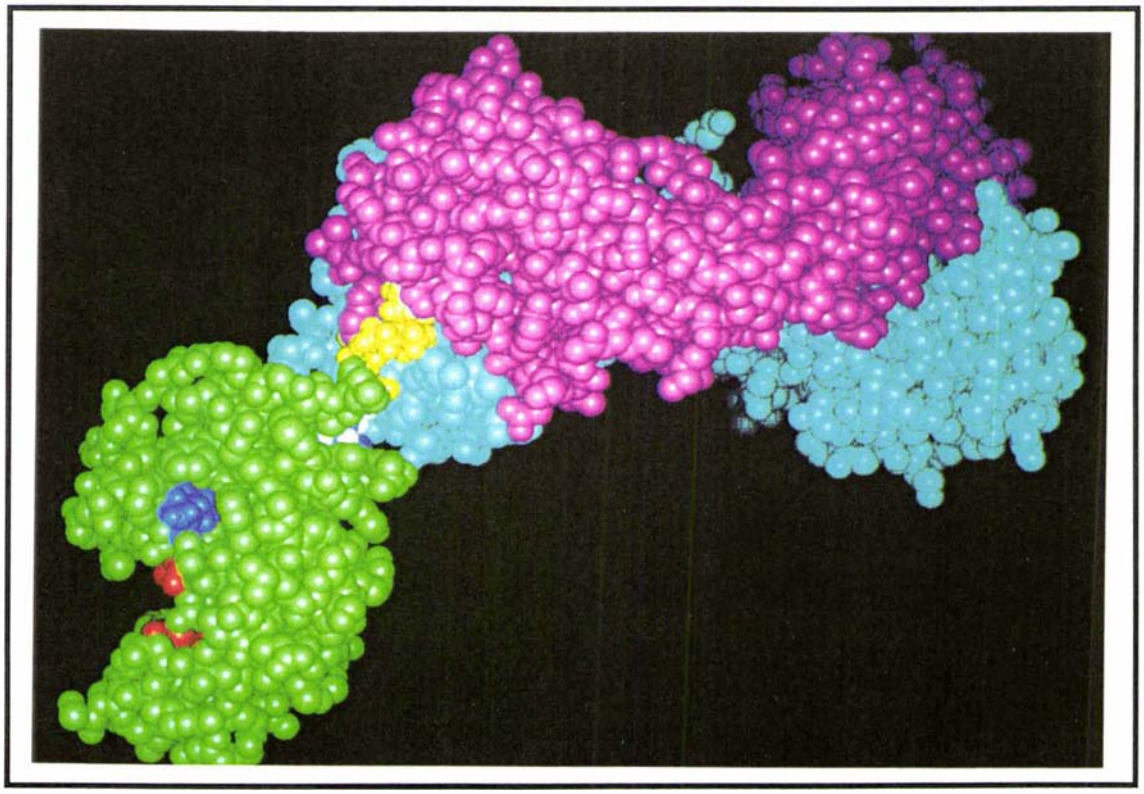

**Fig. 4.3.17** CPK space-filling representation of the computer generated three dimensional structure of the PdG-lysozyme-anti-hapten antibody immune complex when the PdG moiety is attached at lysine residue 13. The colour coding is as described in Fig. 4.3.12. For details see text.

different from that observed for the corresponding PdG-lysozyme structure (Fig. 4.3.15). In the estrone glucuronide-lysozyme conjugate the Fab fragment protrudes much further forward of the enzymatic active site The antibody fragment lies in a similar orientation to that seen in the PdG-lysozyme conjugate, although on the opposite side of the lysozyme molecule, when the PdG moiety is attached to lysine residue 116 (Fig. 4.3.12). Thus, binding of the Fab structure to the E1G moiety (Fig. 4.3.16) would be expected to physically prevent the close approach and binding of the large bacterial substrate to the active site cleft, irrespective of any effects on the productive binding of the cell wall polymer into the active site.

The fitting of the pregnanediol glucuronide-lysozyme and estrone glucuronide-lysozyme conjugate molecules into the progesterone antibody binding site can give only a broad picture of the three dimensional structure upon the binding of an anti-PdG or anti-E1G antibody. However, the results clearly show that both the identity of the steroid and the position of acylation play a part in determining the orientation of the antibody with respect to the enzymatic active site. The importance of the acylation position can be seen best in the three dimensional structure represented in Fig. 4.3.17. In this structure the pregnanediol glucuronide moiety was attached to the lysozyme molecule at lysine residue 13. Although there were no conjugates actually found where lysine residue 13 was acylated, the computer generated structure shows that if this were the case, the binding of an anti-PdG antibody to a hapten attached at this position on the lysozyme molecule would not be expected to inhibit the lytic activity of the enzyme. The structure clearly shows the Fab fragment is oriented on the opposite side of the lysozyme molecule with respect to the active site, and cannot therefore, interfere with the binding of the large bacterial substrate by either of the mechanisms discussed above. Even allowing for rotation about the carbon-carbon bonds of the lysine side chain it would not be possible to orientate the Fab fragment so that it would cause enough steric hindrance to inactivate the lytic activity of the enzyme. Since lysine 13 was not acylated in any of the conjugates this prediction could not be tested experimentally.

The fortunate fact that neither lysine residue 1 or 13 of the lysozyme molecule were acylated with the steroid glucuronides is therefore extremely important to the success of the assay system. If these residues were acylated in conjugates with low substitution levels it would result in conjugates which could not be inhibited to any great extent upon binding of an anti-hapten antibody based on the three dimensional structures generated and discussed above. Thus the lysozyme system is perfect for the Ovarian Monitor system since only highly inhibitable conjugates are obtained upon acylation with either PdG or E1G.

The inhibitory effect of the anti-E1G and anti-PdG antibodies on the lytic activity of the Ovarian Monitor conjugates is therefore the result of a combination of factors, such as the nature of the hapten, the orientation of the hapten with respect to the active site, the size of the substrate, the size of the enzyme itself and the length and rigidity of the link between the hapten and the enzyme. However, the fact that there is still residual activity for the purified conjugates, even in the presence of excess anti-hapten antibody, shows that binding and cleavage of the bacterial substrate is still possible in the presence of excess antibody, although only at an extremely slow rate. The low residual activity may be due to kinetic effects, such as the competition that exists between the *Micrococcus lysodeikticus* substrate and the antibody for the conjugate. During the time period required for an assay, it is possible for equilibration to occur and the equilibrium to shift from complete binding to the antiserum towards partial binding to both the cell wall *Micrococcus lysodeikticus* substrate and the antibody. Hence a more detailed analysis of the kinetic effects and kinetic mechanisms at work in the assay system is needed, and this is the topic of discussion in chapter five.

## 4.4 Conclusions

The large degree of inhibition observed in the lytic activity of the steroid glucuronide-lysozyme conjugates upon the binding of an anti-hapten antibody is due to steric hindrance of the active site as suggested by Rubenstein *et al.* [107] and not conformational changes. However, the steric hindrance does not operate simply by blockage of the active site but rather by (1) providing a physical barrier to approach by the large bacterial substrate, (2) by disrupting the binding of the long bacterial cell wall polymer into the lysozyme active site cleft by blocking of one end of the active site cleft by the antibody combining site, or (3) a combination of (1) and (2). One question which still needs to be addressed, is what affect the size of the bacterial substrate has on the degree of inhibition observed. This question is one of the topics for discussion in chapter five.

# Chapter Five

# The Kinetics and Mechanism of the Estrone Glucuronide-Lysozyme-Anti-Estrone Glucuronide Antibody Binding Reaction

## 5.1 Introduction

### 5.1.1 The Mechanism of Lysozyme Action

Sir Alexander Fleming is perhaps most renowned for his discovery of penicillin which is generally accepted as "a milestone in the history of medical progress" [233]. However, seven years before this Fleming discovered the enzyme lysozyme [234], which has since been extensively studied and has contributed much to our present understanding of enzymology. Fleming also discovered a gram-positive species of bacteria, *Micrococcus lysodeikticus*, which was particularly susceptible to the action of lysozyme [234] and is still used almost universally in assaying its activity. Later Berger and Weiser [235] showed that lysozyme also degrades chitin, a linear $\beta(1\rightarrow4)$ linked polymer of N-acetylglucosamine, and many kinetic studies now use chitin derived oligosaccharides as the lysozyme substrate. Fleming also reported that lysozyme was present in many animal and plant tissues [234] and it is now known that the enzyme is extensively distributed throughout the plant and animal kingdoms [236]. The most easily accessible and concentrated source of lysozyme was found to be hen egg white, and hence most of the work on lysozyme has been undertaken with hen egg white lysozyme (HEWL). The greatest advancement in the understanding of the catalytic mechanism of lysozyme came with the solving of the three dimensional structure of hen egg white lysozyme in 1965 [237] (see chapter two, Figs. 2.1.1 and 2.1.2). Although the exact mechanistic details of lysozyme activity are still under debate, a general understanding of the complex reaction sequence and stereoelectronic effects which occur during the lysozyme reaction is now known and accepted by the scientific community.

Early work examined the activity of lysozyme on the *Micrococcus lysodeikticus* bacterial substrate. In 1952 Salton [238] showed that the substrate was located within the bacterial cell wall and in 1963 Jeanloz *et al.* [239] showed that a tetrasaccharide from a lysozyme digest of the substrate consisted of a series of $\beta(1\rightarrow4)$ linkages between alternating N-acetylglucosamine (GlcNAc or NAG) and N-acetylmuramic acid (MurNAc or NAM)

sugar units, as shown in Fig. 5.1.1. Earlier, Berger and Weiser [235] had shown that lysozyme possessed β(1→4) glucosamine activity in experiments with an N-acetylglucosamine linear chitin polymer (Fig. 5.1.2). It was later shown that lysozyme cleaves the glycosidic bond between the C-1 NAM sugar residue and the C-4 NAG sugar residue in the cell wall. The glycosidic bond between C-1 of the NAG residue and C-4 of the NAM residue is not cleaved. The three dimensional crystal structure of lysozyme, as published in 1965 [237], clearly showed the active site cleft, and the crystal structure of an enzyme-substrate complex unambiguously identified the participating functional groups in the active site region [240].

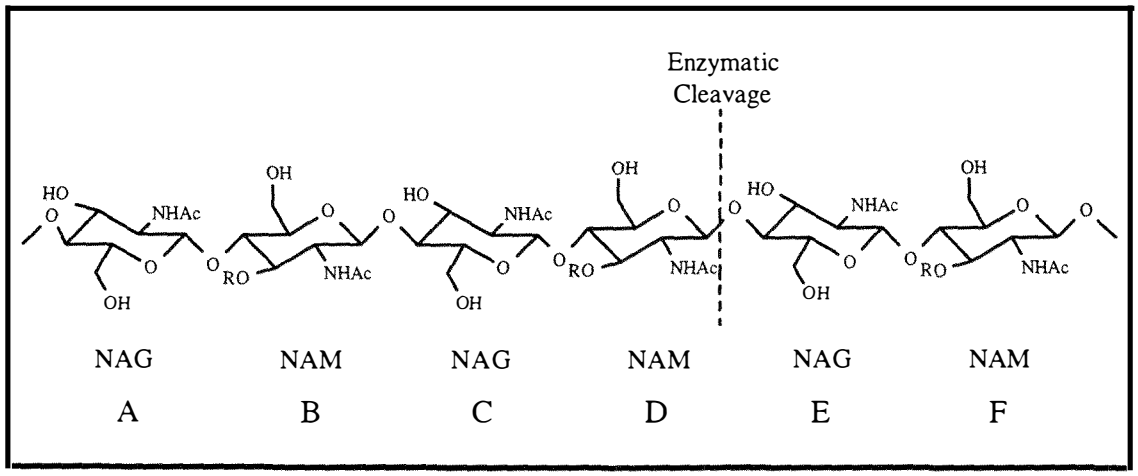


**Fig. 5.1.1** The structure of the polysaccharide component of the *Micrococcus lysodeikticus* bacteria cell wall. The cell wall consists of alternating N-acetylglucosamine (NAG) and N-acetylmuramic acid (NAM) sugar residues. NHAc refers to the N-acetyl or acetamido moiety found in both NAG and NAM sugars. R refers to the lactyl or $OCH(CH_3)COOH$ moiety found in NAM sugar residues. Six saccharide units are thought to bind to successive sites in the lysozyme active site labelled A through F. Lysozyme cleaves the glycosidic bond between the C-1 of the NAM residue and the C-4 of the NAG residue between the sugar residues bound at sites D and E, as indicated in the diagram.

Because small oligosaccharides bound in the actual active site of the enzyme can be co-crystallised with lysozyme, most of the mechanistic studies on hen egg white lysozyme have been undertaken with the small oligosaccharide complexes. The crystal structure of lysozyme with tri-(N-acetylglucosamine) (tri-NAG) bound in the active site, clearly defined the location of the active site and showed tri-NAG occupied about half of the active site cleft. These three binding saccharide units were designated A, B, and C and three additional sugar units have since been fitted into the rest of the active site cleft by computer modelling [241]. These additional saccharide units are labelled D, E, and F, confirming that the active site cleft of hen egg white lysozyme consists of an extended binding site. The six binding subsites (A-F) can accommodate a linear hexasaccharide and the structure is held in place by hydrogen bonds between the oligosaccharide and the side chains of nearby amino acid residues. Although there are no electrostatic interactions

between the oligosaccharide and the enzyme many van der Waals interactions exist further stabilising the enzyme-substrate complex.

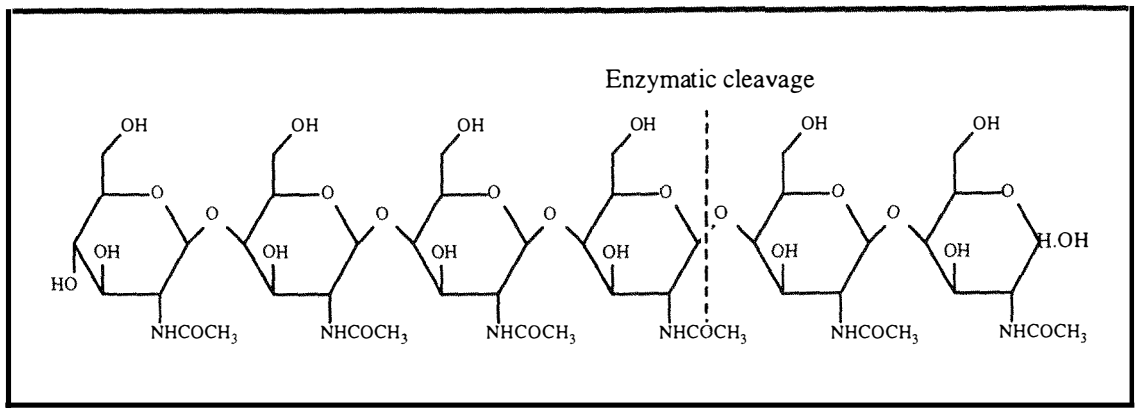


**Fig. 5.1.2** The site of hydrolysis of the chitin derived $(GlcNAc)_6$ hexa N-acetylglucosamine oligosaccharide moiety by lysozyme. Lysozyme cleaves the β-glycosidic bond between the fourth and fifth sugar residues of $(GlcNAc)_6$ to give $(GlcNAc)_4$ and $(GlcNAc)_2$ as products.

As shown by the tri-NAG crystal structure [241], the non-reducing end of the substrate binds into subsites A-C without the need for adjustment of the conformation of the oligosaccharide. However, in order to achieve satisfactory binding of the two terminal sugars (which were fitted into the active site subsites E and F as mentioned above) in the hexasaccharide structure, without incurring serious non-bonded interactions, it was necessary to adjust the conformation of the sugar in subsite D from the ground state chair conformation to a half-chair conformation [241]. This obviously results in a cost in free energy in the binding of the sugar residue bound in subsite D. Crystallographic evidence also indicates that this distortion of the D sugar ring may be necessary [242-243].

However, in what manner does the actual bacterial NAG-NAM structure bind and which bond is cleaved? Because tri-NAG is stable when bound in the A-C subsites in the active site cleft, the bond between residues A-B and B-C obviously cannot be cleaved. The actual bond cleaved in the bacterial substrate was known to be a NAM-NAG linkage and because a NAM residue cannot fit into subsite C a NAG residue must be bound there. This ruled out cleavage between sugar residues C-D and E-F and as a result left the D-E bond as the only remaining candidate for the cleavage site [244] (Fig. 5.1.3). The NAG-NAM polymer must therefore bind so that a NAG residue occupies the A subsite and a NAM residue the F subsite. As a result a NAM sugar residue binds at subsite D and a NAG sugar residue at subsite E and the enzyme catalyses the hydrolysis of the β(1→4) link between these two sugar molecules using the functional groups situated at residues Glu 35 and Asp 52 as described in Figs. 5.1.3 and 5.1.4.

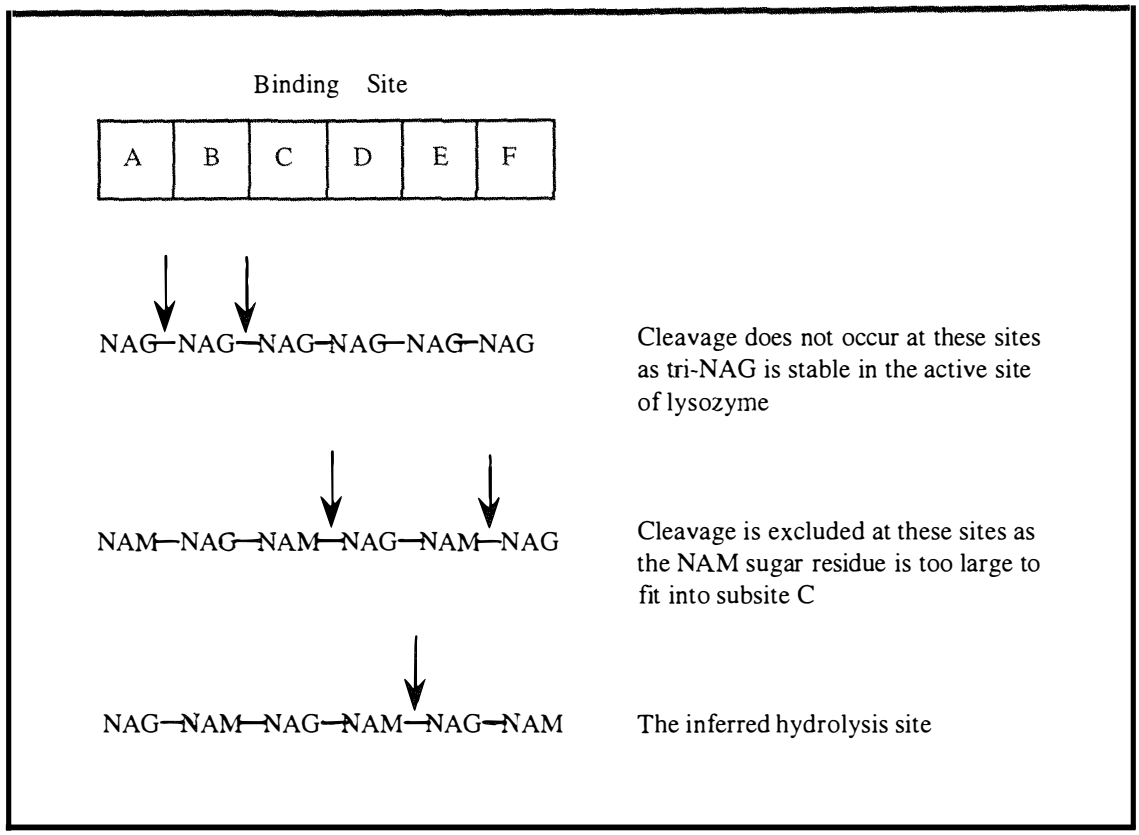


**Fig. 5.1.3** The steps in deducing that it is the glycosidic bond between the sugar residues in subsites D and E is that cleaved by lysozyme

Identification of the bond which is hydrolysed in turn allowed the identification of the catalytic groups which must be in close proximity to the glycosidic bond cleaved. Close to the anomeric centre of the D ring of the bound sugar, where bond cleavage must occur, are two carboxyl groups, those of glutamic acid residue 35 (Glu-35) and aspartic acid residue 52 (Asp-52). Chemical modification of these two groups destroys the catalytic activity of the enzyme [245-247] and thus these two carboxylic acid groups have been identified as being responsible for the chemical catalysis. Despite the identification of the catalytic groups, the mechanistic problem of how one COOH group (Glu-35), assisted by a second $COO^-$ group (Asp-52), can catalyse the hydrolysis of the unreactive glycosidic linkage of an oligosaccharide remained. Although much debate still rages over this problem, at least in a broad outline, it is thought that the mechanistic details are as depicted in Fig. 5.1.4 and proceed as follows;

1. The COOH group of Glu-35 participates as a general acid, donating a proton to the leaving group glycosidic oxygen atom between the sugar D and E rings. This results in the cleavage of the bond between C-1 of the D ring and the glycosidic oxygen which remains attached to the E ring.

2. The dimer oligosaccharide, consisting of the sugar residues bound to subsites E and F, is then free to diffuse away from the enzyme.

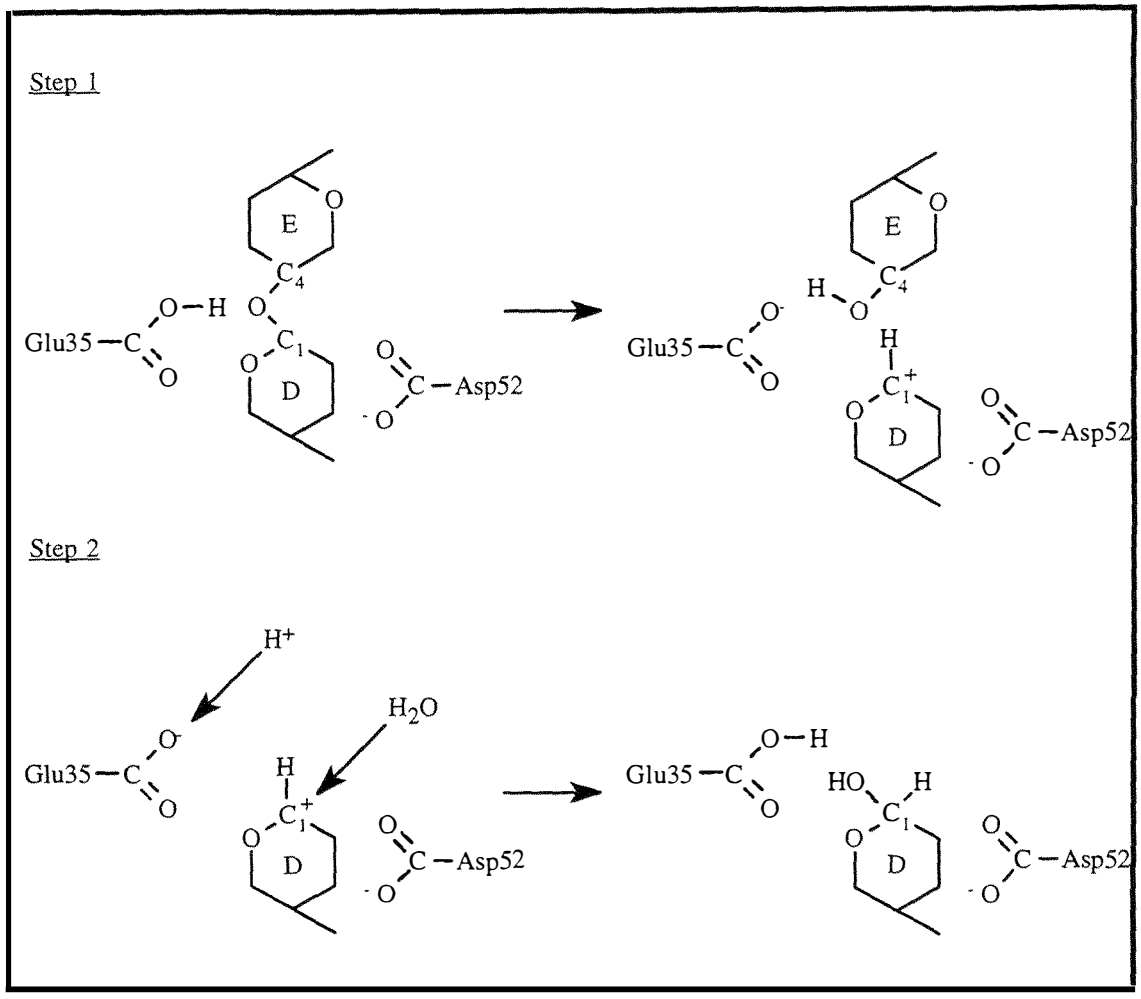


**Fig. 5.1.4** The hydrolysis of substrate by lysozyme. In the first step of catalysis, an $H^+$ ion is transferred from Glu 35 to the oxygen atom of the glycosidic bond, which is cleaved, and a carbonium ion intermediate is formed. In the second step, the cleavage reaction is completed by the addition of OH from a water molecule to the carbonium ion and $H^+$ to the side chain of Glu 35. N.B. only the skeletons of the D and E sugar residues are shown.

3. The cleavage of the bond results in the formation of a carbocation at position C-1 of the D-ring. The negative charge on the nearby ionised Asp-52 $COO^-$ group stabilises the formation of the carbocation by favouring its development. The D ring distorted half-chair conformation allows further stabilisation of the carbocation transition state. The half-chair conformation of the D ring is already close to that required in the transition state and allows the positive charge located at carbon C-1 to be shared between C-1 and the sugar ring oxygen.

4. Finally, the reactive carbocation reacts with a hydroxyl group from the aqueous environment and Glu-35 is re-protonated, thus completing the cycle.

A large amount of experimental support and evidence now exists so that the above mechanism is widely accepted. More recent evidence suggests that Asp-52 has a second role in catalysis other than stabilisation of the metastable oxocarbonium intermediate through charge-charge interactions. It is proposed that Asp-52 also interacts with the active site NAM sugar residue (bound at subsite D) *via* a hydrogen bond with the O-3' lactyl group of the sugar residue so as to help strain the pyranose ring into the more reactive half-chair conformation [243, 248]. Recently the role of electrostatics in the enzymatic mechanism have also come under investigation, suggesting that the electrostatic component may play a much larger role in the catalytic mechanism than previously considered [249].

### 5.1.2 Measurement of Lysozyme Activity

The turbidimetric method for the assay of the lytic activity of lysozyme provides one of the quickest and easiest methods for the detection of the enzymatic activity of lysozyme. The method is based on the decrease in optical density of a suspension of cell walls from the bacterial substrate *Micrococcus lysodeikticus*, or of the intact cells. Although there are many variations on the exact procedure [250-251], those of Shugar [252] and Jolles [253] are the most widely used. The observed change in absorbance (or transmission) measured is due to the light scattering of the bacterial cell and is therefore only indirectly related to the enzymatic activity. Although the turbidimetric assay of lytic activity is easy to perform it is extremely sensitive to changes in pH, ionic strength and even the instrument used to measure the changes in absorbance. For these reasons it is difficult to compare results obtained in different places or with different instruments and as a result great care must be taken when discussing the kinetic properties as determined by turbidimetric assay.

Measurement of lysozyme activity by the hydrolysis of oligosaccharides is much less popular than the turbidimetric method. The measurement of lysozyme activity in this way is much more technically demanding and time consuming than the turbidimetric method, but has allowed more precise measurement of the kinetic parameters. Lysozyme activity measured in this way (using oligosaccharides) is less sensitive to ionic strength effects and chemical modification of the positively charged amino groups within the lysozyme structure. Kinetic studies with the small oligosaccharide substrates may however be complicated by both transfer reactions (such as the transglycosylation of $NAG_4 + NAG_2$ to form $NAG_6$) and non-productive binding. In transglycosylation reactions, the products of the cleavage reaction bound to sites A-D (for $NAG_2$ as a product of the cleavage of $NAG_4$, the $NAG_2$ product is bound in subsites C and D) react with another sugar residue (ROH) instead of $OH^-$ or $H_2O$. Therefore the transglycosylation reaction of $NAG_2$ bound

in subsites C and D with $NAG_4$ (of which two sugar residues bind into subsites E and F) gives $NAG_6$. Fortunately, these transglycosylation reactions are very slow under the conditions utilised for hydrolysis experiments.

### 5.1.3 Mechanistic Detail of the Ovarian Monitor Assay System

The three dimensional models generated in chapter four implied that the large size of the bacterial substrate, relative to lysozyme, was a key factor in the extensive inhibition of the enzymatic activity observed for the lysozyme-steroid glucuronide conjugates in the presence of excess anti-steroid glucuronide antibody. Lysozyme will also cleave chitin derived oligosaccharides [254] which are tiny compared to the extremely large *Micrococcus lysodeikticus* cell wall. If the lysozyme conjugates are not inactivated by the anti-steroid glucuronide antibodies using the small oligosaccharides as substrates this has important consequences for the future design of new inhibitable enzyme systems capable of producing colours. Most of the enzyme systems capable of producing colours (such as horseradish peroxidase) use small chromogenic substrates and such systems have not shown the extensive degree of inhibition observed with lysozyme systems. The characterised conjugates and conjugate-antibody immune complex models can therefore be used as probes for the steric requirements of the active site cleft, by comparing the levels of activity in the presence, and absence, of excess anti-steroid glucuronide antibody for the oligosaccharide and *Micrococcus lysodeikticus* substrates. The effect of the steroid glucuronide acylation position and the protrusion of the antibody into the active site of the enzyme, relative to the size of the substrate, can also be investigated.

## 5.2 Experimental

### 5.2.1 Apparatus

Fab purifications were performed on a Pharmacia Fast Protein Liquid Chromatography (FPLC) system at room temperature. This system consisted of two P-500 pumps, an LCC-500 liquid chromatography controller, an MV-7 motor valve injector, a P-1 peristaltic pump, a Pharmacia mixer and a 280 nm single-path UV-1 monitor which was coupled to a two channel Pharmacia chart recorder. Purifications were performed on a Pharmacia Superdex G-75 gel filtration column. SDS-PAGE was undertaken on a Protean® II xi system, from Bio-Rad Laboratories, Richmond, CA 94804. All other apparatus was as described in the methods section. The curve fitting software program GraphPad Prism™ (Version 2.0) was to used to fit data on an IBM compatible computer.

### 5.2.2 Reagents

The monoclonal antibody to estrone glucuronide (isotype IgG1 [98]) was generated from Balb/c mice using standard methodology and was a generous gift from Dr. Keith Henderson (AgResearch, Wallaceville Research Centre, Upper Hutt, New Zealand). Pepsin A powder (EC 3.4.23.1, containing 80% lactose) was from BDH Biochemicals Ltd, Poole, England. The mixed anhydride estrone glucuronide-lysozyme E3 conjugate used in all experiments was prepared as described in section 3.2.3.3 after purification on a Butyl Sepharose column. *Micrococcus lysodeikticus* was from Sigma Chemical Co. (St. Louis, MO, U.S.A.) and was prepared by triturating 7.5 mg/mL with 75 mM tris maleate buffer in a glass homogenator and then sonicating the suspension for five minutes. The bacterial suspension was kept on ice and resonicated every 1-2 hours. Hexa-N-acetyl-chitohexaose [$(GlcNAc)_6$] from the Seikagaku Corporation, Tokyo, Japan, was a generous gift from Professor P. A. Sullivan (Department of Biochemistry, Massey University, Palmerston North, New Zealand). All other chemicals and reagents were analytical reagent grade or better. All buffers were filtered and degassed, and stock tris-maleate buffer prepared as described in chapter two (section 2.2.2).

### 5.2.3 Methods

*5.2.3.1 Preparation of estrone glucuronide monoclonal antibody Fab fragments*

Fab fragments of the estrone glucuronide monoclonal antibody were prepared essentially as previously described [255-257] *via* the formation of $F(ab')_2$ fragments using pepsin digestion at pH 3.5. Pepsin A powder (20.5 mg), was dissolved in sodium citrate buffer (0.1 M, pH 3.50, 1 mL), and then an aliquot of the resulting solution (200 μL) was

added to a sample of freeze dried estrone glucuronide monoclonal antibody powder (36.4 mg) dissolved in the same buffer (10 mL) in a 5 mL pyrex screw top test tube. This weight of monoclonal antibody powder contained monoclonal antibody (approximately 10.9 mg), with the remainder consisting of ammonium sulfate used in the purification and other buffer salts. Digestion was allowed to proceed for 4.0 hours at 37°C with mixing by inversion every 30 minutes. Digestion was halted by rapidly freezing the digest solution which was then stored at -10°C until the reduction step and purification by gel filtration chromatography. An aliquot (20 μL) for analysis by sodium dodecyl sulfate polyacrylamide gel electrophoresis (SDS-PAGE, see section 5.2.3.3) was taken upon completion of the digestion period. After analysis by SDS-PAGE indicated that digestion was complete (by the absence of any uncleaved IgG and the presence of $F(ab')_2$ fragments), the solution was thawed and dialysed extensively against 0.1 M tris-HCl (pH 7.5) at 4°C. If digestion was incomplete the sample was incubated at 37°C for a further one hour or until SDS-PAGE analysis confirmed that digestion of the intact IgG molecule was complete.

After dialysis against tris-HCl buffer (0.1 M, pH 7.5), the peptic digest solution containing $F(ab')_2$ was equilibrated at 37°C at which time an aliquot (1100 μL) of a 0.1 M cysteine solution in the same buffer was added. The resulting solution was allowed to incubate at 37°C, with gentle shaking, for 2.5 hours. Upon completion of the incubation period, 1 M iodoacetic acid (2 mL) in tris-HCl buffer (0.1 M, pH 7.5) was added and the solution left to incubate at room temperature in the dark for 45 minutes. The reaction mixture was then dialysed against a solution consisting of 0.15 M NaCl + 0.05 M sodium dihydrogen phosphate dihydrate buffer (pH 7.5) in readiness for gel filtration chromatography. The dialysis step was also helpful in removing any unreacted reagents and small impurities.

*5.2.3.2 Purification of Fab fragments*

Purification of the intact Fab fragments was achieved by gel filtration. After the sample had been filtered to remove insoluble material, the dialysed Fab solution (1 mL) was loaded onto a Pharmacia Superdex G-75 gel filtration column pre-equilibrated with 0.15 M NaCl + 0.05 M sodium dihydrogen phosphate dihydrate buffer (pH 7.5). The column was then run using an isocratic gradient at a flow rate of 0.3 mL/min. Detection of the protein material was carried out at a wavelength of 280 nm and fractions were collected manually into 1 mL Eppendorf tubes. The fractions were then analysed by SDS-PAGE (see section 5.2.3.3) to locate the Fab containing fractions. The Fab containing fractions were then pooled, concentrated through a Centricon® concentration membrane (Mr cut off 10 000) and stored at -10°C.

*5.2.3.3 SDS-PAGE analysis of the fragmentation products during the preparation of Fab fragments from the intact IgG estrone glucuronide monoclonal antibody*

The fragmentation patterns obtained during the IgG digestion and Fab gel purification procedure were analysed by either reduced, or non-reduced, sodium dodecyl sulfate polyacrylamide gel electrophoresis (SDS-PAGE) as first described by Laemmli [258] and discussed by Parham [257]. Large gels (160 x 200 mm) consisting of a 10% acrylamide running gel and a 4% acrylamide stacking gel were run. The running gel was prepared as follows: Milli-Q water (24.25 mL); 1.5 M tris-HCl (pH 8.8, 12.5 mL); 10% sodium dodecyl sulfate (0.5 mL); 40% acrylamide solution (12.5 mL); ammonium persulfate (300 μL of a freshly prepared 50 mg/500 μL solution); and N, N, N', N',-tetramethylethylenediamine (30 μL) were mixed and the running gel poured. The stacking gel was prepared from Milli-Q water (6.4 mL); 0.5 M tris-HCl (pH 6.8, 2.5 mL); 10% sodium dodecyl sulfate (0.1 mL); 40% acrylamide solution (1.0 mL); ammonium persulfate (50 μL of a freshly prepared 50 mg/500 μL solution); and N, N, N', N',-tetramethylethylenediamine (10 μL) which were mixed, poured, the combs inserted and the stacking gel allowed to set.

Gels were run at a constant current (40 mAmps/gel i.e. 80 mAmps for two gels) until the bromophenol blue dye in the sample buffer had almost reached the bottom of the gel. The electrode running buffer consisted of tris-HCl (15 g), glycine (72 g) and SDS (5 g) made up to 1 L with Milli-Q water and then diluted 1/5 before use. A Pharmacia Electrophoresis Calibration Kit for the determination of low molecular weight proteins was used as a marker and run on all gels. The calibration kit contained the following marker proteins; phosphorylase b (Mr 94 000), bovine serum albumin (Mr 67 000), ovalbumin (Mr 43 000), carbonic anhydrase (Mr 30 000), soybean trypsin inhibitor (Mr 20 100), and α-lactalbumin (Mr 14 400). The intact IgG molecule (Mr ~ 150 000) could also be used as a marker. Both the marker solution and samples were prepared in a sample buffer consisting of Milli-Q water (17 mL), 0.5 M tris-HCl (pH 6.8, 12 mL), glycerol (4.8 mL), 10% SDS (9 mL) and 0.5% bromophenol blue (2 mL). Typically the sample solutions were diluted 1/2 with the sample buffer and an aliquot loaded into the gel wells. Reduced samples were prepared with a sample buffer consisting of 950 μL of the non-reduced sample buffer + 50 μL of β-mercaptoethanol. All samples were prepared in 1 mL Eppendorf tubes and heated at 100°C in a dry bath for 5 minutes immediately prior to loading them into the wells formed by the combs in the stacking gel.

*5.2.3.4 Measurement of the displacement off-rate constants of the estrone glucuronide polyclonal and monoclonal antibodies, and the monoclonal Fab fragment, from the conjugate-antibody (or conjugate-Fab) immune complexes*

An assay mixture was prepared with the appropriate dilution of the mixed anhydride estrone glucuronide-lysozyme conjugate E3 (5 μL) such that it gave an appropriate change in transmission (ΔT) upon the addition of the *Micrococcus lysodeikticus* solution (10 μL) over 20 minutes (ΔT~350). This conjugate dilution and volume (5 μL) was then used in all lytic experiments described in section 5.2.3.4. The reaction was followed by recording the transmission value every 10 seconds for the first two minutes, every 30 seconds for the following six minutes and then every few minutes for the remainder of the twenty minute assay period so that a clearing curve was generated. The initial rate of the reaction was calculated by the measurement of the slope of a tangent to the resulting clearing curve as this part of the curve fits to the straight line equation $y = mx + c$. The time over which the reaction rate was linear (the initial rate period) was determined visually from the clearing curve to be for the first three-four minutes under the conditions specified above and initial rate experiments were therefore followed for four minutes. The initial rate for each incubation period was calculated manually by plotting the time of the reading against the transmission recorded to give a straight line ($y = mx + c$) and was expressed as the change in transmission per minute ($\Delta T\ min^{-1}$). An antibody titration was also undertaken with the polyclonal and monoclonal antibodies, and the Fab fragment (prepared as described in sections 5.2.3.1 and 5.2.3.2) to determine the optimum dilution required to give the maximum inhibition of the lytic activity upon the addition of 5 μL of the antibody solution.

The displacement off-rate constants ($k1_{off}$, as described below and in scheme 5.2.1) of the antibodies from the immune complex were determined using the initial rate method as described below.

The following solutions were placed in the plastic 1 mL cuvette;

| | | |
|---|---|---|
| 1. | mixed anhydride E1G-lysozyme conjugate E3 (dilution as determined above) | 5 μL |
| 2. | E1G antibody (dilution as determined above) | 5 μL |
| 3. | 40 mM tris-maleate buffer (pH 7.0) | 280 μL |

The solutions were mixed by vortexing, the cuvettes capped and then pre-incubated at 40°C using a specifically designed heating block for 30 minutes. Solution 2 (E1G antibody) was changed depending on the antibody displacement off-rate constant under study i.e. polyclonal, monoclonal or Fab fragment. Both solution 1 and 2 dilutions were

prepared in 40 mM tris-maleate buffer. After the pre-incubation period, E1G (50 µL of a 500 000 nmol/24 hours solution (138 889 nmol/L) prepared in 40 mM tris-maleate buffer) was added to the reaction mixture which was vortexed (time zero) and incubated at 40°C in a heating block for the required time period. For the polyclonal antibody experiments incubation times ranging from 0-480 minutes were employed. Time points from 10 minutes onwards were set up in a single batch while those less than 10 minutes were set up individually to accommodate the 4 minute assay time. This was necessary as the 0-10 minute time points were less than 4 minutes apart.

After the required incubation period (0-480 minute) the initial rate assay was initiated by the addition of 10 µL of a 7.5 mg/mL solution of the bacterial substrate *Micrococcus lysodeikticus* (in 75 mM tris-maleate buffer pH 7.0). After vortex-mixing, the initial rate assay was followed using the Ovarian Monitor for four minutes. The transmission value was noted every 10 seconds for the first two minutes and then every 30 seconds for the remaining two minutes. Several control assays were also run, without the addition of the E1G solution, to ensure that the enzymatic activity did not decrease over the time period during which the solutions were incubated.

The 30 minute pre-incubation period allowed after the mixing of the conjugate and the antibody in tris-maleate buffer is necessary to allow the reaction

$$AB + Conj \rightleftharpoons Conj\text{-}AB \qquad \text{Eqn. 1}$$

to approach equilibrium, where AB represents the antibody in question, Conj the estrone glucuronide-lysozyme conjugate, and Conj-AB the bound immune complex. A large excess of free estrone glucuronide is then added to the reaction mixture. The excess E1G binds to the free antibody in equation one to form an antibody-E1G immune complex as described in scheme 5.2.1 below.

In scheme 5.2.1 it is shown that if the concentration of E1G in the assay mixture is much greater than the concentration of everything else we should see a single exponential (one per antibody population) since the $k1_{on}$ step for AB + Conj binding is effectively removed, as is the $k3_{off}$ step for AB-E1G. Therefore, the presence of excess E1G in the assay mixture has the effect of removing any free antibody so that all of it essentially ends up bound to E1G. Since the experiment starts with all of the conjugate bound to the antibody this forces the top equilibrium shown in scheme 5.2.1 to the left, resulting in the dissociation of the conjugate-antibody immune complex. As this dissociation occurs, the large excess of E1G binds to the antibody preventing it from re-binding to the conjugate. This results in the amount of free conjugate (equation 1) increasing and the rate of this

increase was measurement by monitoring the corresponding increase in the initial rates of the conjugate lytic activity in the reaction mixture at various time points as described in the methods section.

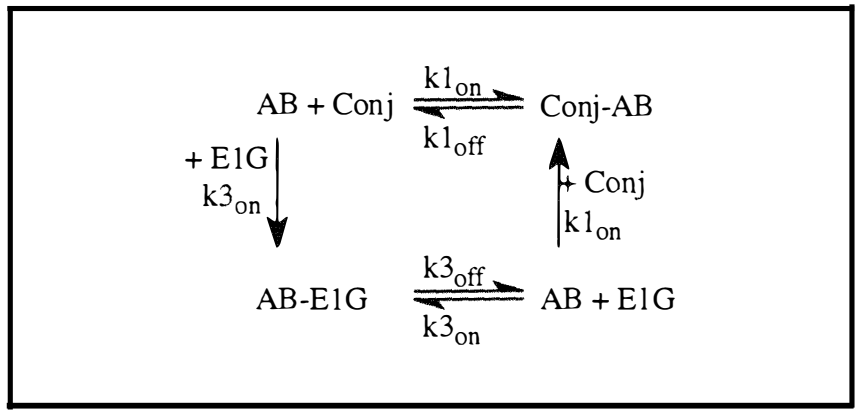


**Scheme 5.2.1** The reactions occurring in the assay reaction mixture during displacement off-rate constant ($k1_{off}$) measurements

The rate of displacement of estrone glucuronide-lysozyme conjugate family E3 from each antibody, or antibody fragment, was calculated by plotting the initial enzymatic rate against the sample incubation time (see Figs. 5.3.7-5.3.10). The curve fitting program Prism™ was used to determine the displacement off-rate constant $k1_{off}$. For a single phase exponential increasing with time, where only one antibody population exists (as in the case of the monoclonal antibody and Fab fragment), the data was fitted to the equation

$$Y = Yo + Ymax\ (1\text{-}exp(-k1_{off}t))$$

where Y = the initial rate calculated for any given incubation time, Yo = the initial rate after a 0 minute incubation time (blank), Ymax = the maximum initial rate when all of the conjugate is free, $k1_{off}$ = the displacement off-rate constant for dissociation of the estrone glucuronide-lysozyme E3 conjugate from the antibody of interest (or Fab fragment), and t = the incubation time in minutes.

For a two phase exponential increase in the initial enzymatic rate of reaction (where two major populations of antibody exist) the equation was modified to

$$Y = Yo + Ymax1\ (1\text{-}exp(-k1_{off}t)) + Ymax2\ (1\text{-}exp(-k2_{off}t))$$

where $k1_{off}$ and $k2_{off}$ are the displacement off-rate constants of two different populations of antibody respectively. The goodness of fit was reported as $R^2$, the square of the correlation coefficient.

*5.2.3.5 Measurement of the apparent dissociation constant ($K_d$) for the E3 conjugate-monoclonal antibody immune complex*

The lytic activity of increasing amounts of conjugate, with a fixed amount of *Micrococcus lysodeikticus* substrate, was measured with an Ovarian Monitor [91]. The appropriate volume of the mixed anhydride E1G-lysozyme E3 conjugate (diluted with 40 mM tris-maleate buffer, pH 7.0) was mixed with enough 40 mM tris-maleate buffer (pH 7.0) to give a total volume of 340 µL. The enzyme solution was then pre-incubated for 5 minutes at 40°C using a heating block before the assay was initiated by the addition and vortex-mixing of 10 µL of a 7.5 mg/mL solution of the bacterial substrate *Micrococcus lysodeikticus* (in 75 mM tris-maleate buffer, pH 7.0). The initial transmission value was then noted and after 20 minutes the final transmission recorded. The solution was kept at 40°C during the 20 minute incubation period by placing the cuvette in a heating block. The rate of reaction was recorded as the change in transmission (ΔT) per 20 minutes. A plot of the reaction rate (ΔT) against the volume of conjugate gave a straight line, confirming that the reaction rate (ΔT) was proportional to the concentration of conjugate used in the assay.

A titration was undertaken by preparing solutions with a fixed amount of monoclonal antibody (5 µL) of an appropriate dilution, pre-mixed with a fixed amount of the *Micrococcus lysodeikticus* substrate (10 µL of a 7.5 mg/mL solution) and 40 mM tris-maleate buffer (pH 7.0), and carrying out a series of assays with increasing amounts of conjugate (added last to the assay), as used in the experiment in the absence of antibody described above. The rate of reaction was again recorded as the change in transmission (ΔT) per 20 minutes. The concentration of conjugate in the assay was determined from the $A_{280}$ measurement, assuming the same absorption coefficient for both the conjugate solution and an equivalent lysozyme solution. The concentration of a stock conjugate solution was therefore calculated using $E^{1\%}_{1\,cm} = 26.4$ at 280 nm and from this stock concentration the concentration of E3 conjugate in each assay could be calculated.

From the two curves (in the presence and absence of monoclonal antibody) the concentration of bound conjugate can be derived as discussed in the results section (section 5.3.3). A plot of the concentration of bound conjugate ($C_B$) in the assay against the concentration of free conjugate ($C_F$) gives a binding curve which can be fitted by non-linear regression using the software program Prism™ and the one site binding (hyperbola) equation

$$Y = \frac{B_{max}.X}{K_d + X}$$

where $B_{max}$ is the maximal binding, X is the concentration of free conjugate in the assay, $K_d$ is the apparent dissociation constant and Y is the concentration of bound conjugate. The Prism™ software was also used to transform the data into a linear form and create a Scatchard plot as discussed in the results section.

*5.2.3.6 Lytic activity of the mixed anhydride E1G-lysozyme E3 conjugate as measured by the hydrolysis of the non-bacterial hexa-N-acetyl-chitohexaose substrate*

The lytic activity of both lysozyme and the E1G-lysozyme E3 conjugate (in the presence and absence of E1G antibody) were measured by the rate of hydrolysis of the non-bacterial substrate hexa-N-acetyl-chitohexaose [$(GlcNAc)_6$] in 40 mM sodium acetate buffer (pH 5.20) at 40°C. The rate of reaction was determined by following the disappearance of the $(GlcNAc)_6$ substrate peak by HPLC analysis on a YMC-Pack $NH_2$ column (250 x 4.6 mm I.D., YMC Co. Ltd., Japan) connected to a Gilson Refractive Index Detector. Each timed aliquot (200 µL) from the assay mixture was diluted to 600 µL with 400 µL of acetonitrile, mixed thoroughly and then spun at 13 000 rpm in a microcentrifuge. An aliquot of the resulting solution (500 µL) was injected onto the column pre-equilibrated with 65% aqueous acetonitrile and eluted at a flow rate of 1 mL/min using an isocratic gradient. The profiles were recorded and the peak areas integrated on an Apple Macintosh computer using the Chart V3.0 and Peaks V1.3 programs, *via* the MacLab™ hardware system from Analog Digital Instruments Pty Ltd., Castle Hill, New South Wales, Australia. The column was calibrated with a standard mixture of di-N-acetyl-chitobiose [$(GlcNAc)_2$], tetra-N-acetyl-chitotetraose [$(GlcNAc)_4$] and hexa-N-acetyl-chitohexaose [$(GlcNAc)_6$] in 65% aqueous acetonitrile solution.

In a typical assay, 2063 µL of a 0.2 mg/mL solution of $(GlcNAc)_6$ (162 µM in sodium acetate buffer, pH 5.20) was placed into a 10 mL plastic tube and the solution pre-equilibrated at 40°C in a water bath for 30 minutes. Sodium acetate buffer (40 mM, pH 5.20) was also added so that the final volume of the assay mixture, after the addition of conjugate and antibody, was 2.2 mL. Appropriate amounts of lysozyme and conjugate solutions (6 µmol/L), prepared in 40 mM sodium acetate buffer (pH 5.20), were also pre-equilibrated in an eppendorf tube at 40°C for 30 minutes. The concentration of the conjugate solution was calculated from the absorbance at 280 nm (using an $E^{1\%}_{1\,cm}$ value of 26.4) as described in section 5.2.3.5. The assay mixture was such that the final concentration of either the lysozyme or the conjugate solution was 100 nmol/L, and the concentration of $(GlcNAc)_6$ was 152 µmol/L. In assays measuring the inhibition of the conjugate by the polyclonal anti-estrone glucuronide antibody, the appropriate amounts of conjugate and antibody were pre-mixed and pre-equilibrated at 40°C for 30 minutes. After the pre-equilibration time, the required volume of lysozyme, conjugate or pre-mixed conjugate-antiserum was added to the $(GlcNAc)_6$ solution, vortex mixed and time zero

recorded. Aliquots of 200 µL were then removed from the reaction mixture after 0, 10, 20, 30, 40, 50, 60, 90, 120 and 180 minutes, placed in an eppendorf tube and heated in a boiling water bath for 5 minutes to quench the reaction. Each aliquot was then stored at -10•C until analysis by HPLC.

## 5.3 Results

### 5.3.1 Preparation of Estrone Glucuronide Monoclonal Antibody Fab Fragments

Digestion of the estrone glucuronide monoclonal antibody with pepsin at pH 3.50 was complete after 2-4 hours at 37°C as shown by SDS-PAGE (Fig. 5.3.1). SDS-PAGE analysis also confirmed that the reaction mixture contained no high molecular weight impurities upon the completion of digestion, there being only one high molecular weight band present ($F(ab')_2$). This band had a relative molecular mass (Mr) of approximately 110 000 on comparison with the original starting material (Mr ~ 150 000) and the various molecular weight markers (Fig. 5.3.1). A low molecular weight band could be seen at the gel front (Fig. 5.3.1) due to the peptide fragments produced upon the proteolytic cleavage of the Fc fraction. SDS-PAGE analysis of the resulting $F(ab')_2$ fraction in the presence of β-mercaptoethanol gave a doublet of protein bands, one under the other, with an apparent mean molecular mass of approximately 25 000.

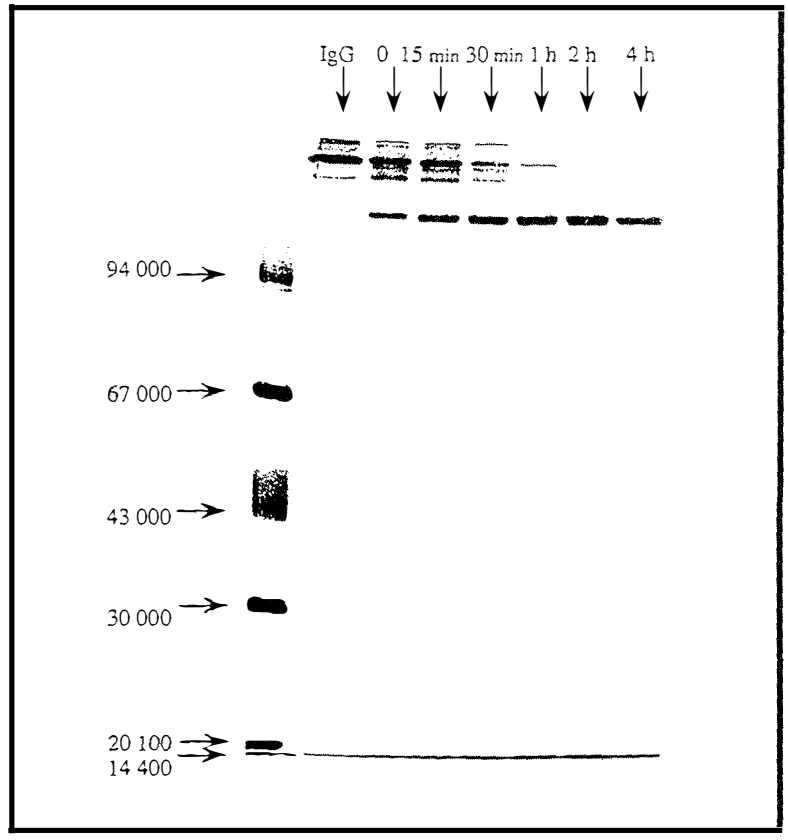


**Fig. 5.3.1** SDS-polyacrylamide gel electrophoresis (SDS-PAGE) analysis of the peptic digestion of IgG anti-estrone glucuronide monoclonal antibody as described in the text. The molecular markers are shown on the left hand side and the time at which samples were removed from the digestion are indicated along the top of the figure. The digestion appears to be over after 2 hours of incubation. The intact IgG can be seen in the first sample lane. The 0 min time sample shows that digestion begins very rapidly as product can already be observed.

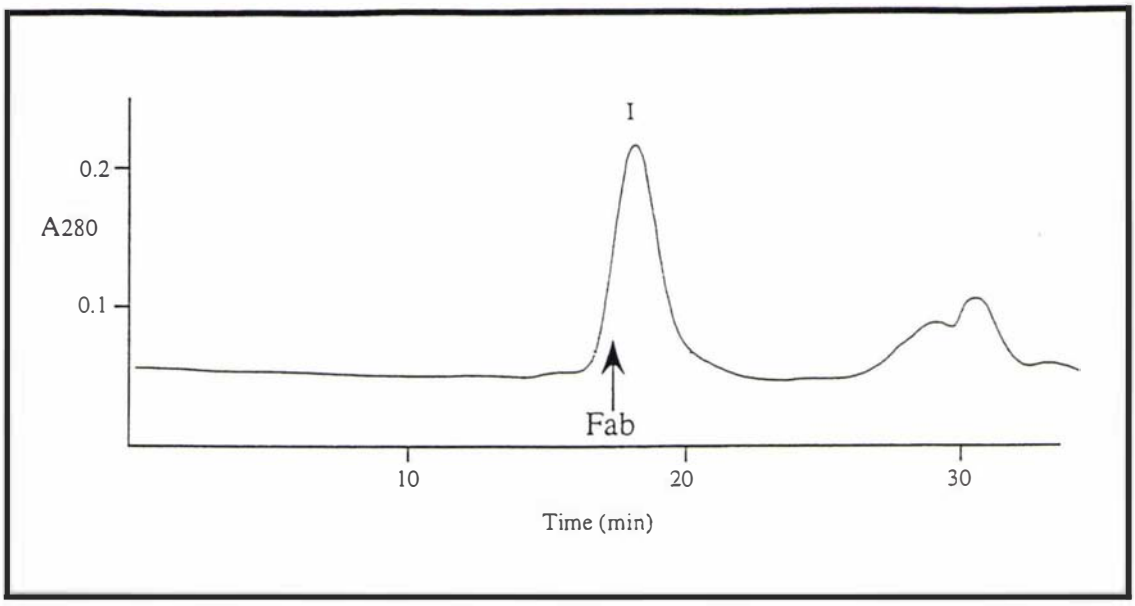


**Fig. 5.3.2** The elution profile resulting from the purification of Fab fragments on a Superdex G-75 gel filtration column. The fragments were produced by the peptic digestion of IgG anti-estrone glucuronide monoclonal antibody to give $F(ab')_2$ fragments. The $F(ab')_2$ fragments were then reduced with cysteine to give Fab fragments as described in the text.

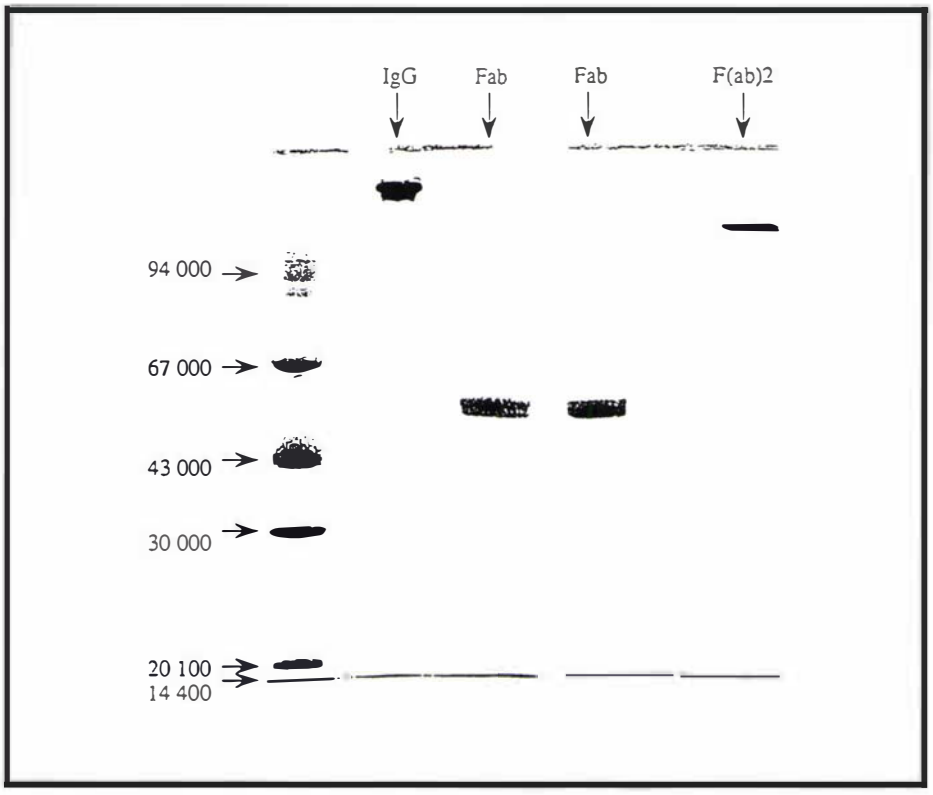


**Fig. 5.3.3** SDS-polyacrylamide gel electrophoresis (SDS-PAGE) analysis of IgG anti-estrone glucuronide monoclonal antibodies, $F(ab')_2$ fragments, and purified Fab fragments. All fractions appear free of other molecular weight fragments. Each fragment shows the expected migration pattern and exhibits the correct molecular weight for IgG, $F(ab')_2$, and Fab fragments as described by Parham [257]. The molecular markers are shown on the left hand side.

After dialysis, the $F(ab')_2$ fragments were reduced with cysteine to give Fab fragments. The resulting Fab fragments were dialysed into pH 7.5, 50 mM sodium dihydrogen phosphate dihydrate buffer containing 0.15 M NaCl and purified by gel filtration chromatography. The resulting elution profile consisted of a large initial peak (I) followed later in the gradient by several smaller, broader peaks (Fig. 5.3.2). SDS-PAGE analysis of the peaks confirmed that the largest, earliest eluting peak (I) had an apparent molecular weight (Mr) ~ 50 000 as expected for an IgG Fab fragment (Fig. 5.3.3). The other peaks consisted of low molecular weight impurities and were discarded. SDS-PAGE analysis of the starting material (intact monoclonal IgG), $F(ab')_2$ fragment, and purified Fab fragment confirmed that all the fragments showed the expected migration patterns and exhibited the correct molecular weight (Fig. 5.3.3) as described by Parham [257]. Each fraction was free of impurities and inhibited the lytic activity of estrone glucuronide-lysozyme conjugates, when present in the assay mixture, by 85-90%.

### 5.3.2 Displacement Off-Rate Constants of the Estrone Glucuronide Polyclonal and Monoclonal Antibodies and the Monoclonal Fab Fragment from the Conjugate-Antibody (or Conjugate-Fab) Immune Complexes

A typical clearing curve generated for the clearance of a *Micrococcus lysodeikticus* solution by the mixed anhydride estrone glucuronide-lysozyme E3 conjugate under the conditions described in the methods section is shown in Fig. 5.3.4. The clearing curve generated under these conditions is not linear but curved and can be shown to fit second order kinetics (rate $\alpha$ [substrate]$^2$) when the data is converted to absorbance over the duration of the assay. However, although the clearing curve follows second order kinetics the rate of clearing with respect to time is constant for about the first 180 seconds (see Fig. 5.3.4). During this time the clearing curve data fits a zero order rate equation and thus an initial rate could be calculated from these data. From a plot of the recorded transmission for the first 180 seconds (as shown in Fig. 5.3.5) the initial rate of clearance was calculated as the change in transmission per minute (41.86 $\Delta T\ min^{-1}$).

The addition of E1G antibody (polyclonal, monoclonal or Fab fragment) to the assay mixture resulted in the inhibition of the initial lytic activity by 87-93% as shown for the polyclonal antibody (93% inhibition) in Fig. 5.3.4. The effect of this on the initial rate can be seen in Fig. 5.3.5. The initial rate of clearance in the presence of the polyclonal antibody was calculated as 3.46 $\Delta T\ min^{-1}$, a decrease of 92% in the initial rate. The initial rate of clearance in the presence of the estrone glucuronide monoclonal antibody was 4.63 $\Delta T\ min^{-1}$ (89% decrease from the control rate) and in the presence of the Fab fragment the initial rate was 4.59 $\Delta T\ min^{-1}$ (90% decrease from the control rate).

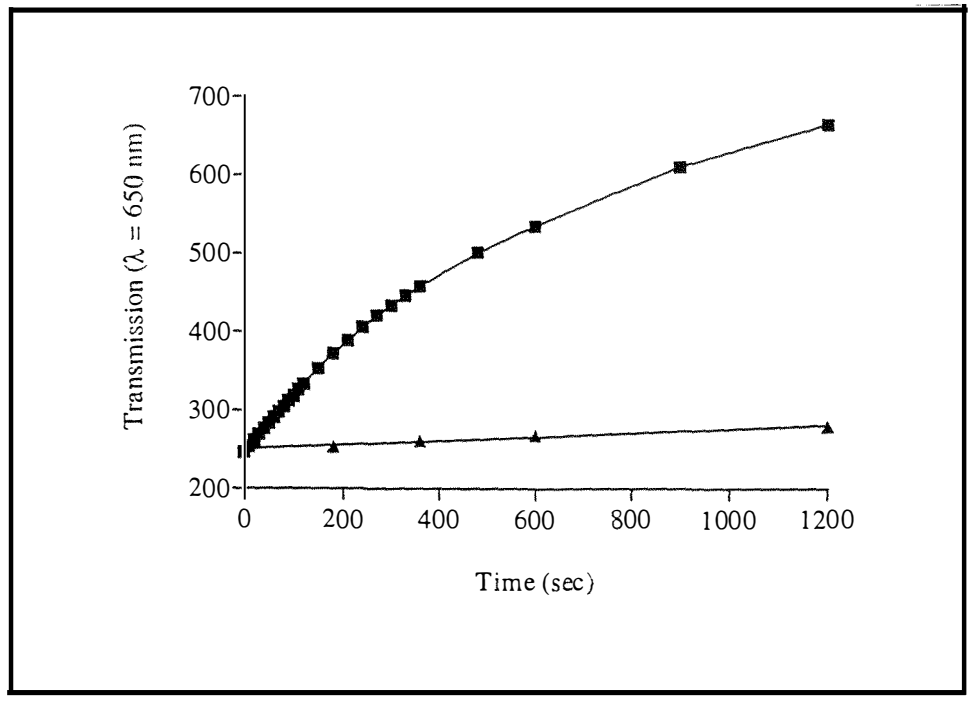


**Fig. 5.3.4** A typical twenty minute clearing curve of a *Micrococcus lysodeikticus* solution by a mixed anhydride estrone glucuronide-lysozyme E3 conjugate solution in the presence (▲) and absence (■) of excess polyclonal anti-estrone glucuronide antibody as described in the text. The extensive inhibition observed on the enzymatic activity of the conjugate in the presence of excess polyclonal anti-E1G antibody is clearly shown.

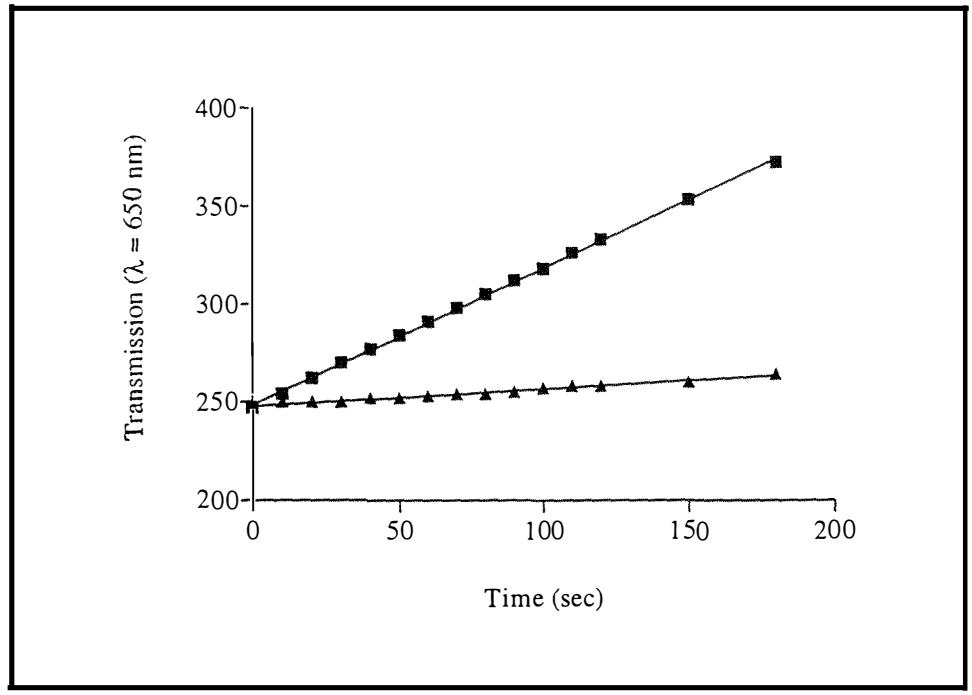


**Fig. 5.3.5** A typical initial rate plot (over 180 seconds) for the clearing of a *Micrococcus lysodeikticus* solution by an E1G-lysozyme mixed anhydride E3 conjugate solution in the presence (▲) and absence (■) of excess polyclonal anti-E1G antibody as described in the text. The extensive inhibition on the lytic activity of the conjugate, in the presence of excess polyclonal anti-E1G antibody, is clearly shown.

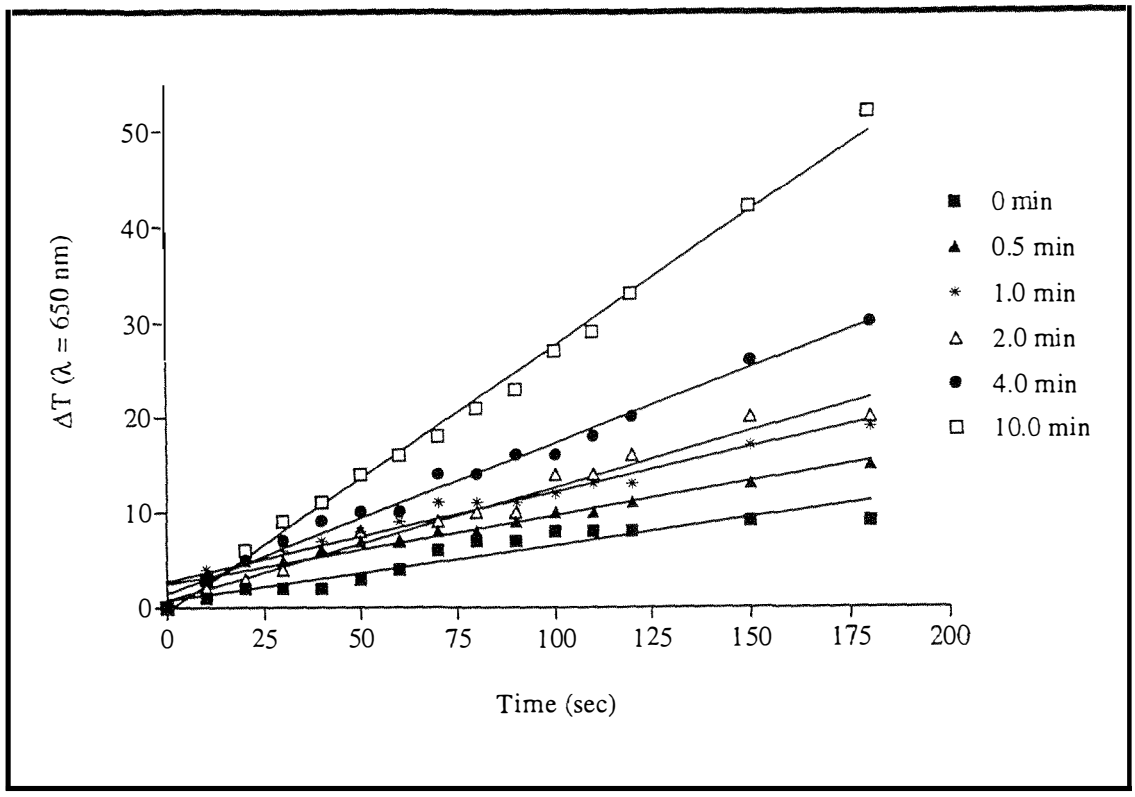


**Fig. 5.3.6** The effect on the initial rate of clearing of a *Micrococcus lysodeikticus* solution by an E1G-lysozyme mixed anhydride E3 conjugate solution in the presence of excess polyclonal anti-E1G antibody upon the addition of excess free estrone glucuronide to the assay system. As the length of time after the addition of the free E1G increases, the initial rate of clearing of the *Micrococcus lysodeikticus* solution can also be seen to increase.

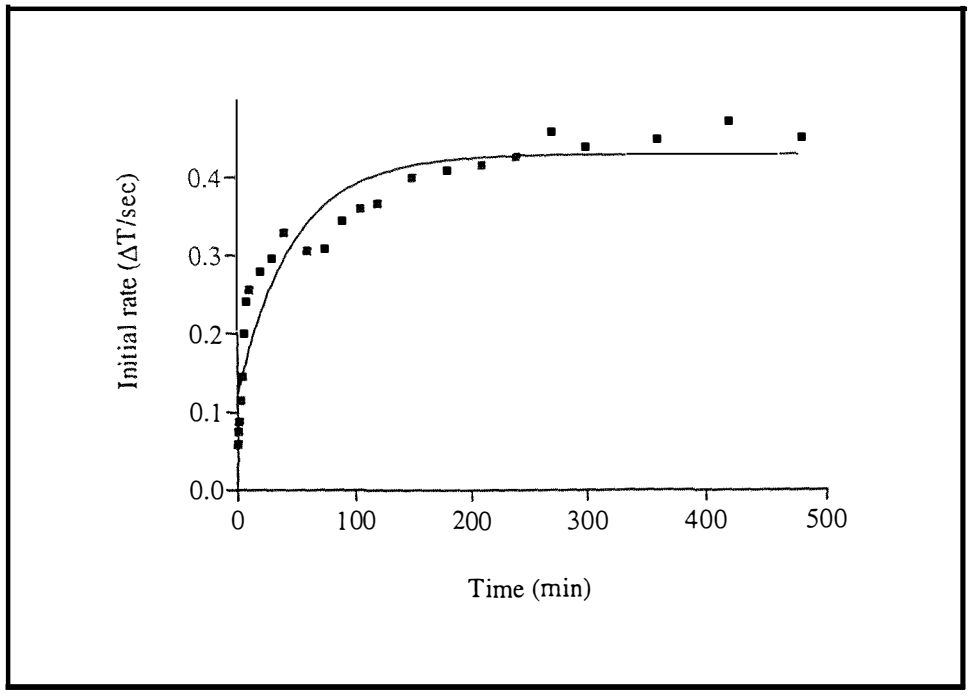


**Fig. 5.3.7** Single exponential fit to the initial rate data obtained for the clearing of a *Micrococcus lysodeikticus* solution by an E1G-lysozyme conjugate solution in the presence of excess polyclonal anti-estrone glucuronide antibody after the addition of excess, free estrone glucuronide. The calculated results are shown in Table 5.3.1.

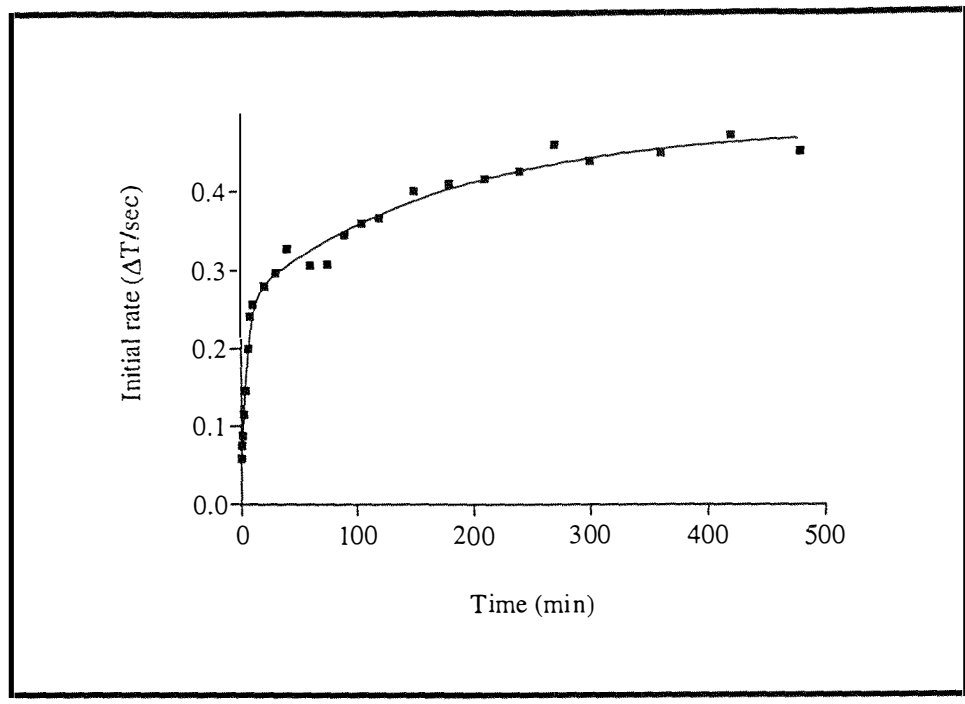


**Fig. 5.3.8** Two phase exponential fit to the initial rate data obtained for the clearing of a *Micrococcus lysodeikticus* solution by an E1G-lysozyme conjugate solution in the presence of excess polyclonal anti-estrone glucuronide antibody after the addition of excess, free estrone glucuronide. The calculated results are shown in Table 5.3.1.

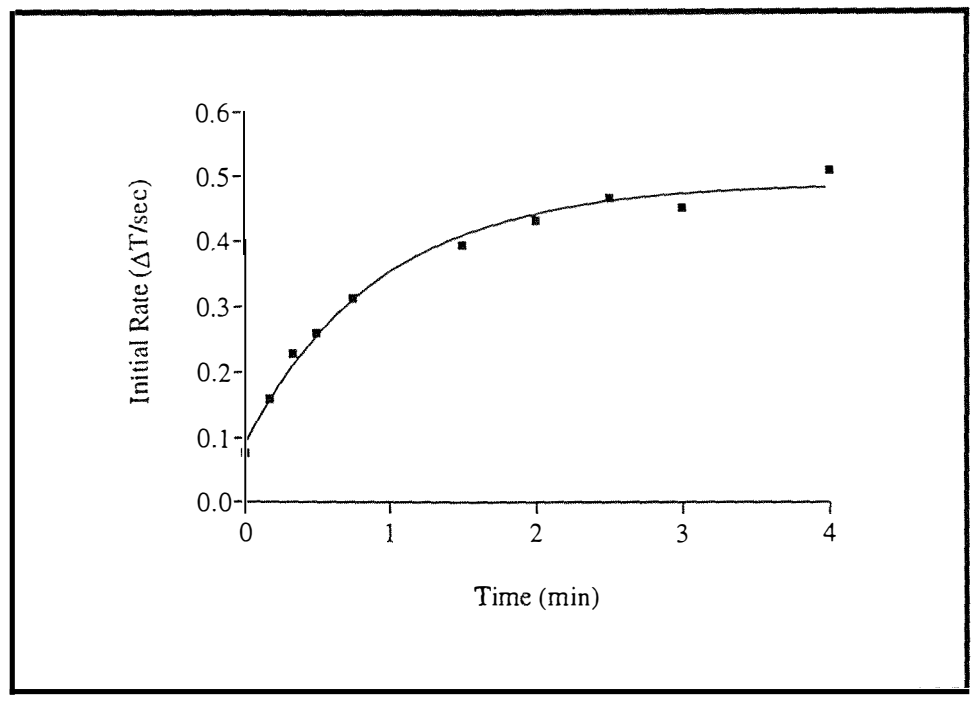


**Fig. 5.3.9** Single exponential fit to the initial rate data obtained for the clearing of a *Micrococcus lysodeikticus* solution by an E1G-lysozyme conjugate solution in the presence of excess monoclonal anti-estrone glucuronide antibody after the addition of excess, free estrone glucuronide. The calculated results are shown in Table 5.3.1.

**Table 5.3.1**

Calculated displacement off-rate constants for the various E1G antibodies from the mixed anhydride E1G-lysozyme E3 conjugate-antibody immune complex

| Parameter | Polyclonal Antibody (Single Exponential) | Polyclonal Antibody (Two Phase Exponential) | Monoclonal Antibody | Fab (Antigen Binding Fragment) |
|---|---|---|---|---|
| Ymax1 (ΔT/sec) | 0.3039 ± 0.0212 | 0.2105 ± 0.0150 | 0.3963 ± 0.0163 | 0.3916 ± 0.0151 |
| $k1_{off}$ ($sec^{-1}$) | $3.50 \times 10^{-4}$ $\pm 7.7 \times 10^{-5}$ | $3.15 \times 10^{-3}$ $\pm 5.1 \times 10^{-4}$ | $1.78 \times 10^{-2}$ $\pm 2.2 \times 10^{-3}$ | $2.06 \times 10^{-2}$ $\pm 2.0 \times 10^{-3}$ |
| Ymax2 (ΔT/sec) | | 0.2203 ± 0.0146 | | |
| $k2_{off}$ ($sec^{-1}$) | | $9.41 \times 10^{-5}$ $\pm 2.08 \times 10^{-5}$ | | |
| Goodness Of Fit ($R^2$) | 0.9037 | 0.9900 | 0.9886 | 0.9932 |

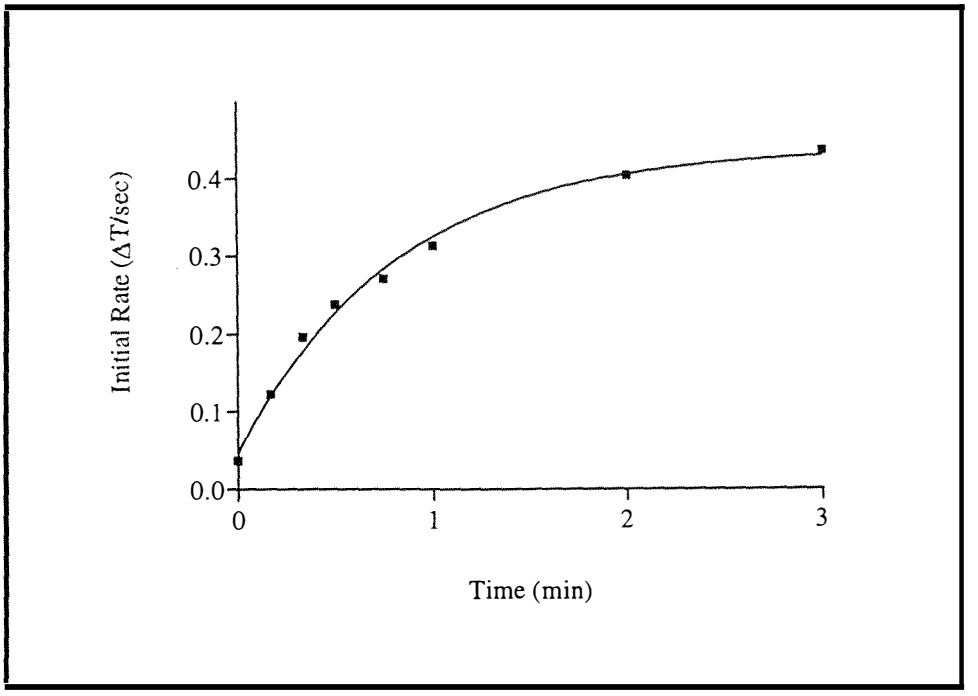


**Fig. 5.3.10** Single exponential fit to the initial rate data obtained for the clearing of a *Micrococcus lysodeikticus* solution by an E1G-lysozyme conjugate solution in the presence of excess anti-estrone glucuronide monoclonal antibody Fab fragments after the addition of excess, free estrone glucuronide. The calculated results are shown in Table 5.3.1.

The effect of the addition of excess estrone glucuronide to the inhibited assay system on the initial rate for the polyclonal antibody system is shown in Fig. 5.3.6. As the time of incubation of the assay after the addition of free, excess estrone glucuronide increases, the initial rate can also be seen to increase as shown in Fig. 5.3.6. For each of the assay time points the initial rate was calculated as the change in transmission per second. A plot of the initial rate against the incubation time (after the addition of the E1G) generated the curves shown in Figs. 5.3.7-5.3.10. The displacement off-rate constants calculated from these curves as described in the methods section are presented in Table 5.3.1.

### 5.3.3 Apparent Dissociation Constant ($K_d$) Measurements for the Conjugate-Monoclonal Antibody Immune Complex

When a titration was performed with a fixed amount of the estrone glucuronide monoclonal antibody pre-mixed with increasing amounts of conjugate there was an initial non-linear increase in the magnitude of the value of the end point assay (after 20 min) as a function of the conjugate concentration. Eventually, as the amount of conjugate in the assay was increased, the change in transmission over twenty minutes became a linear function of the conjugate concentration (see Fig. 5.3.11). The final slope of this line was within experimental error the same as for a set of assays undertaken with increasing amounts of conjugate but in the absence of any antibody. From these data the amount of

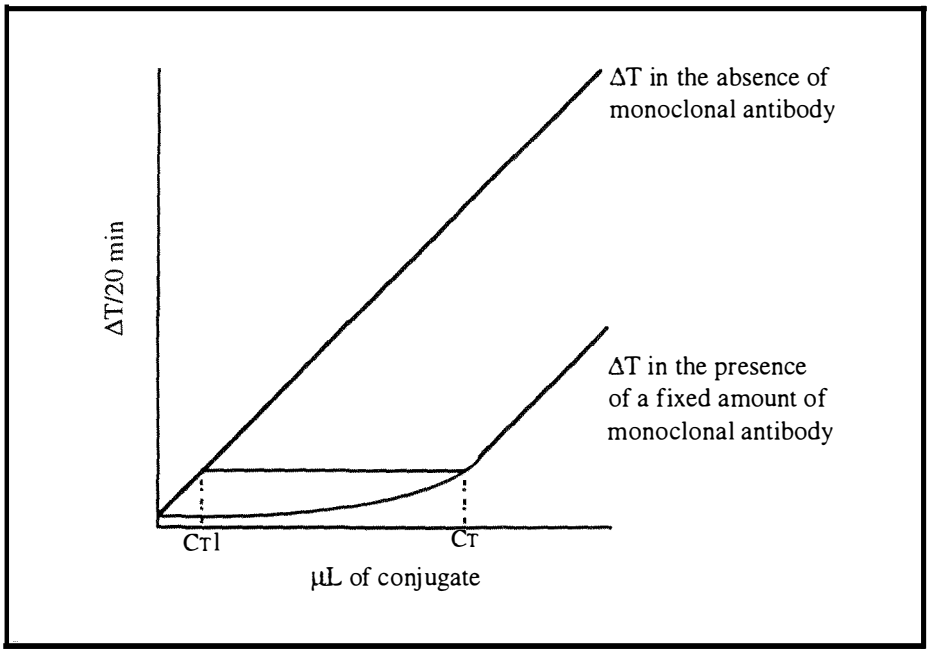


**Fig. 5.3.11** Method 1 for determining $C_T$ and $C_T1$ giving the same lytic rate (ΔT/20 min) when calculating the concentration of conjugate bound ($C_B$) in the presence of a fixed amount of monoclonal antibody

conjugate bound ($C_B$) for any given total volume of conjugate ($C_T$) in the presence of a fixed amount of antibody, can be calculated by two methods as described below. Both methods assume that the maximum extent of inhibition of the lytic activity in the presence of excess antibody will be the same for all total conjugate concentrations.

The first method (Method 1) of calculating the amount of conjugate bound ($C_B$) for any total conjugate concentration ($C_T$) in the presence of a fixed concentration of antibody is to compare the volumes of conjugate which give the same lytic activity ($\Delta T$) in the presence and absence of antibody as shown in Fig. 5.3.11. At any total conjugate concentration ($C_T$) the lytic activity is the sum of the activity of the bound conjugate ($k_BC_B$, where $k_B$ is the catalytic constant for the bound conjugate and $C_B$ is the concentration of bound conjugate) and the free conjugate ($k_FC_F$, where $k_F$ is the catalytic constant for the free conjugate and $C_F$ is the concentration of free conjugate). Therefore the rate ($\Delta T$/20 min) can be expressed in terms of

$$\Delta T/20 \text{ min} = k_FC_F + k_BC_B$$

and this equation may also be written in terms of the total conjugate concentration ($C_T$) where

$$\Delta T/20 \text{ min} = k_F(C_T - C_B) + k_BC_B$$

or

$$\Delta T/20 \text{ min} = k_FC_T - k_FC_B + k_BC_B$$

or

$$\Delta T/20 \text{ min} = k_FC_T - (k_F - k_B)C_B$$

When two points of equal lytic activity are compared on the control line ($\Delta T$ in the absence of monoclonal antibody, see Fig. 5.3.11) and the titration curve in the presence of a fixed amount of monoclonal antibody (see Fig. 5.3.11, i.e. the control and titration rates are equal) then

$$k_FC_T1 = k_FC_T - (k_F - k_B)C_B$$

where $C_T$ is the total concentration of conjugate giving the rate $\Delta T$ in the titration curve and $C_T1$ is the total concentration of conjugate giving the rate $\Delta T$ in the control experiment in the absence of antibody. This equation can be rearranged so that

$$(k_F - k_B)C_B = k_FC_T - k_FC_T1$$

or

$$(k_F - k_B)C_B = k_F(C_T - C_T1)$$

It therefore follows that the concentration of bound conjugate ($C_B$) is;

$$C_B = \frac{k_F}{k_F - k_B}(C_T - C_T1)$$

$$= \frac{1}{1 - \frac{k_B}{k_F}}(C_T - C_T1) \qquad \text{eqn. 1}$$

Since from a titration with excess monoclonal antibody the maximum extent of inhibition of the enzymatic rate was 87%, and assuming that all total conjugate concentrations will be inhibited to the same amount in the presence of excess monoclonal antibody, $K_B$ can be written in terms of $K_F$;

$$k_B = 0.13k_F$$

Hence, it follows that $\frac{k_B}{k_F} = 0.13$

and substituting this into equation 1

$$C_B = \frac{1}{1 - 0.13}(C_T - C_T1)$$

$$= 1.15\,(C_T - C_T1) \qquad \text{eqn. 2}$$

Therefore, the concentration of conjugate bound ($C_B$) can be calculated for every total conjugate volume ($C_T$) in the presence of a fixed amount of monoclonal antibody. Hence, the concentration of free conjugate ($C_F$) may also be calculated as $C_F = C_T - C_B$ at each value of $C_T$, and a plot of $C_B$ versus $C_F$ may be used to calculate $B_{max}$ and $K_d$ as described in section 5.2.3.5 where $B_{max}$ is the asymptote to the curve of $C_B$ v $C_F$ and may be taken as the total concentration of antibody binding sites. Also if there are two binding sites per antibody molecule the concentration of monoclonal antibody in the assay is equal to $B_{max}/2$. The curve generated from the plot of $C_B$ v $C_F$, according to method 1, is shown in Fig. 5.3.12. From this curve (Fig. 5.3.13) the variables were calculated as;

$B_{max} = 2.784 \pm 0.399$ nmol/L

$K_d = 0.198 \pm 0.077$ nmol/L

and the goodness of fit $R^2 = 0.956$.

Linear transformation of the data gave a Scatchard plot (Fig. 5.3.13), whereby $C_B/C_F$ is plotted against $C_B$, for which a straight line is obtained and whose slope is the negative

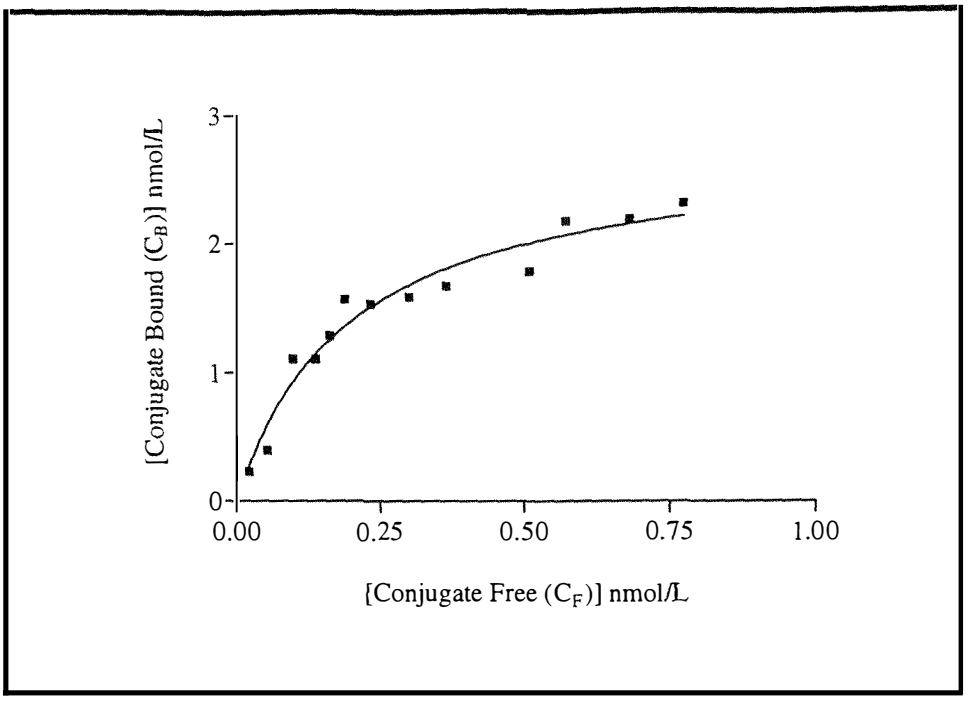


**Fig. 5.3.12** Binding curve for the binding of lysozyme-estrone glucuronide mixed anhydride E3 conjugate by monoclonal anti-E1G antibody with increasing conjugate concentrations and a constant antibody concentration when the $C_B$ and $C_F$ data are calculated by method 1 (see text for details).

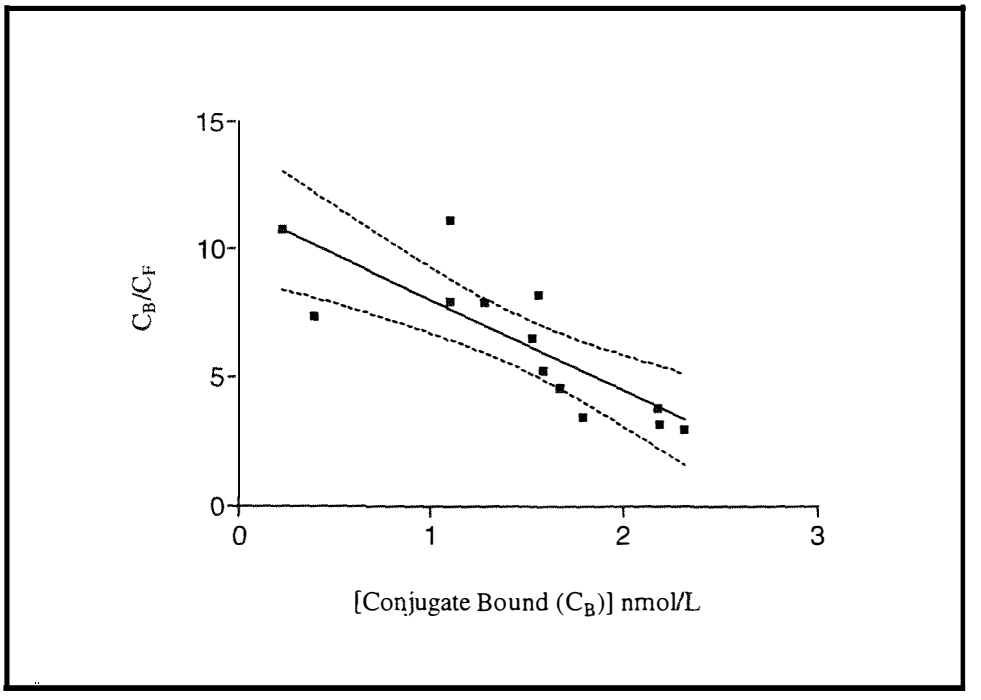


**Fig. 5.3.13** Scatchard plot for the binding of lysozyme-E1G E3 mixed anhydride conjugate by monoclonal anti-E1G antibody with increasing conjugate concentrations and a constant antibody concentration when the $C_B$ and $C_F$ data are calculated by method 1 (see text for details). The 95% confidence levels are shown (- - -).

inverse of the apparent dissociation constant ($K_d$) and the X intercept gives $B_{max}$. From the Scatchard plot the variables were calculated as;

$B_{max}$ = 3.271 nmol/L

$K_d$ = 0.283 ± 0.313 nmol/L

and the goodness of fit $R^2$ = 0.661.

The second method (Method 2) for calculating the amount of conjugate bound ($C_B$) for a given total volume of conjugate ($C_T$) in the titration curve is to compare the lytic activities ($\Delta T$/20 min) for a total volume of conjugate in the presence and absence of a fixed amount of monoclonal antibody as shown in Fig. 5.3.14.

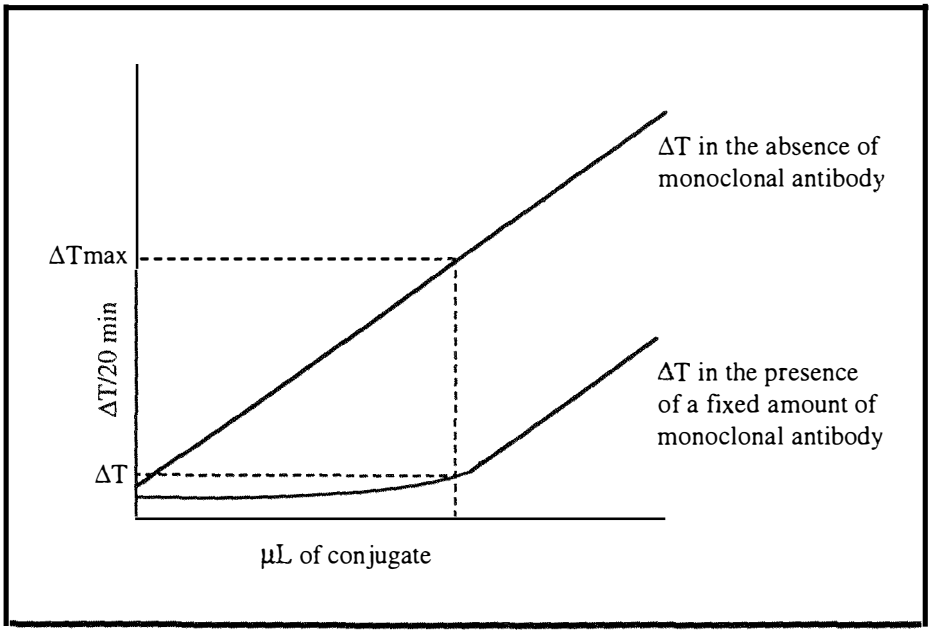


**Fig. 5.3.14** Method 2 for determining the concentration of conjugate bound ($C_B$) in the presence of a fixed amount of monoclonal antibody using the difference in the lytic activity for a given total concentration of conjugate ($C_T$)

As shown above in the derivation of method 1, the lytic rate for a given total concentration (or volume) of conjugate may be described as

$$\Delta T = k_F C_T + (k_B - k_F) C_B \qquad \text{eqn. 3}$$

From the control line (in the absence of antibody) the maximum $\Delta T$ is obtained (or $\Delta T_{max}$) for each total volume of conjugate. Therefore $\Delta T_{max} = k_F C_T$ and substituting this into equation 3 gives

$$\Delta T = \Delta T_{max} + (k_B - k_F) C_B$$

or $$C_B = \frac{\Delta T_{max} - \Delta T}{k_F - k_B} \qquad \text{eqn. 4}$$

If we assume that in the presence of excess antibody all of the conjugate will be bound, and the minimum $\Delta T$ is obtained (or $\Delta T_{min}$) for each volume of conjugate, then the concentration of conjugate bound ($C_B$) and the total conjugate concentration ($C_T$) will be equal and

$$\Delta T_{min} = k_B C_B \quad \text{or} \quad \Delta T_{min} = k_B C_T \text{ (as } C_B = C_T)$$

Therefore, $$k_B = \frac{\Delta T_{min}}{C_T}$$

and $$k_F = \frac{\Delta T_{max}}{C_T} \quad \text{(from } \Delta T_{max} = k_F C_T).$$

Thus $k_F - k_B$ from the denominator in equation 4 can be expressed as

$$k_F - k_B = \frac{\Delta T_{max} - \Delta T_{min}}{C_T}$$

and substituting this into equation 4 gives

$$C_B = \frac{(\Delta T_{max} - \Delta T)C_T}{\Delta T_{max} - \Delta T_{min}}$$

or $$\frac{C_B}{C_T} = \frac{(\Delta T_{max} - \Delta T)}{\Delta T_{max} - \Delta T_{min}} \qquad \text{eqn. 5}$$

Since the titration of conjugate with excess antibody showed that the maximum extent of inhibition by the monoclonal antibody was 87% we can calculate $\Delta T_{min}$ as

$$\Delta T_{min} = 0.13 \Delta T_{max}.$$

Thus, the concentration of conjugate bound ($C_B$) can be calculated for every total conjugate volume ($C_T$) in the presence of a fixed amount of monoclonal antibody, and hence the concentration of free conjugate ($C_F$). A plot of $C_B$ versus $C_F$ may be fitted (as described for method 1 above) to generate the curve shown in Fig. 5.3.15. From this the variables were calculated as

$B_{max}$ = 2.584 ± 0.739 nmol/L

$K_d$ = 0.359 ± 0.260 nmol/L

and the goodness of fit, $R^2$ = 0.897.

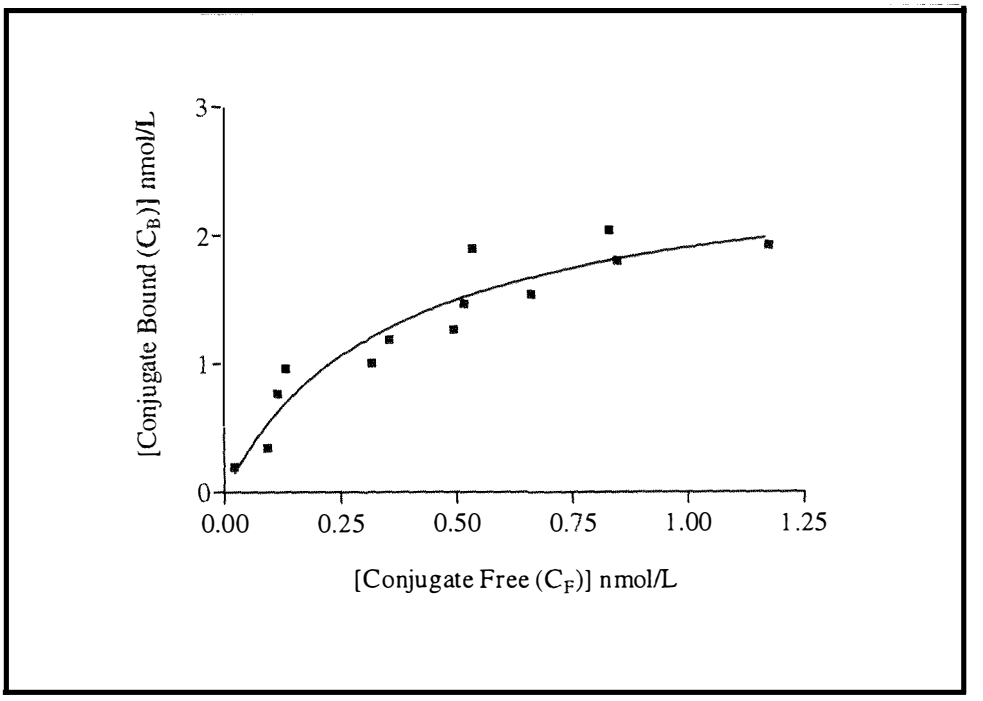


**Fig. 5.3.15** Binding curve for the reaction of lysozyme-estrone glucuronide mixed anhydride E3 conjugate with monoclonal anti-E1G antibody at increasing conjugate concentrations and a constant antibody concentration when the $C_B$ and $C_F$ data are calculated by method 2 (see text for details).

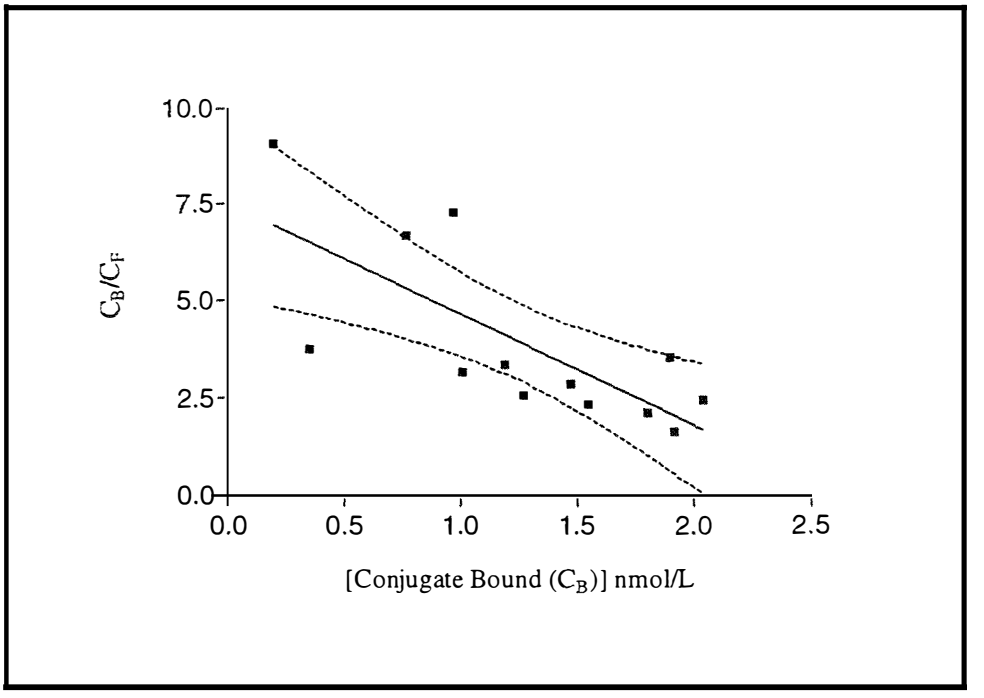


**Fig. 5.3.16** Scatchard plot for the binding of lysozyme-E1G E3 mixed anhydride conjugate by monoclonal anti-E1G antibody with increasing conjugate concentrations and a constant antibody concentration when the $C_B$ and $C_F$ data are calculated by method 2 (see text for details). The 95% confidence levels are shown (- - -).

Linear transformation of the data gave a Scatchard plot (Fig. 5.3.16) from which the variables were calculated as

$$B_{max} = 2.642 \text{ nmol/L}$$
$$K_d = 0.353 \pm 0.578 \text{ nmol/L}$$

and the goodness of fit $R^2 = 0.542$.

From the average of the non-linear fit to the data calculated by method 1 and method 2, the concentration of monoclonal antibody ([MCAB]) in the titration experiment was calculated as

$$[MCAB] = B_{max}/2$$
$$= 2.684/2$$
$$= 1.342 \text{ nmol/L}.$$

### 5.3.4 Lytic Activity of the Mixed Anhydride Estrone Glucuronide E3 Conjugate as Measured by the Hydrolysis of the Non-Bacterial Hexa-N-Acetyl-Chitohexaose Substrate, $(GlcNAc)_6$

A typical profile for a $(GlcNAc)_6$ standard analysis by HPLC on the YMC-Pack $NH_2$ column, as recorded *via* a MacLab™ system, is shown in Fig. 5.3.17. The $(GlcNAc)_6$ peak eluted (highlighted in black in Fig. 5.3.17) approximately 11.5 minutes after the injection point and the area under the peak was integrated and reported as $mV^2$ (millivolts$^2$). Two earlier peaks also eluted from the column and these are due to a loading peak (the first large peak in Fig. 5.3.17) and a buffer peak (the second large peak in Fig. 5.3.17) as shown by analysis of the buffer in the absence of $(GlcNAc)_6$.

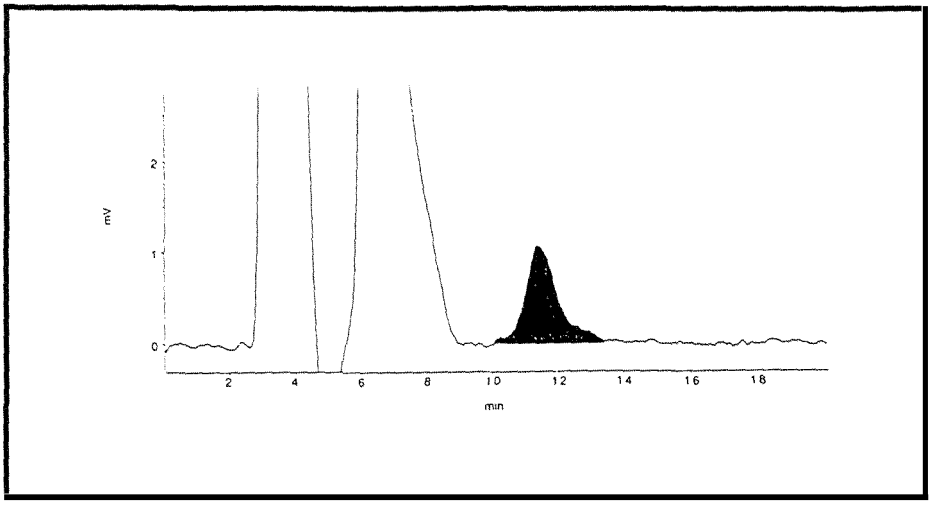


**Fig. 5.3.17** A typical elution profile of $(GlcNAc)_6$ (shaded peak) when analysed by HPLC on a YMC-Pack $NH_2$ column under the conditions described in the text as recorded on a MacLab™ system

Analysis of several standard samples of $(GlcNAc)_6$ produced the standard curve shown in Fig. 5.3.18. From the standard curve the concentration of $(GlcNAc)_6$ in any sample could be calculated from the peak area after HPLC analysis. The disappearance of the $(GlcNAc)_6$ substrate peak with time as the reaction proceeded could be visually detected when timed aliquots were analysed by HPLC, as shown in Fig. 5.3.19. Lysozyme cleaves $(GlcNAc)_6$ to give $(GlcNAc)_4$ and $(GlcNAc)_2$ (as shown in Fig. 5.1.2) and in principle the appearance of the product peaks could also be monitored. The appearance of the $(GlcNAc)_4$ product peak can be seen on the right hand edge of the buffer peak (Fig. 5.3.19d), however this peak was not well enough resolved to integrate the area beneath it. The $(GlcNAc)_2$ peak was completely covered by the buffer peak, as shown by analysis of a sample in the absence of buffer.

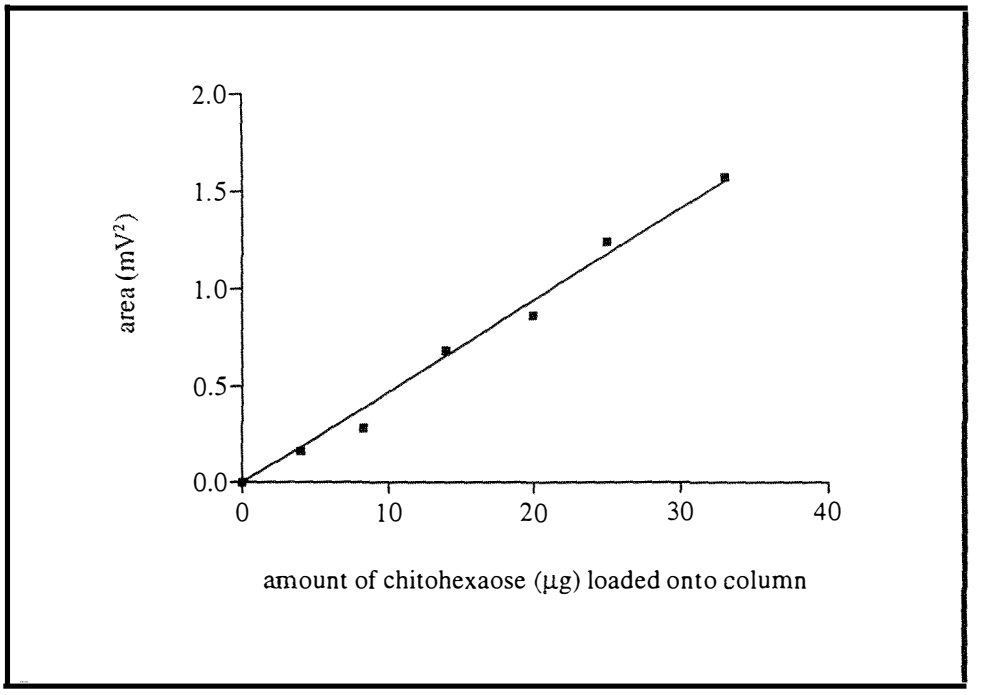


**Fig. 5.3.18** A $(GlcNAc)_6$ standard curve generated from HPLC data showing the relationship between the amount of chitohexaose injected onto the column and the area under the eluted $(GlcNAc)_6$ peak

Once all of the points from a kinetic run were analysed by HPLC and the areas under the $(GlcNAc)_6$ peak integrated and converted to micrograms of $(GlcNAc)_6$ using the standard curve in Fig. 5.3.18, it was necessary to divide the calculated number of micrograms by 5/6 as only 500 μL of the 600 μL sample was injected. A plot of the amount of $(GlcNAc)_6$ substrate remaining against time gave a straight line (Fig. 5.3.20) where $y = mx + c$ and m (the slope) is negative. By changing the sign of the slope the rate of hydrolysis, and hence the rate of reaction, was calculated and reported as the micrograms of $(GlcNAc)_6$ hydrolysed per minute ($\mu g\ min^{-1}$). Once assay points began to significantly

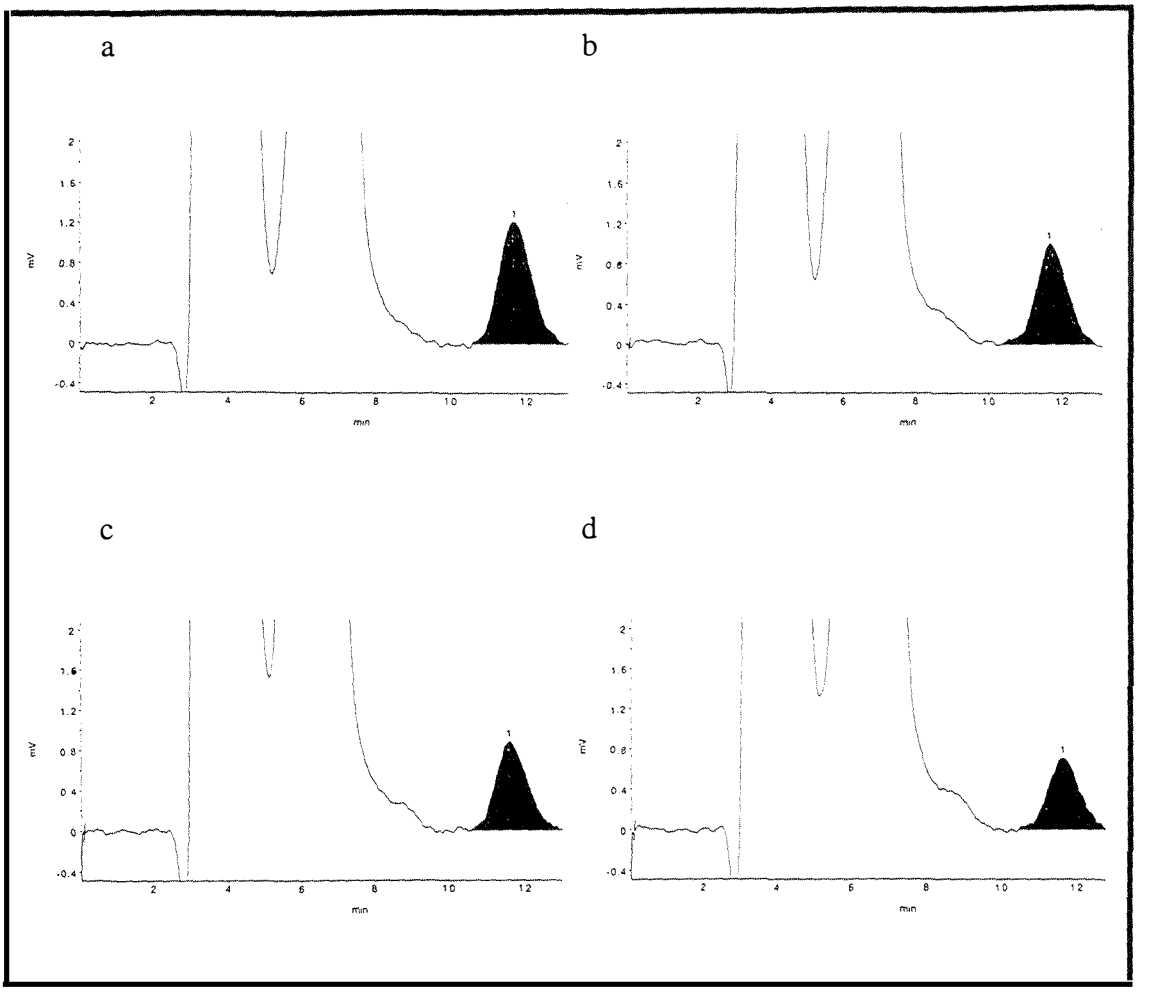


**Fig. 5.3.19** Time series showing the rate of hydrolysis of the $(GlcNAc)_6$ substrate by an E1G-lysozyme conjugate solution (E3). The rate of hydrolysis of the substrate is monitored by measuring the disappearance of the $(GlcNAc)_6$ substrate peak (shaded peak) as a function of assay time. The time points are referenced to the beginning of the assay, that is, the time of addition of the conjugate to the substrate (time 0). The profiles shown are those in which the assay system contains 100.3 μL of undiluted polyclonal antibody as described in the text. (a) 0 min after addition, (b) 10 min after addition, (c) 20 min after addition, and (d) 30 min after addition.

deviate from a straight line (at long incubation times) they were discarded from the calculations.

The rate of hydrolysis of the $(GlcNAc)_6$ substrate by native hen egg white lysozyme (at a concentration of 100 nM) under the conditions specified in the methods section was found to be

duplicate 1 = 0.111 μg $min^{-1}$ $R^2 = 0.997$

duplicate 2 = 0.121 μg $min^{-1}$ $R^2 = 0.774$

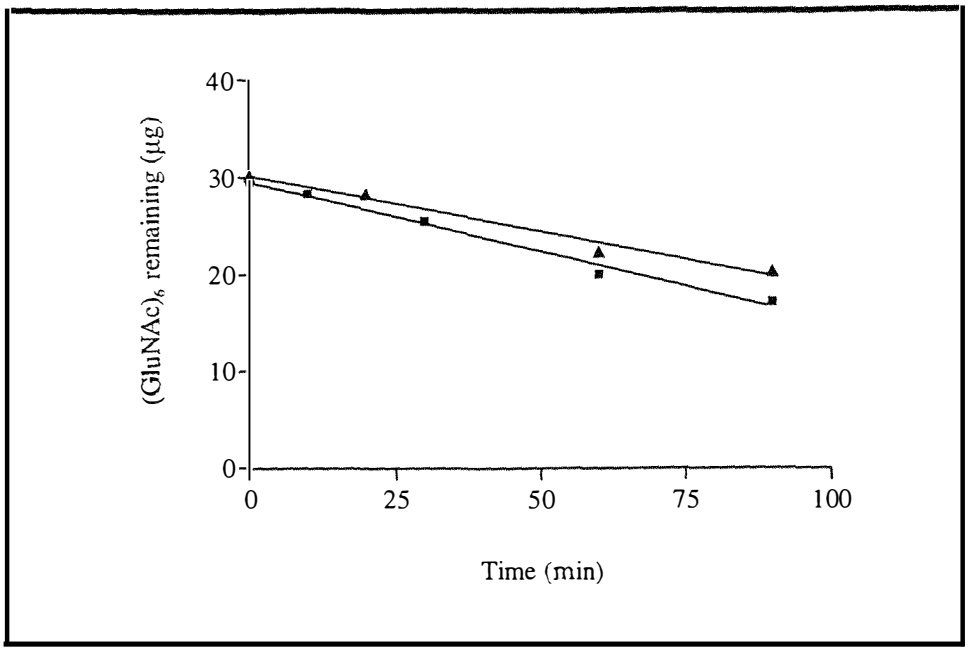


**Fig. 5.3.20** A plot showing the rate of hydrolysis of $(GlcNAc)_6$ by an E1G-lysozyme conjugate solution as a function of time. The rate profile shown is that for the assay system containing 20 μL of a 1/20 diluted polyclonal antibody solution. Two duplicate experimental assay runs are shown.

**Table 5.3.2**

The reaction rates (calculated as described above and in the methods section) for the hydrolysis of $(GlcNAc)_6$ by the mixed anhydride estrone glucuronide-lysozyme conjugate E3 in the absence and presence of various amounts of polyclonal estrone glucuronide antibody

| Volume antibody (μL) | Antibody dilution factor† | Rate of hydrolysis from analysed data* (μg $min^{-1}$) | Volume adjusted rate (μg $min^{-1}$ $mL^{-1}$) | Rate of hydrolysis (μM $min^{-1}$) | Time to exhaust initial [substrate] (min) |
|---|---|---|---|---|---|
| - | - | 0.114 | 0.570 | 0.46 | 330 |
| - | - | 0.119 | 0.595 | 0.48 | 317 |
| 100.3 | 0 | 0.389 | 1.945 | 1.57 | 97 |
| 100.3 | 0 | 0.416 | 2.080 | 1.68 | 91 |
| 20.0 | 1/2 | 0.161 | 0.805 | 0.65 | 234 |
| 20.0 | 1/2 | 0.172 | 0.860 | 0.70 | 217 |
| 20.0 | 1/20 | 0.139 | 0.695 | 0.56 | 271 |
| 20.0 | 1/20 | 0.127 | 0.635 | 0.51 | 298 |

**Key**

† = antibody dilution factor before addition to the assay mixture (see methods)

* = data calculated from 200 μL aliquot analysis (see text for details)

for the 200 μL aliquots. The rates were averaged (0.116 μg $min^{-1}$) and allowances made for volume, giving a rate of 0.58 μg $min^{-1}$ $mL^{-1}$ (0.46 μM $min^{-1}$). As the original concentration of $(GlcNAc)_6$ in the assay mixture was 152 μM it can be shown that all of the $(GlcNAc)_6$ substrate in the assay will be hydrolysed in approximately 330 minutes. The reaction rates calculated for the mixed anhydride conjugate (E3) in the presence and absence of the estrone glucuronide polyclonal antibody are presented in Table 5.3.2.

## 5.4 Discussion

### 5.4.1 Preparation of Fab Fragments from the Estrone Glucuronide Monoclonal Antibody

The proteolytic digestion of the intact monoclonal IgG antibody with pepsin resulted in the formation of $F(ab')_2$ fragments in good yield. The resulting Fc fragments are unstable and were completely degraded during the pepsin treatment in agreement with Parham [256]. Pepsin cleaves immunoglobulins on the carboxy-terminal side of the disulfide bonds that hold the two heavy chains together to produce a bivalent fragment, $F(ab')_2$, with both antigen binding sites intact as depicted in Fig. 5.4.1. However, peptic digestion of mouse derived monoclonal antibodies to produce $F(ab')_2$ fragments has proven to be difficult and unreliable for most antibody isotypes [257]. Only isotype IgG1 has been shown to behave predicably and produce high yields of $F(ab')_2$ product [256]. The estrone glucuronide monoclonal antibody used in the methods described above has

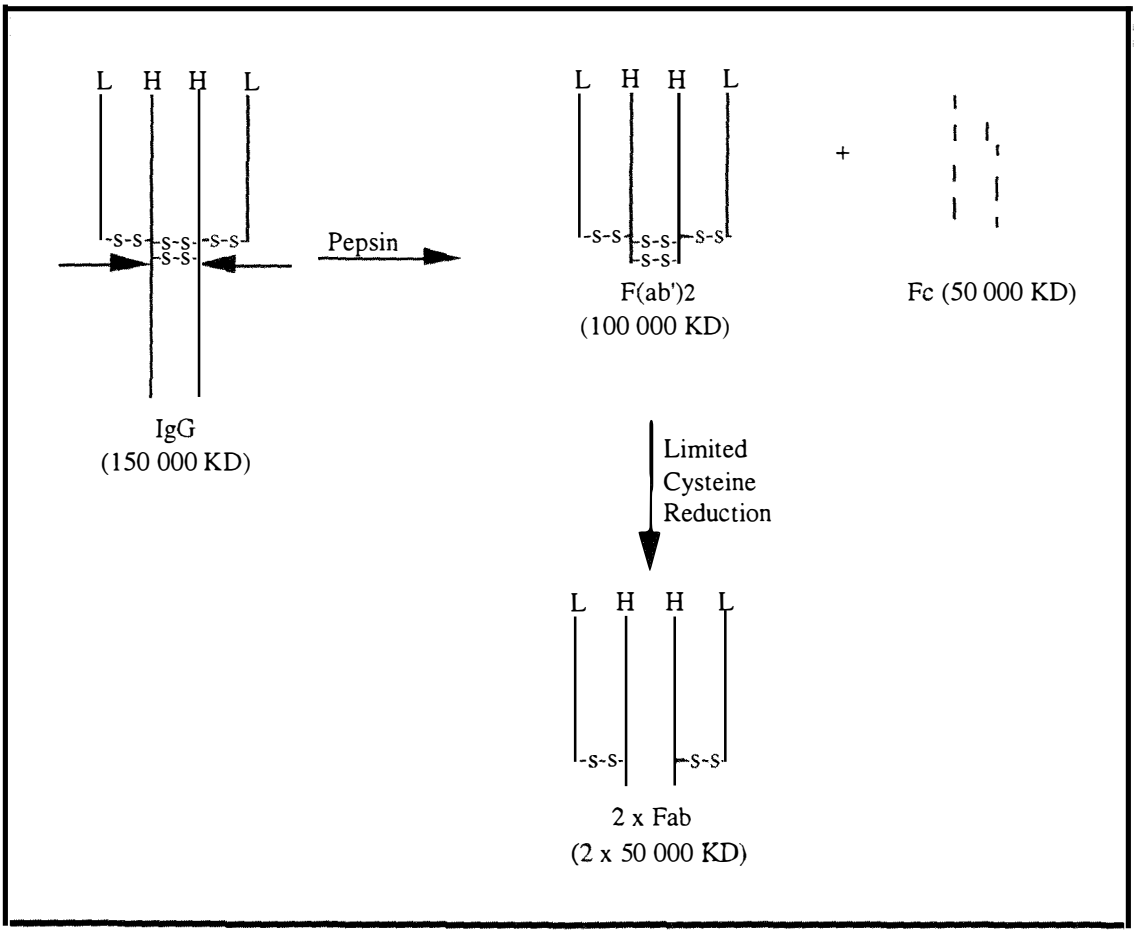


**Fig. 5.4.1** The preparation of Fab fragments from IgG estrone glucuronide monoclonal antibody as described in the text

previously been characterised as isotype IgG1 [98], and pepsin could therefore be used to remove the Fc portion of the immunoglobulin molecule. Because the $F(ab')_2$ products of peptic digestion of IgG1 antibodies are stable, it is possible to exhaustively digest the immunoglobulin with a high yield of $F(ab')_2$ product provided the pH of the digest solution is buffered at pH 3.50 [256-257] (see Fig. 5.3.1). This removes the need to separate uncleaved IgG from $F(ab')_2$ fragments and a simple dialysis step is all that is required before the selective reduction of the $F(ab')_2$ bivalent fragment to the univalent (one antigen binding site) Fab fragment.

SDS-PAGE techniques were used to analyse all digestion experiments and the purity of products. The distance that a polypeptide chain migrates has been shown to be proportional to the logarithm of the relative molecular mass [257]. The method therefore separates polypeptide chains under denaturing SDS conditions according to molecular weight (i.e. size). This is particularly useful for the analysis of immunoglobulins and the fragments arising from their proteolytic digestion. Under non-reducing conditions IgG migrates as a single band with an apparent molecular weight of ~ 150 000 [257]. The divalent $F(ab')_2$ and univalent Fab fragments also migrate as single bands under non-reducing conditions with apparent molecular weights of ~ 110 000 and 50 000 respectively. It is therefore possible to identify IgG, $F(ab')_2$ and Fab unambiguously by SDS-PAGE without using indirect and difficult methods such as immunodiffusion and immunoelectrophoresis.

Analytical experiments using small amounts of monoclonal antibody showed that after 2-4 hours all of the IgG was cleaved as shown in Fig. 5.3.1. Not all of the IgG initially dissolved in the digest buffer although this material tended to go into solution as the digest proceeded so that after 1/2-1 hour all of the IgG containing material had dissolved. If the digest was allowed to run longer than 4-5 hours an impurity with an apparent molecular weight of ~ 65 000 was seen (as shown by SDS-PAGE) as previously reported by Parham [256]. To prevent the appearance of this impurity all digests were followed by SDS-PAGE and terminated by dialysis against 0.1 M tris-HCl (pH 7.5) at 4°C as soon as the last of the intact IgG disappeared. Digests treated in this way showed no traces of high molecular weight impurities (Fig. 5.3.3).

Mild conditions of reduction with cysteine were used to break the H-H inter-heavy chain disulfide bonds [257] of the bivalent $F(ab')_2$ fragment (as depicted in Fig. 5.4.1) to give two univalent Fab fragments. Mild conditions ensured that the H-L disulfide bond between the heavy and light chains remained intact. After alkylation of the reduced Fab fragments with iodoacetic acid and dialysis against 0.15 M NaCl + 0.05 M sodium dihydrogen phosphate dihydrate buffer (pH 7.5), the reaction mixture was purified by gel

filtration chromatography to give active Fab fragments which were pure when analysed by SDS-PAGE (Fig. 5.3.3). The gel filtration step proved necessary to remove low molecular weight impurities which could not be removed by dialysis.

Attempts were made to prepare Fab fragments directly from the intact IgG molecule by cleavage with cysteine activated papain. The principal sites of papain cleavage are on the amino-terminal side of the H-H inter-heavy chain disulfide bonds that hold the two heavy chains together. As a result digestion with cysteine activated papain yields the two univalent Fab domains and an intact Fc fragment. However, attempts to produce Fab fragments in this way from the estrone glucuronide IgG antibody resulted in a number of products. Although Fab and Fc fragments were produced a number of other products of both high and low molecular weights were also generated. Separation and purification of the Fab fragments from the reaction mixture proved to be difficult and as a result all Fab fragments for kinetic experiments were produced by the peptic digestion method outlined above.

### 5.4.2 Displacement Off-Rate Constants for Displacement of E1G-Lysozyme Conjugate E3 from the Estrone Glucuronide Polyclonal and Monoclonal Antibodies, and the Monoclonal Fab Fragment

Although the conjugate clearing curve obtained under the conditions described in methods was not linear over the twenty minute assay period (Fig. 5.3.4), it did initially display a sufficiently straight line relationship to allow an initial rate to be calculated (Fig. 5.3.5). The initial rates calculated for the clearing of the *Micrococcus lysodeikticus* solution by the estrone glucuronide-lysozyme E3 conjugate were 25% faster in the presence of the monoclonal antibody and Fab fragment than in the presence of the polyclonal antibody. Thus the polyclonal antibody was the most effective in inhibiting the lytic activity of the estrone glucuronide-lysozyme conjugate. It was also apparent that the absence of the Fc fragment in the Fab molecule did not effect the binding required to inhibit the lytic activity as there was no significant difference between the initial rates calculated in the presence of the monoclonal antibody or the Fab fragment. This is not to say that the removal of the Fc fragment has not effected the kinetics and parameters of the Fab-estrone glucuronide recognition and coupling (e.g. strength of binding) but rather that binding leading to the successful inactivation of the lysozyme conjugate is not lessened by the absence of the Fc fragment.

When a single exponential was fitted to the polyclonal antibody data (Fig. 5.3.7) a displacement off-rate constant $k1_{off} = 3.5 \times 10^{-4}\ s^{-1}$ was obtained. However, the fit of the data was not good ($R^2 = 0.9037$) and this could be seen easily by visual inspection of

the fitted curve (Fig. 5.3.7). It is not surprising that a single exponential did not fit the polyclonal antibody data well. In a polyclonal antibody population it is unlikely that there will be only one major population of antibody which binds to, and inactivates, the conjugate. A two phase exponential was therefore fit to the polyclonal antibody data (Fig. 5.3.8) which gave a much better fit ($R^2$ = 0.9900 v 0.9037 for the single phase exponential) and this could also be seen by visual inspection of the generated curve (Fig. 5.3.8). Of the two displacement off-rate constants calculated from the two phase exponential fit one was faster ($k1_{off} = 3.15 \times 10^{-3}\ s^{-1}$) and one slower ($k2_{off} = 9.41 \times 10^{-5}\ s^{-1}$) than for the single exponential fit.

The superiority of the two phase exponential fit suggests that at least two major populations of antibody exist within the polyclonal antibody preparation. From the calculated displacement off-rate constants and using the equation

$$t_{1/2} = \frac{\ln 2}{k}$$

where $t_{1/2}$ is defined as the half-life or the length of time required for half of the bound antibody (see equation 1, Fig. 5.4.2) to dissociate from the immune complex, the half lives for the two polyclonal antibody populations can be calculated. The time for half of the bound antibody in equation 1 (Fig. 5.4.2) to dissociate from the immune complex for the first population of antibody is 220 seconds (3.7 min) and the time for the second population is 7 266 seconds (122.8 min). The first population therefore dissociates from the immune complex relatively quickly compared to the second population. Even 500 minutes after the excess E1G is added to the conjugate-antibody mixture, the initial rate is still significantly below (~ 60% of the control rate) a control assay in the absence of antibody. It is impossible to identify whether this is due to the existence of another population (a third or fourth population of antibody) because the displacement off-rate constants of these would be too slow to be measured. The control rate also begins to decline after about 500 minutes and it is therefore not possible to continue the experiment until the second population has completely dissociated and determine whether the control rate has been achieved.

Because the assay time for the measurement of estrone glucuronide in the Ovarian Monitor is only 20 minutes (1 200 seconds) the relatively slow displacement off-rate constants (particularly of the second population) must be considered in the assay design. It is necessary to mix the fixed amount of antibody in the assay system (section 1.5) with the sample of interest (containing the analyte to be measured) before allowing the antibody to mix with the lysozyme conjugate. By mixing in this order the sample analyte

can bind to the antibody first and only after the analyte has bound can the conjugate bind to any remaining free antibody. As a result the lytic activity measured will be dependent on the amount of free conjugate, which in turn, will be dependent on the level of analyte in the sample of interest. However, if the antibody and the estrone glucuronide-lysozyme conjugate are allowed to react prior to the addition of the E1G sample a considerable loss of lytic activity will result even after pro-longed incubation periods of the mixture due to the small displacement off-rate constants of the polyclonal antibody populations. In this case, the lytic activity observed would be lower than that directly related to the sample analyte concentration giving a falsely low measurement for the level of E1G in the sample of interest. Furthermore, in the presence of the *Micrococcus lysodeikticus* substrate during the assay procedure, there will be some equilibration as the substrate competes with the antibody for the conjugate and the sample analyte competes with the conjugate for the antibody as shown in Fig. 5.4.2. As a result of this equilibration occurring during the assay procedure, more conjugate will become free and the lytic activity will slowly increase over the assay time. Thus, the percentage inhibition after 20 minutes may be significantly less than that observed from the initial rates.

A single exponential fit is all that is required for the monoclonal and Fab fragment displacement off-rate data as there is only one population of antibody present. As a result the goodness of fit of both sets of data was very high (Table 5.3.1). The calculated displacement off-rate constants for the two antibodies were similar ($1.78 \times 10^{-2}$ $s^{-1}$ for the monoclonal and $2.06 \times 10^{-2}$ $s^{-1}$ for the Fab fragment) as reported in Table 5.3.1. This shows that the removal of the Fc fragment from the intact IgG (to give the Fab fragment) has no effect on the kinetic parameters of the binding of conjugated estrone glucuronide to the monoclonal antibody fragment. This is not surprising as the binding dynamics in the antibody binding site are spatially far removed from the Fc portion of the antibody molecule. However, the displacement off-rate constants of the monoclonal antibody and Fab fragment were approximately 6 times faster than the first polyclonal antibody population and 204 times faster than the second polyclonal antibody population. Half life calculations show that the time for half of the bound monoclonal antibody (or Fab fragment) to dissociate from the immune complex is only 36 seconds. The fast displacement off-rate constants of the monoclonal antibody and Fab fragment mean that if these were to be used in the assay system of twenty minutes duration, the order of mixing will have a much less dramatic effect on the measurement of the analyte concentration than in the case of the polyclonal antibody. However, as the displacement off-rate constant of eqn. 1 (Fig. 5.4.2) is so fast (for the monoclonal antibody) the substrate will also be able to compete more effectively for the free conjugate further shifting the equilibrium of eqn. 1 to the left hand side during the assay time. This results in a greater

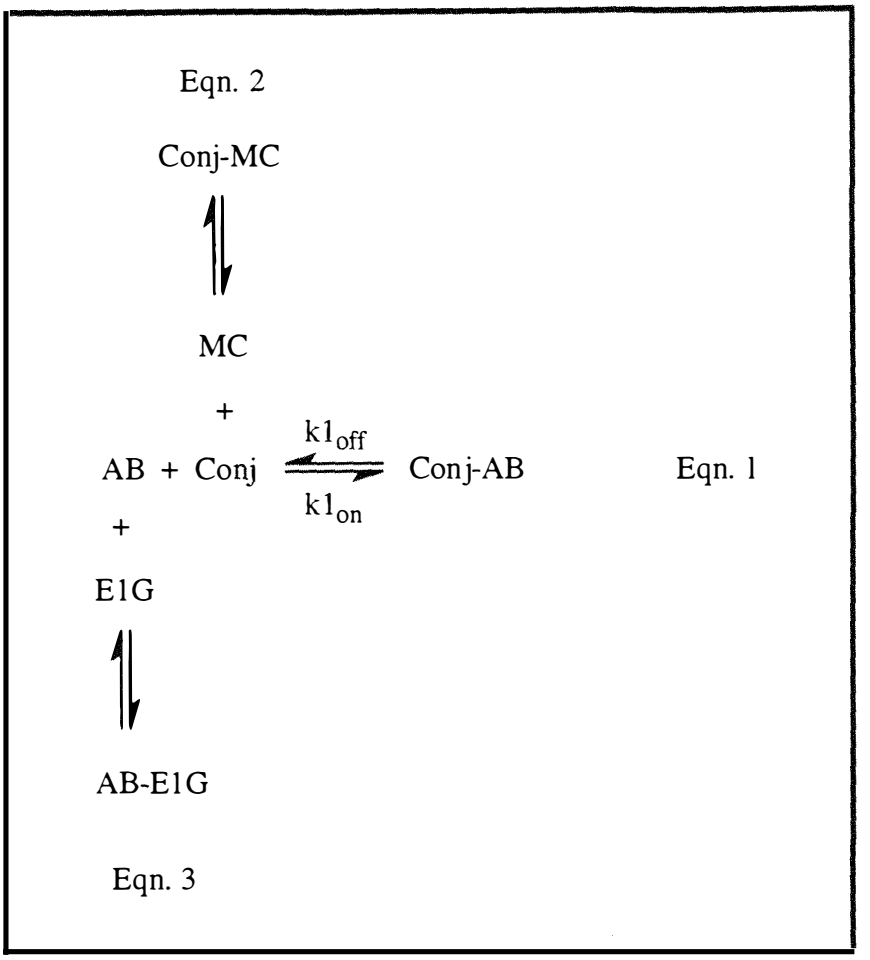


**Fig. 5.4.2** The implications of the slow displacement off-rate constants on the Ovarian Monitor assay system where Conj is the steroid glucuronide-lysozyme conjugate (in this case estrone glucuronide-lysozyme), AB is the antibody and MC is the *Micrococcus lysodeikticus* substrate. Although the displacement off-rate constants for eqn. 1 are small, in the presence of the *Micrococcus lysodeikticus* substrate and the sample analyte (E1G in this case) the competition between the antibody and the substrate for the conjugate, and the E1G and the conjugate for the antibody, means more conjugate will be free (and able to cleave substrate) as eqns. 2 and 3 approach equilibrium. Therefore the observed lytic activity will increase due to the increase in the amount of free conjugate in the assay mixture.

concentration of free conjugate than that determined by the antibody-analyte reaction. As a result of this, the lytic activity observed would be higher at any sample analyte concentration than with the polyclonal antibody, even for the zero standard. Hence, less inhibition will be observed for the zero standard and the discrimination between similar analyte estrone glucuronide concentrations diminished. It is this factor which makes the monoclonal antibody less suitable for the Ovarian Monitor assay than the more heterogeneous polyclonal antibodies.

### 5.4.3 Apparent Dissociation Constant ($K_d$) Measurements for the Conjugate-Monoclonal Antibody Immune Complex

In fitting the data collected from the dissociation constant experiments to a rectangular hyperbola (Fig. 5.3.11) the following assumptions were made;

1. That the reaction

$$AB + Conj \rightleftharpoons Conj\text{-}AB \qquad \text{Eqn. 1}$$

has reached equilibrium,

2. That binding is reversible, and

3. That there is no cooperativity (i.e. the binding of conjugate to one antibody binding site does not alter the affinity of another binding site).

The fit of the data by the non-linear regression method was much better than when estimating the values of $K_d$ and $B_{max}$ by linearising the data to create a Scatchard plot ($R^2$ = 0.956 v 0.661 for method 1 and $R^2$ = 0.897 v 0.542 for method 2, see section 5.3.3). This is because during the transformation of the data into a linear form, the experimental error is distorted and this violates the assumptions of linear regression [259]. The calculated values for $K_d$ and $B_{max}$ from the Scatchard plot are therefore likely to be further from the true value than those calculated by non-linear regression methods. Despite this the values calculated by both methods lie within experimental error of each other. However, for calculations involving $K_d$ and $B_{max}$ the values calculated using the non-linear regression method were used.

The kinetic and thermodynamic parameters of the E1G-lysozyme conjugate-monoclonal antibody binding system can be used to calculate the affinity constant ($K_a$) of the antibody for the lysozyme conjugated estrone glucuronide moiety. Since $K_a$ is the inverse of $K_d$, a value of $K_a = 3.60 \times 10^9\ M^{-1}$ may be calculated.

If we consider the reaction

$$AB + Conj \rightleftharpoons Conj\text{-}AB \qquad \text{Eqn. 1}$$

at equilibrium and both the dissociation off-rate constant ($k_{off}$) and the apparent dissociation constant ($K_d$) are known, then the association rate constant can be calculated as

$$k_{on} = \frac{k_{off}}{K_d}$$
$$= \frac{1.78 \times 10^{-2}}{0.278 \times 10^{-9}}$$
$$= 6.40 \times 10^{7}\ M^{-1}s^{-1}.$$

The binding affinity of the monoclonal antibody for the lysozyme conjugated estrone glucuronide molecule is similar to that obtained for the high affinity DB3 progesterone antibody ($K_a \sim 10^9\ M^{-1}$) [203] when binding unconjugated steroid. Although the estrone glucuronide monoclonal antibody has a high binding affinity ($\sim 10^9\ M^{-1}$), the production of extremely high affinity monoclonal antibodies is difficult as they make up only a small proportion of the total number of antibodies produced by hybridoma techniques [260]. However, even the production of high affinity antibodies does not mean that the required specificity will always be meet [220]. Cross-reactivity studies for the estrone glucuronide monoclonal antibody used in this study have been published by Henderson *et al.* [98] which show that the antibody cross-reacts with estrone-3-sulphate (18%) and estrone (7%). For these reasons (the difficulty in developing high affinity monoclonal antibodies and the low specificity of many monoclonal antibodies) polyclonal antibodies are often more suited to homogeneous enzyme immunoassay than monoclonal antibodies.

The dissociation constant was not determined for the Fab fragment of the monoclonal antibody since the $K_d$ value for the Fab fragment should be the same as that for the monoclonal antibody if assumption 2 above is correct (although $B_{max}$ will differ as there is only one binding site per molecule). It may have also proven difficult to measure $K_d$ for the Fab fragment as previous experiments of this type have reported that the resulting Scatchard plots of the binding curves are convex and the number of binding sites is only half of the expected number [232]. Fab fragments are therefore not considered appropriate for this type of experiment [232]. It has been suggested that the over-complex binding curves of Fab fragments is due to protein dimerisation [261] and single site cooperativity [262]. However, de Lauzon *et al.* [232] have suggested that it is difficult to explain why cooperativity stemming from protein conformational changes upon steroid binding should occur with Fab fragments but not with the intact IgG. de Lauzon *et al.* [232] suggest that it is more likely that the Fab fragments are unstable in relatively low ionic strength medium but are stabilised by the presence of their ligand accounting for the convex curves.

It was not possible to determine the $K_d$ value for the polyclonal antibody population(s) using the method outlined above as a titration curve could not be obtained. When a titration was attempted with a fixed amount of the estrone glucuronide polyclonal antibody pre-mixed with increasing amounts of conjugate there was not an initial non-linear increase in the rate of the end point assay (after 20 min) as a function of the conjugate concentration. Instead the slope of this line was parallel to the x axis until sufficient conjugate had been added to the assay so that all of the antibody was inactivated. At this point the extra conjugate then gave a line parallel to the control line in the absence of antibody. Hence the association constant ($K_a$) for the polyclonal antibody must be significantly larger than $10^9$ $M^{-1}$.

### 5.4.4 Lytic Activity of the Mixed Anhydride Estrone Glucuronide E3 Conjugate as Measured by the Hydrolysis of the Non-Bacterial Hexa-N-Acetyl-Chitohexaose Substrate, $(GlcNAc)_6$

The assay of lysozyme activity, as measured by monitoring the hydrolysis of the chitin derived substrate $(GlcNAc)_6$ (which consists of six β (1→4) linked N-acetylglucosamine units, Fig. 5.1.2) to produce $(GlcNAc)_4$ and $(GlcNAc)_2$, was much more time consuming and technically demanding than the turbidimetric method. Despite this the method has been considered more suitable for kinetic studies as the substrate is less complex than the bacteria cell wall and the reaction is less dependent on ionic strength (see introduction to this chapter). The size of the substrate probably plays a crucial role in the inhibition of lysozyme activity upon the binding of anti-hapten antibodies to conjugated steroid glucuronides (see chapter four). The pH rate profiles of the bacterial and saccharide substrates also differ significantly and more importantly, for work involving steroid glucuronide-lysozyme conjugates, it has previously been shown that acetylation of the amino groups in lysozyme does not affect the small substrate lytic activity [263]. Much of the early work on the binding and hydrolysis of saccharides by lysozyme was undertaken in the mid 1960's by Rupley and colleagues [253, 264] and has been well summarised by Imoto *et al.* [265] who list the kinetic parameters for the hydrolysis of $(GlcNAc)_6$ by hen egg white lysozyme at pH 5.2 and 40°C as

| | |
|---|---|
| $k_{cat}$ ($s^{-1}$) | 0.15 |
| $K_m$ (M) | $8.5 \times 10^{-6}$ |
| $k_{cat}/K_m$ ($s^{-1}$ $M^{-1}$) | 18 000 |

They also report a pH optimum near pH 5 without the ionic strength effects observed with the bacterial substrate. From the kinetic parameters above, the assay system reported in the methods section was established in 40 mM sodium acetate buffer (pH 5.20) at

40°C. The initial concentration of $(GlcNAc)_6$ in the assay was 152 μmol/L (17.9 x $K_m$) so that the enzyme was operating under conditions approaching $V_{max}$.

The $(GlcNAc)_6$ concentration in any one assay, at any one time, could be followed conveniently by HPLC analysis on a YMC-Pack $NH_2$ column (see Fig. 5.3.17). However, the presence of a large injection peak (3-4.5 minutes into the elution profile) followed shortly after by a large buffer peak (5.5-8.5 minutes into the elution profile) prevented the reaction being followed by measuring the rate of appearance of the product peaks ($(GlcNAc)_2$ and $(GlcNAc)_4$). Nevertheless, tracking of the $(GlcNAc)_6$ substrate peak was sufficiently accurate to allow the calculation of the rate of hydrolysis.

The rate of hydrolysis of the $(GlcNAc)_6$ substrate by a 100 nM solution of lysozyme, under the conditions specified in the methods section, was found to be 0.46 μM $min^{-1}$. Considering the difficulty and number of steps involved in the assay procedure, the agreement of the duplicates was very good, and the final error was less than ± 5%. The rate of hydrolysis of $(GlcNAc)_6$ by the mixed anhydride E3 conjugate was similar (0.47 μM $min^{-1}$) confirming the results published earlier by Imoto *et al.* [263] that acetylation of amino groups does not affect the small substrate lytic activity.

The reason for the observed difference in the activity of the estrone glucuronide-lysozyme conjugate relative to the native enzyme in the lytic assay system has been proposed to relate to the nature of the complex interaction between the bacterial substrate and the enzyme. Both the lysozyme molecule and the cell wall of the *Micrococcus lysodeikticus* molecule possess highly charged areas, resulting in the existence of electrostatic fields. Although lysozyme has an overall net positive charge at the pH values under which lytic activity assays are undertaken, Dao-Pin *et al.* [249] have shown that hen egg white lysozyme possesses both a negatively and positively charged lobe. This results in the formation of a large potential difference, which exists across the active site cleft of the lysozyme molecule and it has been suggested that this potential plays an important role in determining the rate of lysis [249]. Price and Pethig [198] have also shown that the *Micrococcus lysodeikticus* cell wall possesses an electrostatic field whose net charge is negative and this must be considered in any electrostatic model.

It is thought that the positive electrostatic field on the lysozyme molecule helps attract the negatively charged *Micrococcus lysodeikticus* cleavage sites towards the lysozyme molecule. Previous work with lysozyme has shown that once more than four lysine residues are acylated the lytic activity of the enzyme is destroyed [121]. However, although lysozyme derivatives with less than four lysine residues acylated retain lytic activity, the activity decreases as the number of acylated residues increases. Clearly, a

possible reason for this is that as the net positive charge on the conjugated lysozyme decreases the attraction between the enzyme and the *Micrococcus lysodeikticus* substrate also decreases, which in turn is reflected in the lytic activity. Further evidence for this can be seen in the results presented in chapter three whereby steroid glucuronide-lysozyme conjugates with higher substitution levels have much lower specific activities than those with lower substitution ratios. Not only will conjugation effect the net positive charge, it will also effect the potential which exists across the active site cleft, particularly for conjugates acylated at lysine residue 33 which lies at the bottom end of the active site cleft. If this potential plays a significant role in the rate of the lytic activity (as discussed in the introduction to this chapter) a reduction in its size would result in a decrease in the observed lytic activity. The electrostatic effect is not relevant in the binding of neutral oligosaccharides which bind directly into the active site cleft and hence the rate of the hydrolysis of $(GlcNAc)_6$ is not effected by the modification of the charge on the lysozyme molecule upon conjugation of the lysine residues as observed experimentally.

The apparent increase in the rate of hydrolysis of the $(GlcNAc)_6$ substrate by the estrone glucuronide-lysozyme conjugate in the presence of excess anti-estrone glucuronide polyclonal antibody is difficult to explain. When a large excess of polyclonal antibody was present the rate of hydrolysis was 3.5 times faster than in the absence of polyclonal antibody. As the data in Table 5.3.2 shows, the rate of hydrolysis increased as the amount of antibody added increased. There are two distinct binding modes for the hexasaccharide substrate of hen egg white lysozyme, a left-sided binding mode and a right-sided binding mode [266-267]. The preferred binding mode is the one which involves the left side of the active site in which the terminal (reducing sugar) binds to a β-sheet region. In this binding mode, the sugar residue which binds in the D-site of the active site adopts a full chair conformation (i.e. no distortion of the D-site saccharide residue is required) [266-267]. Inspection of the lysozyme molecule shows it may be possible for the polyclonal antibody to block or sterically hinder access of the hexasaccharide to the right-sided binding mode leaving access only to the left-sided binding mode. If this was the case only the more favoured binding mode may be possible resulting in an observed increase in the rate of the hydrolysis of the $(GlcNAc)_6$ substrate by the estrone glucuronide-lysozyme conjugate in the bound immune complex. It is also possible that the fingers of the antibody that protrude into the active site (as discussed in chapter four) help the binding of the polymer by increasing the distortion in the sugar ring bound at subsite D, which is necessary to allow sugar residues E and F to bind. In either event the antibody does not prevent the productive binding of substrate into the active site (as suggested in chapter 4).

Therefore, the source of inhibition when using the large bacterial substrate must be due to the antibody preventing the physical approach of the giant *Micrococcus lysodeikticus* molecule close enough to the active site to allow binding and cleavage (i.e. steric hindrance as first proposed by Rubenstein *et al.* [107]). The large bacterial substrate must not only have access to the active site, but must be able to wrap around it (subsites a-f) so that the half chair conformation of the sugar ring bound at subsite D is achieved. This is necessary so that the transition state carbonium ion intermediate can be formed (see Fig. 5.1.4). The source of inhibition when using the large bacterial substrate can therefore be described in terms of the antibody preventing access to the required transition state, that is to say, steric inhibition of access to the transition state.

From the detailed analysis of the lysozyme system sufficient information is now available that in principle it may be possible to design an inhibitable small substrate. For example, it may be possible to synthesise an oligosaccharide substrate which can be inhibited upon binding of an antibody by extending the length of the chitohexaose moiety with a conformationally rigid structure. This extension would have to be long enough to interact with the bound antibodies so that steric access to the transition state was again prevented. If this could be achieved experimentally it would show that a giant substrate such as *Micrococcus lysodeikticus* is not necessary to exhibit extensive inhibition of lysozyme conjugates. However, it should be noted that it is not possible to extend this approach generally to other enzyme systems which use small substrates unless the following parameters are known:

1) The three dimensional structure of the enzyme.
2) The acylation positions in the enzyme conjugates.
3) A model or crystal structure of the Fab-conjugate three dimensional structure so that the topography of the immune complex is known.
4) The geometry of the active site.
5) The enzyme mechanism.

If these parameters are known then in principle one could design a small substrate which could be subject to the same steric restraints or interference for enzymes producing colour. This information is not currently available for any other enzyme system (except lysozyme) and given the amount of information required to produce inhibitable conjugates of other enzymes, lysozyme will continue to be the best example of a practical homogeneous enzyme immunoassay system. Unless procedures can be developed which control the site of acylation in other enzymes (such as horseradish peroxidase) the hope of synthesising an inhibitable conjugate in the immediate future seems remote. Therefore

colour assays will most probably continue to be solid phase systems which do not rely on obtaining highly inhibitable conjugates.

## 5.5 Conclusions

When designing assay systems it is apparent that the type of antibody (monoclonal v polyclonal) used must be considered and the kinetic properties analysed to obtain the most sensitive system. The kinetic parameters of any given antibody may also influence assay procedure and the order of mixing of reagents. The large degree of inhibition observed for the lytic activity of the steroid glucuronide-lysozyme conjugates upon the binding of an anti-hapten antibody is due to steric hindrance of the large bacterial substrate (*Micrococcus lysodeikticus*). However, when lysozyme activity was measured by the rate of hydrolysis of the small chitin derived oligosaccharide $(GlcNAc)_6$, excess antibody did not inhibit the observed activity, in fact it accelerated it. This may explain why high levels of inhibition have not been observed for immunoassays based on horseradish peroxidase type systems. Horseradish peroxidase works on substrates which are much, much smaller than the bacterial cell wall of lysozyme and these small substrates may still be able to access the active site, even in the presence of antibody much as the $(GlcNAc)_6$ substrate can still access the active site cleft of estrone glucuronide conjugated lysozyme, even in the presence of a large excess of anti-estrone glucuronide antibody. These results suggest that if attempts are to be made to produce inhibitable enzyme conjugates by manipulating the size of the substrate then large, somewhat rigid matrices would seem to be the best vehicles to which to attach substrates. Controlling the sites of acylation of the enzyme is also likely to be important.

# Chapter Six

# Studies Toward the Development of a Colour Test Immunoassay For the Detection of the Fertile Period

## 6.1 Introduction

To date, very few examples of colour test systems for the determination of ovulation or the fertile period have been published in the literature. The majority of these test systems rely on the use of enzymes such as horseradish peroxidase which have substrates that change colour during, or after, the enzymatic reaction. The colour development is usually a direct measure of the amount of bound or free enzyme conjugate, or a measurement of the colour development resulting from an enzyme labelled second antibody which detects binding of the first antibody (see references 40, 88, 95 for example). In this second system the first antibody ($AB_1$) binds to either immobilised hapten, conjugate, or another antibody and the amount of bound antibody ($AB_1$) is then measured by the binding of the second antibody ($AB_2$) to which an enzyme capable of producing colour is attached. A number of enzymes such as horseradish peroxidase (HRP) [98, 111-112] and alkaline phosphatase [98, 113] have now been linked to steroid glucuronides for use in enzyme immunoassays to measure urinary concentrations of these haptens. The most widely used enzyme label for this purpose is horseradish peroxidase (HRP), a plant peroxidase which consists of two parts, a glycoprotein and a protohemin [268-269]. Peroxidases catalyse the reaction

$$H_2O_2 + AH_2 \rightarrow 2H_2O + A$$

in which hydrogen peroxide ($H_2O_2$) is reduced to water by a reductant ($AH_2$). By changing the reductant ($AH_2$, the substrate) various colour changes can be observed as the reaction proceeds.

Unfortunately, horseradish peroxidase-hapten conjugates whereby the enzyme is conjugated directly to a hapten molecule do not exhibit the extensive degree of inhibition upon the binding of an antibody to a conjugated hapten that is observed in the Ovarian

Monitor lysozyme based immunoassay system. Thus solution assay systems such as that in the Ovarian Monitor which rely on homogeneous enzyme immunoassay principles have not been possible with horseradish peroxidase. There are several other problems associated with the use of HRP for enzyme immunoassay, particularly:

(1) The difficulty in obtaining steroid glucuronide conjugates of HRP using traditional coupling procedures such as the mixed anhydride procedure or the active ester procedure [108].

(2) The difficulty involved in the purification of HRP conjugates. It has proven difficult to separate HRP-hapten conjugates from unreacted starting materials (unreacted HRP and unreacted steroid glucuronide) after conjugation reactions.

(3) The instability of HRP or HRP-hapten conjugates when stored at relatively low concentrations.

In the last 10-15 years a number of colour and test strip type assays have been developed for the measurement of a variety of proteins and small analytes (for example see references 40, 88, 95, 110, 270-276). The majority of these systems are based on visual detection of the concentration of the molecule of interest by changes in the intensity of the colour produced with changing analyte concentrations. In recent years the development of coloured dyes [88], coloured latex or polystyrene beads (or microspheres) [277], and inorganic colloidal particles (particularly colloidal gold) [278-286] for labelling in immunoassays has meant an enzyme capable of producing colour is not an absolute necessity for colour strip immunoassay tests. Instead, either the enzyme conjugate or an antibody is labelled with colloidal gold or coloured latex beads. Upon binding of the labelled molecule, the cumulative effect is the development of a coloured product (or band) on the solid phase which is proportional to the amount of label captured. The enzyme itself does not take part in the immunoassay but is a handle or label for the hapten of interest which captures the antibody. In some cases this label may not be required and the antigen can be used on its own, however small organic antigens by themselves are too small to label with the coloured reagents. The latex beads have become particularly popular for use in solid phase colour tests and several companies now market tests using microspheres and chromatographic test strips where the sample moves up the strip by capillary action (Table 6.1.1).

The way in which these tests work can be explained using the Unipath Clearblue Easy® system (developed as a home pregnancy test) [277] as an example. In this test, small dark blue microspheres are coated with a primary antibody (Ab1-μs) raised to human

chorionic gonadotrophin (HCG). The microsphere coated antibody (Ab1-μs) is dried onto one part of a nitrocellulose strip (which acts as the solid phase) and a second antibody for a different epitope (Ab2) to HCG is immobilised on another part of the nitrocellulose strip. The strip is dipped in urine at one end and as the urine moves up the strip by capillary action it picks up the blue microspheres (Ab1-μs), remobilising it and carries it up the strip. When the flow reaches the immobilised Ab2, the dyed microspheres with HCG are captured by Ab2 to form a blue line as a result of the sandwich formed (Ab1-μs-HCG-Ab2). This blue line signals a positive pregnancy. If a woman is not pregnant, then there will be no HCG present in the urine, the sandwich will not form and no blue line will be seen (i.e. a negative pregnancy test).

Hand in hand with the advancement in dyes, microspheres and metal colloids for labels in immunoassay has been the advancement in solid phase supports. The most commonly used solid phase supports for immunoassay are membrane strips consisting of nitrocellulose or nylon. Of these two types of membrane nitrocellulose based strips have become the most popular, particularly when designing capillary action colour test strips. In recent years the type of membrane used and the methods for immobilising and remobilising proteins and antigens on these membranes has been the subject of much investigation (for example see references 95, 277, 280, 282, 288-291). As a result a large number of membrane handling procedures and solid phase immunoassay formats are now published in the literature.

Although the technology and techniques required for the development of a colour test for the measurement of urinary estrone glucuronide and pregnanediol glucuronide levels appear to be available, in reality developing such a test is much more complex. Designing a colour test in which the colour signal is proportional to increasing levels of analyte is an even more difficult problem. The characterisation details described in the previous chapters mean that it may now be possible to extend the Ovarian Monitor hen egg white lysozyme system to develop a colour test for the measurement of estrone glucuronide and pregnanediol glucuronide.

Access to the extensive information now available on the Ovarian Monitor immunoassay system is a huge advantage when attempting to convert the system to a colour test with the precision and reliability of the Ovarian Monitor. However, in developing such a new (or modified) system it is necessary to repeat and advance previous work undertaken with other assay systems and membrane formats. It is imperative that the techniques and assay formats of other systems are mastered in order to apply them to any new system derived from the Ovarian Monitor. For this reason the following chapter is split into three

**Table 6.1.1**

Chromatographic strip and sandwich colour tests for various analytes using microsphere dyed latex particles for the measurement and visualisation of bound label (from Bangs [277])

| Company | Commercial Name of Test(s) | Analyte measured |
|---|---|---|
| Unipath | Clearblue Easy®, Clearview | HCG<br>LH<br>Strep A<br>Chlamydia |
| | Personal Contraceptive System | Estrone glucuronide & LH† |
| Carter Wallace | First Response® | HCG |
| Abbott | Test Pack Plus | HCG<br>Strep A |
| Johnson & Johnson | (Fact Plus-OEM by Abbott) | HCG |
| Drug Screening Systems | # | Cocaine<br>Heroin/Opiates |
| Pacific Biotech/<br>Hybritech | CARDS+ -OS | HCG<br>Strep A<br>Strep B |
| Biosite Diagnostics | Triage™ | Panel of 8 DAU's* |
| Quidel | Conceive™ | LH |
| Eiken | OC-H or OC-Hemocatch | fecal occult blood (hemoglobin) |

**Key**
HCG = human chorionic gonadotrophin
LH = luteinising hormone
Strep = streptococcus
† = reference [287]
* = an eight analyte DAU (drugs of abuse) test panel
# = unknown

sections. The first deals with the establishment of colour test immunoassays on membranes using horseradish peroxidase directly conjugated with estrone glucuronide and various methods of visually detecting the bound and free conjugate. The second section investigates the possibility of using one of these formats with the hen egg white lysozyme system. The third section discusses a possible new and exciting assay format

based on the characterisation results and parameters reported in the chapters 2-5. The proposed format is an extension of the Ovarian Monitor, utilising the steroid glucuronide conjugates of hen egg white lysozyme, anti-steroid glucuronide antibodies and monoclonal antibodies specific to certain epitopes (or defined surface areas) of the lysozyme molecule. If successful it will constitute an excellent example of the rational design of an immunoassay system based on the accumulation of fundamental research data collected over 20-30 years.

## 6.2 Colour Test Formats for the Measurement of Urinary E1G and PdG Levels using Steroid Glucuronide-Horseradish Peroxidase Conjugates

### 6.2.1 Introduction

Preliminary colour test formats for the measurement of urinary levels of estrone glucuronide were set-up under the guidance of Dr. Roger Collin (Toxinology and Food Safety, Ruakura Agricultural Research Centre, Hamilton, New Zealand) using estrone glucuronide-horseradish peroxidase conjugates. Dr. Collin has developed colour based horseradish peroxidase immunoassays for the measurement of sporidesmin, the toxin which causes facial eczema in domestic ruminants such as sheep and cattle which graze pasture [292]. Two different colour test immunoassay formats were investigated. The first format (immunofiltration) utilises the enzymatic properties of horseradish peroxidase to produce a colour change resulting from the reduction of hydrogen peroxide. The second format (capillary action colour test strip) uses the HRP-E1G conjugate as a capture molecule, the colour development resulting from the binding of colloidal gold labelled antibody to estrone glucuronide attached to the capture molecule.

### 6.2.2 Apparatus, Reagents, and Methods

*6.2.2.1 Apparatus*

All chromatographic procedures were performed on a Pharmacia fast protein liquid chromatography (FPLC) system at room temperature as described in section 2.2.1. Chromatographic analysis and procedures were performed on prepacked Mono-S strong cation-exchange and Alkyl Superose hydrophobic interaction columns HR 5/5 (50 x 5 mm I.D.).

Immunofiltration experiments were undertaken using a specially designed, two part Perspex block as shown in Fig. 6.2.1. The block consisted of a solid base into which two bolts were set. The bolts were placed 8 cm apart so that filter papers could be placed down the bolts when holes were punched with a regular hole punch. The top half of the block had two holes placed so that it could be slipped over the bolts and bolted into place against the base using wingnuts. It also had a series of holes of approximately 1 cm diameter drilled into it. These holes acted as wells, when the top half was screwed to the bottom half, into which reagents could be placed.

The microplate reader and software used was from Bio-Rad and belonged to AgResearch, Ruakura, Hamilton, New Zealand.

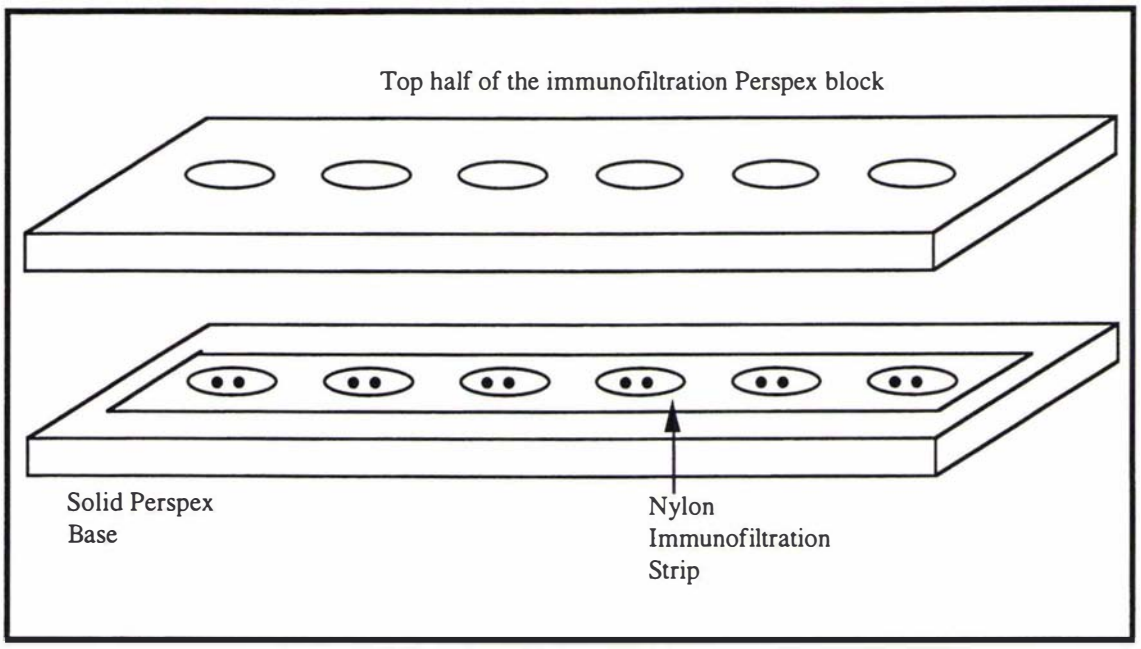


**Fig. 6.2.1** The immunofiltration apparatus described in the apparatus section. The base consists of a solid Perspex block upon which filter papers are placed. The immunofiltration strip is then placed on top of the filter papers and the top of the block is then placed over the strip so that wells are formed between the top Perspex block and the test strip. Reagents can then be placed into the wells, which are pulled through the test strip by capillary action into the filter papers below. The top block is held in place by bolts attached to the bottom block which pass through holes in the top block. The apparatus is then screwed together. For more details see text and sections 6.2.2.1 and 6.2.2.6.

### *6.2.2.2 Reagents*

The following reagents were used and obtained from the sources indicated: horseradish peroxidase, bovine serum albumin (fraction V), sodium caseinate (C-8652) and tetramethylbenzidine (TMB) were from Sigma Chemical Co. (St. Louis, MO, U.S.A.). Estrone glucuronide (E1G) was synthesised as described in section 2.2.3.2. Anti-horseradish peroxidase antibodies were a generous gift from Dr. R. Collin (Toxinology and Food Safety, Ruakura Agricultural Research Centre, Hamilton, New Zealand). Nylon membrane (Pall Biosupport membrane, Biodyne B transfer membrane, 0.45 μm, BNBZF3R) was from Pall Europe Ltd., Portsmouth, England and was purchased from A. M. E. Industries, 6 Perclo Place, Hamilton, New Zealand. Laminated nitrocellulose membranes (Nitroflow V (NT 5000), 5 μm) were purchased from Gelman Sciences, New South Wales, Australia. All other chemicals and reagents were analytical reagent grade or better.

Ion-exchange and hydrophobic interaction chromatography buffers were prepared as described in chapter two. All buffers were filtered and degassed using 0.2 μm filters (Millipore) before use. Samples were filtered through Millipore GVWP 013 00 filters (0.2 μm).

Stock (10 X) saline phosphate buffer (PBS) was prepared from NaCl (80 g), KCl (2.0 g), $Na_2HPO_4$ (14.4 g) and $KH_2PO_4$ (2.4 g). The solution was prepared by dissolving the required amounts in sequence in 900 mL of Milli-Q water. The volume was then made up to 1000 mL with Milli-Q water to give a final pH of approximately 6.8. PBS buffer for use was prepared by diluting the stock solution 1/10 with Milli-Q water to give a pH of pH 7.3-7.5.

*6.2.2.3 Preparation of an estrone glucuronide-horseradish peroxidase conjugate*

Conjugation of horseradish peroxidase (HRP) with estrone glucuronide was achieved by the mixed anhydride procedure of Erlanger *et al.* [116] as described in section 3.2.3.1 (and scheme 3.2.1) at a 40.4:1 ratio of E1G[H] to HRP. Conditions for the mixed anhydride coupling reaction were as follows: E1G[H] (4.5 mg, 10.1 μmol), dimethylformamide (72 μL), tri-n-butylamine (2.4 μL, 10 μmol), isobutylchloroformate (1.3 μL, 9.99 μmol), horseradish peroxidase (10 mg, 0.24 μmol) dissolved in 1.3 mL of Milli-Q water at 0°C, pH 8.39. At the completion of the conjugation reaction, the reaction mixture was dialysed into 50 mM sodium dihydrogen phosphate buffer (pH 6.60) to remove unreacted estrone glucuronide.

*6.2.2.4 Ion-exchange and hydrophobic interaction chromatography analysis of the estrone glucuronide-horseradish peroxidase conjugation reaction mixture*

The estrone glucuronide-horseradish peroxidase conjugation reaction was analysed by Mono-S 7 M urea cation-exchange chromatography and Alkyl Superose hydrophobic interaction chromatography as described in section 2.2.3.6. The resulting chromatographic profiles were standardised and compared with the profile of unconjugated, native horseradish peroxidase under the same conditions.

*6.2.2.5 Purification of the estrone glucuronide polyclonal antibody from other serum proteins*

Estrone glucuronide polyclonal antibody from sheep sera (prepared as described in sections 2.2.3.8 and 2.2.3.9) was purified from other serum proteins using an E-Z-SEP™ polyclonal antibody purification kit from Middlesex Sciences, Inc., Foxborough, MA, U.S.A (marketed by Pharmacia Biotech). The concentration of protein in the antiserum before and after purification was determined using a commercially available protein assay (the bicinchoninic acid protein assay (Pierce)) and reading the resulting (blank corrected) absorbance with a Bio-Rad microplate reader at a wavelength of 562 nm. The protein concentrations were determined using the standard curve obtained from the absorbance values of a set of bovine serum albumin standards with accurate and known concentrations. The purity of the antibody was determined by comparison against

the unpurified serum when analysed by non-reduced SDS-PAGE as described in section 5.2.3.3.

*6.2.2.6 Preparation of nylon membranes for use in, and the procedures involved in, immunofiltration experiments for the detection of estrone glucuronide levels*

All immunofiltration experiments were undertaken using nylon membrane as the solid phase support and unpurified estrone glucuronide-horseradish peroxidase conjugate (i.e. the conjugation reaction mixture was used as E1G-HRP conjugate). The nylon membrane was prepared for immunofiltration experiments as follows:

1. The nylon membrane was marked with a template and cut into strips. When handling the membrane latex gloves were used to prevent hand oils and proteins from contacting the membrane surface. The strips contained six reaction centres, each of which could be aligned with a well in the Perspex block (Figs. 6.2.1 and 6.2.2). Each reaction centre had two indentations marked into the membrane (without damaging the membrane) so that small volumes could be placed into these indentations to prevent the liquid from dispersing and spreading through the membrane.

2. A dilution series using the anti-estrone glucuronide antibody was prepared. The dilutions were prepared with saline phosphate buffer (PBS) containing 0.05% bovine serum albumin (BSA). Dilutions of both unpurified antiserum and purified estrone glucuronide antibody (purified as described in section 6.2.2.5) were prepared. A sample of antibody (diluted by a factor of 1/5) was serially diluted (by a factor of 2) to give a 1/10, 1/20, 1/40, 1/80, 1/160, 1/320, 1/640 dilution series.

3. Anti-estrone glucuronide antibody was immobilised on the nylon membrane by placing 2 μL spots of the diluted antibody solutions into the small indentations on the nylon membrane. Both purified and unpurified antibody membranes were prepared. The membrane was then allowed to air dry for 30 minutes.

4. Remaining protein binding sites on the membrane were blocked to prevent non-specific binding of the probe (HRP-E1G conjugate) to the membrane. This was achieved by immersing the membrane strips in a 1% solution of sodium caseinate. The strips were then allowed to air dry overnight and stored under desiccant conditions. The sodium caseinate solution was prepared by bringing the required amount of Milli-Q water to the boil and then adding the sodium caseinate powder with rapid stirring to the boiling water. The solution was then left with rapid stirring for 10 minutes. The sodium caseinate solution was left to cool to room temperature before use and the solution was discarded immediately after use.

The prepared nylon strips looked similar to that depicted in Fig. 6.2.2 although the antibody spots could not be seen. However, the position of the immobilised antibody could be detected by the indentations on the membrane surface into which the antibody was placed. Nylon strips prepared for immunochromatography were used immediately or stored in air tight plastic bags containing silica gel.

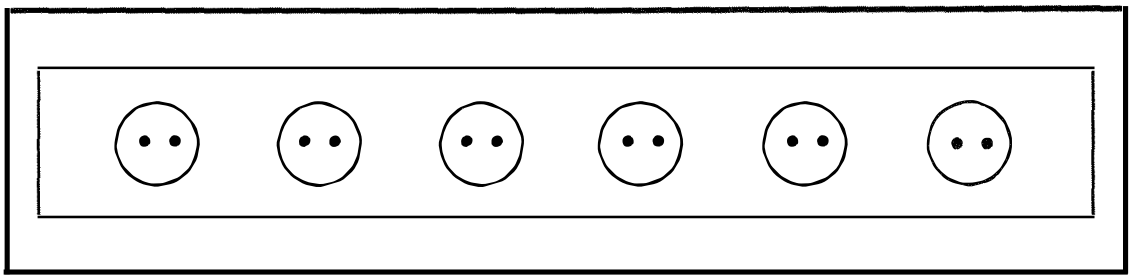

**Fig. 6.2.2** A schematic diagram of a nylon immunofiltration membrane with immobilised anti-estrone glucuronide antibody (represented by the dots). The membrane is placed in a Perspex block (see Fig. 6.2.1) in which the wet chemistry takes place. For more details see text.

Once the nylon strips were prepared, immunofiltration experiments were run according to the following procedure:

1. Filter papers (usually handy towels) were placed over the bolts on the base of the Perspex block. The purpose of the filter papers is to draw the liquid through the membrane and act as solvent absorption (or sink) papers.

2. The prepared nylon membrane was then placed on top of the filter papers, and the top of the Perspex block was placed over the membrane so that the holes in the Perspex block aligned with the membrane reaction centres. This formed a well above the immobilised antibody (see Fig. 6.2.1). Care must be taken in aligning the block. The antibody spots must be as close to the centre of each well as possible to prevent colour distortion upon undertaking the wet chemistry.

3. Into the well was placed 400 μL of sample (urine) or standard which was allowed to run through the membrane. If sample or standard was not run and the system was being tested, at this stage the membrane was washed with 400 μL of Milli-Q water containing 0.05% Tween 20.

4. As soon as the last of the liquid in step 3 had run through the membrane, and before it began to dry, 100 μL of the horseradish peroxidase-estrone glucuronide conjugate was placed in the well and allowed to run through the membrane. The volume and dilution of conjugate was adjusted as required to obtain better sensitivity and colour formation.

5. The membrane was washed with 400 μL of a Milli-Q water solution containing NaCl (0.85%) and Tween 20 (0.025%). It is important that the strip is not allowed to dry between steps 4 and 5 to prevent any chance of non-specific immobilisation of the conjugate onto the nylon membrane. The conjugate must only be allowed to immobilise by binding to the immobilised antibody.

6. In the last step a stock TMB solution was prepared from TMB (50.4 mg), acetone (1 mL), and methanol (9 mL). A citrate buffer solution was also prepared consisting of sodium citrate (4.41 g), 1 M KOH (25 mL), 30% $H_2O_2$ (36 μL) and Milli-Q water to give a solution with a final pH of approximately pH 3.74. A developing solution was prepared from 100 μL of the stock TMB solution and 900 μL of the citrate buffer solution. This must be made up and mixed immediately prior to use. The resulting solution (100 μL) was placed in each well and the colour reaction left to proceed (a nice green colour develops where the antibody spots are immobilised if any HRP-E1G conjugate is bound). After 3 minutes the membrane was removed from the Perspex block and a record of the assay made by photocopying the membrane. The membrane was then discarded. If the reaction was allowed to proceed beyond 3 minutes the background colour became very intense. The remaining developing solution was then discarded as after 5-10 minutes it turns dark green.

*6.2.2.7 Preparation of nitrocellulose membranes for use in, and the procedures involved in, colloidal gold systems for the detection of estrone glucuronide levels*

All colloidal gold experiments were undertaken using laminated nitrocellulose membrane as the solid phase support and unpurified estrone glucuronide-horseradish peroxidase as the conjugate. Colloidal gold was prepared using a method similar to that published by Ferns [293] as described by Coco Martin *et al.* [283] and Ching *et al.* [294]. Aqueous gold chloride ($HAuCl_4.3H_2O$, 200 mL, 0.01%) was brought to the boil and 2 mL of 1% sodium citrate solution was added. The boiling was then continued for 5-10 minutes until the solution rapidly changed from pale yellow in colour to purple-red. The solution was then cooled and stored at 4°C. Colloidal gold stored in this way was stable for several months.

Antibody-colloidal gold (immunogold) was prepared using a method similar to that of Coco Martin *et al.* [283]. Anti-estrone glucuronide antibody-colloidal gold was prepared with both unpurified antiserum and purified antibody (which had been purified as described in section 6.2.2.5). Preparation of immunogold involves a series of steps as outlined below.

1. A series of eight antibody solutions, diluted to different concentrations with Milli-Q water, were initially prepared. The dilutions were undertaken serially, so that a dilution series of 1/5, 1/10, 1/20, 1/40, 1/80, 1/160, 1/320, 1/640 diluted antibody was prepared.

2. After the pH of the colloidal gold solution had been adjusted to pH 7.70 with potassium carbonate (0.02 M), 10 mL aliquots of the pH adjusted colloidal gold solution were pipetted into eight SS34 centrifuge tubes.

3. Into each of the centrifuge tubes was added one of the eight antibody dilutions (100 μL) with vigorous vortex mixing. This was essential at this stage to obtain uniform complex formation. Each centrifuge tube was then left to stand at room temperature for 5 minutes before the addition, with vortex mixing, of 150 μL of 20% BSA in PBS. After the addition of the BSA solution the immunogold solutions were placed in a centrifuge (Sorvall Superspeed RC2-B) and spun at 6 000 rpm in a SS34 rotor for one hour at room temperature.

4. After centrifugation the supernatant was removed from each tube using a Pasteur pipette. It is not possible to decant the supernatant due to the soft nature of the pellet. The colloidal gold conjugate (immunogold) in each pellet was then resuspended in 500 μL of 2% BSA in PBS. The resulting solution was sonicated and then transferred to a 1 mL Eppendorf tube.

5. The immunogold solution was placed in a microcentrifuge and spun at 6 000 rpm for 10 minutes. At the completion of centrifugation, the supernatant was once again removed, the pellet resuspended in 500 μL of 2% BSA in PBS, the solution sonicated and spun again at 6 000 rpm for 10 minutes. This procedure was repeated twice more before the pellet was finally resuspended in 500 μL of 2% BSA in PBS for the last time, sonicated and stored at 4°C until required for use. If the immunogold solution had been stored for sometime before use it was necessary to resonicate the solution.

Laminated nitrocellulose membrane sheets were cut into strips of approximately 0.6 x 4 cm in size. Three bands of undiluted horseradish peroxidase-estrone glucuronide conjugate were immobilised on the middle of each strip by application with a Helena Thin Layer Chromatography (TLC) Applicator as shown in Fig. 6.2.3. The membrane strips were then allowed to air dry for 60 minutes and used immediately, or stored over silica gel.

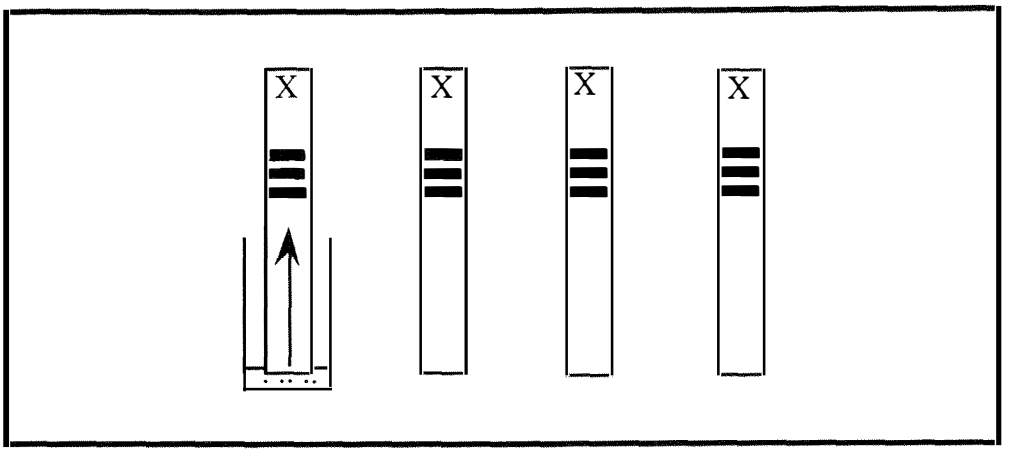


**Fig. 6.2.3** The make-up of nitrocellulose solid phase test strips for immunogold chromatography immunoassay as described in the text. Three bands of HRP-E1G conjugate are immobilised onto one end of each strip. The strip is then placed in a small reservoir of immunogold (antibody labelled with colloidal gold) which is allowed to flow up the strip (as shown in the left test strip) and bind to the immobilised conjugate. The colloidal gold particles produce a typical pinkish-red colour when they bind to the conjugate and accumulate at the surface of the membrane resulting in the formation of bands where conjugate has been immobilised. At the spot marked X filter paper can be attached (simply by stapling it to the membrane) so that extra liquid can be drawn up the test strip by capillary action.

The immunogold test strips were run as described in Fig. 6.2.3. Immunogold solution was placed in the bottom of a small, plastic vial. The immunogold was then diluted with 2% BSA in PBS (as required to obtain the maximum sensitivity) to give a final volume of 50 μL. If sample or standard was to be tested this was introduced and allowed to react with the immunogold. The volume was adjusted for the introduction of sample by adding less 2% BSA in PBS solution so that the final volume remained at 50 μL. Alternatively, the assay format was changed so that the final volume was 100 μL. The colloidal gold-antibody (immunogold) was then left for a few minutes to react with the sample or standard solution. A test strip was then placed into the immunogold solution and the solution allowed to run up the strip by capillary action. Extra filter paper could be attached to the top of the strip so as to allow the running of larger volumes (see Fig. 6.2.3).

### 6.2.3 Results and Discussion

*6.2.3.1 The preparation and analysis of an estrone glucuronide-horseradish peroxidase conjugate*

The estrone glucuronide-horseradish peroxidase conjugate was prepared by the mixed anhydride method as described in section 6.2.2.3. In preparing the conjugate, a large excess of estrone glucuronide (40.4:1) was used as Rajkowski and Cittanova [111] had previously shown that large excesses of steroid glucuronides are required to achieve moderate acylation levels of horseradish peroxidase. Despite this, the level of acylation achieved by Rajkowski and Cittanova [111] was still very low. As a result it is an

expensive exercise to couple steroid glucuronides directly to horseradish peroxidase in this way and the results are generally poor with very low yields. The extensive glycosylation of the horseradish peroxidase surface may, in part, prevent or limit the surface of the protein available for acylation resulting in the low coupling levels of steroid glucuronides observed. If this is the case, use of deglycosylated horseradish peroxidase in acylation procedures may overcome the problem.

The estrone glucuronide-horseradish peroxidase conjugation reaction mixture was analysed by both Mono-S cation-exchange and Alkyl Superose hydrophobic exchange chromatography. The Mono-S 7 M urea chromatographic profile of (a) native, unconjugated horseradish peroxidase, and (b) the conjugation reaction mixture are shown in Figs. 6.2.4a and 6.2.4b respectively. In the native chromatographic profile (Fig. 6.2.4a) a large break through peak (peak I) was observed in the void volume which was brown in colour followed later in the gradient by a second peak (peak II). The initial peak

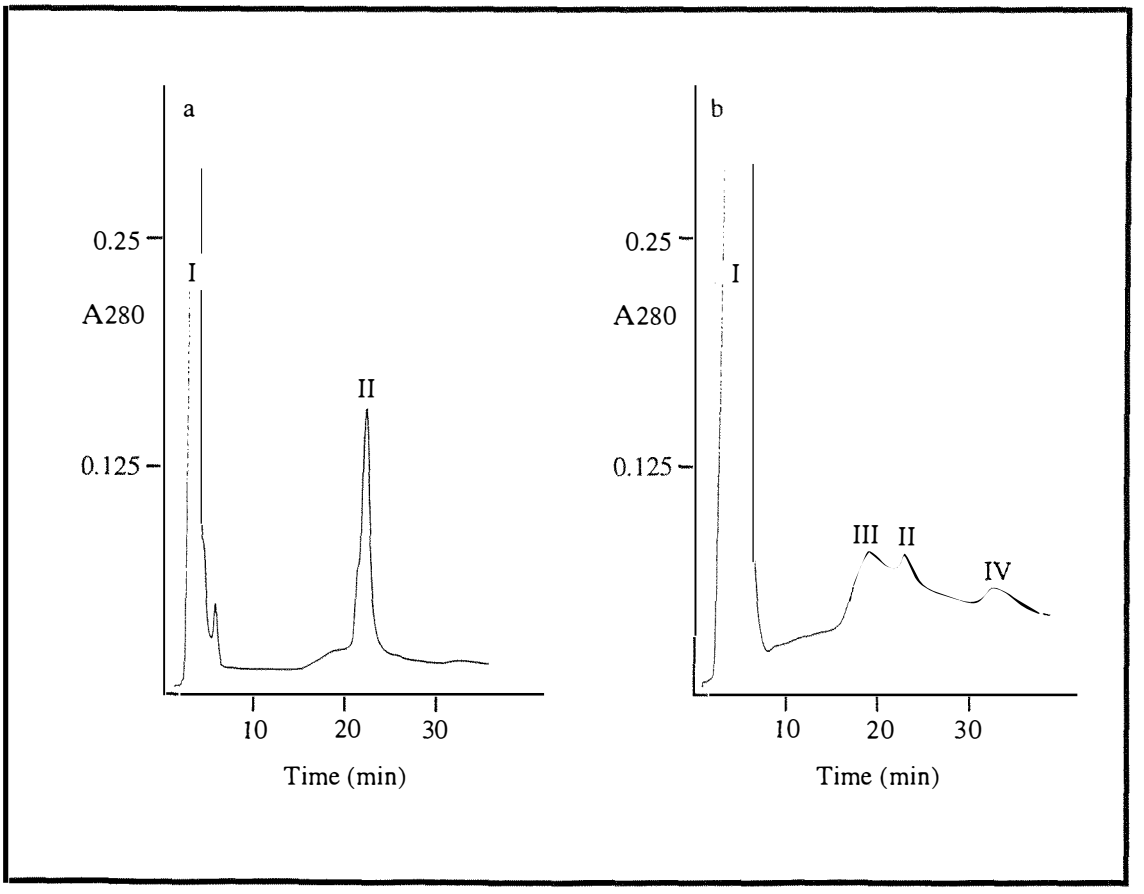


**Fig. 6.2.4** Native horseradish peroxidase (a) and an estrone glucuronide-horseradish peroxidase mixed anhydride conjugation reaction mixture (b) in 7 M urea on a Mono-S cation-exchange HR 5/5 column. Conditions: buffer A, 7 M urea + 50 mM $NaH_2PO_4$ buffer titrated to pH 6.0 with 1 M NaOH and buffer B, buffer A + 1 M NaCl titrated to pH 6.0 with 1 M NaOH; gradient, 0% B for 5 min, 0-30% B in 40 min at 0.5 mL/min; chart, 0.2 cm/min.

(peak I) was presumably due to (1) the hemin group, which upon denaturation of the horseradish peroxidase structure in 7 M urea solutions dissociates from the protein complex and does not bind to the cation-exchange column, or (2) glycosylated protein which does not bind to the Mono-S column. The second peak (peak II) eluted after 21 minutes (21.33% buffer B) and was presumably due to the horseradish peroxidase apo-protein. The analysis of the estrone glucuronide-horseradish peroxidase conjugate reaction mixture (Fig. 6.2.4b) also showed the initial break through peak (peak I) and the unconjugated, native HRP peak (peak II). In addition two further peaks were observed. The first (peak III) eluted before the native apo-protein peak (18 minutes, 17.3% buffer B) and is presumably due to estrone glucuronide conjugated horseradish peroxidase. The second extra peak (peak IV) eluted after the native apo-protein peak (31.5 minutes, 35.3% buffer B), the composition of which is unknown. The separation between the conjugate peak (peak III) and the native enzyme peak (peak II) was poor and

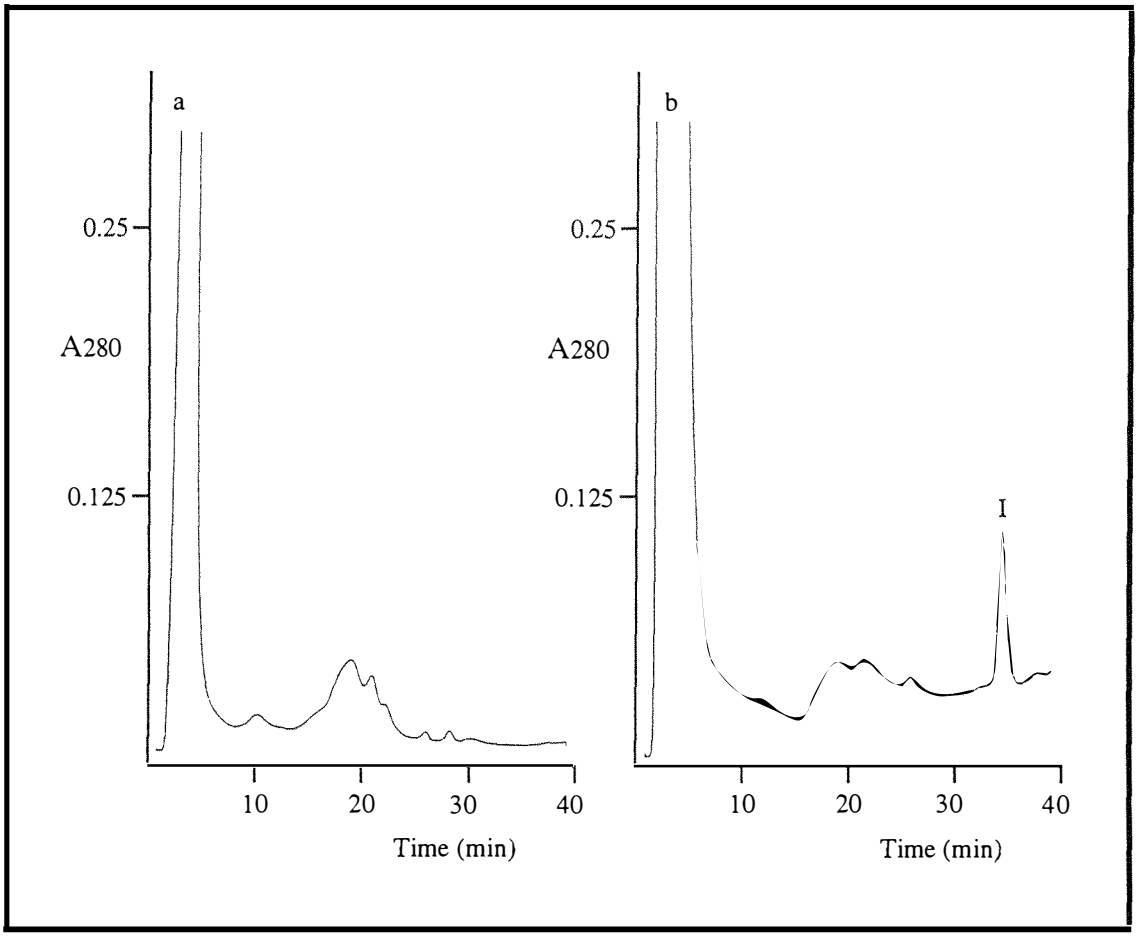


**Fig. 6.2.5** Native horseradish peroxidase (a) and an estrone glucuronide-horseradish peroxidase mixed anhydride conjugation reaction mixture (b) in 1.4 M ammonium sulfate on an Alkyl Superose hydrophobic interaction HR 5/5 column. Conditions: buffer A, 50 mM $NaH_2PO_4$ + 1.4 M $(NH_4)_2SO_4$ titrated to pH 6.6 with 1 M NaOH and buffer B, 50 mM $NaH_2PO_4$ titrated to pH 6.6 with 1 M NaOH; gradient, 0% B for 10 min, 0-100% B in 20 min, 100% B for 15 min; chart, 0.2 cm/min.

chromatography in this way therefore seems unsuitable as a purification method for the separation of unconjugated and conjugated HRP protein products. A further disadvantage of the Mono-S 7 M urea denaturing method is that it results in the removal of the hemin group. This would necessitate renaturing the apo-protein and then re-inserting the hemin group back into the enzyme to obtain an active enzyme which is clearly unsatisfactory.

Chromatographic analysis of native horseradish peroxidase by Alkyl Superose hydrophobic interaction chromatography resulted in the elution of a series of peaks as shown in Fig. 6.2.5a. The chromatogram consisted of a large initial break through peak of material which did not bind to the column followed by several broad peaks which eluted later in the gradient. These later peaks are presumably due to the heterogeneous nature of the horseradish peroxidase enzyme preparation whereby the individual enzyme molecules are glycosylated to various degrees. The chromatogram of the estrone glucuronide-horseradish peroxidase conjugation mixture by Alkyl Superose hydrophobic interaction chromatography (Fig. 6.2.5b) also showed the same pattern of an initial large peak followed by a series of later eluting peaks. In addition to these peaks, an extra peak (peak I) was also observed much later in the gradient (38 minutes, 93% buffer B) which is presumably due to estrone glucuronide conjugated horseradish peroxidase. Although neither of these chromatographic methods (Mono-S or Alkyl Superose) appear ideal for purification procedures they do confirm the presence of some horseradish peroxidase conjugated material.

*6.2.3.2 The purification of the estrone glucuronide polyclonal antibody from other serum proteins*

The estrone glucuronide polyclonal antibody was purified from other serum proteins using a commercially available purification kit. The concentration of protein in the serum sample was calculated from a bovine serum albumin standard curve as 85 mg/mL while the concentration of protein in the purified antibody sample was calculated as 41.5 mg/mL. The purification procedure therefore removed approximately 50% of the protein present in the original serum sample. Analysis of the unpurified serum (lanes 4 and 7, Fig. 6.2.6) and purified antibody (lanes 5 and 8, Fig. 6.2.6) by SDS-polyacrylamide gel electrophoresis (SDS-PAGE) showed that the procedure had removed most of this material consisting of low molecular weight proteins (Fig. 6.2.6). The polyclonal antibody could be easily identified at the top of the gel with a molecular weight ($M_r$) of approximately 150 000. Most of the protein removed by the purification procedure could be assigned to a protein band with a molecular weight of approximately 67 000 which had all but disappeared in the purified antibody sample (Fig. 6.2.6). The purified antibody was therefore almost free of other serum proteins after the purification process.

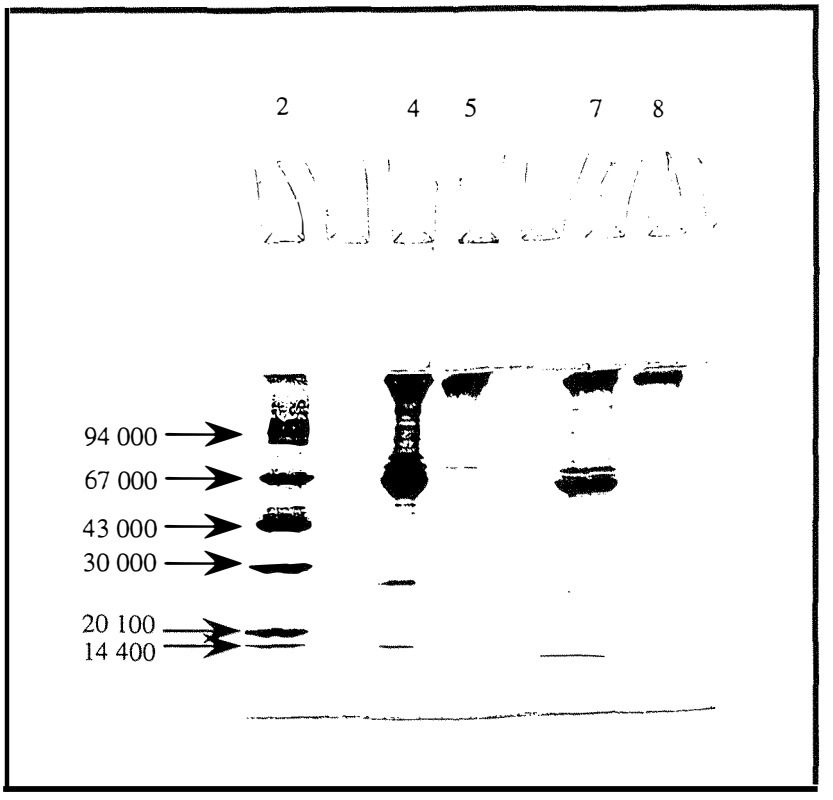


**Fig. 6.2.6** SDS-polyacrylamide gel electrophoresis (SDS-PAGE) analysis of unpurified anti-estrone glucuronide antiserum (lanes 4 and 7) and purified anti-estrone glucuronide antibody (lanes 5 and 8) as described in the text. The molecular markers are shown on the left hand side.

*6.2.3.3 Immunofiltration colour tests for the measurement of estrone glucuronide levels*

Immunofiltration strips were prepared with both purified and unpurified polyclonal anti-estrone glucuronide antibody. The assay format relies on the competition between the sample analyte and the estrone glucuronide-horseradish peroxidase conjugate for the immobilised anti-estrone glucuronide antibody binding sites. In the final step of the immunofiltration assay format, the amount of free antibody (that not bound by antigen in the sample or standard step) is indirectly measured by determining the amount of HRP-E1G conjugate bound and immobilised by the antibody. This was achieved by visual inspection of the intensity of the colour reaction of HRP with $H_2O_2$ and the substrate tetramethylbenzidine (TMB). Fig. 6.2.7 shows a developed nylon test strip with unpurified anti-estrone glucuronide antibody immobilised in two spots per reaction centre and using 100 μL of the appropriately diluted solution of HRP-E1G conjugate in the absence of sample or standard. From this test run in the absence of sample (or standard) the best colour development of the spot which did not also give high background development was found to be obtained using a HRP-E1G conjugate dilution of 1/10 000. All immunofiltration experiments were therefore run using this dilution of the conjugation reaction mixture. Less dilute samples gave high backgrounds and this interfered with the colour development at the immobilised antibody positions.

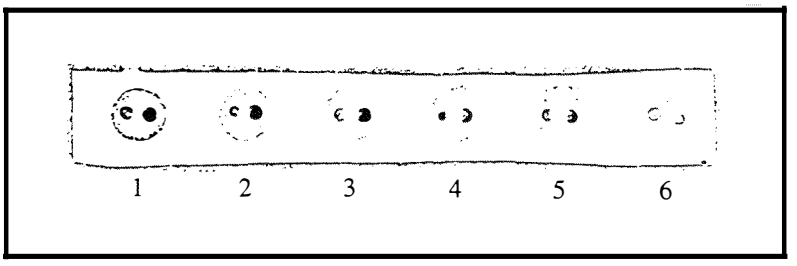


**Fig. 6.2.7** A nylon immunofiltration test strip run using various concentrations of estrone glucuronide-horseradish peroxidase conjugation reaction mixture. The dilutions used in each well (100 µL) from left to right are 1/10 000, 1/15 000, 1/20 000, 1/25 000, 1/30 000, and 1/35 000. Spots in each reaction centre on the left hand side contain immobilised polyclonal anti-estrone glucuronide antibody diluted by 1/160 while the right hand spots contain 1/80 diluted immobilised antibody.

Fig. 6.2.8 shows the change in the intensity of the colour with increasing concentrations of estrone glucuronide standards, where purified antibody diluted by 1/160 is immobilised at the left hand spot and purified antibody diluted by a factor of 1/80 is immobilised at the right hand spot of each reaction centre. As the concentration of estrone glucuronide increased, the colour intensity decreased, such that at the top standard concentration no colour could be detected. Both purified and unpurified antibody immobilised immunofiltration strips were run. The purified antibody gave less intense background colour development than the unpurified antibody and was thus the antibody preparation of choice.

Fig. 6.2.9 shows another set of standards run using the nylon membrane immunofiltration format and the colour intensity decrease associated with increasing estrone glucuronide concentrations. The reaction centres in wells 5 and 6 (Fig. 6.2.9) contain anti-horseradish peroxidase antibody immobilised on the right hand side and the left hand spot of wells 5 and 6 contain 1/80 diluted purified anti-E1G antibody. The left hand spots of wells 1-4 contain 1/80 diluted purified anti-E1G antibody while the right hand spots contain 1/160 diluted purified anti-E1G antibody. The intense colour development at the right hand spots of wells 5 and 6 (where anti-HRP antibody is bound)

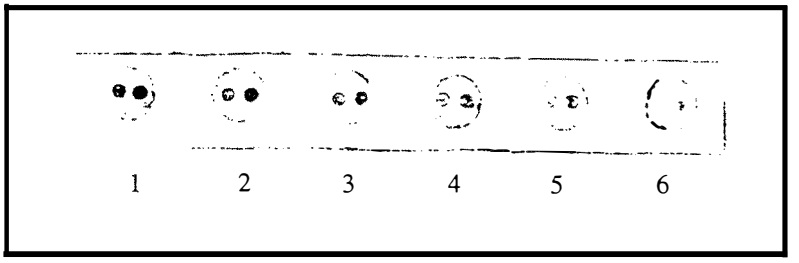


**Fig. 6.2.8** A nylon immunofiltration test strip run using 1/10 000 diluted estrone glucuronide-horseradish peroxidase conjugation reaction mixture (100 µL) and various E1G standards of known concentrations. The left hand spot of each well contains 1/160 diluted immobilised antibody and the right hand spot contains 1/80 diluted immobilised antibody. The strip was run using estrone glucuronide standards of the following concentrations in each well: well 1, 0 nmol/24 h; well 2, 144 nmol/24 h; well 3, 288 nmol/24 h; well 4, 432 nmol/24 h; well 5, 695 nmol/24 h; and well 6, 1 300 nmol/24 h.

confirms the presence of bound HRP. A blank was run in well 6 where no sample or standard was run and this showed that the colour development on the left hand spot (anti-estrone glucuronide antibody) was much less than that on the right hand side. This is to be expected for the unpurified conjugate reaction mixtures. Only estrone glucuronide conjugated horseradish peroxidase will bind to the immobilised anti-E1G antibody. However, both conjugated and unconjugated horseradish peroxidase will bind to the anti-horseradish peroxidase antibody. As a result there will be a higher concentration of enzyme bound at the right hand immobilised antibody spot than the left hand spot (assuming excess antibody is immobilised) and colour development should be more intense at the right hand antibody spot as found experimentally.

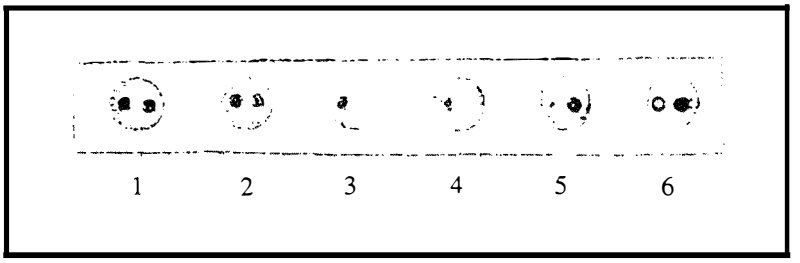


**Fig. 6.2.9** A nylon immunofiltration test strip run using 1/10 000 diluted estrone glucuronide-horseradish peroxidase conjugation reaction mixture (100 μL) and various E1G standards of known concentrations. The left hand spot of each well contains 1/80 diluted immobilised antibody and the right hand spot of wells 1-4 contain 1/160 diluted immobilised antibody. The right hand spots of wells 5-6 also contain immobilised anti-horseradish peroxidase antibody. The strip was run using estrone glucuronide standards of the following concentrations in each well: well 1, 144 nmol/24 h; well 2, 288 nmol/24 h; well 3, 432 nmol/24 h; well 4, 695 nmol/24 h; well 5, 1 300 nmol/24 h; and well 6, 0 nmol/24 h.

Although standard solutions of estrone glucuronide gave a good gradient of colour intensity (as shown in Figs. 6.2.8-6.2.9) it was not possible to get consistent colour development with either diluted, or undiluted, urine samples. While it was possible to distinguish between peak estrone glucuronide days and baseline estrone glucuronide days during a normal menstrual cycle, it was much more difficult to distinguish between baseline days and the days when the estrone glucuronide levels were beginning to rise. This period is the most important when determining the beginning of the fertile period. It is therefore necessary for any useful colour assay to be sensitive enough to be able to distinguish between baseline levels of estrone glucuronide and the first E1G rise day. While this colour assay format did not give the desired sensitivity it may be possible to further refine the assay system. The present assay format gave a positive colour result at low concentrations of steroid glucuronide and a negative colour result (no colour development) at high concentrations of steroid glucuronide. Ideally, as discussed previously, an assay format should produce a positive colour test at high concentrations of steroid glucuronide and a negative colour test at low concentrations of steroid glucuronide.

The estrone glucuronide-horseradish peroxidase conjugation reaction mixture was used in the immunofiltration assay format without further purification since it was not necessary to separate estrone glucuronide conjugated horseradish peroxidase from unconjugated, unreacted horseradish peroxidase. Only the estrone glucuronide conjugated horseradish peroxidase should bind to the immobilised anti-estrone glucuronide antibody, any unconjugated material being washed straight through the nylon membrane. Hence unreacted horseradish peroxidase should not affect the sensitivity of the assay as unreacted lysozyme in the Ovarian Monitor immunoassay would. However, high concentrations of unreacted HRP in the conjugation reaction mixture may effect the background colour development of the assay as all of the unreacted HRP may not be removed during the washing step and non-specific absorption may occur.

The immunofiltration immunoassay works on the principle that the enzymatic activity of horseradish peroxidase is not inhibited upon binding of the estrone glucuronide moiety to the immobilised anti-estrone glucuronide antibody. That no inhibition was occurring upon binding of the conjugated or unconjugated enzyme to the anti-HRP or anti-E1G antibody was clearly shown in Fig. 6.2.9 since if the enzymatic activity was inhibited upon binding, then no colour would be visible. This assay therefore demonstrates the difficulty in designing an enzyme immunoassay format using conjugated horseradish peroxidase whereby the enzymatic activity is extensively inhibited upon the binding of anti-hapten antibody.

*6.2.3.4 Colloidal gold based colour tests for the measurement of estrone glucuronide levels*

Colloidal gold particles produce a typical pinkish-red colour when they bind to, and accumulate at, the surface of a solid phase, thereby avoiding the need for secondary colour development. Fig. 6.2.10 shows typical colour development (seen as bands) resulting from the binding of anti-estrone glucuronide antibody-colloidal gold complexes to estrone glucuronide-horseradish peroxidase conjugate immobilised (in bands) on a nitrocellulose membrane in the absence of estrone glucuronide containing standards or samples. Fig. 6.2.10 clearly shows the increase in the intensity of the colour development observed as the concentration of antibody-colloidal gold used in running the assay increased. However, as the concentration of antibody-colloidal gold increased the background levels of colour also increased (Fig. 6.2.10). The lowest immobilised conjugate band develops with the greatest intensity in all cases (Fig. 6.2.10) as expected. The colloidal gold should bind to the first immobilised strip (lowest strip) until all of the binding sites are occupied. Once this has occurred any remaining colloidal gold flowing up the strip should pass over this binding site and bind to the next strip of immobilised conjugate.

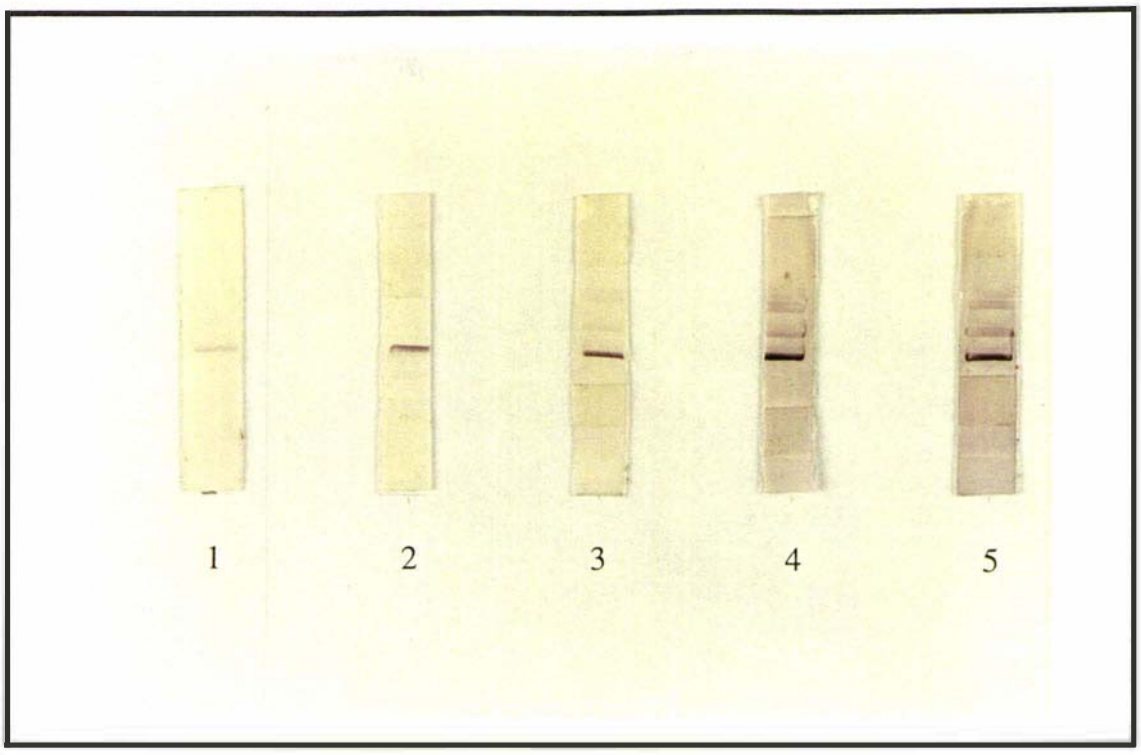


**Fig. 6.2.10** Nitrocellulose immunogold E1G-HRP test strips run and prepared with various concentrations of immunogold as described in the text. The required volume of immunogold was placed in the running tube and diluted to 50 µL with 2% BSA in PBS. The strips were run using immunogold prepared with 1/20 diluted antiserum. The strips had the following amounts of immunogold in the 50 µL running solution: strip 1, 5 µL; strip 2, 10 µL; strip 3, 20 µL; strip 4, 40 µL; and strip 5, 50 µL.

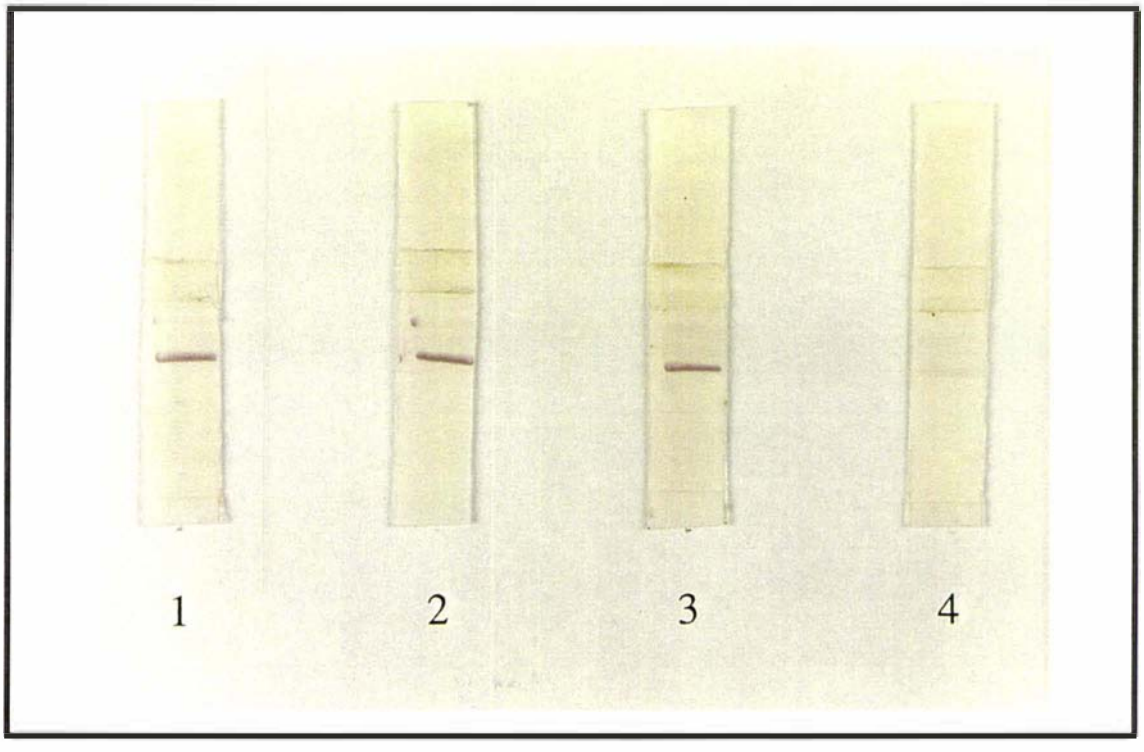


**Fig. 6.2.11** Nitrocellulose immunogold E1G-HRP test strips run using 5 µL of 1/20 diluted antibody prepared immunogold, 35 µL of 2% BSA in PBS, and 10 µL of increasing E1G standard concentrations. The test strips were run with the following E1G standard concentrations: strip 1, 0 nmol/24 h; strip 2, 0.0047 nmol/24 h; strip 3, 0.047 nmol/24 h; and strip 4, 46.8 nmol/24 h.

The estrone glucuronide-horseradish peroxidase conjugate anti-estrone glucuronide antibody colloidal gold system was found to be extremely sensitive to the presence of estrone glucuronide. Fig. 6.2.11 shows that when a standard consisting of a concentration of 46.8 nmol/24 h (13 nmol/L) of estrone glucuronide was used in the assay system, no colour development resulted. The colloidal gold immunoassay format works on the principle of competition between the sample analyte and the immobilised HRP-E1G conjugate for the antibody-colloidal gold complex. Initially, the sample (or standard) containing estrone glucuronide was allowed to mix and bind to the anti-estrone glucuronide antibody-colloidal gold complex. A test strip was then placed in this solution and the solution was allowed to run by capillary action up the strip. Free antibody-colloidal gold complex can bind to the immobilised estrone glucuronide-horseradish peroxidase conjugate and the accumulation of the binding colloidal gold complexes resulted in the formation of the typical pinkish-red colour. However, an antibody-colloidal gold complex which is bound to antigen from the sample, cannot bind the immobilised conjugate and passes over it. Hence the colour development is again inversely proportional to the concentration of E1G in the test or standard sample.

A series of HRP-E1G nitrocellulose strips were run against a set of estrone glucuronide standards of known concentrations and the results are shown in Fig. 6.2.12. The results clearly show that the pinkish-red colour formation decreased as the concentration of estrone glucuronide standard in the assay increased, as expected. Three urine samples were also run under the same conditions, an estrone glucuronide baseline day, a first E1G rise day, and a peak estrone glucuronide day as previously defined by the Ovarian Monitor immunoassay system. The results are shown in Fig. 6.2.13. The peak day urine sample gave no colour development as expected. The baseline day urine did result in colour development, however the colour intensity was much less than the blank shown in Fig. 6.2.12. The baseline level of estrone glucuronide was therefore high enough to neutralise a significant amount of the antibody-colloidal gold and lower the intensity of the colour development. Therefore, there may be a urine blank effect and as a result more antibody (or a greater concentration of immunogold) may be required for running of the urines than for a set of standard estrone glucuronide concentrations. The first rise day colour intensity was slightly less than the baseline day, although without prior knowledge of this fact it would be impossible to attach any significance to the change in colour intensity. However, with further development and refinement of the assay components and concentrations, it may be possible to obtain an assay which has the sensitivity to discriminate between baseline and early rise levels of estrone glucuronide.

In the colloidal gold immunoassay format the horseradish peroxidase enzyme acts only as

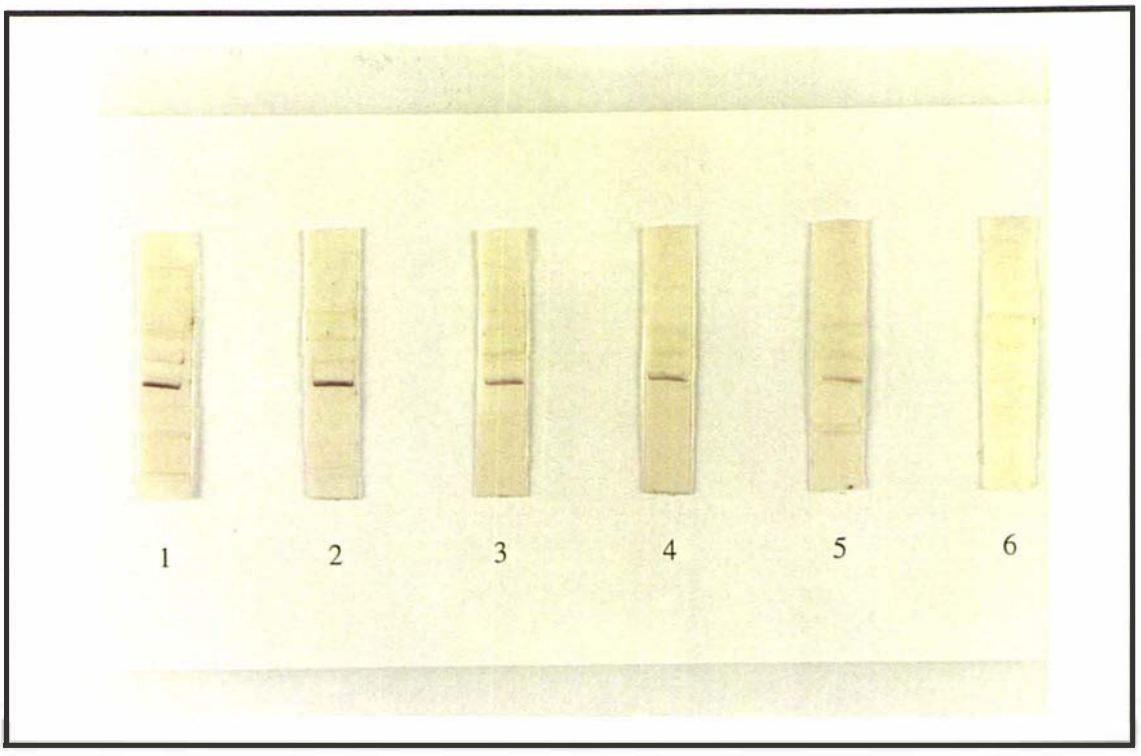


**Fig. 6.2.12** Nitrocellulose immunogold E1G-HRP test strips run using (1) 45 µL of 1/40 diluted antibody prepared immunogold which was further diluted by 1/4 with 2% BSA in PBS and (2) various concentrations of E1G. The test strips were run with the following standards (5 µL): strip 1, Milli-Q water; strip 2, 0 nmol/24 h; strip 3, 23 nmol/24 h; strip 4, 50 nmol/24 h; strip 5, 125 nmol/24 h; and strip 6, 250 nmol/24 h.

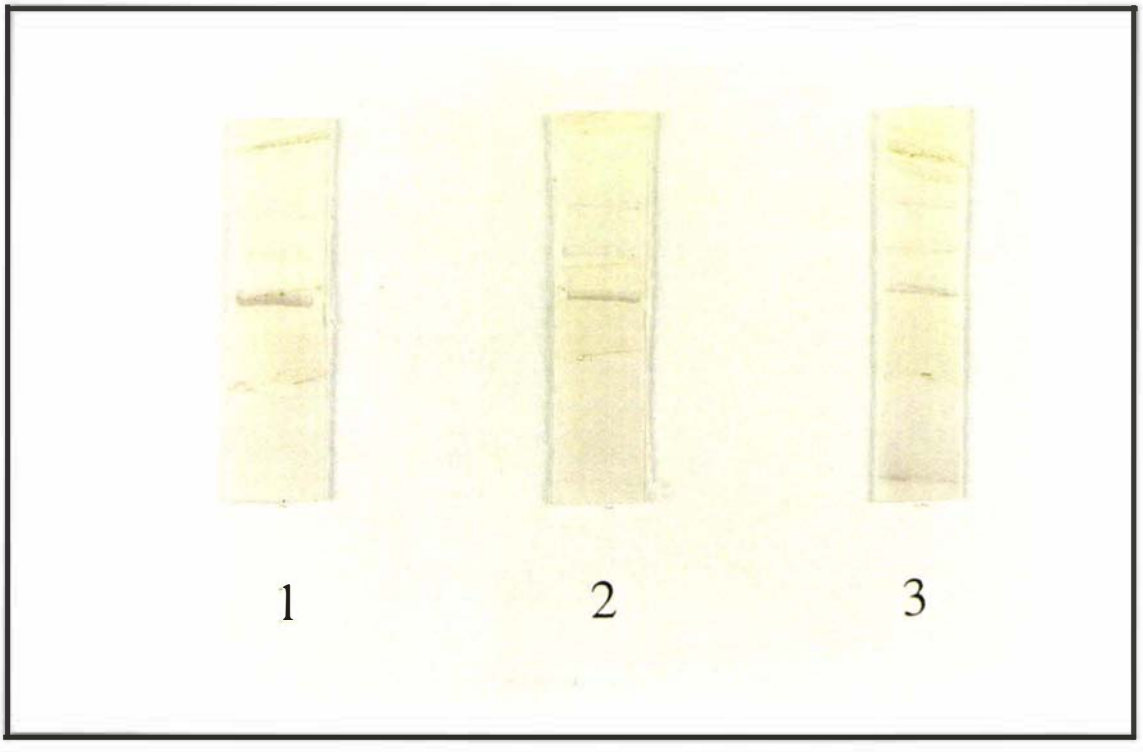


**Fig. 6.2.13** Nitrocellulose immunogold E1G-HRP test strips run using the conditions described in Fig. 6.2.12 and 5 µL of sample urine. The test strips were run using the following urine samples: strip 1, baseline E1G urine; strip 2, first day rise E1G urine; strip 3, peak day E1G urine sample.

a label for the analyte of interest, estrone glucuronide, and its enzymatic activity is not utilised. The HRP-E1G conjugate acts as a capture source to which free antibody-colloidal gold can be bound. These colloidal gold antibody markers have several advantages over the enzymatic markers used in immunodetection techniques. These include (a) the separation of bound and free enzyme label is not required, (b) long-lasting visual results are produced, (c) no costly equipment is required, (d) the total time to run an individual assay is reduced, and (e) all steps and incubations can be carried out in one step at room temperature.

The most likely problem to be encountered with the colloidal gold immunoassay format is obtaining reproducible strips and antibody-colloidal gold preparations. The most important reagent in the colloidal gold immunoassay format is the antibody-colloidal gold complex and obtaining reproducible batches of this, whereby the same amount of colloidal gold is attached to each antibody molecule, is likely to be difficult. The labelling of antibodies with colloidal gold particles is not well understood with the complex phenomenon depending on the stability of the colloid itself, the concentration, conformation and isoelectric point of the antibody, and the ionic strength, pH, and temperature of the suspending medium [283, 295]. The actual labelling process is thought to occur through the physical adsorption of the antibody onto the colloidal gold particles.

Finally, the chemical changes which take place during the labelling of antibodies and the resulting changes in specificity remain unknown. The colloidal gold immunoassay avoids the use of radioactive material and the shelf-life of the reagents is likely to be longer than those of conventional enzyme immunoassay reagents as the enzymatic activity of the enzyme label is not important. The antibody colloidal gold labelled complexes have an intense colour and hence no enzyme-substrate reaction is required to produce a colour. The use of colloidal gold labelled antibodies offers flexibility with regard to the method of assay and the method of detection. Besides the described competitive immunoassay, sandwich immunoassay formats are also possible. The advantage of sandwich type assays are that they can be designed so that a positive colour test is achieved with increasing levels of analyte. The possibilities for a sandwich type immunoassay format, based on the lysozyme system, is further described in section 6.4.

## 6.3 Development of a Lysozyme Colloidal Gold Based Colour Test for the Measurement of Estrone Glucuronide Levels

### 6.3.1 Introduction

A lysozyme-estrone glucuronide conjugate could, in principle, be used as a capture molecule by immobilising it onto a nitrocellulose membrane in much the same way as the estrone glucuronide-horseradish peroxidase conjugate was treated in section 6.2. The colloidal gold labelled antibody could then be run up the strip and allowed to bind to the immobilised lysozyme conjugate producing the typical reddish-pink colour associated with colloidal gold binding, immobilisation and accumulation. This possibility is examined in the following section.

### 6.3.2 Apparatus, Reagents, and Methods

Apparatus, reagents and methods were as described in sections 6.2.2.2 and 6.2.2.7 unless described otherwise. Purified mixed anhydride E3 estrone glucuronide-lysozyme conjugate was immobilised on nitrocellulose strips as described for HRP-E1G conjugates in section 6.2. The mixed anhydride E3 estrone glucuronide-lysozyme conjugate was synthesised and purified as described in chapter 3.

### 6.3.3 Results and Discussion

When nitrocellulose test strips with immobilised E1G-lysozyme conjugate were placed in an anti-estrone glucuronide antibody-colloidal gold solution (prepared with unpurified antiserum) and allowed to run by capillary action (as described in section 6.2) very little colour development was observed. Fig. 6.3.1 shows the increasing colour development observed in the bands when using increasingly concentrated amounts of antibody-colloidal gold and that the background colour and intensity also increased. However, it was also clear that a significant amount (or most) of the antibody-colloidal gold was not actually physically binding to the immobilised E3 estrone glucuronide-lysozyme conjugate. When a large excess of estrone glucuronide was added to the assay, the level of colour development in the bands did not diminish significantly as shown in Fig. 6.3.2. Hence, there was no competition between the free steroid glucuronide and the immobilised conjugate for the anti-E1G-antibody-colloidal gold reagent. This suggests that the apparent antibody-colloidal gold binding observed in Fig. 6.3.1 at the immobilised conjugate strip position was due to non-specific binding of colloidal gold labelled protein to the lysozyme conjugate.

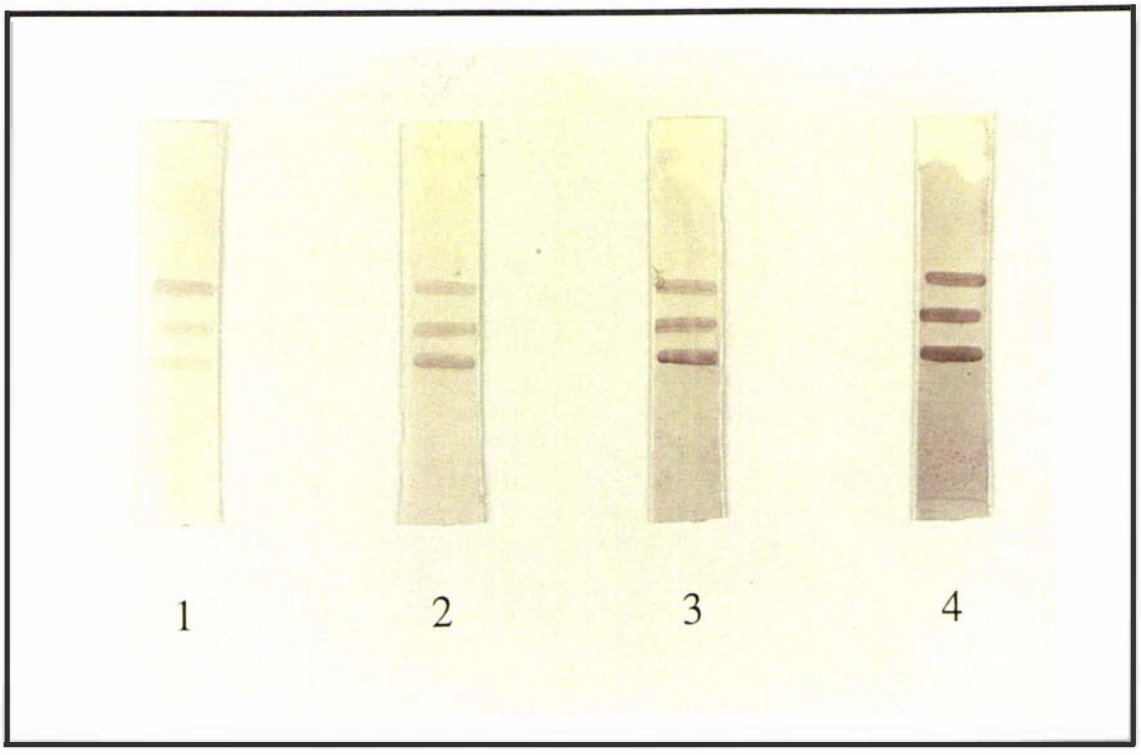


**Fig. 6.3.1** Nitrocellulose immunogold E1G-lysozyme test strips run and prepared as described in the text. The required volume of immunogold was placed in the running tube and diluted to 50 µL with 2% BSA in PBS. The strips were run using immunogold prepared with 1/5 diluted antiserum. The strips had the following amounts of immunogold in the 50 µL running solution: strip 1, 2.5 µL; strip 2, 5 µL; strip 3, 10 µL; and strip 4, 20 µL.

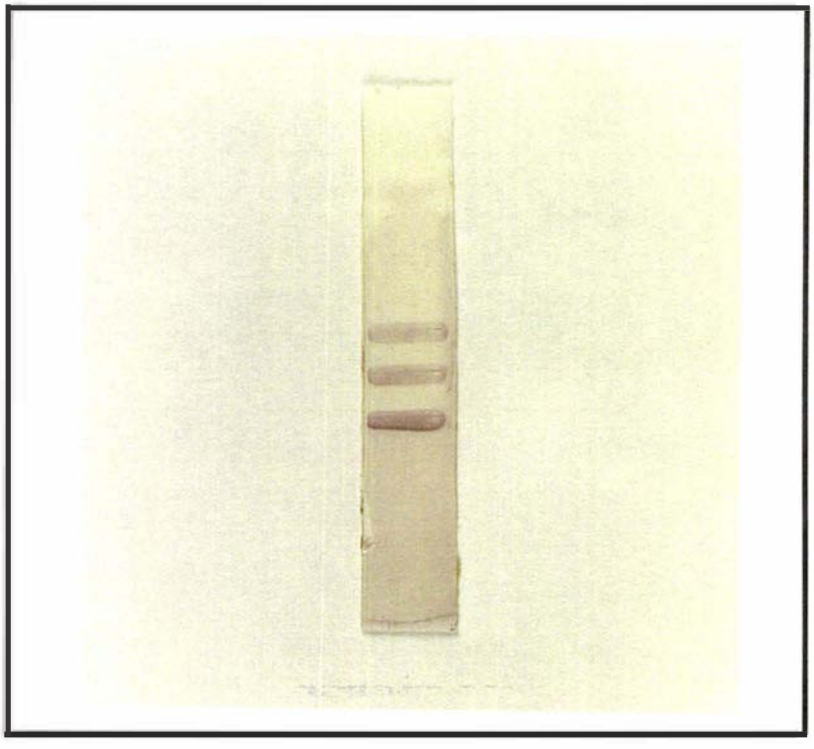

**Fig. 6.3.2** Nitrocellulose immunogold E1G-lysozyme test strip run using 5 µL of 1/5 diluted antibody prepared immunogold, 35 µL of 2% BSA in PBS, and 10 µL of an estrone glucuronide solution whose concentration was 500 000 nmol/24 h.

In agreement with this suggestion, when purified anti-E1G antibody was complexed with colloidal gold and used in the immunoassay, no colour development was observed at the immobilised conjugate positions (Fig. 6.3.3). In fact white bands were observed where the lysozyme-E1G conjugate was immobilised on the nitrocellulose strip and the background became very dark as a result of saturation of the membrane with liquid containing colloidal gold labelled antibody (highlighting further the clear bands with no antibody-colloidal gold). In preparing antibody-colloidal gold with unpurified antiserum, all of the other serum proteins present, as well as the anti-estrone glucuronide antibody, become labelled with colloidal gold. Some of the other serum proteins will presumably carry an overall negative charge at the buffer pH and therefore be attracted to the positively charged lysozyme molecule in much the same way as the negatively charged lysozyme substrate *Micrococcus lysodeikticus* is attracted to the positively charged enzyme. As a result these proteins bind to the lysozyme surface by electrostatic interactions and their accumulation results in the development of a colour as observed in Fig. 6.3.1. However, when these serum proteins were removed no colour development was observed (Fig. 6.3.3), confirming that colloidal gold labelled anti-estrone glucuronide antibody was not binding to the immobilised lysozyme conjugate.

There are two possible reasons why the purified anti-estrone glucuronide antibody-colloidal gold complex did not bind to the immobilised lysozyme conjugate. The first is that upon immobilisation of the E1G-lysozyme conjugate onto the nitrocellulose membrane the hydrophobic estrone glucuronide moiety projects downwards, into the membrane and is inaccessible to the antibody. As a result the antibody-colloidal gold complex cannot bind, and simply passes over it by capillary action. However, in the E1G-HRP nitrocellulose tests described in section 6.2, the antibody-colloidal gold complex does bind to the immobilised estrone glucuronide-horseradish peroxidase conjugate. If the hydrophobic estrone glucuronide moiety was influencing the position in which the conjugate was immobilised then this problem should also be observed in the E1G-HRP system. The fact that this problem was not observed suggests that incorrect orientation of the estrone glucuronide moiety is not the primary reason for the lack of binding observed in the lysozyme system. Furthermore, the fact that non-specific binding to the immobilised E1G-HRP molecule was not observed is consistent with the suggestion that the non-specific binding in the lysozyme system is a result of some non-specific interaction involving the lysozyme moiety and not the estrone glucuronide moiety.

Absolutely no colour was observed at the immobilised estrone glucuronide-lysozyme conjugate sites using purified antibody-colloidal gold while the background became a

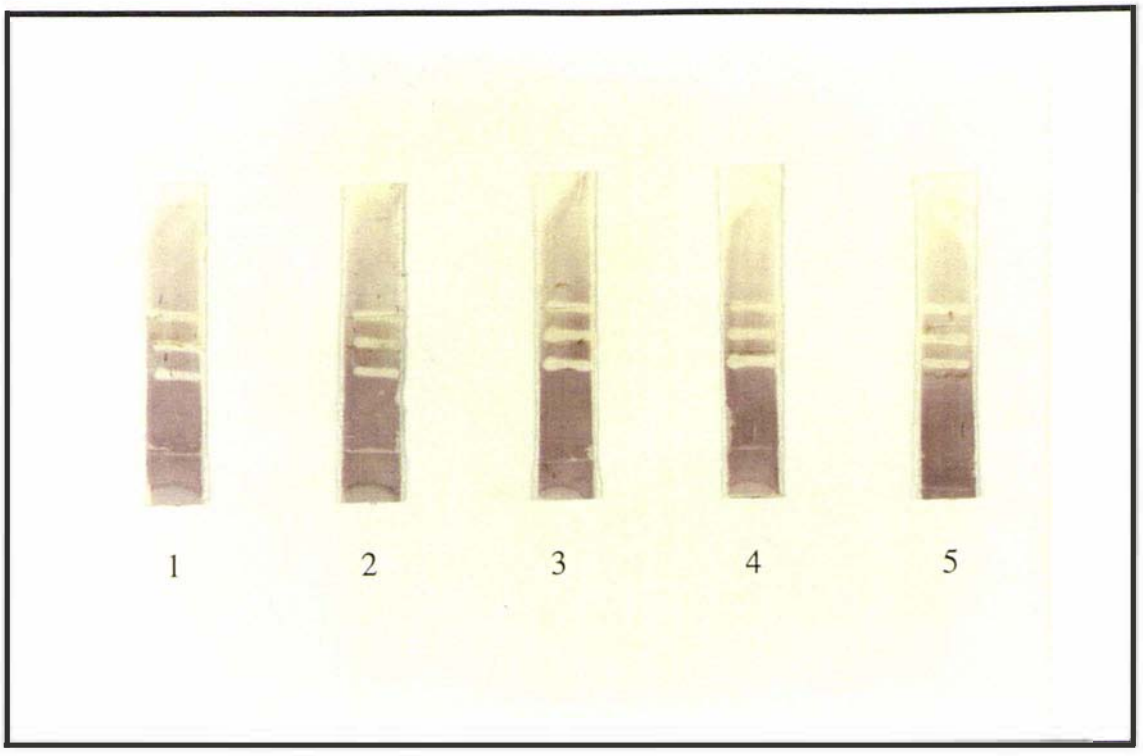


**Fig. 6.3.3** Nitrocellulose immunogold E1G-lysozyme test strips run and prepared with purified anti-E1G antibody as described in the text. The required volume of immunogold was placed in the running tube and diluted to 50 µL with 2% BSA in PBS. The strips were run using immunogold prepared with 1/5 diluted antiserum. The strips had the following amounts of immunogold in the 50 µL running solution: strip 1, 50 µL; strip 2, 25 µL; strip 3, 7.5 µL; strip 4, 3 µL; and strip 5, 1.5 µL.

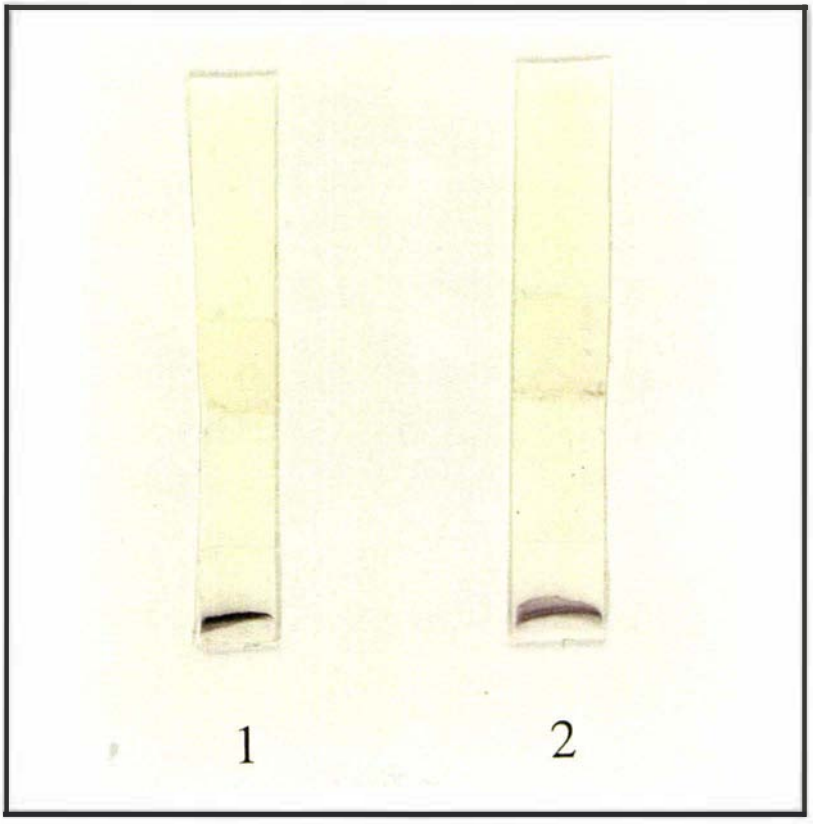


**Fig. 6.3.4** Nitrocellulose immunogold E1G-lysozyme test strip run using 10 µL of immunogold (prepared with purified anti-E1G antibody) and 40 µL of a 20 mg/mL lysozyme solution (strip 1) and 40 µL of a 10 mg/mL lysozyme solution (strip 2).

very dark reddish-pink colour as a result of membrane saturation with the colloidal gold labelled antibody (Fig. 6.3.3). If incorrect orientation of the estrone glucuronide moiety upon immobilisation of the E1G-lysozyme conjugate was the primary reason for the non-binding of the immunogold reagent, then the background and conjugate strip positions should show the same colour intensity. However, Fig. 6.3.3 shows this is clearly not the case. The antibody immunogold reagent is clearly being repelled by the lysozyme conjugate and as a result the anti-estrone glucuronide antibody strip appears to be white.

The reason for this repulsion of the antibody-colloidal gold reagent by the immobilised estrone glucuronide-lysozyme most probably arises from either (1) the conditions used to prepare the antibody immunogold, or (2) the conditions under which the nitrocellulose test strips are run (or a combination of both). In preparing the antibody immunogold complex (see section 6.2.2.7) bovine serum albumin (BSA) is used to complex any unbound colloidal gold reagent which has not been complexed by the antibody of interest. This is necessary as any remaining colloidal gold would bind non-specifically to any protein immobilised on a nitrocellulose test strip when running it. As a result the observed colour intensity would not be proportional to the concentration of analyte in the sample under investigation. Also, at the buffer pH at which the colloidal gold immunoassays are run, the BSA protein will be partially or locally negatively charged on the protein surface. Hence the negatively charged BSA and the positively charged immobilised lysozyme conjugate will be attracted to each other. If the colloidal gold labelled BSA binds to the lysozyme surface due to this electrostatic attraction, this could prevent the anti-estrone glucuronide antibody binding to the immobilised E1G-lysozyme conjugate. However, if this was the case, some non-competitive colour development should be observed due to the non-specific binding of the colloidal gold-labelled BSA to the lysozyme moiety. This was clearly not the case.

A second more likely reason for this apparent repulsion effect may arise from the conditions under which the nitrocellulose test strips are run. The antibody-colloidal gold preparations and analyte samples are diluted with a solution of 2% bovine serum albumin in phosphate buffer saline (PBS). As the liquid runs up the test strip, the solvent front runs well ahead of the colloidal gold labelled antibody. Therefore, the BSA in the solvent is likely to reach the immobilised lysozyme conjugate band before the colloidal gold labelled antibody. If this is the case the positively charged BSA molecule will complex with the negatively charged lysozyme molecule to form a highly stable complex [57]. As a result the BSA may occupy all of the immobilised lysozyme conjugate binding sites. The positively charged BSA moiety would therefore screen the immobilised E1G-lysozyme capture band which would mean that the anti-estrone glucuronide antibody would simply pass over the capture position. The antibody-colloidal gold complex is

presumably also negatively charged at the buffer pH, hence the immobilised BSA molecules and the antibody-colloidal gold complex will repel each other thus accounting for the white bands which form. This repulsion theory may be tested by immobilising the lysozyme conjugate right across the nitrocellulose strip. If the BSA is binding to the estrone glucuronide-lysozyme conjugate and preventing the approach of the immunogold antibody complex, then the purple colour should not be able to cross the immobilisation strip and a very intense background colour should develop below it as the antibody-colloidal gold accumulates.

An attempt was also made to run the lysozyme conjugate immobilised nitrocellulose test strips in antibody-colloidal gold preparations and analyte samples which were diluted down with a solution of 2-10% lysozyme in PBS (instead of BSA) to circumvent the BSA repulsion problem. However, in this case the colloidal gold complex would not run up the strip at all and accumulated at the base of the strip (Fig. 6.3.4). It is difficult to explain why the antibody-colloidal gold would not run up the test strips in the presence of 2% lysozyme solutions. Presumably the reason is related to the highly positively charged nature of the lysozyme molecule, the charge on the antibody-colloidal gold complex and the charge on the nitrocellulose membrane itself.

It is obvious that for the nitrocellulose test strips immobilised with E1G-lysozyme conjugate to be used in an antibody-colloidal gold colour test format, BSA must be replaced as the blocking and running agent of choice. An alternative reagent must be found, ideally one which is neutrally charged and which cannot complicate the immunoassay through electrostatic interactions. Antibody-colloidal gold complexes have been stabilised with, and nitrocellulose membranes blocked and run with, various proteins and reagents including polyethylene glycol [283], animal serum, haemoglobin, ovalbumin, casein, gelatin, polyvinylpyrrolidone, Tween and ethanolamine [282]. Although problems have previously been observed when using Tween 20 with nitrocellulose membranes [289] agents such as polyvinylpyrrolidone, ethanolamine, and casein may be suitable for use with the lysozyme system. Protein reagents are likely to be less useful because of their charged nature at all pH values. Even at the isoelectric point of a protein local areas of charge are likely to exist on the protein surface. Through the use of one or more reagents, it should be possible to design an antibody-colloidal gold immunoassay system which will bind to immobilised estrone glucuronide-lysozyme conjugate, and as a result of accumulation, develop the characteristic pinkish-red colour of captured colloidal gold labelled antibody. It may also prove possible to improve the assay sensitivity by changing from a nitrocellulose solid phase to a nylon based solid phase for immobilisation of the lysozyme conjugate.

## 6.4 The Design of a Possible Solid Phase Sandwich Immunoassay for the Measurement of Estrone Glucuronide Levels using a Lysozyme-Estrone Glucuronide Conjugate

The detailed characterisation of the mixed anhydride estrone glucuronide-lysozyme conjugate, coupled with the current knowledge of the antigenic determinants of hen egg white lysozyme has made it possible to design, on a rational basis, a novel sandwich, solid phase colour immunoassay format for the measurement of estrone glucuronide levels. A considerable knowledge base now exists relating to the structures of the various lysozyme-anti-lysozyme antibody complexes based on published X-ray crystallographic studies [229] and epitope mapping studies [227-229]. This wealth of information was therefore used to help in the design of a possible new immunoassay system utilising hen egg white lysozyme conjugates as immune reagents and monoclonal antibodies to defined epitopic regions of the lysozyme molecule.

Investigations into the antigenic regions of hen egg white lysozyme have defined the structural epitopes of the anti-hen egg white lysozyme monoclonal antibodies. These studies have shown that the antigenic regions of hen egg white lysozyme correspond to structural domains of the enzyme and that the whole surface of the enzyme forms a continuous antigenic surface [228]. A large number of monoclonal antibodies raised against hen egg white lysozyme have now had their epitopes mapped and the results show unique patterns of specificity and unique epitopes exist on the surface of the enzyme [228-229]. As these monoclonal antibodies bind at different sites (or epitopes) on the protein surface, it is possible to bind several antibodies at once to different structural domains of hen egg white lysozyme [228-229]. It is also possible to obtain anti-hen egg white lysozyme monoclonal antibodies which bind to similar epitopes which are in close proximity to each other within the three dimensional tertiary structure of the enzyme and hence cannot bind simultaneously. These antibodies with very closely related epitopes therefore compete for binding sites on the hen egg white lysozyme protein surface. Careful selection of the different monoclonal antibodies gives rise to pairs which co-bind (both antibodies can bind to the protein surface at the same time) or compete with each other for the different epitopes on the enzyme surface and these pairs can be utilised in sandwich immunoassays for hen egg white lysozyme.

The major conjugate product of the mixed anhydride coupling procedure when linking estrone glucuronide to lysozyme is the monoacylated lysozyme conjugate (see chapter 3) which is exclusively acylated at lysine residue 33 in each conjugate molecule. Since the E3 conjugate can be obtained as a homogeneous preparation, the anti-estrone glucuronide

antibody can bind the lysozyme conjugate only in this region of the lysozyme surface. The approximate area where the anti-estrone glucuronide antibody will bind in relation to the protein surface has been modelled by computer graphic simulations as described in chapter four. The surface area of lysozyme which is covered by the bound anti-estrone glucuronide antibody can now be matched to one of the known anti-hen egg white lysozyme monoclonal antibody epitopes [228-229]. The hen egg white monoclonal antibody which binds to this area of the enzyme and the anti-estrone glucuronide antibody should therefore compete with each other for the same general surface area of conjugate E3. This competition between the anti-E1G antibody and a monoclonal anti-hen egg white lysozyme antibody can be used in principle to form the basis of an alternative colour test immunoassay format for the measurement of estrone glucuronide.

The principle reactions behind the proposed solid phase colour immunoassay format for the measurement of estrone glucuronide levels using (1) the mixed anhydride E3 estrone glucuronide-lysozyme conjugate, (2) the anti-estrone glucuronide antibody, and (3) two anti-hen egg white lysozyme monoclonal antibodies are depicted in Fig. 6.4.1. The assay format relies on the competition between the anti-estrone glucuronide antibody and one anti-hen egg white lysozyme antibody (labelled antibody 2 (HEWL-AB2) in Fig. 6.4.1) for the estrone glucuronide-lysozyme conjugate E3 and the non-competitive binding of a second monoclonal anti-hen egg white lysozyme antibody (labelled HEWL-AB1 in Fig. 6.4.1) to the lysozyme conjugate for a different non-overlapping epitope. The assay format presented in Fig. 6.4.1 is therefore proposed to work as follows:

(1) Anti-estrone glucuronide antibody (E1G-AB in Fig. 6.4.1) and an anti-hen egg white lysozyme antibody (HEWL-AB2) which compete for the same region of the estrone glucuronide conjugate are both immobilised on a solid phase membrane. The reagents are immobilised so that the E1G-lysozyme conjugate is below the HEWL-AB2 reagent. Therefore the sample analyte and other reagents come into contact with the lysozyme conjugate as they flow up the test strip before they contact the HEWL-AB2 reagent as shown in Fig. 6.4.1.

(2) A second monoclonal antibody to hen egg white lysozyme (HEWL-AB1), which binds on the opposite side of the lysozyme conjugate relative to the binding region of the competing anti-estrone glucuronide and anti-hen egg white lysozyme second antibody is selected. This second antibody (HEWL-AB1) is selected so that the lysozyme conjugate can co-bind both HEWL-AB1 and either the E1G-AB or the HEWL-AB2 molecule, thus forming a sandwich. The lysozyme conjugate cannot co-bind the E1G-AB and HEWL-AB2 molecules.

(3) The co-binding anti-hen egg white monoclonal antibody (HEWL-AB1) is labelled with either colloidal gold particles (as described in section 6.2.2.7) or latex coloured beads as described by Bangs [277]. The labelled antibody is then allowed to mix with, and bind to, the estrone glucuronide-lysozyme conjugate E3 to form a conjugate-monoclonal antibody reagent (as shown in Fig. 6.4.1) which is coloured due to the colloidal gold or latex beads attached to the antibody.

(4) In the final step of the assay, the coloured E1G-HEWL-HEWL-AB1 reagent is allowed to mix with the sample of interest containing estrone glucuronide. A test strip with the immobilised anti-estrone glucuronide and anti-hen egg white lysozyme antibody HEWL-AB2 is then placed into the running solvent and buffer solution containing the E1G-HEWL-HEWL-AB1 reagent and sample of interest. The test strip is then allowed to run by capillary action.

If the sample under investigation contains low concentrations of analyte then most of the immobilised anti-estrone glucuronide antibody will be free upon the running of the assay. As a result the estrone glucuronide-lysozyme conjugate can bind to the immobilised anti-E1G antibody and hence a sandwich is formed (i.e. the E3 conjugate is sandwiched between the anti-E1G antibody and the coloured HEWL-AB1). Hence a positive colour test would arise at the immobilised anti-E1G antibody position due to the accumulation of the colloidal gold, or latex bead particles attached to HEWL-AB1. A positive colour test at the anti-E1G antibody position would therefore indicate the absence of analyte in the test sample. However, if the test sample contains high concentrations of estrone glucuronide, most, or all, of the immobilised anti-E1G antibody will be bound by the analyte upon the running of the assay and thus neutralised. The E1G-HEWL-HEWL-AB1 reagent should therefore pass over the immobilised anti-E1G antibody and bind further up the strip at the immobilised HEWL-AB2 position. Thus, a high concentration of estrone glucuronide will give rise to a positive colour test at the HEWL-AB2 immobilised antibody due to the accumulation of the colloidal gold, or latex bead, labelled HEWL-AB1 in the sandwich. Under the correct conditions and concentration of reagents, the increase in the intensity of the colour of this band should be directly proportional to the increase in estrone glucuronide levels. Concentrations of estrone glucuronide in between these low and high values would give a gradient of colour intensities observed between the two immobilisation positions. The advantage of this immunoassay format is that a positive colour test is obtained at the immobilised anti-hen egg white lysozyme antibody (HEWL-AB2) position with increasing estrone glucuronide concentrations.

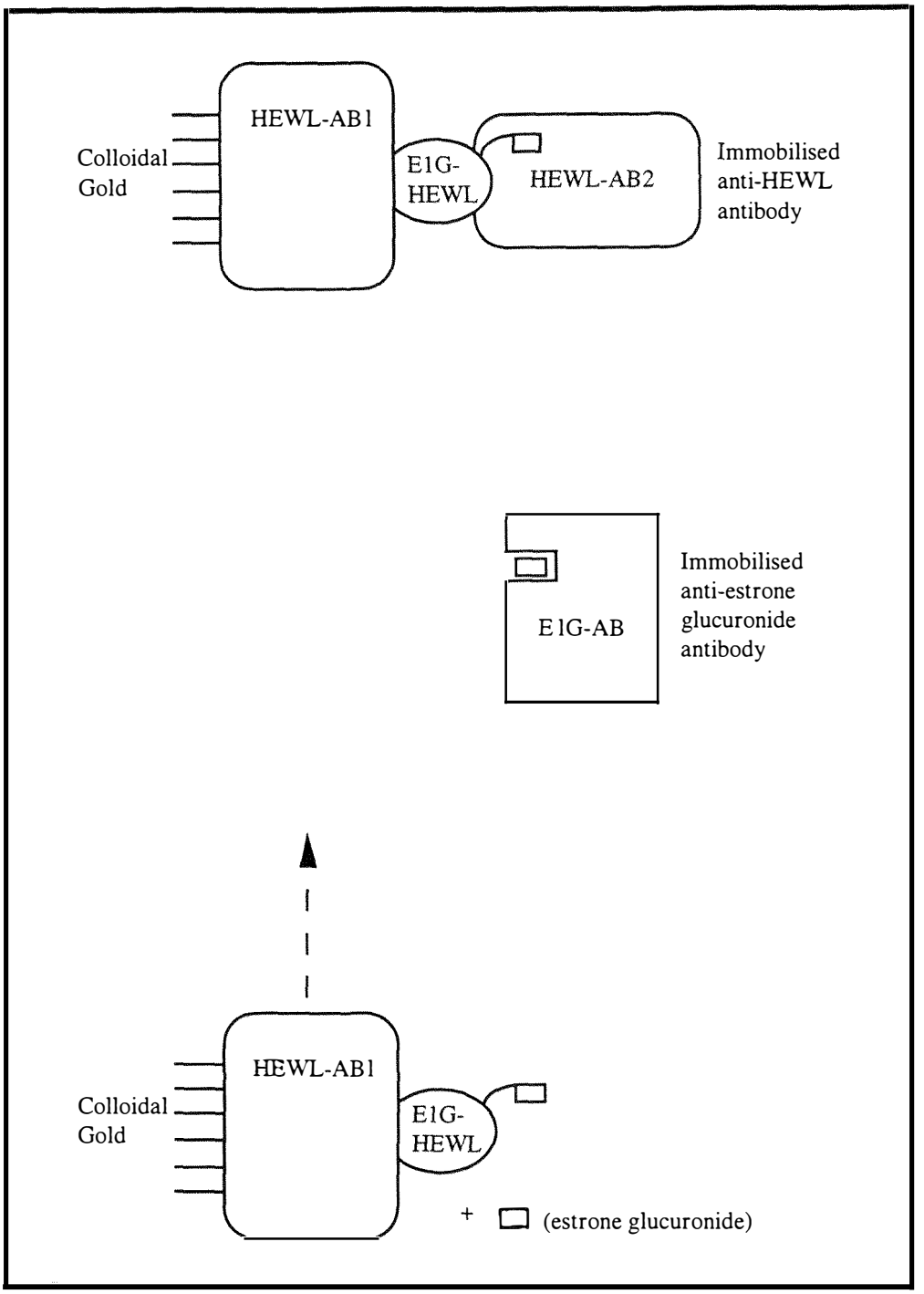


**Fig. 6.4.1** The principles behind the proposed estrone glucuronide-hen egg white lysozyme conjugate sandwich immunoassay colour test as described in the text. In the presence of estrone glucuronide the immobilised anti-estrone glucuronide antibody is neutralised and the colour labelled HEWL-AB1-E1G-lysozyme complex binds to the HEWL-AB2 immobilised antibody giving a positive colour test at this position. In the absence of estrone glucuronide the colour labelled HEWL-AB1-E1G-lysozyme complex binds to the immobilised anti-E1G antibody resulting in the formation of a coloured band at this position. For concentrations in between there will be a gradient of colour between the two immobilisation sites.

If the difference in colour intensity between the menstrual cycle baseline and first rise days could not be visually detected, it may still prove necessary to develop a monitor to detect the changes in colour development. The advantage of having two positions at

which colour may develop in this way, is that a meter would be able to use the ratio of colour intensity between the two positions to calculate the concentration of estrone glucuronide in the sample of interest.

The proposed test format relies on obtaining a steroid glucuronide-lysozyme conjugate which is exclusively acylated at one position on the lysozyme surface. The assay format could therefore be extended to the measurement of pregnanediol glucuronide levels as the characterisation of the mixed anhydride pregnanediol glucuronide-lysozyme conjugates has shown that two of the resulting conjugates are exclusively monoacylated at positions 97 (mixed anhydride P1 conjugate) and 33 (mixed anhydride P3 conjugate) respectively (see chapter three). If the assay format could be extended to PdG levels as well as E1G levels, then both the beginning and end of a woman's fertile period during any given menstrual cycle could be accurately identified and defined by a simple colour test, possibly on the same strip.

This assay format has yet to be tested. The first stage in developing such a test will be to design a membrane system whereby the lysozyme conjugate can be run up the solid phase membrane as discussed in section 6.3. The second stage will be to obtain the required anti-lysozyme monoclonal antibodies required for such a test. Dr. S. J. Smith-Gill (Laboratory of Genetics, National Cancer Institute, National Institutes of Health, Bethesda, MD, U.S.A.) has indicated her willingness to donate the required monoclonal antibodies for initial experiments to begin. Unfortunately these antibodies have not yet been sent to New Zealand and as a result the development and testing of this immunoassay format has been delayed. Once the principles behind the proposed immunoassay format have been shown to be sound, the assay format will have to be refined and developed so that the maximum sensitivity and precision can be obtained. If the sensitivity and precision required for the measurement of estrone glucuronide can be achieved, the proposed format will offer a real alternative colour dipstick type test for the measurement of urinary estrone glucuronide and pregnanediol glucuronide levels. Such a test could have large commercial implications and be of real benefit to women in the home wishing to monitor their own fertility. If this objective can be achieved it will represent a practical end result arising from the detailed fundamental studies of lysozyme and lysozyme conjugate structures.

## 6.5 Conclusions

The work presented in chapter six shows that horseradish peroxidase-steroid glucuronide conjugates may be used either as capture molecules in colloidal gold labelled antibody type assays, or as an enzyme conjugate capable of producing colour in immunofiltration assays. Both these formats may be useful in colour test immunoassays for the measurement of steroid glucuronide levels. However, further work is required before the precision, reliability and sensitivity of such assays could be suitable for home immunoassay solid phase tests for the measurement of urinary steroid glucuronide levels. A much more promising immunoassay format is the proposed sandwich format based on the monoacylated lysozyme conjugates. This format appears the most promising yet to provide a colour test immunoassay which can provide the accuracy, sensitivity and reliability required for the measurement of urinary steroid glucuronide levels for the delineation of the fertile period during a woman's menstrual cycle.

# Chapter Seven

# Crystallographic Studies

## 7.1 Introduction

The structures of the hapten conjugates determined in this work have led to insights into the parameters which are essential in producing inhibition by anti-hapten antibodies. Although the computer generated three dimensional structures presented in chapter 4 are believed to be reasonable approximations of the actual structures, a number of approximations have had to be made. Hence, it is desirable to obtain a true three dimensional structure of at least one of the conjugates to confirm the validity of the approaches taken in this thesis.

The most powerful technique that yields a detailed and precise description of the actual molecular structure, and the subtleties of the inter- and intra-molecular interactions within a small inorganic or organic moiety, or in a macromolecule such as a protein or hapten-antibody immune complex, is X-ray crystallography [296]. Although this technique determines three dimensional structures of molecules in the solid state, there is now evidence to suggest that the solid state structures are very close to the true three dimensional structures found in solution [297]. The agreement of X-ray crystallographic structures with structures obtained by nuclear magnetic resonance (NMR) spectroscopy techniques (where the molecule of interest is studied in solution) is particularly strong evidence. X-ray crystallographic techniques utilise the diffraction of X-ray beams by electrons in a molecule to solve its three dimensional structure. However, this is no easy task as it is not possible to focus X-rays to form an image as can be done in the case of visible light. Instead, an image is formed by applying the mathematical relation known as a Fourier transform to a diffraction pattern by treating diffracted X-ray beams as waves.

### 7.1.1 The Principles of X-ray Crystallographic Analysis

*7.1.1.1 Crystal lattices, the unit cell, and the symmetry in crystal systems*

Any pattern can be described as a regular arrangement of motifs related to each other by specific symmetry elements. A crystal can be likened to a three dimensional pattern where the motifs are individual molecules which can be superimposed on a grid that is termed a

lattice. The repeating unit of a lattice is known as its unit cell and this is the smallest and simplest three dimensional volume element that is completely representative of the whole crystal (Fig. 7.1.1). If the components of the unit cell are known then the entire crystal lattice can be constructed by stacking the unit cells on top of, and beside, each other to form a three dimensional array.

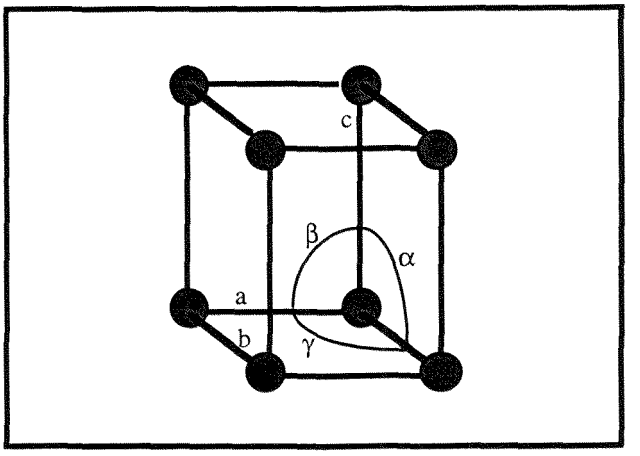


**Fig. 7.1.1** The three dimensional unit cell. The edges a, b, and c intersect at angles $\alpha$, $\beta$, and $\gamma$.

The unit cells of all three dimensional lattices are based on that shown in Fig. 7.1.1 but all differ in shape due to differences in the lengths of a, b, and c, and the angles opposite them, $\alpha$, $\beta$, and $\gamma$. This gives rise to the seven crystal classes listed in Table 7.1.1.

**Table 7.1.1**

Properties of the unit cells of the seven crystal systems

| Crystal System | Edge Lengths | Angles |
|---|---|---|
| cubic | $a = b = c$ | $\alpha = \beta = \gamma = 90^o$ |
| tetragonal | $a = b \neq c$ | $\alpha = \beta = \gamma = 90^o$ |
| orthorhombic | $a \neq b \neq c$ | $\alpha = \beta = \gamma = 90^o$ |
| monoclinic | $a \neq b \neq c$ | $\alpha = \beta = 90^o \neq \gamma$ |
| triclinic | $a \neq b \neq c$ | $\alpha \neq \beta \neq \gamma$ |
| trigonal | $a = b = c$ | $\alpha = \beta = \gamma \neq 90^o, < 120^o$ |
| hexagonal | $a = b \neq c$ | $\alpha = \beta = 90^o, \gamma = 120^o$ |

In 1848, Auguste Bravais showed that only fourteen different kinds of lattice could be formed from these seven unit cells, seven which have lattice points only at the corners of the unit cell and are known as primitive lattices prefaced by the letter P, and seven which

contain lattice points other than those at the corners and are described as non-primitive. These are the face-centred and body-centred lattices as described in Fig. 7.1.2 and have one or more extra set of lattice points per unit cell.

Each crystal system possesses certain types of symmetry based on rotation and reflection. Rotation occurs about an axis and is designated *n* fold (where $n = 1, 2, 3, 4$, or 6) if a rotation of $360°/n$ gives an arrangement equivalent to that initially present. Mirror planes exist when everything on one side of the plane is related by reflection to what is on the other side of the plane and are designated by the letter *m*. Inversion centres (or centrosymmetry) can also exist and are designated as $\bar{n}$. Combination of these three symmetry operations gives rise to 32 point groups by which a crystal system may be described. Each crystal of a different compound produces a characteristic diffraction pattern which also exhibits symmetry. The diffraction symmetry (or Laue symmetry) is centrosymmetric and there are 11 different types which correspond with the 11 centrosymmetric point groups. Identification of which of these point groups describes the diffraction symmetry allows the crystal class (Table 7.1.1) to be established.

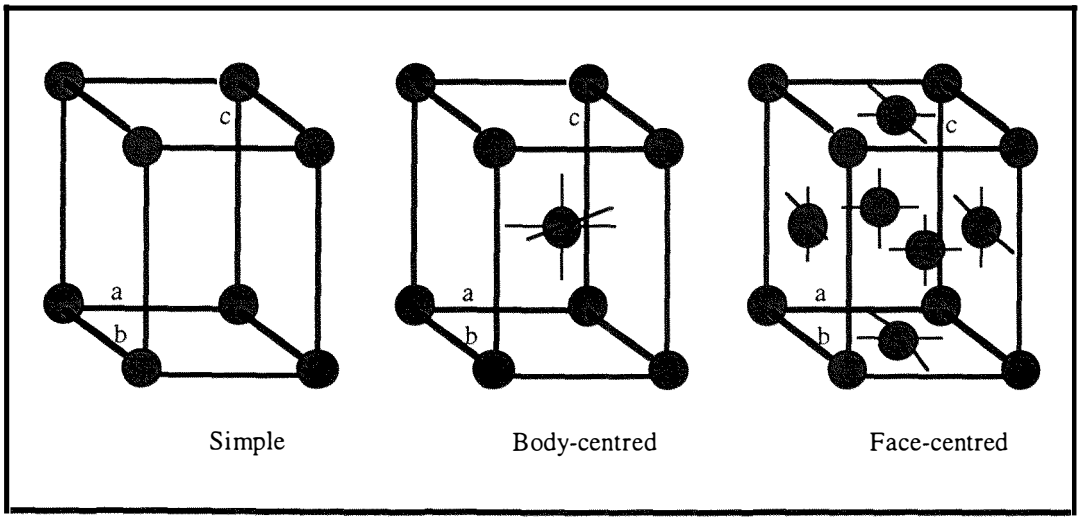


**Fig. 7.1.2** The simple (primitive), body-centred and face-centred lattices as described in the text

Groups of atoms can exhibit the symmetry of all the 32 point groups but, as well, because the crystal is a repeating array, translation is also allowed. When the two translation elements are added to the 32 point groups, 230 unique space groups result. These arise from (a) rotation + translation (screw axis), and (b) mirror plane + translation (glide plane). The space group symmetry therefore refers to the way in which all atoms or groups of atoms are arranged in the crystal. A space group is designated by a capital letter (identifying the lattice type e.g. P = primitive) followed by the point group symbol modified by the introduction of translational symmetry elements. Proteins, because of their chirality, can not crystallise in a space group that involves mirror planes or centres,

which means there are only 11 point groups and 63 space groups that can accommodate protein molecules.

*7.1.1.2 The process of X-ray diffraction*

A crystal acts as a three dimensional diffraction grating since the spacing between the atoms that makeup the molecule is similar to the wavelength of X-rays. The electrons in these atoms diffract (or scatter) the X-rays in various directions that depend on the size and shape of the repeating unit in the crystal. To solve a structure we need to know the intensity of each diffracted beam and the origin of the diffracted beam.

Diffracted X-ray beams have a wave-like nature, each with an amplitude (|F|, a measure of the strength of the beam) and a phase ($\alpha$, the distance of the peak maximum from the point of diffraction). The relationship between the measured intensity and the amplitude may be represented as

$$\text{Intensity} \quad \alpha \quad |F|^2.$$

The diffraction of X-rays by crystals is treated as diffraction by a set of parallel planes that are related to the faces of the unit cell and defined by the labels hkl (Miller indices). Bragg's Law shows that in order to observe any intensity in the emerging, diffracted X-rays the equation

$$2d \sin\theta = n\lambda$$

(where d = spacing of crystal planes, $\theta$ = Bragg angle (angle of reflection), $\lambda$ = the wavelength of the X-rays, and n is an integer) must be fulfilled as shown in Fig. 7.1.3. This is because the waves from different planes of atoms are only in phase when this equation is obeyed. When this happens reinforcement of the waves occurs and intense beams of X-rays are observed. If the waves are out of phase the peak of one wave coincides with the trough of another wave and the two waves cancel each other out with a reduction in intensity (Fig. 7.1.3). Formation of the correct image therefore relies upon recombining the diffracted waves with their correct phases. By measuring the angles at which the X-rays are reflected, it is a simple task to calculate the distances between the planes of atoms within a crystal.

The indices h, k, and l are integers that can have both even and odd values. Although all atoms in the crystal contribute to every diffracted beam, some arrangements of groups of atoms within the cell cancel out exactly the contribution from another. Thus, certain combinations of h, k, and l may give rise to zero intensity diffracted beams. These will

occur in a systematic fashion and are not random effects. For example, for a series of reflections arising from a centred lattice h + k + l will always be an even number i.e. diffracted beams where h + k + l is an odd number are not observed. Identification of such patterns allows the space group to be determined.

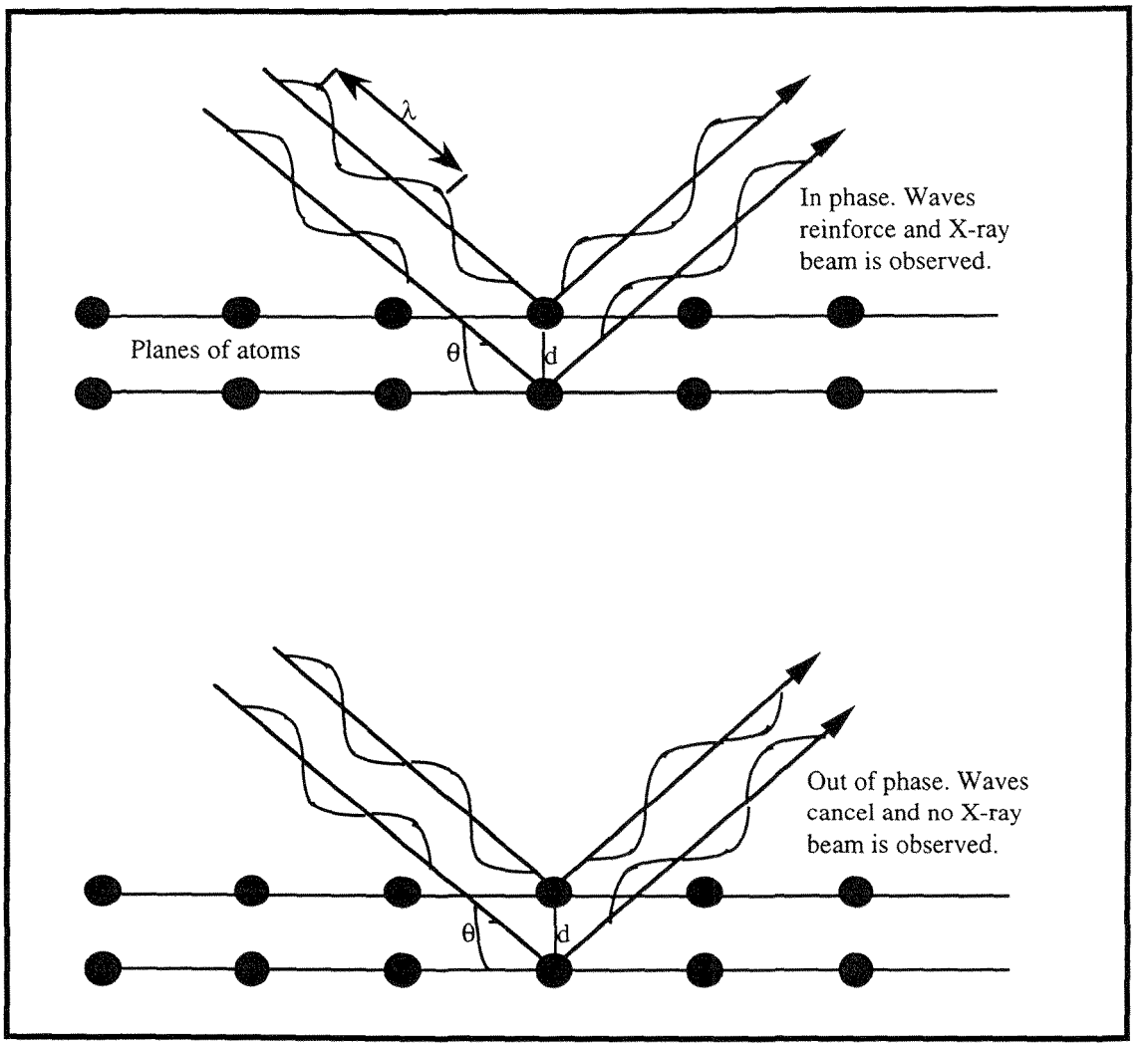


**Fig. 7.1.3** Bragg's law shows that the waves from different planes of atoms are only in phase when the equation $2d \sin\theta = n\lambda$ is obeyed

Every diffracted X-ray beam can be described by the following equation,

$$F^* = |F|\exp(i\alpha)$$

where $F^*$ is a vector called the structure factor, $|F|$ is the structure amplitude and $\alpha$ is the phase. A structure factor is the sum of the Fourier series which describes the reflection hkl. Each atom makes a contribution to both the amplitude and the phase (i.e. $f\exp(i\alpha)$) where $f$ refers to the scattering power or scattering factor of an atom (which is a function of the atomic number of the atom and the scattering angle $\theta$). Thus, $f$ is different for

every atom and for every diffracted beam. The overall structure factor is therefore represented by

$$F^* = f_{atom1}\exp(i\alpha_{atom1}) + f_{atom2}\exp(i\alpha_{atom2}) + .....$$

The phase ($\alpha$) of each atom is related to the atom site (x, y, z) in the unit cell so that

$$\alpha_{atom1} = 2\pi(h\, x_{atom1} + k\, y_{atom1} + l\, z_{atom1}).$$

An electron density map of the structure must then be calculated. The map is calculated at a series of grid points and there is a contribution from every atom at every grid point. The contribution from a single atom will dominate the reflections whose indices correspond to the planes that intersect that atom. The electron density map may be calculated as a Fourier series of two parts, the coefficient and geometric parts, as described by the equation

$$\rho(XYZ) = 1/V \sum\sum\sum F^*\exp[-2\pi i(h\, X + k\, Y + l\, Z)$$

where the summation is over all diffracted beams *hkl*, V is the cell volume, XYZ represent grid points into which the map is divided, and F* is the structure factor. In calculating an electron density map F* (the structure factor) must be known for every diffracted beam. While the structure amplitude can be measured (|F|) the phase cannot be and must therefore be calculated. In crystallography this is known as the phase problem. The phase is commonly determined by two methods, multiple isomorphous replacement (MIR) and molecular replacement. In MIR methods an atom with a large scattering factor (a heavy atom) is added to all unit cells, preferably at identical sites, causing changes in the intensities of the diffraction pattern but not the cell dimensions. The phase of the heavy atom can be determined using Patterson syntheses. This phase can then be used as an approximation of the overall phase for all the atoms in the molecule. Repeating this procedure for up to two different heavy atoms and combining the results improves the likelihood of obtaining the correct phase. Molecular replacement can be used where the coordinates of a related or similar structure are available, and involves trying to match the electron density generated for this model with that of the unknown molecule. For small organic molecules a method known as Direct or Statistical methods may be used. This method is based on establishing statistical relationships between phases and calculates the probability that particular phases have been estimated correctly. Often, not all of the atoms are clear (or some may even be missing) in early maps. A more reliable phase can be estimated by including the contributions of the atoms located.

Electron density maps may be calculated using one of these methods. The electron density map may then be interpreted to give a three dimensional model of the molecule under study. The model at this stage is normally only a rough approximation of the final structure and is most likely to need refinement, which is usually undertaken by a full-matrix least-squares minimisation of a function which involves the positional parameters (x, y, z) and the thermal parameters of every atom in the unit cell. The function minimised is usually either

$$w(|Fo| - |Fc|)^2$$

or

$$w(|Fo|^2 - |Fc|^2)^2$$

where |Fo| = the observed structure amplitude
|Fc| = the calculated structure amplitude
and w is a weight which depends on the accuracy with which the diffracted beam has been measured.

Because of the large number of parameters involved with protein structures compared to the relatively small number of data, information that is known about amino acid and protein structures is included to reduce the number of parameters, thus constraining the refinement.

Finally the calculated three dimensional structure is presented along with a measure of the accuracy of the structure refinement. The simplest and most common measure of accuracy is the R-factor or reliability factor. This is most commonly calculated as

$$R = \frac{\sum(|Fo| - |Fc|)}{\sum|Fo|}$$

where |Fo| = the observed structure amplitude and |Fc| = the calculated structure amplitude.

### 7.1.2 The Rationale for Attempting to Obtain the Three Dimensional Structures of the Components which Constitute the Ovarian Monitor Immunoassay System for Estrone Glucuronide

In order to apply the technique of X-ray crystallography the molecule of interest must first be crystallised. This is particularly difficult to achieve, especially for large macromolecules such as proteins. The crystals must be of a quality and size suitable for high-resolution X-ray diffraction [296]. The difficulty in obtaining quality crystals of many macromolecules of interest (and indeed of many small inorganic and organic molecules) continues to prevent the full utilisation and exploitation of X-ray crystallography as a technique [296].

Despite this problem the three dimensional structures of an ever increasing number of proteins have now been elucidated at atomic resolution. The low resolution structure of hen egg white lysozyme was the first protein structure to be solved using X-ray crystallography and therefore has a special place in history [237]. A high resolution structure of this tetragonal crystal form has since been solved [298]. Hen egg white lysozyme also crystallises in several other polymorphic forms [299] and the three dimensional structures of both the triclinic and monoclinic crystalline forms have been solved at high resolution [118, 300-303]. An orthorhombic form has also been studied but only at low resolution [303]. All of the crystal forms have the same basic three dimensional structure with only small differences in the overall architecture of the molecule. Recently a three dimensional structure in which the lysine residues of lysozyme were methylated has also been reported [223]. The three-dimensional structures of the native lysozyme and the methylated derivative were shown to be very similar with the only significant differences being in two surface loops [223]. In the present study the lysine residues have been acylated with much larger, and more hydrophobic steroid glucuronides, and there is no structural information available to indicate the effect of these on the protein structure.

A number of three dimensional protein antigen-antibody structures have also been solved and among these are several Fab-lysozyme complexes [226]. There are also several published structures of small antigen-Fab complexes one of which is the progesterone-Fab structure [203] used in the modelling of the immune complexes presented in chapter four. However, there are no published three dimensional structures of small antigen-Fab complexes where the antigen is conjugated to another protein as in the case of the steroid glucuronide-lysozyme conjugate-anti-steroid glucuronide immune complexes.

The computer generated three dimensional models of the lysozyme enzyme conjugates and the immune complexes described in chapter four are based on published X-ray structures and provide a great deal of information about the immunoassay system and the parameters involved in its operation. However, a more precise understanding of the intricate details may be provided from the actual X-ray structures of the steroid glucuronides, lysozyme conjugates and the lysozyme conjugate-anti-hapten antibody immune complexes. The advantages of such structure determinations include:

(1) The computer derived models, although likely to be good representations of the actual structures, are still only models and must be treated as such.

(2) Although the actual three dimensional structure of lysozyme is known [237] and was used in the modelling of the lysozyme conjugates, the steroid glucuronide structures were originally unknown so that the steroid glucuronide models were generated using energy minimisation techniques.

(3) In the modelling of the lysozyme conjugate three dimensional structures there was no consideration of any secondary interactions (such as hydrogen bonds, van der Waals bonds, etc.) between the steroid glucuronide moiety and the enzyme surface. The exact orientations of the steroid glucuronides with respect to the lysozyme surface therefore remains undetermined. The three dimensional structures would provide such information.

(4) In the modelling of the lysozyme conjugate-immune complexes the three dimensional structure of a Fab fragment to progesterone [203] was used. This differs from the actual hapten structure (see Fig. 4.3.10) and does not allow for any binding of the antibody to the glucuronide ring. As a result the orientation and position of the real anti-hapten antibody may be closer to the enzyme surface and oriented in a different position with respect to the active site. This may be important in determining the mode of inhibition which inactivates the enzyme conjugate.

(5) Determination of the actual three dimensional structure of an immune complex will accurately define the spatial requirements of the antibody-conjugate interaction.

(6) The computer generated three dimensional models of the immune complexes do not allow for any interactions between the enzyme protein surface and the antibody protein surface. These interactions, together with those involving water molecules, are likely to play an important part in the orientation and stability of the immune complex.

Thus, in summary, because the mixed anhydride E1G-lysozyme E3 conjugate is acylated exclusively at lysine 33 and because it can be purified (see chapters 2 and 3) it is an ideal candidate for protein crystallographic studies. The estrone glucuronide monoclonal antibody Fab fragment prepared in chapter five is also ideal for use in crystallisation studies to solve the three dimensional structure of the lysozyme conjugate-Fab immune complex. The work described in the following chapter describes the efforts to date towards obtaining crystals of, and solving the three dimensional structures of (1) estrone glucuronide, (2) an estrone glucuronide-lysozyme conjugate, and (3) an estrone glucuronide-lysozyme-anti-E1G Fab fragment immune complex, the components of which constitute the Ovarian Monitor immunoassay system for estrone glucuronide.

## 7.2 The X-ray, Three Dimensional Structural Analysis of Estrone Glucuronide (E1G)

Although the crystal structures of many steroids have now been published (for example see Duax, Weeks, and Rohrer [204]) and the structure of estrone has been known for some time [207], there are very few examples of the crystal structures of steroid glucuronides. One of the major reasons for this is the difficulty in obtaining good quality crystals of such moieties. The problem of crystallisation lies in the makeup of such molecules which are amphipathic in nature, consisting of a hydrophobic steroid skeleton and a relatively polar carbohydrate ring due to the presence of several hydroxyl groups and a carboxyl group (see Fig. 7.2.1 for example). Both the recently published estriol 17β-glucuronide structure [209] and the reported estradiol 17β-glucuronide structure of Hadd *et al.* [208] contained a carbohydrate moiety which was acetylated at the sugar hydroxyl groups. Also, in these compounds the glycosidic linkage between the steroid and the glucuronide ring was *via* the C-17 position of the steroid skeleton D-ring. There are no crystal structures of steroid glucuronides so far reported where the glycosidic linkage is located at the C-3 position of the steroid A-ring and the hydroxyl groups and the carboxyl group of the carbohydrate moiety are free.

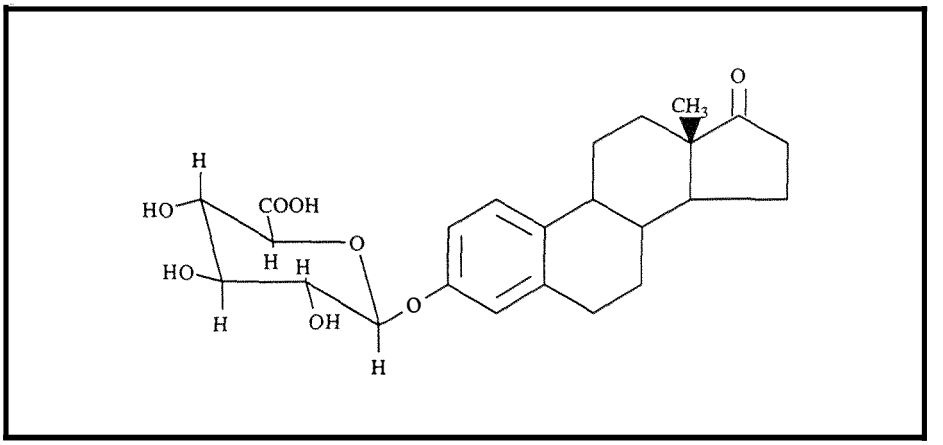


**Fig. 7.2.1** The estrone glucuronide moiety and its amphipathic nature. This can be easily distinguished by the hydrophobic steroid skeleton and the hydrophilic hydroxylated carbohydrate ring making crystallisation difficult.

### 7.2.1 Experimental

17-oxoestra-1,3,5(10)-triene-3-yl-β-D-glucopyranosiduronic acid (estrone glucuronide or E1G, Fig. 7.2.1) was synthesised *via* a Koenigs-Knorr coupling reaction as described in chapter two. Colourless crystals of estrone glucuronide were grown by evaporation from a methanol:Milli-Q water solution at room temperature (Fig. 7.2.2). Data collection was undertaken on a Siemens SMART diffractometer by Associate Professor C. E. F.

Rickard at the University of Auckland (Auckland, New Zealand). The data was processed using Siemens XSCANS (cell refinement) and Siemens SAINT (data reduction). The three dimensional structure was solved by Dr. A. K. Burrell (Department of Chemistry, Massey University, Palmerston North, New Zealand) using the program SHELXS86 [304] and the structure refined using SHELXL93 [305]. Molecular graphics were generated using the program XPMA [306]. The crystal data, data collection and refinement details are listed in Table 7.2.1 below.

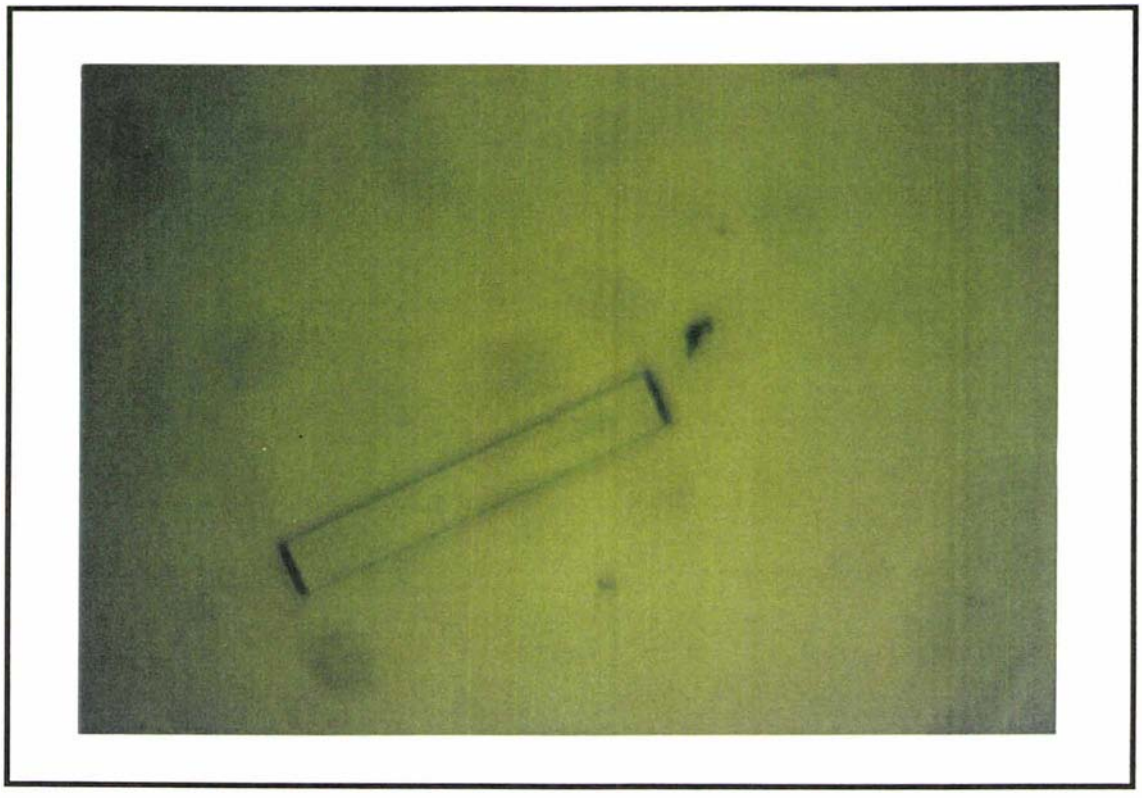

**Fig. 7.2.2** A crystal of estrone glucuronide (magnification unknown)

### 7.2.2 Results and Discussion

Estrone glucuronide crystallises from a water:methanol solution along with a single water molecule. The three dimensional molecular structure, as determined from the X-ray crystallographic data is shown in Fig. 7.2.3. The atomic coordinates, and selected bond distances and angles are listed in Tables 7.2.2, 7.2.3, and 7.2.4 respectively. The hydrogen atom associated with the carboxylic acid group, and those of the solvent water molecule, could not be located and were omitted. All of the bond lengths and angles in the steroid skeleton are in the expected ranges. Ring-A has the expected aromaticity and the non-planar geometries of rings B, C, and D are also as expected from comparison with other steroid molecules whose three dimensional structures have been solved [204].

**Table 7.2.1**

Crystal data, data collection and refinement details for estrone glucuronide

| *Crystal data* | | | |
|---|---|---|---|
| Empirical formula | $C_{24}H_{30}O_8$ | Z | Z = 4 |
| Formula weight | $M_r$ = 461.47 | Density (calculated) | $D_x$ = 1.366 Mg $m^{-3}$ |
| Crystal system | Orthorhombic | X-ray source | Mo Kα radiation |
| Space group | $P2_12_12_1$ | Wavelength | λ = 0.71073 Å |
| Unit cell dimensions | a = 7.0337 (2) Å | Cell parameters from 6916 reflections | |
| | b = 8.3981 (2) Å | Theta range | θ = 1-25° |
| | c = 37.9873 (11) Å | Absorption coefficient | μ = 0.105 $mm^{-1}$ |
| | α = β = γ = 90° | Temperature | T = 293 (2) K |
| Volume | V = 2243.90 (11) $Å^3$ | Crystal size | 0.50 x 0.12 x 0.035 mm |
| *Data collection* | | | |
| Diffractometer | Siemens SMART | Index Ranges | -8≤h≤8 |
| Absorption correction | none | | -8≤k≤10 |
| Measured reflections | 10397 | | -44≤l≤47 |
| Independent reflections | 3111 | Intensity decay | <2% |
| Observed reflections [I>2σ(I)] | 2730 | | |
| *Refinement details* | | | |
| Refinement method | Full-matrix least-squares on $F^2$ | Extinction correction | none |
| Goodness of fit on $F^2$ | S = 1.132 | | |
| Reflections used | 3110 | | |
| Parameters | 337 | | |
| Final R indices | | Atomic scattering factors from International Tables for Crystallography (1992, Vol. C, Tables 4.2.6.8 and 6.1.1.4) | |
| $R[F^2>2s(F^2)]$ | 0.0513 | | |
| $wR(F^2)$ | 0.1330 | | |

The angle between the mean plane of the A-ring of the steroid (C1, C2, C3, C5, C10) and the mean plane of the glucuronide (C19, C20, C21, C22, O3) is 13.97 (43)°, with a torsion angle (C3, O2, C19, C20) of 158.4 (3)°. The structure also clearly shows the carbohydrate ring is in a chair conformation and that all of the hydrogen substituents on the glucuronide ring occupy axial sites, resulting in the adoption of trans positions of hydrogen atoms attached to adjacent carbon atoms with respect to each other. Hence the orientation and position of the critical β-linkage between the carbohydrate moiety and the C-3 position of the steroid A-ring, which determines the orientation of the steroid upon conjugation to lysozyme and its presentation to antibodies in the surrounding environment, is clearly shown. The observed stereochemistry is that predicted from the synthetic route adopted and NMR experiments.

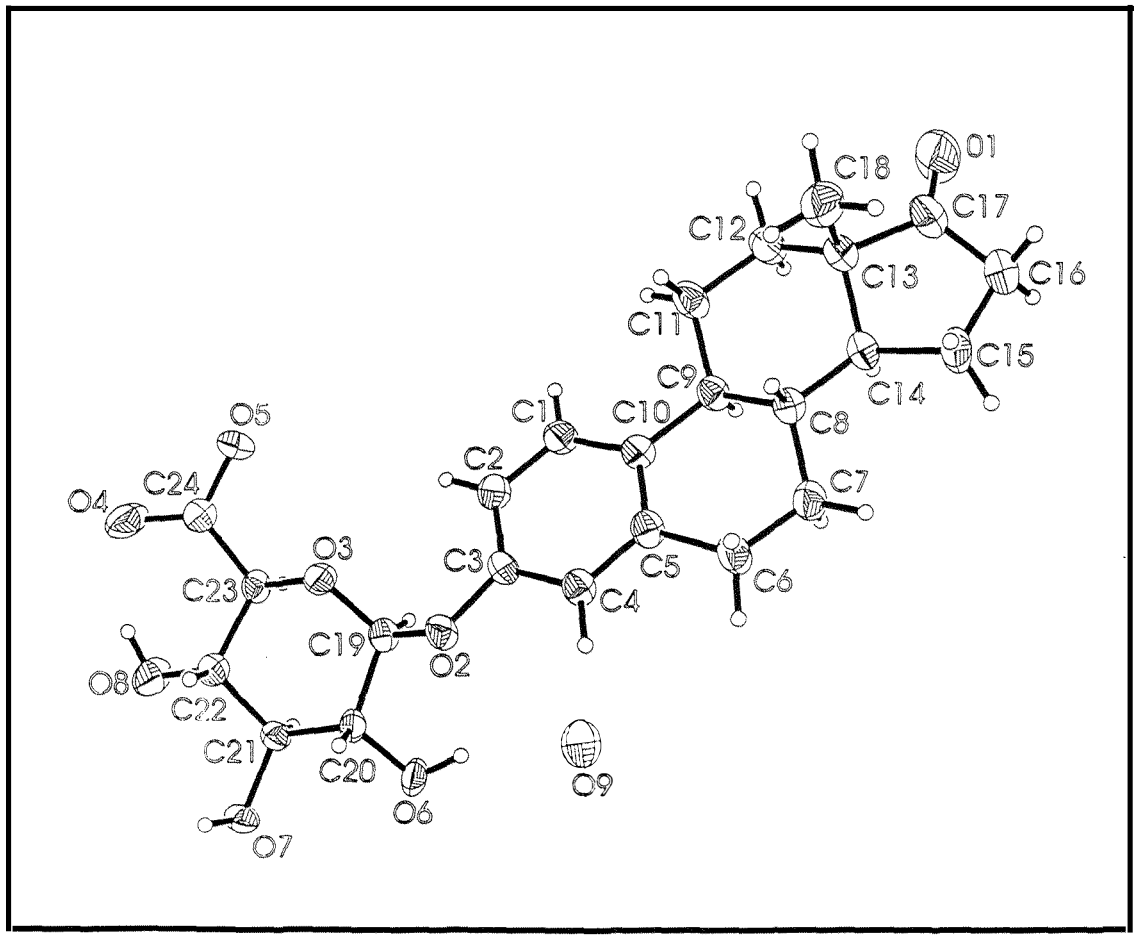


**Fig. 7.2.3** ZORTEP [306] drawing of $C_{24}H_{30}O_8$ (estrone glucuronide hydrate) showing thermal ellipsoids drawn at the 50% probability level (except for hydrogens where arbitrary levels have been used)

**Table 7.2.2**

Fractional atomic coordinates and equivalent isotropic displacement parameters ($Å^2$) for 17-oxoestra-1,3,5(10)-triene-3-yl-β-D-glucopyranosiduronic acid hydrate, $C_{24}H_{30}O_8$

$$U_{eq} = (1/3)\Sigma_i\Sigma_j U_{ij} a_i^* a_j^* \mathbf{a}_i.\mathbf{a}_j.$$

| Atom | x | y | z | $U_{eq}$ |
|---|---|---|---|---|
| O1 | 2.0124 (5) | 1.1109 (5) | 0.18256 (12) | 0.0855 (13) |
| O2 | 0.7639 (3) | 0.4363 (3) | 0.10569 (6) | 0.0313 (6) |
| O3 | 0.5665 (4) | 0.5779 (3) | 0.07031 (6) | 0.0306 (6) |
| O4 | 0.2182 (5) | 0.7641 (3) | 0.02054 (8) | 0.0590 (10) |
| O5 | 0.4759 (4) | 0.8648 (3) | 0.04604 (7) | 0.0381 (7) |
| O6 | 0.7037 (4) | 0.1581 (3) | 0.06395 (7) | 0.0394 (7) |
| O7 | 0.3174 (4) | 0.1537 (3) | 0.03656 (6) | 0.0337 (7) |
| O8 | 0.2151 (4) | 0.4503 (3) | 0.00477 (7) | 0.0483 (8) |
| O9 | 1.0710 (4) | 0.1505 (4) | 0.09133 (8) | 0.0540 (8) |
| C1 | 1.1352 (5) | 0.7461 (5) | 0.10940 (10) | 0.0327 (10) |
| C2 | 0.9718 (6) | 0.6691 (5) | 0.09794 (10) | 0.0321 (10) |
| C3 | 0.9214 (5) | 0.5278 (4) | 0.11394 (9) | 0.0267 (9) |
| C4 | 1.0291 (5) | 0.4705 (5) | 0.14208 (9) | 0.0306 (9) |
| C5 | 1.1922 (5) | 0.5470 (5) | 0.15275 (9) | 0.0314 (9) |
| C6 | 1.3039 (6) | 0.4757 (6) | 0.18346 (11) | 0.0412 (10) |
| C7 | 1.5065 (6) | 0.5360 (5) | 0.18530 (11) | 0.0377 (10) |
| C8 | 1.5105 (5) | 0.7169 (4) | 0.18243 (9) | 0.0283 (8) |
| C9 | 1.4396 (5) | 0.7675 (5) | 0.14549 (9) | 0.0304 (9) |
| C10 | 1.2497 (5) | 0.6883 (4) | 0.13631 (9) | 0.0285 (9) |
| C11 | 1.4438 (6) | 0.9490 (5) | 0.14058 (12) | 0.0389 (10) |
| C12 | 1.6421 (6) | 1.0188 (6) | 0.14840 (12) | 0.0408 (11) |
| C13 | 1.7081 (5) | 0.9712 (5) | 0.18461 (10) | 0.0333 (9) |
| C14 | 1.7074 (5) | 0.7865 (4) | 0.18750 (9) | 0.0280 (8) |
| C15 | 1.8235 (6) | 0.7514 (6) | 0.22101 (12) | 0.0427 (11) |
| C16 | 1.9850 (7) | 0.8726 (6) | 0.21832 (14) | 0.0496 (12) |
| C17 | 1.9158 (6) | 1.0021 (5) | 0.19390 (12) | 0.0464 (11) |
| C18 | 1.5919 (7) | 1.0548 (6) | 0.21328 (12) | 0.0519 (12) |
| C19 | 0.6871 (5) | 0.4435 (4) | 0.07143 (9) | 0.0279 (8) |
| C20 | 0.5747 (5) | 0.2890 (4) | 0.06719 (9) | 0.0262 (8) |
| C21 | 0.4372 (5) | 0.2920 (4) | 0.03636 (9) | 0.0269 (9) |
| C22 | 0.3254 (5) | 0.4468 (5) | 0.03600 (9) | 0.0290 (9) |
| C23 | 0.4641 (5) | 0.5841 (4) | 0.03781 (9) | 0.0269 (9) |
| C24 | 0.3730 (6) | 0.7448 (5) | 0.03429 (10) | 0.0323 (10) |

The crystallographically determined three dimensional structure is similar to that generated by computer modelling in chapter four (section 4.3.1). It is therefore likely that the models of the estrone glucuronide-lysozyme conjugates generated in chapter four will be good representations of the actual three dimensional structures. The computer three dimensional structure of the pregnanediol glucuronide moiety generated in chapter four is therefore also likely to be a good representation of the actual or real structure.

**Table 7.2.3**

Selected bond distances (Å) for 17-oxoestra-1,3,5(10)-triene-3-yl-β-D-glucopyranosiduronic acid hydrate, $C_{24}H_{30}O_8$

| Bond | Distance | Bond | Distance |
|---|---|---|---|
| O1 --- C17 | 1.216 (5) | C7 --- C8 | 1.523 (6) |
| O2 --- C3 | 1.384 (4) | C8 --- C14 | 1.516 (5) |
| O2 --- C19 | 1.410 (4) | C8 --- C9 | 1.549 (5) |
| O3 --- C19 | 1.413 (4) | C9 --- C10 | 1.532 (5) |
| O3 --- C23 | 1.430 (4) | C9 --- C11 | 1.535 (6) |
| O4 --- C24 | 1.219 (5) | C11 --- C12 | 1.542 (6) |
| O5 --- C24 | 1.318 (5) | C12 --- C13 | 1.506 (6) |
| O6 --- C20 | 1.431 (4) | C13 --- C17 | 1.526 (6) |
| O7 --- C21 | 1.435 (4) | C13 --- C18 | 1.532 (6) |
| O8 --- C22 | 1.418 (4) | C13 --- C14 | 1.555 (5) |
| C1 --- C2 | 1.388 (5) | C14 --- C15 | 1.541 (5) |
| C1 --- C10 | 1.389 (5) | C15 --- C16 | 1.528 (7) |
| C2 --- C3 | 1.380 (5) | C16 --- C17 | 1.510 (7) |
| C3 --- C4 | 1.397 (5) | C19 --- C20 | 1.528 (5) |
| C4 --- C5 | 1.377 (5) | C20 --- C21 | 1.519 (5) |
| C5 --- C10 | 1.400 (5) | C21 --- C22 | 1.519 (5) |
| C5 --- C6 | 1.529 (5) | C22 --- C23 | 1.512 (5) |
| C6 --- C7 | 1.514 (6) | C23 --- C24 | 1.500 (5) |

**Table 7.2.4**

Selected bond angles (°) for 17-oxoestra-1,3,5(10)-triene-3-yl-β-D-glucopyranosiduronic acid hydrate, $C_{24}H_{30}O_8$

| Bond | Angle | Bond | Angle |
|---|---|---|---|
| C3 --- O2 --- C19 | 119.5 (3) | C17 --- C13 --- C14 | 99.0 (3) |
| C19 --- O3 --- C23 | 110.9 (3) | C18 --- C13 --- C14 | 113.9 (3) |
| C2 --- C1 --- C10 | 123.2 (4) | C8 --- C14 --- C15 | 121.1 (3) |
| C3 --- C2 --- C1 | 118.4 (4) | C8 --- C14 --- C13 | 112.2 (3) |
| C2 --- C3 --- O2 | 125.7 (3) | C15 --- C14 --- C13 | 104.3 (3) |
| C2 --- C3 --- C4 | 119.7 (3) | C16 --- C15 --- C14 | 102.2 (3) |
| O2 --- C3 --- C4 | 114.5 (3) | C17 --- C16 --- C15 | 106.3 (4) |
| C5 --- C4 --- C3 | 120.9 (4) | O1 --- C17 --- C16 | 125.3 (4) |
| C4 --- C5 --- C10 | 120.5 (3) | O1 --- C17 --- C13 | 125.6 (4) |
| C4 --- C5 --- C6 | 118.0 (3) | C16 --- C17 --- C13 | 109.2 (4) |
| C10 --- C5 --- C6 | 121.6 (3) | O3 --- C19 --- O2 | 107.0 (3) |
| C7 --- C6 --- C5 | 112.8 (3) | O3 --- C19 --- C20 | 111.4 (3) |
| C6 --- C7 --- C8 | 110.3 (4) | O2 --- C19 ---- C20 | 105.0 (3) |
| C14 --- C8 --- C7 | 113.1 (3) | O6 --- C20 --- C19 | 109.5 (3) |
| C14 --- C8 --- C9 | 107.3 (3) | O6 --- C20 --- C21 | 110.5 (3) |
| C7 --- C8 --- C9 | 109.5 (3) | C19 --- C20 - C21 | 113.4 (3) |
| C10 --- C9 --- C11 | 114.8 (3) | O7 --- C21 --- C22 | 112.9 (3) |
| C10 --- C9 --- C8 | 111.5 (3) | O7 --- C21 --- C20 | 110.9 (3) |
| C11 --- C9 --- C8 | 112.1 (3) | C22 --- C21 --- C20 | 110.5 (3) |
| C5 --- C10 --- C1 | 117.2 (3) | O8 --- C22 --- C21 | 108.0 (3) |
| C5 --- C10 --- C9 | 121.2 (3) | O8 --- C22 --- C23 | 112.0 (3) |
| C1 --- C10 --- C9 | 121.4 (3) | C21 --- C22 --- C23 | 108.6 (3) |
| C9 --- C11 --- C12 | 111.8 (4) | O3 --- C23 --- C24 | 108.9 (3) |
| C13 --- C12 --- C11 | 110.7 (4) | O3 --- C23 --- C22 | 109.7 (3) |
| C12 --- C13 --- C17 | 117.5 (4) | C24 --- C23 --- C22 | 114.0 (3) |
| C12 --- C13 --- C18 | 111.3 (4) | O4 --- C24 --- O5 | 122.3 (4) |
| C17 --- C13 --- C18 | 105.6 (3) | O4 --- C24 --- C23 | 122.7 (4) |
| C12 --- C13 --- C14 | 109.2 (3) | O5 - C24 --- C23 | 115.0 (3) |

## 7.3 Crystallisation and X-ray Studies of an Estrone Glucuronide-Lysozyme Conjugate

Characterisation of the estrone glucuronide-lysozyme E3 conjugate family showed that the estrone glucuronide moiety was exclusively attached to the lysozyme molecule *via* the side chain of lysine residue 33. Thus only one type of macromolecule was present, unlike the active ester E1G-lysozyme conjugate family E1 where two types of macromolecule were present, one where the lysozyme molecule is conjugated with estrone glucuronide at lysine residue 97, and one where the lysozyme molecule is conjugated with estrone glucuronide at lysine residue 116 (see chapters three and four for details). The mixed anhydride estrone glucuronide-lysozyme E3 conjugate was shown to be inhibited by > 90% in the presence of excess anti-estrone glucuronide antibody after purification by cation-exchange and hydrophobic interaction chromatography (see chapters two and three). The conjugate was free of all other conjugate products and unreacted, unconjugated, native lysozyme by both Mono-S 7 M urea chromatography analysis and acid polyacrylamide gel electrophoresis analysis as described in chapters two and three. The conjugate was thus considered of sufficient purity for crystallisation studies.

### 7.3.1 Initial Crystallisation Studies

Initial attempts at crystallising the E3 estrone glucuronide conjugate were undertaken using a factorial screening method, whereby a large range of conditions (i.e. pH, precipitant, concentration etc.) are screened [307]. The hanging drop method of McPherson [296] was used at room temperature to create a supersaturated state from which crystals may grow. This method involves placing a drop of protein solution on a siliconised microscope cover slip and adding an equal volume of the well buffer solution (containing buffer, precipitant, metal salt, etc.) to the drop. The cover slip is then carefully inverted and sealed (usually with Vaseline) over a much larger volume of buffer solution (the reservoir) in a well and left. Tissue culture trays (Linbro model FB-16-24-TC) consisting of 24 wells are ideal for such experiments, the reservoir being placed in the well and the coverslip sealed over the top. Once the well is sealed a vapour diffusion gradient between the droplet and the well reservoir is established. Through the vapour diffusion gradient the concentration of the precipitant in the droplet gradually changes until it becomes the same as that of the reservoir [296]. Because the volume of the reservoir is much larger than that of the drop, the final equilibrium conditions are essentially the same as those initially determined for the reservoir.

The advantage of this system for crystallisation trials is that only small amounts of protein are required. For the factorial screen, 1 μL drops of a 10 mg/mL solution of the E3

estrone glucuronide-lysozyme conjugate in Milli-Q water were used. To these were added 1 μL of reservoir buffer solution. Thus a large number of conditions can be screened without using large amounts of precious protein material. A further advantage of this set up is that the tissue culture plates can be moved easily with minimum disturbance of the hanging drop and easily examined under a microscope for signs of crystallisation [296]. Unfortunately, the initial factorial screen provided few conditions which looked promising for crystallisation of the estrone glucuronide-lysozyme conjugate. No conditions were found which resulted in crystal growth and only a few conditions resulted in precipitates.

As the conditions under which native hen egg white lysozyme crystallises are known, extra trays were set up using conditions similar to those used by Moult *et al.* [299] in growing triclinic crystals of lysozyme. A trial using sodium nitrate as the precipitant and ammonium acetate as the buffer solution was undertaken, screening between pH 4.50 and pH 5.50 (0.1 M ammonium acetate) and a precipitant concentration ranging between 1 and 6% sodium nitrate. A further trial was also set up using conditions similar to those employed to obtain crystals of hen egg white lysozyme which contained methylated lysine residues [223] (pH 7.00 to pH 8.50, 0.1 M tris buffer, precipitant concentration 1.0-2.0 M magnesium sulfate). All crystallisation trials were undertaken at room temperature.

The high pH trials (pH 7.00 to pH 8.50, 0.1 M tris buffer) produced a large number of precipitates. Further trials were therefore carried out at pH 7.75 using a variety of buffers, precipitants and protein concentrations. When ammonium nitrate (1.0 M) was used as the precipitant in either HEPES, EPPS, or phosphate buffer (0.1 M, pH 7.75), thin crystalline plates were formed with butterfly like structures at a protein concentration of 10 mg/mL. However, the crystals were extremely thin and could not be handled without breaking. Further attempts to refine the crystallisation conditions and improve upon these crystals were without success.

The trials undertaken at lower pH (4.50-5.50) using sodium nitrate as the precipitant gave small, cubic shaped crystals under a variety of conditions. The best crystals were grown from a solution that contained 3% sodium nitrate and 0.1 M ammonium acetate buffer (pH 4.90) using a protein concentration of 10 mg/mL. Fig. 7.3.1 shows a photograph of the best crystals of the mixed anhydride estrone glucuronide-lysozyme E3 conjugate grown under these conditions. Although these were the best crystals obtained, they were still extremely small and not large enough for X-ray diffraction studies. Attempts to grow larger crystals by changing the protein concentration, the temperature and reservoir composition failed to improve crystal size. The technique of macroseeding [308-309] was

therefore employed in an attempt to enlarge the small crystals into crystals suitable for X-ray diffraction studies. This involves taking the small pregrown crystals, exhaustively washing them in specific solutions and then introducing them individually into a pre-equilibrated protein solution. The seeding experiments were undertaken using sitting drops on purpose built bridges (Micro Bridges, Hampton Research, Luguna Hills, CA 92653, U.S.A.). The advantage of this technique over the hanging drop technique is that the crystal can be washed in the bridge and then the equilibrated protein solution introduced, the reservoir solution placed in the well and the well sealed with a cover slip.

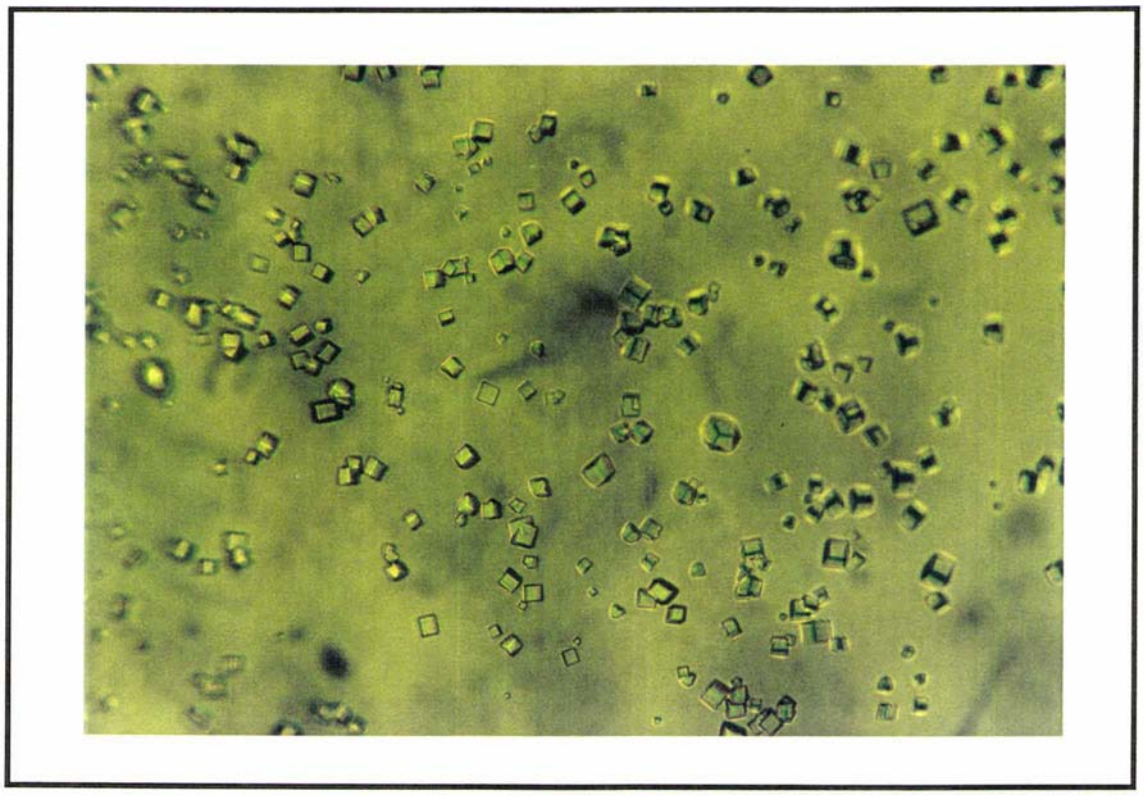

**Fig. 7.3.1** Cubic crystals of the mixed anhydride estrone glucuronide-lysozyme E3 conjugate grown under the conditions described in section 7.3.1

Although macroseeding of crystals such as those shown in Fig. 7.3.1 did give enlarged crystals, the rate of growth was extremely slow and the increase in size was small. Crystals which had been re-seeded several times were still very small and only 2-3 times larger than the size of the initial crystals. Under the conditions in which the seeded crystals grew, spontaneous nucleation also occurred and as a result a shower of microcrystals was always observed despite enormous care being taken to exclude potential nucleation sites. While reducing the protein concentration in the pre-equilibrated drop stopped this spontaneous nucleation, it also prevented the growth of the seeded crystal.

Despite the fact that the seeded crystals were still small, one of the larger crystals was mounted in a capillary tube and placed in an X-ray beam to determine how well it would diffract. All the data were collected on an R-Axis IIC imaging plate system with monochromated Cu Kα radiation from a Rigaku RU rotating anode generator operating at 50 KV and 100 mA.

The crystal placed in the X-ray beam diffracted poorly. Very few spots were observed even with stills collected over a 60 minute exposure time. An attempt to process the data was made using (1) the software provided by the image plate system (R-axis software programs) on a VAX station 4000 computer system, and (2) the software package Denzo on a Silicon Graphics Workstation. The data processing of the collected stills showed that the symmetry of the crystal was most likely primitive cubic with preliminary unit cell dimensions of

$$a = 104.17 \text{ Å}, b = 105.24 \text{ Å}, c = 105.65 \text{ Å}$$
$$\alpha = 89.96^{o}, \beta = 89.32^{o}, \gamma = 89.18^{o}$$

where $a = b = c$ and $\alpha = \beta = \gamma = 90^{o}$. The corresponding space group could not be determined. Unfortunately, because the crystals diffracted so poorly they were not of sufficient quality for X-ray diffraction studies and were abandoned.

### 7.3.2 Further Crystallisation Studies

Further crystallisation trials were undertaken with the estrone glucuronide-lysozyme E3 conjugate using sodium nitrate as the precipitant, 0.1 M ammonium acetate (pH 4.90) as the buffer solution and polyethylene glycol (PEG, $M_r = 6000$) as an additive. Trials were undertaken using 20 μL sitting drops in bridges at room temperature. Precipitant conditions of 3-6% sodium nitrate and 1-6% PEG 6000 were screened. A number of conditions resulted in crystal growth.

The best crystals were obtained using a protein concentration of 10 mg/mL, precipitant concentrations of 5-6% sodium nitrate and 4-6% PEG 6000, and were colourless and diamond in shape as shown in Fig. 7.3.2. These crystals were much larger than the crystals obtained in the absence of PEG 6000 (see Fig. 7.3.1). The best crystals were also larger than those grown in the absence of PEG 6000 even after several seeding experiments as described in section 7.3.1 above. Several of these larger crystals were mounted in capillary tubes and several still images were taken in an attempt to find the crystal orientation and the unit cell dimensions in order to determine their suitability for

X-ray diffraction studies. One crystal was considered suitable for more advanced studies and the results of these studies are discussed in section 7.3.3.

### 7.3.3 Data Collection, Processing and Structure Determination from an Estrone Glucuronide-Lysozyme Conjugate Crystal

Data was collected from a crystal grown using a protein concentration of 10 mg/mL, in 6% sodium nitrate, 0.1 M ammonium acetate (pH 4.90), 4% PEG 6000 as described in section 7.3.2. The data collection and initial data processing was undertaken by Dr. G. E. Norris (Department of Biochemistry, Massey University, Palmerston North, New Zealand). Further data processing and the structure determination was undertaken by Dr. P. D. Jeffrey (Department of Biochemistry, Massey University, Palmerston North, New Zealand). All data processing and structural determination calculations were undertaken on a Silicon Graphics Workstation using the software described.

*7.3.3.1 Data collection*

All data were collected on an R-axis IIC imaging plate system with monochromated Cu Kα radiation from a Rigaku RU200 rotating anode generator operating at 50 KV and 100 mA at room temperature. The unit cell and orientation matrix of the crystal were determined by collecting six still images at various ϕ angles from 0° to 145° and auto-indexing the observed reflections using the software package Denzo. The data collection comprised 42 frames, each with an oscillation angle (or range) of 2° covering a total of 84°, and each frame was exposed for a total of 60 minutes. The crystal was stable in the X-ray beam for the entire collection period.

*7.3.3.2 Data processing*

Initial processing of the collected data was undertaken using the software package Denzo. The X-ray data were then scaled using the software package Scalepack. The crystal was shown to be tetragonal and belong to the space group $P4_32_12$, and have cell dimensions

$$a=b=78.5\ \text{Å},\ c=39.1\ \text{Å};\ \alpha=\beta=\gamma=90^{\circ}.$$

Table 7.3.1 lists the data processing statistics for the collected data set. Table 7.3.2 gives the data processing statistics as a function of resolution. It can be seen that the completeness level remains high, even out to a resolution of 2.10 Å with a cumulative completeness of 94.7% (Table 7.3.2). The number of intensities greater than $3\sigma$ can be seen to fall off with increasing resolution from 2.91 Å. A total of 80.8% of all reflections (5 798) had an intensity greater than $3\sigma$ (Table 7.3.2). The linear R factor for all

**Table 7.3.1**

Data processing statistics for the estrone glucuronide-lysozyme E3 conjugate data

| Parameter | Value |
|---|---|
| Resolution (Å) | 2.10 |
| Number of observations (reflections) | 24 976 |
| Unique Observations (reflections) | 7 176 |
| % completeness (to 2.10 Å) | 94.7 |
| R factor for scaling (%) | 9.1 |

**Table 7.3.2**

Statistics for the scaled R-Axis estrone glucuronide-lysozyme E3 conjugate data as a function of resolution

| Resolution (Å) | | Reflections | Completeness in shell (%) | I > 3σ (%) | Linear R factor (%) |
|---|---|---|---|---|---|
| Lower limit | Upper limit | | | | |
| 99.00 | 4.20 | 990 | 94.4 | 97.2 | 5.9 |
| 4.20 | 3.33 | 942 | 97.2 | 96.3 | 7.7 |
| 3.33 | 2.91 | 906 | 96.4 | 90.5 | 10.0 |
| 2.91 | 2.65 | 885 | 95.6 | 84.4 | 12.5 |
| 2.65 | 2.46 | 885 | 95.5 | 77.3 | 14.3 |
| 2.46 | 2.31 | 857 | 94.2 | 70.9 | 16.4 |
| 2.31 | 2.20 | 877 | 93.2 | 67.6 | 19.2 |
| 2.20 | 2.10 | 834 | 90.8 | 58.5 | 21.7 |
| All Reflections | | 7176 | 94.7 | 80.8 | 9.1 |

reflections in the scaled data was 9.1%. The overall data set was poor with high mosaicity (0.8) and some splitting of the data was observed. Despite this the data was merged with an R value of 9.1% although the R factor and percentage of reflections with an intensity > 3σ was poor for data at high resolution (Table 6.3.2).

*7.3.3.3 Structure determination*

The three dimensional structure of the E3 estrone glucuronide-lysozyme conjugate was solved and refined by Dr. P. D. Jeffrey (Department of Biochemistry, Massey University, Palmerston North, New Zealand) by molecular replacement with the software package X-PLOR (Version 3.1 A system for X-ray Crystallography and NMR (1992), Axel, T., Brünger, Yale University Press).

*7.3.3.4 Molecular replacement*

Molecular replacement was first used in the early 1960's by Rossman and Blow [310] to use structural redundancy, a consequence of noncrystallographic symmetry, for phase determination. The technique uses the three dimensional model of a related protein as a search model. The search model is placed in the unit cell of the unknown protein and rotated and translated through the unit cell until the diffraction pattern calculated from it gives the best agreement with the observed diffraction pattern of the unknown protein. This generates an approximate structure of the unknown protein in the correct unit cell and approximate phases can be calculated. Finally, an electron density map can be calculated with real amplitudes and approximate phases. The actual technique of molecular replacement therefore involves three steps:

1. Determining the orientation of the unknown molecule in its unit cell by rotation of the search model.

2. Finding the position of the oriented model in the unit cell (translation).

3. Calculating an initial set of phases from the structure factors of the known protein which can in turn be used to calculate electron density maps for improvement (or correction) of the model.

The first step (or the rotation function) determines the correct orientation of the model in the crystal lattice. This search is undertaken by finding maximum overlaps between the Patterson functions of the search and target structures. Patterson functions are maps of interatomic vectors and when the Patterson function of the model is superimposed onto that of the target, the product of the two Patterson functions should be a large value. The second step (or translation function) takes the search model which has been oriented correctly in the unit cell and uses a translation function to translate the model into the correct position.

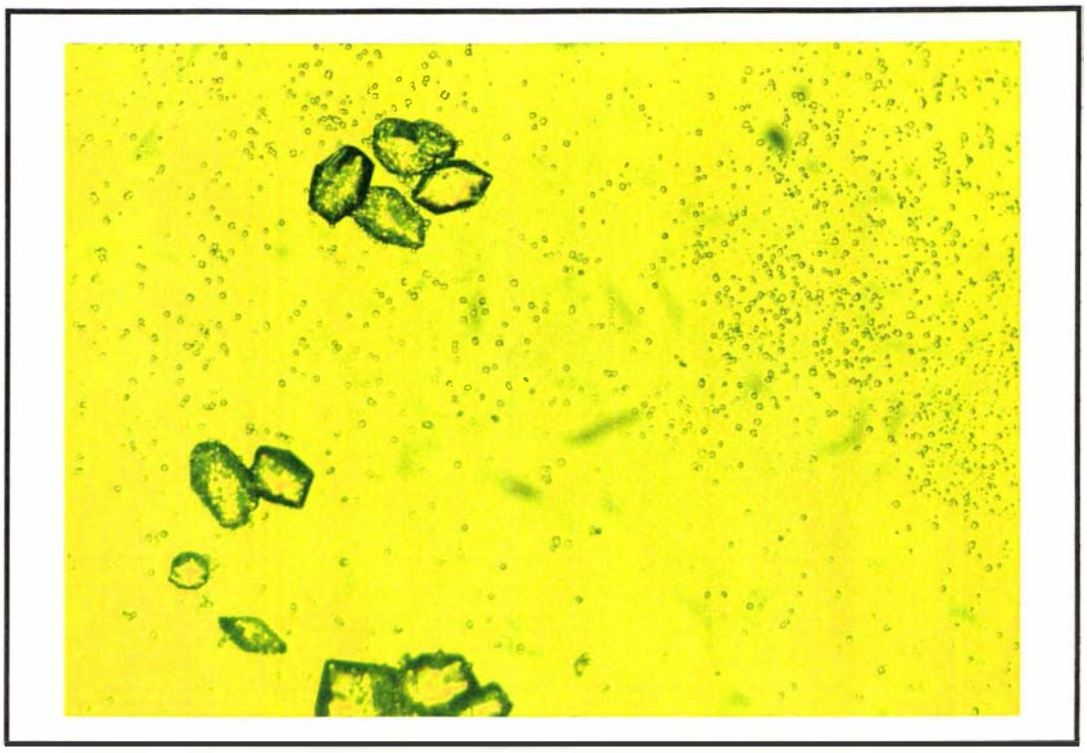

**Fig. 7.3.2** Diamond shaped crystals of the mixed anhydride estrone glucuronide-lysozyme E3 conjugate grown under the conditions described in section 7.3.2. Note the shower of microcrystals.

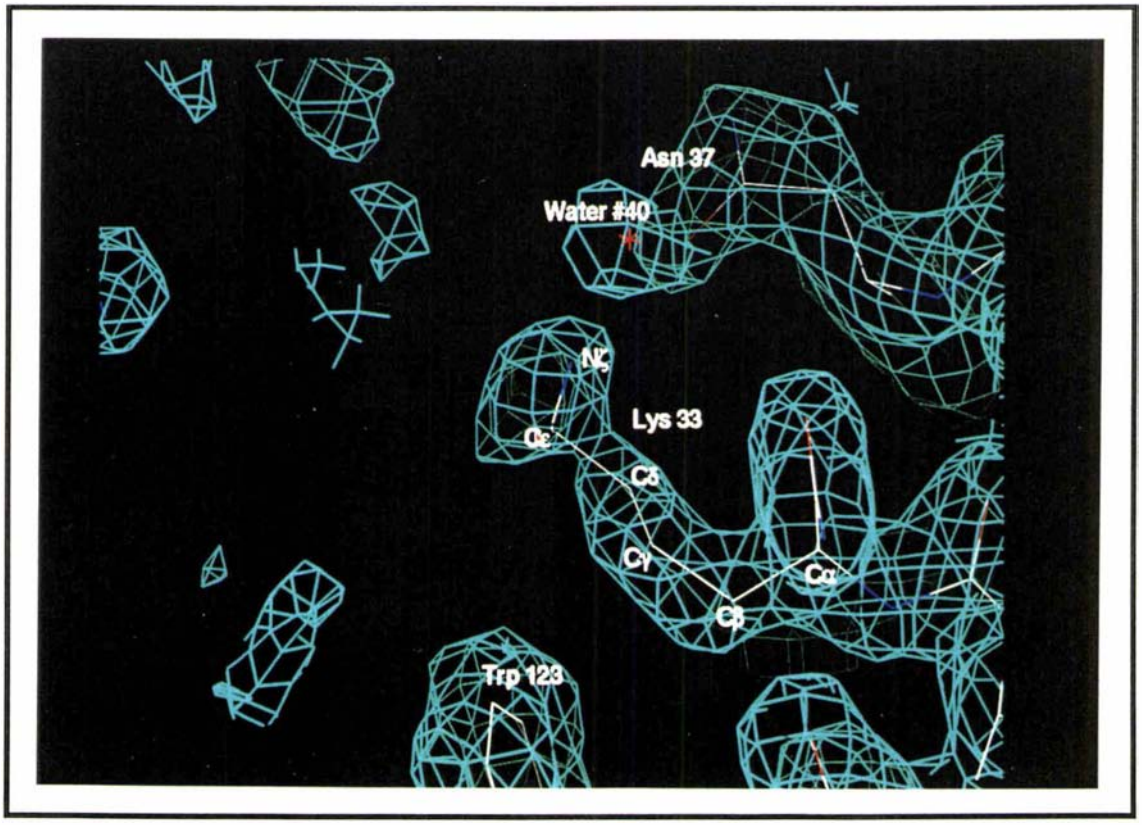


**Fig. 7.3.3** Final electron density map (contoured at a level of 0.9σ) of the estrone glucuronide-lysozyme E3 conjugate showing lysine residue 33 and the surrounding environment. Note that there is no defined electron density for the Nζ atom of lysine residue 33 and the absence of any defined electron density around lysine residue 33 where the steroid glucuronide moiety should be located. However, even though the steroid glucuronide moiety cannot be seen, there is a large hole in the electron density around lysine residue 33 where an estrone glucuronide molecule could fit in the crystal packing.

*7.3.3.5 X-PLOR*

The X-PLOR program suite (Version 3.1 A system for X-ray Crystallography and NMR (1992), Axel, T., Brünger, Yale University Press) is specifically designed for computational structural biology. X-PLOR stands for the exploration of conformational space of macromolecules restrained to regions allowed by combination of empirical energy function and experimental data. As this suggests, the program is based on an energy minimisation approach. The constant energy function is minimised by a series of gradient descent, simulated annealing, and conformational search procedures. As well as the molecular replacement system the program suite incorporates a structure refinement package.

*7.3.3.6 Results and discussion of the structure determination*

The three dimensional structure of the estrone glucuronide-lysozyme conjugate was solved using the refined X-ray coordinates for hen egg white lysozyme as determined in the tetragonal crystal form (P. D. Jeffrey, unpublished results [311]). Native lysozyme, in the tetragonal form, crystallises in the same space group as the crystal under study ($P4_32_12$ [237, 311-312]) with approximately the same unit cell dimensions (a = b = 79.1 Å, c = 37.9 Å [237, 312] v a = b = 78.5 Å, c = 39.1 Å). The coordinates for this structure were thus used directly to generate a model and refined using the software package XPLOR. All measured X-ray data from 2.10-6.00 Å consisting of 6 809 reflections were used for refinement. The reflections were divided into a test set (T) and a working set (W) where the test set was a random selection of 520 (or 7.6%) of the observed (6 809) reflections. The refinement was carried out with the working set only (6289 reflections), and the free R factor [313] was calculated using the test set of reflections where,

$$R_T^{free} = \frac{\sum_{hkl<T} | \, |Fo| - k|Fc| \, |}{\sum_{hkl<T} |Fo|}$$

where hkl<T is all of the reflections belonging to the test set T. The free R factor is therefore unbiased by the refinement procedure. This is important as the normal crystallographic R-factor can reach very low levels in the refinement of protein structural models that appear later to be incorrect because the number of model parameters is taken to high. The free R factor for the calculated three dimensional structure was 25.17% while the final R factor for the refined data was 17.35% as reported in Tables 7.3.3 and 7.3.4.

**Table 7.3.3**

Statistics for the unrefined test set of R-Axis estrone glucuronide-lysozyme reflections as a function of resolution

| Resolution (Å) | | Reflections | Free R factor (%) | Accumulative Free R factor (%) |
|---|---|---|---|---|
| Lower limit | Upper limit | | | |
| 6.00 | 3.85 | 69 | 23.87 | 23.87 |
| 3.85 | 3.20 | 70 | 23.29 | 23.60 |
| 3.20 | 2.85 | 78 | 27.10 | 24.53 |
| 2.85 | 2.61 | 56 | 22.87 | 24.31 |
| 2.61 | 2.44 | 56 | 24.19 | 24.30 |
| 2.44 | 2.30 | 71 | 27.43 | 24.65 |
| 2.30 | 2.19 | 69 | 29.19 | 25.06 |
| 2.19 | 2.10 | 51 | 27.42 | 25.17 |
| All Reflections | | 520 | | 25.17 |

**Table 7.3.4**

Statistics for the refined working set of R-Axis estrone glucuronide-lysozyme reflections as a function of resolution

| Resolution (Å) | | Reflections | R factor (%) | Accumulative R factor (%) |
|---|---|---|---|---|
| Lower limit | Upper limit | | | |
| 6.00 | 3.85 | 848 | 13.42 | 13.42 |
| 3.85 | 3.20 | 830 | 14.85 | 14.06 |
| 3.20 | 2.85 | 790 | 17.82 | 14.92 |
| 2.85 | 2.61 | 790 | 18.91 | 15.55 |
| 2.61 | 2.44 | 798 | 20.01 | 16.09 |
| 2.44 | 2.30 | 765 | 20.96 | 16.55 |
| 2.30 | 2.19 | 742 | 20.86 | 16.89 |
| 2.19 | 2.10 | 726 | 23.89 | 17.35 |
| All Reflections | | 6289 | | 17.35 |

The three dimensional molecular structure of the estrone glucuronide-lysozyme conjugate was solved and refined to 2.10 Å with a crystallographic R factor of 17.35. The structure was isomorphous with the native lysozyme structure. Unfortunately there was no electron density visible for the steroid glucuronide group which was known to be attached at lysine residue 33, even when the map was contoured at a low level (0.9σ) (Fig. 7.3.3). Although the four $CH_2$ groups of lysine residue 33 were reasonably well defined there was no ordered density for Nζ. In comparison most of the other lysine Nζ groups were better ordered than residue 33, although the Nζ group of lysine residue 97 was also not visible. In the orthorhombic $P2_12_12_1$ crystal structure of lysine methylated lysozyme solved by Rypniewski *et al.* [223], three of the lysine residues have disordered side chains (Lys 13, Lys 97, and Lys 116). Disordered lysine residues are common to many structures due to the mobile nature of the side chain.

Characterisation of the mixed anhydride E3 estrone glucuronide conjugate by mass spectroscopy had shown that only one estrone glucuronide moiety was attached, and tryptic mapping confirmed that this was attached at lysine residue 33 only (see chapter three). If we assume that the estrone glucuronide moiety is attached at lysine 33 and look at the crystal packing it is clear that there is space in the three dimensional packing for an estrone glucuronide moiety to fit near the Nζ atom of lysine 33 (Fig. 7.3.3). Despite this only very weak, disordered electron density can be seen in this area. Examination of the structure shows that it is not possible for an estrone glucuronide moiety to be attached at any of the other lysine residues as there is not enough room between the packed lysozyme molecules.

If the estrone glucuronide molecule is attached at lysine residue 33, why can we not see electron density? A possible explanation is disorder, or the ability of the lysine-estrone glucuronide moiety to adopt several conformations. Fig. 7.3.4 shows a two dimensional representation of the estrone glucuronide-lysine attachment site and the most likely positions (angles and bonds, labelled a-h) about which rotation or movement may take place.

Positions a through d can be ruled out immediately as sources of the disorder as these carbon atoms can be clearly seen in the electron density map. Rotation is possible at positions g and h, however the thermal ellipsoids drawn at the 50% probability level for the estrone glucuronide structure reported in Fig. 7.2.3 are relatively small, indicating good order and limited, if any, mobility in the crystal packing of the steroid in this structure. It is therefore unlikely that there is a great deal of rotation about these bonds in the conjugate structure, although obviously the packing of the steroid in the small organic structure is different. If this area is involved in rotation and distortion, it cannot be the

sole source of the disorder in the electron density map as electron density should be observed for the carbohydrate moiety. If the source of the disorder was position f, clear and ordered electron density should be observed for the peptide type bond between the glucuronide carboxyl group and the Nζ of the lysine residue. This leaves position e as the only real potential source of disorder. The Nζ of the lysine side chain is probably quite mobile itself and this would result in disorder of the steroid glucuronide moiety if the steroid glucuronide was not secured into place, or restricted in movement, by secondary or crystal packing interactions.

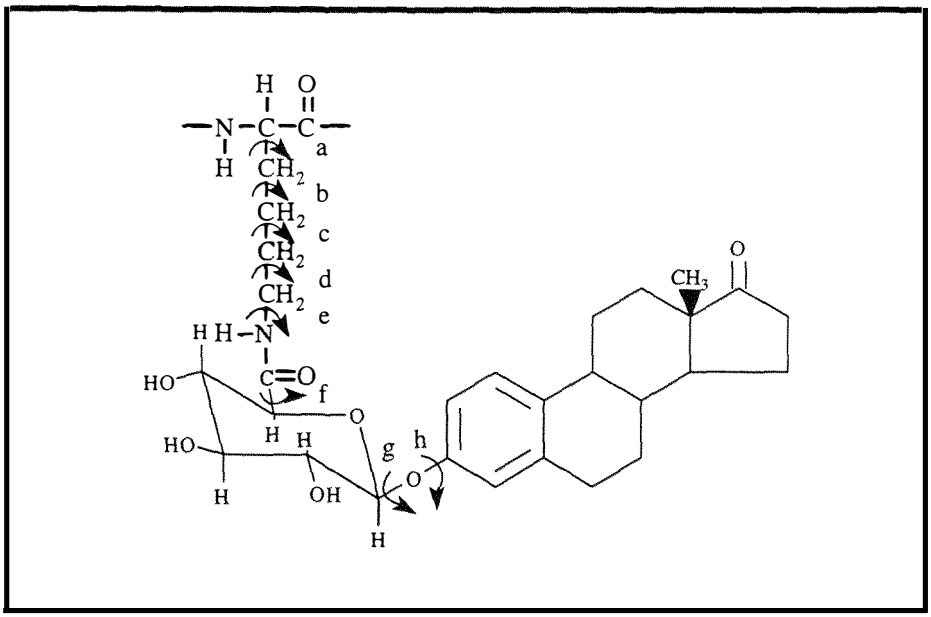


**Fig. 7.3.4** A two dimensional representation of the estrone glucuronide-lysine conjugation site. The lysine side chain is shown attached to the carboxyl group of the steroid glucuronide carbohydrate moiety *via* a peptide type bond which is rigid and has no freedom of rotation about it. The angles and bonds about which free rotation is possible are labelled a-h. Rotation about any of these bonds would lead to disorder in the three dimensional crystal structure of the estrone glucuronide-lysozyme conjugate. For details see text.

Despite the fact that the estrone glucuronide moiety could not be detected, the three dimensional structure does show that conjugation of lysozyme in this manner produces limited changes in the overall and local three dimensional structure of the enzyme. It may yet be possible to grow better and larger crystals of the estrone glucuronide-lysozyme E3 conjugate where the steroid glucuronide moiety is not so mobile. The structure of a tetragonal $P4_32_12$ lysozyme crystal has already been solved from a data set collected at 100 K and the structure shows little change from that obtained at 298 K [314]. The B-factors of side chain residues in the low temperature crystal study were lower than those from a room temperature structure indicating a more ordered structure. If larger crystals could be obtained which diffracted better than that used in the current study, it may be possible to slow down any movement of the estrone glucuronide moiety by freezing the

crystal and collecting a data set at a much lower temperature (well below 0°C) where any mobility exhibited by the steroid glucuronide would be restricted.

---

## 7.4 Crystallisation Studies of Estrone Glucuronide-Lysozyme Conjugate-Fab Immune Complexes

Although the crystal structures of many protein-antigen and small hapten molecule-antigen complexes have now been published (for example see Davies and Padlan [224] and Laver [315]), there are no examples of the crystal structures of hapten-anti-hapten antibody complexes where the hapten is conjugated to an enzyme whose activity is extensively inhibited upon the binding of the anti-hapten antibody. The three dimensional structures of all the antibody-antigen complexes solved to date have utilised the Fab fragments of monoclonal antibodies rather than the intact antibody. The reason for this is that the Fab fragment is univalent, that is to say, it can only bind one antigen molecule. However, the intact monoclonal antibody is bivalent and can bind two antigen molecules which may complicate solving any three dimensional structure. The intact monoclonal antibody is also extremely large ($M_r$ ~ 150 000) whereas the Fab fragment is only a third of this size. For these reasons the use of Fab fragments is favoured for crystallisation experiments of antigen-antibody immune complexes. Polyclonal antibodies are of no practical use in crystallisation experiments because of their inherent heterogeneity.

A three dimensional structure of the estrone glucuronide-lysozyme-anti-estrone glucuronide antibody immune complex should show the spatial requirements of such antibody binding and lead to an understanding of the precise details of the mechanism by which the enzymic activity of the enzyme conjugate is inhibited. A three dimensional structure of the immune complex would also provide the structure of the estrone glucuronide-lysozyme conjugate and allow investigation of the effect of the location and orientation of the hapten (in the enzyme conjugates) upon the binding of the anti-hapten antibodies. Further evidence on the binding requirements of the anti-hapten antibodies, in addition to the evidence discussed in chapters four and five, will aid in defining the parameters which need to be present in the successful design of enzyme systems which are likely to produce colours with the degree of inhibition shown by the lysozyme system.

### 7.4.1 Initial Crystallisation Attempts

In all crystallisation attempts the estrone glucuronide-lysozyme conjugate utilised was that described in section 7.3 above. The Fab fragments were prepared by pepsin cleavage of

an intact anti-estrone glucuronide monoclonal antibody and purified by gel filtration chromatography as described in sections 5.2.3.1-5.2.3.3. The final Fab products were pure by both gel filtration chromatographic analysis (section 5.2.3.2) and SDS-polyacrylamide gel electrophoresis (SDS-PAGE) analysis as described in section 5.2.3.3. The concentration of E1G-lysozyme conjugate used in crystallisation experiments was 10 mg/mL. The amount of Fab required to neutralise this (or form the immune complex) was calculated from the volume required to inhibit the lytic activity of a known concentration of the lysozyme conjugate by 90% as measured using the Ovarian Monitor. The Fab solution was then concentrated using a Centricon® concentration membrane device so that the addition of one volume of Fab to an equivalent volume of E1G-lysozyme conjugate would neutralise the lysozyme conjugate. Crystallisation experiments were carried out with such a mixture of Fab and E1G-lysozyme conjugate, the mix being prepared just before use each time.

As there are now a number of anti-lysozyme Fab fragment-lysozyme [199-202, 224, 229-231, 316-317] and small antigen-antibody [203, 224] three dimensional structures, the conditions under which these complexes crystallised were the starting point in an attempt to crystallise the E1G-lysozyme-Fab immune complex. All crystallisation trials were undertaken using the hanging drop method of McPherson [296] as described in section 7.3.1. Initial trials were undertaken between pH 8.02 and pH 5.50 (buffers pH 6.50-8.02, 0.1 M EPPS; pH 6.0, 0.1 M PIPES; pH 5.50, 0.1 M ammonium acetate) and polyethylene glycol (PEG) 6000 (14-20%) as the precipitant. No crystals grew under any of the conditions, although there seemed to be a relationship between pH and PEG concentration as precipitates formed at lower PEG concentrations at lower pH values.

Further crystallisation trials were undertaken between pH 6.0-8.0 and precipitant concentrations of 12-22% PEG. At pH 7.0 and 12% PEG, chunky type crystals grew such as those shown in Fig. 7.4.1. However, when these crystals were placed in an X-ray beam they diffracted very poorly and very few spots could be observed. Despite further attempts to grow larger, or more ordered crystals by varying the protein concentration, buffer, or precipitant, better crystals were not obtained.

Recently, an isoelectric focusing gel run of the Fab fragments used in the crystallisation studies, shows that despite the fact that the Fab fragments appear pure by SDS-PAGE analysis, the Fab product is actually heterogeneous. The isoelectric focusing gel shows several bands of protein whose isoelectric points are quite different. Two major populations of Fab product exist, one with a low isoelectric point (pH 5-6) and one with a much higher isoelectric point (pH 8-9). This heterogeneity observed in the Fab products is not unusual [311] (although this was not known at the time of the initial crystallisation

experiments) and is due to cleavage of the intact monoclonal antibody (when producing the Fab fragments) at more than one position. This results in several Fab families being produced which differ by having several amino acid residues more, or less, than each other and this has a vast effect on the isoelectric point of the Fab fragment produced. Such heterogeneity is very likely to prevent crystallisation of the Fab fragments.

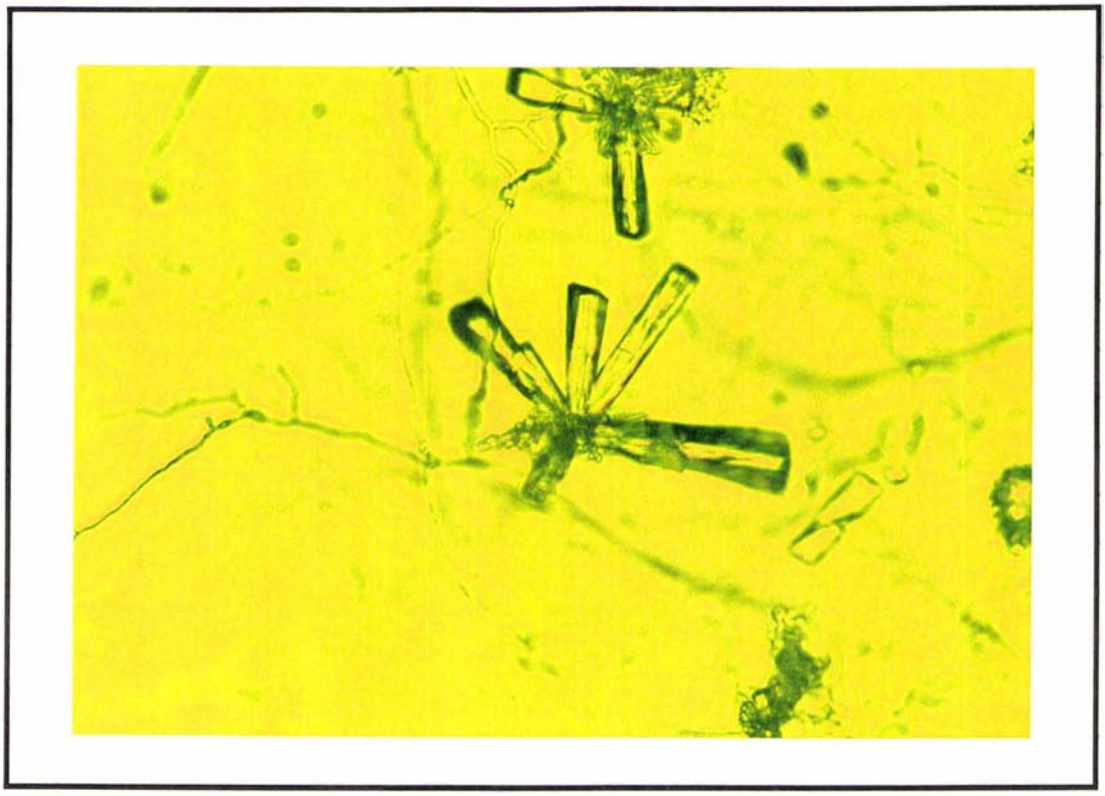

**Fig. 7.4.1** The chunky type crystals grown under conditions of 0.1 M EPPS (pH 7.0) and 12% PEG 6000 in attempts to obtain crystals of the estrone glucuronide-lysozyme-anti-estrone glucuronide Fab fragment immune complex as described in the text

### 7.4.2 Future Crystallisation Attempts

The initial focus of the crystallisation trials was on conditions under which other Fab complexes have crystallised. It is now obvious that a much wider screen of conditions will be required to find the optimum conditions under which the best estrone glucuronide-lysozyme-anti-estrone glucuronide Fab fragment complex crystals can be grown and that further purification of the Fab fragments may also be required. The flexibility of the lysine side chain as discussed in section 7.3 may prove to be a problem in attempts to crystallise the complex. Although binding of the Fab fragment to the steroid will lock the steroid in place there is no guarantee that it will have a similar effect on the lysine sidechain. For this reason future attempts at crystallisation should also focus on obtaining crystals of the steroid glucuronide-Fab complex. Future crystallisation trials should be focused towards obtaining crystals of suitable quality for X-ray diffraction studies of

both (if possible), or either of, the estrone glucuronide-lysozyme-anti-estrone glucuronide Fab immune complex or the estrone glucuronide-anti-estrone glucuronide Fab complex.

## 7.5 Conclusions

To be able to apply the technique of X-ray crystallography, good quality crystals of the molecule of interest must first be obtained which will give strong X-ray diffraction patterns when placed in an X-ray beam. The growing of good quality crystals is still somewhat of a black art which limits the utilisation and exploitation of X-ray crystallography. Unfortunately this obstacle has also proven to be a problem in the current study outlined above. However, the X-ray crystallographic study outlined above is still only in its infancy. With further trials it may be possible to obtain better quality crystals which will reveal the three dimensional structure of the estrone glucuronide conjugate moiety and the lysozyme conjugate-Fab immune complex. As the three dimensional structure of the lysozyme conjugate-Fab immune complex will also reveal the structure of the estrone glucuronide-lysozyme molecule, it is recommended that future crystallisation trials concentrate on obtaining good quality crystals of this.

# Summary

The work presented in the preceding chapters represents the most detailed analysis of a homogeneous enzyme immunoassay system undertaken to date. The importance of (1) the acylation procedure utilised in synthesising steroid glucuronide-lysozyme conjugates, (2) the purity of the conjugate material used in homogeneous enzyme immunoassay, (3) the type of antibody used in homogeneous enzyme immunoassay (polyclonal v monoclonal), (4) the spatial requirements of the antibody binding site in steroid glucuronide-lysozyme conjugates, and (5) the size of the substrate have all been determined. The results also show that the kinetic parameters must be considered if the best results are to be obtained from any homogeneous enzyme immunoassay system. The characterisation results suggested that two areas of work require further investigation.

The first of these is the continuation of X-ray crystallographic studies towards the three dimensional structure of an estrone glucuronide-lysozyme-anti-estrone glucuronide Fab fragment immune complex. Such a three dimensional structure should unambiguously show the spatial requirements of antibody binding and the mechanism by which the enzymatic activity of the enzyme conjugate is inhibited. The structure would also reveal the three dimensional structure of the estrone glucuronide-lysozyme conjugate and allow further investigation into the effect of the location and orientation of the hapten upon the binding of the anti-hapten antibodies.

The second and most exciting area of work which requires immediate attention is the testing of the assay format proposed in chapter six. This format appears the most promising yet proposed to provide a colour test immunoassay which has the accuracy, sensitivity and reliability required for the measurement of urinary steroid glucuronide levels for the delineation of the fertile period during a woman's menstrual cycle. Initially, a membrane system must be designed whereby the lysozyme conjugate can be run up the solid phase membrane as discussed in section 6.3. Following this the principles behind the proposed immunoassay format must be tested and if this is successful the assay format will have to be refined and developed so that the maximum sensitivity and precision can be obtained. If this is successful the proposed solid phase immunoassay format will offer a real alternative colour dipstick type test for the measurement of urinary steroid glucuronide levels. Such a test could have large commercial implications and be of real benefit to women in the home wishing to monitor their own fertility. Because of the simplicity of the proposed test, the assay system would be very portable and could be

used by women in their own homes without the need for technical instruction upon how to use the system. If this objective can be achieved it will represent a practical end result arising from the detailed fundamental studies of lysozyme and lysozyme conjugate structures.

# Bibliography


1. Villee, C. A., Walker, W. F., Jr., and Barnes, R. D. (1984) *General Zoology*, 6th edn., chapter 12, pp. 279, CBS College Publishing, Saunders College Publishing, Tokyo, Japan.

2. Hillier, S., Whitelaw, P., and Smyth, C. (1994) Sex steroid metabolism in the ovary, *The Biochemist* Apr/May, 22-26.

3. Collins, W. P. (1991) The evolution of reference methods to monitor ovulation, *Am. J. Obstet. Gynecol.* **6,** 1994-1996.

4. Martinez, A. R., Zinaman, M. J., Jennings, V. H., and Lamprecht, V. M. (1995) Prediction and detection of the fertile period: the markers, *Int. J. Fertil.* **40,** 139-155.

5. Wilcox, A. J., Weinberg, C. R., and Baird, D. D. (1995) Timing of sexual intercourse in relation to ovulation, *N. Engl. J. Med.* **333,** 1517-1521.

6. Adlercreutz, H., Brown, J., Collins, W., Goebelsman, U., Kellie, A., Campbell, H., Spieler, J., and Braissand, G. (World Health Organisation, Task Force on Methods for the Determination of the Fertile Period) (1982) The measurement of urinary steroid glucuronides as indices of the fertile period in women, *J. Steroid Biochem.* **17,** 695-702.

7. World Health Organisation Task Force on Methods for the Determination of the Fertile Period (1983) Temporal relationships between indices of the fertile period, *Fertil. Steril.* **39,** 647-655.

8. Cortesi, S., Fortunato, A., Marzot, E., and Soffiati, G. (1991) Simultaneous dosage of oestrone-3-glycuronide and pregnanediol-3-glycuronide in urines to monitor the fertile period in the woman, *Acta Europaea Fertilitatis* **22,** 27-31.

9. Wilson, M. A. (1980) The ovulation method of birth regulation. The latest advances for achieving or postponing pregnancy-naturally, chapter 2, pp. 3-23, Van Nostrand Reinhold Co., New York.

10. Scheele, F., and Schoemaker, J. (1996) The role of follicle-stimulating hormone in the selection of follicles in human ovaries: a survey of the literature and a proposed model, *Gynecol. Endocrinol.* **10,** 55-66.

11. Baird, D. T. (1987) A model for follicular selection and ovulation: lessons from superovulation, *J. Steroid Biochem.* **27,** 15-23.

12. Glasier, A. F., Baird, D. T., and Hillier, S. G. (1989) FSH and the control of follicular growth, *J. Steroid Biochem.* **32,** 167-170.

13. van Dessel, H. J. H. M. T., Schipper, I., Pache, T. D., van Geldorp, H., de Jong, F. H., and Fauser, B. C. J. M. (1996) Normal human follicle development: an evaluation of correlations with oestradiol, androstenedione and progesterone levels in individual follicles, *Clin. Endocrinol.* **44,** 191-198.

14. Ireland, J. J. (1987) Control of follicular growth and development, *J. Reprod. Fert.* **Suppl. 34,** 39-54.

15. Zeleznik, A. J., and Kubik, C. J. (1986) Ovarian responses in Macaques to pulsatile infusion of follicle-stimulating hormone (FSH) and luteinizing hormone: Increased sensitivity of the maturing follicle to FSH, *Endocrinology* **119,** 2025-2032.

16. Brown, J. B. (1978) Pituitary control of ovarian function - concepts derived from gonadotrophin therapy, *Austr. NZ J. Obstet. Gynaecol.* **18,** 47-54.

17. Hsueh, A. J. W., Bisack, T. A., Jia, X. C., Dahl, K. D., Fauser, B. C. J. M., Galway, A. B., Czekala, N., Pavlou, S. N., Papkov, H., Keene, J., and Boime, I. (1989) Granulosa cells as hormone targets: the role of biologically active follicle stimulating hormone in reproduction, *Rec. Pro. Horm. Res.* **45,** 209-273.

18. McNatty, K. P. (1981) Hormonal correlates of follicular development in the human ovary, *Aust. J. Biol. Sci.* **34,** 249-268.

19. Picton, H. M., and McNeilly, A. S. (1991) Evidence to support a follicle stimulating hormone threshold theory for follicle selection in ewes chronically treated with gonadotropin-releasing hormone agonist, *J. Reprod. Fertil.* **93,** 43-51.

20. Schoemaker, J., van Weissenbruch, M. M., Scheele, F., and van der Meer, M. (1993) The FSH threshold concept in clinical ovulation induction, *Baillieres Clin. Obstet. Gynaecol.* **7,** 297-308.

21. van Weissenbruch, M. M., Schoemaker, H. C., Drexhage, H. A., and Schoemaker, J. (1993) Pharmacodynamics of human menopausal gonadotropin (HMG) and follicle stimulating hormone (FSH). The importance of the FSH concentration in initiating follicular growth in polycystic ovary-like disease, *Hum. Reprod.* **6,** 813-821.

22. Yen, S. S. C., and Tsai, C. C. (1971) The biphasic pattern in the feedback action of ethinyl estradiol on the release of pituitary FSH and LH, *J. Clin. Endocinol. Metab.* **33,** 882-887.

23. Collins, W. P. (1989) Biochemical indices of potential fertility, *Int. J. Gynecol. Obstet.* **Suppl. 1,** 35-43.

24. Burger, H. G. (1989) Estradiol: the physiological basis of the fertile period, *Int. J. Gynecol. Obstet.* **Suppl. 1,** 5-9.

25. Hoff, J. D., Quigley, M. E., and Yen, S. S. C. (1983) Hormonal dynamics at midcycle: a reevaluation, *J. Clin. Endocrinol. Metab.* **57,** 792-796.

26. Liu, J. H., and Yen, S. S. C. (1983) Induction of midcycle gonadotropin surge by ovarian steroids in women: a critical evaluation, *J. Clin. Endocrinol. Metab.* **57,** 797-802.

27. Karsch, F. J. (1987) Central actions of ovarian steroids in the feedback regulation of pulsatile secretion of luteinising hormone, *Ann. Rev. Physiol.* **49,** 365-382.

28. Austin, C. R. (1975) Sperm fertility, viability and persistence in the female tract, *J. Reprod. Fertil. Suppl.* **22,** 75-89.

29. World Health Organisation Task Force on Methods for the Determination of the Fertile Period (1980) Temporal relationships between ovulation and defined changes in the concentration of plasma estradiol-17β, luteinizing hormone, follicle-stimulating hormone, and progesterone. I. Probit analysis, *Am. J. Obstet. Gynecol.* **138,** 383-390.

30. Bhavnani, B. R., and Woolever, C. A. (1979) Alternate pathways of steroid biosynthesis and the origin, metabolism, and biological effects of ring B unsaturated estrogens, in *Steroid Biochemistry* (Hobkirk, R., ed.) Vol. II, chapter 1, pp. 1-50, CRC Press, Inc., Florida.

31. Stryer, L. (1988) Biosynthesis of membrane lipids and steroid hormones, in *Biochemistry*, 3rd edn., chapter 23, pp. 402, W. H. Freeman and Company, New York.

32. Lehoux, J. -G. (1979) Factors controlling the biosynthesis of aldosterone, in *Steroid Biochemistry* (Hobkirk, R., ed.) Vol. II, chapter 2, pp. 55-56, CRC Press, Inc., Florida.

33. Fishman, J. (1982) Biochemical mechanism of aromatization, *Cancer Research* **Suppl. 42,** 3277s-3280s.

34. Musey, P. I., Wright, K., Preedy, J. R. K., and Collins, D. C. (1979) Formation and metabolism of steroid conjugates: effect of conjugation on excretion and tissue distribution, in *Steroid Biochemistry* (Hobkirk, R., ed.) Vol. II, chapter 3, pp. 81-131, CRC Press, Inc., Florida.

35. Serra, G. B. (ed.) (1983) *Comprehensive Endocrinology - The Ovary*, pp. 432, Raven Press, New York.

36. Acros, M., Gurpide, E., Vande Wiele, R. L., and Lieberman, S. (1964) Precursors of urinary pregnanediol and their influence on the determination of the secretory rate of progesterone, *J. Clin. Endocrinol. Metab.* **24,** 237-245.

37. Munro, C. J., Stabenfeldt, G. H., Cragun, J. R., Addiego, L. A., Overstreet, J. W., and Lasley, B. L. (1991) Relationship of serum estradiol and progesterone concentrations to the excretion profiles of their major urinary metabolites as measured by enzyme immunoassay and radioimmunoassay, *Clin. Chem.* **37,** 838-844.

38. Hobrick, P., and Nilsen, M. (1974) Early urinary conjugated metabolites of intravenously injected (6.7-$^{3}$H)-estradiol-17β in the human subject, *J. Steroid Biochem.* **5,** 15-20.

39. Musey, P. I., Green, R. N., and Hobkirk, R. (1972) The role of an enterohepatic system in the metabolism of 17β-E2-17G in the human female, *J. Clin. Endocrin. Metab.* **35,** 448-457.

40. Brown, J. B. (1955) Urinary excretion of estrogens during the menstrual cycle, *Lancet* **1,** 320-323.

41. Rae, M. H., Mole, P. A., and Paterson, C. R. (1988) Evaluation of urinary oestrogen assays after the menopause and their potential for screening, *Clin. Chim. Acta* **176,** 71-82.

42. Lasley, B. L., Shideler, S. E., and Munro, C. J. (1991) A prototype for ovulation detection: pros and cons, *Am. J. Obstet. Gynecol.* **165,** 2003-2007.

43. Queenan, J. T., O'Brien, G. D., Baine, L. M., Simpson, J., Collins, W. P., and Campbell, S. (1980) Ultrasound scanning of ovaries to detect ovulation in women, *Fertil. Steril.* **34,** 99-105.

44. World Health Organisation (WHO) (1980) Special programme of research development and research training in human reproduction, ninth annual report, WHO December (1980).

45. World Health Organisation (1988) Natural family planning. A guide to provision of services, chapter 1, pp. 1, World Health Organisation, Geneva, Switzerland.

46. Ogino, K. (1930) Ovulationstermin und Konzephonstermin, *Zentralblatt fur Gynaek.* **54,** 464-479.

47. Gross, B. A. (1989) Clinical indicators of the fertile period, *Int. J. Gynecol. Obstet.* **Suppl. 1,** 45-51.

48. Baird, D. T., and Fraser, I. S. (1975) Concentrations of estrone and estradiol 17β in follicular fluid and ovarian venous blood of women, *Clin. Endocrinol.* **4,** 259-266.

49. Baker, T. S., Jennison, K., and Kellie, A. E. (1980) A possible method for the detection of ovulation and the determination of the duration of the fertile period, *J. Steroid Biochem.* **12,** 411-415.

50. Billings, E. L., Billings, J. J., Brown, J. B., and Burger, H. G. (1972) Symptoms and hormonal changes accompanying ovulation, *Lancet* **1,** 282-284.

51. Collins, W. P., Collins, P. O., Kilpatrick, M. J., Manning, P. A., Pike, J. M., and Tyler, J. P. (1979) The concentrations of urinary oestrone-3-glucuronide, LH and pregnanediol-3-glucuronide as indices of ovarian function, *Acta Endocrinol (Copenh)* **90,** 336-348.

52. Adlercreutz, H., Lehtinen, T., and Kairento, A. -L. (1980) Prediction of ovulation by urinary estrogen assays, *J. Steroid Biochem.* **12,** 395-401.

53. Stanczyk, F. Z., Miyakawa, I., and Goebelsman, U. (1980) Direct radioimmunoassay of urinary estrogen and pregnanediol glucuronides during menstrual cycles, *Am. J. Obstet. Gynecol.* **137,** 443-450.

54. Blackwell, L. F., and Brown, J. B. (1992) Application of time-series analysis for the recognition of increases in urinary estrogens as markers for the beginning of the potentially fertile period, *Steroids* **57,** 554-562.

55. Lewis, J. G., Manley, L., Whitlow, J. C., and Elder, P. A. (1994) Re-examining steroid hormone metabolites as ovulation markers using monoclonal antibodies, *Steroids* **59,** 288-291.

56. Trigg, D. W. (1964) Monitoring a forecasting system, *Operat. Res. Q.* **15,** 271-274.

57. Blackwell, L. F. (personal communication).

58. Kesner, J. S., Wright, D. M., Schrader, S. M., Chin, N. W., and Krieg, E. F., Jr. (1992) Methods of monitoring menstrual function in field studies: efficacy of methods, *Reprod. Toxicol.* **6,** 385-400.

59. Marrian, C. F. (1930) The chemistry of oestrin. 4) The chemical nature of crystalline preparations, *Biochem. J.* **24,** 1021-1030.

60. Astwood, E. B. (1938) A six hour assay for the quantitative determination of estrogen, *Endocrinology* **23,** 25-31.

61. Kober, S. (1938) The colorimetric estimation of the oestrogenic hormones. 2) Oestrone, *Biochem. J.* **32,** 357-365.

62. Brown, J. B. (1955) A chemical method for the determination of estriol, oestrone and oestradiol in human urine, *Biochem. J.* **60,** 185-193.

63. Hashimoto, Y., and Neeman, M. (1963) Isolation and characterization of estriol 16α-glucosiduronic acid from human pregnancy urine, *J. Biol. Chem.* **238,** 1273-1282.

64. Murphy, B. P., Engelberg, W., and Pattee, C. J. (1963) Simple method for the determination of plasma corticoids, *J. Clin. Endocrinol. Metab.* **23,** 293-300.

65. Abraham, G. E. (1969) Solid-phase radioimmunoassay of estradiol-17β, *J. Clin. Endocrinol. Metab.* **29,** 866-870.

66. van Weemen, B. K., Bosch, A. M. G., Dawson, E. C., and Schuurs, A. H. W. M. (1979) Enzyme-immunoassay of steroids: possibilities and pitfalls, *J. Steroid Biochem.* **11,** 147-151.

67. Ji, A. J., Nunez, M. F., Machacek, D., Ferguson, J. E., Iossi, M. F., Kao, P. C., and Landers, J. P. (1995) Separation of urinary estrogens by micellar electrokinetic chromatography, *J. Chromatogr. B* **669,** 15-26.

68. Gosling, J. P. (1990) A decade of development in immunoassay methodology, *Clin. Chem.* **36,** 1408-1427.

69. Hage, D. S. (1993) Immunoassays, *Anal. Chem.* **65,** 420-424.

70. Kellie, A. E. (1975) The radioimmunoassay of steroid conjugates, *J. Steroid Biochem.* **6,** 277-281.

71. Baker, T. S., Jennison, K. M., and Kellie, A. E. (1979) The direct radioimmunoassay of estrogen glucuronides in human female urine, *Biochem. J.* **177,** 729-738.

72. Samarajerwa, P., Cooley, G., and Kellie, A. E. (1979) The radioimmunoassay of pregnanediol-3α-glucuronide, *J. Steroid Biochem.* **11,** 1165-1171.

73. Schiphorst, L. E. M., Collins, W. P., and Royston, J. P. (1985) An estrogen test to determine the times of potential fertility in women, *Fertil. Steril.* **44,** 328-334.

74. Luppa, P., Hauck, S., Schwab, I., Birkmayer, C., and Hauptmann, H. (1995) 6α-biotinylated estrone: novel tracer in competitive chemiluminescence immunoassay of estrone in serum, *Clin. Chem.* **41,** 564-570.

75. Kohen, F., Kim, J. B., Barnard, G., and Linder, H. R. (1980) An assay for urinary estriol-16α-glucuronide based on antibody-enhanced chemiluminescence, *Steroids* **36,** 405-419.

76. Eshhar, Z., Kim, J. B., Barnard, G., and Collins, W. P. (1981) Use of monoclonal antibodies to pregnanediol-3α-glucuronide for the development of a solid phase chemiluminescence immunoassay, *Steroids* **38,** 89-109.

77. Burd, J. F., Wong, R. C., Feeney, J. E., Carrico, R. J., and Boguslaski, R. C. (1977) Homogeneous reactant-labelled fluorescent immunoassay for therapeutic drugs exemplified by gentamicin determination in human serum, *Clin. Chem.* **23,** 1402-1408.

78. Barnard, G., Kohen, F., Mikola, H., and Lövgren, T. (1989) Measurement of estrone-3-glucuronide in urine by rapid, homogeneous time-resolved fluoroimmunoassay, *Clin. Chem.* **35,** 555-559.

79. Barnard, G., O'Reilly, C., Dennis, K., and Collins, W. (1989) A nonseparation, time-resolved fluoroimmunoassay to monitor ovarian function and predict potential fertility in women, *Fertil. Steril.* **52,** 60-65.

80. Karsilayan, H., Kohen, F., and Barnard, G. (1992) Progress in the development of sensitive time-resolved fluorescence immunoassays for the measurement of oestradiol in serum, *Commun. Lab. Med.* **2,** 39-47.

81. Mikola, H., Sundell, A. -C., and Hänninen, E. (1993) Labeling of estradiol and testosterone alkyloxime derivatives with a europium chelate for time-resolved fluoroimmunoassays, *Steroids* **58,** 330-334.

82. Kesner, J. S., Knecht, E. A., Krieg, E. F., Jr., Barnard, G., Mikola, H. J., Kohen, F., Gani, M. M., and Coley, J. (1994) Validations of time-resolved fluoroimmunoassays for urinary estrone 3-glucuronide and pregnanediol 3-glucuronide, *Steroids* **59,** 205-211.

83. Barnard, G., Osher, J., Lichter, S., Gayer, B., De Boever, J., Limor, R., Ayalon, D., and Kohen, F. (1995) The measurement of progesterone in serum by a non-competitive idiometric assay, *Steroids* **60,** 824-829.

84. Schuurs, A. H. W. M., and van Weemen, B. K. (1980) Enzyme-immunoassay: a powerful analytical tool, *J. Immunoassay* **1,** 229-249.

85. Porstmann, T., and Kiessig, S. T. (1992) Enzyme immunoassay techniques. An overview, *J. Immunol. Methods* **150,** 5-21.

86. Silván, G., Illera, J. C., and Illera, M. (1993) Determination of follicular fluid estradiol levels by enzyme-linked immunosorbent assay, *Steroids* **58,** 324-329.

87. Cuisset, B., Pradelles, P., Kime, D. E., Kühn, E. R., Babin, P., Davail, S., and Le Menn, F. (1994) Enzyme immunoassay for 11-ketotestosterone using acetylcholinesterase as label: application to the measurement of 11-ketotestosterone in plasma of Siberian sturgeon, *Comp. Biochem. Physiol.* **108C,** 229-241.

88. Chatterton, R. T. (1982) Method of ovulation detection and indicator strip for use therein, Eur. Pat. Appl. EP 0 075 193 A1 (*Chem. Abstr.* **99,** 17314x).

89. Brown, J. B., Blackwell, L. F., Cox, R. I., Holmes, J. M., and Smith, M. A. (1988) Chemical and homogeneous enzyme immunoassay methods for the measurement of estrogens and pregnanediol and their glucuronides in urine, *Prog. Clin. Biol. Res.* **285,** 119-138.

90. Dhar, T. K., Samanta, A. K., and Ali, E. (1988) Homogeneous enzyme immunoassay of estradiol using estradiol-3-O-carboxymethyl ether as hapten, *Steroids* **51,** 519-526.

91. Brown, J. B., Blackwell, L. F., Holmes, J., and Smyth, K. (1989) New assays for identifying the fertile period, *Int. J. Gynecol. Obstet.* **Suppl. 1,** 111-122.

92. Lewis, J. G., Clifford, J. K., and Elder, P. A. (1990) Monoclonal antibodies to pregnanediol-3-glucuronide: application to a direct enzyme-linked immunosorbent assay of urine, *Steroids* **55,** 314-318.

93. Sauer, M. V., and Paulson, R. J. (1991) Utility and predictive value of a rapid measurement of urinary pregnanediol glucuronide by enzyme immunoassay in an infertility practice, *Fertil. Steril.* **56,** 823-826.

94. Bouve, J., De Boever, J., Leyseele, D., Bosmans, E., Dubois, P., Kohen, F., and Vandekerckhove, D. (1992) Direct enzyme immunoassay of estradiol in serum of women enrolled in an in vitro fertilization and embryo transfer program, *Clin. Chem.* **38,** 1409-1413.

95. De Lauzon, S., Desfosses, B., Christeff, N., Hanquez, C., and Cittanova, N. (1992) A direct dot-enzyme immunoassay to detect human ovulation, *J. Steroid Biochem. Molec. Biol.* **42,** 223-228.

96. Wergeland, R., Mørkrid, L., and Åbyholm, T. (1993) Evaluation of the Abbott IMx estradiol assay, *J. Clin. Immunoassay* **16,** 238-243.

97. O'Rorke, A., Kane, M. M., Gosling, J. P., Tallon, D. F., and Fottrell, P. F. (1994) Development and validation of a monoclonal antibody enzyme immunoassay for measuring progesterone in siliva, *Clin. Chem.* **40,** 454-458.

98. Henderson, K. M., Camberis, M., and Hardie, A. H. (1995) Evaluation of antibody- and antigen-coated enzymeimmunoassays for measuring oestrone-3-glucuronide concentrations in urine, *Clin. Chim. Acta* **243,** 191-203.

99. Mares, A., De Boever, J., Osher, J., Quiroga, S., Barnard, G., and Kohen, F. (1995) A direct non-competitive idiometric enzyme immunoassay for serum oestradiol, *J. Immunol. Methods* **181,** 83-90.

100. Mares, A., De Boever, J., Stans, G., Bosmans, E., and Kohen, F. (1995) Synthesis of a novel biotin-estradiol conjugate and its use for the development of a direct, broad range enzyme immunoassay for plasma estradiol, *J. Immunol. Methods* **183,** 211-219.

101. Miller, P. B., and Soules, M. R. (1996) The usefulness of a urinary LH kit for ovulation prediction during menstrual cycles of normal women, *Obstet. Gynecol.* **87,** 13-17.

102. Kirkpatrick, J. F., Kincy, V., Bancroft, K., Shideler, S. E., and Lasley, B. L. (1991) Oestrous cycle of the North American bison (*Bison bison*) characterized by urinary pregnanediol-3-glucuronide, *J. Reprod. Fert.* **93,** 541-547.

103. Chapeau, C., King, G. J., and Elmar, B. (1993) Fecal estrogens in one primate and several ungulate species during various reproductive stages, *Anim. Reprod. Sci.* **34,** 167-175.

104. Hatzidakis, G., Katrakili, K., and Krambovitis, E. (1993) Development of a direct and specific enzymeimmunoassay for the measurement of oestrone sulfate in bovine milk, *J. Reprod. Fert.* **98,** 235-240.

105. Jenkins, S. H. (1992) Homogeneous enzyme immunoassay, *J. Immunol. Methods* **150,** 91-97.

106. Schneider, R. S., Lindquist, P., Wong, E. T., Rubenstein, K. E., and Ullman, E. F. (1973) Homogeneous enzyme immunoassay for opiates in urine, *Clin. Chem.* **19,** 821-825.

107. Rubenstein, K. E., Schneider, R. S., and Ullman, E. F. (1972) "Homogeneous" enzyme immunoassay. A new immunological technique, *Biochem. Biophys. Res. Comm.* **47,** 846-851.

108. Brown, J. B., Holmes, J., and Barker, G. (1991) Use of the Home Ovarian Monitor in pregnancy avoidance, *Am. J. Obstet. Gynecol.* **165,** 2008-2011.

109. Daviaud, J., Fournet, D., Ballongue, C., Guillem, G. -P., Leblanc, A., Casellas, C., and Pau, B. (1993) Reliability and feasibility of pregnancy home-use tests: laboratory validation and diagnostic evaluation by 638 volunteers, *Clin. Chem.* **39,** 53-59.

110. Unipath, (1994) The UNIPATH Personal Contraceptive System, UNIPATH promotional brochure, Unipath Ltd., Bedford, UK.

111. Rajkowski, K. M., and Cittanova, N. (1981) The efficiency of different coupling procedures for the linkage of oestriol-16α-glucuronide, oestrone-3-glucuronide and pregnanediol-3α-glucuronide to four different enzymes, *J. Steroid Biochem.* **14,** 861-866.

112. Stabenfeldt, G. H., Daels, P. F., Munro, C. J., Kindahl, H., and Hughes, J. P. (1991) An oestrogen conjugate enzyme immunoassay for monitoring pregnancy in the mare: limitations of the assay between days 40 and 70 of gestation, *J. Reprod. Fert.* **Suppl 44,** 37-44.

113. March, S. C., and Shlpchandler, M. T. (1984) Alkaline phosphatase labelled steroid hormones glucuronides, Eur. Pat. Appl. EP 114 615 A2.

114. Brown, J. B., Blackwell, L. F., Billings, J. J., Conway, B., Cox, R. I., Garrett, G., Holmes, J. M., and Smith, M. A. (1987) Natural family planning, *Am. J. Obstet. Gynecol.* **157,** 1082-1089.

115. Thornton, S. J., Pepperell, R. J., and Brown, J. B. (1990) Home monitoring of gonadotrophin ovulation induction using the Ovarian Monitor, *Fertility and Sterility* **54,** 1076-1082.

116. Erlanger, B. F., Borek, F., Beiser, S. M., and Lieberman, S. (1959) Steroid-protein conjugates II: Preparation and characterisation of conjugates of bovine serum albumin and progesterone deoxycorticosterone and estrone, *J. Biol. Chem.* **234,** 1090-1094.

117. Canfield, R. E. (1963) The amino acid sequence of egg white lysozyme, *J. Biol. Chem.* **238,** 2698-2707.

118. Ramanadham, M., Sieker, L. C., and Jensen, L. H. (1990) Refinement of triclinic lysozyme: II. The method of stereochemically restrained least squares, *Acta Cryst.* **B46,** 63-69.

119. Gani, M., Coley, J., Piron, J., Humphreys, A. S., Arevalo, J., Wilson, I. A., and Taussig, M. J. (1994) Monoclonal antibodies against progesterone: effect of steroid-carrier coupling position on antibody specificity, *J. Steroid Biochem. Molec. Biol.* **48,** 277-282.

120. Habeeb, A. F. S. A., and Atassi, M. Z. (1970) Enzymic and immunochemical properties of lysozyme. Evaluation of several amino group reversible blocking reagents, *Biochemistry* **9,** 4939-4944.

121. Habeeb, A. F. S. A., and Atassi, M. Z. (1971) Enzymic and immunochemical properties of lysozyme-V Derivatives modified at lysine residues by guanidination, acetylation, succinylation or maleylation, *Immunochemistry* **8,** 1047-1059.

122. Exley, D., and Abuknesha, R. (1977) The preparation and purification of a β-D-galactosidase-oestradiol-17β conjugate for enzyme immunoassay, *FEBS Lett.* **79,** 301-304.

123. Rubenstein, K. E., and Ullman, E. F. (1974) Enzyme amplification assay, U.S Patent 3, 817, 837.

124. Still, W. C., Kahn, M., and Mitra, A. (1978) Rapid chromatographic technique for preparative separations with moderate resolution, *J. Org. Chem.* **43,** 2923-2925.

125. Bollenback, G. N., Long, J. W., Benjamin, D. G., and Lindquist, J. A. (1955) The synthesis of aryl-D-glucopyranosiduronic acids, *J. Am. Chem. Soc.* **77,** 3310-3315.

126. Conrow, R. B., and Bernstein, S. (1971) Steroid conjugates. VI. An improved Koenigs-Knorr synthesis of aryl glucuronides using cadmium carbonate, a new and effective catalyst, *J. Org. Chem.* **36,** 863-870.

127. Mattox, V. R., Goodrich, J. E., and Vrieze, W. D. (1969) Synthesis of C-21 glucosiduronates of cortisone and related corticosteroids, *Biochemistry* **8,** 1188-1199.

128. Numazawa, M., Nagaoka, M., Tsuji, M., and Osawa, Y. (1983) Novel and efficient synthesis of estriol and its 16-glucuronide *via* 2,4,16α-tribromoestrone, *J. Chem. Soc. Perkin Trans.* **I,** 121-125.

129. Elce, J. S., Carpenter, J. G. D., and Kellie, A. E. (1967) The synthesis of estrogen monoglucuronides, *J. Chem. Soc.* **(C),** 542-550.

130. Remmele, R. L., Jr., and Stushnoff, C. (1994) Low-temperature IR spectroscopy reveals four stages of water loss during lyophilization of hen egg white lysozyme, *Biopolymers* **34,** 365-370.

131. Habeeb, A. F. S. A. (1968) Microheterogeneity of human serum albumin: evidence for differences in reducibility of disulfide linkages, *Can. J. Biochem.* **46,** 789-795.

132. Sashidhar, R. B., Capoor, A. K., and Ramana, D. (1994) Quantitation of ε-amino group using amino acids as reference standards by trinitrobenzene sulfonic acid. A simple spectrophotometric method for the estimation of hapten to carrier protein ratio, *J. Immunol. Methods* **167,** 121-127.

133. Fields, R. (1972) The rapid determination of amino groups with TNBS, *Methods in Enzymology* **25,** 464-468.

134. Brown, J. B., MacLeod, S. C., MacNaughtan, C., Smith, M. A., and Smyth, B. (1968) A rapid method for estimating estrogens in urine using a semi-automatic extractor, *J. Endocrinol.* **42,** 5-15.

135. Wu, Y., and Blackwell, L. F. (1993) The synthesis of estriol 16- and 17-monoglucuronide from estriol, *Steroids* **58,** 452-456.

136. Lemieux, R. U., Hendriks, K. B., Stick, R. V., and James, K. (1975) Halide ion catalyzed glycosidation reactions. Syntheses of α-linked disaccharides, *J. Am. Chem. Soc.* **97,** 4056-4062.

137. Wallace, J. E., and Schroeder, L. R. (1977) Koenigs-Knorr reactions. Part 3. Mechanistic study of mercury(II) cyanide promoted reactions of 2-O-acetyl-3,4,6-tri-O-methyl-α-D-glucopyranosyl bromide with cyclohexanol in benzene-nitromethane, *J. Chem. Soc. Perkin Trans.* **II,** 795-802.

138. Banoub, J., and Bundle, D. R. (1979) 1,2-orthoacetate intermediates in silver trifluoromethanesulphonate promoted Koenigs-Knorr synthesis of disaccharide glycosides, *Can. J. Chem.* **57,** 2091-2097.

139. Garegg, P. J., Konradsson, P., Kvarnström, I., Norberg, T., Svensson, S. C. T., and Wigilius, B. (1985) Studies on Koenigs-Knorr glycosidations, *Acta Chem. Scand. B* **39,** 569-577.

140. Sehgal, D., and Vijay, I. K. (1994) A method for the high efficiency of water-soluble carbodiimide-mediated amidation, *Anal. Biochem.* **218,** 87-91.

141. Verhamme, I. M. A., Van Dedem, G. W. K., and Lauwers, A. R. (1988) Ionic-strength-dependent substrate inhibition of the lysis of *Micrococcus luteus* by hen egg-white lysozyme, *Eur. J. Biochem.* **172,** 615-620.

142. Maeda, Y., Koga, H., Yamada, H., Ueda, T., and Imoto, T. (1995) Effective renaturation of reduced lysozyme by gentle removal of urea, *Protein Eng.* **8,** 201-205.

143. Henry, M. P. (1990) High-performance ion-exchange chromatography of proteins: A review of methods and mechanisms, in *High Performance Liquid Chromatography In Biotechnology* (Hancock, W. S., ed.) chapter 10, pp. 224, J. Wiley and Sons, New York, NY.

144. Kopaciewicz, W., Rounds, M. A., Fausnaugh, J., and Regnier, F. E. (1983) Retention model for high-performance ion-exchange chromatography, *J. Chromatogr.* **266,** 3-21.

145. Kopaciewicz, W., and Regnier, F. E. (1986) Synthesis of cation-exchange stationary phase using an absorbed polymeric coating, *J. Chromatogr.* **358,** 107-118.

146. Boyd, S., and Yamazaki, H. (1994) Use of polyvinyl alcohol as a stabilizer of peroxidase-antibody conjugate for enzyme immunoassay, *Biotechn. Techn.* **8,** 123-128.

147. Gibson, T. D., Hulbert, J. N., and Woodward, J. R. (1993) Preservation of shelf life of enzyme based analytical systems using a combination of sugars, sugar alcohols and cationic polymers or zinc ions, *Anal. Chim. Acta* **279,** 185-192.

148. Gibson, T. D., Hulbert, J. N., Parker, S. M., Woodward, J. R., and Higgins, I. J. (1992) Extended shelf life of enzyme-based biosensors using a novel stabilization system, *Biosensors and Bioelect.* **7,** 701-708.

149. Gibson, T. D., Higgins, I. J., and Woodward, J. R. (1992) Stabilization of analytical enzymes using a novel polymer-carbohydrate system and the production of a stabilized, single reagent for alcohol analysis, *Analyst* **117,** 1293-1297.

150. Maeda, Y., Ueda, T., Yamada, H., and Imoto, T. (1994) The role of net charge on the renaturation of reduced lysozyme by the sulfhydryl-disulfide interchange reaction, *Protein Engng* **7,** 1249-1254.

151. Lee, C. -L., Atassi, M. Z., and Habeeb, A. F. S. A. (1975) Enzymic and immunochemical properties of lysozyme IX. Conformation and immunochemistry of derivatives succinylated at certain lysine residues, *Biochim. Biophys. Acta* **400,** 423-432.

152. Suckau, D., Mak, M., and Przybylski, M. (1992) Protein surface topology-probing by selective chemical modification and mass spectrometric peptide mapping, *Proc. Natl. Acad. Sci. USA* **89,** 5630-5634.

153. Burnens, A., Demotz, S., Corradin, G., Binz, H., and Bosshard, H. R. (1987) Epitope mapping by chemical modification of free and antibody-bound protein antigen, *Science* **235,** 780-783.

154. Riordan, J. F., and Vallee, B. L. (1972) Acetylation, in Enzyme structure Part B, Section VIII. Modification reactions (eds. Hirs, C. H. W., and Timasheff, S. N.) *Methods Enzymol.* **25,** 494-499.

155. Hosoda, H., Tsukamoto, R., and Nambara, T. (1989) Sensitivity of steroid enzyme immunoassays. Comparison of four label enzymes in an assay system using a monoclonal anti-steroid antibody, *Chem. Pharm. Bull.* **37,** 1834-1837.

156. Hosoda, H., Fukuda, K., and Gotoh, Y. (1991) Enzyme labeling in steroid immunoassays. Comparison of the *p*-nitrophenyl ester and N-succinimidyl ester methods, *Chem. Pharm. Bull.* **39,** 2373-2377.

157. Charbonneau, H. (1989) Strategies for obtaining partial amino acid sequence data, in *A Practical Guide to Protein and Peptide Purification for Microsequencing*, (Matsudaira, P. T., ed.) Chapter 1, pp. 21, Academic Press, San Diego.

158. Reisfeld, R. A., Lewis, U. J., and Williams, D. E. (1962) Disk electrophoresis of basic proteins and peptides on polyacrylamide gels, *Nature* **195,** 281-283.

159. Medrano, J. F., and Sharrow, L. (1989) Milk protein typing of bovine mammary gland tissue used to generate a complementary deoxyribonucleic acid library, *J. Dairy Sci.* **72,** 3190-3196.

160. Harwig, S. S. L., Chen, N. P., Park, A. S. K., and Lehrer, R. I. (1993) Purification of cysteine-rich bioactive peptides from leukocytes by continuous acid-urea-polyacrylamide gel electrophoresis, *Anal. Biochem.* **208,** 382-386.

161. Takahashi, N., and Hirose, M. (1990) Determination of sulfhydryl groups and disulfide bonds in a protein by polyacrylamide gel electrophoresis, *Anal. Biochem.* **188,** 359-365.

162. Hirose, M., Takahashi, N., Oe, H., and Doi, E. (1988) Analyses of intramolecular disulfide bonds in proteins by polyacrylamide gel electrophoresis following two-step alkylation, *Anal. Biochem.* **168,** 193-201.

163. Rutherfurd, K. J., Chen, S., and Shively, J. E. (1991) Isolation and amino acid sequence analysis of bovine adrenal 3β-hydroxysteroid dehydrogenase/steroid isomerase, *Biochemistry* **30,** 8108-8116.

164. Rutherfurd, K. J., Chen, S., and Shively, J. E. (1991) Affinity labeling of bovine adrenal 3β-hydroxysteroid dehydrogenase/steroid isomerase by 5'-[p-(fluorosulfonyl)benzoyl]adenosine, *Biochemistry* **30,** 8116-8123.

165. Bruton, C. J., and Hartley, B. S. (1970) Chemical studies on methionyl-tRNA synthetase from *Escherichia coli*, *J. Mol. Biol.* **52,** 165-178.

166. Bailey, J. M. (1995) Chemical methods of protein sequence analysis, *J. Chromatogr.* **705,** 47-65.

167. Siuzdak, G. (1994) The emergence of mass spectrometry in biochemical research, *Proc. Natl. Acad. Sci. USA* **91,** 11290-11297.

168. Mann, M., and Wilm, M. (1995) Electrospray mass spectrometry for protein characterization, *TIBS* **20,** 219-224.

169. Nguyen, D. N., Becker, G. W., and Riggin, R. M. (1995) Protein mass spectrometry: applications to analytical biotechnology, *J. Chromatogr.* **705,** 21-45.

170. Hofstadler, S. A., Bakhtiar, R., and Smith, R. D. (1996) Electrospray ionization mass spectrometry. Part I. Instrumentation and spectral interpretation, *J. Chem. Educ.* **73,** A82-A88.

171. Hrkal, Z. (1979) Gel-type techniques, in *Journal of Chromatography Library. Electrophoresis - a survey of techniques and applications part A: techniques*, (Deyl, Z., ed.) **18,** pp. 121, Elsevier Scientific Publishing Company, Amsterdam.

172. Canfield, R. E. (1963) Peptides derived from tryptic digestion of egg white lysozyme, *J. Biol. Chem.* **238,** 2691-2697.

173. Noda, Y., Fujiwara, K., Yamamoto, K., Fukuno, T., and Segawa, S. (1994) Specificity of trypsin digestion and conformational flexibility at different sites of unfolded lysozyme, *Biopolymers* **34,** 217-226.

174. Okazaki, K., Imoto, T., Yamada, H., Kuroki, R., and Fujita, K. (1982) Specificity of trypsin. Cleavage of aspartic acid 101 derivatives of lysozyme by trypsin, *J. Biol. Chem.* **257,** 12559-12562.

175. Yamada, H., Ueda, T., Kuroki, R., Fukumura, T., Yasukochi, T., Hirabayashi, T., Fujita, K., and Imoto, T. (1985) Isolation and characterization of 101-β-lysozyme that possesses the β-aspartyl sequence at aspartic acid-101, *Biochemistry* **24,** 7953-7959.

176. Switzer, R. C. III, Merril, C. R., and Shifrin, S. (1979) A highly sensitive silver stain for detecting proteins and peptides in polyacrylamide gels, *Anal. Biochem.* **98,** 231-237.

177. Tsai, C. -M., and Frasch, C. E. (1982) A sensitive silver stain for detecting lipopolysaccharides in polyacrylamide gels, *Anal. Biochem.* **119,** 115-119.

178. Dubray, G., and Bezard, G. (1982) A highly sensitive periodic acid-silver stain for 1,2-diol groups of glycoproteins and polysaccharides in polyacrylamide gels, *Anal. Biochem.* **119,** 325-329.

179. Mattox, V. R., Litwiller, R. D., and Nelson, A. N. (1979) A comparison of procedures for attaching steroidal glucosiduronic acids to bovine serum albumin, *J. Steroid Biochem.* **10,** 167-172.

180. Vaughan, J. R., and Osata, R. L. (1952) The preparation of peptides using mixed carbonic carboxylic acid anhydrides, *J. Am. Chem. Soc.* **74,** 676-678.

181. Nakamura, S., Gohya, Y., Losso, J. N., Nakai, S., and Kato, A. (1996) Protective effect of lysozyme-galactomannan or lysozyme-palmitic acid conjugates against *Edwardsiella tarda* infection in carp, *Cyprinus carpio* L., *FEBS Lett.* **383,** 251-254.

182. Frieden, E. H. (1956) "Enzymoid" properties of lysozyme methyl ester, *J. Am. Chem. Soc.* **78,** 961-965.

183. Yamasaki, N., Hayashi, K., and Funatsu, M. (1968) Acetylation of lysozyme: Part II. Mechanism of lysis by lysozyme, *Agr. Biol. Chem.* **32,** 64-68.

184. Davies, R. C., and Neuberger, A. (1969) Modification of lysine and arginine residues of lysozyme and the effect on enzymatic activity, *Biochim. Biophys. Acta* **178,** 306-317.

185. Imoto, T., Johnson, L. N., North, A. C. T., Phillips, D. C., and Ruplet, J. A. (1972) Vertebrate lysozymes, in *The Enzymes* (Boyer, P. D., ed.) 3rd edn, **Vol. VII,** Chapter 21, pp. 781, Academic Press, New York, NY.

186. Price, J. A. R., and Pethig, R. (1986) Surface charge measurements on *Micrococcus lysodeikticus* and the catalytic implications for lysozyme, *Biochim. Biophys. Acta* **889,** 128-135.

187. Smyth, D. G. (1967) Techniques in enzyme hydrolysis, in Enzyme structure, Section V. Cleavage of peptide chains (ed. Hirs, C. H. W.), *Methods Enzymol.* **11,** 214-231.

188. Winter, G. (1986) Manual sequence strategy - a personal view, in *Practical Protein Chemistry*, (Darbre, A., ed.) chapter 10, pp. 349, J. Wiley and Sons Ltd, New York, NY.

189. Kuroki, R., Yamada, H., Moriyama, T., and Imoto, T. (1986) Chemical mutations of the catalytic carboxyl groups in lysozyme to the corresponding amides, *J. Biol. Chem.* **261,** 13571-13574.

190. Inoue, M., Yamada, H., Yasukochi, T., Kuroki, R., Miki, T., Horiuchi, T., and Imoto, T. (1992) Multiple role of hydrophobicity of tryptophan-108 in chicken lysozyme: structural stability, saccharide binding ability, and abnormal $pK_a$ of glutamic acid-35, *Biochemistry* **31,** 5545-5553.

191. Tomizawa, H., Yamada, H., Ueda, T., and Imoto, T. (1994) Isolation and characterization of 101-succinimide lysozyme that possesses the cyclic imide at Asp101-Gly102, *Biochemistry* **33,** 8770-8774.

192. Pike, A. S. C., and Acharya, K. R. (1994) A structural basis for the interaction of urea with lysozyme, *Protein Science* **3,** 706-710.

193. Fujita, Y., and Noda, Y. (1992) Effect of alkylation with different sized substituents on thermal stability of lysozyme, *Int. J. Peptide Protein Res.* **40,** 103-109.

194. Gerken, T. A., Jentoft, J. E., Jentoft, N., and Dearborn, D. G. (1982) Intramolecular interactions of amino groups in $^{13}C$ reductively methylated hen egg-white lysozyme, *J. Biol. Chem.* **257,** 2894-2900.

195. Eagleson, M., and Scott, T. (1988) *Concise Encyclopedia Biochemistry*, 2nd edn., pp. 147, Walter de Gruyter & Co., Berlin, Germany.

196. Stryer, L. (1988) *Biochemistry*, 3rd edn., chapter 17, pp. 402, W. H. Freeman and Company, New York.

197. Hamaguchi, K. (1958) Studies on the denaturation of lysozyme. II. Urea denaturation, *J. Biochem. (Tokyo)* **45,** 79-88.

198. Parente, E. S., and Wetlaufer, D. B. (1984) Influence of urea on the high-performance cation-exchange chromatography of hen egg white lysozyme, *J. Chromatogr.* **288,** 389-398.

199. Fischmann, T. O., Bentley, G. A., Bhat, T. N., Boulot, G., Mariuzza, R. A., Phillips, S. E. V., Tello, D., and Poljak, R. J. (1991) Crystallographic refinement of the three-dimensional structure of the FabD1.3-lysozyme complex at 2.5-Å resolution, *J. Biol. Chem.* **266,** 12915-12920.

200. Braden, B. C., Souchon, H., Eiselé, J. L., Bentley, G. A., Bhat, T. N., Navaza, J., and Poljack, R. J. (1994) Three dimensional structures of the free and the antigen complexed Fab from monoclonal antilysozyme antibody D44.1, *J. Mol. Biol.* **243,** 767-781.

201. Sheriff, S., Silverton, E. W., Padlan, E. A., Cohen, G. H., Smith-Gill, S. J., Finzel, B. C., and Davies, D. R. (1987) Three-dimensional structure of an antibody-antigen complex, *Proc. Natl. Acad. Sci. USA* **84,** 8075-8079.

202. Padlan, E. A., Silverton, E. W., Sheriff, S., Cohen, G., Smith-Gill, S. J., and Davies, D. R. (1989) Structure of an antibody-antigen complex: Crystal structure of the HyHEL-10 Fab-lysozyme complex, *Proc. Natl. Acad. Sci. USA* **86,** 5938-5942.

203. Arevalo, J. H., Stura, E. A., Taussig, M. J., and Wilson, I. A. (1993) Three-dimensional structure of an anti-steroid Fab' and progesterone-Fab' complex, *J. Mol. Biol.* **231,** 103-118.

204. Duax, W. L., Weeks, C. M., and Rohrer, D. C. (1976) Crystal structures of steroids, in *Topics in Stereochemistry*, (Eliel, E. L., and Allinger, N., eds.) pp. 271-383, Wiley, New York.

205. Cook, B., and Beastall, G. H. (1987) Measurement of steroid hormone concentrations in blood, urine and tissues, in *Steroid hormones - a practical approach*, (Green, B., and Leake, R. E., eds.) chapter 1, pp. 1-3, IRL Press Limited, Oxford, England.

206. Cooper, A., Norton, D. A., and Hauptman, H. (1969) Estrogenic steroids. III. The crystal and molecular structure of estriol, *Acta Cryst.* **B25,** 814-828.

207. Busetta, P. B., Courseille, C., and Hospital, M. (1973) Structures cristallines et moléculaires de trois formes polymorphes de l'oestrone, *Acta Cryst.* **B29,** 298-313.

208. Hadd, H. E., Slikker, W., Miller, D. W., Jr., Helton, E. D., Duax, W., Strong, P. D., and Swenson, D. C. (1983) Synthesis and characterization of the anomeric pair of 17β-glucuronides of ethynylestradiol, *J. Steroid Biochem.* **18,** 81-87.

209. Wu, Y., Waters, J. M., and Blackwell, L. F. (1996) X-ray crystal structure analysis and $^{13}C$ NMR investigation of estriol 16- and 17-monoglucuronide derivatives, *J. Chem. Soc. Perkin Trans. II* **7,** 1449-1453.

210. Ohrt, J. M., Cooper, A., and Norton, D. A. (1969) Crystal and molecular structure of 3β-17α-dihydroxy-16β-bromo-5α-pregnane-11,20-dione and its comparison with the related -16β-bromo-3β-acetate and -21-bromo-3β-ol analogs, *Acta Cryst.* **B25,** 41-51.

211. Roberts, P. J., Coppola, J. C., Isaacs, N. W., and Kennard, O. (1973) Crystal and molecular structure of cortisol (11β, 17α, 21-trihydroxy-pregn-4-ene-3,20-dione) methanol solvate, *J. Chem. Soc. Perkin Trans. II* , 774-781.

212. Duax, W. L., and Osawa, Y. (1980) Steroid structure and function-VI. The molecular conformation of 19-hydroxy-4-androstene-3,17-dione, as an intermediate for estrogen synthetase, *J. Steroid Biochem.* **13,** 383-386.

213. Danilova, N. P. (1994) ELISA screening of monoclonal antibodies to haptens: influence of the chemical structure of hapten-protein conjugates, *J. Immunol. Methods* **173,** 111-117.

214. Goodrow, M. H., Sanborn, J. R., Stoutamire, D. W., Gee, S. J., and Hammock, B. D. (1995) Strategies for immunoassay hapten design, *ACS Symposium Series* **586,** chapter 9, 119-139.

215. Lindner, H. R., Perel, E., Friedlander, A., and Zeitlin, A. (1972) Specificity of antibodies to ovarian hormones in relation to the site of attachment of the steroid hapten to the peptide carrier, *Steroids* **19,** 357-375.

216. Van Weemen, B. K., and Schuurs, A. H. W. M. (1975) The influence of heterologous combinations of antiserum and enzyme-labeled estrogen on the characteristics of estrogen enzyme-immunoassays, *Immunochemistry* **12,** 667-670.

217. Hosoda, H., Kobayashi, N., and Nambara, T. (1983) Effect of bridge heterologous combination on sensitivity in enzyme immunoassay for 11-deoxycortisol, *Chem. Pharm. Bull.* **31,** 953-958.

218. Hosoda, H., Kobayashi, N., Ishii, N., and Nambara, T. (1986) Bridging phenomena in steroid immunoassays. The effect of bridge length on sensitivity in enzyme immunoassay, *Chem. Pharm. Bull.* **34,** 2105-2111.

219. Pratt, J. J. (1978) Steroid immunoassay in clinical chemistry, *Clin. Chem.* **24,** 1869-1890.

220. Fránek, M. (1987) Structural aspects of steroid-antibody specificity, *J. Steroid Biochem.* **28,** 95-108.

221. Bermúdez, J. A., Coronado, V., Mijares, A., León, C., Velázquez, A., Noble, P., and Mateos, J. L. (1975) Stereochemical approach to increase the specificity of steroid antibodies, *J. Steroid Biochem.* **6,** 283-290.

222. Podestá, A., and Montagnoli, G. (1994) Specificity in protein-ligand interactions: a model from estrone-antiserum binding, *Biochim. Biophys. Acta* **1200,** 291-296.

223. Rypniewski, W. R., Holden, H. M., and Rayment, I. (1993) Structural consequences of reductive methylation of lysine residues in hen egg white lysozyme: An x-ray analysis at 1.8-Å resolution, *Biochemistry* **32,** 9851-9858.

224. Davies, D. R., and Padlan, E. A. (1990) Antibody-antigen complexes, *Annu. Rev. Biochem.* **59,** 439-473.

225. Davies, D. R., and Cohen, G. H. (1996) Interactions of protein antigens with antibodies, *Proc. Natl. Acad. Sci. USA* **93,** 7-12.

226. Jones, S., and Thornton, J. M. (1996) Principles of protein-protein interactions, *Proc. Natl. Acad. Sci. USA* **93,** 13-20.

227. Smith-Gill, S. J., Wilson, A. C., Potter, M., Prager, E. M., Feldmann, R. J., and Mainhart, C. R. (1982) Mapping the antigenic epitope for a monoclonal antibody against lysozyme, *J. Immunol.* **128,** 314-322.

228. Smith-Gill, S. J., Lavoie, T. B., and Mainhart, C. R. (1984) Antigenic regions defined by monoclonal antibodies correspond to structural domains of avian lysozyme, *J. Immunol.* **133,** 384-393.

229. Grivel, J.-C., and Smith-Gill, S. J. (1996) Lysozyme: Antigenic structure as defined by antibody and T cell responses, in *Structure of Antigens*, (Van Regenmortel, M. H. V., ed.) **3,** chapter 5, pp. 91-154, CRC Press, Inc., Boca Raton, Florida, USA.

230. Amit, A. G., Mariuzza, R. A., Phillips, S. E. V., and Poljak, R. J. (1986) Three-dimensional structure of an antigen-antibody complex at 2.8 Å resolution, *Science* **233,** 747-753.

231. Cohen, G. H., Sheriff, S., and Davies, D. R. (1996) Refined structure of the monoclonal antibody HyHEL-5 with its antigen hen egg-white lysozyme, *Acta Cryst.* **D52,** 315-326.

232. de Lauzon, S., Rajkowski, K. M., and Cittanova, N. (1994) Investigation of a 17β-estradiol-monoclonal antiestradiol antibody binding mechanism using dilute solutions of organic solvents, *J. Steroid Biochem. Molec. Biol.* **48,** 225-233.

233. Fleming, A. (1955) The discovery of penicillin, *Brit. Med. J.* **1,** 711-??

234. Fleming, A. (1922) On a remarkable bacteriolytic element found in tissues and secretions, *Proc. Roy. Soc. London* **B93,** 306-317.

235. Berger, L. R., and Weiser, R. S. (1959) The β-glucosaminidase activity of egg-white lysozyme, *Biochim. Biophys. Acta* 26, 517-521.

236. Jolles, P., and Jolles, J. (1984) What's new in lysozyme research, *Mol. Cell. Biochem.* **63,** 165-189.

237. Blake, C. C. F., Koenig, D. F., Mair, G. A., North, A. C. T., Phillips, D. C., and Sarma, V. R, (1965) Structure of hen egg-white lysozyme. A three-dimensional fourier synthesis at 2 Å resolution, *Nature* **206,** 757-761.

238. Salton, M. R. J. (1952) Cell wall of *Micrococcus lysodeikticus* as the substrate of lysozyme, *Nature* **170,** 746-747.

239. Jeanloz, R. W., Sharon, N., and Flowers, H. M. (1963) The chemical structure of a disaccharide isolated from *Micrococcus lysodeikticus* cell wall, *Biochem. Biophys. Res. Commun.* **13,** 20-25.

240. Johnson, L. N., and Phillips, D. C. (1965) Structure of some crystalline lysozyme-inhibitor complexes determined by x-ray analysis at 6 Å resolution, *Nature* **206,** 761-763.

241. Kirby, A. J. (1987) Mechanism and stereoelectronic effects in the lysozyme reaction, *Crit. Rev. Biochem.* **22,** 283-315.

242. Ford, L. O., Johnson, L. N., Machin, P. A., Phillips, D. C., and Tjian, R. (1974) Crystal structure of a lysozyme-tetrasaccharide lactone complex, *J. Mol. Biol.* **88,** 349-371.

243. Strynadka, N. C. J., and James, M. N. G. (1991) Lysozyme revisited: crystallographic evidence for distortion of an N-acetylmuramic acid residue bound in site D, *J. Mol. Biol.* **220,** 401-424.

244. Stryer, L. (1988) Mechanisms of enzyme action, in *Biochemistry*, 3rd edn. chapter 9, pp. 206, W. H. Freeman and Company, New York.

245. Parsons, S. M., Jao, L., Dahlquist, F. W., Borders, C. L., Jr., Groff, T., Racs, J., and Raftery, M. A. (1969) The nature of the amino acid side chains which are critical for the activity of lysozyme, *Biochemistry* **8,** 700-712.

246. Eshdat, Y., Dunn, A., and Sharon, N. (1974) Chemical conversion of aspartic acid 52, a catalytic residue in hen egg-white lysozyme, to homoserine, *Proc. Natl. Acad. Sci. U.S.A.* **71,** 1658-1662.

247. Yamada, H., Imoto, T., and Noshita, S. (1982) Modification of catalytic groups in lysozyme with ethyleneimine, *Biochemistry* **21,** 2187-2192.

248. Matsumura, I., and Kirsch, J. F. (1996) Is aspartate 52 essential for catalysis by chicken egg white lysozyme? The role of natural substrate-assisted hydrolysis, *Biochemistry* **35,** 1881-1889.

249. Dao-Pin, S., Liao, D. -I., and Remington, S. J. (1989) Electrostatic fields in the active sites of lysozymes, *Proc. Natl. Acad. Sci. U.S.A.* **86,** 5361-5365.

250. Gorin, G., Wang, S. -F., and Papapavlou, L. (1971) Assay of lysozyme by its lytic action on *M. lysodeikticus* cells, *Anal. Biochem.* **39,** 113-127.

251. Mörsky, P. (1983) Turbidimetric determination of lysozyme with *Micrococcus lysodeikticus* cells: reexamination of reaction conditions, *Anal. Biochem.* **128,** 77-85.

252. Shugar, D. (1952) Ultra-violet inactivation of lysozyme, *Biochim. Biophys. Acta* **8,** 302-310.

253. Jolles, P. (1962) Lysozymes from rabbits spleen and dog spleen, *Meth. Enzymol.* **5,** 137-140.

254. Rupley, J. A., and Gates, V. (1967) Studies on the enzymic activity of lysozyme, II. The hydrolysis and transfer reactions of N-acetylglucosamine oligosaccharides, *Proc. Natl. Acad. Sci. U.S.A.* **57,** 496-510.

255. Lamoyi, E., and Nisonoff, A. (1983) Preparation of $F(ab')_2$ fragments from mouse IgG of various subclasses, *J. Immunol. Meth.* **56,** 235-243.

256. Parham, P. (1983) On the fragmentation of monoclonal IgG1, IgG2a, and IgG2b from BALB/c mice, *J. Immunol.* **131,** 2895-2902.

257. Parham, P. (1986) Preparation and purification of active fragments from mouse monoclonal antibodies, in *Handbook of Experimental Immunology in Four Volumes, Volume 1: Immunochemistry* (Weir, D. M., ed.) Blackwell Scientific Publications, Oxford, Great Britain, 4th edn, **vol. 1,** chapter 14.

258. Laemmli, U. K. (1970) Cleavage of structural proteins during the assembly of the head of bacteriophage $T_4$, *Nature* **227,** 680-685.

259. GraphPad Prism™ (Version 2.0), (1994) User's Guide, GraphPad Software, Inc., 10855 Sorrento Valley Road #203, San Diego, CA 92121, U.S.A.

260. Fantl, V. E., and Wang, D. Y., (1984) Simultaneous production of monoclonal antibodies to dehydroepiandrosterone, oestradiol, progesterone and testosterone, *J. Endocr.* **100,** 367-376.

261. Gordon, M. S., and Notides, A. C. (1986) Computer modelling of estradiol interactions with the estradiol receptor, *J. Steroid Biochem.* **25,** 177-181.

262. Kaufman, M. and Pinsky, L. (1989) A single-site allosteric model of intracellular androgen-receptor interaction, *J. Steroid Biochem.* **32,** 113-119.

263. Imoto, T., Johnson, L. N., North, A. C. T., Phillips, D. C., and Ruplet, J. A. (1972) Vertebrate lysozymes, in *The Enzymes* (Boyer, P. D., ed.) 3rd edn, **Vol. VII,** Chapter 21, pp. 840, Academic Press, New York, NY.

264. Rupley, J. A., Butler, L., Gerring, M., Hartdegen, F. J., and Pecoraro, R. (1967) Studies on the enzymic activity of lysozyme, III. The binding of saccharides, *Biochemistry* **57,** 1088-1095.

265. Imoto, T., Johnson, L. N., North, A. C. T., Phillips, D. C., and Ruplet, J. A. (1972) Vertebrate lysozymes, in *The Enzymes* (Boyer, P. D., ed.) 3rd edn, **Vol. VII,** Chapter 21, Academic Press, New York, NY.

266. Smith-Gill, S. J., Rupley, J. A., Pincus, M. R., Carty, R. P., and Scheraga, H. A. (1984) Experimental identification of a theoretically predicted "left-sided" binding mode for $(GlcNAc)_6$ in the active site of lysozyme, *Biochemistry* **23,** 993-997.

267. Pincus, M. R., and Scheraga, H. A. (1981) Prediction of the three-dimensional structures of complexes of lysozyme with cell wall substrates, *Biochemistry* **20,** 3960-3965.

268. Welinder, K. G. (1979) Amino acid sequence studies of horseradish peroxidase. Amino and carboxyl termini, cyanogen bromide and tryptic fragments, the complete sequence, and some structural characteristics of horseradish peroxidase C, *Eur. J. Biochem.* **96,** 483-502.

269. Welinder, K. G. (1985) Plant peroxidases, Their primary, secondary and tertiary structures, and relation to cytochrome c peroxidase, *Eur. J. Biochem.* **151,** 497-504.

270. Litman, D. J., Lee, R. H., Jeong, H. J., Tom, H. K., Stiso, S. N., Sizto, N. C., and Ullman, E. F. (1983) An internally referenced test strip immunoassay for morphine, *Clin. Chem.* **29,** 1598-1603.

271. Chen, R., Li, T. M., Merrick, H., Parrish, R. F., Bruno, V., Kwong, A., Stiso, C., and Litman, D. J. (1987) An internal clock reaction used in a one-step enzyme immunochromatographic assay of theophylline in whole blood, *Clin. Chem.* **33,** 1521-1525.

272. Li, T. M., Chen, R., Leeder, S., Stiso, S. N., Sizto, N. C., Zuk, R. F., and Litman, D. J. (1987) One-step enzyme immunochromatographic assay for theophylline, *Anal. Biochem.* **166,** 276-283.

273. Allen, M. P., DeLizza, A., Ramel, U., Jeong, H., and Singh, P. (1990) A noninstrumental quantitative test system and its application for determining cholesterol concentration in whole blood, *Clin. Chem.* **36,** 1591-1597.

274. Monaco, F., Gianelli, M., Dimanico, U., and Mutani, R. (1990) A simple and disposable visual measuring device to assay antiepileptic drugs from whole blood samples, *Ther. Drug Monit.* **12,** 359-361.

275. Ramadass, P., Meerarani, S., and Padmanaban, V. D. (1993) Dipstick enzyme immunoassay for rinderpest antibody in cattle, *Vet. Microbiol.* **36,** 385-388.

276. Fernández, D., Valle, I., Llamos, R., Guerra, M., Sorell, L., and Gavilondo, J. (1994) Rapid detection of rotavirus in faeces using a dipstick system with monoclonal antibodies and colloidal gold as marker, *J. Virol. Methods* **48,** 315-323.

277. Bangs, L. B. (1994) Review of "commercial latex diagnostic tests" (immunological applications of microspheres) Workshop Notes, The Latex Course (January 12th 1994), Bangs Laboratories, Inc., Carmel, IN.

278. Leuvering, J. H. W., Thal, P. J. H. M., van der Waart, M., and Schuurs, A. H. W. M. (1980) Sol particle immunoassay (SPIA), *J. Immunoassay* **1,** 77-91.

279. Leuvering, J. H. W., Thal, P. J. H. M., van der Waart, M., and Schuurs, A. H. W. M. (1981) A sol particle agglutination assay for human chorionic gonadotrophin, *J. Immunol. Methods* **45,** 183-194.

280. Hsu, Y. -H. (1984) Immunogold for detection of antigen on nitrocellulose paper, *Anal. Biochem.* **142,** 221-225.

281. Moeremans, M., Daneels, G., Van Dijck, A., Langanger, G., and De Mey, J. (1984) Sensitive visualization of antigen-antibody reactions in dot and blot immune overlay assays with immunogold and immunogold/silver staining, *J. Immunol. Methods* **74,** 353-360.

282. Stott, D. I. (1989) Immunoblotting and dot blotting, *J. Immunol. Methods* **119,** 153-187.

283. Coco Martin, J. M., Pàques, M., van der Velden-de Groot, T. A. M., and Beuvery, E. C. (1990) Characterisation of antibody labelled colloidal gold particles and their applicability in a sol particle immunoassay (SPIA), *J. Immunoassay* **11,** 31-47.

284. Gupta, R., Talwar, G. P., and Gupta, S. K. (1992) Rapid antibody capture assay for detection of group-A streptococci using monoclonal antibody and colloidal gold-monospecific polyvalent antibody conjugate, *J. Immunoassay* **13,** 441-455.

285. Bradshaw, P., Fitzgerald, D., Stephens, L., Baddam, S., Doe, J., Hua, J., and Chandler, H. (1995) FlexSure® test device: qualitative immunochromatographic test format, *Clin. Chem.* **41,** 1360-1363.

286. Dykman, L. A., Matora, L. Y., and Bogatyrev, V. A. (1996) Use of colloidal gold to obtain antibiotin antibodies, *J. Microbiol. Methods* **24,** 247-248.

287. May, K. (Unipath Ltd., Bedford, UK, personal communication).

288. Hendry, R. M., and Herrmann, J. E. (1980) Immobilization of antibodies on nylon for use in enzyme-linked immunoassay, *J. Immunol. Methods* **35,** 285-296.

289. Hoffman, W. L., and Jump, A. A. (1986) Tween 20 removes antibodies and other proteins from nitrocellulose, *J. Immunol. Methods* **94,** 191-196.

290. Gregorius, K., Mouritsen, S., and Elsner, H. I. (1995) Hydrocoating: a new method for coupling biomolecules to solid phases, *J. Immunol. Methods* **181,** 65-73.

291. Steinitz, M., and Tamir, S. (1995) An improved method to create nitrocellulose particles suitable for the immobilization of antigen and antibody, *J. Immunol. Methods* **187,** 171-177.

292. Collin, R. (personal communication).

293. Frens, G. (1973) Controlled nucleation for the regulation of the particle size in monodisperse gold suspensions, *Nature Phys. Sci.* **241,** 20-22.

294. Ching, S., Gordon, J., and Billing, P. A. (1989) Process for immunochromatography with colloidal particles, Eur. Pat. Appl. EP 299 428 A2.

295. Geoghegan, W. D., and Ackerman, G. A. (1977) Adsorption of horseradish peroxidase, ovomucoid and anti-immunoglobulin to colloidal gold for the indirect detection of concanavalin A, wheat germ agglutinin and goat anti-human immunoglobulin G on cell surfaces at the electron microscopic level: A new method, theory and application, *J. Histochem. Cytochem.* **11,** 1187-1200.

296. McPherson, A. (1990) Current approaches to macromolecular crystallization, *Eur. J. Biochem.* **189,** 1-23.

297. Rhodes, G. (1993) Crystallography made crystal clear. A guide for users of macromolecular models, Academic Press, Inc., San Diego.

298. Kundrot, C. E., and Richards, F. M. (1987) Crystal structure of hen egg-white lysozyme at a hydrostatic pressure of 1000 atmospheres, J. *Mol. Biol.* **193,** 157-170.

299. Steinrauf, L. K. (1959) Preliminary X-ray data for some new crystalline forms of β-lactoglobulin and hen egg-white lysozyme, *Acta Cryst.* **12,** 77-78.

300. Moult, J., Yonath, A., Traub, W., Smilansky, A., Podjarny, A., Rabinovich, D., and Saya, A. (1976) The structure of triclinic lysozyme at 2.5 Å resolution, *J. Mol. Biol.* **100,** 179-195.

301. Hogle, J., Rao, S. T., Mallikarjunan, M., Beddell, C., McMullan, R. K., and Sundaralingam, M. (1981) Studies of monoclinic hen egg white lysozyme. I. Structure solution at 4 Å resolution and molecular-packing comparisons with tetragonal and triclinic lysozymes, *Acta Cryst.* **B37,** 591-597.

302. Hodsdon, J. M., Brown, G. M., Sieker, L. C., and Jensen, L. H. (1990) Refinement of triclinic lysozyme: I. Fourier and least-squares methods, *Acta Cryst.* **B46,** 54-62.

303. Rao, S. T., and Sundaralingam, M. (1996) Studies of monoclinic hen egg-white lysozyme. IV. X-ray refinement at 1.8 Å resolution and a comparison of the variable regions in the polymorphic forms, *Acta Cryst.* **D52,** 170-175.

304. Sheldrick, G. M. (1986) SHELXS86. A program for the solution of crystal structures from diffraction data, University of Göttingen, Germany.

305. Sheldrick, G. M. (1993) SHELXL93. Fortran-77 program for the refinement of crystal structures from diffraction data, University of Göttingen, Germany.

306. Zsolnai, L. (1994) XPMA. A program for Molecular Graphics, University of Heidelburg, Germany.

307. Jancarik, J., and Kim, S. -H. (1991) Sparse matrix sampling: a screening method for crystallisation of proteins, *J. Appl. Cryst.* **24,** 409-411.

308. Thaller, C., Weaver, L. H., Eichele, G., Wilson, E., Karlsson, R., and Jansonius, J. N. (1981) Repeated seeding technique for growing large single crystals of proteins, *J. Mol. Biol.* **147,** 465-469.

309. Stura, E. A., and Wilson, I. A. (1990) Analytical and production seeding techniques, *METHODS: A companion to methods in Enzymology* **1,** 38-49.

310. Rossman, M. G., and Blow, D. M. (1962) The detection of sub-units within the crystallographic asymmetric unit, *Acta Cryst.* **15,** 24-31.

311. Jeffrey, P. D. (personal communication).

312. Phillips, D. C. (1967) The hen egg-white lysozyme molecule, *Proc. Natl. Acad. Sci. U.S.A.* **57,** 484-495.

313. Brünger, A. T. (1992) Free R value: a novel statistical quantity for assessing the accuracy of crystal structures, *Nature* **355,** 472-475.

314. Young, A. C. M., Tilton, R. F., and Dewan, J. C. (1994) Thermal expansion of hen egg-white lysozyme. Comparison of the 1.9 Å resolution structures of the tetragonal form of the enzyme at 100 K and 298 K, *J. Mol. Biol.* **235,** 302-317.

315. Laver, W. G. (1990) Crystallization of antibody-protein complexes, *METHODS: A companion to methods in Enzymology* **1,** 70-74.

316. Mariuzza, R. A., Jankovic, D. L., Boulot, G., Amit, A. G., Saludjian, P., Le Guern, A., Mazié, J. C., and Poljak, R. J. (1983) Preliminary crystallographic study of the complex between the Fab fragment of a monoclonal anti-lysozyme antibody and its antigen, *J. Mol. Biol.* **170,** 1055-1058.

317. Silverton, E. W., Padlan, E. A., Davies, D. R., Smith-Gill, S., and Potter, M. (1984) Crystalline monoclonal antibody Fabs complexed to hen egg white lysozyme, *J. Mol. Biol.* **180,** 761-765.